To the Graduate Council:

I am submitting herewith a dissertation written by Wataru Minoshima entitled "Experimental and Theoretical Investigation of Multiaxial Elongational Flow and Processing of Polymer Melts." I have examined the final copy of this dissertation for form and content and recommend that it be accepted in partial fulfillment of the requirements for the degree of Doctor of Philosophy, with a major in Polymer Engineering.

James L. White, Major Professor

We have read this dissertation and recommend its acceptance:

Accepted for the Council:

The Graduate School

EXPERIMENTAL AND THEORETICAL INVESTIGATION OF MULTIAXIAL ELONGATIONAL FLOW AND PROCESSING OF POLYMER MELTS

A Dissertation

Presented for the

Doctor of Philosophy

Degree

The University of Tennessee, Knoxville

Wataru Minoshima

August 1983

Lord, when thou wentest out
of Seir, when thou marchest out
of the field of Edom, the earth
trembled, and the heavens dropped,
the clouds also dropped water,
The mountains melted from
before the Lord, even that Sinai
from before the Lord God of Israel,

Judges 5

ACKNOWLEDGMENTS

The author is indebted to the many persons who have been of assistance in various ways to make the investigation possible.

First and foremost, I would like to express my sincere appreciation to Professor James L. White, the author's advisor and mentor over the past seven years, for his guidance during the course of the research. Professor White's support and encouragement have given me the perseverance needed to complete this dissertation.

The author is also very grateful to Professor Donald C. Bogue and Professor Jirō Shimizu of the Tokyo Institute of Technology for their helpful comments and suggestions.

The cooperation of several individuals who provided direct help in the research studies themselves is also acknowledged. To these individuals, the author offers his appreciation for their generous help on several matters: Dr. Ramesh N. Shroff of Chemplex Company for providing GPC data for eleven samples; Dr. George N. Foster of Union Carbide for supplying four samples and molecular characterization data; Mr. R. T. Werkman of Phillips Petroleum Company for providing molecular characterization data and helping to provide four samples; Dr. James M. Rieke of Dow Chemical for providing GPC data and polystyrene samples; Dr. George Vassilatos of E. I. duPont deNemours and Co., Messrs. Mike A. Smith and R. F. Martinovich of Phillips Petroleum Company, Mr. W. J. Pearson of Dow Chemical, and Dr. David C. Huang and Mr. Larry Dowd of Chemplex Company for

providing samples; Mr. Peter Herh of Rheometric Inc. for measuring dynamic properties of three samples; Mr. Alan P. Richards of American Enka for making "pellet" samples from strand-like samples. And sincere appreciation goes to Dr. Yoshiaki Ide of Celanese Research Company for his supplying research notes on the disturbance growth of filaments during uniaxially stretching; and, finally, to Professor Toshirō Masuda of Kyoto University for supplying unpublished research data.

Also, the financial support of the National Science Foundation and the Polymer Consortium of The University of Tennessee, Knoxville is acknowledged.

Thanks are also extended to all of the faculty members and students who have made useful suggestions and provided a stimulating environment during the author's seven years' study. Special thanks are extended to Mr. Howell B. Thompson of the Machine Shop and to Mr. Ted Long of the Electronics Shop.

A special note of appreciation is given to Miss Jennifer Leslie, secretary in the Polymer Engineering Department, who helped the author many times in his job as a staff assistant.

The tedious task of typing was performed by Ms. Maxine Martin, to whom the author is extremely grateful.

Finally, the author wishes to express his appreciation to his parents and his younger brother, Kohji, for their support and encouragement.

ABSTRACT

Several of the most important polymer processing operations involve the deformation of melt streams in the absence of walls. Such processes in which applied stresses act in the absence of walls result in elongation of polymer melts. This includes uniaxial elongation for melt spinning, multiaxial elongation for film casting, tubular blown film extrusion, thermoforming, blow molding and stretch blow molding. One of the most important problems associated with these operations is the influence of the rheological properties of the melts on the ability to form the desired products. To understand these processes we must be concerned with the behavior of polymer melts in elongational flow, especially multiaxial elongational flow.

Instabilities undergoing multiaxial elongational flow (including uniaxial extension) were considered in both isolated (batch) systems and continuous systems. Major attention was given to the differences in geometry, conservation equations (such as the continuity and force balance equation), and rheological properties.

The growth of disturbances in isolated sheets and annular cylinders of viscoelastic fluids, Newtonian fluids, and elastic solids undergoing multiaxial elongational flow was considered. Both stable and unstable flow were of concern in the film extrusion processes (including a melt spinning process). Unstable flows in the draw down and blowing processes were considered. An attempt was made

to develop a general perspective of the response or processability undergoing continuous multiaxial elongation (including uniaxial extension) of polymer melts as functions of their rheological properties (such as steady shear flow behavior and uniaxial elongational flow behavior) and in terms of a convected Maxwell model. This was correlated with molecular structure such as molecular weight, molecular weight distribution, and degree of long chain branching.

TABLE OF CONTENTS

CHAPTER PAGE

LIST OF TABLES

LIST OF FIGURES

FIGURE PAGE

FIGURE PAGE

FIGURE PAGE

CHAPTER I

INTRODUCTION

Polymer melt forming operations are of two general types. In extrusion and injection molding, forming occurs between walls in heated dies and molds. This involves shearing motions of melts. Several of the most important polymer processing operations, however, involve the deformation of melt streams in the absence of walls. Such processes in which applied stresses act in the absence of walls result in elongation of polymer melts. This includes uniaxial elongation for melt spinning, but multiaxial elongation for film casting, tubular blown film extrusion, thermoforming and blow molding.

One of the most important problems associated with these operations is the influence of the rheological properties of the melt on the ability to form the desired products. However, it has scarcely been for a decade that extensional flow has received any significant scientific attention, and there is far from complete understanding. To understand these processes one must be concerned with the behavior of polymer melts in elongational flow, especially multiaxial elongational flow.

Both stable and unstable flow are of concern in the cast and tubular blown film extrusion processes. Unstable flows are well known in both the die (called "extrudate distortion" or "melt fracture") and in the drawdown and blowing process (called "draw resonance" and "bubble instabilities"). The close relationship of

instabilities to system geometry requires their study in experiments approaching industrial conditions.

Generally, industrial researchers have found the processability of polymer melts can be traced to a combination of the fluid mechanics of the process and the rheological properties of the melts. The problem of processability investigations often reduce to careful rheological studies and to the determination of the relationship of specific rheological properties and response to molecular structure.

In this dissertation we will investigate the elongational flow (uniaxial and multiaxial including biaxial and planar deformation) of polymer melts and investigate various multiaxial processing operations of the same melts under quasi-industrial conditions. We shall attempt to develop a general perspective of the response or processability of these melts as a function of their rheological properties. This will be correlated with molecular structure.

CHAPTER II

BACKGROUND

A. EXTENSIONAL POLYMER PROCESSING

There exist two groups of polymer processing operations based on extensional flow. These are continuous and batch processes. Continuous methods involve a range of fiber and film manufacturing processes. Batch methods are blow molding, stretch blow molding and thermoforming processes.

Continuous filaments may be produced by extruding molten polymers through a spinneret having single or multiple orifices and drawing down with a take-up device. The molten polymer is solidified by a surrounding air or quench bath. This process first appeared in an English patent of 1845 by Brooman [B-16]. Films, on the other hand, are formed by (i) extrusion from a slit die and taking up on a rotating roll (or through a quench bath) or (ii) extruding vertically from an annular die forming a cylinder shaped bubble into which air is blown to generate an internal pressure which expands the annular film. The bubble is cooled by an external air blast or with an internal cooling cylinder. This is followed by eventual take-up on a series of rotating rolls. The former process is called film casting and later tubular blown film extrusion. Fibers may be made from film by a splitting process [O-3].

The most important continuous film process is tubular blown film extrusion which is widely used for polyethylene. Bewley as early as 1845 used an external mandrel [B-10]; it had the same shape as within the die and simply extended below it. It clearly was intended to maintain a shape, not to develop a new one or orientation. The tubular film process based on inflation of an emerging film with air dated to 1949 [F-21,S-7]. Mandrel procedures have been applied to extrusion of tubular film extrusion since 1955 [G-3]. The primary purpose of this external mandrel was to increase cooling rate on the bubble in order to increase productivity (high flow rate) and secondarily to maintain bubble stability. Blown polyethylene film is used extensively in packaging and for construction and agriculture applications. Clear nonshrink biaxially oriented polypropylene films are similarly used for many packaging applications. Shrink wrap plastic packaging, which is produced by the conventional blown film methods, is a rapidly growing segment of overwrap packaging. Polyethylene, poly(vinyl chloride), polypropylene, and poly(vinylidene chloride) are the most common films used for shrink wrapping.

A small amount (10 $\sim$ 20%) of film is produced by the slit die extrusion method (film casting). Rapid chilling gives better film gloss and clarity. The physical properties of cast film are also different from blown film: thickness variations are less, and cast film has a low degree of orientation as compared with blown film.

For different applications varying degrees of orientation are described. This may be accomplished by a secondary stretching of

the film under controlled conditions to create more molecular orientation and then freeze this orientation by rapid cooling. This frozen orientation can be released when the film is heated. The film then pulls back toward its original unstretched dimensions. This is the common shrinkable film. The other type of oriented film is heat set film which is manufactured by holding the stretched film at a high temperature just below its melting point. Such films have improved properties and are not normal shrink films. They will, however, shrink if reheated above their heat set temperature.

Highly uniaxial oriented film may be produced by either tubular blowing or casting by using heated differential speed rolls prior to wind up. Some blown biaxially oriented film is produced by the double-bubble process [D-9]. In this process, the film is blown into a small bubble, cooled quickly, and passed through pulling rolls. After the rolls, the tube is reheated to a temperature just below its melting point and further expanded by internal pressure with or without existence of a mandrel, while at the same time film speed along the machine direction is increased by another set of pulling rolls. Another way to introduce biaxial orientation in film, especially for casting film, is simultaneous or sequential stretching in the transverse direction with apparatus known as a tenter frame [A-10, M-4,W-23], which consists of two endless chains equipped with gripper clamps mounted on a Y frame and enclosed in an oven. Heat setting is usually accomplished at the exit end of the tenter frame.

Batch inflation of finite membrances of polymer melts, i.e., blow molding, dates to a patent of Carpenter in 1881 [C-2]. This

process sees various modifications chief among which is stretch blow molding [W-28]. Today there are three major techniques. These are extrusion blow molding, injection blow molding, and stretch blow molding.

The basic process of extrusion blow molding consists of three stages: (1) melting or plasticating a resin, (2) formation of a hollow tube or parison; (3) inflating the parison to form the end product. Two methods are employed for parison formation: continuous extrusion for smaller size and intermittent extrusion for large and heavier products. Injection blow molding differs from extrusion blow molding in that the parison is injection molded on a blowing rod instead of being extruded as a tube in free air. Since the distribution of the material is determined in the injection mold, the process is more uniform and more automatic with few variables to worry about. Stretch blow molding (also called orientation blow molding) is capable of producing containers with marked orientation in both machine and transverse directions. All blow molding processes induce orientation in the transverse direction, but none in the machine direction in the case of extrusion blow molding and only a moderate amount in the case of injection molding. There are two different types of processes. One is simultaneous stretch blow molding in which a hollow tube is stretched radially by the blown air and mechanically stretched along the vertical axis. The other one is sequential blow molding in which the parison is preformed by injection molding or tube extrusion and stretched to preform to the full length of mold on the blowing rod and then expand radially by blown air.

Practically any thermoplastic material can be blow molded. Polyethylenes, rigid poly(vinyl chloride), and poly(ethylene terephthalate) are used in quantity in the blow molding of containers, bottles, toys, household and industrial products. Poly(ethylene terephthalate) is processed by the stretch blow molding method.

Thermoforming, another example of extensional batch process, is the process of forming thermoplastic sheet into a product by an application of heat and pressure. This process can be dated at least back to a 1901 patent of Thurber [T-4]. This process includes new development such as the Dow "scrapless" thermoforming process [A-9]. The process uses a combination of compression molding of an extruded sheet and thermoforming to form a part that has no scrap. There exists other processes such as an injection thermoformer, called a "monoformer," of Hayssen Manufacturing [S-9]. This process uses a combination of injection molding, compression molding, and thermoforming. In thermoforming a heat softened sheet assumes a shape by being forced into a mold where it cools and solidifies. The forming pressure may be developed by a vacuum (against atmospheric pressure), compressed air, or by mating matched molds. The major plastics used for this process are high impact polystyrene and ABS. The major products are packaging and disposable containers. Other low-volume products produced in this manner are refrigerator door liners, heavy-duty pallets, exterior signs, sail boats, snowmobile shrouds, etc.

B. ELONGATIONAL FLOW

B-1. General

Although simple shear flow has been most widely studied, the occurrence of elongational flow in polymer processing operations such as melt spinning, film casting, tubular film extrusion, blown molding and thermoforming makes it an important area of study. This includes not only uniaxial elongational flow but also biaxial and planar elongational flow. For incompressible fluids the kinematics (deformation rate tensor $\underset{\sim}{d}$) of elongational flow can be expressed in terms of two independent deformation rates (E_1, E_2).

$$\underset{\sim}{d} = \frac{1}{2}\left[\nabla \underset{\sim}{v} + (\nabla \underset{\sim}{v})^T\right] = \begin{vmatrix} E_1 & 0 & 0 \\ 0 & E_2 & 0 \\ 0 & 0 & E_3 \end{vmatrix}$$

$$= \begin{vmatrix} E_1 & 0 & 0 \\ 0 & E_2 & 0 \\ 0 & 0 & -(E_1 + E_2) \end{vmatrix}$$

$$= E_1 \begin{vmatrix} 1 & 0 & 0 \\ 0 & E_2/E_1 & 0 \\ 0 & 0 & -(1 + E_2/E_1) \end{vmatrix} \qquad (2.1)$$

where "1" is in the machine direction, "2" is in the transverse direction, and "3" is in the free surface direction. Various possibilities exist. For uniaxial extension [P-11,T-10],

$$\frac{E_2}{E_1} = -0.5 \quad \text{or} \quad E_2 = E_3 = -0.5\, E_1 \tag{2.2a}$$

while for planar extension [D-5,P-11]

$$\frac{E_2}{E_1} = 0 \quad \text{or } E_2 = 0, \quad E_3 = -E_1 \tag{2.2b}$$

and for equal biaxial extension [D-6,P-11]

$$\frac{E_2}{E_1} = 1.0 \quad \text{or} \quad E_2 = E_1 = -2E_3 \,. \tag{2.2c}$$

The total stress is usually divided into two parts for convenience:

$$\underset{\sim}{\sigma} = -p\,\underset{\sim}{I} + \underset{\sim}{P} = -p\underset{\sim}{I} + \begin{vmatrix} P_{11} & 0 & 0 \\ 0 & P_{22} & 0 \\ 0 & 0 & P_{33} \end{vmatrix} \tag{2.3}$$

where p is an isotropic pressure and $\underset{\sim}{P}$ is the extra stress tensor associated with deformation. When a fluid is in the static condition ($\underset{\sim}{P} = 0$), "p" is identified as the hydrostatic pressure. In a dynamic situation for incompressible fluids "p" should be considered as a scalar value to be determined by boundary conditions. For elongational

flow there exists at least one free surface as a boundary condition so that elongational viscosities are determined as the measurable material function. In general, it is only possible to determine extensional viscosities as true material parameters under steady state conditions in which either constant strain rate or constant stress is achieved.

Reviews of research on elongational flow have been written by Cogswell [C-18,C-19], Dealy [D-1], White [W-14], and Petrie [P-11].

B-2. Uniaxial Elongational Flow

As early as 1906, Trouton [T-10] showed that the uniaxial elongational viscosity of a Newtonian fluid was three times the shear viscosity. This fact is equivalent to Young's modulus for an incompressible solid being three times the shear modulus.

From the mid-1960's there were several investigators who measured the uniaxial elongational viscosity of polymer melts with different experimental methods. There were often difficulties in measuring the elongational viscosity under controlled kinematics. Various methods of elongational viscosity measurement have been developed for highly viscous melts. These involve constant elongational rate, constant stress, and various approximate procedures using more gross techniques. Such experiments should be carried out at constant elongational rate or stress, if they are to specify true material properties.

A constant elongational rate apparatus was originally developed by Ballman [B-3]. Later instruments were developed and used by

Meissner [M-18,M-19,M-20,M-21,M-22,M-23,R-2], Vinogradov, Fikhman, Raduchevich and Malkin [V-1,V-2,V-5,V-6], Stevenson [S-28], Macosko and Lorntson [M-1], Everage and Ballman [E-2], Ide and White [I-1,I-3, I-4], Laun and Munstedt [L-3,L-4,M-46,M-47,M-48,M-49], Minoshima, White, and Spruiell [M-40,M-42], Koyama and Ishizuka [I-7,K-13,K-14, K-15], Au-Yeung, Macosko and Raju [A-12], and the author with Yamane, Suetsugu and White. This was first described in a paper by Yamane and White [Y-2].

Constant stress experiments were also carried out by Cogswell [C-15,C-17,C-18,C-20], Vinogradov, Fikhman, and Radushkevich [V-4], Munstedt and Laun [L-3,M-45,M-46,M-47,M-48,M-49], and Agrawell, Lee, Lorntson, Richardson, Wissbrun and Metzner [A-5]. These techniques are applicable only for high viscosity materials.

Everage and Ballman [E-4] who were concerned with lower viscosity melts such as polycondensates developed a converging flow rheometer with a lubricated layer which is steady in both Lagrangian (constant deformation rate) and Eulerian senses.

The view one develops on the basis of these experiments is that with pure melts, there are two classes of responses. Polymers such as low density polyethylene (LDPE) [C-16,C-17,I-4,L-3,L-4,M-20,M-22, M-23,M-48,M-49], polystyrene (PS) [E-2,I-4,M-45,M-46,M-47,T-3,V-4, V-5], and narrow molecular weight distribution polypropylene (PP) [M-42] may be stretched uniformly. At low stretch rates, the elongational viscosity, χ, remained constant (around three times the zero shear viscosity ($3\eta_0$). This has been also observed for

monodisperse hydrogenated polybutadienes [A-12]. At high elongation rates χ increases and some evidence exists that it may go through a maximum and then decrease [L-4,M-46,M-47,M-48,M-49]. Broad molecular weight distribution linear polymers such as most high density polyethyrenes (HDPE), polypropylenes (PP), and polybutene-1s (PB-1) stretch out in a non-uniform manner and fail by necking [I-4,M-42, Y-2]. This would seem to indicate a decreasing elongational viscosity function with elongation rate. However, there exists some question as to whether steady state elongational viscosities have been achieved.

Uniaxial elongational flow of filled systems was studied by Lobe and White [L-6], Chan, White, and Oyanagi [C-5], Tanaka and White [T-3], and Suetsugu and White [S-30]. Generally the addition of particulate solids causes the elongational viscosity to become a decreasing function of strain rate.

B-3. Other Elongational Flows

Investigations of multiaxial elongational flow behavior have been fewer. Denson and his co-workers [D-5,D-6,D-7,J-1,J-2] using sheet inflation experiments have investigated both equal biaxial extension and planar extension (transverse dimension fixed in length). This method, also called the bubble inflation technique, was originally initiated by Treloar [T-8] in 1944, and used by Treloar and Rivlin and Saunders [R-7] to test the theory of nonlinear large strain elasticity. Similar experiments have been reported by Maerker and Schowalter [M-3], Baily [B-2] and Rhi-Sausi and Dealy [R-6].

While various other techniques have been suggested, little actual experimental apparatus has been developed. Orthogonal stagnation flow within a lubricated die, which is similar to Everage and Ballman's technique [E-4] for uniaxial elongational viscosity measurement, has been proposed by Winter, Macosko and Bennett [W-26] for planar and equal biaxial elongational flow. This technique was actually used by van Aken and Janeschitz-Kriegl [A-6,A-7] for equal biaxial elongational viscosity measurement. A lubricated squeezing flow was also used by Chatraei, Macosko and Winter [C-9] as a method of measuring equal biaxial elongational viscosity. Stephenson and Meissner [M-23,S-27] have described a planar equal biaxial stretching apparatus.

There appears to be little in the way of experimental results for those elongational flows. Clearly, for equal biaxial elongational flow, the viscosity function for the polymer melts studied is six times the zero shear viscosity. At low strain rates and the planar extensional viscosity four times the zero shear viscosity. This is expected from the theory of Newtonian fluids. Nonlinear viscoelastic theories indicate that Newtonian fluid response should be expected in long duration slow flows.

C. ELONGATIONAL FLOW IN POLYMER PROCESSING

In all polymer processing operations involving extrusion, such as melt spinning, film casting, tubular blown film extrusion, blow molding, thermoforming and simple extrusion itself, a smooth

extrudate surface and controlled final dimensions are prime necessities. These considerations involve the matter of extrusion and melt stretching behavior and associated instabilities which in turn involve viscoelastic properties and the associated molecular parameters of the materials. Polymer processing operations are carried out under nonisothermal conditions so that we must solve simultaneously not only the equation of motion with the appropriate constitutive equation and continuity but also the energy equation [P-12,T-1].

C-1. Melt Spinning

Melt spinning produces a small diameter fiber by means of the extrusion of a polymer melt through a capillary die. The molten polymer rod exiting from die is drawn down by a take-up device. The molten polymer is solidified by surrounding air or quench bath.

C-1-a. Kinematics. The velocity field of the flow in the region between the die and the freezing point has been given

$$V_1 = V_1 (x_1, x_2), \quad v_2 = v_2 (x_1, x_2), \quad v_3 = v_3 (x_1, x_3) \quad (2.4a)$$

where "1" denotes the axial direction and "3" the radial direction. The velocity field intuitively has been assumed flat across the thread by most researchers with the exception of those of Matovich and Pearson [M-11] and Kase [K-4]. They considered this problem by expanding the velocity and other variables into series and substituting them into the continuity and momentum equation. Kase [K-4] obtained

numerical results using a Newtonian fluid model with temperature dependent viscosity and showed that under all conceivable melt spinning conditions the distribution of velocity across the thread is so small that the flow field can safely be regarded flat and purely uniaxial elongation. Eq. (2.4a) can be rewritten

$$v_1 = v_1(x_1), \quad v_2(x_2) = v_3(x_3) . \tag{2.4b}$$

The deformation rate tensor is

$$\underset{\sim}{d} = \frac{\partial v_1}{\partial x_1} \begin{vmatrix} 1 & 0 & 0 \\ 0 & -0.5 & 0 \\ 0 & 0 & -0.5 \end{vmatrix} . \tag{2.5}$$

C-1-b. Force balance. Several forces act on the descending fiber take-up force, F_L, gravitation, F_{grav}, frictional drag, F_{drag}, inertial force, F_{inert}, and rheological force, F_{rheo}. If we make a balance between position "x_1," and "L," we obtain

$$F_{rheo} = F_L + F_{grav} - F_{drag} - \rho Q (v_L - v_{x_1}) \tag{2.6}$$

where ρ is the density of polymer and Q volumetric flow rate.

There have been numerous attempts to estimate the relative magnitudes of the acting forces F_L, F_{grav}, and F_{drag}. The greatest difficulties have been associated with the air drag force, which becomes quite important at high take-up speed. Extensive studies of the air drag force were made by Hamana, Matsui, and Kato [H-2],

Anderson [A-11], Fukuda [F-20], Sano and Orii [S-5], Matsui [M-12], Bankar, Spruiell, and White [B-4], and Chen, White, Spruiell, and Goswami [C-12]. In the force balance equation, inertia and surface tension forces are generally small. Gravitational and frictional drag tend to counterbalance each other; the former is important at low take-up velocities and the latter at high take-up velocities. Ziabicki and Kedzierska [Z-7], Han and Lamonte [H-7] and Bankar, Spruiell, and White [B-4], showed the spinline forces F_{grav}, F_{drag}, F_{inert}, and F_{rheo} as a function of spinline position.

The acting stress is

$$\sigma_{11}(x_1) = \frac{4F_{rheo}}{\pi d^2(x_1)} = \frac{F_{rheo}}{Q} v_1(x_1) . \qquad (2.7a)$$

Therefore the uniaxial elongational viscosity, χ_{sp}, can be represented by

$$\chi_{sp}(x_1) = \frac{F_{rheo}\, v_1(x_1)/Q}{dv_1/dx_1} . \qquad (2.7b)$$

The velocity distribution along the fiber axis should be the same as the stress distribution.

C-1-c. Experimental studies of steady state spinline behavior. Various experimental studies [K-8,M-32,Z-7] of descending streams of viscous Newtonian fluids have been carried out. These generally involve the action of gravity and externally applied forces. The results of such experiments are in agreement with $\chi_{sp} = 3\eta_0$.

Isothermal experimental studies by Acierno et al. [A-2], Han and Lamonte [H-7], Bankar, Spruiell, and White [B-4], Minoshima, White, and Spruiell [M-40,M-41], Ishizuka and Koyama [I-8], and Yamane and White [Y-1] show elongational viscosities vary with elongation rates. These data show no consistent trend. These authors find that for LDPE and Nylon 6, χ_{sp} increases with dv_1/dx_1 or is constant, for HDPE, PP, and PB-1 decrease with dv_1/dx_1 and for PS and narrow molecular weight distribution PP of Minoshima, White, and Spruiell [M-40,M-41] are either constant or slightly decreasing. Most data also show that χ_{sp} is larger than Trouton viscosity.

Nonisothermal melt spinning studies usually correlate the interaction of temperature and threadline diameter profiles. The key is the χ_{sp} (T) function which is empirically determined. These equations have the form

$$\chi_{sp}(T) = A \exp(B/T) \ . \tag{2.8}$$

The classical study of heat transfer during melt spinning of fibers is that of Kase and Matsuo [K-6] who determined a relationship between Nusselt number and Reynolds number for air blowing longitudinally along a hot wire. They [K-8] have reported an experimental study of the melt spinning of PP and polyester fibers to check their theory. Variations in extrusion rate, take-up velocity, ambient temperature, air velocity, etc. were studied. The agreement between theory and experiment is reasonably good.

C-1-d. Experimental studies of unstable spinline behavior. Various conditions can arise which lead to vibrating spinlines and fluctuating fiber diameters. The later phenomena have received the most study. One may divide this response into "forced oscillations" and "natural oscillations." The former are due to periodic fluctuations in flow rate, melt temperature, heat transfer coefficient, etc. The latter are natural instabilities, notably draw resonances which occurs at a critical drawdown ratio dependent on the rheological properties of the melt during melt spinning.

Forced oscillations due to changes of cooling or changes of take-up speed were first studied by Kase and Matsuo [K-8] both theoretically and experimentally, and later studied by Minoshima, White, and Spruiell [M-40,M-41].

The instability, draw resonance, involves cyclic fluctuations in fiber diameter and tension. It was described by Freeman and Coplan [F-14], Kase and Matsuo [K-9], Han, Lamonte, Shah, Kim, and Apte [H-4,H-6,H-13], Weinberger, Cruz-Saenz and Donnelly [W-8], White and Ide [W-17], Matsumoto and Bogue [M-16], Minoshima, White, and Spruiell [M-41], Chang and Denn [C-7], Nam and Bogue [N-2], and Yamane and White [Y-1]. Draw resonance was observed at or above certain drawdown ratios. The experimental observations sometimes appear conflicting. Kase and Matsuo [K-9], White and Ide [W-17], and Minoshima, White, and Spruiell [M-41] observed that nonisothermal melt spinning is more stable than isothermal spinning; however, Han, Lamonte, and Shah [H-13], Matsumoto and Bogue [M-16] (their PS sample), and Han and Apte [H-4] observed the opposite. Matsumoto and Bogue

[M-7] also suggest that the passage through a rheological transition temperature (T_g or T_m) may induce major disturbances and diameter variations.

White and Ide [W-17] and later Minoshima, White, and Spruiell [M-41] argue that draw resonance in a spinline is the analog of ductile failure of an extending filament. This shows good agreement of experimental results that draw resonance readily occur in HDPE, PP, and poly(ethylene terephthalate) (PET), strain rate softening melts, and not LDPE, a strain rate hardening melt. Even in the same polymer family draw resonance readily occurs under both isothermal and nonisothermal conditions only in melts which exhibit strain rate softening χ_{sp} [M-41]. The above rheological character has been related to molecular weight distribution indicating narrowing the molecular weight distribution tends to show strain rate hardening χ_{sp} and spinline stabilization [M-41]. Minoshima, White, and Spruiell [M-41] and Ghijsels and Ente [G-5] showed that narrowing the molecular weight distribution of PP makes the spinline stable.

C-2. Film Casting

Film casting is a process whereby a thin sheet of hot molten polymer is extrudated through a slit die and falls into a quench bath or onto a chilled roll. Film is normally drawn down to reduce its thickness to the desired value. Chill roll cast film gives more uniform film thickness.

C-2-a. Kinematics. Pearson [P-1] has pointed out that the process may be interpreted to operate two-dimensionally. Later this

assumption was used by Middleman [M-35]. There is no lateral force so that the flow is in some sense equivalent to the axisymmetric situation in melt spinning.

The velocity field of the flow in the region between the die and freezing line has been given assuming purely uniaxial elongation (flat velocity profile cross the film)

$$v_1 = v_1 (x_1), \quad v_2 = v_2 (x_1, x_2), \quad v_3 = v_3 (x_1, x_3) , \tag{2.9}$$

where "1" indicates machine direction, "2" transverse direction, and "3" perpendicular to the 1-2 plane. The deformation rate tensor is represented as

$$\underset{\sim}{d} = \begin{vmatrix} \frac{\partial v_1}{\partial x_1} & \frac{1}{2}\frac{\partial v_2}{\partial x_1} & \frac{1}{2}\frac{\partial v_3}{\partial x_1} \\ \frac{1}{2}\frac{\partial v_2}{\partial x_1} & -\frac{1}{2}\frac{\partial v_1}{\partial x_1} & 0 \\ \frac{1}{2}\frac{\partial v_3}{\partial x_1} & 0 & -\frac{1}{2}\frac{\partial v_1}{\partial x_1} \end{vmatrix} . \tag{2.10}$$

C-2-b. Force balance. The force balance equation is essentially the same as the melt spinning one. If we make a balance between position "x_1" and "L," we obtain

$$F_{rheo} = F_L + F_{grav} - F_{drag} - \rho Q (v_L - v_{x_1}) . \tag{2.11}$$

The acting stress is

$$\sigma_{11}(x_1) = \frac{F_{rheo}}{hW} = \frac{F_{rheo}}{Q} v_1(x_1) , \qquad (2.12)$$

where "h" is the thickness of the film and "W" the width of the film.

C-2-c. Experimental studies of stable and unstable film casting. Several experiments have been reported in film casting by Bergonzoni and DiCresce [B-5] and Kase [K-5]. Kase showed that surging in film casting is essentially the same phenomena as draw resonance in melt spinning. Bergonzoni and DiCresce [B-5] also studied draw resonance of various PP melts and found the higher the molecular weight the more severe the draw resonance.

C-3. Tubular Blown Film Extrusion

The blown film extrusion process produces a thin film by means of the extrusion of a polymer melt through an annular die. The molten polymer tube exiting from the die is drawn upward by a take-up device. At the bottom of the die, air is blown and inflates the tube to form a bubble. An air ring is also used to cool rapidly the hot bubble and solidify it at some distance above the die. Then, the inflated solidified bubble is flattened as it passes through the nip rolls. The nip rolls, driven by constant torque or constant speed, provide the axial tension needed to pull the film upward, and they form an air-tight seal so that a constant pressure, slightly above atmospheric pressure, is maintained in the inflated bubble. The pressure inside the bubble is controlled by adjusting the air supply to the bottom of the die.

C-3-a. Kinematics. The kinematics of the flow in the region between the die and the freeze line have been discussed from a simple physical viewpoint by Pearson and Petrie [P-4] using the theory of thin shells as an assumption. The assumptions made are that the film thickness, h, is small compared with other dimensions of the bubble and its radii of curvature (i.e., $h \ll R$), permitting one to approximate the curved film by a plane film, and for the velocity gradients to be approximated locally by those of a plane film being extended biaxially.

The cylindrical coordinates (r,ϕ,z) are related with the local Cartesian coordinates (ν_1,ν_2,ν_3) at a point p in the film where ν_1 is in the direction of flow (meridional direction), ν_2 is in the transverse (hoop) direction, and ν_3 is normal to the film. In the definition the origin p is taken on the inner surface; the ν_3-axis meets the outer surface at ν_3 of h. Let (v_1,v_2,v_3) be velocity components in the coordinates (ν_1,ν_2,ν_3). The deformation rate tensor may be written as

$$d_{ij}(\nu_1,\nu_2,\nu_3) = \frac{Q \cos\theta}{2\pi Rh} \begin{vmatrix} -\left(\frac{1}{R}\frac{dR}{dz} + \frac{1}{h}\frac{dh}{dz}\right) & 0 & 0 \\ 0 & \frac{1}{R}\frac{dR}{dz} & 0 \\ 0 & 0 & \frac{1}{h}\frac{dh}{dz} \end{vmatrix}, \quad (2.13)$$

where R is the radius of the bubble and θ is the angle between parallel to film in the meridional direction and "z" direction.

Basic experimental studies of kinematics are reported by Ast [A-13,A-14], Farber and Dealy [F-1], Han and Park [H-8], Iwakura, Yoshinari and Fujimura [I-10], Swerdlow, Cogswell and Krul [S-31], and Kanai and White [K-2]. Farber and Dealy [F-1] and Kanai and White discuss motion picture techniques for following deformation history. Han and Park use photographs and carry out experiments ranging from uniaxial to biaxial extension through variation of the air pressure within the bubble. Iwakura et al. use photographs and carry out planar extension with no deformation along the machine direction under isothermal conditions.

C-3-b. Force balance. The dynamics of the tubular film process are somewhat more complex due to the expansion of the bubble. A force balance equation was first developed by Alfrey [A-8] and Pearson [P-1] applying thin shell theory. Later the dynamics of this process were developed by Pearson and Petrie [P-4,P-5], Petrie [P-7,P-8] and Han and Park [H-8].

The force balance equations are essentially those used for membrane theory. These are a balance of force over the whole cross section in the machine direction ("z" direction) and the other local balance between the forces in the film and the pressure difference across it. If we make a balance between position "z" and "L" where L is above the freeze line, we obtain

$$F_{rheo} = F_L - \pi (R_f^2 - R^2)\Delta p - F_{grav} - F_{drag} - F_{inert} \qquad (2.14)$$

where

$$F_{rheo} = 2\pi R h \sigma_{11} \cos \theta \ . \qquad (2.15a)$$

Here R is the radius of the bubble at an arbitrary position, R_f the maximum radius, h the thickness of film, Δp the pressure difference, θ the angle between the tangent to the film and the vertical, σ_{11} the stress in the film in the machine direction, ρ the density of polymer, and Q volumetric flow rate. For constant volumetric flow rate, Eqn. (2.15a) is reduced to

$$\sigma_{11}(z) = \frac{F_{rheo} v_1(z)}{Q \cos \theta} \ . \qquad (2.15b)$$

The radial force balance has the form, which neglects gravity, inertia, drag force, and surface tension,

$$\frac{\Delta P}{h} = \frac{\sigma_{11}}{R_M} + \frac{\sigma_{22}}{R_H} \ . \qquad (2.16)$$

Here σ_{22} is the circumferential (hoop) stress in the film, and R_M and R_H are the principal radii of curvature in the meridional direction and hoop direction, respectively.

$$R_H = r \sec \theta \ , \qquad (2.17a)$$

$$R_M = - \frac{\sec^3 \theta}{\left(\frac{d^2 r}{dz^2}\right)} \ . \qquad (2.17b)$$

The effects of gravity and inertia on Newtonian fluids were examined by Petrie [P-8]. He found that the effect of gravity is small for small scale experiments but can be expected to be large for

larger scale units. The effect of inertia appears to be negligible for all practical purposes.

C-3-c. Experimental studies of stable blown film extrusion. Some measurements of bubble shapes, velocity or strain rate as functions of machine variable (take-up speed, volumetric flow rate and air pressure) were studied by Ast [A-13,A-15], Farber and Dealy [F-1], Han and Park [H-8], Wagner [W-1,W-2,W-3], Swerdlow, Cogswell and Krul [S-31], and Kanai and White [K-2].

It was observed that the bubble shape was extremely sensitive to the valiation in air pressure within the bubble and also take-up speed [H-8].

Experimental studies of heat transfer in blown film extrusion have been reported by Zeppenfeld [Z-4], Menges and Predohl [M-29,M-30, M-31], Ast [A-13,A-14,A-15], Wagner [W-1,W-2,W-3], and Kanai and White [K-2].

C-3-d. Experimental studies of the unstable blown film extrusion. An instability occurs in the blown film extrusion which is different from melt fracture or draw resonance in melt spinning processes. This is the bubble instability. This phenemenon is discussed in detail by Han and Park [H-10] and Han and Shetty [H-11]. Periodic variations in bubble diameter are found to arise. This wavy surface is imparted to the bubble, when the size of disturbance was greater than a critical value. Han et al. suggest blown film process is very sensitive to a disturbance in processing variables, such as

a mass flow rate, air pressure, temperature, and take-up speed. They find their LDPE to be more unstable than HDPE. It is not clear whether this is due to differences in operating conditions.

D. RHEOLOGICAL BEHAVIOR OF POLYMER MELTS

In general, rheology, especially polymer melt rheology, combines two quite different approaches; a phenomenological approach which aims to find a common relation between stress and strain history for many polymers and a molecular based approach which looks for understanding of flow behavior in terms of molecular structure and mechanisms [B-17,B-18,G-8].

D-1. Basic Viscoelastic Theory

The analysis of flow problems requires the solution of the equations of conservation of mass, the equation of motion, the equation of conservation of energy, and a constitutive equation, which relates the stress tensor to the deformation history [P-12,T-1].

One of the fundamental problems of rheology is to establish the relationship between the stress and the deformation rate [B-11,B-13, H-3,L-9]. Polymeric liquids show elastic or memory effects in the sense that the present stress state depends on the previous history of deformation [B-11,B-13,H-3,L-9,T-11]. They are thus viscoelastic fluids. Viscoelasticity theory, which originated in one dimensional mechanical models for small strains, has been generalized to three dimensional large strain models [B-11,B-13,H-3]. The total stress is usually divided into two parts for convenience:

$$\underset{\sim}{\sigma} = -p\underset{\sim}{I} + \underset{\sim}{P} \tag{2.18}$$

where p is an isotropic pressure and $\underset{\sim}{P}$ is the extra stress tensor associated with deformation. When a fluid is in the static condition, i.e., $\underset{\sim}{P}$ being zero, p is identified as the hydrostatic pressure. In a dynamic situation for incompressible fluids p should be considered as a scalar value to be determined by boundary conditions.

The historical development of viscoelastic constitutive models begins with Maxwell's equation [M-17]:

$$P + \tau \frac{dP}{dt} = G\tau \frac{d\gamma}{dt} , \quad G\tau = \eta , \tag{2.19}$$

where P is the stress, γ is the strain, G is the elastic modulus, and τ denotes the relaxation time. This is the simplest viscoelastic fluid model in one dimensional linear form.

The first generalization of Eqn. (2.19) independent of coordinate system and valid for large deformations was given by Zaremba [Z-1]. Zaremba argued that the constitutive equation of a material should be framed in a coordinate system embedded in the material; that is, from the point of view of an observer attached to material points. However, human observers are in a stationary coordinate system fixed in a space, and so it is necessary to transform tensors from a convected to a stationary coordinate system. As the constitutive equation relates stress to deformation, it should be independent of translation and rigid rotation of material. Thus Zaremba [Z-1] considered an embedded coordinate system which translates and rotates with a material point.

Zaremba's theory predicts non-Newtonian viscosity and normal stresses in simple shear flow. Oldroyd [O-6] considered a coordinate system which translates, rotates, and deforms with the fluid which he termed a convected coordinate system. In succeeding years other generalizations were described by Noll [N-4], White and Metzner [W-19], Williams and Bird [W-24], and Spriggs and Bird [S-25,S-26]. When one tries to apply some of these constitutive equations for various flow problems, one encounters difficulty because of the number of material constants. The expression developed by White and Metzner [W-19] is the simplest but still describes many important features of nonlinear viscoelasticity [I-3,I-3]. This is written as

$$\underset{\sim}{P} + \tau \frac{\delta \underset{\sim}{P}}{\delta t} = 2\eta \underset{\sim}{d} \quad , \quad \eta = G\tau \ , \tag{2.20a}$$

where

$$\underset{\sim}{d} = \frac{1}{2} [\nabla \underset{\sim}{v} + (\nabla \underset{\sim}{v})^T] \ , \tag{2.20b}$$

$$\frac{\delta \underset{\sim}{P}}{\delta t} = \frac{\delta \underset{\sim}{P}}{\delta t} + (\underset{\sim}{v} \cdot \nabla)\underset{\sim}{P} - \nabla \underset{\sim}{v} \cdot \underset{\sim}{P} - \underset{\sim}{P} \cdot \nabla \underset{\sim}{v} \ . \tag{2.20c}$$

White and Metzner [W-19] proposed that the relaxation time τ is a function of the second invariant d, i.e.,

$$\tau(II_d) = \tau(\text{tr } \underset{\sim}{d}^2) \ . \tag{2.21}$$

Integral theories are based on Boltzmann's superposition principle [B-14] which represents the stress response to a series of infinitesimal strains.

$$\underset{\sim}{P}(t) = \sum_i G(t-t_i)\Delta\gamma = \int_{-\infty}^{t} G(t-s)\,\frac{d\gamma}{dt}\,ds \ , \qquad (2.22)$$

where $G(t)$ is a relaxation modulus at time t, γ is strain, and s is time.

The one dimensional Boltzmann constitutive equation is limited to infinitesimal deformations. It is necessary to extend the Boltzmann theory to be valid at large deformation and to describe non-linear viscoelastic behaviors. The first generalization to finite strain was considered by Oldroyd [O-6] and more specifically by Lodge [L-7] at about the same time Yamamoto [Y-3,Y-4,Y-5] and Lodge [L-8] developed nonlinear generalization of Boltzmann's equation based on network theories of flexible polymer chains. A general constitutive theory accounting for nonlinear effects was developed by Green and Rivlin [G-1] presuming that the stress is general hereditary functional of the deformation history. An equivalent but more elegant formulation of the Green and Rivlin concept has been given by Noll [N-4] and later Coleman and Noll [C-23]. This is expressed as a function of strain history

$$\underset{\sim}{P} = F\,[\underset{\sim}{e}\,(t-s)]_{s=-\infty}^{s=t} \ . \qquad (2.23)$$

Here $\underset{\sim}{e}(t)$ is a strain measure which we may take as a Finger deformation. The constitutive equations of a single integral type can be written as the following equation which is generally equivalent to Eqn. (2.23).

$$\underset{\sim}{P}(t) = \int_{-\infty}^{t} [m_1 (t-s)\ \underset{\sim}{c}^{-1} (t-s) + m_2 (t-s)\ \underset{\sim}{c} (t-s)]\ ds\ , \quad (2.24a)$$

$$= \int_{-\infty}^{t} m (t-s)\ [(1 + \frac{\varepsilon}{2})\ \underset{\sim}{c}^{-1} (t-s) + \frac{\varepsilon}{2}\ \underset{\sim}{c} (t-s)]\ ds\ , \quad (2.24b)$$

where $\underset{\sim}{c}^{-1}$ is the Finger deformation tensor and $\underset{\sim}{c}$ is the Cauchy deformation tensor. This form was first used by Bernstein, Kearsley and Zapas [B-8]. The memory functions m_1 (t-s), m_2 (t-s), or m (t-s) are dependent upon the invariants of $\underset{\sim}{c}^{-1}$, $\underset{\sim}{c}$, $\underset{\sim}{d}$, or $\underset{\sim}{P}$. Many constitutive equations of this type have been proposed.

The memory function m of many of these constitutive equations can be written

$$m_1(t,t') = \sum_i \frac{G_i}{\tau_i\ f_i} \exp(- \int_{-t'}^{t} \frac{dt''}{\tau_i\ g_i}) \ . \quad (2.25)$$

Here G_i are relaxation moduli, τ_i are relaxation times, and f_i and g_i are functions of tensor invariants at time t' and t" ($t' \leq t'' \leq t$). In memory function for linear viscoelastic response may be expressed

$$m_1(t-s) = \sum_i \frac{G_i}{\tau_i} \exp(- \frac{t}{\tau_i}) \ , \quad (2.26a)$$

$$= \int_0^{\infty} \frac{H(\tau)}{\tau} \exp(- \frac{t}{\tau}) d\ \ell n\ \tau \ . \quad (2.26b)$$

Eqn. (2.26) represents the case for $f_i = g_i = 1$. This form $m_2 = 0$ is called Lodge's fluid. The nature of the constitutive equation will be dependent upon which invariant functions f_i and g_i are used.

Another important form of the memory function m (t-s) has been suggested by Bogue [B-12] and later modified by Bogue and White [B-13]. This form has been found to successfully correlate data on bulk polymers by Middleman [M-34], Chen and Bogue [C-10], Chen, Hagler, Abbott, Bogue and White [C-11], Takaki and Bogue [T-2], Furuta, Lobe and White [F-22] and Ide and White [I-1,I-4]. This form is:

$$m_1(t-s) = \sum_i \frac{G_i}{\tau_{i\ eff}} \exp\left(-\frac{t}{\tau_{i\ eff}}\right) , \tag{2.27a}$$

$$\tau_{i\ eff} = \frac{\tau_i}{1 + a\ \tau_i \langle II_d^{1/2} \rangle} , \tag{2.27b}$$

$$\langle II_d^{1/2} \rangle = \frac{1}{z} \int_0^z [2tr\ \underset{\sim}{d}^2]^{1/2}\ dz , \tag{2.27c}$$

where z = t-s is time running back from the present.

The previous formulations are for isothermal behavior. Traditionally, the effect of temperature has been considered in rheology through using temperature dependent viscosity functions. A more general perspective is suggested by the time-temperature superposition behavior observed in small strain viscoelastic behavior [F-2,W-25]. This approach was formalized by Morland and Lee [M-44] in terms of the linear viscoelastic theory. In the continuum mechanics, a series of papers by Crochet and Naghdi [C-25,C-26] present non-isothermal theory based on the Coleman's thermodynamics of simple material [C-21]. A specific nonlinear formulation of integral type

was developed by Matsui and Bogue [M-14] and Matsumoto and Bogue [M-15]. It was used to represent the rheological behavior of molten polystyrene in experiments with programmed temperature fields. They proposed a constitutive equation of form

$$\underset{\sim}{\sigma} = -p\underset{\sim}{I} + \sum_i \frac{T(t)}{T_0} \int_{-\infty}^{t} \frac{G_i}{\tau_i(t)} \exp\left[- \int_{-t'}^{t} \frac{dt''}{\tau_i(t'')} \right] \underset{\sim}{C}^{-1}(t,t')dt' \ , \tag{2.28}$$

which may be seen to derive from Eqn. (2.24) in the special case of $m_2(z)$ being zero. Marrucci [M-5] has approached this problem using an elastic dumbbell (bead-spring) model, and derived a modified form of Eqn. (2.20) in which Eqn. (2.20a) is replaced with

$$\underset{\sim}{P}\left(1 - \tau \frac{D \ \ell n \ T}{Dt}\right) + \tau \frac{\delta \underset{\sim}{P}}{\delta t} = 2G \ \tau \ \underset{\sim}{d} \ , \tag{2.29}$$

where τ is considered to depend on temperature. Eqn. (2.29) was applied to non-isothermal melt spinning analyses by Fisher and Denn [F-6]. A slightly modified form of Eqn. (2.29) has been developed by Gupta and Metzner [G-12].

D-2. Theoretical Studies of Elongational Flow

D-2-a. Uniaxial elongational flow. Qualitatively, shear flow of all polymer melts follow a similar pattern whereas uniaxial elongational flow shows significant difference from polymer to polymer [C-18,I-2,I-3,I-4,M-42].

The nonlinear character of the elongational viscosity was first described by Yamamoto [Y-5] in 1957. He showed that, depending upon

the constitutive equation, the elongational viscosity first increases with elongational rate and then either goes to infinity in the region of $\tau E \gtrsim 0.5$ or decreases after exhibiting a maximum. The infinite elongational viscosity at finite elongational rate was later described by Lodge in his monograph [L-9] using a constitutive equation with constant relaxation times. It was, however, pointed out by Denn and Marrucci [D-2] that the infinite stress indicates a never achievable steady state and one should rather consider the transient stress build-up.

Various researchers have compared transient uniaxial elongational stress development of range of constitutive equations using material parameters obtained from shear experiments or stress relaxation experiments with experimental results. Petrie [P-9,P-11] discussed in detail uniaxial elongational flow at constant strain, strain rate, velocity, stress, and force for several Maxwell models.

Studies of stability of uniaxial elongational flow considering nonlinear viscoelastic behavior of polymer melts were initiated by Chang and Lodge [C-6], Ide and White [I-1,I-2,I-3,W-16] and Acierno and LaMantia [A-3] using stability analysis techniques. Roughly they predict that the influence of elasticity is to stabilize the filaments. Ide and White [I-2,I-3,I-4] also note that in strain rate softening materials, the neck continues to grow and ductile failure results. This theory investigated through the deformation dependence of τ, using a convected Maxwell model (Eqn. 2.19) with τ given by an expression similar to Eqn. (2.27b) where τ depends on II_d through

a parameter "a." They reported that filament stability and elongation-to-break depend on $\tau_0 E$ and "a." At fixed $\tau_0 E$, filament stability decreases with increasing "a." At small "a," stability increases with increasing $\tau_0 E$ while for "a" > $1/\sqrt{3}$ stability decreases with increasing $\tau_0 E$. For smaller "a," ductile failure can occur for small $\tau_0 E$, but cohesive fracture should be the case of failure at large $\tau_0 E$.

D-2-b. Multiaxial elongational flow. Several nonlinear viscoelastic constitutive equations have been tested for biaxial (equal) elongational flow experiment by Joye et al. [J-1,J-2]. Joye et al. [J-2] compared steady state biaxial elongational viscosity with a Rivlin-Ericksen third order fluid [B-13,T-11,W-11], Oldroyd three constants model [B-12,B-13] using dynamic data. Another type of constitutive equation in which f_i and g_i in Eqn. (2.25) are functions of some invariant of stress were compared with deformation and stress growth data of Denson et al. [D-6,J-1,J-2] by Acierno et al. [A-3].

Transient stress build-up during the early periods of biaxial deformation was considered by White [W-13] using nonlinear integral constitutive equations represented by Eqns. (2.24) and (2.27). He showed that for low deformation rates it was possible to apply the creeping flow Navier-Stokes equations, and for high deformation rates the response approached that of an elastic solid subjected to finite deformations.

Stevenson et al. [S-29] suggested a general method for classifying steady, isochoric elongational flow.

Studies of stability of biaxial elongational flow of polymer melts were initiated by White [W-13] using stability analysis techniques. Roughly he predicted that the perimeter around a nonhomogeneity exhibits considerable reinforcing behavior and prevents the growth of geometric (thickness and nonuniformity) and low viscosity (hot spot) defects, and high viscosity (gel) defects will not neck down as rapidly as a lower viscosity perimeter.

D-3. The Effects of Molecular Structure on Elongational Flow

Studies of the effect of molecular parameter on the rheological response of polymer melts in elongational flow have been strongly related to instabilities and failure studies. Because of strong industrial interest in this kind of flow (e.g., melt spinning and film extrusion), commercial broad molecular weight distribution samples have often been employed. Thus detailed data on the effect of molecular parameters were generally unavailable. In recent years systematic studies of stress-strain and failure in elongation for narrow molecular weight distribution materials and their blends, as well as commercial broad molecular weight distribution materials, have been investigated. However, as will be seen, the data are still sparse compared with shear flow experimental results.

Using typical data of narrow molecular weight distribution PS, White and Ide [I-1,I-2,W-16] by presuming a melt behaved like a Newtonian fluid below the entanglement molecular weight and a convected

Maxwell model above it predicted the elongation-to-break, $L(t_b)/L(0)$, as a function of molecular weight at a constant elongation rate. At low molecular weight a capillary failure occurs, at an intermediate molecular weight ($M_w > M_c$) a ductile failure occurs (viscoelastic fluid), at high molecular weight a cohesive failure occurs at a critical stress. In between the two regions the critical strain reaches a maximum.

When one looks at the failure mechanism and uniaxial elongational viscosity of various polymers, there exist two polymer groups. One consists of HDPE and PP (normal or broad molecular weight distribution) which fail by a ductile mechanism and show strain rate softening. The other group consists of LDPE, PS and PP (narrow molecular weight distribution) which fail by a cohesive fracture and show strain rate hardening. These results are explained by Ide and White's interpretation [I-3,I-4] and by deformation rate dependent relative relaxation time, $d \log \bar{\tau}/d \log \dot{\gamma}$.

D-4. Rheological Properties of Polyethylene Melts

There have been a number of experimental rheological studies of PE melts, but these generally do not provide a detailed discussion of the polymer used. Concerning polyethylene, one must remember that commercial polymers possess a broad range of molecular weights, of molecular weight distributions, and of chain branching, all of which depend on the means of manufacture. For example, the Ziegler-type of catalyst can produce a linear HDPE with a range of molecular weights and molecular weight distributions. On the other hand, the

Phillips-type of catalyst produce a HDPE with long chain branching and only limited molecular weight distributions; this type of catalyst cannot produce a narrow molecular weight distribution HDPE (the Ziegler-type can produce a narrow molecular weight distribution HDPE). Conventional broad molecular weight distribution high pressure PE (LDPE) has a more complex molecular structure than conventional narrow molecular weight distribution high pressure PE, because of the existence of a higher degree of long chain branching (and also short chain branching). It is also known that linear low density polyethylene (LLDPE) has a relatively narrow molecular weight distribution and almost no long chain branching [F-9,F-11]. In addition to these complexities in the molecular structure of polyethylenes, there exists peculiar phenomena in conventional high pressure LDPE known as shear modification. The rheological properties of LDPE are strongly dependent upon the previous shearing histories even without a change in the molecular structure [F-15,F-20,H-17,R-9,R-10,R-13]. The changed rheological properties can be reversed to the original states by two means; one is to keep the shear modified LDPE under high temperature for several hours (heat treatment), and the other is to dissolve shear modified LDPE (solvent treatment). This phenomenon is also observed in acetal polymers [P-14] and ethylene-vinylacetate copolymers [R-12]. Both polymers also contain long chain branching.

In general, studies of molecular weight distribution effects in recent years have tended to utilize anonically polymerized systems [G-8,G-10,M-6,M-8,M-36,M-38,N-3,O-1,O-7,P-13,R-1]. Studies also exist for fractionated polymer melts [G-8,M-37]. The early literature

has been reviewed by Graessley [G-8]. Certain trends in the behavior are clear in this literature. The zero shear viscosity increases with the 3.5 power of the weight average molecular weight. Broadening the molecular weight distribution increases the non-Newtonian character (shear rate dependence) of the viscosity function. The principal normal stress difference-shear stress relationship is independent of the temperature and molecular weight but is very strongly dependent upon the molecular weight distribution. The same trends are also found for a series of specially prepared polypropylenes of varying molecular weight and distribution [M-40,M-42]. Information on the effect of molecular weight distribution on uniaxial elongational flow exists only for a series of polypropylenes of various molecular weights and distributions [M-40,M-42].

Studies of the long chain branching effect have also been done using anionically polymerized and well-characterized star-like polymers [G-9,I-9,K-1,K-18,M-7,M-10,N-5,O-2,R-3,R-8,U-1,U-2,W-27,Y-7]; comb-like polymers [F-17,F-18,N-5]; and randomly branched polymers [M-9]. These are all monodisperse polymers. The zero shear viscosity is decreased by long chain branching in the low molecular weight region but increases more rapidly with molecular weight, above certain molecular weights [G-9,K-18,M-7,M-10,O-2,R-3,R-8]. The viscosity crosses that for linear polymers. The steady-state compliance for the long chain branched polymer is about one order (decade) higher than that for the linear polymer [F-17,F-18,I-9,M-7, O-2,R-8]. Some researchers have reported that the steady-state compliance is approximately proportional to the molecular weight, even

for relatively high molecular weights [G-9,M-10,U-1,U-2]. There is apparently no literature on the effect of long chain branching on uniaxial elongational viscosity.

There exist many studies of the rheological properties of HDPE, conventional LDPE, and their fractionated samples. For HDPE shear viscosity related studies such as the examination of the molecular weight dependent zero shear viscosity (η_0) [K-17,M-27,R-4,S-3,S-8, T-7], Cox-Meltz relationship [C-24,K-17,M-2,M-27], and Graessley's theory for non-Newtonian shear viscosity [G-7,I-5,S-2,S-21] are available. Some researchers have investigated the first normal stress difference [H-4,H-12,H-15,I-5,K-11,K-17,M-28,S-4,S-23,W-5], extrudate swell [B-1,F-19,K-10,M-26,S-15], and the onset of extrudate distortion [S-15] for molecularly well-characterized samples. For molecularly characterized conventional LDPE, the shear viscosity studies such as the primary normal stress difference [H-5,H-12,M-22,W-5] zero shear viscosity [K-16,M-27,M-39,P-6] and Graessley's theory for non-Newtonian shear viscosity [K-17,S-21], and elasticity related studies such as primary normal stress difference [H-5,H-12,M-22,W-5] and extrudate swell [M-25,R-11,W-22] appear in the literature. Relatively little has appeared on the effect of molecular weight and its distribution on the uniaxial elongational flow behavior in PE. Studies on conventional LDPE's and HDPE's have been carried out by Munstedt and Laun [M-49], and on HDPE's by Koyama and Ishizuka [K-15]. Monodisperse linear hydrogenated polybutadienes have also been studied [A-10]. Some additional studies of HDPE [C-5,I-4] and LDPE

[C-16,C-17,L-3,L-4,M-20,M-22,M-23,M-48] are available. Data on the shear flow characterization and the uniaxial elongational flow behavior of LLDPE are rare [F-12,S-10].

E. ANALYSIS OF PROCESSING OPERATIONS

E-1. Theoretical Studies of Melt Spinning

E-1-a. Theoretical studies of stable melt spinning. The steady state spinline dynamics beyond the extrudate swell region were first considered by Ziabicki and Kedzierska [Z-5,Z-6,Z-7] who made a detailed analysis for the isothermal case where the fluid has constant properties along the spinline. Further considerations of the analysis of the isothermal spinning process were made by Matovich and Pearson [M-1], Bogue and White [B-13] and Acierno, Dalton, Rodriguez and White [A-2]. Acierno et al. carried out isothermal melt spinning experiments and interpreted them in terms of both elongational viscosities and a more rigorous nonlinear viscoelastic theory. Similar isothermal melt spinning studies were carried out by Chen et al. [C-11], Lamonte and Han [L-2], and Spearot and Metzner [S-24]. Zeichner [Z-2], Denn, Petrie and Avenas [D-4], Fisher and Denn [F-3,F-4,F-5,F-6], White and Ide [W-16], and Minoshima, White, and Spruiell [M-40,M-41] have been of isothermal melt spinning of viscoelastic fluids using a convected Maxwell model, and Ronca [R-15] also discussed using the Lodge general temporary network model [R-14]. Denn and Marrucci [D-3] examined the effect of a relaxation time spectrum and concluded that they could explain the observation that

relaxation times obtained with a Maxwell type model from spinning experiments are larger than those measured in dynamic or normal stress measurements.

The above analyses were carried out with respect to the Eulerian coordinates system (threadline spinning distance). Hyun and Ballman [H-20] considered the steady state solution for the isothermal melt spinning of Newtonian, power law and a Maxwell fluid with respect to both the Lagrangian coordinates (threadline residence time) and the Eulerian coordinates to demonstrate the unity of two coordinate systems in revealing different characteristics of the spinning process.

The problem of nonisothermal effects in spinline dynamics was first considered by Kase and Matsuo [K-6] using a temperature dependent elongational viscosity. This is further expanded and examined by Yasuda, Sugiyama and Yanagawa [Y-6] and George [G-2]. Lamonte and Han [L-2] proposed an analysis using temperature and deformation rate dependent elongational viscosity. Abbott and White [A-1] and Matsui and Bogue [M-13] suggested a method of carrying out analyses using a nonlinear integral theory with temperature dependent relaxation functions. An important problem is the heat transfer coefficient. Generally the experimentally determined relation of Kase and Matsuo [K-6] has been used.

A basic problem in the viscoelastic fluid analyses is initial conditions. If the melt remembers its past history, will not flow in the spinneret influence it? This problem has been realized by

many investigators beginning with Acierno, Dalton, Rodriguez and White [A-2], but they were not fully able to cope with it. Denn, Petrie and Avenas [D-4] and Fisher and Denn [F-5] argue that for the theory using a convected Maxwell model only the initial stress need be considered. Matsui and Bogue [M-13], Petrie [P-10], and Nam and Bogue [N-2] have included the influence of Poiseville flow in the spinneret in their analysis.

E-1-b. Theoretical studies of unstable melt spinning. The analysis of diameter fluctuation (draw resonance or natural oscillation) is due to Kase and co-workers [I-6,K-6,K-8] and by Pearson, Matovich and Shah [P-2,S-11,S-12,S-14], Fisher and Denn [F-3,F-4,F-5,F-6], Hyun [H-18,H-19], Chang, Denn and Geyling [C-7, C-8], and by Geyling [G-4]. Rheological aspects are considered by White and Ide [W-17] and Minoshima, White and Spruiell [M-40,M-41].

Kase, Matsuo and Yoshimoto [K-9], Pearson, Matovich and Shah [P-2], and Gelder [G-1] analyzed the problem of isothermal melt spinning of Newtonian fluid using continuity and force balance. A linear perturbation analysis was carried out, and it was shown that the system becomes unstable when the draw ratios v_L/v_0 exceed 20.21.

Shah and Pearson [S-14] and Ishihara and Kase [I-6] have studied this problem using power law constitutive equation (χ varies with dv_1/dx_1 to a power) and found that if χ increases with E, stability is increased. Zeichner [Z-2] performed a linearized stability analysis for an isothermal viscoelastic fluid using a convected Maxwell model. They found the stability increased with $\tau v_1(0)/L$,

the Weissenberg number. Fisher and Denn [F-5,F-6] generalized the theory of both the isothermal and nonisothermal viscoelastic fluid using a convected Maxwell model in which viscosity obeys a power law. They predicted a complex effect of elasticity. For the isothermal case, first the critical drawdown ratio (onset of draw resonance) decreases with increasing elasticity, after the Weissenberg number reaches about 0.01 the critical drawdown ratio begins to increase, indicating a stabilizing effect of elasticity. And shortly thereafter the stability envelope turns back on itself, indicating existence of stable region at high drawdown ratio. They also showed the effect of nonlinearity based on the power law "n" in shear viscosity. Increasing deformation rate softening shear viscosity (i.e., lowering n value) tends to destabilize the spinline, smaller critical drawdown ratio at fixed Weissenberg number.

White and Ide [W-17] and later Minoshima, White and Spruiell [M-40,M-41,W-20] argue that draw resonance in a spinline is the analog of ductile failure of an extending filament. The materials with stronger strain rate softening, for which the neck continues to grow and ductile failure results in the isolated stretching of a filament, are sensitive to the disturbances and result resonance readily occur from lower drawdown ratio. This is the case of HDPE, PP (except narrow molecular weight distribution ones), and poly(ethylene terephthalate). On the other hand, materials with strain rate hardening character are insensitive to the disturbances and heal them out, resulting in absence of draw resonance. LDPE is the

example of this case. The strain rate dependent character can be restated in terms of spinline viscosities. The spinline elongational viscosities of strain rate softening material decrease with increasing velocity gradient; however, those of strain rate hardening increase with increasing velocity gradient.

The influence of a spinline temperature gradient was investigated by Shah and Pearson [S-11,S-12], Kase [K-5] and Fisher and Denn [F-6]. For the Newtonian fluids case, decreases in the ratio T_{air}/T_{melt} lead one from an unstable to a stable region, provided one is at a draw ratio above the critical value and provided that one avoids extremes in the Stanton number N_{st}, which is defined as the following equation.

$$N_{st} = \frac{h}{\rho C_p V^*} , \tag{2.30a}$$

$$V^* = \frac{Dv}{4L} , \tag{2.30b}$$

where h is heat transfer coefficient at thread surface, ρ is density of polymer melt, C_p is specific heat of melt, D is diameter of fiber at spinneret, v is thread velocity at spinneret and L is spinline length. Solidification of samples stabilize the spinline even in a high Stanton number region. Similar effects on spinline temperature gradient for a Maxwell fluid are suggested at fixed values of elasticity by Fisher and Denn [F-6].

There are experimental observations that cannot be fit into the above theory; Han and co-workers [H-6,H-13] have shown that spinning into air is sometimes destabilizing, compared to spinning into an

isothermal chamber and that the length of the die has an effect on the draw resonance. The latter effect is also observed by Matsumoto and Bogue [M-16]. These authors also suggest that the passage through a rheological transition temperature (T_g or T_m) may induce major disturbances and diameter variations.

E-2. Theoretical Studies of Tubular Blown Film Extrusion

The steady state behavior of blown film extrusion was first considered by Pearson and Petrie [P-4,P-5], later by Han and Park [H-9], Petrie [P-7,P-8] and Wagner [W-1,W-2].

The solution for the dynamics of blown film extrusion for isothermal Newtonian fluid is rather complex and Pearson and Petrie [P-4,P-5] were only able to give numerical solutions by neglecting gravity, inertia, drag force, and surface tension. Han and Park [H-9] consider a power law fluid and Petrie [P-7,P-8] has investigated a convected Maxwell model behavior and a neo-Hookean nonlinear elastic model. Han and Park found that decreasing "n" gives rise to a larger bubble radius and lower bubble temperature at fixed dimensionless distance from the die exit. In convected Maxwell models there are difficulties in the numerical solution arising from the predictable inherent instability of the systems of equations [P-7]. Petrie found that effects of the nonzero relaxation time are that a tube of constant radius is not dynamically possible. He found that elasticity reduces blow ratio and increases the thickness reduction, both favoring an increase in machine direction drawing as opposed to transverse drawing.

Nonisothermal modelling of blown film extrusion has been reported by Petrie [P-8], Han and Park [H-9], and Wagner [W-1,W-2]. Petrie combines the Pearson-Petrie Newtonian fluid model which has temperature dependent viscosity and density with Ast's temperature profiles, and found that velocity and deformation rate predictions appear more sensitive to details of temperature profile and melt rheology than bubble shape. Wagner combines the Pearson-Petrie Newtonian fluid model which has temperature dependent viscosity and density and energy balance equation with assuming: (1) heat transfer between the inner surface and the air trapped within the bubble is negligible; (2) the heat of crystallization is negligible; (3) the heat conduction in the film is negligible; (4) the cooling of the bubble is controlled by radiative and convective heat transfer; (5) the heat generation due to the frictional force is negligible. Also he has examined the neo-Hookean nonlinear elastic model and the temperature dependent integral Maxwell model. Han and Park combine the power law fluid which has temperature dependent viscosity and energy balance equations with the same assumptions as Wagner. They find that the accuracy of predicted bubble shapes and temperature profiles depends very much on the numerical values of the overall heat transfer coefficient and the emissivity coefficient.

Bubble instability was theoretically analyzed by Yeow [Y-9] for the isothermal Newtonian fluid using an assumption that the infinitesimal disturbances possess axisymmetry. He correlated the

stability domains in terms of take-up force vs. inflation bubble pressure and drawdown ratio vs. blow-up ratio.

CHAPTER III

MATERIALS

A. GENERAL

The materials used in this study were polyethylenes (PE), polypropylenes (PP), and polystyrenes (PS). These materials were chosen as to represent a variety of rheological properties and molecular structure. They are listed in Tables III-1, III-2, III-3, III-4, and III-5.

Polyethylenes included eight high density polyethylenes (HDPE), four linear low density polyethylenes (LLDPE), and four conventional low density polyethylenes (LDPE). Five of the samples were Marlex® made by Phillips Petroleum Company, three samples Alathon® by E. I. du Pont deNemours & Co., three samples Chemplex® by Chemplex Company, two samples of G® and two samples of DFD® by Union Carbide Co., and two samples Dowlex® by Dow Chemical Co. The molecular weight distribution (MWD) of the HDPE samples and two Chemplex LDPE samples were kindly supplied to us by Dr. Ramesh N. Shroff of Chemplex Company. The degree of long chain branching (LCB) of the Marlex samples (HDPE) was supplied by Mr. R. T. Werkman. Molecular characterization data of two Union Carbide LLDPE and two Union Carbide LDPE were measured and supplied to us by Dr. George N. Foster of Union Carbide. They are also listed in Tables III-1, III-2, and III-3.

Table III.1. High Density Polyethylenes Used in the Experiments

Commercial Name	Code	Melt Index	$M_w \times 10^{-4}$	M_w/M_n	M_z/M_w	M_{z+1}/M_z	Degree of Long Chain Branching (per 10^5 C Atoms)	ρ (Density)	Lot Number
Chemplex 6109E	HDPE-1	0.85	14.4_9	9.64_6	6.35_5	2.56_8	-	0.96	35199
Marlex 6009	HDPE-2	0.90	17.3_2	14.10_8	8.28_9	2.47_7	1.1	0.963	0170339
Marlex 6030	HDPE-3	3.0	11.6_8	7.10_4	7.84_1	2.89_5	1.0	0.964	03300797
Marlex 6050	HDPE-4	5.0	11.4_0	8.08_3	7.11_6	2.47_7	-	0.96	0130798
Marlex 6080	HDPE-5	8.0	9.28_7	4.66_8	6.55_6	3.32_7	-	0.962	0181220
Alathon 7030	HDPE-11	2.8	11.6_8	3.35_5	2.97_4	2.26_3	-	0.960	956440
Alathon 7040	HDPE-12	6.0	9.28_1	3.59_2	3.11_3	2.57_4	-	0.960	955766
Alathon 7050	HDPE-13	12.0	7.10_3	3.05_9	2.70_6	2.57_2	-	0.960	055737

Table III-2. Linear Low Density Polyethylenes Used in the Experiments

Commercial Name	Code	Melt Index	$M_w \times 10^{-4}$	M_w/M_n	Shape of MWD	Degree of Long Chain Branching (per 10^3 C Atoms)	ρ (Density)	Lot Number
G-7047	LLDPE-1	1.1	10.8	3.81	log normal	less than 0.1	0.9181	-
G-7040	LLDPE-2	2.1	8.37	3.36	log normal	less than 0.1	0.9190	-
Dowlex 2032	LLDPE-3	2.0	-	-	-	-	0.926	TB613013
Dowlex 2047	LLDPE-4	2.3	-	-	-	-	0.917	TB9149032

Table III-3. Low Density Polyethylenes Used in the Experiments

Commercial Name	Code	Melt Index	$M_w \times 10^{-4}$	M_w/M_n	M_z/M_w	M_{z+1}/M_z	Degree of Long Chain Branching (per 10^3 C Atoms)	ρ (Density)	Lot Number
DFD 4140	LDPE-1	2.01	23.5	11.19	-	-	3.4	0.9182	-
Chemplex 1005F	LDPE-2	3.5	20.0_8	8.35_6	5.26_3	2.03_2	high	0.919	494A3
DFD 0332	LDDE-11	1.86	11.2	4.11	-	-	1.6	0.9234	-
Chemplex 3405CA+B	LDPE-12	3.5	8.44_7	3.29_3	5.61_4	4.89_3	low	0.923	78839

Table III-4. Polypropylenes Used in the Experiments

Code	Previous Code	Melt Index	$M_w x 10^{-5}$	M_w/M_n	M_z/M_w	Sample Number
PP-1	PP-H-R-B	5.0	3.03_4	9.04	3.57	8531-106-2
PP-2	PP-M-R	12.4	2.78_9	7.83	4.82	8531-106-5
PP-11	PP-H-N	4.2	2.83_6	6.37	2.59	8531-106-1
PP-12	PP-M-N	11.6	2.31_5	4.67	2.81	8531-106-4
PP-13	PP-L-N	25.0	1.78_7	4.62	2.47	8531-106-7

Table III-5. Polystyrenes Used in the Experiments

Commercial Name	Code	Melt Index	$M_w \times 10^{-5}$	M_w/M_n	M_z/M_n	Lot Number	Reference
Dow Styron 678U	PS-1	12	2.14	2.6	-	-	Lobe and White [L-5] Tanaka and White [T-4]
Dow Styron 685D	PS-2	1.6	3.06	1.91	1.61	MM319960	-

To a first approximation the HDPE samples can be subdivided into two groups as either narrow, regular (or broad) molecular weight distributions (MWD). Similarly, LDPE samples can be subdivided into two groups: low degree of LCB with narrow MWD, and high degree of LCB with regular or broad MWD. The code names of HDPE samples with narrow MWD and LDPE samples with a low degree of LCB have two digit numbers (for example, HDPE-11 or LDPE-12). On the other hand, other HDPE and LDPE samples have only a one digit number (for example, HDPE-1 or LDPE-2).

We have identified the LLDPE samples with a single digit. These polymers generally have a narrow MWD ($M_w/M_n \simeq 3 \sim 4$) [F-9].

GPC curves of eight HDPE and two Chemplex LDPE samples are shown in Appendix A. Narrow MWD HDPE (HDPE-11, -12, and -13) and LDPE with low degree of LCB (LDPE-11 and -12) have approximately log normal MWD shapes. GPC curves of LDPE with a high degree of LCB (LDPE-1 and -2) have shoulders in their high molecular weight regions [F-9]. The MWD shape of LDPE-1 and LDPE-11 are similar to those of HP-LDPE-A and HP-LDPE-C of Foster et al. [F-10], respectively [F-9]. Usually LLDPE have narrow MWD with log normal shapes [F-9].

Polypropylene samples, with varying molecular weights and molecular weight distributions, were made by Diamond Shamrock Co. (now part of ARCO). The molecular weight distributions were measured and supplied to us by ARCO. They were already rheologically characterized by the present author [M-40,M-41,M-42]. They are listed in Table III-4 including the code names previously used by

the author. The MWD shape of these samples is approximately log normal.

Two PS materials were also used. One of the PS samples (Dow Styron 678U) was previously used by Lobe and White [L-6] and Tanaka and White [T-3]. The other PS sample is Dow Styron 685D. The MWD characterization was measured and supplied to us by Dr. James M. Rieke of Dow Chemical Co. They are also listed in Table III-5.

B. STABILIZATION

Samples used in the rheological characterization experiments (Chapter IV) and in melt spinning (Chapter XI) had additional stabilizer added to prevent thermal oxidation. Stabilizer in the amount of 0.07 weight percent of BHT (2,6 di-tert-Butyl Hydroxy Toluene) was added to HDPE, LDPE, PP, and PS samples. Similarly, 0.1 weight percent of Irganox 1076 were added to LLDPE-3 and -4. LLDPE-1 and -2 were supplied in granular shape. After adding 0.12 weight percent of Irganox 1076 in LLDPE-1 and -2, they were extruded at 155°C using a Brabender extruder (3/4-inch diameter, L/D = 10) at screw speed of 20 rpm to form strands. "Pellet" samples were made from these strands by Mr. Alan P. Rickards at American Enka. They (the pellet samples of LLDPE-1 and -2) were used for the steady shear flow and the melt spinning experiments.

CHAPTER IV

RHEOLOGICAL PROPERTIES OF POLYETHYLENES

A. INTRODUCTION

Polyethylene (PE) has long been one of the most important commercial thermoplastics. It is widely used for films, bottles, sheets, fibers, and injection molded products.

Until recently there were only two types of polyethylene. These were high density polyethylene (HDPE), manufactured by several low pressure processes and low density polyethylene (LDPE), manufactured by several high pressure processes. HDPE is an almost linear polymer; HDPE manufactured by a Ziegler-type catalyst is a linear polymer, and by a Phillips-type catalyst is a nearly linear polymer, with only one or two long chain branchings (LCB) per 10^5 C atoms [W-9]. The actual values are shown in Table III-1 (page 49). LDPE has a complex molecular structure because of the existence of short and long chain branching [A-16,B-7,B-15,C-27,C-28,H-14,K-12, S-16,S-17,S-18,S-19,W-4]. Recently a new type of polyethylene, known as linear low density polyethylene (LLDPE), has been developed. LLDPE has a density similar to that of LDPE; however, it is a linear polyolefin with short chain branching. LLDPE is manufactured by copolymerization of ethylene and α-olefins, such as butene-1 or octane-1 at low pressures. LLDPE is used in film extrusion, injection and rotational molding, sheet and pipe extrusion, and wire and cable

coating, and as a blow molding resin. The flow properties of molten polyethylene, as in the other case of other thermoplastics, are of great importance in determining the processing characteristics. In the present chapter, we describe a detailed study of the rheological properties of polyethylenes, including high density, linear low density, and low density polyethylene; also we consider various molecular weights and molecular weight distributions and various degrees of long chain branching. We consider the implications of these results in terms of nonlinear viscoelastic constitutive equations and in terms of molecular structure.

B. EXPERIMENTAL

B-1. Materials

A series of HDPE, LDPE, and LLDPE materials were used. They are listed in Tables III-1, III-2, and III-3 (Chapter III, pages 49-51) with molecular characterization data. Pellets of materials containing additional stabilizer (Chapter III, Section B) were compression molded at 170°C to form a sheet of 1.5 mm thickness for making the shear flow measurements. For the uniaxial elongational flow experiments, filament samples were prepared by extrusion from a Brabender extruder (3/4-inch diameter, L/D = 10). A die with a diameter of 3 mm and an L/D ratio of 11.5 was used. The extrusion speeds and temperature were varied, depending on the material; temperatures ranged from 135°C to 175°C, rotation speeds from 12 rpm to 20 rpm.

B-2. Rheological Measurements

Complete rheological measurements were carried out at 180°C.

B-2-a. Steady shear flow measurements. The steady laminar shear viscosity η and the principal normal stress difference $N_1 (= \sigma_{11} - \sigma_{22})$ were measured in a Rheometrics Mechanical Spectrometer (model RMS 7200), using a cone-plate geometry of dimensions 25 mm diameter and cone angle 0.1 radian. After placing a sheet-like sample between the cone and the plate, 10 to 15 minutes were allowed reaching thermal equilibrium for relaxing out compression stresses. During this period both the upper cone and the lower plate were rotated freely at a rotation speed of 0.1 radian/sec. Then an additional one minute was allowed to pass after stopping the rotation. Only one measurement was carried out on each sample.

For the cone angle α and the radius R, the shear rate is given by [W-7]:

$$\dot{\gamma} = \Omega/\alpha \ , \tag{4.1}$$

where Ω is the rotational speed of the cone. The shear stress σ_{12} is determined from the torque M and the principal normal stress difference N_1, as determined from the normal force F. These are given by [W-7]:

$$\eta = \sigma_{12}/\dot{\gamma} = \frac{3}{2} (M/\pi R^2)/\dot{\gamma} \ , \tag{4.2a}$$

$$N_1 = \sigma_{11} - \sigma_{22} = 2F/(\pi R^2) \ . \tag{4.2b}$$

B-2-b. Uniaxial elongational flow measurement. The elongational viscosity was determined as a function of elongational rate and time, using an apparatus recently developed by the author in cooperation with others in our laboratory (H. Yamane, Y. Suetsugu, and Dr. J. L. White). This was first described in a paper by Yamane and White [Y-2]. This development was, in fact, an upgrading of a previous instrument, the Ide-White apparatus [I-4]. It consists of a constant temperature silicone oil bath, a force transducer, and a take-up device (see Figure 4.1). An AC operated linear variable differential transformer (LVDT) (model FTA-G-50, Schaevitz Co., Pennsauken, NJ) was used with a Digital Transducer Readout (model DTR-450, Schaevitz Co.). The maximum linear operating region is ±50 g. The output is recorded on a single chart pen recorder (model SR-206, Health Company, Benton Harbor, MI). A double-gear shaped roller device was used as the take-up device. These gears were driven with a motor equipped with a controller. Two 1/15 Hp motors were used: one 1.6 rpm maximum, and a second 12 rpm maximum. The motor speed was controlled by a B & B controller type ST-12. A silicone oil (Dow Corning Fluid 200: kinematic viscosity 100 centistokes and density 0.968 g/cm^3 at 25°C) was used. The temperature was controlled by a phase angle fired temperature controller (model 2122 PA 03C, Athena Controls, Inc., West Conshohocken, PA).

The filament sample was attached on one end to the LVDT. Ten minutes were allowed for the filament to reach thermal equilibrium and to eliminate frozen-in stresses and orientation. The other end was clamped to the two-gear take-up device. Then, the filament

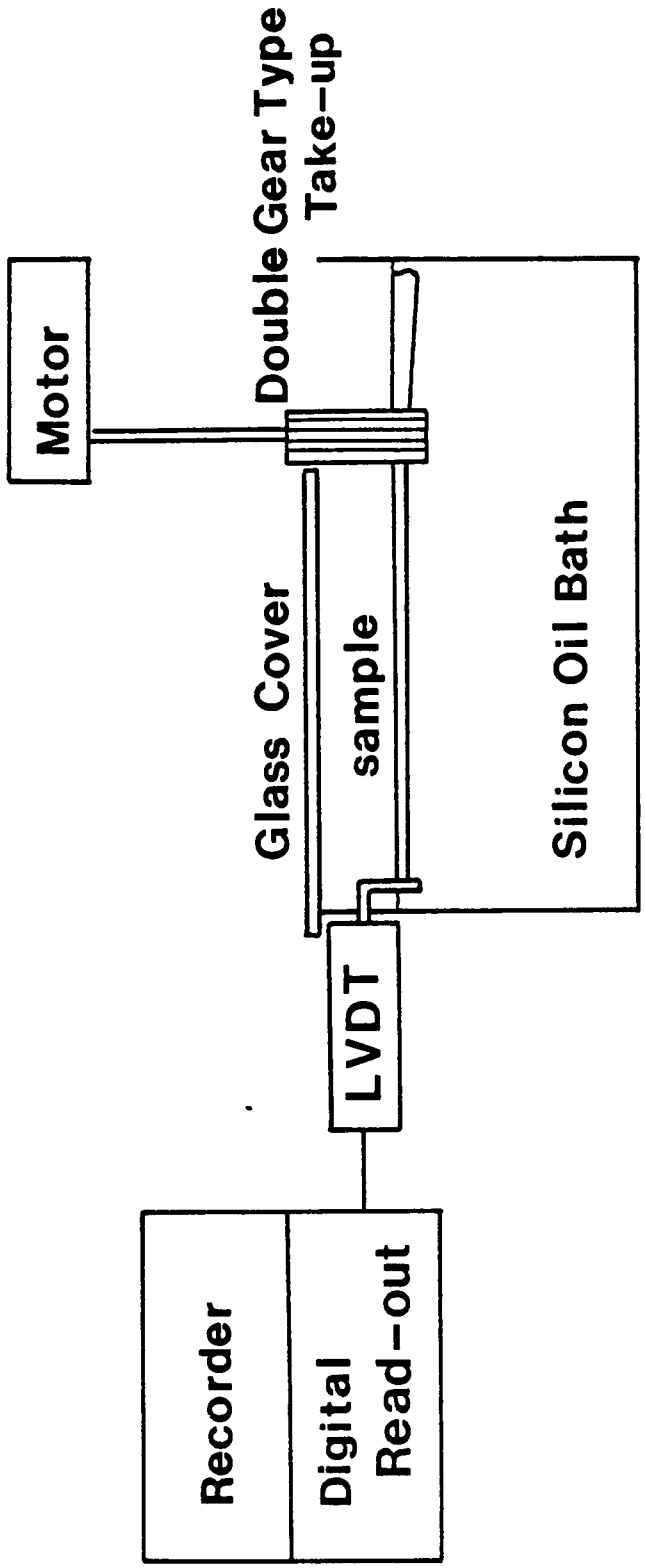

Figure 4.1. Uniaxial elongational rheometer.

was stretched at a constant elongational rate. For each material, the measured cross-section area of the filament at room temperature was corrected to 180°C, using dilatometory data and a shrinkage factor.

The elongational rate E is determined by

$$E = \frac{1}{L}\frac{dL}{dt} = \frac{v_L}{L} \ . \tag{4.3}$$

In the present experiment, the deformation length L and the rotational speed v_L remained constant with time, thus providing a condition of constant strain rate. As long as the filament deforms uniformly, the tensile stress $\sigma_{11}(t)$ and the (apparent) uniaxial elongational viscosity $\chi(t)$ can be determined by

$$\sigma_{11}(t) = \frac{F(t)}{A_0} \exp(Et) \ , \tag{4.4a}$$

$$\chi(t) = \sigma_{11}(t)/E \ , \tag{4.4b}$$

where F(t) is the total force, and A_0 is the cross-sectional area of the melted filament before stretching.

A qualitative study on the nature of the nonuniformities was also carried out, in addition to observations made on the failure mechanism during the constant elongational rate experiments. The filament samples, which were marked with notches, were inserted in a hot silicon oil bath at 180°C and then stretched out by "hand pulling" after removal from an oil bath.

C. RESULTS OF SHEAR FLOW

C-1. Shear Viscosity

The steady shear viscosity η is plotted as a function of shear rate $\dot{\gamma}$ in Figures 4.2, 4.3, and 4.4 for HDPE, LLDPE, and LDPE, respectively. The viscosity functions generally fall in the same order as the molecular weights and approximately inversely with the melt indices. At low shear rates, the shear viscosity is a constant (η_0). At higher shear rates it is a decreasing function. It is noted that: (i) narrow molecular weight distribution (MWD) HDPE, such as HDPE-11, -12, and -13 behave in a quite Newtonian manner (η is a weak decreasing function of $\dot{\gamma}$) compared with other HDPE samples; (ii) LLDPE behaves similarly to narrow MWD HDPE; (iii) LDPE (LDPE-11 and -12), which has a low degree of long chain branching (LCB) and at the same time has a narrow MWD, behaves in a relatively Newtonian manner compared with other LDPE; and (iv) LLDPE behaves somewhere between narrow MWD HDPE and a LDPE with a low degree of LCB.

C-2. Principal Normal Stress Difference

The principal normal stress difference N_1 is plotted as a function of shear stress σ_{12} in Figures 4.5, 4.6, and 4.7 for HDPE, LLDPE, and LDPE, respectively, with the PS-1 data [T-3] (see Table III-5, page 53). We adopt this type of plot following the suggestion of Oda, White, and Clark [O-1], who found for polystyrenes (PS) that it is independent of temperature and the average molecular

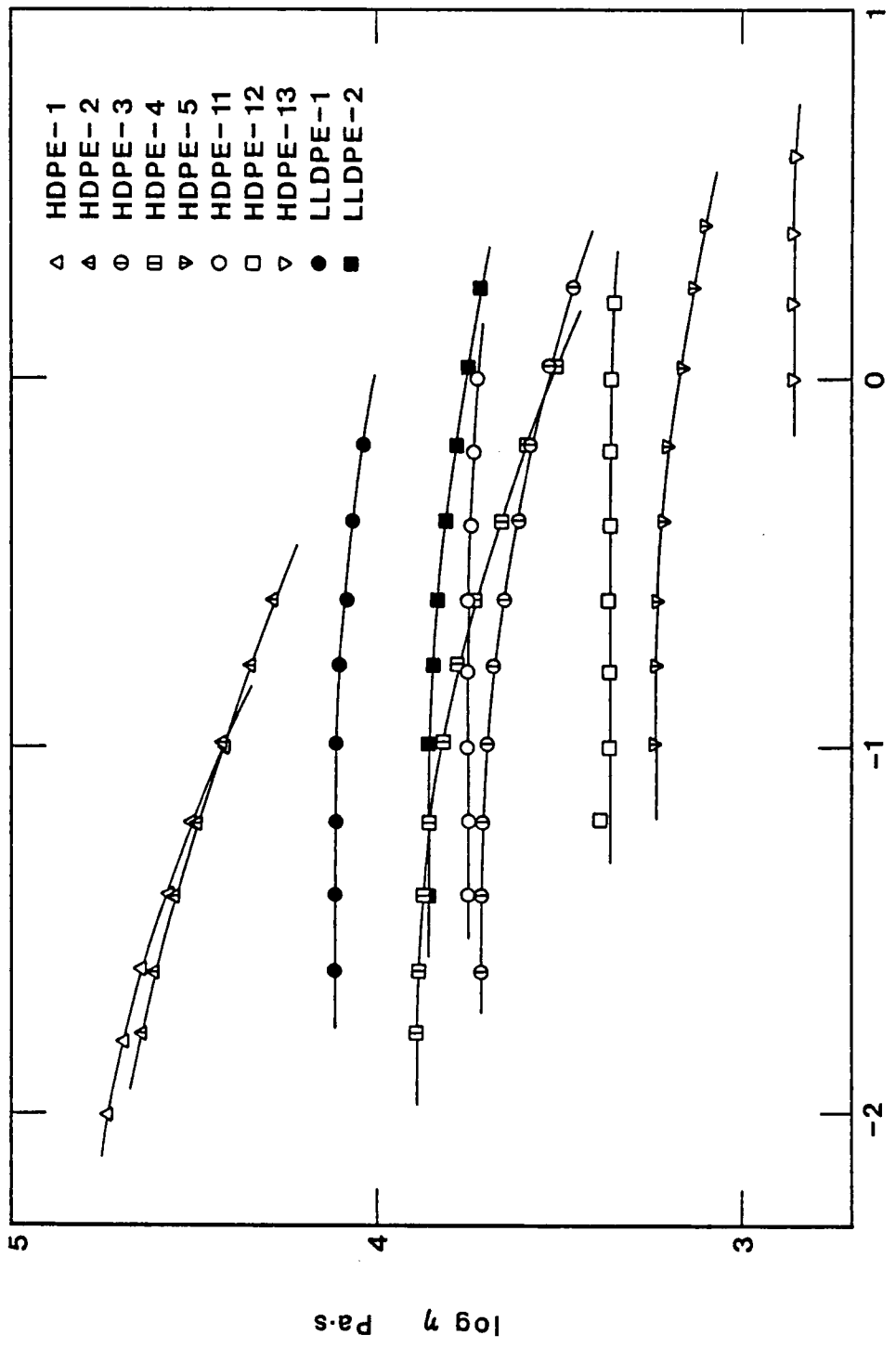

Figure 4.2. Steady shear viscosity as a function of shear rate for high density polyethylenes.

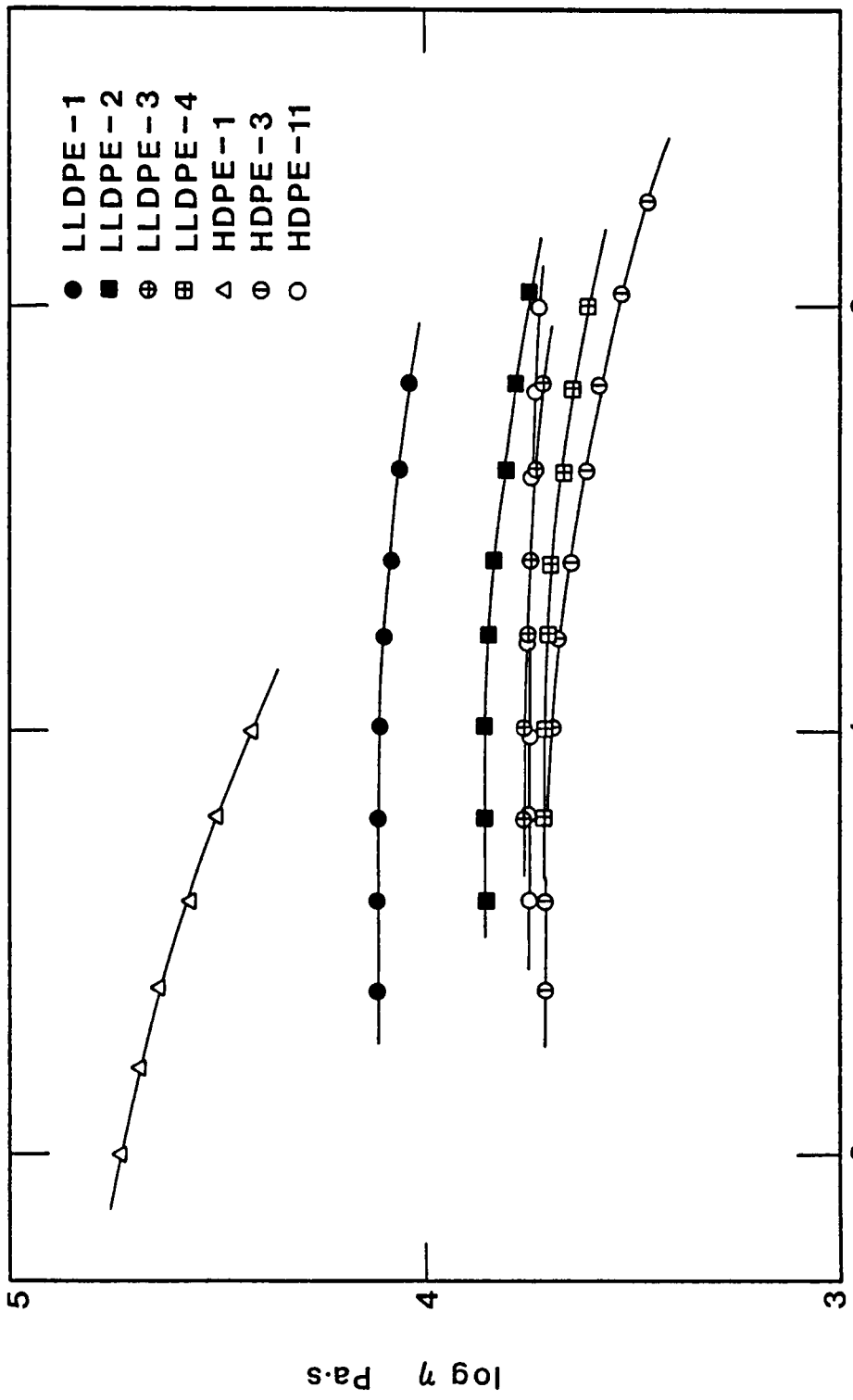

Figure 4.3. Steady shear viscosity as a function of shear rate for linear low density polyethylenes.

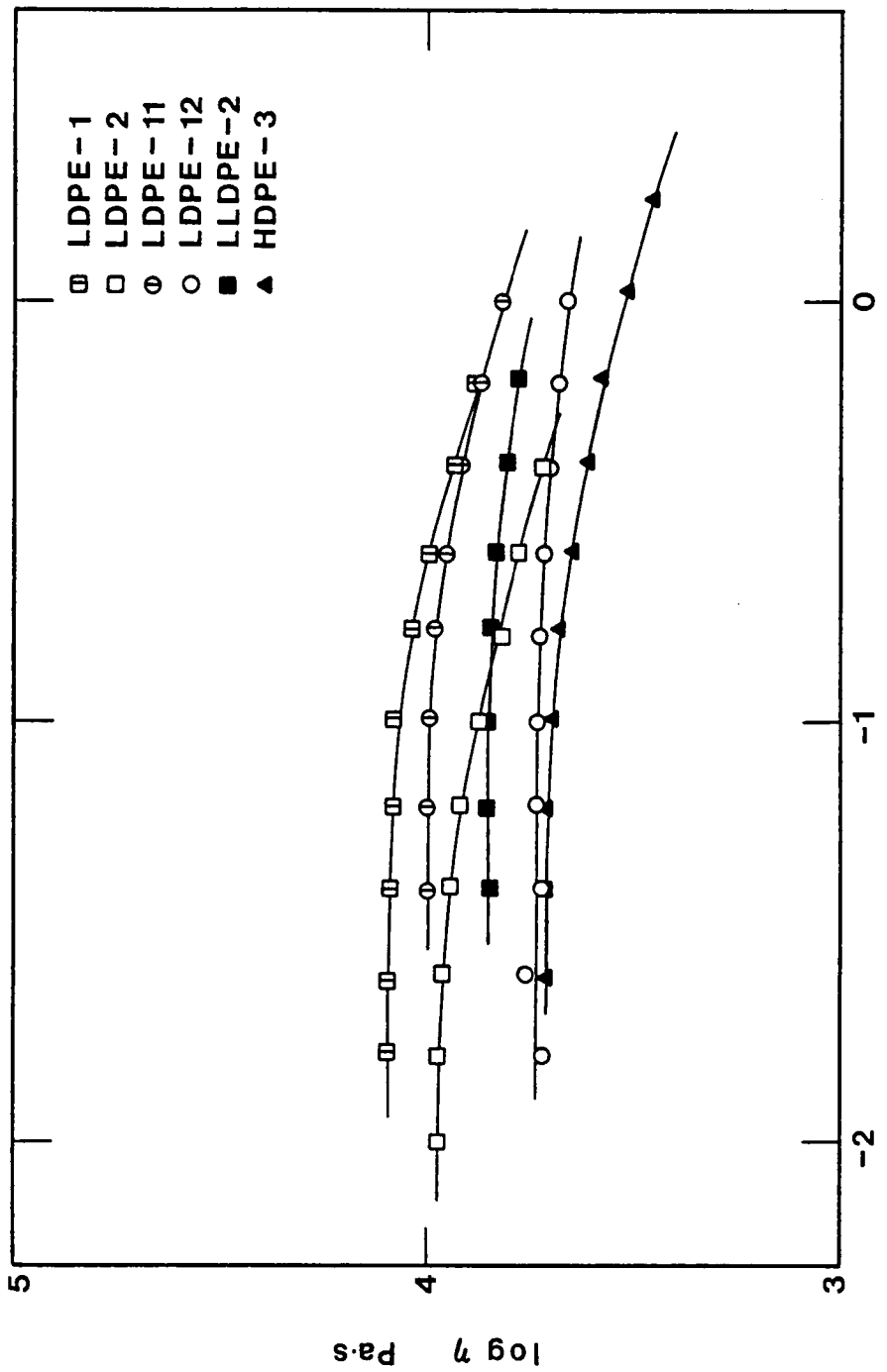

Figure 4.4. Steady shear viscosity as a function of shear rate for low density polyethylenes.

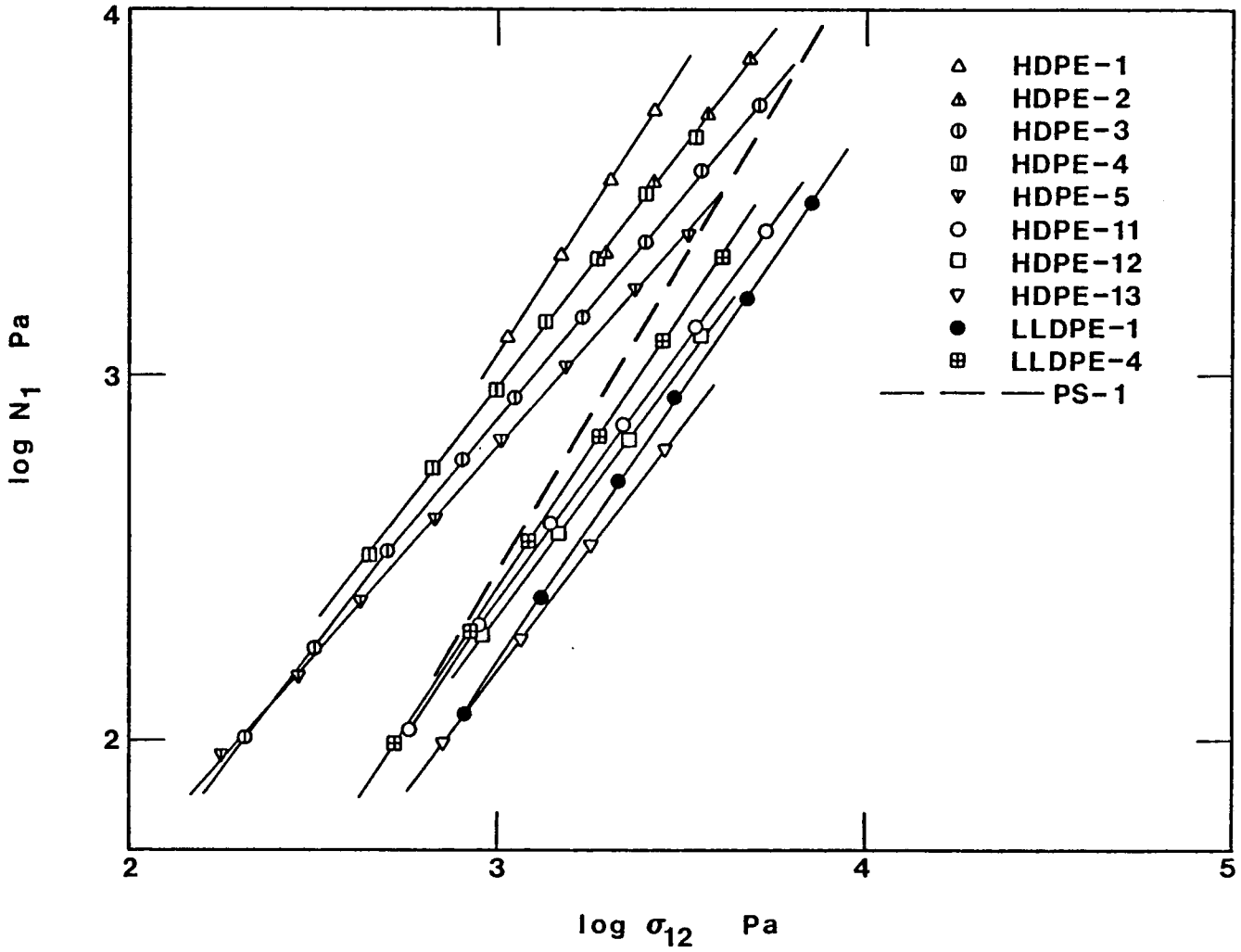

Figure 4.5. Principal normal stress difference as a function of shear stress for high density polyethylenes.

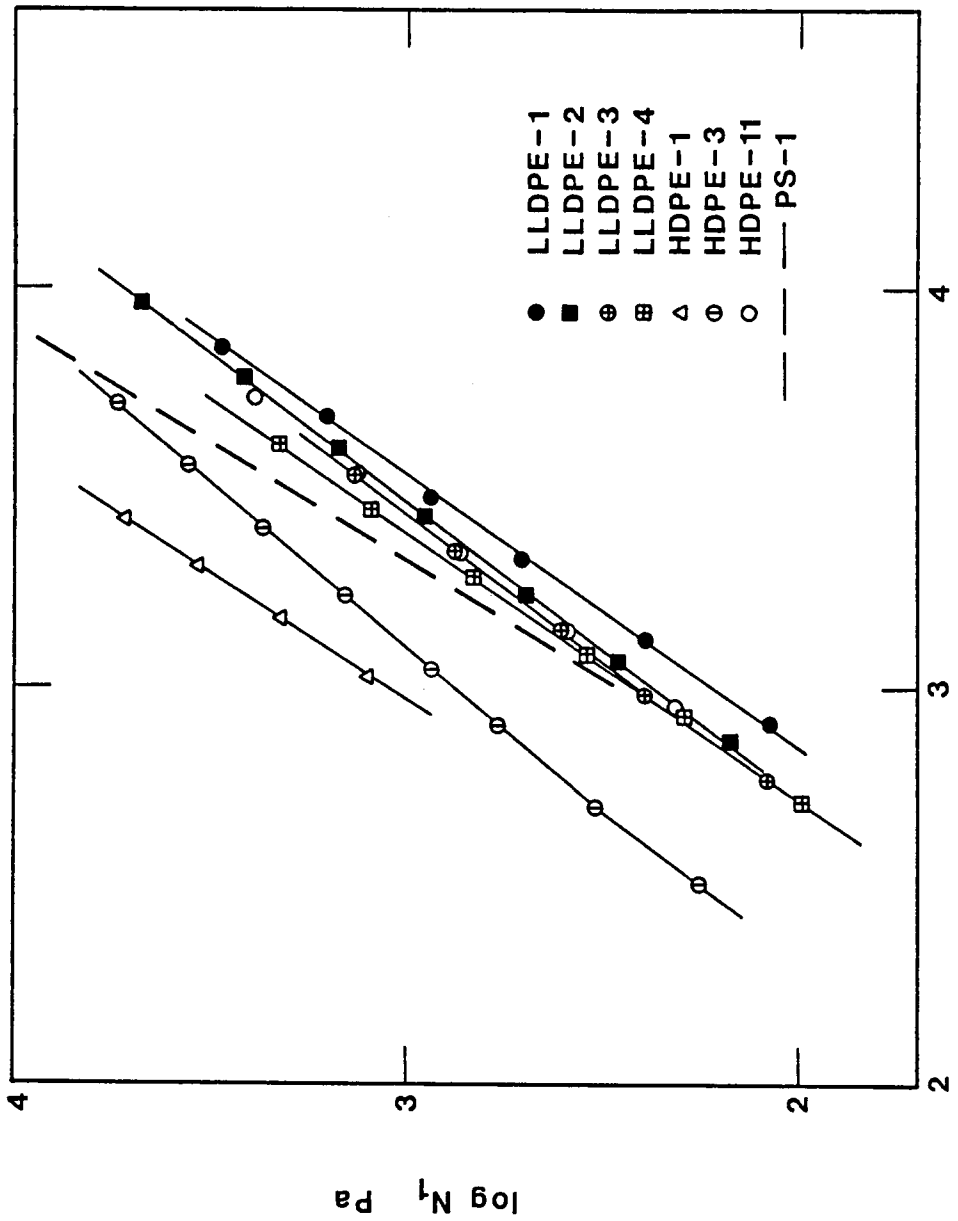

Figure 4.6. Principal normal stress difference as a function of shear stress for linear low density polyethylenes.

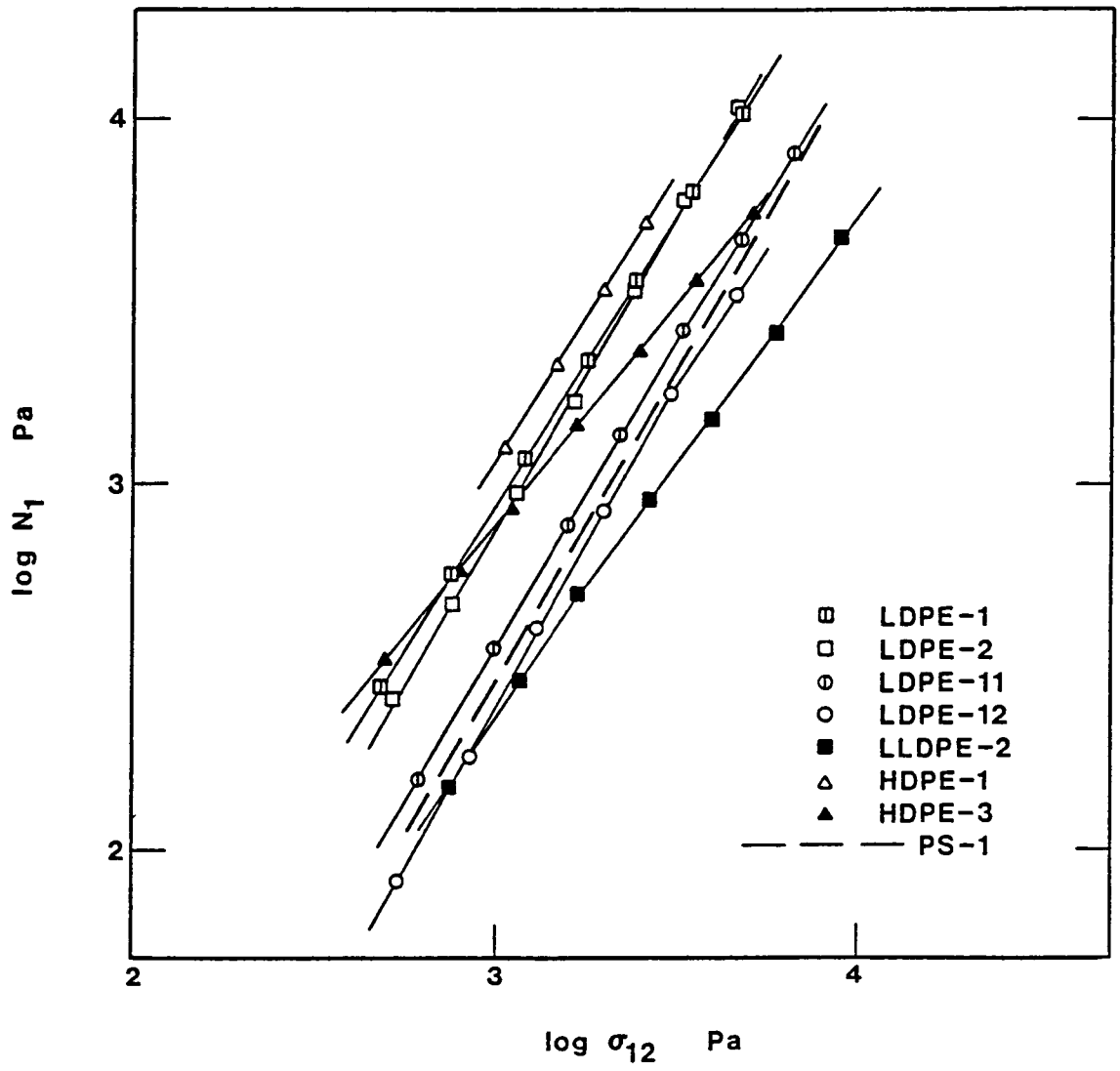

Figure 4.7. Principal normal stress difference as a function of shear stress for low density polyethylenes.

weight, but strongly dependent on the molecular weight distribution. The principal normal stress difference of linear PE (HDPE and LLDPE) increases with the molecular weight distribution at a fixed shear stress. Again it is found that LLDPE behaves in a manner similar to narrow MWD HDPE (HDPE-11, -12, and -13). However, the gradient ($d \log N_1 / d \log \sigma_{12}$) of LLDPE is larger than that of a narrow MWD HDPE. LDPE's having a higher degree of LCB and a broad MWD have the largest principal normal stress difference at a fixed shear stress.

D. INTERPRETATION OF SHEAR FLOW DATA

We will attempt in this section to give a more critical discussion of shear flow rheological properties in terms of molecular structure, such as molecular weight, molecular weight distribution, and degree of long chain branching.

D-1. Shear Viscosity

In Figure 4.8 we plot the zero shear viscosity η_0 of HDPE as a function of the weight average molecular weight M_w. For samples which did not show any Newtonian viscosity (HDPE-1 and -2), η_0 was estimated using Sabia's equation [S-1]. We obtained the result that η_0 varies with about the 3.9th power of M_w.

$$\eta_0 \sim M_w^{3.9} \quad . \tag{4.5}$$

The 3.9th power dependence on M_w is greater than the well-known 3.5th power, as is generally the case for melts with flexible polymer chains. The 3.4 $\sim$ 3.6th power for the fractioned linear PE has been

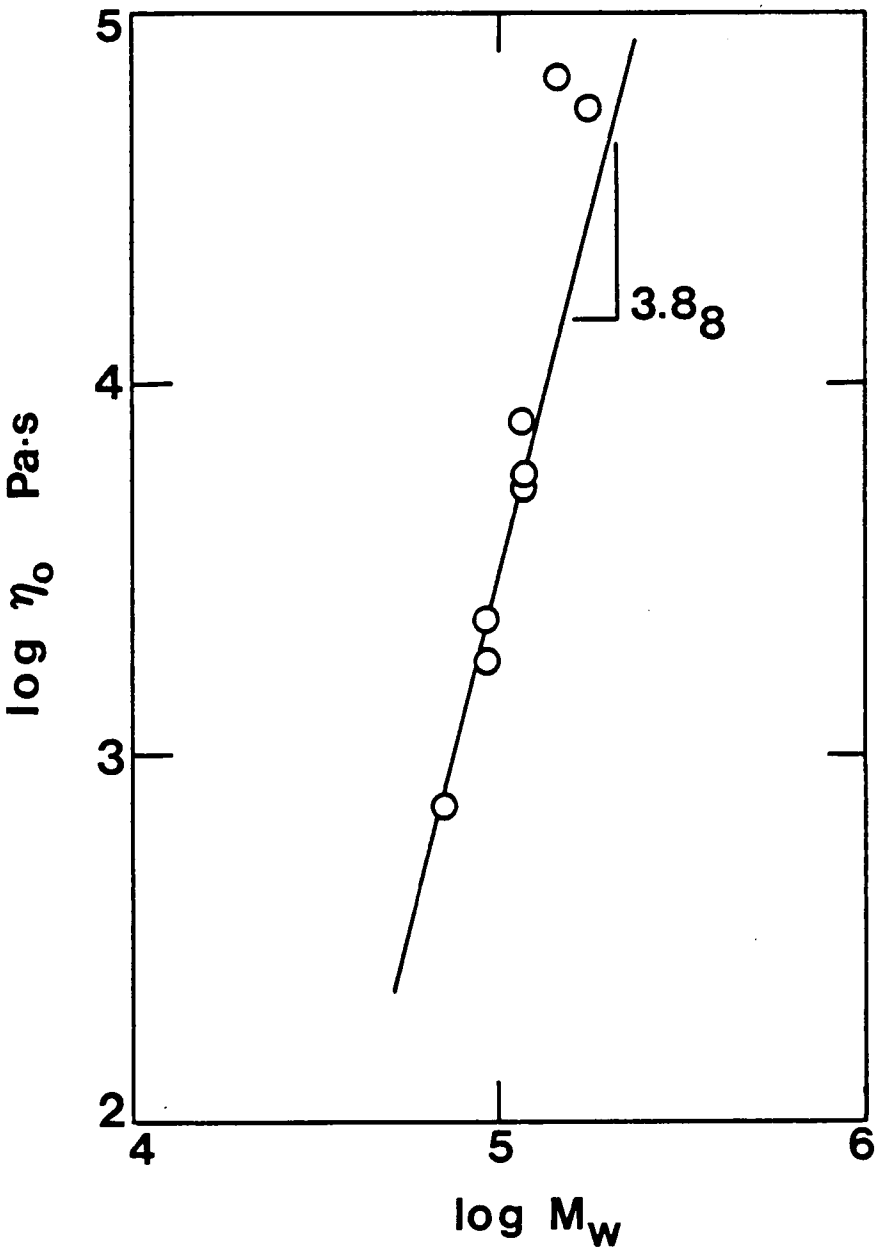

Figure 4.8. Zero shear viscosity as a function of weight average molecular weight for high density polyethylenes.

reported [K-17,M-27,R-4,S-3,S-8,T-7]. Polydispersity is evidentally the cause of this higher power dependence [S-3]. However, there still exists some discrepancy in the case of HDPE-11, -12, and -13. Zeichner and Patel [Z-3] reported for log normal MWD polypropylene (PP) that

$$\eta_0 \sim M_w^{3.6} \cdot (M_w/M_n)^{0.84} \quad . \tag{4.6}$$

However, Saeda [S-3] showed a more complex effect of MWD on the molecular weight dependence of η_0, in the case of a Phillips-type commercial linear HDPE:

$$\eta_0 \sim M_w^m \cdot (MWD)^n \tag{4.7}$$

where the power m is also a function of MWD and increases with broadening of the MWD. Various correlations between η_0 and M_w (based on Eqn. (4.7)) were attempted; however, no better method of correlation was found. This may be responsible for not considering the actual MWD shape (only the ratio of moments was used).

In Figure 4.9, as suggested by Vinogradov and Malkin [V-3] and others [C-4], we plot the following function for linear PE:

$$\eta/\eta_0 = F(\eta_0\dot{\gamma}) \quad . \tag{4.8}$$

The data correlate much better when plotted in this manner, but show a tendency to separate on the basis of MWD, with η/η_0 falling off more rapidly with $\eta_0\dot{\gamma}$ in the broader MWD samples, the same as with PP [M-42]. Very much the same behavior is found in the formulation and master plots of η/η_0 developed by Graessley and his colleagues

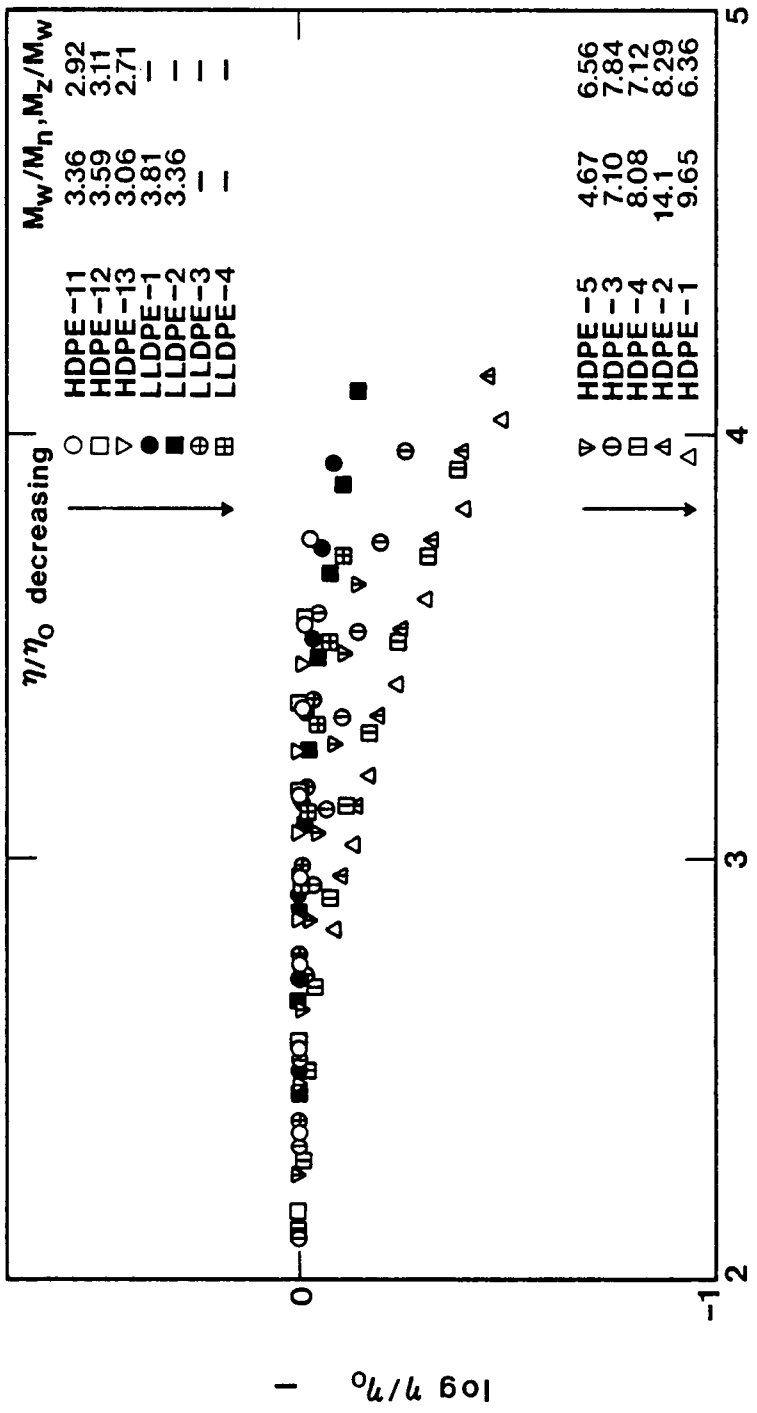

Figure 4.9. η/η_0 as a function of $\eta_0\dot{\gamma}$ for linear polyethylenes.

[G-6,G-8,G-10], and applied by others [I-5,S-2]. In Figure 4.10, the η/η_0 for linear PE at $\eta_0\dot{\gamma} = 3 \times 10^3$ Pa as a function of MWD (such as M_w/M_n and M_z/M_w) are plotted. This clearly shows that η/η_0 falls off more rapidly with $\eta_0\dot{\gamma}$ in the broader MWD samples. The plot of η/η_0-MWD shows a better correlation by using M_w/M_n to represent the MWD. However, Figure 4.10 suggests the need for a better representation of the MWD which can take into account the actual distribution shape. We give our attention now to LLDPE. In Figures 4.9 and 4.10, the η/η_0 function of LLDPE falls off more quickly than that of narrow MWD HDPE (HDPE-11, -12, and -13). However, the N_1 function for LLDPE is almost the same as that for narrow MWD HDPE. Saed, Suzuki, and Yamaguchi [S-2] reported that the η/η_0 function for fractionated ethyl-branched polyethenes fall off more rapidly with $\eta_0 M_w \dot{\gamma}$ than fractioned linear polyethyenes. Therefore, we must conclude that the existence of short chain branching makes shear viscosity more shear rate softening.

We now turn to the η/η_0-$\eta_0\dot{\gamma}$ relationship for LDPE. This is plotted in Figure 4.11. η/η_0 falls off more rapidly with $\eta_0\dot{\gamma}$ in the broader MWD samples and with higher degree of LCB. The effects of LCB are not clear because the broad MWD LDPE has a higher degree of LCB. The correlation of η/η_0 with $\eta_0\dot{\gamma}$ for LDPE in the literature was also carried out (using the data from Shroff and Shida [S-20] and Mendelson, Bowles and Finger [M-27]). However, the effect of MWD and LCB in LDPE on the η/η_0-$\eta_0\dot{\gamma}$ function could not be clearly distinguished: generally the same effects of MWD and LCB, as shown in Figure 4.11, were observed.

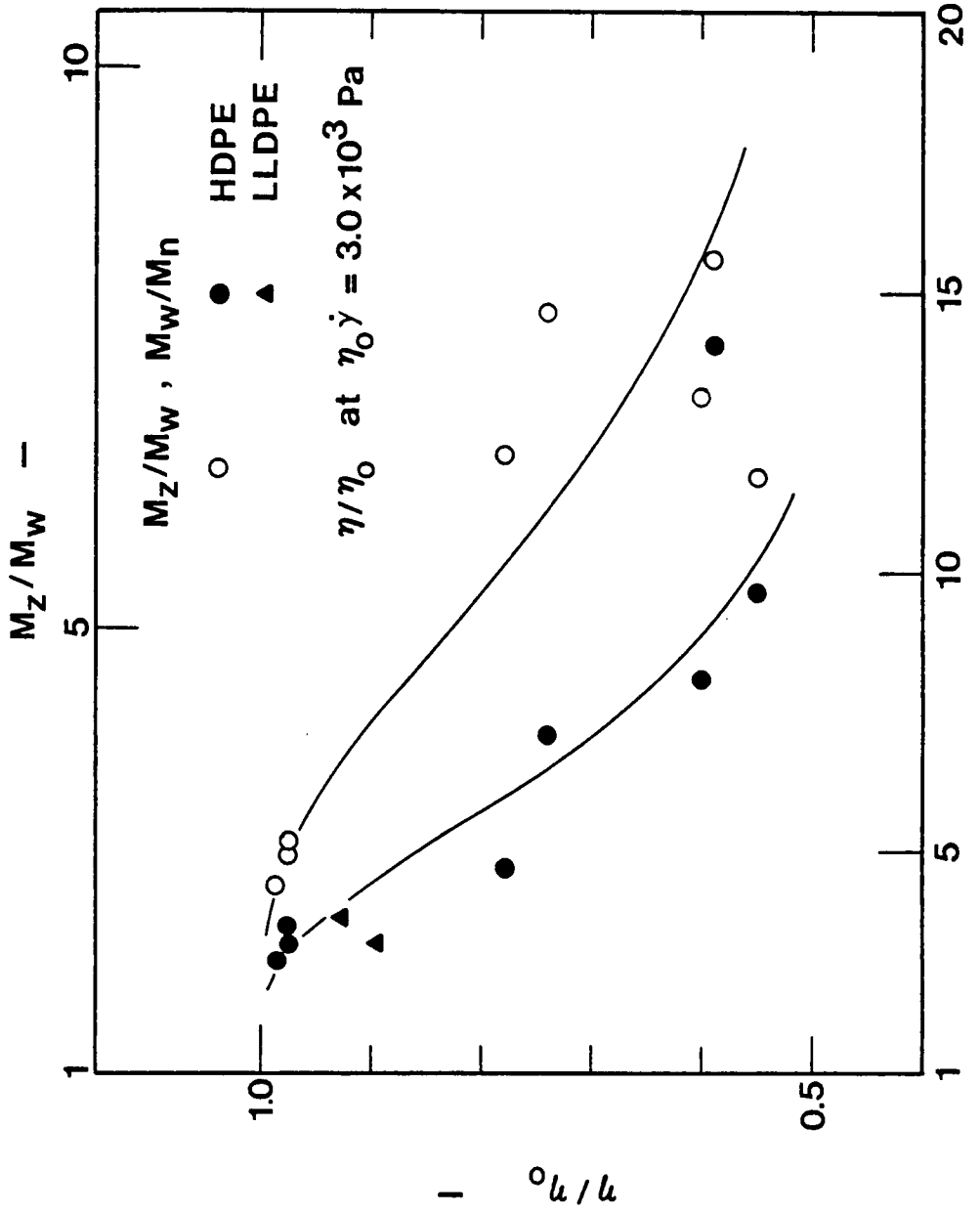

Figure 4.10. η/η_0 (at $\eta_0\dot{\gamma}$ = 3 x 10^3 Pa) as a function of molecular weight distributin.

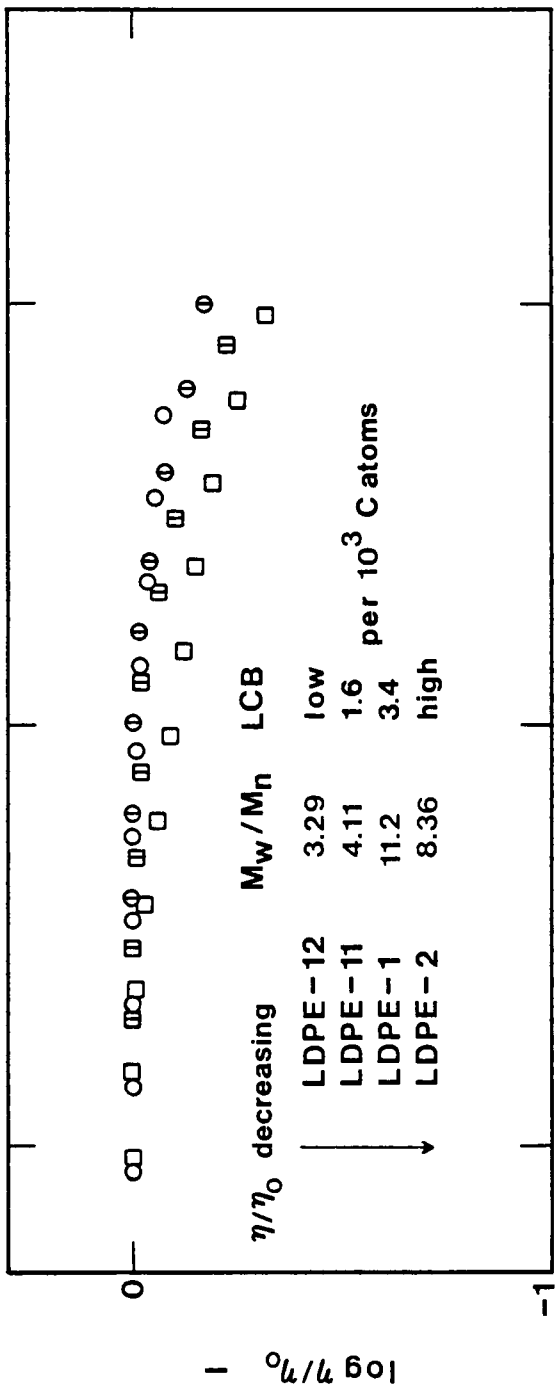

Figure 4.11. η/η_0 as a function of $\eta_0\dot{\gamma}$ for low density polyethylenes.

In Figure 4.12, we plot the η/η_0-$\eta_0\dot{\gamma}$ function for linear and star-branched (four star and six star branched) anionically polymerized polyisoprene (PI) data for a 40 weight percent TD (tetradecane) solution. These data were supplied to us by Professor T. Masuda of Kyoto University. Some of the data have appeared in the papers of Graessley, Masuda, Roovers, and Hadjichristidis [G-9]. All of the samples are narrow MWD and well-characterized by dilute solution methods [H-1]. The same sample names as were used by Graessley et al. [G-9] are shown. These samples are considered to have monodisperse MWD. η/η_0 falls off more rapidly with $\eta_0\dot{\gamma}$ with increasing number of branches. The magnitude of η/η_0 falls in the order (at fixed $\eta_0\dot{\gamma}$) as follows:

Linear PI > Four Star PI > Six Star PI .

We conclude that the effect on the shear viscosity of LCB, in star-branched polymers, is shear rate softening. No data on the η-$\dot{\gamma}$ function for comb-branched polymers are available. LDPE has a more complicated branched structure than star-branched polymers. The existence of LCB makes the hydrodynamic volume small, depending on what the LCB structure is (star-branched, comb-branched, or randomly branched polymer). Therefore, we conclude that the effect of LCB in LDPE on shear viscosity is to cause a shear rate softening effect.

D-2. Principal Normal Stress Differences

The correlation of the principal normal stress difference N_1 with the shear stress σ_{12} of linear PE, as shown in Figures 4.5 and

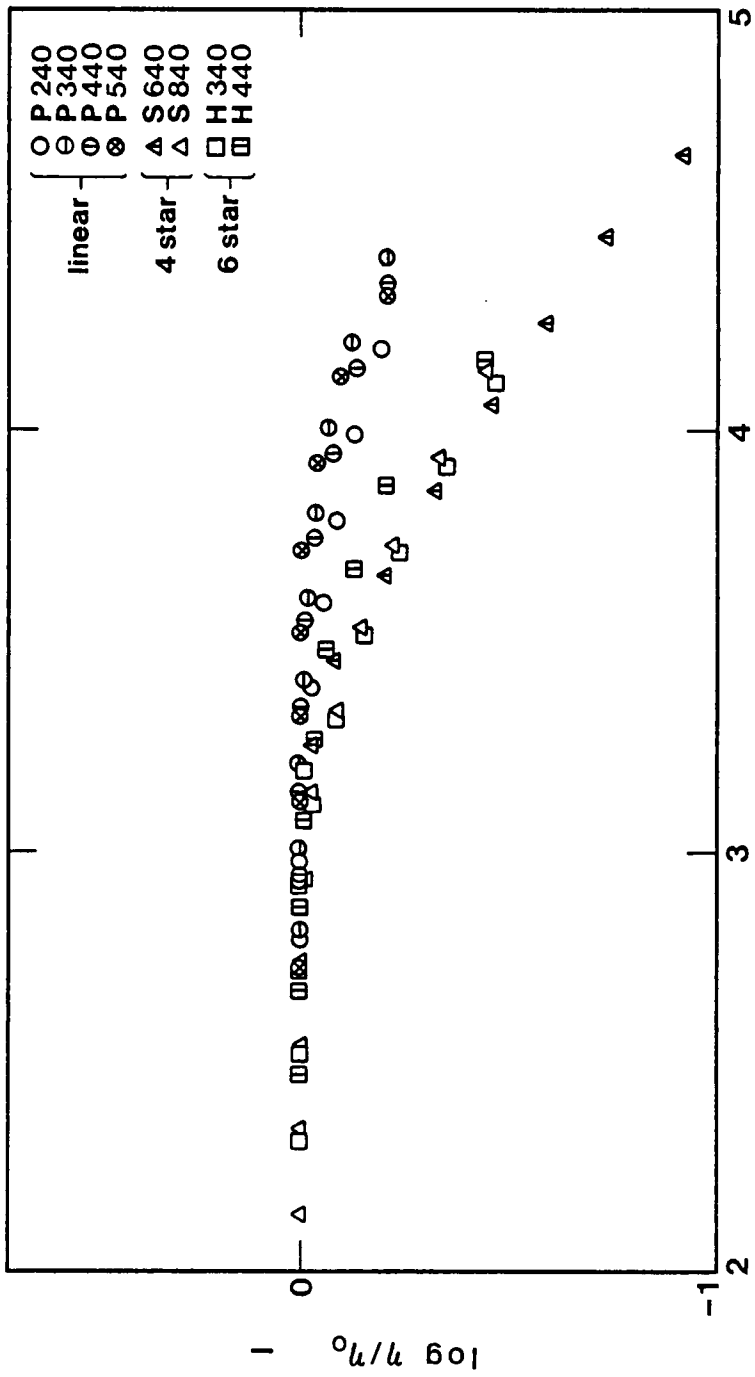

Figure 4.12. η/η_0 as a function of $\eta_0\dot{\gamma}$ for monodisperse polyisoprenes (40 weight percent tetradecane solution: linear, 4 star and 6 star-branched polymer.

4.6, is very similar to the results of Oda, White, and Clark [O-1] and Racin and Bogue [R-1] for polystyrene (PS); Minoshima, White, and Spruiell for polypropylene (PP) [M-42]; and Ishida, Shiga, and Sakamoto for HDPE [I-5]. It is generally known that N_1 for the linear polymers, at fixed σ_{12}, is greater for the broader MWD samples. The slope of the log N_1-log σ_{12} plot for the linear broader MWD's is lower; that is, if we write

$$N_1 = A\ \sigma_{12}^{\ b} \ . \tag{4.9}$$

the value of "b" is smaller. However, if we look carefully at Figure 4.5 (page 66), we note that the N_1-σ_{12} function for HDPE is not simply a function of M_w/M_n, M_z/M_w, or M_{z+1}/M_z. There are two questions: (i) Why is N_1 for narrow MWD HDPE, at fixed σ_{12}, greater for the higher MW samples?; and (ii) why is N_1 for HDPE-1 greater than that for HDPE-2 at fixed σ_{12}? (or, differently stated, why is the slope of the log N_1-log σ_{12} plot for HDPE-1 larger than that for HDPE-2?). These two questions about the function N_1 for HDPE will be considered after examining this function for LLDPE and LDPE (Figures 4.6 and 4.7, pages 67 and 68). LLDPE shows similar values in the N_1-σ_{12} function for narrow MWD HDPE materials (HDPE-11, -12, and -13), as expected from the MWD data. However, the slope of the log N_1-log σ_{12} plot for LLDPE is greater than that for narrow MWD HDPE. The question is why? Among the various LDPE materials, the values for N_1, at fixed σ_{12}, are greater for the samples with broad MWD and with a high degree of LCB. The slope of the log N_1-log σ_{12}

plot of LDPE is the highest among the polyethylenes. No effects of MWD or LCB are seen. The slopes of the various log N_1-log σ_{12} plots fall in the order

LDPE > LLDPE $\geq$ narrow MWD HDPE > moderate and broad MWD HDPE .

Let us now consider the question: Why does LDPE have the highest slope?

First we consider the effect of LCB on the principal normal stress difference. In Figure 4.13 we plot the function N_1-σ_{12} for linear and star-branched (four star and six star branched) anionically polymerized polyisoprene (PI). These are the same samples described in connection with the LCB effects on shear viscosity (Section D-1). These data were supplied to us by Professor T. Masuda of Kyoto University. All of these samples have a narrow MWD and are well-characterized by dilute solution methods [H-1]. These samples are considered to have monodisperse MWD. The values of N_1 for the star-branched polymers, at fixed σ_{12}, are larger than those for the linear polymers. Both star-branched and linear polymers have slopes in the plots of log N_1-log σ_{12} of 2.0. No effect of the number of LCB on the value of N_1 is found. In Eqn. (4.9), the constant "A" increases with the occurrence of LCB.

We now return to the matter of the nature of the function N_1 for linear PE. Kume, Takahashi, Masuda, and Onogi [K-17] reported that the function N_1 for fractioned HDPE ($M_w = 5.94 \times 10^4 \sim 2.03 \times 10^5$, $M_w/M_n = 1.19 \sim 1.59$, $M_z/M_w = 1.24 \sim 1.63$) increases with MW at fixed

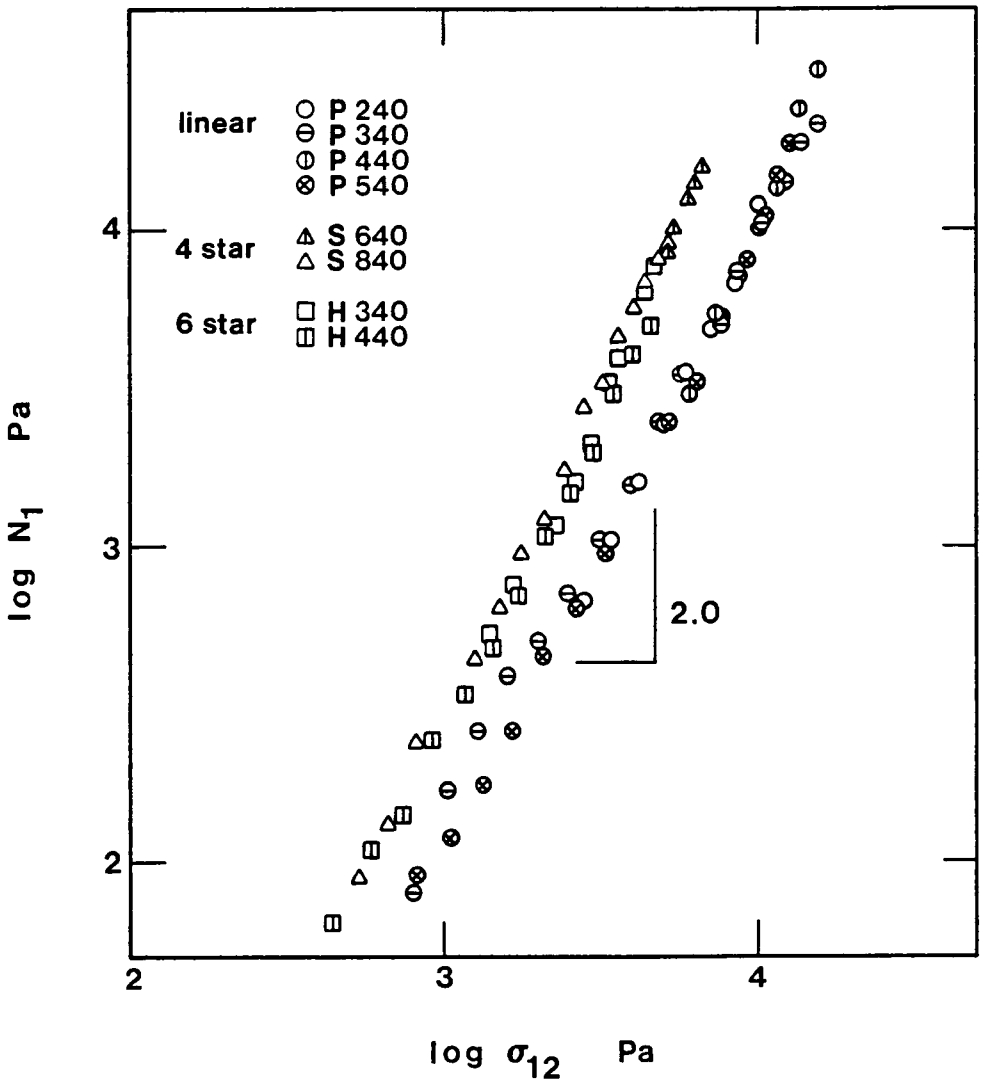

Figure 4.13. Principal normal stress difference as a function of shear stress for monodisperse polyisoprenes (40 weight percent tetradecane solution: linear, 4 star and 6 star-branched polymer).

σ_{12}. However, their fractioned samples showed increasing MWD with increasing MW. Their stress levels are well above 10^4 Pa, which is the limit of the cone and plate type of measurement. They also presented steady state compliance data (Je) obtained from dynamic measurements. Their Je values show a 12.1 power dependence in the Je-M_z/M_w relationship. It is known that Je is proportional to M_z/M_w with exponents in the range 3.5 to 3.7, for non-polar linear flexible chains, such as those of polystyrene and polymethyl disiloxane [M-8, M-37]. Kume et al. [K-17] suggested that the effects of MW on Je are important in the case of very narrow MWD HDPE materials and the effects of MWD are dominant for rather broad MWD HDPE (commercial HDPE). If we introduce the second-order fluid (low deformation rate) asymptote, N_1 may be expressed in terms of Je [C-22] as follows:

$$N_1 = 2\ Je\ \eta_0^2\ \dot{\gamma}^2 = 2\ Je\ \sigma_{12}^2 \ . \qquad (4.10)$$

In Figure 4.14, we plot Je for our HDPE data (defined as $N_1/2\sigma_{12}^2$ at $\sigma_{12} = 10^3$ Pa) in comparison with the data of Kume et al. [K-17], Mills [M-37], Wales [W-6], and Shroff et al. [S-22]. All data, except Kume's, are obtained from the principal normal stress differences; Wales and Shroff's data are estimated at $\sigma_{12} = 10^3$ Pa. Figure 4.14 seems to support Kume's argument as to the effect of MWD and MW on Je. However, one must be careful about fractionated HDPE samples. There are two possibilities which might make the Je values so high: (i) the existence of high MW fractions which cannot be detected by GPC, or (ii) the existence of long chain branching. Recent studies

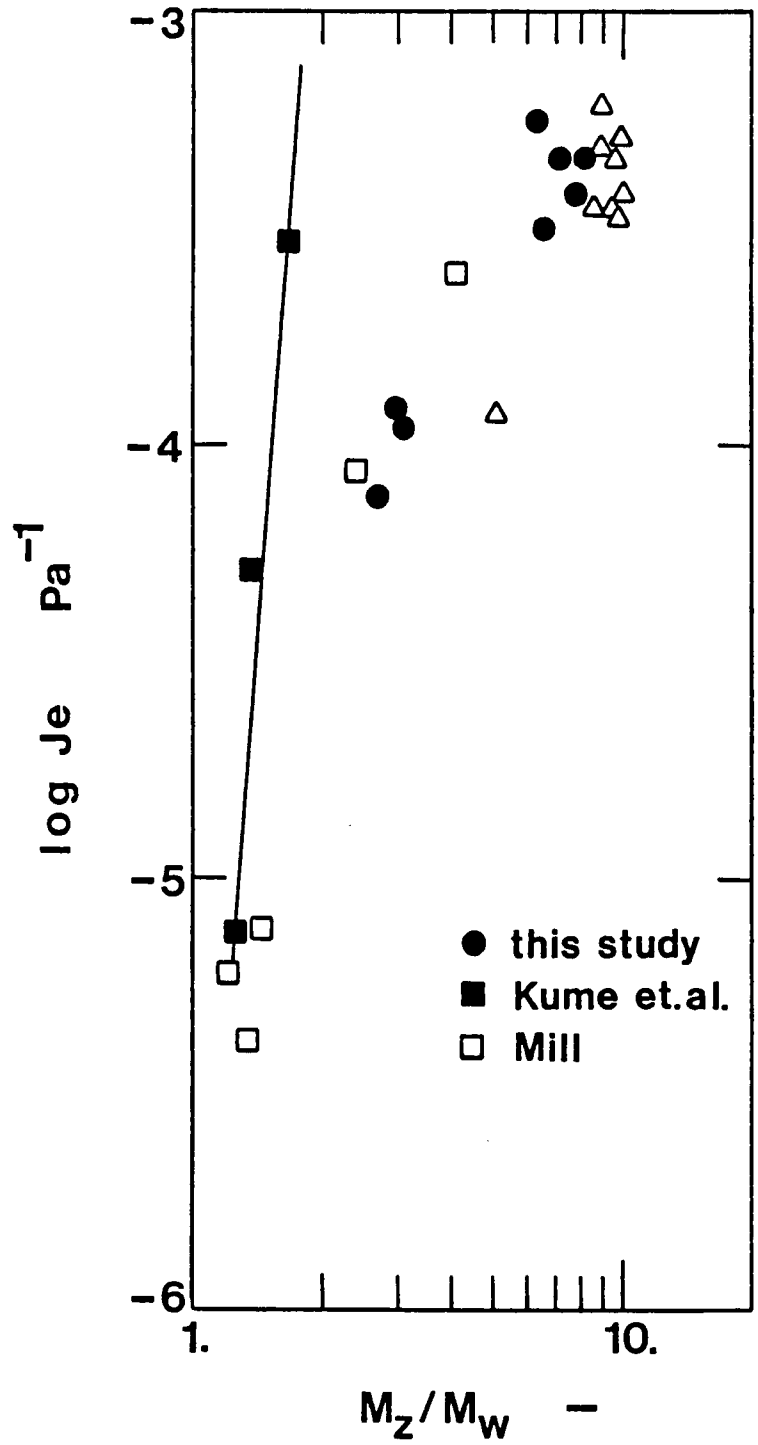

Figure 4.14. Je as a function of M_z/M_w for high density polyethylenes.

of the dynamic rheological properties of monodisperse hydrogenated polybutadiene, which do not have any possibility of having LCB or high MW fractions, suggest a MW dependence of Je in the case of monodisperse linear PE (Je is estimated from their G' and G" data) [R-31]. This also supports Kume's results for HDPE that Je increases with MW for very narrow MWD samples; and also it supports the idea that the effects of MWD on Je are dominant in broad MWD samples. This may explain why the values of N_1, at fixed σ_{12}, for narrow MWD HDPE (HDPE-11, -12, and -13) increase with increasing MW. The slope of the log N_1-log σ_{12} plots and the values of N_1 at fixed σ_{12} for HDPE-1 are higher than those for other moderate and broad MWD HDPE (note that HDPE-1 is not the broadest MWD nor the highest MW sample). This may be explained by the existence of a higher level of LCB compared with other HDPE samples. Unfortunately the degree of LCB in HDPE-1 is not known.

Saed et al. [S-2] showed that the value of η/η_0 for fractionated ethyl-branched PE samples falls off more rapidly with $\eta_0 M_w \dot{\gamma}$ than does the same function for fractionated linear PE. This suggests that the effects of short chain branching (SCB) may be similar to those of LCB, even though the effects of SCB are weaker than those of LCB. It is certainly a fact that the slopes of the log N_1-log σ_{12} plots for LLDPE are greater than those of narrow MWD HDPE. The effects of LCB, SCB, and MWD on N_1 will be discussed again in terms of the nonlinearity of the convected Maxwell model (see Sections D-3-b and F).

D-3. Implications in the Constitutive Equations

D-3-a. Characteristic time. In nonlinear viscoelastic constitutive equations, the nonlinearity of the memory function is often tied to the time average deformation rate dependence of the relaxation times. In the special case in which the deformation rate is independent of the time, the nonlinearity of the memory function is tied to the deformation rate dependence of the relaxation time (for reviews see Middleman [M-33], Han [H-3], and White [W-15]). Recently Ide and White [I-3,W-17], White and Kondo [W-18], and White and Minoshima [W-20] have re-emphasized the importance of this dependence on hydrodynamic response in flow problems, especially those involving elongational deformations.

The usually defined characteristic time is

$$\bar{\tau}(\dot{\gamma}) = \frac{\Psi_1}{2\eta} = \frac{N_1}{2\sigma_{12}\dot{\gamma}} . \tag{4.11}$$

The relaxation time $\bar{\tau}$ falls off more rapidly as MWD broadens [M-42, W-18,W-20].

The $\bar{\tau}$ - $\dot{\gamma}$ dependence is related to the slope of the N_1-σ_{12} plots. This may be shown by combining Eqns. (4.8) and (4.9)

$$\bar{\tau} = \frac{N_1}{2\sigma_{12}\dot{\gamma}} = \frac{A\,\sigma_{12}^{\,b}}{2\sigma_{12}\dot{\gamma}}$$

$$= B\,\eta^{b-1}\dot{\gamma}^{b-2} = B\,\dot{\gamma}^{b-2}\,[\eta_0 F(\eta_0\dot{\gamma})]^{b-1} . \tag{4.12}$$

For monodisperse polymer melts Oda et al. [O-1] find "b" is 2.0, as expected, which leads to

$$\bar{\tau} = B\eta = B\eta_0 F(\eta_0\dot{\gamma}) \ , \tag{4.13a}$$

indicating that $\bar{\tau}$ falls off at the same rate as does η. As MWD broadens "b" decreases to values of the order 1.5, giving

$$\bar{\tau}(\dot{\gamma}) = B[\frac{\eta_0}{\dot{\gamma}} F(\eta_0\dot{\gamma})]^{0.5} \ . \tag{4.13b}$$

Even if the $\eta(\dot{\gamma})$ functions are the same for narrow and broad MWD samples, $\bar{\tau}$ should decrease more rapidly for broad MWD.

More detailed arguments are presented by White and Minoshima [W-20].

D-3-b. Material parameter determination and molecular structure effects in the constitutive equations. The qualitative features of shear flow may be interpreted in terms of nonlinear viscoelastic constitutive equations. The simplest expression for doing this is the convected Maxwell (White-Metzner) type of constitutive equation used by Ide and White [I-3,W-17] and Minoshima, Spruiell, and White [M-41,M-42]. This expression has the form

$$\underset{\sim}{\sigma} = -p\underset{\sim}{I} + \underset{\sim}{P} \ , \tag{4.14a}$$

$$\underset{\sim}{P} = 2G\tau\underset{\sim}{d} - \tau \frac{\delta \underset{\sim}{P}}{\delta t} \ , \tag{4.14b}$$

where

$$\tau = \frac{\tau_0}{1 + a\,\tau_0\,II_d^{1/2}} \tag{4.14c}$$

This form for τ was suggested by Bogue [B-12]. II_d is the second invariant of $\underset{\sim}{d}$ where $\underset{\sim}{d}$ is the strain rate (or rate of deformation tensor. $\delta(\ )/\delta t$ is Oldroyd's contravariant convected derivative.

In steady shear flow Eqn. (4.14) is written as

$$\sigma_{12} = \eta\dot{\gamma}\ , \tag{4.15a}$$

$$\eta = \frac{G\,\tau_0}{1 + a\,\tau_0\,\dot{\gamma}}\ , \tag{4.15b}$$

$$N_1 = 2G\,\tau^2\,\dot{\gamma}^2 = 2\sigma_{12}^2/G = \Psi_1\dot{\gamma}^2\ , \tag{4.15c}$$

$$\bar{\tau} = \tau = \frac{\tau_0}{1 + a\,\tau_0\,\dot{\gamma}}\ , \tag{4.15d}$$

with $N_2 (= \sigma_{22} - \sigma_{33})$ equal to zero.

There are several ways to determine the material constants G, τ, and "a", based on shear flow data (details are given by Yamane [Y-1]). These are as follows:

(i) Method A

First determine τ_0 based upon Eqn. (4.15d) which leads to

$$1/\tau = 1/\tau_0 + a\,\dot{\gamma}\ . \tag{4.16a}$$

Then determine G using the zero shear viscosity

$$G = \eta_0/\tau_0\ . \tag{4.16b}$$

Finally, determine "a" using Eqns. (4.15b), (4.15c), and (4.15d).

(ii) Method B

First determine G using Eqn. (4.15c)

$$G = 2\sigma_{12}^2/N_1\Big|_{\text{at some } \sigma_{12}} \quad . \tag{4.17a}$$

Then determine τ_0 using the zero shear viscosity

$$\tau_0 = \eta_0/G \quad . \tag{4.17b}$$

Finally, determine "a" using Eqns. (4.15b), (4.15c), and (4.15d).

The material parameters for the PE samples used in this chapter, as well as those for the polypropylene (PP) samples (see Table III-4, page 52), will be determined in the following.

The material parameters determined using Method A are listed in Table IV-1. Here, $1/\tau$ for any sample is not a linear relation with $\dot{\gamma}$, as expected from Eqn. (4.16a). A weighted linear (least squares) method was employed to obtain a best fit. Less emphasis was put on the τ values in the lowest and highest shear rate regimes, because of the lesser accuracy of the N_1 data in those regimes. Less than a 10% difference between an actual τ value and a calculated τ value is allowed. However, it is permitted to have larger differences between the actual τ values and the calculated τ values at the highest and lowest shear rates, if that is necessary. In Figures 4.15a through

Table IV-1. Material Parameters from Method A

Polymer	τ sec	G Pa x 10^{-3}	"a" (-) Based on η	"a" (-) Based on N_1	"a" (-) Based on τ
HDPE-1	42.4	1.53	0.4	0.55	0.80
HDPE-2	45.7	1.20	0.25	0.6	1.40
HDPE-3	8.78	0.592	0.1	0.55	2.08
HDPE-4	7.55	1.04	0.2	0.6	1.43
HDPE-5	4.75	0.367	0.05	0.5	2.76
HDPE-11	1.13	4.98	0.1	1.2	3.66
HDPE-12	0.620	3.71	0.05	1.5	5.22
HDPE-13	0.142	5.06	0.05	1.5	7.77
LLDPE-1	1.68	7.82	0.2	1.4	4.82
LLDPE-2	1.54	4.66	0.2	1.2	4.10
LLDPE-3	1.73	3.34	0.1	1.4	4.34
LLDPE-4	1.29	4.00	0.2	1.2	3.59
LDPE-1	8.74	1.43	0.1	0.4	0.88
LDPE-2	4.06	2.32	0.4	0.5	0.80
LDPE-11	2.29	4.33	0.2	0.6	1.43
LDPE-12	0.844	6.44	0.2	0.8	1.70
PP-1	11.1	1.77	0.3	0.8	1.82
PP-2	7.47	1.16	0.25	0.7	1.65
PP-11	2.80	3.57	0.2	1.4	3.67
PP-12	1.83	2.57	0.2	1.0	3.03
PP-13	0.462	3.68	0.3	1.3	3.34

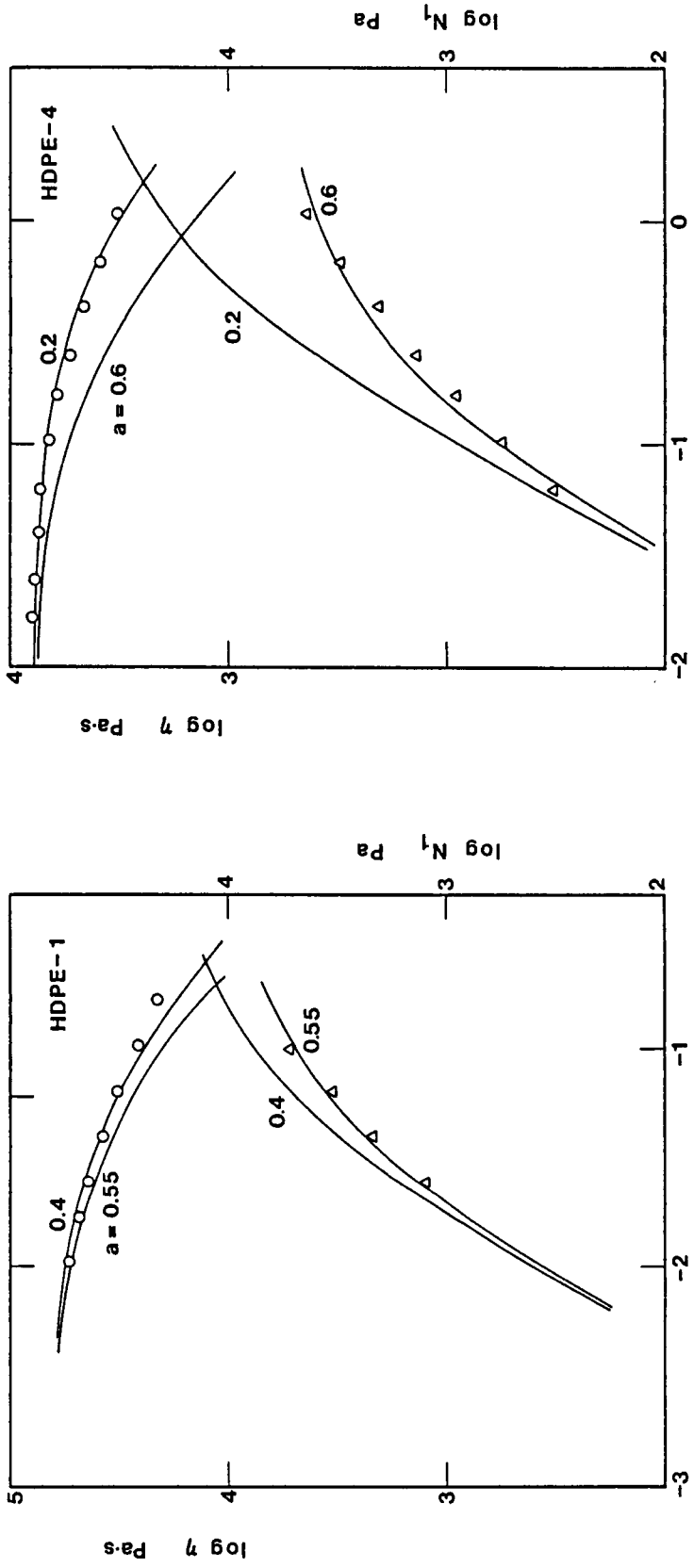

(a) HDPE-1

(b) HDPE-4

Figure 4.15. Comparison of steady shear flow data (n and N_1) with White-Metzner model (from Method A).

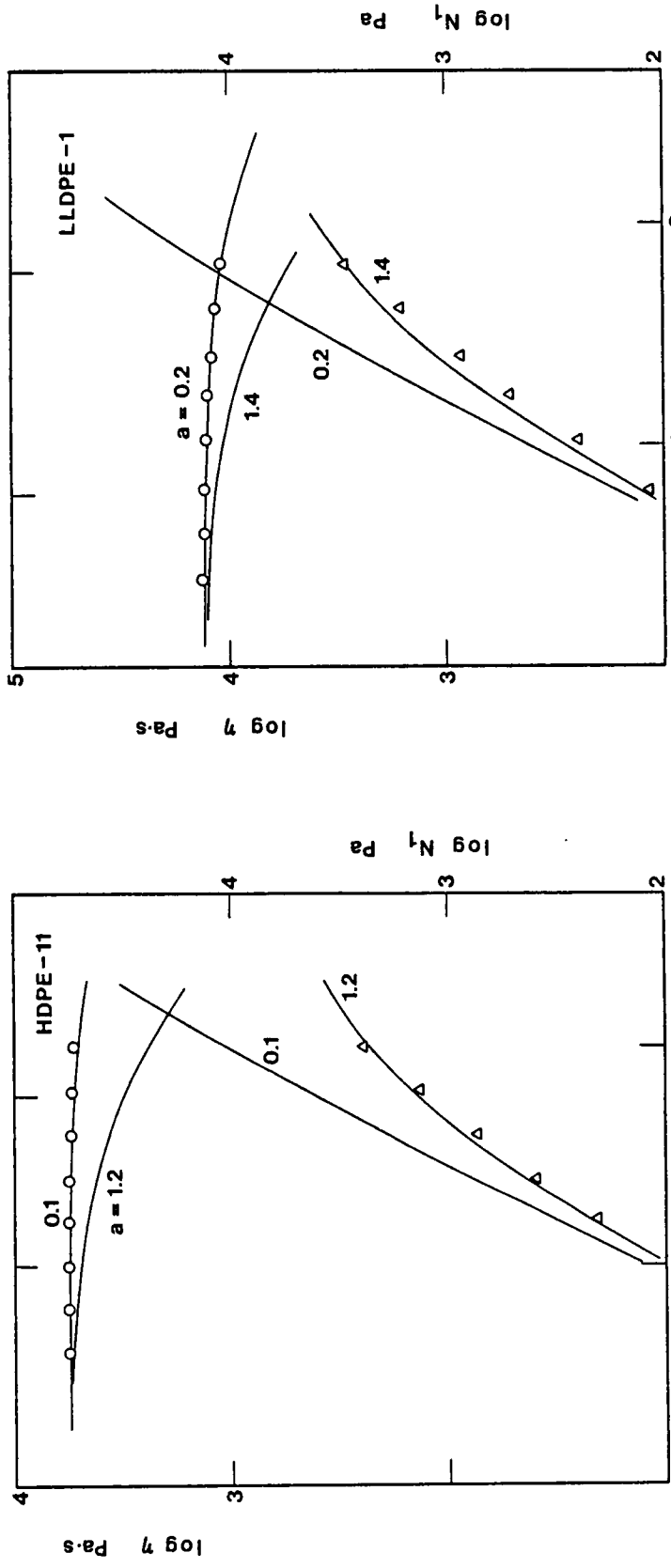

Figure 4.15 (continued)

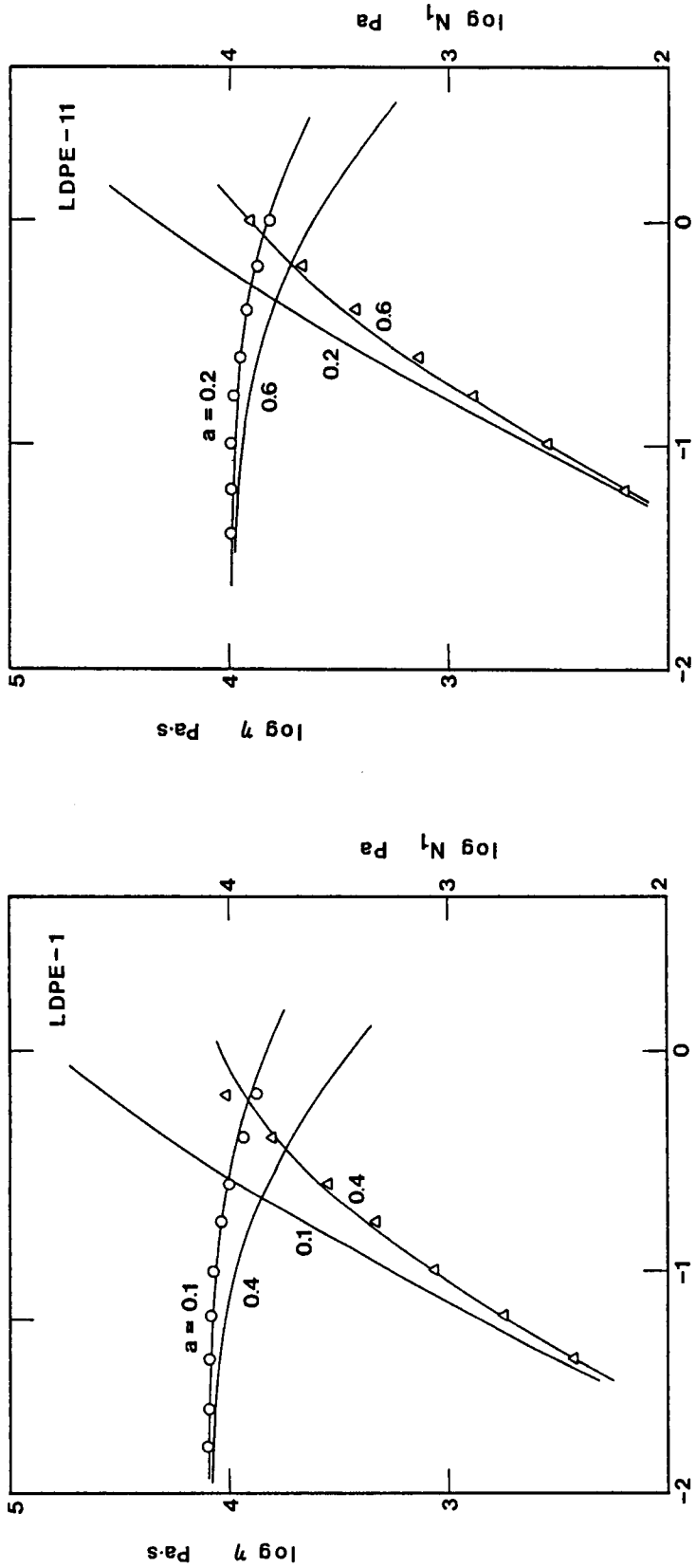

(f) LDPE-11

(e) LDPE-1

Figure 4.15 (continued)

through 4.15f, the model prediction for different values of "a", for six polymers which have typical rheological behavior, is presented. The actual data are shown by circles (for η) and triangles (for N_1). In Table IV-2 the material properties determined by Method B are listed. Here, G is calculated using N_1 values at $_{12} = 10^3$ Pa. In Figures 4.16a through 4.16f, the model prediction for different "a" values, for the same polymer, are shown.

Generally, the predictions based on the two methods (Methods A and B) show good agreement with the experimental data, if we use different "a" values for η and N_1. In Method A the difference in the "a" values for η and N_1 are sometimes very large. For example, narrow MWD HDPE materials need "a" values for η of 0.05 $\sim$ 0.1 and for N_1 of 1.2 $\sim$ 1.5. This effect is also observed for LLDPE and narrow MWD PP. The need for having so different "a" values for η and N_1 is improved by employing Method B.

The best fit values for "a", based on shear flow properties, are shown in Table IV-3. They show clear effects of MWD. The narrow MWD linear samples have "a" values of 0.1 to 0.45. The moderate and broad MWD linear samples have "a" values of 0.5 to 0.8. The results, except for LDPE, indicate that "a" increases with the breadth of the distribution. The low value of "a" for the LDPE is obviously associated with LCB (the strain rate hardening effects on τ by LCB overcome the strain rate softening effects caused by the breadth of the MWD).

Table IV-2. Material Parameters from Method B

Polymer	τ sec	G Pa x 10^{-3}	"a" (-) Based on η	"a" (-) Based on N_1	"a" (-) Based on Best Fit for η and N_1
HDPE-1	36.5	1.80	0.5	0.6	0.55
HDPE-2	25.3	2.17	0.5	0.7	0.6
HDPE-3	1.95	2.67	0.5	0.65	0.6
HDPE-4	3.58	2.20	0.5	0.7	0.6
HDPE-5	0.548	3.18	0.5	0.9	0.5
HDPE-11	0.690	8.16	0.1	0.9	0.1
HDPE-12	0.253	9.09	0.1	1.1	0.1
HDPE-13	0.0549	13.1	0.1	1.0	0.1
LLDPE-1	1.07	12.2	0.3	1.3	0.3
LLDPE-2	0.828	8.70	0.35	1.1	0.35
LLDPE-3	0.744	7.75	0.3	1.0	0.3
LLDPE-4	0.670	7.66	0.4	1.1	0.4
LDPE-1	5.42	2.30	0.2	0.35	0.25
LDPE-2	3.43	2.74	0.4	0.4	0.4
LDPE-11	1.74	5.70	0.3	0.6	0.3
LDPE-12	0.673	8.08	0.3	0.6	0.3
PP-1	5.96	3.31	0.75	0.9	0.8
PP-2	3.23	2.69	0.6	0.8	0.7
PP-11	1.36	7.38	0.4	1.0	0.4
PP-12	0.841	5.59	0.45	0.9	0.45
PP-13	0.237	7.17	0.45	0.9	0.45

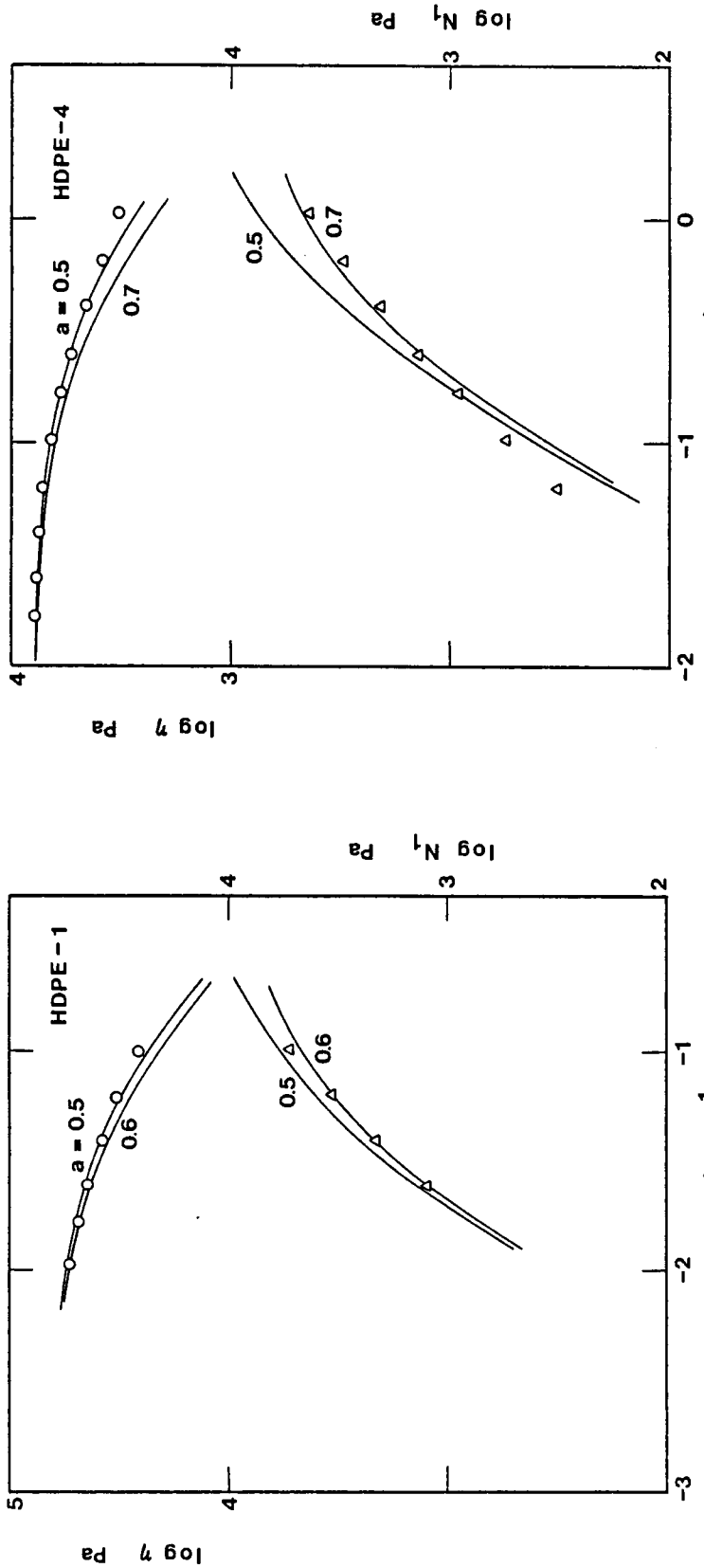

(a) HDPE-1 (b) HDPE-4

Figure 4.16. Comparison of steady shear flow data (η and N_1) with White-Metzner model (from Method B).

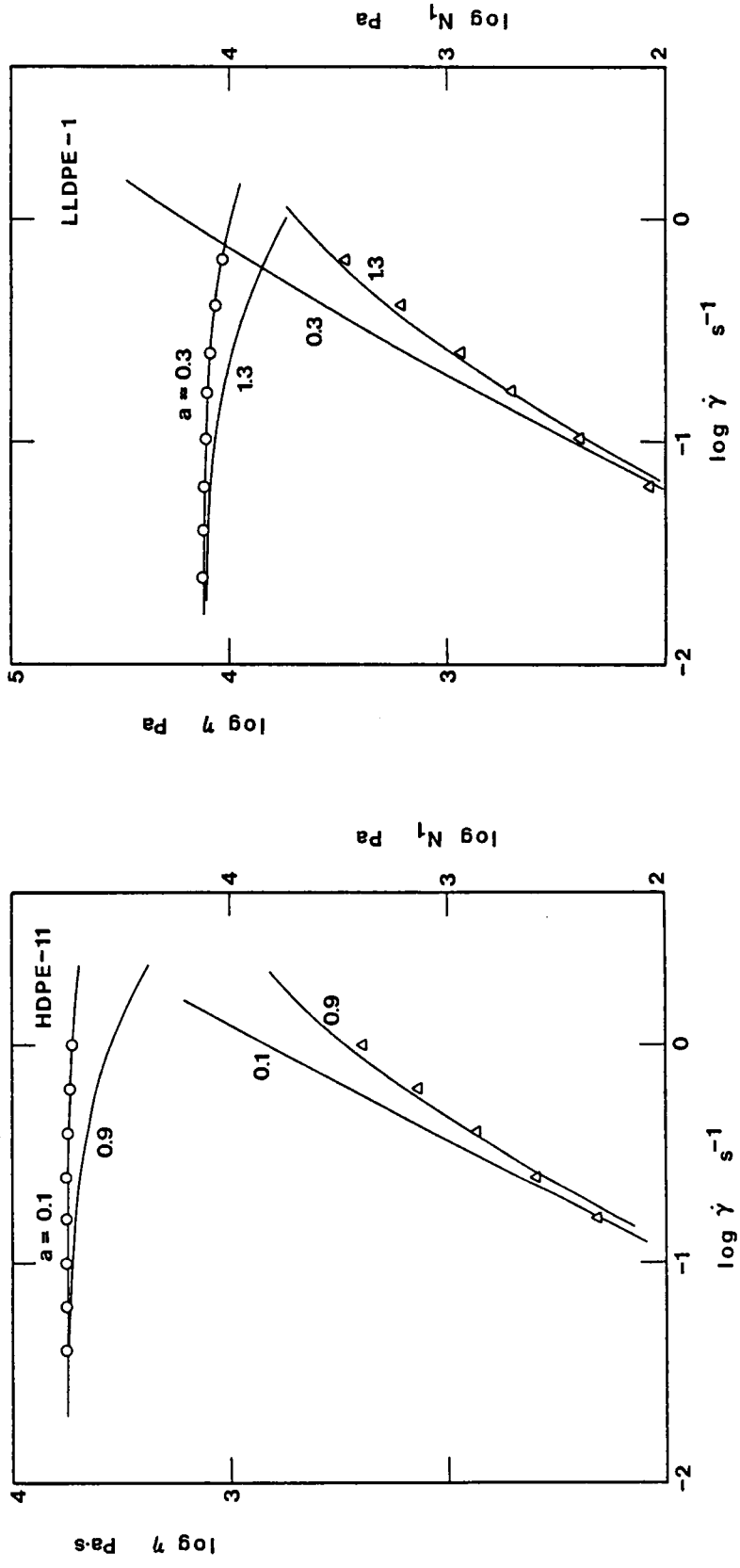

(c) HDPE-11

(d) LLDPE-1

Figure 4.16 (continued)

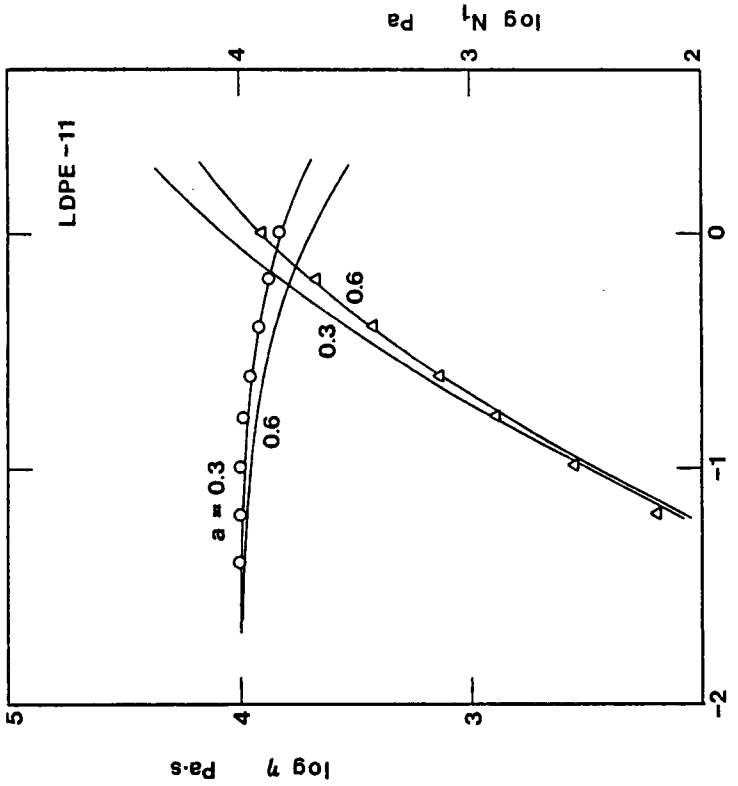

(f) LDPE-11

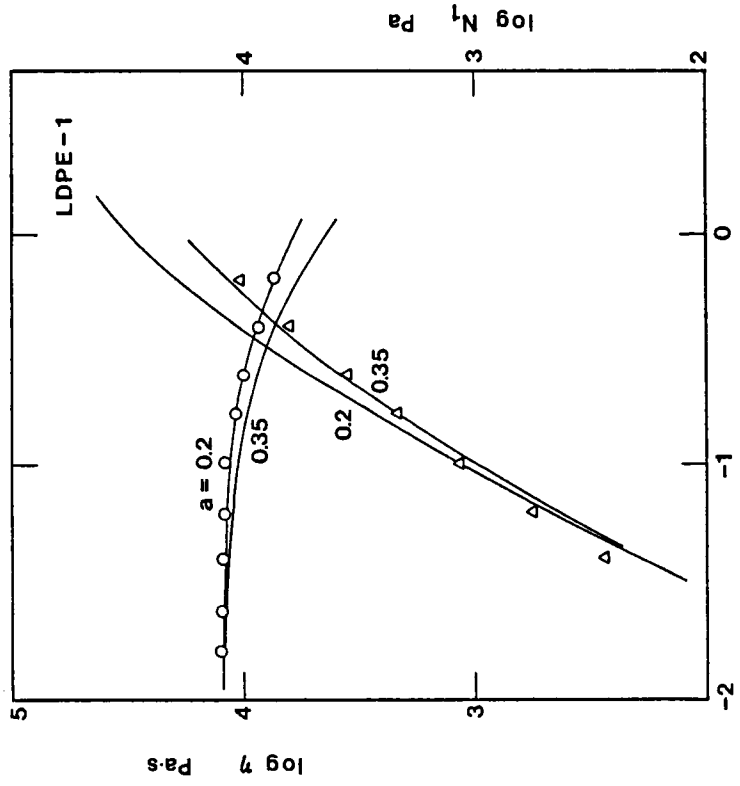

(e) LDPE-1

Figure 4.16 (continued)

Table IV-3. "a" Parameter in Eqn. (4.14c) for Relaxation Time of the Convected Maxwell Model

Polymer	"a"	M_w/M_n	M_z/M_w
HDPE-13	0.1	3.06	2.71
HDPE-11	0.1	3.36	2.97
HDPE-12	0.1	3.59	3.11
HDPE-5	0.5	4.67	6.56
HDPE-3	0.6	7.10	7.84
HDPE-4	0.6	8.08	7.12
HDPE-1	0.55	9.65	6.36
HDPE-2	0.6	14.1	8.29
LLDPE-2	0.35	3.36	-
LLDPE-1	0.3	3.81	-
PP-13	0.45	4.62	2.47
PP-12	0.45	4.67	2.81
PP-11	0.4	6.37	2.59
PP-2	0.7	7.83	4.82
PP-1	0.8	9.04	3.57
LDPE-1	0.25	11.2	-
LDPE-2	0.4	8.36	5.26
LDPE-11	0.3	4.11	-
LDPE-12	0.3	3.29	5.61
PS*	0.3 ∿ 0.65	2 ∿ 4	
PP*	0.6 ∿ 1.3	7 ∿ 10	
HDPE*	0.6 ∿ 1.4	7 ∿ 30	
LDPE*	0.2 ∿ 0.6	7 ∿ 30	

*From analysis of literature data on commercial polymers.

E. UNIAXIAL ELONGATIONAL FLOW

E-1. Results

Uniaxial elongational viscosities were measured only for HDPE-1, HDPE-11, LDPE-1, and LPPE-11. Kanai and White [K-2] have reported uniaxial elongational viscosities for HDPE-2, LLDPE-2, which are the same lot samples that we used here. The data for other samples will appear elsewhere.

The developing elongational viscosities χ are shown as a function of elongational rate E and time t in Figures 4.17-4.20. We plot only the data where obvious nonuniform stretching was not observed.

HDPE-1 exhibits local deformation (necking) near the point of maximum stress, and this is followed by ductile failure. The narrow MWD HDPE, LDPE, and LLDPE samples elongated uniformly and in some cases fractured abruptly, probably by a defect mechanism. Fracture (which may be described as a cohesive failure) actually occurred only in LDPE-1 at E = 0,1 and 0.05 sec^{-1}, which are pointed out by the arrow marks in Figure 4.19. This is illustrated in Figures 4.21-4.23 for HDPE, LLDPE, and LDPE, respectively (hand-pulled filaments were painted by black color). They clearly show that broad or regular MWD HDPE filaments exhibit necks and are nonuniform, whereas narrow MWD HDPE, LLDPE, and LDPE samples possess a higher uniformity.

There are two types of stress build-up. One type, shown by narrow MWD HDPE, LLDPE [K-2], and LDPE of low degree of LCB, exhibits monotonic increasing stress build-up to an asymptotic value; this

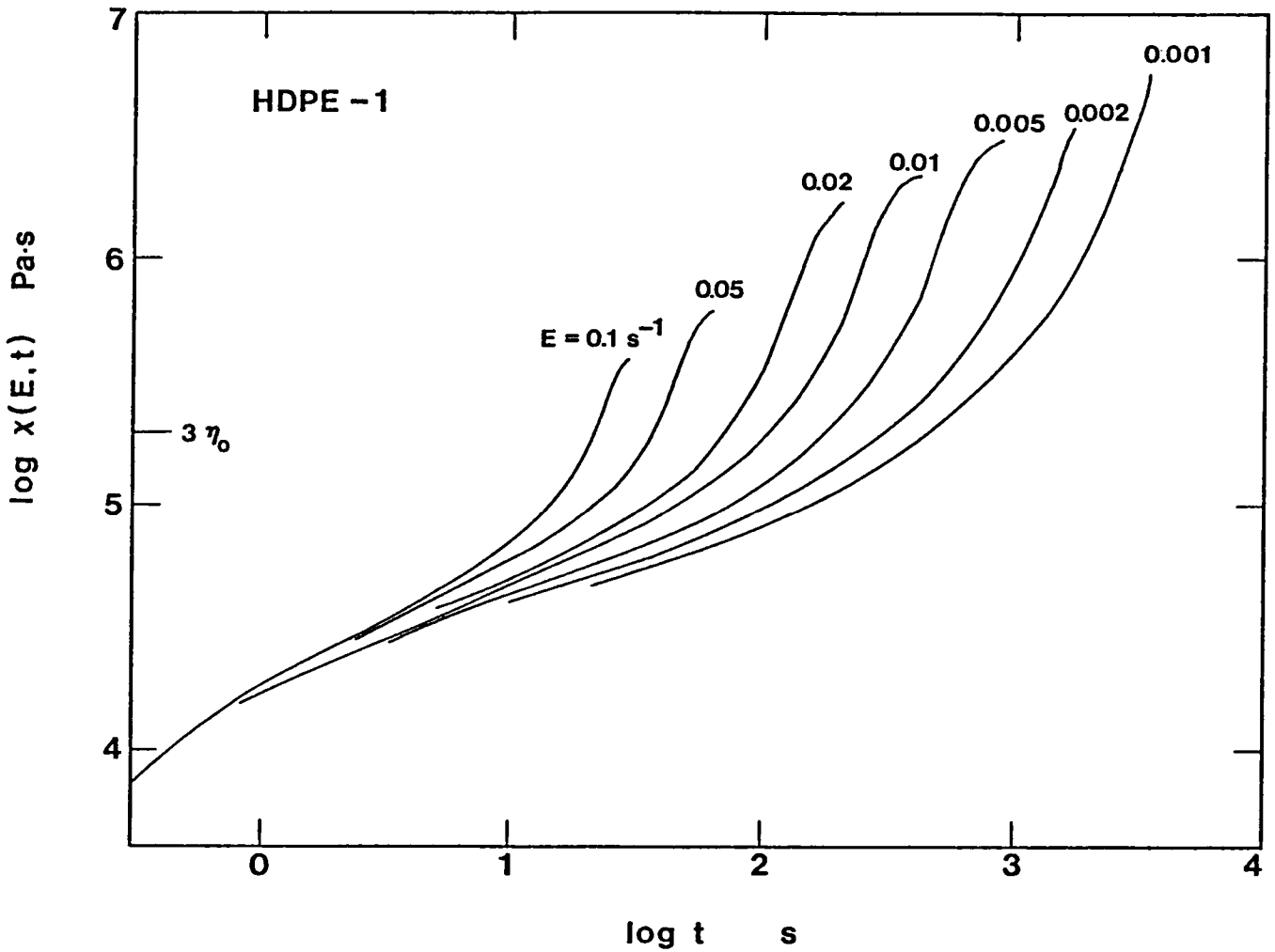

Figure 4.17. Elongational viscosity of HDPE-1 as a function of time and elongation rate.

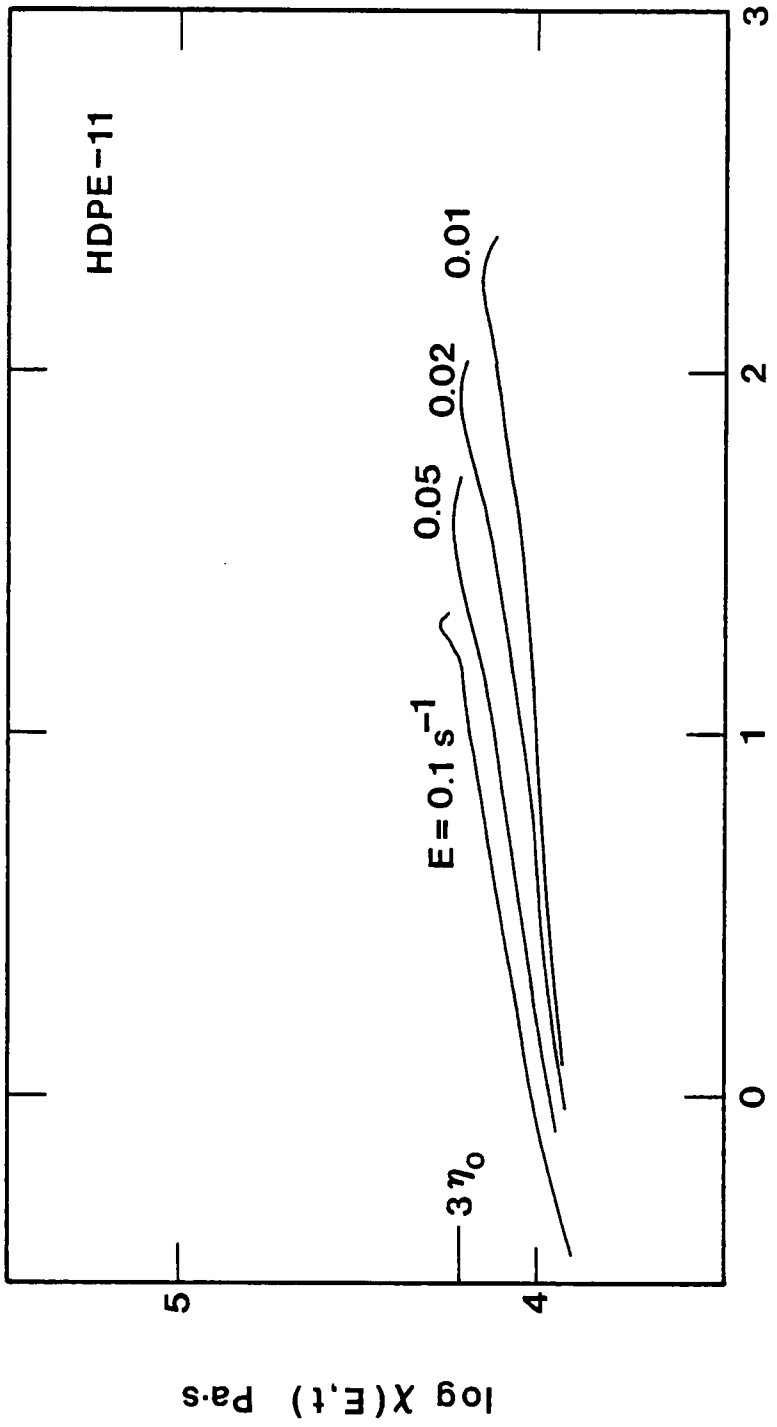

Figure 4.18. Elongational viscosity of HDPE-11 as a function of time and elongation rate.

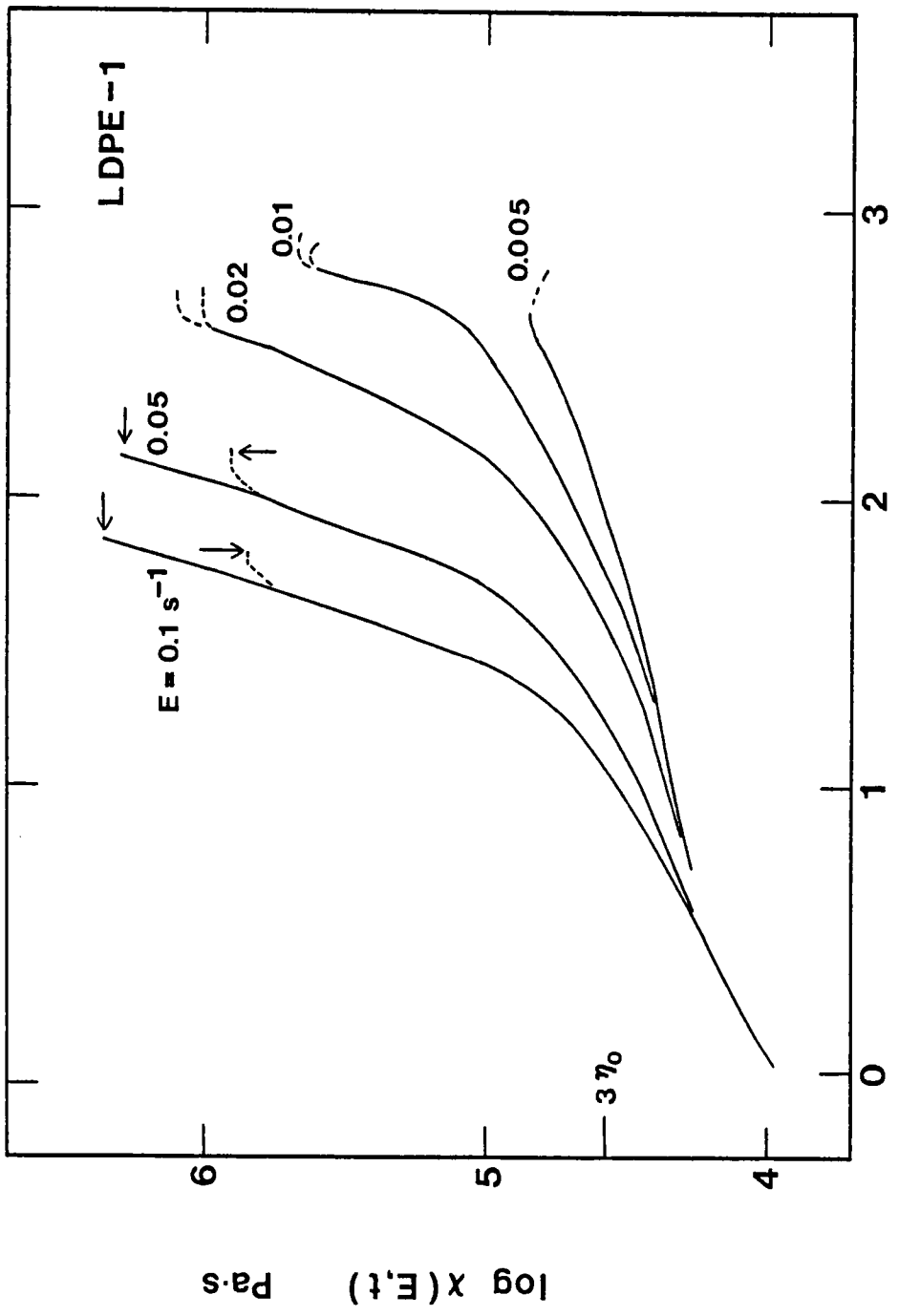

Figure 4.19. Elongational viscosity of LDPE-1 as a function of time and elongation rate.

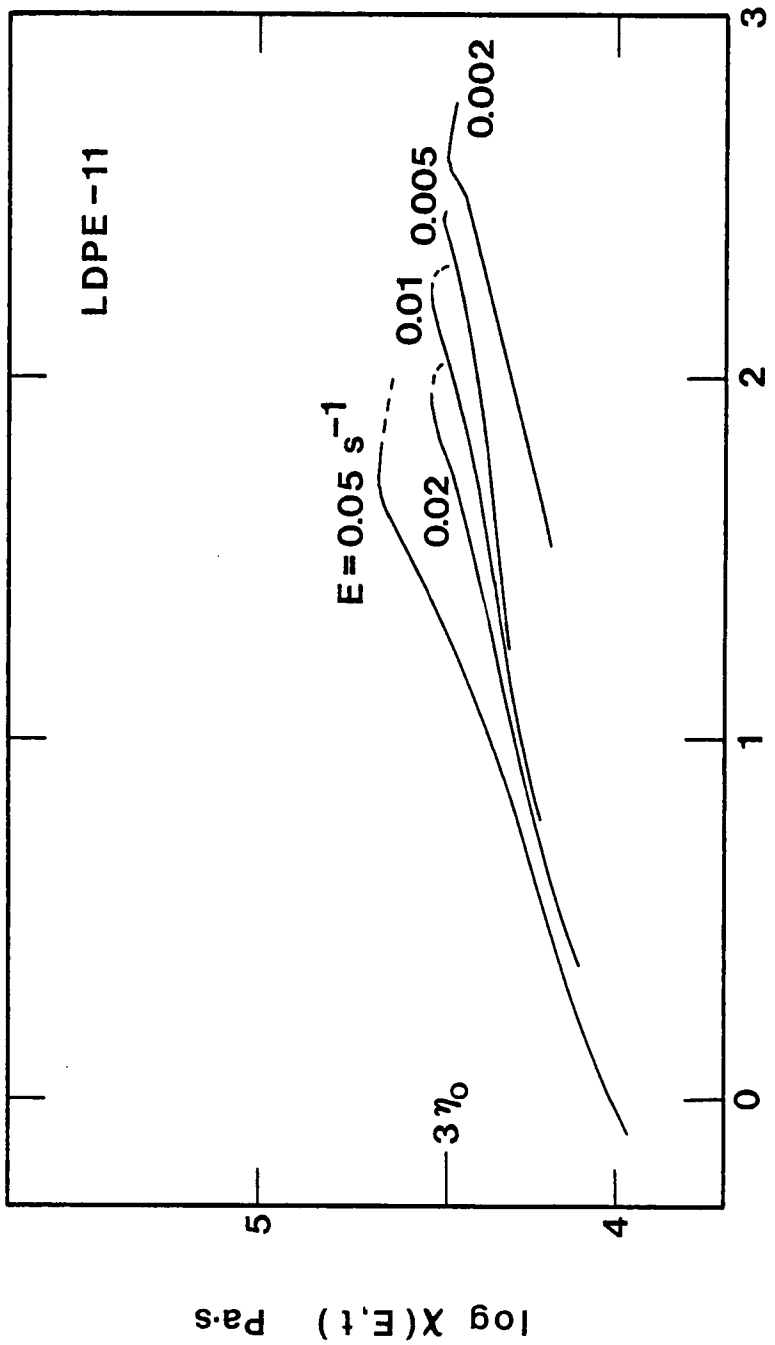

Figure 4.20. Elongational viscosity of LDPE-11 as a function of time and elongation rate.

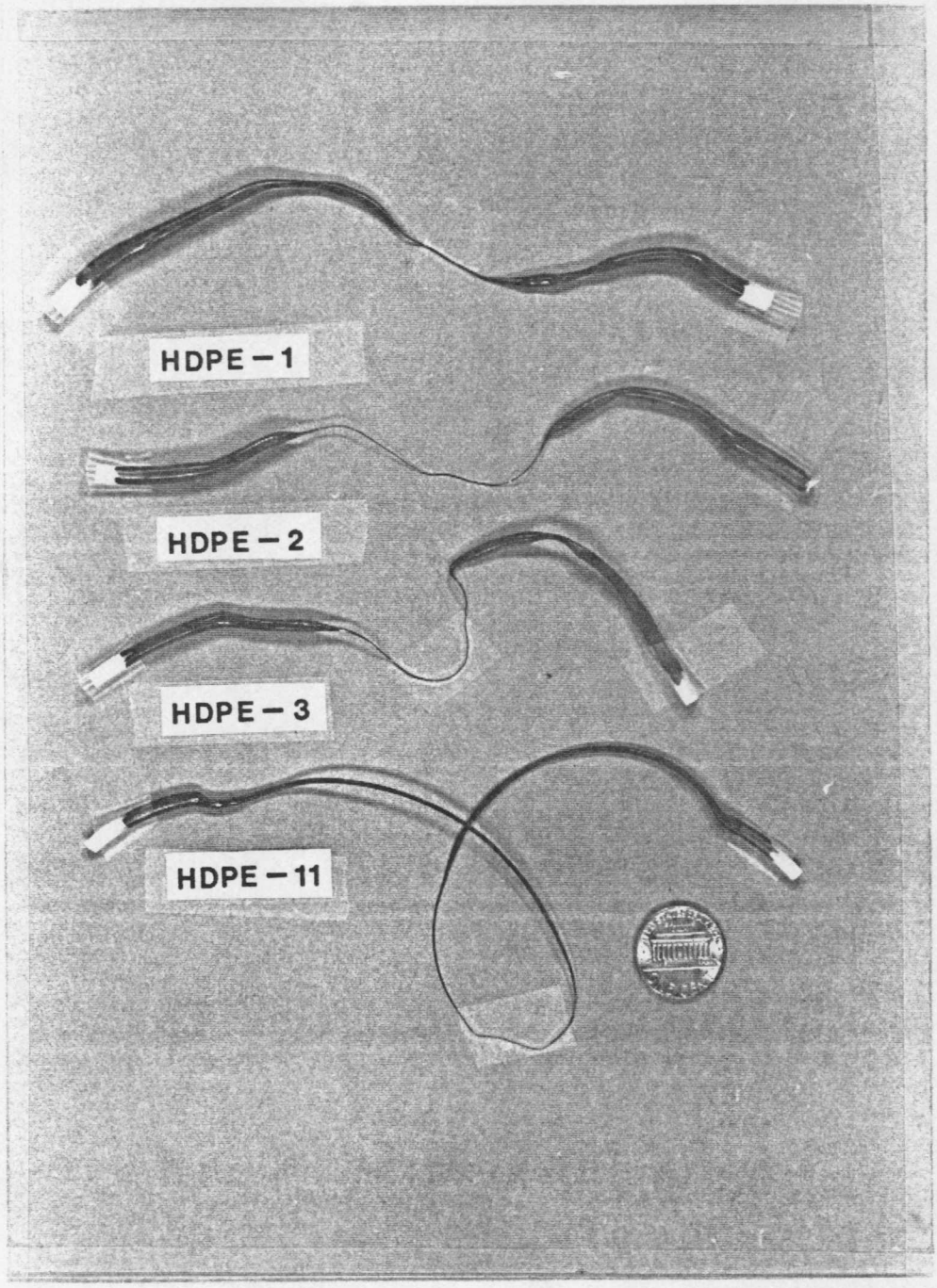

Figure 4.21. Elongated filaments of high density polyethylenes.

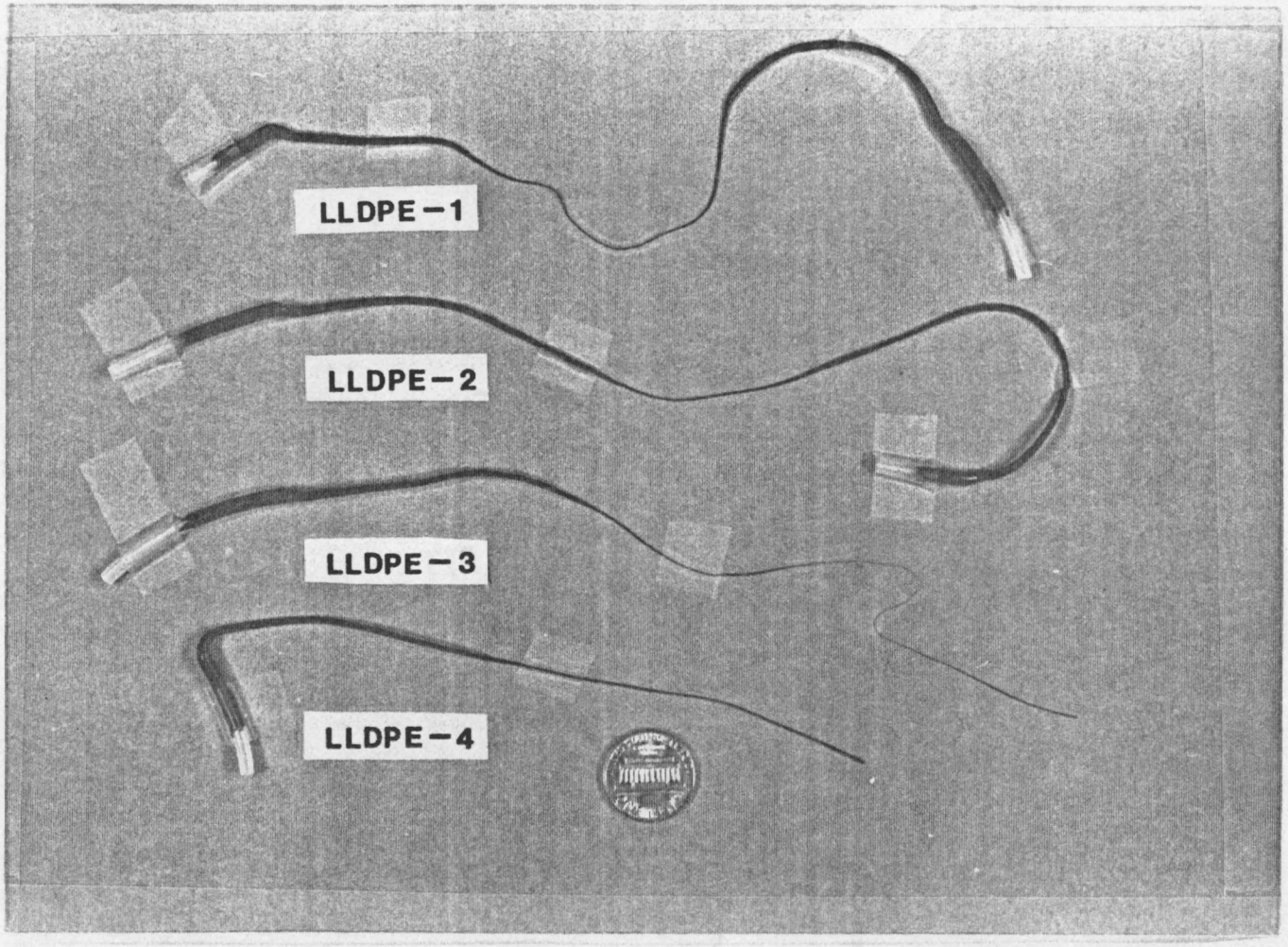

Figure 4.22. Elongated filaments of linear low density polyethylenes.

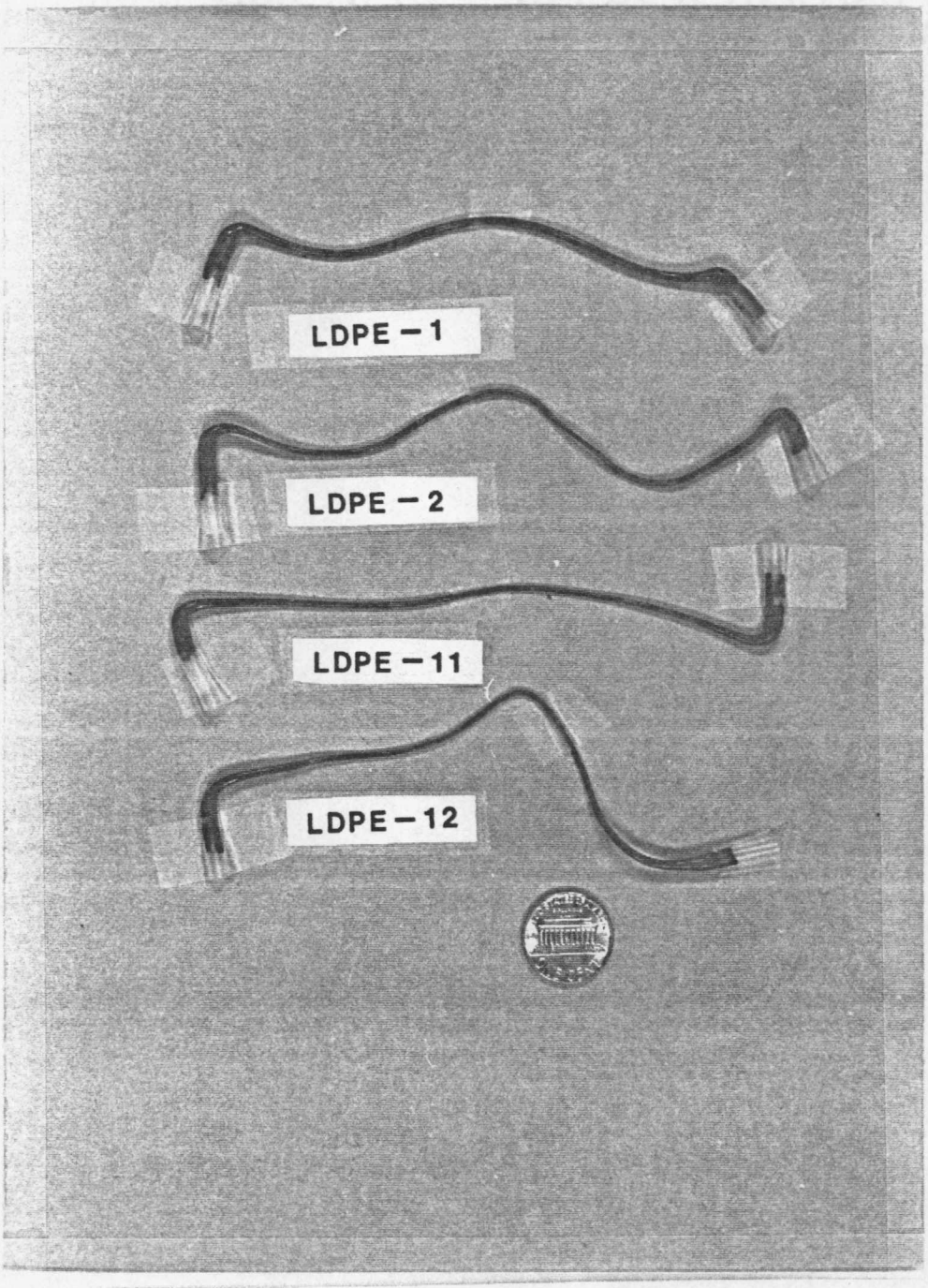

Figure 4.23. Elongated filaments of low density polyethylenes.

value is close to three times the zero shear viscosity ($3\eta_0$) at low elongation rate. It shows higher values at higher deformation rates. The other type, shown by HDPE of moderate and broad MWD and by LDPE of high degree of LCB, exhibits a strong strain hardening effect after achieving a certain strain level. However, the latter type shows two subclassifications. One, shown by moderate and broad MWD HDPE, never shows a constant viscosity value because of a ductile instability. The other, shown by LDPE of high degree of LCB, exhibits constant viscosity after a sharp stress build-up in the log χ-log t plots. The values of these constant viscosities scattered sometimes by as much as 20 to 30%, depending on the experimental run. However, there is almost no scatter in the region where the stress is still building. This is clear in Figure 4.24, which shows plots of log χ vs. Et for LDPE-1. The strain hardening stress build-up of HDPE-1 and LDPE-1 behaves in a somewhat different way; LDPE-1 exhibits stronger strain hardening stress build-up than does HDPE-1.

The reduced steady (or maximum) elongational viscosity $\chi/3\eta_0$ - E is shown in Figure 4.25. There is no doubt that narrow MWD HDPE (HDPE-11) and LDPE with a low degree of LCB (LDPE-11) achieved steady state at any E. LDPE-1 is also believed to have achieved steady state, except at E = 0.1 and 0.05 sec^{-1}. At these E values, LDPE-1 sometimes show constant χ for 0.4 $\sim$ 0.5 (as measured by the Hencky strain) just before fracture; during this period no fluctuation of diameter was observed. This constant χ may be due to a defect mechanism. There is no doubt that broad MWD HDPE never achieved steady state because of a ductile instability.

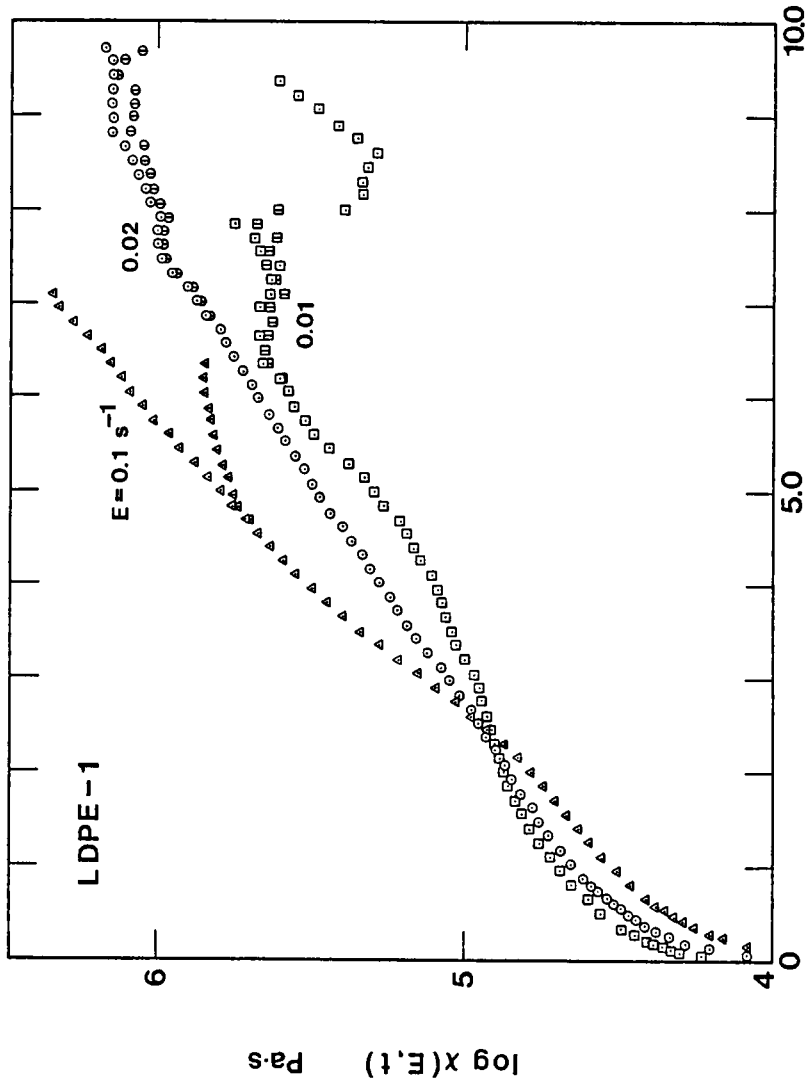

Figure 4.24. Elongational viscosity of LDPE-1 as a function of strain Et and elongation rate.

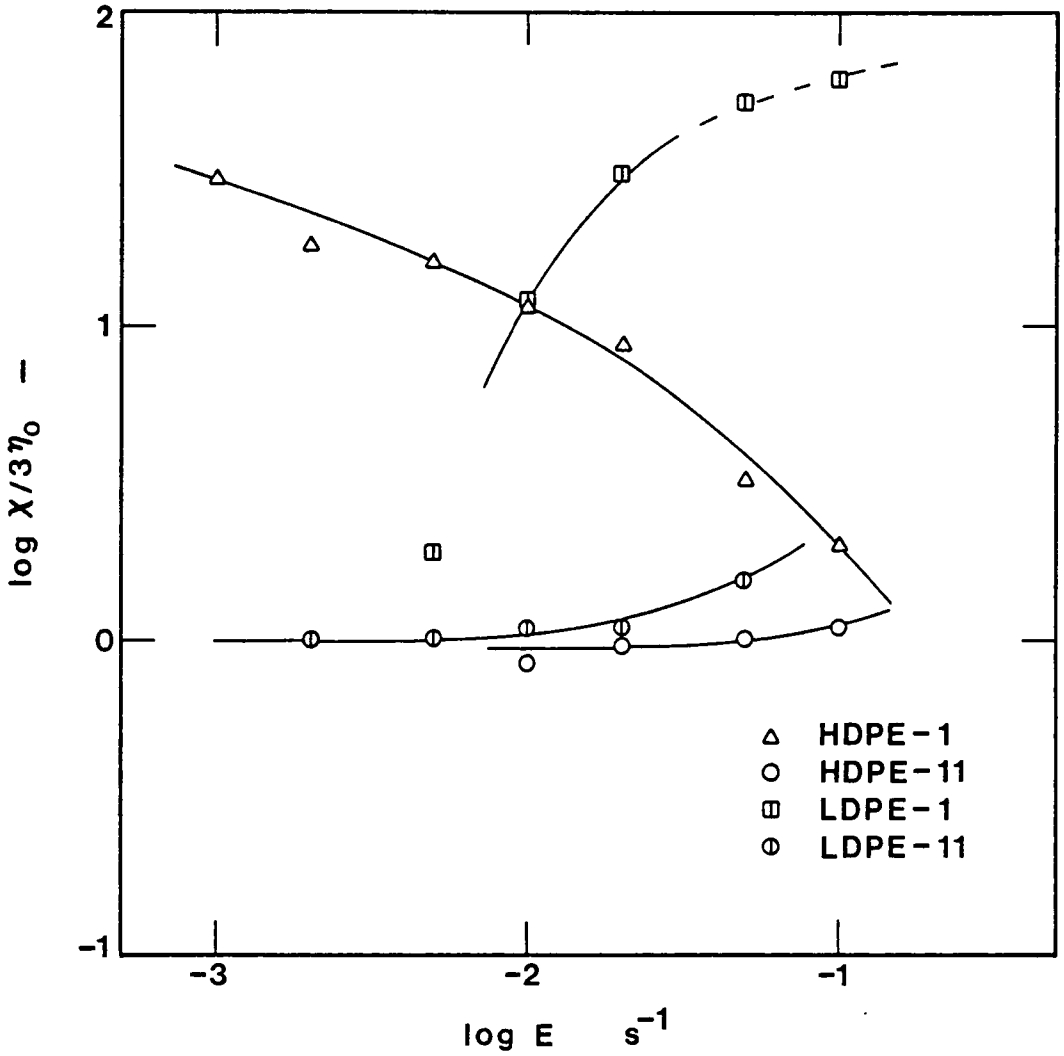

Figure 4.25. Reduced steady state (or maximum) elongational viscosity as a function of elongation rate.

For narrow MWD HDPE and LDPE with low degree of LCB, one obtains a constant χ at low E which is about three times the zero shear viscosity ($3\eta_0$). At higher E, χ increases. χ for LDPE with high degree of LCB increases with E. For the broad MWD HDPE, the maximum elongational viscosity is a decreasing function of E.

Elongation-to-break is plotted in Figure 4.26, where Et_b is the elongation-to-break as measured by the Hencky strain ($Et_b = \ell n[L(t_b)/L(0)]$). HDPE-1 and LDPE-1 at E = 0.1 and 0.05 sec^{-1} actually exhibit filament failure, but not the other cases. The elongation-to-break of "unfailed" filaments was determined by assuming that the final diameter of the filament is the same as diameter of the failed samples. For linear polymers, the elongation-to-break of the narrow MWD samples exceeds that for broader MWD samples. The effects of LCB are difficult to detect, except for the cohesive fracture in LDPE-1 at E = 0.1 and 0.05 sec^{-1}.

E-2. Interpretation

During the uniaxial elongational stretching of the linear moderate and broad MWD filaments, necks are observed. The material in the necked region deforms more rapidly than the sample as a whole. A theory of stability having to do with the necking of polymer melt filaments was given by Ide and White [I-2,I-3].

The free-elongation data of Figure 4.17 (for HDPE-1) may be significantly influenced by the stress-elongation rate characteristics in the neck (when they develop), as opposed to the sample as a whole.

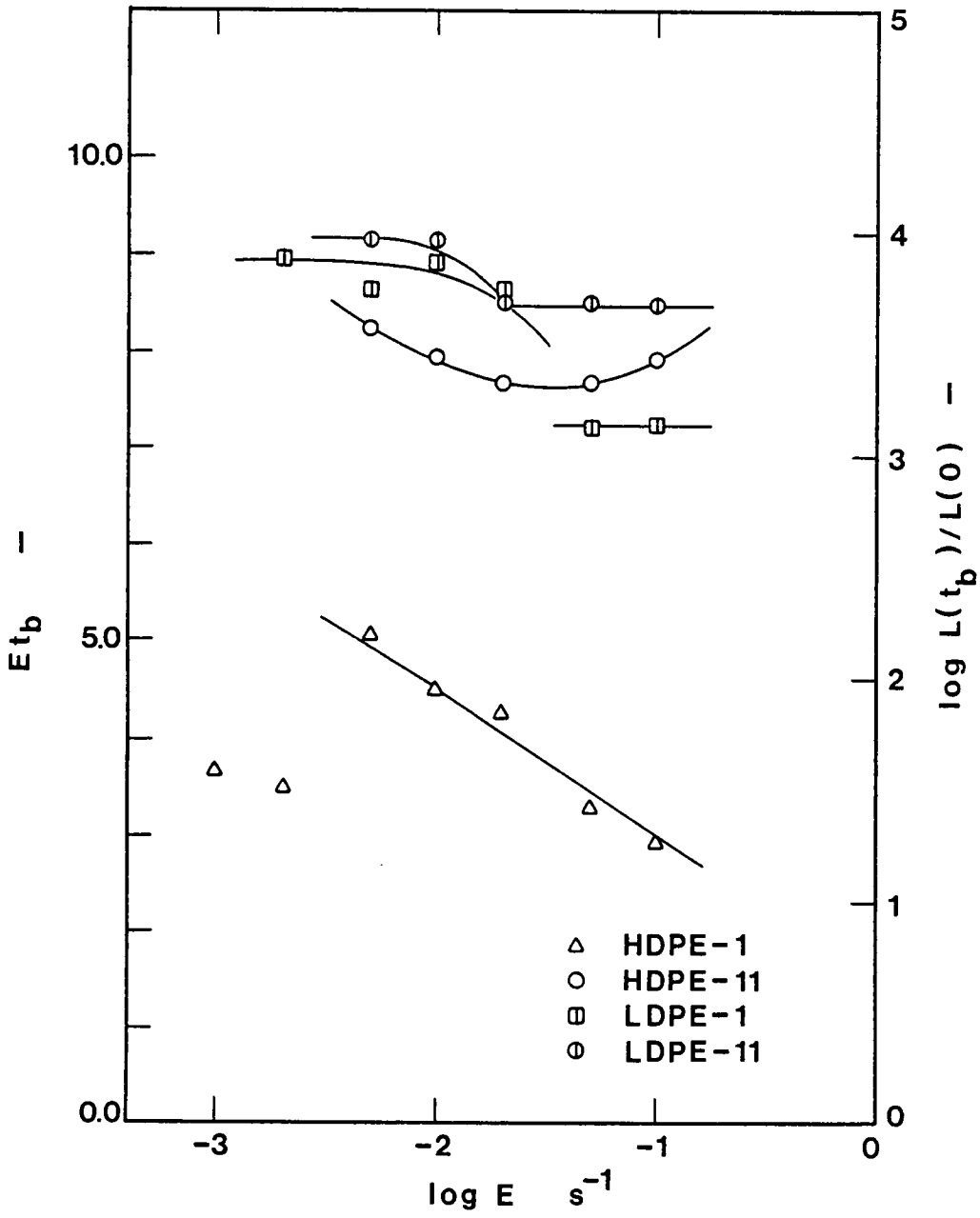

Figure 4.26. Elongation-to-break as a function of elongation rate.

It is not known at what point on these curves the necks develop. However, only the data where no visible necks were observed are plotted. If we continue to plot after visible necks are observed, the curves immediately reach a maximum and then decrease with time. These curves have been reported for linear moderate and broad MWD filaments, such as HDPE and PP [C-5,I-3,I-4,M-42,Y-2]. If we look carefully at Figu re 4.17, we notice that the slope of the log χ-log t plot decreases just before reaching the maximum point. This may be caused by the start of necks, although this is not visible, because the strain is too small to reach to a steady state (compare with LDPE-1, which has τ_0 = 5.42 sec, and with HDPE-1, which has τ_0 = 36.5 sec; see Table IV-2, page 93).

Our steady state (or maximum elongational viscosity χ data on linear PE suggest that the effect of MWD dominates in determining the character of linear polymer melts. Narrow MWD linear polymers (HDPE, monodispersed linear hydrogenated polybutadiene, PP, and PS) [A-12,E-2,I-4,M-42,M-46,M-47,T-3] shown constant values of $\chi(= 3\eta_0)$ at low elongational rates (or τE_1), and then become an increasing function. On the other hand, χ of moderate and broad MWD linear polymers exhibits a decreasing function of E; also $\chi/3\eta_0$ values at low E are very large. Similar behavior has been observed earlier [C-5,I-4,M-49,Y-2]. For moderate and broad MWD HDPE (M_w = 2.20 x 10^5 and 2.19 x 10^5, M_w/M_n = 12 and 9, respectively) Munsted and Laun [M-49] reported the existence of a maximum in the χ-E plot. At low E, $\chi/3\eta_0$ is unity, and after reaching the maximum

value, $\chi/3\eta_0$ decreases with E. However, they also report for HDPE (M_w = 1.52 x 10^5 and 9.80 x 10^4, M_w/M_n = 13 and 10, respectively) that $\chi/3\eta_0$ is a decreasing function of E and unity at low E. It is not clear what the cause of the difference in HDPE is.

Considering LDPE in an overall way, it is not easy to separate the effects of MWD and LCB on elongational flow. However, based on our data and those of Munstedt and Laun on LDPE with different degrees of LCB and MWD [M-49], we may reasonably summarize the behavior as follows: the strain rate hardening character on uniaxial elongational viscosity increases with extent of LCB and the effects of LCB overcome those of MWD.

The observed failure mechanisms are consistent with the trend in the steady state (or maximum) elongational viscosity χ. The neck development in the moderate and broad MWD linear samples indicates a decreasing elongational viscosity character. The uniformly stretched filaments of the narrow MWD linear polymers and also the branched (LCB) polymers, where defects are healed, presumably have increasing viscosity functions (compare Ide and White [I-4] and Minoshima, White and Spruiell [M-42]).

F. SOME COMMENTS ON A CONVECTED MAXWELL MODEL

In the previous section (Section D-3-b) we have described two different ways of determining the material parameters based upon the convected Maxwell (White-Metzner) model (Eqn. 4.14). The material properties are listed in Tables IV-1 and IV-2 (pages 88 and 93). If

we look at these tables, we see a systematic difference in the "a" values in the shear viscosity function and in the principal normal stress difference function. Such differences are less for moderate and broad MWD linear polymers and highly branched (LCB) polymers. On the other hand, the differences for narrow MWD linear polymers are very large. Similarly, LDPE with broad MWD and higher degree of LCB show less differences in the "a" values than do LDPE with narrow MWD and a lower degree of LCB.

More specifically, Ψ_1 ($= N_1/\dot{\gamma}^2$) of narrow MWD linear polymers (HDPE, PP, and LLDPE) falls off more rapidly with shear rate than does η for these polymers, as expected from Eqn. (4.15). The difference between the shear rate dependency of η and Ψ_1 becomes less by the presence of LCB and broadening MWD. If data in wider shear rate ranges were available, these varying shear rate dependencies in η and N_1 might be negligible. However, Eqn. (4.15) predicts a second power dependence of N_1 on σ_{12}. This is true only for monodisperse polymers. It is generally known, as indicated previously, that the slope of the log N_1-log σ_{12} plot decreases with the breadth of MWD and that N_1, at fixed σ_{12}, increases with the breadth of MWD in linear polymers. LDPE with broad MWD and a high degree of LCB has the highest slope in the log N_1-log σ_{12} plot among the various PE samples (including narrow MWD HDPE) (see Section D-2).

According to Eqns. (4.14) and (4.15), η/η_0 for a convected Maxwell model is given by

$$\eta/\eta_0 = \tau/\tau_0 = \frac{1}{1 + a\,\tau_0\,\dot{\gamma}}\,, \tag{4.18a}$$

$$= \frac{1}{1 + a\,Je\,\tau_0\,\dot{\gamma}} \tag{4.18b}$$

where Je (= 1/G) is the steady state compliance. In Figure 4.27 we plot η/η_0-Je $\eta_0\,\dot{\gamma}$ for linear and star-branched (four star and six star) anionically polymerized polyisopre (PI) of a 40 weight percent TD (tetradecane) solution. These data were supplied to us by T. Masuda of Kyoto University. Some of the data have appeared in Graessley et al. [G-9]. Figure 4.27 indicates that the presence of LCB has a deformation rate softening effect on relaxation time; the "a" value becomes large by increasing the LCB. It is difficult to believe that their star-branched polymer has a broader MWD than linear PI (see G-9 and H-1). This is inconsistent with the "a" values for LDPE being smaller than those for PP (including narrow MWD samples) and moderate and broad MWD HDPE (see Tables IV-1 and IV-2, pages 88 and 93).

These phenomena suggest that the effect of shear rate on the relaxation intensity and the relaxation time is different. This leads to the following form for the convected Maxwell model

$$\underset{\sim}{\sigma} = -p\underset{\sim}{I} + \underset{\sim}{P}\,, \tag{4.19a}$$

$$\underset{\sim}{P} = 2G_0\tau_0\,\frac{g^2}{f}\,\underset{\sim}{d} - \tau_0 g\,\frac{\delta \underset{\sim}{P}}{\delta t}\,, \tag{4.19b}$$

where the relaxation intensity and the relaxation time change with

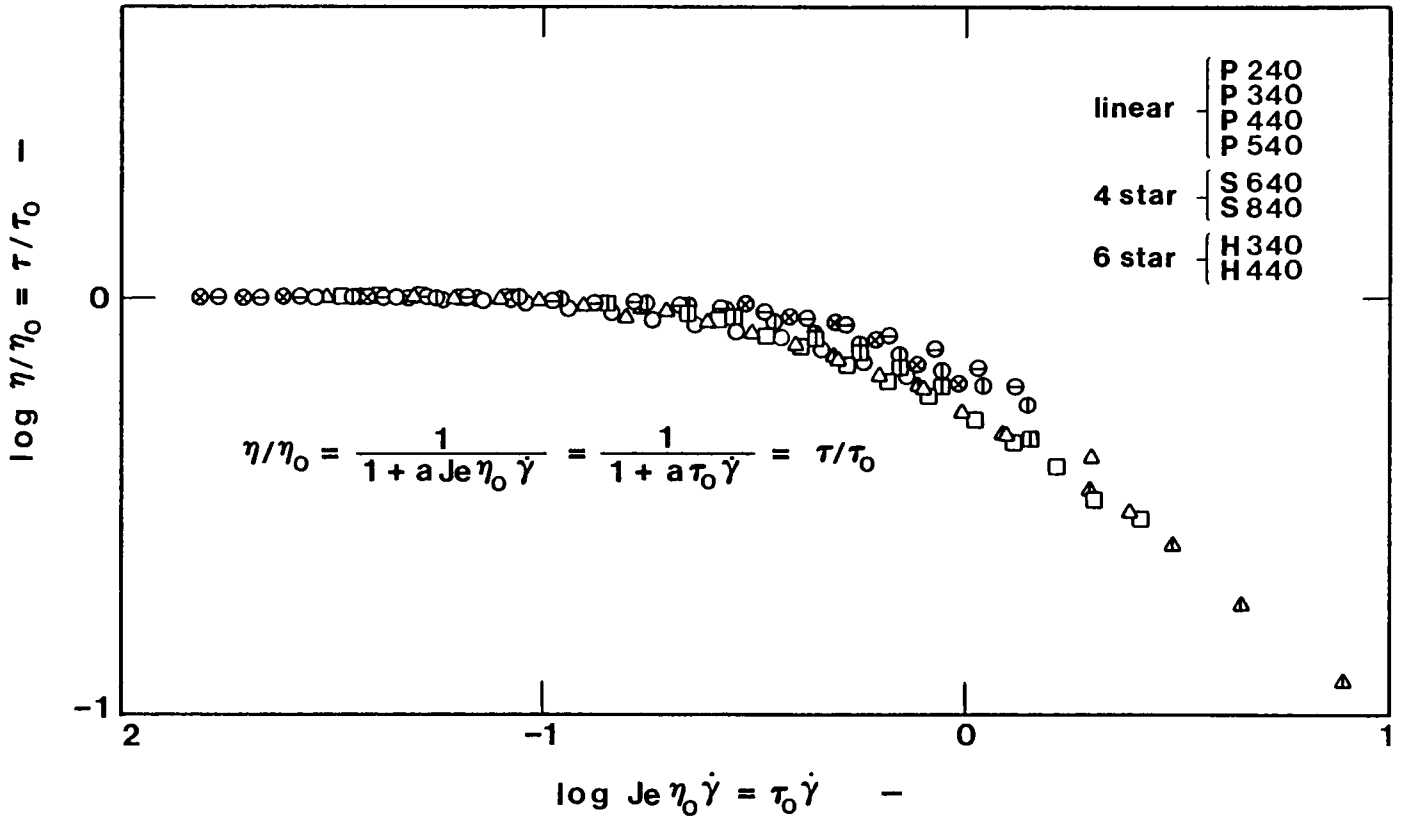

Figure 4.27. η/η_0 as a function of $Je\eta_0\dot{\gamma}$ for monodisperse polyisoprenes (40 weight percent tetradecane solution: linear, 4 star and 6 star-branched polymers).

deformation, as indicated with the factors of "f" and "g", which are functions of tensor invariants, respectively (see the more detailed formulation of Eqn. 4.19 in Chapter XIII). Eqn. (4.14) is a special case of Eqn. (4.19) where

$$g = f = \frac{\tau(II_d)}{\tau(II_d = 0)} , \tag{4.20a}$$

$$= \frac{1}{1 + a\,\tau_0 II_d^{1/2}} . \tag{4.20b}$$

In the steady shear flow Eqn. (4.19) is written as

$$\eta = \sigma_{12}/\dot{\gamma} = G_0\tau_0 g^2/f , \tag{4.21a}$$

$$\Psi_1 = N_1/\dot{\gamma}^2 = 2G_0\tau_0^2 g^3/f , \tag{4.21b}$$

$$N_1 = \frac{\sigma_{12}^2}{G_0}\frac{f}{g} , \tag{4.21c}$$

$$\tau = \tau_0 g . \tag{4.21d}$$

For uniaxial elongational flow

$$\sigma_{11} = P_{11} - P_{33} = \frac{2\tau_0 G_0 E g^2/f}{1-2\tau_0 gE}\left[1-e^{-(1-2\tau_0 gE)t/(\tau_0 g)}\right]$$

$$+ \frac{\tau_0 G_0 E g^2/f}{1+\tau_0 gE}\left[1-e^{-(1+\tau_0 gE)t/(\tau_0 g)}\right] \tag{4.22a}$$

The steady state elongational viscosity is given by

$$\chi = \sigma_{11}/E = \frac{3\tau_0 G_0 g^2/f}{(1-2\tau_0 gE)\ (1+\tau_0 gE)} \quad . \tag{4.22b}$$

As a special case, we may take "g" and "f" to be functions of the second invariant of the deformation rate tensor. There is a good possibility that we can eliminate contradictions and inconsistencies in Eqn. (4.14), as previously mentioned, by introducing proper functionalities for "g" and "f". However, these functionalities (or at least one of the functionalities) should not be similar to Eqn. (4.20). If the functionalities for "g" and "f" are given similar to Eqn. (4.20), then

$$g = \frac{1}{1 + a\ \tau_0\ II_d^{1/2}} \ , \tag{4.23a}$$

$$f = \frac{1}{1 + b\ \tau_0\ II_d^{1/2}} \ . \tag{4.23b}$$

The steady state uniaxial elongational viscosity exhibits a maximum under certain combinations of "a" and "b" (such as a = 1.2 and $b \geq 2.0$). However, the maximum values in steady state elongational viscosity ($\chi_{max}/3\eta_0$) never reach 2.0 for the case where $0.0 \leq a \leq 4.0$ and $0.0 \leq b \leq 4.0$.

G. SUMMARY

An experimental study of steady shear and uniaxial elongational flow rheological properties of a series of high density, linear low

density, and low density polyethylene melts of varying molecular weight and distribution and different degree of long chain branching has been carried out. Broadening the molecular weight distribution increases the non-Newtonian character of the shear viscosity functions and increases the principal normal stress differences at fixed shear stress. Increasing the degree of long chain branching increases the non-Newtonian character of shear viscosity functions and increases the principal normal stress differences at fixed shear stress. However, the existence of long chain branching in polydisperse systems makes the principal normal stress difference and shear stress relationship more linear than linear polydisperse systems. Uniaxial elongational flow studies indicate that linear polyethylenes of moderate and broad molecular weight distribution readily fail by neck development; also the elongational viscosity appears to decrease with increasing elongation rate. For polyethylenes of narrow molecular weight distribution (including low density polyethylenes), the elongational viscosity is an increasing function of elongational rate and never fails. Highly branched low density polyethylene exhibits cohesive fracture at high elongation rate and the elongational viscosity strongly increases with elongation rate. Finally, the implications of these experimental results in developing a constitutive equation was developed.

CHAPTER V

MULTIAXIAL ELONGATIONAL FLOW OF VISCOELASTIC FLUIDS: CONVECTED MAXWELL MODEL

A. INTRODUCTION

Simple shear flow in polymer processing operations has been very widely studied. The occurrence of elongational flows in polymer processing operations (such as melt spinning, film casting, tubular blown film extrusion, blow molding and thermoforming) makes it an important area for study. This includes not only uniaxial elongational flow but also biaxial and planar elongational flow. This makes it necessary to develop a general perspective of various elongational flows.

In this chapter we present a general analysis of the homogeneous elongational flow of incompressible fluids, which includes a kinematical classification of these flows, geometrical effects, and characterization of the elongational viscosity under various kinematical conditions.

B. CLASSIFICATION OF ELONGATIONAL FLOW

B-1. Kinematical Classification

For incompressible fluids, the kinematics of elongational flow can be expressed in terms of two independent deformation rates

(E_1, E_2). The physical components* of the deformation rate tensor $\underset{\sim}{d}$ are defined as

$$\underset{\sim}{d} = \frac{1}{2}\left[\nabla\underset{\sim}{v} + (\nabla\underset{\sim}{v})^T\right] = \begin{vmatrix} E_1 & 0 & 0 \\ 0 & E_2 & 0 \\ 0 & 0 & E_3 \end{vmatrix}$$

$$= E_1 \begin{vmatrix} 1 & 0 & 0 \\ 0 & E_2/E_1 & 0 \\ 0 & 0 & -(1+E_2/E_1) \end{vmatrix}, \qquad (5.1)$$

where "1" is in the machine direction, "2" in the transverse direction, and "3" in the free surface direction. Various possibilities exist. For uniaxial extension [M-24,P-11,T-10],

$$E_2/E_1 = -0.5, \text{ or } E_2 = E_3 = -0.5\ E_1\ , \qquad (5.2a)$$

while for planar extension [D-5,M-24,P-11],

$$E_2/E_1 = 0, \text{ or } E_2 = 0,\ E_3 = -E_1\ , \qquad (5.2b)$$

and for equal biaxial extension [D-6,M-24,P-11],

$$E_2/E_1 = 1.0, \text{ or } E_2 = E_1 = -2E_3\ , \qquad (5.2c)$$

---

*Throughout this dissertation (except Chapter XIII) physical components (coming from contravariant transformations) will be used, even though these physical components are written in the same notation as covariant components (i.e., A_{ij} and B_k means A(ij) and B(k), respectively).

The total stress is usually divided into two parts for convenience:

$$\underset{\sim}{\sigma} = -p\underset{\sim}{I} + \underset{\sim}{P} = -p\underset{\sim}{I} + \begin{vmatrix} P_{11} & 0 & 0 \\ 0 & P_{22} & 0 \\ 0 & 0 & P_{33} \end{vmatrix}, \tag{5.3}$$

where p is an isotropic pressure and $\underset{\sim}{P}$ is the extra stress tensor associated with the deformation. When a fluid is in the static condition ($\underset{\sim}{P} = 0$), "p" is identified as the hydrostatic pressure. In a dynamic situation for incompressible fluids "p" is considered as a scalar quantity to be determined by boundary conditions. For elongational flow there exists at least one free surface as a boundary condition so that the elongational viscosity is determined as the measurable material function.

In general, it is only possible to determine extensional viscosities as true material functions under steady state conditions—in which either constant strain rate or constant stress is achieved. In other words, it is necessary to carry out elongational viscosity measurements under steady state conditions in both the Lagrangian and the Eulerian senses. The elongational viscosity is defined by

$$\chi = \frac{\sigma_{11}}{E_1} = \frac{P_{11} - P_{33}}{E_1} . \quad * \tag{5.4}$$

---

*The definition shown in Eqn. (5.4) is effective only when $\sigma_{33} = 0$. Under the conditions of an external hydrostatic pressure $p_e (\sigma_{33} = p_e)$, compression mode, it is useful to define the elongational viscosity as:

$$\chi = \frac{\sigma_{11} - \sigma_{33}}{E_1} = \frac{P_{11} - P_{33}}{E_1} .$$

It is possible to apply further restrictions on the kinematics from definitions of the relative magnitudes of the stretch rates:

$$E_1 \geq E_2 \geq E_3 \ . \tag{5.5a}$$

This leads to

$$-0.5 \leq E_2/E_1 \leq 1.0 \ . \tag{5.5b}$$

By this restriction one may avoid confusion. For example, uniaxial compression and equal biaxial extension are essentially the same ($E_2/E_1 = 1$); however, these deformation modes are different deformations without the restriction given by Eqn. (5.5). Similarly, equal biaxial compression and uniaxial extension are the same deformation modes ($E_2/E_1 = -0.5$). Eqn. (5.5) suggests that two of the extreme deformation modes among extension are uniaxial extension and equal biaxial extension. Other extension modes, including compression, lie between uniaxial and equal biaxial elongation. Generally in this dissertation we shall consider:

$$E_1 > 0 \text{ and } E_3 < 0 \ . \tag{5.6a}$$

This leads to

$$E_2/E_1 > -0.5 \ , \tag{5.6b}$$

This definition for elongational viscosity has been used for lubricated orthogonal stagnation flow [A-6,A-7,W-25] and lubricated squeezing flow [C-9,C-19], where the driving force on the deformation is the external hydrostatic pressure.

where again "1" is the machine direction, "2" is the transverse direction, and "3" is the free surface direction.

B-2. Geometrical Effects

Several different geometries can be suggested for understanding polymer processing operations and material property determination, i.e., elongational viscosity measurements. These include stretching (or compressing) of sheets, cylinders, annular cylinders, and hollow spheres.

B-2-a. Stretching of sheets. Consider the steady state elongational flow of a fluid sheet having constant thickness and a "1,2,3" Cartesian coordinate system embedded in the sheet with "3" normal to the sheet and "1" and "2" in the directions of stretch (Figure 5.1). We take the velocity field in the sheet as:

$$v_1 = v_1(x_1),\ v_2 = v_2(x_2),\ v_3 = v_3(x_3)\ . \tag{5.7a}$$

The deformation rate tensor is given by:

$$\underset{\sim}{d} = \begin{vmatrix} \frac{\partial v_1}{\partial x_1} & 0 & 0 \\ 0 & \frac{\partial v_2}{\partial x_2} & 0 \\ 0 & 0 & \frac{\partial v_3}{\partial x_3} \end{vmatrix}\ . \tag{5.7b}$$

The velocity gradients will be expressed as

$$\frac{\partial v_1}{\partial x_1} = E_1,\ \frac{\partial v_2}{\partial x_2} = E_2,\ \frac{\partial v_i}{\partial x_j} = 0\ (i \neq j)\ . \tag{5.8}$$

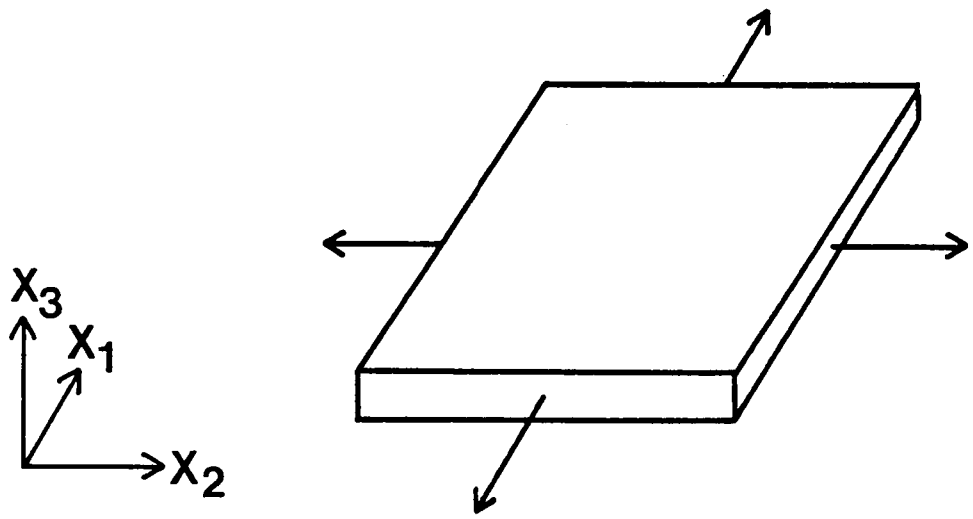

$$v_1 = E_1 x_1$$
$$v_2 = E_2 x_2$$
$$v_3 = E_3 x_3$$

$$\Sigma E_i = 0$$

Figure 5.1. Elongational flow of a sheet.

The velocity gradient normal to the sheet may be written

$$\frac{\partial v_3}{\partial x_3} = E_3 = \frac{1}{h}\frac{Dh}{Dt} = \frac{1}{h}\frac{dh}{dt} . \tag{5.9}$$

The velocity gradients are interrelated for a continuous fluid by the continuity equation. Presuming incompressibility:

$$\frac{\partial v_1}{\partial x_1} + \frac{\partial v_2}{\partial x_2} + \frac{\partial v_3}{\partial x_3} = 0 . \tag{5.10a}$$

$$\frac{\partial v_3}{\partial x_3} = \frac{1}{h}\frac{dh}{dt} = -(E_1 + E_2) , \tag{5.10b}$$

$$h = h(0)\exp[-(E_1+E_2)t] = h(0)\exp[-(1+E_2/E_1)E_1 t] , \tag{5.10c}$$

where E_1 and E_2 are considered as constant stretch rates.

B-2-b. Stretching of cylindrical filaments and compression of discs. Consider the steady state elongational flow of a fluid cylinder or disc of radius R and filament length L or disc thickness h (Figure 5.2). The velocity field is

$$v_z = v_z(z),\ v_r = v_r(r),\ v_\phi = cr , \tag{5.11a}$$

where c is a constant (for elongation flow c is zero). The deformation rate is

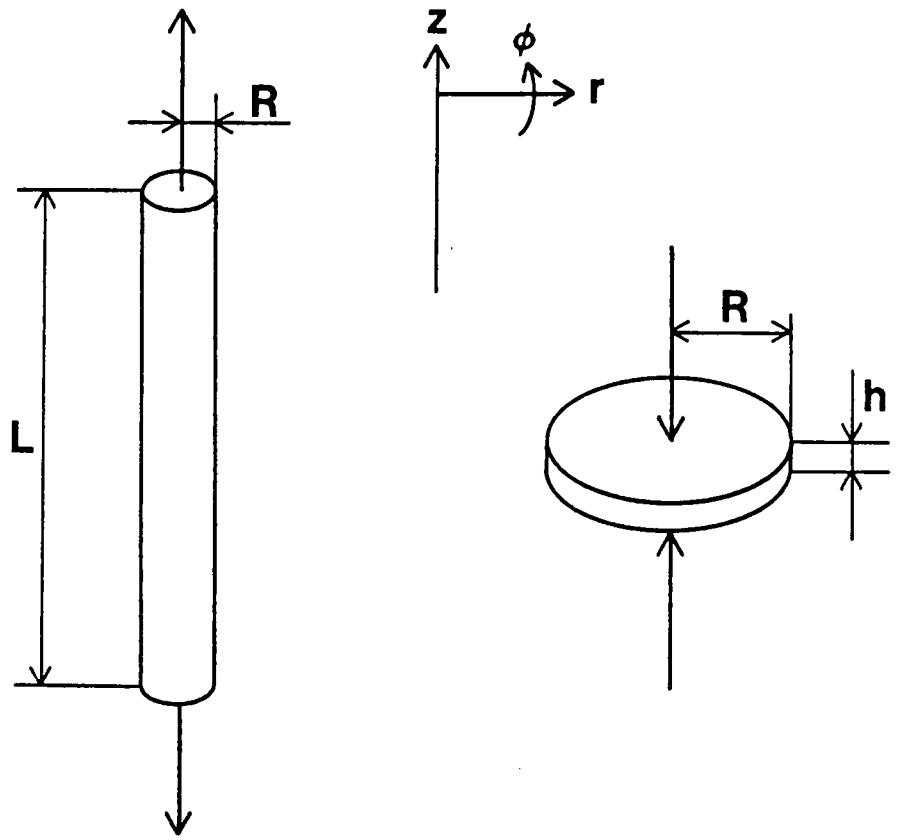

Figure 5.2. Elongational flow of a cylindrical filament and a disc.

$$\underset{\sim}{d}(z,\phi,r) = \begin{vmatrix} \frac{\partial v_z}{\partial z} & 0 & 0 \\ 0 & \frac{v_r}{r} & 0 \\ 0 & 0 & \frac{\partial v_r}{\partial r} \end{vmatrix} . \qquad (5.11b)$$

At the center of the cylinder or the disc ($r = 0.0$), v_r is zero, and on the outer surface ($r = R$), $v_r = DR/Dt$, so that, assuming a flat velocity profile, we obtain

$$d_{rr} = \frac{\partial v_r}{\partial r} = \frac{1}{R}\frac{DR}{Dt} = \frac{1}{R}\frac{dR}{dt} . \qquad (5.12a)$$

Also, by neglecting the variation of $\partial v_z/\partial z$ with z, we have

$$d_{zz} = \frac{\partial v_z}{\partial z} = \frac{1}{L}\frac{DL}{Dt} = \frac{1}{L}\frac{dL}{dt} \quad \text{or} \quad = \frac{1}{h}\frac{dh}{dt} . \qquad (5.12b)$$

Similarly, we obtain

$$d_{\phi\phi} = \frac{v_r}{r} = \frac{1}{R}\frac{dR}{dt} . \qquad (5.12c)$$

There exist two possibilities as to which direction is the machine direction ("1" direction). One case is

$$E_1 = E_z = \frac{1}{L}\frac{dL}{dt}, \quad E_2 = E_\phi = \frac{1}{R}\frac{dR}{dt}, \quad E_3 = E_r = \frac{1}{T}\frac{dR}{dt} . \qquad (5.13)$$

From the continuity equation, we have

$$\frac{1}{L}\frac{dL}{dt} = -\frac{2}{R}\frac{dR}{dt}, \quad E_z = E_1 = -2E_\phi = -2E_r . \qquad (5.14)$$

This is the case of uniaxial extension. The other case is

$$E_1 = E_r = \frac{1}{R}\frac{dR}{dt}, \quad E_2 = E_\phi = \frac{1}{R}\frac{dR}{dt}, \quad E_3 = E_z = \frac{1}{h}\frac{dh}{dt} . \tag{5.15}$$

From the continuity equation, we have

$$\frac{1}{R}\frac{dR}{dt} = -\frac{2}{h}\frac{dh}{dt}, \quad E_r = E_1 = E_\phi = -\frac{1}{2}E_z . \tag{5.16}$$

This is the case of equal biaxial extension (or one may say "uniaxial compression").

B-2-c. Elongation of an annular cylinder. Consider the multiaxial elongational flow of an annular cylinder of radius R, annular thickness h and length L (Figure 5.3). The velocity field is

$$v_z = v_z(z), \quad v_r = v_r(r), \quad v_\phi = cr , \tag{5.17a}$$

where c is a constant (for extensional flow c is zero). The deformation rate tensor is

$$\underset{\sim}{d}(z,\phi,r) = \begin{vmatrix} \frac{\partial v_z}{\partial z} & 0 & 0 \\ 0 & \frac{v_r}{r} & 0 \\ 0 & 0 & \frac{\partial v_r}{\partial r} \end{vmatrix} . \tag{5.17b}$$

On the inner surface of the annulus, v_r is zero, and on the outer surface $v_r = Dh/Dt$, so that, neglecting the variation of $\partial v_r/\partial r$ with r by assuming that the thickness h is small compared with other dimensions of the annulus (i.e., $h \ll R$), we obtain

$$d_{rr} = \frac{\partial v_r}{\partial r} = \frac{1}{h}\frac{Dh}{Dt} = \frac{1}{h}\frac{dh}{dt} . \tag{5.18a}$$

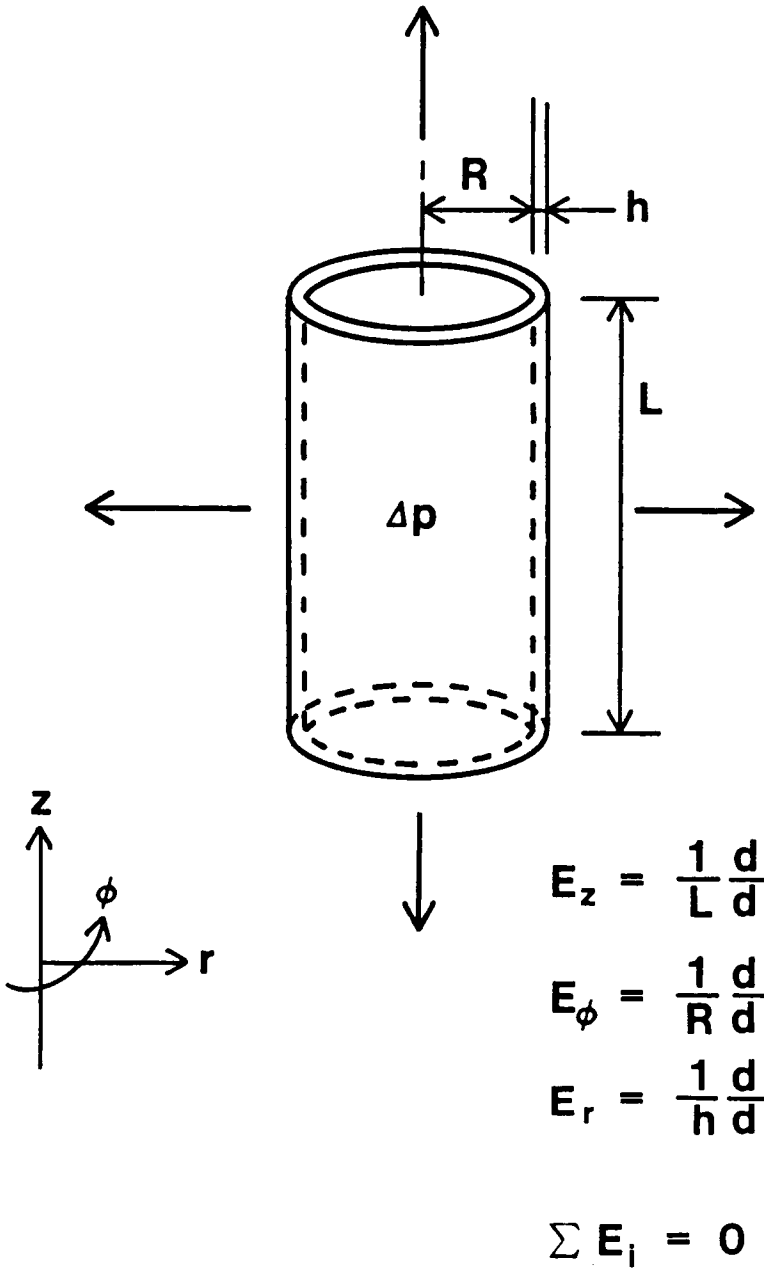

Figure 5.3. Elongational flow of an annular cylinder.

Also, by neglecting the variation of $\partial v_z/\partial z$ with z, we have

$$d_{zz} = \frac{\partial v_z}{\partial z} = \frac{1}{L}\frac{DL}{Dt} = \frac{1}{L}\frac{dL}{dt} . \tag{5.18b}$$

Similarly, we obtain

$$d_{\phi\phi} = \frac{v_r}{r} = \frac{1}{R}\frac{dR}{dt} . \tag{5.18c}$$

We may write

$$E_z = \frac{1}{L}\frac{dL}{dt}, \quad E_\phi = \frac{1}{R}\frac{dR}{dt}, \quad E_r = \frac{1}{h}\frac{dh}{dt} . \tag{5.19}$$

From the continuity equation, we have

$$E_z + E_\phi + E_r = 0 . \tag{5.20}$$

Various possibilities of deformation exist. For uniaxial extension of an annular cylinder

$$\frac{1}{R}\frac{dR}{dt} = \frac{1}{h}\frac{dh}{dt} < 0 \text{ or } E_r = E_\phi = -\frac{1}{2}E_z < 0 . \tag{5.21a}$$

For inflation of an annular cylinder

$$\frac{1}{L}\frac{dL}{dt} = 0, \quad \frac{1}{R}\frac{dR}{dt} = -\frac{1}{h}\frac{dh}{dt} > 0 ,$$

or

$$E_z = 0, \quad E_\phi = -E_r > 0 . \tag{5.21b}$$

For simultaneous drawdown and inflation

$$\frac{1}{L}\frac{dL}{dt} > 0, \quad \frac{1}{R}\frac{dR}{dt} > 0, \quad \frac{1}{h}\frac{dh}{dt} < 0 ,$$

or

$$E_z > 0, \quad E_\phi > 0, \quad E_r = -(E_z + E_\phi) \ . \tag{5.21c}$$

B-2-d. Expansion of a hollow sphere. Consider the expansion of a hollow sphere of radius R and bubble thickness h. The velocity profile is

$$v_r = v_r(r), \quad v_\phi = cr, \quad v_\psi = cr \sin\theta \ , \tag{5.22a}$$

where c is zero (for elongation flow c is zero). The deformation rate tensor is

$$\underset{\sim}{d}(r,\phi,\psi) = \begin{vmatrix} \frac{\partial v_r}{\partial r} & 0 & 0 \\ 0 & \frac{v_r}{r} & 0 \\ 0 & 0 & \frac{v_r}{r} \end{vmatrix} \ . \tag{5.22b}$$

On the inner surface of the bubble, v_r is zero, and on the outer of the sphere $v_r = Dh/Dt$, so that, neglecting the variation of $\partial v_r/\partial r$ with r by assuming that the thickness h is small compared with the other dimensions of the hollow space (i.e., $h << R$), we have

$$d_{rr} = \frac{\partial v_r}{\partial r} = \frac{1}{h}\frac{Dh}{Dt} \quad \frac{1}{h}\frac{dh}{dt} \ . \tag{5.23a}$$

Similarly, we obtain

$$d_{\phi\phi} = d_{\psi\psi} = \frac{v_r}{r} = \frac{1}{R}\frac{dR}{dt} \ . \tag{5.23b}$$

We may write

$$E_1 = E_\phi = \frac{1}{R}\frac{dR}{dt}, \quad E_2 = E_\psi = \frac{1}{R}\frac{dR}{dt}, \quad E_3 = E_r = \frac{1}{h}\frac{dh}{dt} . \tag{5.24a}$$

From the continuity equation, we have

$$\frac{2}{R}\frac{dR}{dt} = -\frac{1}{h}\frac{Dh}{Dt}, \quad E_\phi = E_1 = E_\psi = -\frac{1}{2}E_r . \tag{5.24b}$$

This is the case of equal biaxial elongation.

C. ELONGATIONAL VISCOSITY

In the previous section, the kinematics of elongational flow (including compressive flow) is described in terms of an elongation rate along the "machine direction" E_1, the "transverse direction" E_2, and the "free surface direction" E_3. The dynamics of extensional flow will be described for a Newtonian fluid and a viscoelastic fluid, especially for a convected Maxwell model in terms of the elongation rates E_1, E_2, and E_3.

C-1. Newtonian Fluids

The stress tensor in a Newtonian fluid may be expressed by

$$\underset{\sim}{\sigma} = -p\underset{\sim}{I} + 2\eta\,\underset{\sim}{d} . \tag{5.25}$$

For a multiaxial elongational flow one writes

$$\begin{aligned} \sigma_{11} &= -p + 2\eta E_1 , \\ \sigma_{22} &= -p + 2\eta E_2 , \\ \sigma_{33} &= -p + 2\eta E_3 . \end{aligned} \tag{5.26a,b,c}$$

The normal stress in the "3" direction is zero (the existence of external hydrostatic pressure, p_e, makes σ_{33} be p_e; see Eqn. (5.4) and footnote on page 121).

$$\sigma_{33} = -p + 2\eta E_3 = 0 \ . \tag{5.27}$$

Using Eqn. (5.27) to eliminate p and Eqn. (5.1) to eliminate E_3 yields:

$$\sigma_{11} = 2\eta(2E_1+E_2) = 2\eta(2+E_2/E_1)\ E_1 \ , \tag{5.28a}$$

$$\sigma_{22} = 2\eta(E_1+2E_2) = 2\eta(1+2E_2/E_1)\ E_1 \ . \tag{5.28b}$$

The elongational viscosity defined by Eqn. (5.4) is given by

$$\chi = \frac{\sigma_{11}}{E_1} = 2\eta(2+E_2/E_1) \ . \tag{5.29}$$

For uniaxial extension defined by Eqn. (5.2a), we have

$$\sigma_{11} = 3\eta\ E_1, \quad \sigma_{22} = 0, \quad \chi = 3\eta \ . \tag{5.30a}$$

For planar extension defined by Eqn. (5.2b), this leads to

$$\sigma_{11} = 4\eta\ E_1, \quad \sigma_{22} = 2\eta\ E_1, \quad \chi = 4\eta \ . \tag{5.30b}$$

For equal biaxial extension defined by Eqn. (5.2c), this leads to

$$\sigma_{11} = 6\eta\ E_1, \quad \sigma_{22} = 6\eta\ E_1, \quad \chi = 6\eta \ . \tag{5.30c}$$

C-2. Viscoelastic Fluids

C-2-a. Constitutive equation. We shall take the rheological character of the viscoelastic fluid to be represented by the convected Maxwell model [D-2,I-2,I-3,M-42,W-16,W-18]

$$\sigma_{ij} = -p\delta_{ij} + P_{ij} , \tag{5.31a}$$

$$P_{ij} = 2\tau G d_{ij} - \tau \frac{\delta P_{ij}}{\delta t} , \tag{5.31b}$$

where $\delta P_{ij}/\delta t$ is the contravariant convected derivative defined by

$$\frac{\delta P_{ij}}{\delta t} = \frac{DP_{ij}}{Dt} - P_{im}\frac{\partial v_j}{\partial x_m} - \frac{\partial v_i}{\partial x_m} P_{mj} . \tag{5.31c}$$

Generally the relaxation time, τ, is considered to depend upon the deformation rate. It has been taken to be of form [I-3,W-16]

$$\tau = \frac{\tau_0}{1 + a\tau_0 II_d^{1/2}} , \tag{5.32}$$

where II_d is the second invariant $\underset{\sim}{d}$, which we take as 2 tr $\underset{\sim}{d}^2$.

In simple shear flow the stress field is predicted to be of form

$$\begin{aligned} \sigma_{12} &= G\tau\dot{\gamma}, \\ N_1 &= 2G\tau^2\dot{\gamma}^2, \\ N_2 &= 0, \end{aligned} \tag{5.33a,b,c}$$

with τ from Eqn. (5.32) being

$$\tau = \frac{\tau_0}{1 + a\tau_0\dot{\gamma}} . \tag{5.34}$$

The deformation rate dependence of τ through Eqns. (5.32) and (5.34) define the non-Newtonian shear viscosity in this model.

C-2-b. Elongational flow. For a multiaxial elongational flow, Eqn. (5.31b) takes the form

$$P_{11} = 2\tau GE_1 - \tau\left(\frac{\partial P_{11}}{\partial t} - 2E_1P_{11}\right),$$

$$P_{22} = 2\tau GE_2 - \tau\left(\frac{\partial P_{22}}{\partial t} - 2E_2P_{22}\right), \qquad (5.35a,b,c)$$

$$P_{33} = 2\tau GE_3 - \tau\left(\frac{\partial P_{33}}{\partial t} - 2E_3P_{33}\right).$$

In a biaxially stretched sheet, this is subject to the boundary condition (existence of external hydrostatic pressure, p_e, makes σ_{33} be p_e; see Eqn. (5.4) and footnote on page 121)

$$\sigma_{33} = -p + P_{33} = 0 . \qquad (5.36)$$

If we take as an initial condition that the sheet is in virgin condition at time $t = 0$, Eqns. (5.35) with (5.36) may be solved to yield for constant stretch rates E_j

$$\sigma_{jj}(t) = P_{jj} - P_{33} = \frac{2\tau GE_j}{1-2\tau E_j}\left[1 - e^{-(1-2\tau E_j)t/\tau}\right]$$

$$- \frac{2\tau GE_3}{1-2\tau E_3}\left[1 - e^{-(1-2\tau E_3)t/\tau}\right] \text{ (j not summed)}, \qquad (5.37)$$

where j may be "1" or "2" and E_3 is $-(E_1 + E_2)$.

The steady state forms for σ_{11} and σ_{22} are

$$\sigma_{jj} = \frac{2\tau GE_j}{1-2\tau E_j} - \frac{2\tau GE_3}{1-2\tau E_3} ,$$
$$= \frac{2\tau G(E_j-E_3)}{(1-2\tau E_j)(1-2\tau E_3)} , \qquad (5.38)$$

or more specifically

$$\sigma_{11} = \frac{2\tau G(2E_1+E_2)}{(1-2\tau E_1)[1+2\tau(E_1+E_2)]} , \qquad (5.39a)$$

$$\sigma_{22} = \frac{2\tau G(2E_2+E_1)}{(1-2\tau E_2)[1+2\tau(E_1+E_2)]} . \qquad (5.39b)$$

For small τE_j, the expressions for σ_{11} and σ_{22} are

$$\sigma_{11} = 2\tau G(2+E_2/E_1)E_1[1-2\tau(E_2/E_1)E_1+O(\tau E_1)^2] , \qquad (5.40a)$$

$$\sigma_{22} = 2\tau G(1+2E_2/E_1)E_1[1-2\tau E_1+O(\tau E_1)^2] . \qquad (5.40b)$$

The characteristics of these functions vary with (E_2/E_1). We will consider several cases.

Uniaxial extension:

$$\sigma_{11} = 3\tau GE_1[1+\tau E_1+O(\tau E_1)^2] , \qquad (5.41a)$$

$$\sigma_{22} = 0 . \qquad (5.41b)$$

Planar extension:

$$\sigma_{11} = 4\tau GE_1[1+O(\tau E_1)^2] , \qquad (5.42a)$$

$$\sigma_{22} = 2\tau GE_1[1-2\tau E_1+O(\tau E_1)^2] . \qquad (5.42b)$$

Equal biaxial extension:

$$\sigma_{11} = \sigma_{22} = 6\tau GE[1-2\tau E_1+O(\tau E_1)^2] \ . \tag{5.43}$$

The stress has the Newtonian value at low τE_1. The elongational viscosity, σ_{11}/E_1, at first increases for uniaxial extension and when E_2/E_1 is less than zero. When E_2/E_1 is greater than zero, including equal biaxial extension, the elongational viscosity σ_{11}/E_1 at first decreases. The effect of E_2/E_1 is deformation rate softening. However, for all values of E_2/E_1

$$\lim_{E_1 \to 1/2\tau} \frac{\sigma_{11}}{E_1} = \infty \ . \tag{5.44}$$

This is shown in Figure 5.4. When E_2/E_1 is greater than zero, σ_{11}/E_1 exhibits a minimum.

It should be noted from Eqn. (5.38) that the deformation-rate softening character in elongational viscosity is dominated by P_{33} term. The P_{11}/E_1 component in σ_{11}/E_1 is a monotonic increasing function of τE_1, i.e., the qualitative nature of P_{11}/E_1 does not depend upon the kinematics (E_2/E_1). On the other hand, the P_{33} component determines the qualitative nature of the elongational viscosity.

We now consider the deformation rate dependence of the relaxation time τ. The invariant $II_d^{1/2}$ of Eqn. (5.32) may be expressed in the form

$$II_d^{1/2} = \sqrt{2\mathrm{tr}\underset{\sim}{d}^2} = 2[(E_2/E_1)^2 + E_2/E_1 + 1]^{1/2} E_1 = KE_1 \ , \tag{5.45}$$

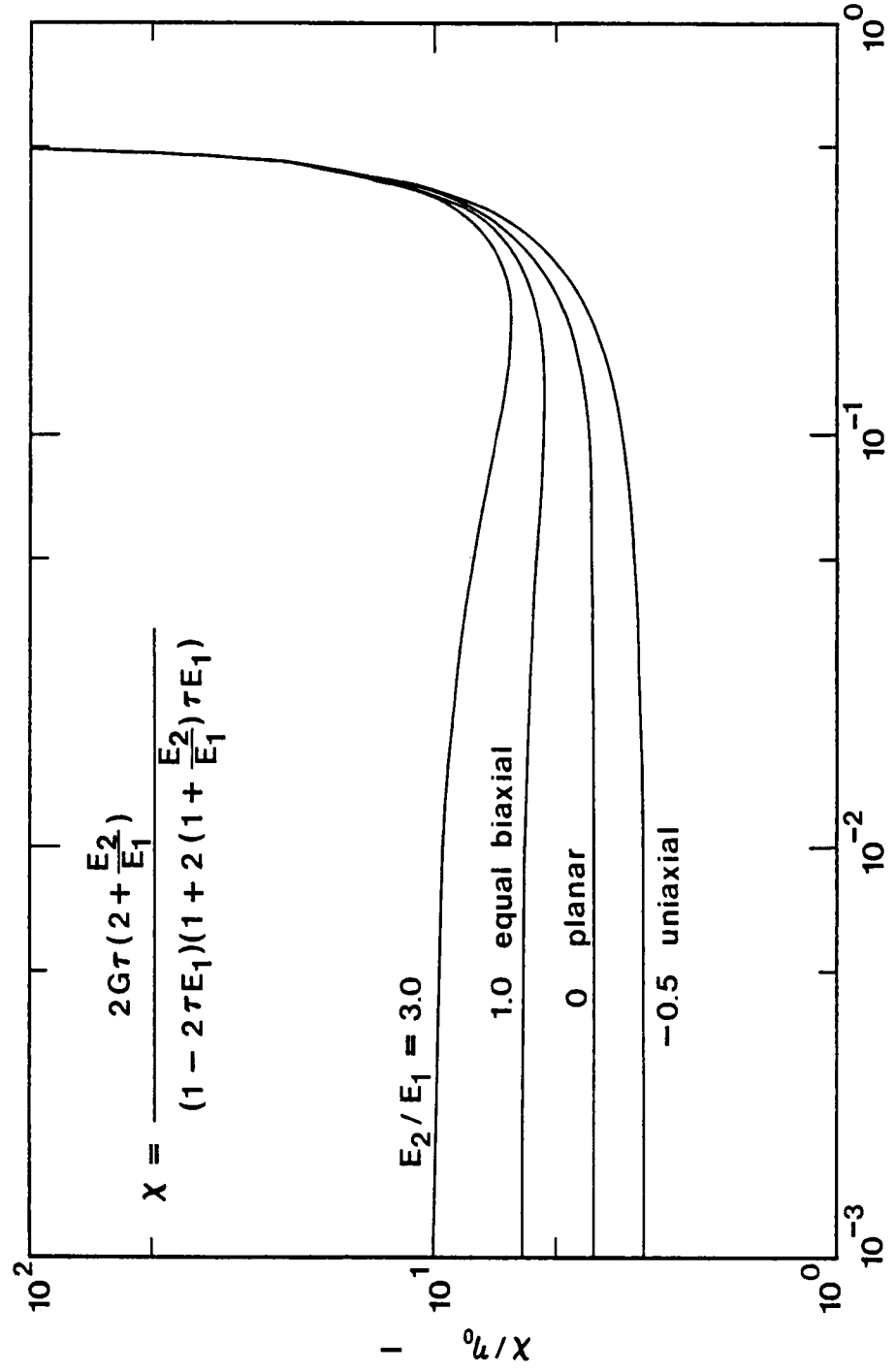

Figure 5.4. Elongational viscosity for a convected Maxwell model with a constant relaxation time as a function of τE_1 for various E_2/E_1.

which makes Eqn. (5.32) take the form

$$\tau = \frac{\tau_0}{1+aK\tau_0 E_1} . \tag{5.46}$$

Introducing Eqn. (5.46) into Eqn. (5.39) gives

$$\sigma_{11} = \frac{2G\tau_0(2+E_2/E_1)(1+aK\tau_0E_1)E_1}{[1-(2-aK)\tau_0E_1][1+(2+aK+2E_2/E_1)\tau_0E_1]} , \tag{5.47a}$$

$$\sigma_{22} = \frac{2G\tau_0(1+2E_2/E_1)(1+aK\tau_0E_1)E_1}{[1-(2E_2/E_1-aK)\tau_0E_1][1+(2+aK+2E_2/E_1)\tau_0E_1]} . \tag{5.47b}$$

For small $\tau_0 E_1$, we may expand Eqn. (5.47) to give

$$\sigma_{11} = 2G\tau_0E_1(2+E_2/E_1)[1-(aK+2E_2/E_1)\tau_0E_1+O(\tau E_1)^2] , \tag{5.48a}$$

$$\sigma_{22} = 2G\tau_0E_1(1+2E_2/E_1)[1-(2+aK)\tau_0E_1+O(\tau E_1)^2] . \tag{5.48b}$$

The elongational viscosity is now an increasing function only when

$$a < \frac{2}{K}\left(-\frac{E_2}{E_1}\right) . \tag{5.49}$$

This is possible in uniaxial extension where K is $\sqrt{3}$ and E_2/E_1 is $(-1/2)$. "a" must be less than 0.577 for the elongational viscosity to be an increasing function. For planar extension and equal biaxial extension, σ_{11}/E will always be a decreasing function at low E_1.

σ_{11} will rise to infinity according to Eqn. (5.47a) when

$$E_1 \to \frac{1}{(2-aK)\tau_0} . \tag{5.50}$$

This can only occur for values of a for which

$$a < 2/K \ . \tag{5.51}$$

This is $2/\sqrt{3}$ for uniaxial extension, unity for planar extension and $1/\sqrt{3}$ for biaxial extension. The dependence of σ_{11}/E_1 upon "a" is shown in Figure 5.5.

The above discussion indicates that increasing E_2/E_1 and the deformation rate dependence of the relaxation time have similar effects on the elongational viscosity. Both tend to decrease its rate of increase and to transform it into a decreasing function.

D. SUMMARY

Various multiaxial elongational flows, including compressive flow, are classified in terms of two individual elongation rates E_1, the elongation rate along the machine direction, and E_2, the elongation rate along the transverse direction, for various geometries. Elongational viscosities are described for a Newtonian fluid and a convected Maxwell model. It is shown that increasing the lateral stretching (larger E_2/E_1 values) makes the elongational viscosities more deformation rate softening.

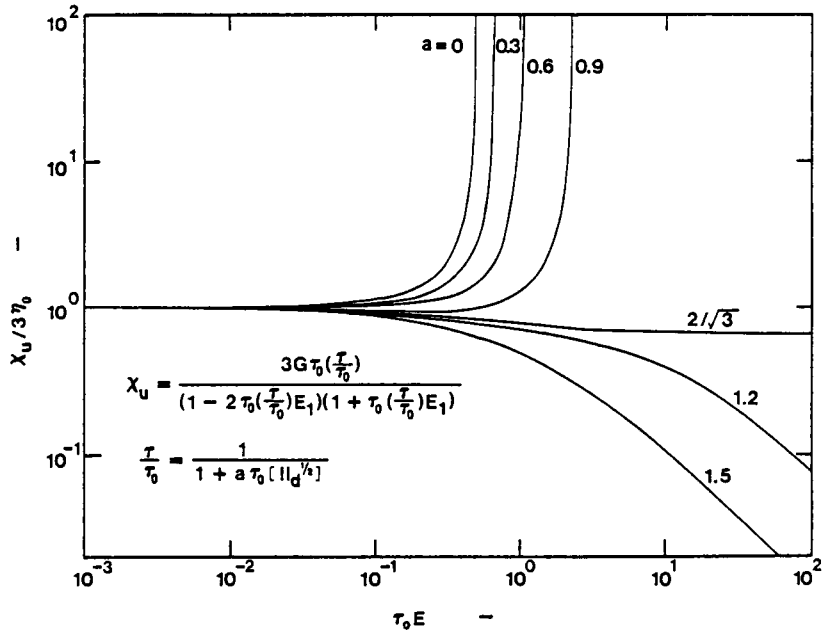

(a) Uniaxial elongational viscosity

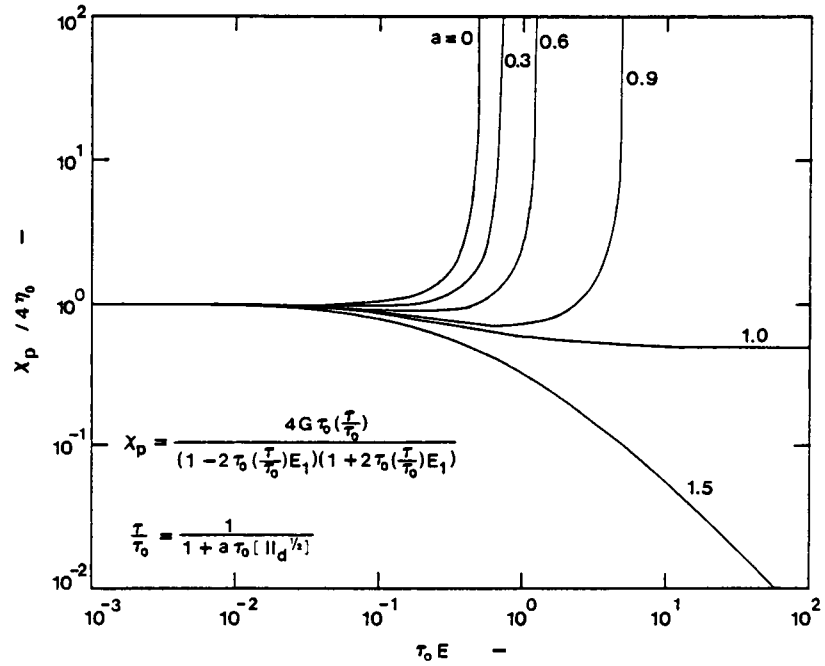

(b) Planar elongational viscosity

Figure 5.5. Elongational viscosity for a convected Maxwell model with a deformation rate dependent relaxation time.

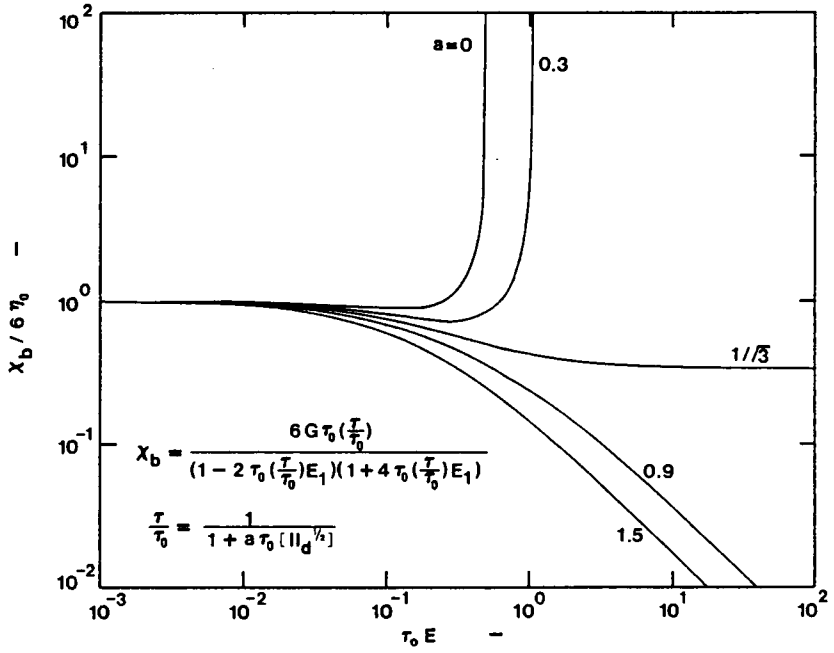

(c) Equal biaxial elongational viscosity

Figure 5.5 (continued)

CHAPTER VI

MULTIAXIAL ELONGATIONAL FLOW OF SHEETS AND ANNULAR CYLINDERS: GROWTH OF DISTURBANCES AND GENERAL FORMULATION

A. INTRODUCTION

A problem of basic interest in the flow of polymer melts is the instabilities which arise during the stretching of filaments and sheets. The characteristics of the failure of molten polymer filaments during uniaxial stretching has been reported in experiments by Ide and White [I-1,I-2,I-3,I-4,W-17]. Theoretical analyses of the growth of disturbances in Newtonian and viscoelastic fluid filaments have been given by Chang and Lodge [C-6] and by Ide and White [I-2, I-3,W-17]. In recent years, attention has increasingly been given to polymer processing operations involving the multiaxial stretching of sheets and films. This has led us to become concerned with basic studies of the growth of disturbances in fluid sheets, and annular cylinders. There have been few basic investigations of this problem. Indeed, the only closely related study that we are aware of is that of White several years ago [W-13].

It is our purpose here to present a theoretical investigation of the growth of disturbances in Newtonian fluid sheets and annuli. We give special attention to the force balance and continuity equation which represent the state of growth of disturbances.

B. ELONGATION OF A FLAT SHEET: GROWTH OF DISTURBANCES

B-1. Homogeneous Deformation

Consider the steady state elongational flow of a fluid sheet having constant thickness and a "1, 2, 3" Cartesian coordinate system embedded in the sheet with "3" normal to the sheet and "1" and "2" in the directions of stretch (Figure 6.1a). The "1" direction is taken as the "machine direction." We take the velocity field in the sheet as

$$v_1 = v_1(x_1),\ v_2 = v_2(x_2),\ v_3 = v_3(x_3)\ . \tag{6.1a}$$

The deformation rate tensor is given by:

$$\underset{\sim}{d} = \frac{1}{2}\left[\nabla\underset{\sim}{v} + (\nabla\underset{\sim}{v})^T\right] = \begin{vmatrix} \frac{\partial v_1}{\partial x_1} & 0 & 0 \\ 0 & \frac{\partial v_2}{\partial x_2} & 0 \\ 0 & 0 & \frac{\partial v_3}{\partial x_3} \end{vmatrix}\ . \tag{6.1b}$$

The velocity gradients will be expressed as

$$\frac{\partial v_1}{\partial x_1} = E_1 > 0\ ,\ \frac{\partial v_2}{\partial x_2} = E_2\ ,\ \frac{\partial v_i}{\partial x_j} = 0\ (i \neq j)\ . \tag{6.1c}$$

The velocity gradient normal to the sheet may be written

$$\frac{\partial v_3}{\partial x_3} = E_3 = \frac{1}{h}\frac{Dh}{Dt} = \frac{1}{h}\frac{dh}{dt} < 0\ . \tag{6.1d}$$

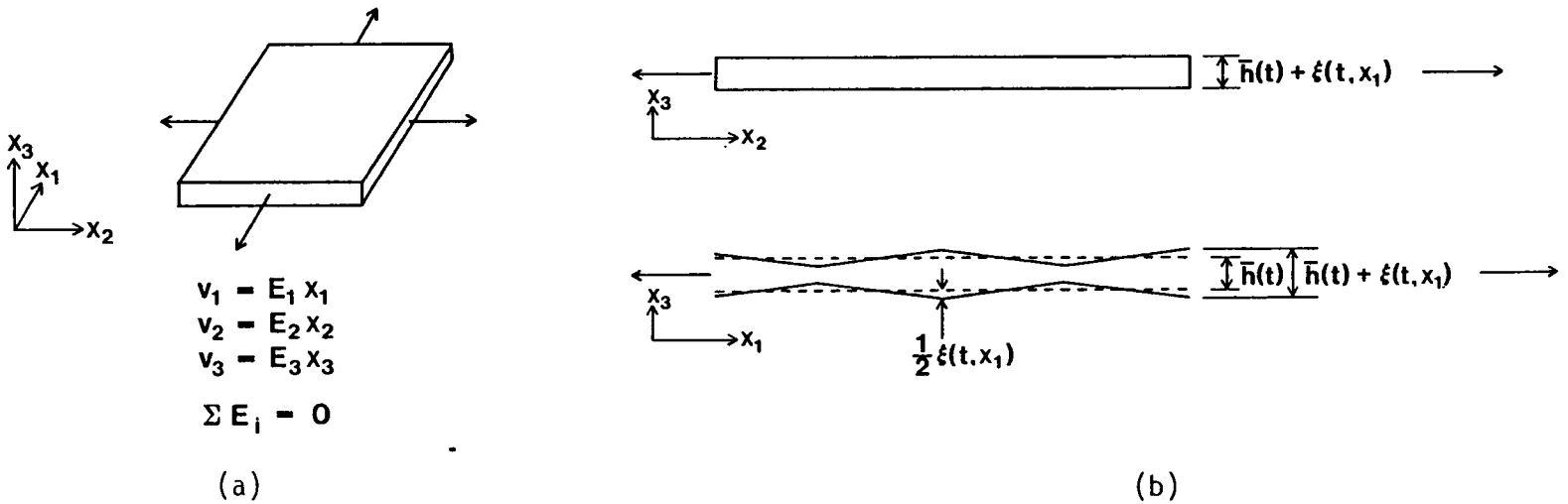

Figure 6.1. (a) Elongational flow of a sheet; (b) disturbances in a stretched sheet.

The velocity gradients are interrelated for a continuous fluid by the continuity equation. Presuming incompressibility:

$$\frac{\partial v_1}{\partial x_1} + \frac{\partial v_2}{\partial x_2} + \frac{\partial v_3}{\partial x_3} = 0 \ , \tag{6.2a}$$

$$\frac{\partial v_3}{\partial x_3} = \frac{1}{h}\frac{dh}{dt} = -(E_1 + E_2) \ , \tag{6.2b}$$

$$h = h(0)\ \exp[-(E_1+E_2)t] = h(0)\ \exp[-(1+E_2/E_1)E,t] \ , \tag{6.2c}$$

where E_1 and E_2 are considered as constant stretch rates. There arise here the value of E_2/E_1 or $(\partial v_2/\partial x_2)/(\partial v_1/\partial x_1)$, which is a characteristic value of the extensional flow.

B-2. Conservation Equations: Perturbed State

We now introduce a disturbance into the flow of the flat sheet along the lines:

$$\underset{\sim}{v} = \overline{\underset{\sim}{v}} + \underset{\sim}{v}' \ , \tag{6.3a}$$

$$h = \overline{h} + \xi \ , \tag{6.3b}$$

$$\underset{\sim}{q} = \overline{\underset{\sim}{q}} + \underset{\sim}{q}' \ , \tag{6.3c}$$

where a superposed bar indicates the steady state.

Let us first consider kinematics of the flow by introducing Eqns. (6.3a) and (6.3b). It follows,

$$\frac{\partial v_3}{\partial x_3} = \frac{1}{\bar{h} + \xi} \frac{D(\bar{h} + \xi)}{Dt} . \tag{6.4a}$$

After linearization we obtain

$$\frac{\partial v_3}{\partial x_3} = \frac{1}{\bar{h}} \frac{\partial \bar{h}}{\partial t} + \frac{1}{\bar{h}} \frac{D\xi}{Dt} - \frac{\xi}{\bar{h}^2} \frac{\partial \bar{h}}{\partial t} . \tag{6.4b}$$

If we introduce Eqn. (6.3a) into Eqn. (6.2a), using Eqn. (6.4b), we obtain

$$\left(\frac{\partial \bar{v}_1}{\partial x_1} + \frac{\partial v_1'}{\partial x_1}\right) + \left(\frac{\partial \bar{v}_2}{\partial x_2} + \frac{\partial v_2'}{\partial x_2}\right) + \left(\frac{\partial \bar{v}_3}{\partial x_3} + \frac{1}{\bar{h}} \frac{D\xi}{Dt} - \frac{\xi}{\bar{h}^2} \frac{\partial \bar{h}}{\partial t}\right) = 0 . \tag{6.5}$$

Noting that the steady state form must also satisfy Eqn. (6.2a), we obtain

$$\frac{\partial v_1'}{\partial x_1} + \frac{\partial v_2'}{\partial x_2} + \frac{1}{\bar{h}} \frac{D\xi}{Dt} - \frac{\xi}{\bar{h}^2} \frac{\partial \bar{h}}{\partial t} = 0 . \tag{6.6}$$

If we limit ourselves to disturbances in the 1-3 plane, i.e., v_2' is zero, we may write

$$\frac{\partial v_1'}{\partial x_1} = E_1' = - \frac{\partial v_3'}{\partial x_3} = - E_3' = \frac{1}{\bar{h}} \left(\frac{D\xi}{Dt} - \frac{\xi}{\bar{h}} \frac{\partial \bar{h}}{\partial t}\right) = - \frac{D}{Dt} \left[\frac{\xi}{\bar{h}}\right] . \tag{6.7}$$

We consider a force F_1 to be applied in the "1" direction to a sheet (Figure 6.1). A uniform disturbance $\xi(x_1)$ is introduced. This causes a disturbance in the cross-section of the 2-3 plane of A'. It follows that if we write

$$A = \bar{A} + A' \ , \tag{6.8a}$$

$$\sigma_{11} = \bar{\sigma}_{11} + \sigma'_{11} \ , \tag{6.8b}$$

the perturbed force balance equation is

$$\rho\{\bar{A}\ (\frac{\partial v'_1}{\partial t} + \bar{v}_1 \frac{\partial v'_1}{\partial x_1} + v'_1 \frac{\partial \bar{v}_1}{\partial x_1}) + A'\ (\frac{\partial \bar{v}_1}{\partial t} + \bar{v}_1 \frac{\partial \bar{v}_1}{\partial x_1})\}$$

$$= \frac{\partial}{\partial x_1} (\bar{A}\ \sigma'_{11} + A'\ \bar{\sigma}_{11}) \ . \tag{6.9}$$

By neglecting inertia in the left-hand side of Eqn. (6.9), one obtains

$$\frac{\partial}{\partial x_1} (\bar{A}\ \sigma'_{11} + A'\ \bar{\sigma}_{11}) = 0 \ . \tag{6.10}$$

Eqn. (6.10) is equivalent to

$$\bar{A}\ \sigma'_{11} + A'\ \bar{\sigma}_{11} = 0 \ . \tag{6.11}$$

Noting that:

$$A = W(\bar{h} + \xi),\ \bar{A} = W\bar{h},\ A' = W\xi \ , \tag{6.12a,b,c}$$

we may write Eqn. (6.11)

$$\sigma'_{11} + \bar{\sigma}_{11}\ [\frac{\xi}{\bar{h}}] = 0 \ . \tag{6.13a}$$

or

$$(P'_{11} - P'_{33}) + (\overline{P}_{11} - \overline{P}_{33})[\frac{\xi}{\overline{h}}] = 0 \ . \qquad (6.13b)$$

B-3. Newtonian Fluid Sheets: Growth of Disturbances

The stress tensor in a Newtonian fluid may be expressed by

$$\underset{\sim}{\sigma} = - p\underset{\sim}{I} + 2\eta \underset{\sim}{d} \ , \qquad (6.14a)$$

or

$$\sigma_{ii} = - p + 2\eta \frac{\partial v_i}{\partial x_i} \qquad (i \text{ not summed}) \ . \qquad (6.14b)$$

The normal stress in the "3" direction is zero, so that

$$\sigma_{ii} = 2\eta \left(\frac{\partial v_i}{\partial x_i} - \frac{\partial v_3}{\partial x_3} \right) \qquad (i \neq 3, \ i \text{ not summed}) \ . \qquad (6.15)$$

The growth of disturbances in a sheet is governed by Eqns. (6.7) and (6.13). The mean stress and disturbed stress are

$$\overline{\sigma}_{11} = - p + 2\eta E_1 = 2\eta(2E_1 + E_2) \ , \qquad (6.16a)$$

$$\sigma'_{11} = - p' + 2\eta \frac{\partial v'_1}{\partial x_1} = 2\eta \left(2 \frac{\partial v'_1}{\partial x_1} + \frac{\partial v'_2}{\partial x_2} \right) \ . \qquad (6.16b)$$

Taking $\partial v'_2/\partial x_2$ as zero and introducing Eqn. (6.7) gives

$$\sigma'_{11} = - \frac{4\eta}{\overline{h}} \left(\frac{D\xi}{Dt} - (E_1 + E_2)\xi \right) \ . \qquad (6.16c)$$

It follows that

$$-\frac{4\eta}{\bar{h}}\left(\frac{D\xi}{Dt} - (E_1 + E_2)\xi\right) + 2\eta(2E_1 + E_2)\frac{\xi}{\bar{h}} = 0 \ , \qquad (6.17a)$$

or

$$\frac{D\xi}{Dt} + \frac{1}{2}E_2\xi = 0 \ . \qquad (6.17b)$$

Let the disturbance be periodic along the "1" direction:

$$\xi(t,x) = \hat{\xi}(t)e^{ikx_1} \ . \qquad (6.18a)$$

The wave number k decreases with time because of the extension of the film. Under constant strain rate E_1 deformation

$$k(t) = k(0)e^{-E_1 t} \ . \qquad (6.18b)$$

This leads to

$$\frac{D\xi}{Dt} = \frac{\partial\xi}{\partial t} + \bar{v}_1\frac{\partial\xi}{x_1} = \frac{\partial\hat{\xi}}{\partial t}e^{ikx_1} \ . \qquad (6.19)$$

Eqn. (6.17) can be rewritten with the aid of Eqn. (6.19) for a constant strain rate deformation:

$$\frac{1}{\hat{\xi}}\frac{\partial\hat{\xi}}{\partial t} = -\frac{1}{2}E_2 = -\frac{1}{2}\left(\frac{E_2}{E_1}\right)E_1 \ . \qquad (6.20)$$

The disturbances vary exponentially in time according to

$$\hat{\xi}(t) = \hat{\xi}(0)\exp(-\frac{1}{2}E_2 t) = \hat{\xi}(0)\exp[-\frac{1}{2}(E_2/E_1)E_1 t] \ . \qquad (6.21)$$

This is summarized in Figure 6.2.

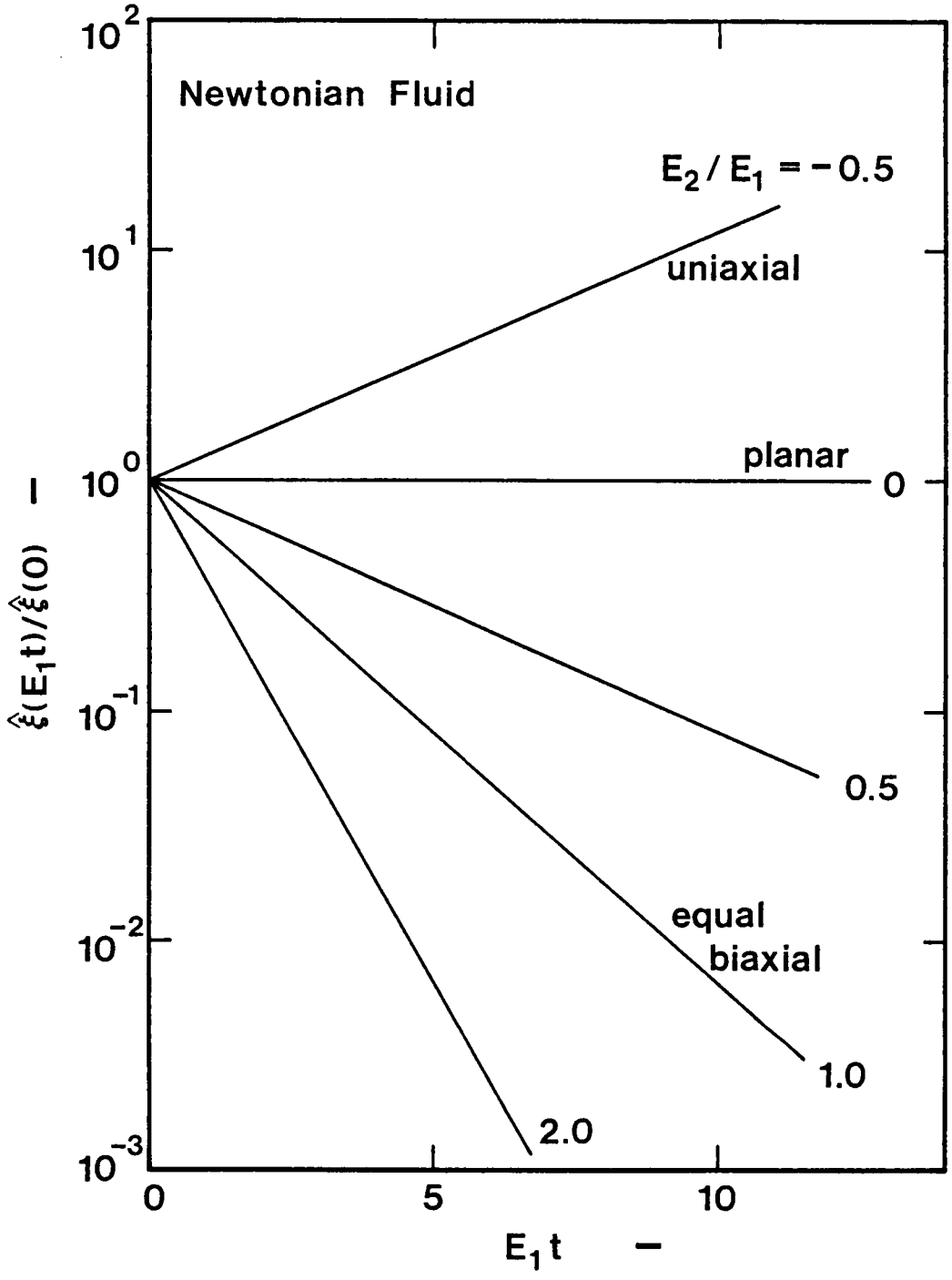

Figure 6.2. Growth of disturbance $\hat{\xi}(E_1 t)/\hat{\xi}(0)$ as a function of $E_1 t$ for various E_2/E_1 in the stretching of a sheet.

For uniaxial extension, where E_2 is $(-1/2)E_1$, we have

$$\hat{\xi}(t) = \hat{\xi}(0) \exp(\frac{1}{4} E_1 t) \ . \tag{6.22a}$$

For planar extension, where E_2 is zero

$$\hat{\xi}(t) = \hat{\xi}(0) \ . \tag{6.22b}$$

For equal biaxial extension, where E_2 is E_1

$$\hat{\xi}(t) = \hat{\xi}(0) \exp(-\frac{1}{2} E_1 t) \tag{6.22c}$$

In uniaxial extension, the disturbance grows. Increasing the deformation rates in the transverse direction, parallel to the disturbance, decreases the rate of growth of disturbances.

B-4. Ductile Failure

The usefulness of the analysis developed in the previous section is that it allows the investigation of the relationship between the kinematics of the deformation of sheets and the eventual occurrence of failure.

It is noted from Eqn. (6.2c) that the sheet thins more rapidly than the defect growth rate as we increase lateral stretching. We take the criterion of failure to be

$$\hat{\xi}(t_b) = \overline{h}(t_b) = \overline{h}(0) \exp[-(1 + E_2/E_1)E_1 t] \ , \tag{6.23}$$

where t_b is the time at failure. By combining Eqns. (6.21) and (6.23), the elongation to break of films of length $L(t_b)$, length

along the "1" direction, and area $A(t_b)$, area in the 1-2 plane, are given as

$$\frac{L(t_b)}{L(0)} = \exp(E_1 t_b) = \exp\left[\frac{2}{(2+E_2/E_1)} \ln \frac{\bar{h}(0)}{\hat{\xi}(0)}\right] , \tag{6.24a}$$

and

$$\frac{A(t_b)}{A(0)} = \exp(E_1 t_b + E_2 t_b) = \exp\left\{\left[2 - \frac{2}{(2+E_2/E_1)}\right] \ln \frac{\bar{h}(0)}{\hat{\xi}(0)}\right\} . \tag{6.24b}$$

Eqns. (6.24) indicate that increasing deformation rates in the transverse direction make the elongation-to-break of the flat sheets decrease in the "1" direction (i.e., machine direction). However, the relative stretched area at break increases with increasing strain rates in the transverse direction.

Although from Eqn. (6.23) the size of the defects is decreased by the lateral stretching of the sheets, the homogeneous decrease in thickness is much greater and the defect size reaches the mean thickness level earlier, resulting in failure.

It is also useful to consider a "normalized disturbance," which is defined as $\hat{\xi}(t)/\bar{h}(t)$, the ratio of the defect size and the mean thickness,

$$\frac{\hat{\xi}(t)/\bar{h}(t)}{\hat{\xi}(0)/\bar{h}(0)} = \exp\left[\left(1 + \frac{E_2/E_1}{2}\right)E_1 t\right] . \tag{6.25}$$

In these terms lateral stretching is destabilizing.

B-5. Additional Comments: Disturbances Along the Transverse Direction

In previous sections (Sections B-2 and B-3) we have described the growth of disturbance where thickness varies only along the "1" direction, i.e., $\xi = \xi(t,x_1)$ or limit disturbances in the 1-3 plane, and E_1 is assumed to have a positive value. It is necessary to describe certain less restricted states.

First we consider elongational flow where $E_1 \leq 0$; however, disturbances are still limited in the 1-3 plane (i.e., $v_2' = 0$). The driving force of this deformation is acting along the "2" direction not along the "1" direction, so that it is not necessary to consider Euler buckling, as occurs during the compression of columns. The growth of disturbances in a sheet is still governed by the previously described conservation equations, Eqns. (6.7) and (6.13). Therefore, the growth of disturbances of a Newtonian fluid sheet is given by

$$\frac{D\xi}{Dt} + \frac{1}{2} E_2 \xi = 0 \ . \tag{6.26a}$$

Applying the periodic disturbance given by Eqn. (6.18) leads to

$$\frac{\partial \hat{\xi}}{\partial t} + \frac{1}{2} E_2 \hat{\xi} = 0 \ . \tag{6.26b}$$

and

$$E_1 \leq 0, \quad E_2 > 0 \ . \tag{6.26c}$$

E_1 is assumed to be less than zero (i.e., a compression mode based upon the x_1 direction), so that this applied restriction on the

kinematics automatically makes E_2 have a positive value and the elongation rate in the "machine direction." This allows us to change the problem from one of the growth of disturbances undergoing compression, where disturbances are along the "1" direction (in the 1-3 plane) (see Figure 6.3a), to one undergoing extension where disturbances are along the transverse direction (in the 2-3 plane) (see Figure 6.3b). Then, we can interchange the subscript "1", which represents the transverse direction, in Eqns. (6.26), applied disturbance defined by Eqn. (6.18), and conservation equations. Therefore, the governing continuity and force balance equation are:

$$\frac{\partial v_2'}{\partial x_2} + \frac{1}{\bar{h}} \frac{D\xi}{Dt} - \frac{\xi}{\bar{h}^2} \frac{\partial \bar{h}}{\partial t} = 0 \ , \tag{6.27a}$$

$$\frac{\partial v_2'}{\partial x_2} = E_2' = - \frac{\partial v_3'}{\partial x_3} = - \frac{1}{\bar{h}} \left(\frac{D\xi}{Dt} - \frac{\xi}{\bar{h}} \frac{\partial \bar{h}}{\partial t} \right) = - \frac{D}{Dt} \left(\frac{\xi}{\bar{h}} \right) \ , \tag{6.27b}$$

and

$$(P_{22}' - P_{33}') + (\bar{P}_{22} - \bar{P}_{33}) \left(\frac{\xi}{\bar{h}} \right) = 0 \tag{6.28}$$

where the disturbance exists along the transverse direction as $\xi(t,x_2)$. Eqns. (6.27) and (6.28) can also be derived by limiting the disturbances in the 2-3 plane, i.e., v_1' is zero in Eqn. (6.6) and making force balance along the "2" direction similar to Eqn. (6.11).

For a Newtonian fluid sheet the growth of disturbances is described by

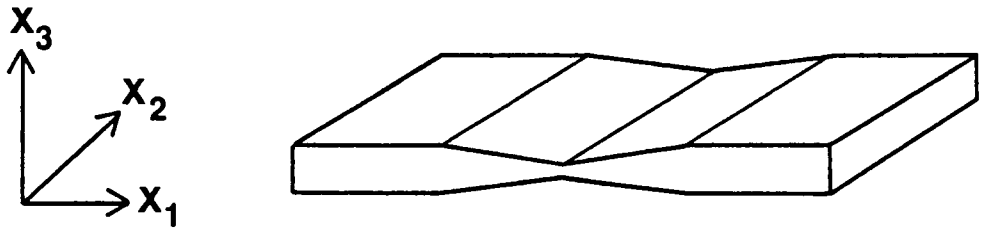

(a) Disturbances along the machine direction

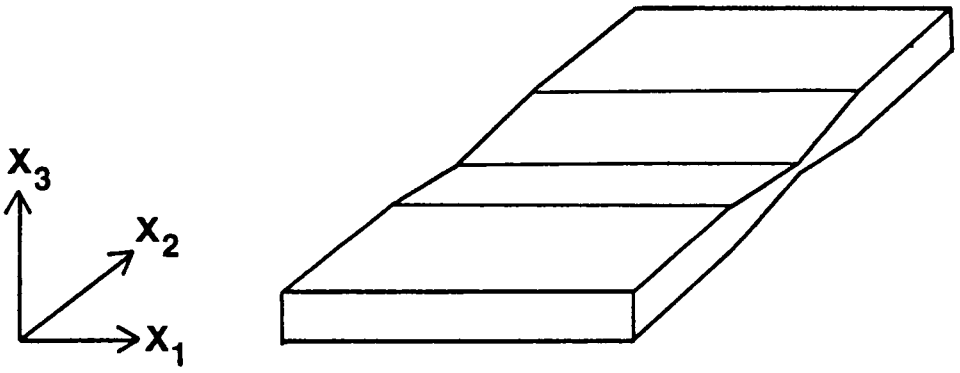

(b) Disturbances along the transverse direction

Figure 6.3. Disturbances in a stretched sheet.

$$\frac{\partial \hat{\xi}}{\partial t} + \frac{1}{2} E_1 \hat{\xi} = 0 \qquad (6.29a)$$

where

$$E_2 \leq 0, \; E_1 > 0 \qquad (6.29b)$$

or

$$0 \geq E_2/E_1 \geq - 0.5 \; . \qquad (6.29c)$$

One notes that Eqn. (6.29a) is the equation which represents the growth of disturbances, that is, in the cross-section of the 2-3 plane or $\xi(t,x_2)$. Consequently, the applied restriction on the kinematics can be expressed as:

$$E_1 > 0, \; E_2/E_1 \geq - 0.5 \; , \qquad (6.30)$$

because there is not any reason to apply Eqn. (6.29b) or (6.29c) from a mathematical point of view. However, once the ratio of elongation rate E_2/E_1 exceeds zero, the growth of disturbances may be expressed by letting the "2" direction be the "machine direction." This case has been already described in Sections B-2, B-3, and B-4. The consideration of disturbances being along the transverse direction $\xi(t,x_2)$ is necessary only when E_2/E_1 is less than unity.

The normalized disturbance, the elongation-to-break of films of length $L(t_b)$, length along the "1" direction, and area $A(t_b)$, area in the 1-2 plane, are given by

$$\frac{\hat{\xi}(t)/\bar{h}(t)}{\hat{\xi}(0)/\bar{h}(0)} = \exp\left[\left(\frac{1}{2} + E_2/E_1\right)E_1 t\right] , \tag{6.31a}$$

$$\frac{L(t_b)}{L(0)} = \exp\left[\left(\frac{2}{1 + 2E_2/E_1)}\right) \ell n \frac{\bar{h}(0)}{\hat{\xi}(0)}\right] . \tag{6.31b}$$

$$\frac{A(t_b)}{A(0)} = \exp\left[\left[1 + \frac{1}{(1 + 2E_2/E_1)}\right] \ell n \frac{\bar{h}(0)}{\hat{\xi}(0)}\right] , \tag{6.31c}$$

where

$$E_1 \geq 0 \text{ and } 1.0 \geq E_2/E_1 \geq -0.5 . \tag{6.31d}$$

The limitation on the kinematics given by Eqn. (6.31d) has to again be noted. Eqn. (6.31) suggests that the disturbance along the transverse direction, $\xi(t,x_2)$, is less destabilizing than a disturbance along the machine direction, $\xi(t,x_1)$. Indeed, uniaxial elongation stretching never leads to failure with the transverse direction disturbance. Equal biaxial elongation conditions give the same elongation to break for disturbances both along the machine direction and along the transverse direction, if the magnitudes of the disturbances are the same.

In general, there exist disturbances both in the machine direction and in the transverse direction. If the magnitude of the disturbances in both directions are the same, the disturbances in the direction which have the highest strain rate are dominant, i.e., it may allow us to consider disturbances only in the direction which has the highest strain rate. If we define the "1" direction to be the

one with the highest strain rate, we need to consider the growth of disturbances only

$$1.0 \geq E_2/E_1 \geq -0.5 \ .$$

C. ELONGATION OF AN ANNULAR CYLINDER

C-1. Homogeneous Deformation

Consider the multiaxial elongational flow of an annular cylinder of radius R, annular thickness h, and length L (Figure 6.4). The velocity field is

$$v_z = v_z(z), \quad v_r = v_r(r), \quad v_\phi = cr \ , \tag{6.32a}$$

where c is a constant (for elongational flow c is zero). The deformation rate tensor is

$$\underset{\sim}{d}(z,\phi,r) = \begin{vmatrix} \frac{\partial v_z}{\partial z} & 0 & 0 \\ 0 & \frac{v_r}{r} & 0 \\ 0 & 0 & \frac{\partial v_r}{\partial r} \end{vmatrix} \ . \tag{6.32b}$$

On the inner surface of the annulus, v_r is zero, and on the outer surface $v_r = Dh/Dt$, so that, neglecting the variation of $\partial v_r/\partial r$ with r by assuming that the thickness h is small compared with other dimensions of the annulus (i.e., $h << R$), we obtain

$$d_{rr} = \frac{\partial v_r}{\partial r} = \frac{1}{h}\frac{Dh}{Dt} = \frac{1}{h}\frac{dh}{dt} \ . \tag{6.33a}$$

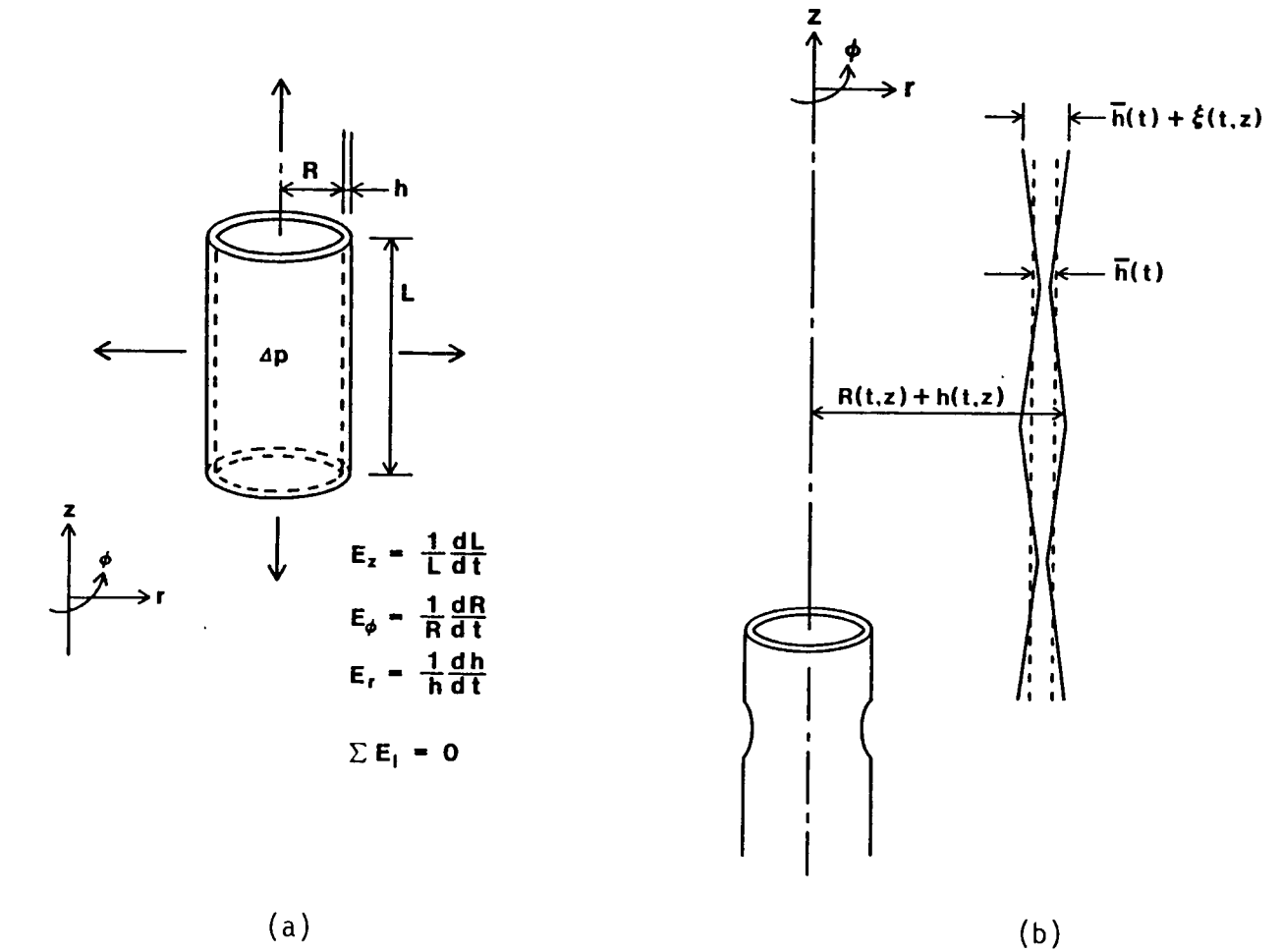

Figure 6.4. (a) Elongational flow of an annular cylinder; (b) disturbances in a stretched annular cylinder.

Also, by neglecting the variation of $\partial v_z/\partial z$ with z, we have

$$d_{zz} = \frac{\partial v_z}{\partial z} = \frac{1}{L}\frac{dL}{dt} . \tag{6.33b}$$

Similarly, we obtain

$$d_{\phi\phi} = \frac{v_r}{r} = \frac{1}{R}\frac{dR}{dt} . \tag{6.33c}$$

We may write

$$E_z = \frac{1}{L}\frac{dL}{dt}, \quad E_\phi = \frac{1}{R}\frac{dR}{dt}, \quad E_r = \frac{1}{h}\frac{dh}{dt} . \tag{6.34}$$

From the continuity equation, we have

$$E_z + E_\phi + E_r = 0 . \tag{6.35}$$

Various possibilities for the deformation exist. For uniaxial extension of an annular cylinder

$$\frac{1}{R}\frac{dR}{dt} = \frac{1}{h}\frac{dh}{dt} < 0 \text{ or } E_r = E_\phi = -\frac{1}{2}E_z < 0 . \tag{6.36a}$$

For inflation of an annular cylinder

$$\frac{1}{L}\frac{dL}{dt} = 0, \quad \frac{1}{R}\frac{dR}{dt} = -\frac{1}{h}\frac{dh}{dt} > 0$$

or

$$E_z = 0, \quad E_\phi = -E_r > 0 . \tag{6.36b}$$

For simultaneous drawdown and inflation

$$\frac{1}{L}\frac{dL}{dt} > 0, \quad \frac{1}{R}\frac{dR}{dt} > 0, \quad \frac{1}{h}\frac{dh}{dt} > 0 \ ,$$

or

$$E_z > 0, \quad E_\phi > 0, \quad E_r = -(E_z + E_\phi) \ . \tag{6.36c}$$

We consider force F_z to be applied in the "z" direction to the annulus and an internal pressure Δp to the annulus (Figure 6.4). The force balances may be expressed from simple membrane theory [F-8, L-10] by neglecting gravity and inertia

$$F_z = 2\pi R h \sigma_{zz} = A\sigma_{zz} \ , \tag{6.37a}$$

$$\frac{h}{R}\sigma_{\phi\phi} = \Delta p \ . \tag{6.37b}$$

C-2. Newtonian Fluid Annular Cylinders: Stable Flow

The stable deformation of a Newtonian fluid cylinder annulus, to which is applied a force F_z and a bubble pressure difference Δp will now be considered. The stress field is

$$\sigma_{zz} = -p + 2\eta\frac{\partial v_z}{\partial z} = -p + 2\eta\frac{1}{L}\frac{dL}{dt} \ , \tag{6.38a}$$

$$\sigma_{\phi\phi} = -p + 2\eta\frac{v_r}{r} = -p + 2\eta\frac{1}{R}\frac{dR}{dt} \ , \tag{6.38b}$$

$$\sigma_{rr} = -p + 2\eta\frac{\partial v_r}{\partial r} = -p + 2\eta\frac{1}{h}\frac{dh}{dt} \ . \tag{6.38c}$$

The boundary condition is

$$\sigma_{rr} = - p + 2\eta \frac{1}{h} \frac{dh}{dt} = 0 \ , \tag{6.39a}$$

$$p = 2\eta \frac{1}{h} \frac{dh}{dt} \ . \tag{6.39b}$$

The applied tension and pressure may be written from Eqn. (6.37)

$$F_z = 2\pi Rh2\eta(2 + \kappa) \frac{1}{L} \frac{dL}{dt} \ , \tag{6.40a}$$

$$\Delta p = \frac{h}{R} 2\eta\left(2 + \frac{1}{\kappa}\right) \frac{1}{R} \frac{dR}{dt} \ , \tag{6.40b}$$

where we have written:

$$\frac{1}{R} \frac{dR}{dt} = \kappa\left(\frac{1}{L} \frac{dL}{dt}\right) \ . \tag{6.40c}$$

For uniaxial extension of an annulus cylinder

$$\frac{1}{R} \frac{dR}{dt} = \frac{1}{h} \frac{dh}{dt}, \ \kappa = - \frac{1}{2} \ , \tag{6.41a}$$

$$F_z = 2\pi Rh3\eta \frac{1}{L} \frac{dL}{dt} = 6\pi Rh\eta \frac{1}{L} \frac{dL}{dt} \ , \tag{6.41b}$$

$$\Delta p = 0 \ . \tag{6.41c}$$

For the inflation of an annular cylinder

$$\frac{1}{R} \frac{dR}{dt} = - \frac{1}{h} \frac{dh}{dt}, \ \kappa \to \infty \ , \tag{6.42a}$$

$$F_z = 0 \ , \tag{6.42b}$$

$$\Delta p = 4\eta \frac{h}{R^2} \frac{dR}{dt} . \tag{6.42c}$$

C-3. Growth of Disturbances: Disturbances Along the Machine Direction

We now consider the influence of disturbances on the flow of an annulus cylinder. We write

$$\underset{\sim}{v} = \overline{\underset{\sim}{v}} + \underset{\sim}{v}' , \tag{6.43a}$$

with disturbances

$$h = \overline{h} + \xi, \; R = \overline{R} + R' . \tag{6.43b}$$

In this section, we will neglect the R' disturbance and also assume the axisymmetric condition

$$\frac{\partial}{\partial \phi} = 0 . \tag{6.44}$$

We may write:

$$d_{rr} = \frac{\partial v_r}{\partial r} = \frac{1}{(\overline{h} + \xi)} \frac{D}{Dt} (\overline{h} + \xi) . \tag{6.45a}$$

After linearization this becomes:

$$\frac{\partial v_r}{\partial r} = \frac{1}{\overline{h}} \frac{\partial \overline{h}}{\partial t} + \frac{1}{\overline{h}} \frac{D\xi}{Dt} - \frac{\xi}{\overline{h}^2} \frac{\partial \overline{h}}{\partial t} . \tag{6.45b}$$

Similarly

$$d_{\phi\phi} = \frac{v_r}{r} = \frac{1}{R} \frac{\partial R}{\partial t} . \tag{6.46}$$

From the continuity equation, we must have

$$\frac{\partial v'_z}{\partial z} + \frac{1}{\bar{h}} \frac{D\xi}{dt} - \frac{\xi}{\bar{h}^2} \frac{\partial \bar{h}}{\partial t} = 0 \ , \tag{6.47a}$$

or

$$E'_z = \frac{\partial v'_z}{\partial z} \ ,$$

$$E'_\phi = 0 \ , \tag{6.47b}$$

$$E'_r = \frac{1}{\bar{h}} \frac{D\xi}{dt} - \frac{\xi}{\bar{h}^2} \frac{\partial \bar{h}}{\partial t} = \frac{D}{Dt} \left(\frac{\xi}{\bar{h}} \right) \ .$$

If we introduce a disturbance $\xi(z)$ into the annular cylinder, we may write

$$A = \bar{A} + A', \ \sigma_{zz} = \bar{\sigma}_{zz} + \sigma'_{zz} \ , \tag{6.48a}$$

where

$$\bar{A} = 2\pi R\bar{h}, \ A' = 2\pi R\xi \ . \tag{6.48b}$$

The perturbed force balance is

$$\bar{A}\sigma'_{zz} + A'\bar{\sigma}_{zz} = 0 \ . \tag{6.49}$$

Introducing Eqn. (6.48) into Eqn. (6.49) leads to

$$\sigma'_{zz} + \bar{\sigma}_{zz} \left(\frac{\xi}{\bar{h}} \right) = 0 \ , \tag{6.50a}$$

or

$$(P'_{zz} - P'_{rr}) + (\bar{P}_{zz} - \bar{P}_{rr}) \left(\frac{\xi}{\bar{h}} \right) = 0 \ . \tag{6.50b}$$

The perturbed conservation equations, the governing equations for the growth of disturbance of an annular cylinder, Eqns. (6.47) and (6.50), are essentially the same as the case of a flat film being stretched. Here, the "z" direction and the "r" direction can be taken as the "1" direction or the machine direction and the "3" direction or the free surface direction in Section B in this chapter, respectively. We can expect exactly the same growth of disturbances in cylindrical annuli shapes as in flat sheet shapes; in the latter case, one presumes that the disturbances are along the machine direction.

For a Newtonian fluid the perturbed stresses are

$$\sigma'_{zz} = 2\eta\left(\frac{\partial v'_z}{\partial z} - \frac{\partial v'_r}{\partial r}\right) , \tag{6.51a}$$

$$\sigma'_{\phi\phi} = 2\eta\left(\frac{v'_r}{r} - \frac{\partial v'_r}{\partial r}\right) . \tag{6.51b}$$

Taking v'_r as zero (neglecting variation of radius R) and introducing Eqn. (6.47) into Eqn. (6.51a) gives

$$\sigma'_{zz} = 4\eta\left(-\frac{1}{\bar{h}}\frac{D\xi}{Dt} + \frac{\xi}{\bar{h}^2}\frac{\partial \bar{h}}{\partial t}\right) . \tag{6.52}$$

From Eqns. (6.34), (6.38), (6.50), and (6.52)

$$\frac{D\xi}{Dt} + \frac{1}{2}E_\phi \xi = 0 . \tag{6.53}$$

By assuming the disturbances are periodic along the "z" direction

which is similar to Eqn. (6.18) and constant strain rate deformation. Eqn. (6.53) can be written as

$$\frac{1}{\hat{\xi}} \frac{\partial \hat{\xi}}{\partial t} = - \frac{1}{2} E_\phi = - \frac{1}{2} \left(\frac{E_\phi}{E_z} \right) E_z \ , \tag{6.54}$$

which has the solution

$$\hat{\xi}(t) = \hat{\xi}(0) \exp[- \tfrac{1}{2}(E_\phi/E_2)E_z t] \ . \tag{6.55}$$

For uniaxial deformation

$$\hat{\xi}(t) = \hat{\xi}(0) \exp[\tfrac{1}{4} E_z t] \ . \tag{6.56a}$$

For planar extension

$$\hat{\xi}(t) = \hat{\xi}(0) \ , \tag{6.56b}$$

while, for equal biaxial extension,

$$\hat{\xi}(t) = \hat{\xi}(0) \exp[- \tfrac{1}{2} E_z t] \ . \tag{6.56c}$$

This has the same form as for the planar sheet.

C-4. Growth of Disturbances: Disturbances Along the Hoop Direction

In previous sections we have described the growth of disturbances of annular cylinders which have disturbances along the "z" direction. We now turn our attention to the effects of disturbances along the hoop direction of the annuli.

The introduced disturbance is

$$\underset{\sim}{v} = \overline{\underset{\sim}{v}} + \underset{\sim}{v}' \tag{6.57a}$$

$$h = \overline{h} + \xi(t,\phi) \tag{6.57b}$$

$$R = \overline{R} + R' \tag{6.57c}$$

and

$$\frac{\partial}{\partial z} = 0 \ . \tag{6.57d}$$

We again neglect R' disturbances (i.e., $R = \overline{R}(t)$). We may write deformation rates as

$$d_{rr} = \frac{\partial v_r}{\partial r} = \frac{1}{(\overline{h} + \xi)} \frac{D}{Dt} (\overline{h} + \xi) \ . \tag{6.58a}$$

After linearization this becomes:

$$\frac{\partial v_r}{\partial r} = \frac{1}{\overline{h}} \frac{\partial \overline{h}}{\partial t} + \frac{1}{\overline{h}} \frac{D\xi}{Dt} - \frac{\xi}{\overline{h}^2} \frac{\partial \overline{h}}{\partial t} \ . \tag{6.58b}$$

Similarly

$$d_{zz} = \frac{\partial v_z}{\partial z} = \frac{1}{L} \frac{dL}{dt} \ , \tag{6.59}$$

$$d_{\phi\phi} = \frac{v_r}{r} + \frac{1}{r} \frac{\partial v_\phi}{\partial \phi} = \frac{1}{R} \frac{dR}{dt} + \frac{1}{r} \frac{\partial v'_\phi}{\partial \phi} \ . \tag{6.60}$$

From the continuity equation, we have

$$\frac{1}{R}\frac{\partial v'_\phi}{\partial \phi} + \frac{1}{\bar{h}}\frac{D\xi}{Dt} - \frac{\xi}{\bar{h}^2}\frac{\partial \bar{h}}{\partial t} = 0 \tag{6.61a}$$

or

$$E'_z = 0 \ ,$$

$$E'_\phi = \frac{1}{r}\frac{\partial v'_\phi}{\partial \phi} + \frac{\partial v'_r}{r} \ , \tag{6.61b}$$

$$E'_r = \frac{1}{\bar{h}}\frac{D\xi}{Dt} - \frac{\xi}{\bar{h}^2}\frac{\partial \bar{h}}{\partial t} = \frac{D}{Dt}\left(\frac{\xi}{\bar{h}}\right) \ .$$

Force balances may be expressed with the aid of classical membrane theory [F-8,L-10] by neglecting gravity and inertia

$$\sigma_{\phi\phi}\, h = R\, \Delta p \tag{6.62a}$$

$$\frac{\partial}{\partial z}\left(\sigma_{zz}\, hR\right) = 0 \ . \tag{6.62b}$$

The perturbed force balance equation is given by combining Eqns. (6.57) and (6.62a). After linearization we have

$$\sigma'_{\phi\phi} + \bar{\sigma}_{\phi\phi}\left(\frac{\xi}{\bar{h}}\right) = 0 \tag{6.63a}$$

or

$$(P'_{\phi\phi} - P'_{rr}) + (\bar{P}_{\phi\phi} - \bar{P}_{rr})\left(\frac{\xi}{\bar{h}}\right) 0 \ . \tag{6.63b}$$

For a Newtonian fluid the perturbed stress is

$$\sigma'_{\phi\phi} = 2\eta\left(\frac{1}{r}\frac{\partial v'}{\partial \phi} - \frac{\partial v'_r}{\partial r}\right) \ . \tag{6.64}$$

Taking v_r' as zero (neglecting variation of radius R) and introducing Eqn. (6.61) into Eqn. (6.64) gives

$$\sigma'_{\phi\phi} = 4\eta \left(- \frac{1}{\bar{h}} \frac{D\xi}{Dt} + \frac{\xi}{\bar{h}^2} \frac{\bar{h}}{t} \right) . \tag{6.65}$$

From Eqns. (6.35), (6.39), (6.63), and (6.65)

$$\frac{D\xi}{Dt} + \frac{1}{2} E_z \xi = 0 , \tag{6.66}$$

where

$$\frac{D\xi(\phi)}{Dt} = \frac{\partial \xi(\phi)}{\partial t} + \bar{v}_z \frac{\partial \xi(\phi)}{\partial z} + \bar{v}_r \frac{\partial \xi(\phi)}{\partial r} + \frac{\bar{v}_\phi}{r} \frac{\partial \xi(\phi)}{\partial \phi} = \frac{\partial \xi}{\partial t} . \tag{6.67}$$

Therefore, Eqn. (6.66) leads us to

$$\frac{1}{\xi} \frac{\partial \xi}{\partial t} = - \frac{1}{2} \left(\frac{E_z}{E} \right) E_\phi , \tag{6.68}$$

which has the solution

$$\xi(t) = \xi(0) \exp \left[- \frac{1}{2} \left(\frac{E_z}{E_\phi} \right) E_\phi t \right] . \tag{6.69}$$

Eqns. (6.68) and (6.69) have the same characteristic behavior as we have previously described in Section B-5 in this chapter.

C-5. The Effect of the Variation of Radius: Disturbances Along the Machine Direction

We have assumed annuli with constant radius R during deformation. It might be more useful to include the diameter variation along the

machine direction ("z" direction) with film thickness h being varied as $\xi(t,z)$, $h(t,z) = \bar{h}(t) + \xi(t,z)$.

We shall assume the annular thickness h to be small compared with other dimensions of the cylindrical annulus and its radii of curvature (i.e., $h << R$). This will permit us to approximate the curved film by a plane film, the velocity gradients to be approximated locally by those of a plane film extended multiaxially. The cylindrical coordinates (z, ϕ, r) are related to the local Cartesian coordinates (ν_1, ν_2, ν_3) at a point p in the film where ν_1 is in the "z" direction. However, ν_1 is parallel to the film, ν_2 in the hoop direction, and ν_3 normal to the film (Figure 6.5). The origin p is taken on the inner surface, then ν_3-axis meets the outer surface at ν_3 of h.

Let (v_1, v_2, v_3) be the velocity components in the coordinates (ν_1, ν_2, ν_3). The deformation rate is

$$d_{ij}(\nu_1,\nu_2,\nu_3) = \frac{1}{2}\left[\frac{\partial v_i}{\partial \nu_j} + \frac{\partial v_j}{\partial \nu_i}\right] \tag{6.70}$$

where i or j may be "1", "2", or "3".

On the inner surface, v_3 is zero and at the outer surface $v_3 = Dh/Dt$, so that, neglecting the variation of $\partial v_3/\partial \nu_3$ with ν_3, we obtain

$$d_{33} = \frac{\partial v_3}{\partial \nu_3} = \frac{1}{h}\frac{Dh}{Dt} . \tag{6.71a}$$

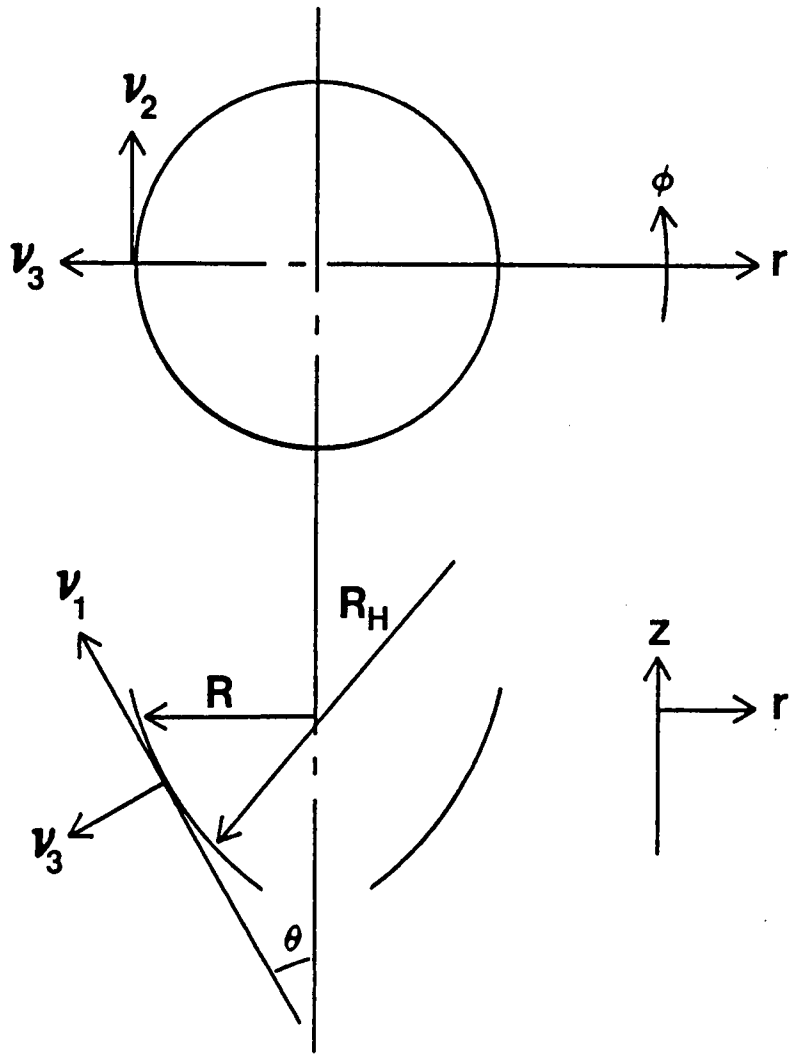

Figure 6.5. Coordinate system: sectional plane and elevation of a portion of an annular film.

Similarly, using the axisymmetry condition and the relation $v_2 = r \tan \phi$, we have

$$d_{22} = \frac{\partial v_2}{\partial v_2} = \frac{1}{R} \frac{DR}{Dt} . \tag{6.71b}$$

We may write

$$E_1 = \frac{\partial v_1}{\partial v_1}, \quad E_2 = \frac{1}{R} \frac{DR}{Dt}, \quad E_3 = \frac{1}{h} \frac{Dh}{Dt} . \tag{6.72}$$

From the continuity equation, we have

$$E_1 + E_2 + E_3 = 0 . \tag{6.73}$$

Treating R and h as functions of z, and using

$$\frac{\partial z}{\partial v_1} = \cos \theta , \tag{6.74a}$$

and

$$\frac{Dv_1}{Dt} = v_1(1 + \sec \theta) , \tag{6.74b}$$

we obtain instead of Eqn. (6.72)

$$d_{11} = E_1 = \cos \theta \frac{\partial v_1}{\partial z} , \tag{6.75a}$$

$$d_{22} = E_2 = \frac{1}{R}\left(\frac{\partial R}{\partial t} + v_1 \cos \theta \frac{\partial R}{\partial z}\right), \tag{6.75b}$$

$$d_{33} = E_3 = \frac{1}{h}\left(\frac{\partial h}{\partial t} + v_1 \cos \theta \frac{\partial h}{\partial z}\right) . \tag{6.75c}$$

Force balances may be expressed from the classical membrane theory [F-1,L-10] by neglecting gravity and inertia

$$\frac{\partial}{\partial z}\left(\sigma_M\, hR\cos\theta\right) = \Delta pR\tan\theta\ , \tag{6.76a}$$

$$\frac{\sigma_M\, h}{R_M} + \frac{\sigma_H\, h}{R_H} = \Delta p\ , \tag{6.76b}$$

$$\frac{\partial}{\partial \phi}\left(\sigma_H\, h\right) = 0\ , \tag{6.76c}$$

where

$$\sigma_M = \sigma_{\nu_1\nu_1}\ ,\quad \sigma_H = \sigma_{\nu_2\nu_2}\ , \tag{6.77a}$$

$$R_H = R\sec\theta\ , \tag{6.77b}$$

$$R_M = -\sec\theta/\frac{\partial\theta}{\partial z}\ . \tag{6.77c}$$

The disturbances which are applied here are only functions of "z" or "ν_1". The annular thickness varies as

$$h(t,z) = \overline{h}(t) + \xi(t,z)\ , \tag{6.78a}$$

which results

$$\begin{aligned} \underset{\sim}{v} &= \overline{\underset{\sim}{v}} + \underset{\sim}{v}'\ , \\ \underset{\sim}{\sigma} &= \overline{\underset{\sim}{\sigma}} + \underset{\sim}{\sigma}'\ , \\ R &= \overline{R} + R'\ , \\ \theta &= \overline{\theta} + \theta'\ . \end{aligned} \tag{6.78b}$$

It might be possible to make further assumptions such as

$$\frac{\partial R}{\partial z} = \frac{\partial(\bar{R}+R')}{\partial z} = \frac{\partial R'}{\partial z} = \tan\theta' \ . \tag{6.79a}$$

This leads to:

$$\bar{\theta} = 0 \ . \tag{6.79b}$$

We may write

$$d_{11} = \cos\theta \frac{\partial v_1}{\partial z} = \frac{\partial \bar{v}_1}{z} + \frac{\partial v_1'}{\partial z} - \sin\theta' \frac{\partial \bar{v}_1}{\partial z} \ . \tag{6.80a}$$

After linearization this becomes:

$$d_{11} = \frac{\partial \bar{v}_1}{\partial z} + \frac{\partial v_1'}{\partial z} - \theta' \frac{\partial \bar{v}_1}{\partial z} = \frac{1}{L}\frac{dL}{dt} + \frac{\partial v_1'}{\partial z} - \frac{\partial R'}{\partial z}\frac{\partial \bar{v}_1}{\partial z} \ . \tag{6.80b}$$

Similarly:

$$d_{22} = \frac{1}{R}\left(\frac{\partial R}{\partial t} + v_1 \cos\theta \frac{\partial R}{\partial z}\right) = \frac{1}{\bar{R}}\frac{\partial \bar{R}}{\partial t} + \frac{1}{\bar{R}}\left(\frac{\partial R'}{\partial t} + \bar{v}_1 \frac{\partial R'}{\partial z} - \frac{R'}{\bar{R}}\frac{\partial \bar{R}}{\partial t}\right) , \tag{6.81}$$

$$d_{33} = \frac{1}{h}\left(\frac{\partial h}{\partial t} + v_1 \cos\theta \frac{\partial h}{\partial z}\right) = \frac{1}{\bar{h}}\frac{\partial \bar{h}}{\partial t} + \frac{1}{\bar{h}}\left(\frac{\partial \xi}{\partial t} + \bar{v}_1 \frac{\partial \xi}{\partial z} - \frac{\xi}{\bar{h}}\frac{\partial \bar{h}}{\partial t}\right) \ . \tag{6.82}$$

From the continuity equation, we have

$$\left(\frac{\partial v_1'}{\partial z} - \frac{\partial R'}{\partial z}\frac{\partial \bar{v}_1}{\partial z}\right) + \frac{1}{\bar{R}}\left(\frac{\partial R'}{\partial t} + \bar{v}_1 \frac{\partial R'}{\partial z} - \frac{R'}{\bar{R}}\frac{\partial \bar{R}}{\partial t}\right)$$

$$+ \frac{1}{\bar{h}}\left(\frac{\partial \xi}{\partial t} + \bar{v}_1 \frac{\partial \xi}{\partial z} - \frac{\xi}{\bar{h}}\frac{\partial \bar{h}}{\partial t}\right) = 0 \ , \tag{6.83a}$$

or

$$E_1' = \frac{\partial v_1'}{\partial z} - \frac{\partial R'}{\partial z}\frac{\partial \bar{v}_1}{\partial z} ,$$

$$E_2' = \frac{1}{\bar{R}}\left(\frac{\partial R'}{\partial t} + \bar{v}_1 \frac{\partial R'}{\partial z} - \frac{R'}{\bar{R}}\frac{\partial \bar{R}}{\partial t}\right) , \tag{6.83b}$$

$$E_3' = \frac{1}{\bar{h}}\left(\frac{\partial \xi}{\partial t} + \bar{v}_1 \frac{\partial \xi}{\partial z} - \frac{\xi}{\bar{h}}\frac{\partial \bar{h}}{\partial t}\right) .$$

and

$$E_1 = \frac{1}{L}\frac{dL}{dt}, \quad E_2 = \frac{1}{\bar{R}}\frac{\partial \bar{R}}{\partial t}, \quad E_3 = \frac{1}{\bar{h}}\frac{\partial \bar{h}}{\partial t} . \tag{6.84}$$

The perturbed force balance equation is given by combining Eqns. (6.76), (6.77), (6.78), and (6.79). After linearization we have

$$\bar{R}\,\bar{h}\,\sigma_M' + \bar{R}\,\xi\,\bar{\sigma}_M + R'\,\bar{h}\,\bar{\sigma}_M - \bar{R}\,\bar{h}\,\bar{\sigma}_M\frac{\partial R'}{\partial z} - R'\,\bar{h}\,\bar{\sigma}_H = 0 . \tag{6.85}$$

For a Newtonian fluid, the stresses are

$$\bar{\sigma}_M = 2\eta(E_1 - E_3) = 2\eta(-E_2 - 2E_3) , \tag{6.86a}$$

$$\bar{\sigma}_H = 2\eta(E_2 - E_3) , \tag{6.86b}$$

$$\bar{\sigma}_M' = 2\eta(E_1' - E_3') = 2\eta(-E_2' - 2E_3') . \tag{6.86c}$$

Introducing Eqns. (6.83b) and (6.84) into Eqn. (6.86) gives

$$\bar{\sigma}_M = -2\eta\left(\frac{1}{\bar{R}}\frac{\partial \bar{R}}{\partial t} + \frac{2}{\bar{h}}\frac{\partial \bar{h}}{\partial t}\right) , \tag{6.87a}$$

$$\bar{\sigma}_H = 2\eta\left(\frac{1}{\bar{R}}\frac{\partial \bar{R}}{\partial t} - \frac{1}{\bar{h}}\frac{\partial \bar{h}}{\partial t}\right) , \tag{6.87b}$$

$$\sigma'_M = 2\eta \left[\frac{1}{\bar{R}} \left(\frac{\partial R'}{\partial t} + \bar{v}_1 \frac{\partial R'}{\partial z} - \frac{R'}{\bar{R}} \frac{\partial \bar{R}}{\partial t} \right) - \frac{1}{\bar{h}} \left(\frac{\partial \xi}{\partial t} + \bar{v}_1 \frac{\partial \xi}{\partial z} - \frac{\xi}{\bar{h}} \frac{\partial \bar{h}}{\partial t} \right) \right] . \tag{6.87c}$$

From Eqns. (6.85), (6.87), and (6.84)

$$\frac{1}{\bar{R}} \frac{DR'}{Dt} + \frac{2}{\bar{h}} \frac{D\xi}{Dt} - \left[\frac{R'}{\bar{R}} - \kappa \frac{\xi}{\bar{h}} - (2 + \kappa) \frac{\partial R'}{\partial z} \right] E_1 = 0 . \tag{6.88}$$

where

$$\frac{D}{Dt} = \frac{\partial}{\partial t} + \bar{v}_1 \frac{\partial}{\partial z} , \tag{6.89a}$$

$$E_1 = \frac{\partial \bar{v}_1}{\partial z} = \frac{1}{L} \frac{dL}{dt} = - \frac{1}{\bar{R}} \frac{\partial \bar{R}}{\partial t} - \frac{1}{\bar{h}} \frac{\partial \bar{h}}{\partial t} , \tag{6.89b}$$

$$\kappa = \frac{1}{\bar{R}} \frac{\partial \bar{R}}{\partial t} \Big/ \frac{1}{L} \frac{dL}{dt} . \tag{6.89c}$$

To solve Eqn. (6.88), it is necessary to have a relationship between ξ and R'. The total volume of V of the annular cylinder is

$$V = 2\pi \int_0^{L(t)} (\bar{R} + R')(\bar{h} + \xi)(1 + \frac{\partial R'}{\partial z}) dz \tag{6.90}$$

From the continuity equation, Eqn. (6.90) can be rewritten as:

$$\frac{\partial}{\partial t} \int_0^{L(t)} (\bar{R}\xi + R' \bar{h} + \bar{R} \bar{h} \frac{\partial R'}{\partial z}) dz = 0 . \tag{6.91}$$

By assuming the thickness variation is periodic along the "z" direction, which is similar to Eqn. (6.18), and under constant strain rate deformation, we have

$$\frac{D\xi}{Dt} = \frac{D\hat{\xi}e^{ikz}}{Dt} = e^{ikz}\,\frac{\partial\hat{\xi}}{\partial t}\,. \tag{6.92}$$

We may write the diameter variation R' as:

$$R' = \hat{R}(t)\, f(t,z)\,, \tag{6.93a}$$

where

$$\hat{R}(t = 0) = 0\,, \tag{6.93b}$$

$$f(t,\, z = 0) = f(t,\, z = L(t)) = 0\,. \tag{6.93c}$$

And also

$$\begin{aligned} L(t) &= L(0)\,\exp(E_1 t)\,, \\ \overline{R}(t) &= \overline{R}(0)\,\exp(E_2 t)\,, \\ \overline{h}(t) &= \overline{h}(0)\,\exp(E_3 t)\,. \end{aligned} \tag{6.94a,b,c}$$

Combining Eqns. (6.91), (6.92), (6.93), (6.94), and (6.73), we have

$$\begin{aligned} & e^{(2E_1+E_2)t}\left[e^{ik(0)L(0)} - 1\right]\left[\frac{\partial\hat{\xi}(t)}{\partial t} + (E_1 + 1)\hat{\xi}(t)\right] \\ & \quad + i\,\frac{k(0)\overline{h}(0)}{\overline{R}(0)}\,\hat{R}(t)\int_0^{L(t)}\frac{\partial f(t,z)}{\partial z}\,dz \\ & \quad + ik(0)L(0)\overline{h}(0)E_1\,e^{E_1 t}\,\frac{\partial f(t,\, L(t))}{\partial z} = 0\,. \end{aligned} \tag{6.95}$$

Similarly the disturbance growth equation, Eqn. (6.88), becomes by the help of Eqns. (6.92) and (6.93)

$$\frac{\hat{R}}{\bar{R}}\frac{Df(t,z)}{Dt} + \frac{f(t,z)}{\bar{R}} + 2\frac{e^{ikz}}{\bar{h}}\frac{\partial\hat{\xi}}{\partial t}$$

$$- \left[\frac{\hat{R}}{\bar{R}} f(t,z) - \kappa\frac{e^{ikz}}{\bar{h}}\hat{\xi} - (2+\kappa)\hat{R}\frac{\partial f(t,z)}{\partial z}\right] E_1 = 0 \ . \quad (6.96)$$

The disturbance growth of an axisymmetrical annulus of a Newtonian fluid is described by Eqns. (6.96) and (6.95). However, we have three unknowns with only two equations. Unless we have one more equation to represent the functionalities of f(t,z) based upon some physical picture, we cannot obtain a solution for this case.

We have been assuming infinitesimal disturbances in the thickness variation. Therefore, the radius variation is caused by the thickness distribution. These are secondary effects in the propagation of the disturbance growth.

D. SUMMARY

The growth of disturbances in sheets and annular cylinders undergoing multiaxial elongational flow has been described. The governing equations (force balance and continuity) are derived for two different disturbances, one along the machine direction and the other along the transverse (or hoop) direction. It is found that the governing equations for flat sheets and annular cylinders are essentially the same. Detailed analyses are given for a Newtonian fluid undergoing constant stretch rates. Disturbances in the highest strain rate direction dominate the stability of the system. When disturbances are in the machine direction, lateral (or hoop)

stretching of sheets decreases the size of the disturbances but at a less rapid rate than the homogeneous decrease in thickness. The elongation-to-break (limiting strain) in the machine direction is actually decreased. However, the relative stretched area at break increases with increasing strain rates in the transverse (or hoop) direction. Disturbances in the transverse (or hoop) direction cause to produce diametrically opposite effects in the disturbance growth and the elongation-to-break on the lateral stretching of sheets.

CHAPTER VII

MULTIAXIAL ELONGATIONAL FLOW OF VISCOELASTIC SHEETS: INVESTIGATION OF DEFECT GROWTH AND FAILURE

A. INTRODUCTION

Several of the most important polymer processing operations involve the deformation of melt streams in the absence of walls. Such processes, in which applied stresses act in the absence of walls, result the elongation of polymer melts. This includes uniaxial elongation for melt spinning and also multiaxial elongation for film casting, tubular blown film, thermoforming and blow molding.

One of the important problems associated with these operations is the influence of the rheological properties of the melt on the ability to form the desired products. This leads to the study of the instabilities which arise during the stretching of filaments, films, sheets, and annuli.

The characteristics of the failure of molten filaments during uniaxial stretching have been reported in experiments by Ide and White [I-1,I-2,I-3,I-4,W-17]. The growth of disturbances in viscoelastic fluid filaments have been investigated by Chang and Lodge [C-6] and by Ide and White [I-2,I-3,W-16]. In recent years, the authors' attention has increasingly been given to polymer processing operations involving the multiaxial stretching of sheets, films and

annuli. This has led us to concentrate on the stability of fluid sheets. There has been few basic investigations of this problem for viscoelastic materials. Indeed, the only one closely related study that we are aware of is that of White [W-13], carried out several years ago.

In the previous chapter, we have described the growth of disturbances in Newtonian fluid sheets and annular cylinders. It is found that the growth of disturbances in planar sheets and in annuli has been described by the same governing equations (continuity and force balance equations) and disturbances along the machine direction make the system more unstable than along the transverse direction. Lateral stretching of sheets decreases the elongation-to-break (in the machine direction).

It is our purpose in this chapter to present theoretical and experimental investigations of the stability of extensional sheets of viscoelastic fluids undergoing multiaxial elongation.

B. HOMOGENEOUS DEFORMATION OF FLUID SHEETS

B-1. Kinematics

Consider the steady state elongational flow of a fluid sheet having constant thickness h. A "1, 2, 3" cartesian coordinate system embedded in the sheet, with "3" normal to the sheet and "1" and "2" in the direction of stretch; the "1" direction is taken as the machine direction. The strain rate in the "j" direction is given as E_j. Details on the kinematics have already been described in Chapter VI, Section B-1.

B-2. Constitutive Equation

The use of integral constitutive equations, involving a spectrum of relaxation times, is required to quantitatively analyze rheological properties or behavior of polymer melts. However, integral constitutive equations are too complex to apply usefully to analyze the growth of disturbances in deforming viscoelastic fluid sheets. It is necessary to use a constitutive equation which has sufficient complexity to qualitatively represent all the features of viscoelastic behavior, yet is simple enough to be applicable to a problem of the type being considered. We propose that the convected Maxwell model is the most useful constitutive equation for such applications. This has the form [D-2,I-2,I-3,M-42,W-17,W-20]

$$\underset{\sim}{\sigma} = -p\underset{\sim}{I} + \underset{\sim}{P} , \tag{7.1a}$$

$$\underset{\sim}{P} = 2\,\tau\,G\,\underset{\sim}{d} - \tau\,\frac{\delta \underset{\sim}{P}}{\delta t} , \tag{7.1b}$$

where $\delta\underset{\sim}{P}/\delta t$ is the contravariant convected derivative defined by

$$\frac{\delta \underset{\sim}{P}}{\delta t} = \frac{D\underset{\sim}{P}}{Dt} - \underset{\sim}{P} \cdot \nabla\underset{\sim}{v} - \nabla\underset{\sim}{v} \cdot \underset{\sim}{P} . \tag{7.1c}$$

Generally the relaxation time τ is considered to depend on the deformation rate in order to predict non-Newtonian viscosity and uniaxial elongational flow behavior observed in different melts [I-3,I-4,M-42]. This will be taken to be form [I-3,W-17]

$$\tau = \frac{\tau_0}{1 + a\,\tau_0\,II_d^{1/2}} \tag{7.2}$$

where II_d is the second invariant of $\underset{\sim}{d}$, which we take as $2\,tr\,\underset{\sim}{d}^2$.

In simple shear flow, the long duration asymptotic stress field is predicted to be of form

$$\sigma_{12} = G\,\tau\,\dot{\gamma} \tag{7.3a}$$

$$N_1 = \sigma_{11} - \sigma_{22} = 2\,G\,\tau^2\,\dot{\gamma}^2 \tag{7.3b}$$

$$N_2 = \sigma_{22} - \sigma_{33} = 0 \tag{7.3c}$$

with τ from Eqn. (7.2) being

$$\tau = \frac{\tau_0}{1 + a\,\tau_0\,\dot{\gamma}} \tag{7.4}$$

The deformation rate dependence of τ through Eqns. (7.2) and (7.4) defines the non-Newtonian shear viscosity in this model.

B-3. Stable Elongational Flow

For a multiaxial elongational flow of constant strain E_i, Eqn. (7.1b) takes the form

$$P_{11} = 2\,G\,\tau\,E_1 - \tau\left(\frac{\partial P_{11}}{\partial t} - 2E_1\,P_{11}\right), \tag{7.5a}$$

$$P_{22} = 2\,G\,\tau\,E_2 - \tau\left(\frac{\partial P_{22}}{\partial t} - 2E_2\,P_{22}\right), \tag{7.5b}$$

$$P_{33} = 2\,G\,\tau\,E_3 - \tau\left(\frac{\partial P_{33}}{\partial t} - 2E_3\,P_{33}\right). \tag{7.5c}$$

In biaxially stretched sheet, this is subject to the boundary condition

$$\sigma_{33} = - p + P_{33} = 0 \ . \tag{7.6}$$

If we take as an initial condition that the sheet is in virgin condition at time t = 0, Eqns. (7.5) with (7.6) may be solved to yield

$$\sigma_{jj}(t) = P_{jj} - P_{33} = \frac{2G\tau E_j}{1-2\tau E_j}\left(1 - e^{-(1-2\tau E_j)\frac{t}{\tau}}\right) - \frac{2G\tau E_3}{1-2\tau E_3}\left(1 - e^{-(1-2\tau E_3)\frac{t}{\tau}}\right)$$

$$(j \text{ not summed}) \ , \tag{7.7}$$

where j may be "1" or "2" and E_3 is $-(E_1 + E_2)$. The steady state forms for σ_{11} and σ_{22} are

$$\sigma_{jj} = \frac{2G\tau E_j}{1-2\tau E_j} - \frac{2G\tau E_3}{1-2\tau E_3} \ ,$$

$$= \frac{2G\tau(E_j - E_3)}{(1-2\tau E_j)(1-2\tau E_3)} \ . \tag{7.8}$$

For small τE_j, the expressions for σ_{11} and σ_{22} are

$$\sigma_{11} = 2G\tau E_1(2 + E_2/E_1)[1 - 2\tau E_1(E_2/E_1) + O(\tau E_1)^2] \ , \tag{7.9a}$$

$$\sigma_{22} = 2G\tau E_1(1 + 2E_2/E_1)[1 - 2\tau E_1 + O(\tau E_1)^2] \ . \tag{7.9b}$$

The characteristics of these functions varies with E_2/E_1. We will consider several cases.

Uniaxial extension:

$$\sigma_{11} = 3G\tau E_1[1 + \tau E_1 + O(\tau E_1)^2] , \tag{7.10a}$$

$$\sigma_{22} = 0 . \tag{7.10b}$$

Planar extension:

$$\sigma_{11} = 4G\tau E_1[1 + O(\tau E_1)^2] , \tag{7.11a}$$

$$\sigma_{22} = 2G\tau E_1[1 - 2\tau E_1 + O(\tau E_1)^2] . \tag{7.11b}$$

Equal biaxial extension:

$$\sigma_{11} = \sigma_{22} = 6G\tau E_1[1 - 2\tau E_1 + O(\tau E_1)^2] . \tag{7.12}$$

The stress has the Newtonian value at low τE_1. The elongational viscosity, σ_{11}/E_1, at first increases for uniaxial extension and when E_2/E_1 is less than zero. When E_2/E_1 is greater than zero, including equal biaxial extension, the elongational viscosity, σ_{11}/E_1, at first decreases. However, for all value of E_2/E_1

$$\lim_{E_1 \to 1/2\tau} \frac{\sigma_{11}}{E_1} = \infty . \tag{7.13}$$

When E_2/E_1 is greater than zero, elongational viscosity σ_{11}/E_1 exhibits a minimum. The elongational viscosity decreases more quickly by increasing the value of E_2/E_1. The effect of E_2/E_1 results in a kind of deformation rate softening.

It should be noted that deformation rate softening behavior in the elongational viscosity is determined by the P_{33} term. The

P_{11}/E_1 component in the quantity σ_{11}/E_1 is a monotonic increasing function of τE_1, i.e., the qualitative nature of P_{11} does not depend upon the kinematics E_2/E_1. On the other hand, the P_{33} component determines the character of the elongational viscosity. This leads to the important conclusion that we cannot assume $\sigma_{11} \approx P_{11}$ in multiaxial elongational flow, as several researchers have done to analyze uniaxial elongational flow and melt spinning [I-2,I-3,W-17,Z-2]. This may cause some difficulties in analyzing the growth of disturbances in multiaxial elongational flow.

We now consider the deformation rate dependence of the relaxation time τ. The invariant $II_d^{1/2}$ of Eqn. (7.2) may be expressed as

$$II_d^{1/2} = \sqrt{2 \text{ tr } \underset{\sim}{d}^2} = 2[(E_2/E_1)^2 + E_2/E_1 + 1]^{1/2} E_1 = KE_1 , \quad (7.14)$$

which makes Eqn. (7.21) take the form

$$\tau = \frac{\tau_0}{1 + a K \tau_0 E_1} . \quad (7.15)$$

Introducing Eqn. (7.15) into Eqn. (7.8) gives

$$\sigma_{11} = \frac{2G\tau_0 E_1 (2+E_2/E_1)(1+aK\tau_0 E_1)}{[1-(2-aK)\tau_0 E_1][1+(2+aK+2E_2/E_1)\tau_0 E_1]} , \quad (7.16a)$$

$$\sigma_{22} = \frac{2G\tau_0 E_1 (1+2E_2/E_1)(1+aK\tau_0 E_1)}{[1-(2E_2/E_1-aK)\tau_0 E_1][1+(2+aK+2E_2/E_1)\tau_0 E_1]} . \quad (7.16b)$$

The characteristics of Eqn. (7.16) and elongational viscosities on

effects of various multiaxiality E_2/E_1 and the strain rate softening relaxation time have been already described in Chapter V, Section C-2-b.

C. ANALYSES: GROWTH OF DISTURBANCES

C-1. Conservation Equations: Perturbed State

Consider the elongational flow of a liquid sheet. We take the thickness of the sheet to be perturbed by an amount of ξ (see Figure 7.1) so that the velocity and stress fields vary according to

$$\begin{aligned} h &= \bar{h} + \xi \ , \\ \underset{\sim}{v} &= \bar{\underset{\sim}{v}} + \underset{\sim}{v}' \ , \\ \underset{\sim}{\sigma} &= \bar{\underset{\sim}{\sigma}} + \underset{\sim}{\sigma}' \ , \end{aligned} \qquad (7.17a,b,c)$$

where a superposed bar indicates the steady state.

The detailed analysis of the perturbed state has been described in Chapter VI, Section B-2. If we limit ourselves to disturbances in the 1-3 plane, i.e., v_2' is zero or $\xi = \xi(t,x_1)$, the governing conservation equations are

$$\sigma_{11}' + \bar{\sigma}_{11} \left(\frac{\xi}{\bar{h}}\right) = 0 \ , \qquad (7.18a)$$

or

$$(P_{11}' - P_{33}') + (\bar{P}_{11} - \bar{P}_{33}) \left(\frac{\xi}{\bar{h}}\right) = 0 \ , \qquad (7.18b)$$

and

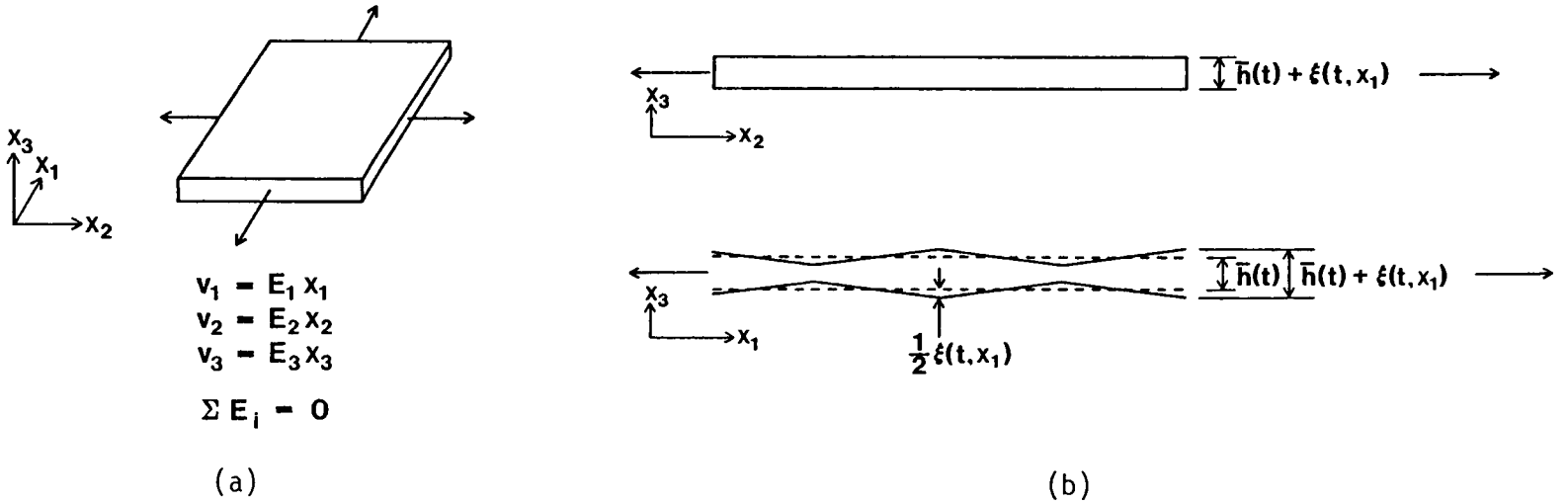

Figure 7.1. (a) Elongational flow of a sheet; (b) disturbances in a stretched sheet.

$$\frac{\partial v_1'}{\partial x_1} = E_1' = -\frac{\partial v_3'}{\partial x_3} = -E_3' = -\frac{1}{\bar{h}}\left(\frac{D\xi}{Dt} - \frac{\xi}{\bar{h}}\frac{\partial \bar{h}}{\partial t}\right) = -\frac{D}{Dt}\left(\frac{\xi}{\bar{h}}\right) . \qquad (7.19)$$

C-2. Perturbed Constitutive Equation

We have introduced disturbances of the form of Eqn. (7.17) into the flow. The stresses σ_{jj} and P_{jj} are perturbed according to

$$\sigma_{jj} = \bar{\sigma}_{jj} + \sigma_{jj}' ,$$
$$p = \bar{p} + p' , \qquad (7.20a,b,c)$$
$$P_{jj} = \bar{P}_{jj} + P_{jj}' .$$

The steady state and the perturbed stresses are given by

$$\bar{P}_{jj} = 2G\bar{\tau}E_j - \bar{\tau}\left(\frac{D\bar{P}_{jj}}{Dt} - 2E_j\bar{P}_{jj}\right) , \qquad (7.21)$$

$$P_{jj}' = 2G\bar{\tau}\frac{\partial v_j'}{\partial x_j} + 2G\tau' E_j - \bar{\tau}\left(\frac{DP_{jj}'}{Dt} - 2E_j P_{jj}' - 2\bar{P}_{jj}\frac{\partial v_j'}{\partial x_j}\right)$$
$$- \tau'\left(\frac{\partial \bar{P}_{jj}}{\partial t} - 2E_j\bar{P}_{jj}\right) , \qquad (7.22)$$

where τ' is the perturbed relaxation time as shown by

$$\tau = \bar{\tau} + \tau' . \qquad (7.23)$$

If the deformation rate dependency of the relaxation time is given by Eqn. (7.2) or (7.15), τ' becomes, under the restriction of the kinematics given by Eqn. (7.19), as follows:

$$\tau' = -a\bar{\tau}^2\frac{(2+E_2/E_1)}{\sqrt{(E_2/E_1)^2+E_2/E_1+1}}E_1' , \qquad (7.24a)$$

$$= -2a\,\bar{\tau}^{2}\,\frac{(2+E_2/E_1)}{K}\,E_1' \ . \qquad (7.24b)$$

The mean stress components are specifically

$$\frac{D\bar{P}_{11}}{Dt} + \left(\frac{1}{\bar{\tau}} - 2E_1\right)\bar{P}_{11} = 2GE_1 \ , \qquad (7.25a)$$

$$\frac{D\bar{P}_{33}}{Dt} + \left(\frac{1}{\bar{\tau}} + 2(1 + E_2/E_1)E_1\right)\bar{P}_{33} = -2G(1 + E_2/E_1)E_1 \ . \qquad (7.25b)$$

The perturbed stress components, with the relaxation time of the form given by Eqn. (7.2) or Eqn. (7.15), become

$$\frac{DP_{11}'}{Dt} + \left(\frac{1}{\bar{\tau}} - 2E_1\right)P_{11}' = 2\left(G + \left(1 - \frac{a(2+E_2/E_1)}{K}\right)\bar{P}_{11}\right)E_1' \ , \qquad (7.26a)$$

$$\frac{DP_{33}'}{Dt} + \left(\frac{1}{\bar{\tau}} + 2(1+E_2/E_1)E_1\right)P_{33}' = -2\left(G + \left(1 + \frac{a(2+E_2/E_1)}{K}\right)\bar{P}_{33}\right)E_1' \ . \qquad (7.26b)$$

C-3. Growth of Disturbance: Viscoelastic Fluid

It is possible to obtain solutions from Eqns. (7.25) and (7.26) at various levels of approximation. The simplest approach is to take τ' to be zero, i.e., to neglect the variation of τ with deformation rate. Even in this simplest case we have to solve six differential equations (Eqns. (7.18), (7.19), (7.25) and (7.26)).

The procedure is rather straightforward but the manipulations are very tedious. Substitute Eqn. (7.18) into Eqn. (7.26b); then the resulting equation is substituted into Eqn. (7.26a) to yield

$$P'_{11} = \frac{-1}{2(2+E_2/E_1)E_1}\left[\frac{D}{Dt}\left(\frac{\xi}{h}(\bar{P}_{11}-\bar{P}_{33})\right) + \left(\frac{1}{\bar{\tau}} + 2(1+E_2/E_1)E_1\right)\frac{\xi}{h}(\bar{P}_{11}-\bar{P}_{33}) + 2\left(2G + \left(1 - \frac{a}{K}(2+E_2/E_1)\right)(\bar{P}_{11}-\bar{P}_{33}) + 2\bar{P}_{33}\right)E'_1\right] . \quad (7.27)$$

Then Eqn. (7.27) is substituted into Eqn. (7.26a) by assuming a constant strain rate deformation. This leads, by help of Eqn. (7.19), to

$$A\frac{D^2\xi}{D(E_1t)^2} + B\frac{D\xi}{D(E_1t)} + C\xi = 0 , \quad (7.28)$$

where

$$A = \left(1 - 2\frac{a}{K}(2+E_2/E_1)\right)\bar{P}_{11} + \left(3 + 2\frac{a}{K}(2+E_2/E_1)\right)\bar{P}_{33} + 4G \quad (7.29a)$$

$$B = 2\left[(3+2E_2/E_1)\left(1 - 2\frac{a}{K}(2+E_2/E_1)\right)\bar{P}_{11} - \left(3 + 2\frac{a}{K}(2+E_2/E_1)\right)\bar{P}_{33} + 2\left(\frac{1}{\bar{\tau}E_1} - \frac{a}{K}(2+E_2/E_1)^2 + E_2/E_1\right)G\right] , \quad (7.29b)$$

$$C = (1+E_2/E_1)(5+3E_2/E_1)\left(1 - 2\frac{a}{K}(2+E_2/E_1)\right)\bar{P}_{11} - (1+E_2/E_1)(3+E_2/E_1)\left(3 + 2\frac{a}{K}(2+E_2/E_1)\right)\bar{P}_{33} + 2\left[\frac{E_2/E_1}{\bar{\tau}E_1} - 2(1+E_2/E_1)\left(\frac{a}{K}(2+E_2/E_1)^2 + 1\right)\right]G , \quad (7.29c)$$

and

$$\bar{\tau}E_1 = \frac{\tau_0 E_1}{1+aK\tau_0 E_1} . \quad (7.29d)$$

$$K = 2[(E_2/E_1)^2 + E_2/E_1 + 1]^{1/2} . \quad (7.29e)$$

$\bar{P}_{11}$ and $\bar{P}_{33}$ are the solution of Eqn. (7.25). These are

$$\bar{P}_{11} = \frac{2G\bar{\tau}E_1}{1-2\bar{\tau}E_1}\left[1 - e^{-(1-2\bar{\tau}E_1)t/\bar{\tau}}\right], \tag{7.30a}$$

$$\bar{P}_{33} = -\frac{2G(1+E_2/E_1)\bar{\tau}E_1}{1+2(1+E_2/E_1)\bar{\tau}E_1}\left(1 - e^{-[1+2(1+E_2/E_1)\bar{\tau}E_1]t/\bar{\tau}}\right). \tag{7.30b}$$

Let the disturbance be periodic along the "1" direction

$$\xi(t,x_1) = \xi(t)e^{ikx_1}. \tag{7.31a}$$

The wave number k decreases with time because of the extension of the film. Under a constant strain rate E_1 deformation,

$$k(t) = k(0)e^{-E_1 t}, \tag{7.31b}$$

this leads to

$$\frac{D\xi}{Dt} = \frac{\partial\xi}{\partial t} + \bar{v}_1\frac{\partial\xi}{\partial x_1} = e^{ikx_1}\frac{\partial\hat{\xi}}{\partial t}, \tag{7.32a}$$

and

$$\frac{D^2\xi}{Dt^2} = \frac{D}{Dt}\left(e^{ikx_1}\frac{\partial\hat{\xi}}{\partial t}\right) = e^{ikx_1}\frac{\partial^2\hat{\xi}}{\partial t^2}. \tag{7.32b}$$

Eqn. (7.28) can be rewritten by the aid of Eqn. (7.32) for a constant rate deformation:

$$A\frac{\partial^2\hat{\xi}}{\partial(E_1 t)^2} + B\frac{\partial\hat{\xi}}{\partial(E_1 t)} + C\hat{\xi} = 0. \tag{7.33}$$

One needs two boundary conditions to solve Eqn. (7.33), which is a second order nonlinear ordinary equation. One of the boundary conditions is the initial disturbance size

$$\hat{\xi}(E_1 t = 0) = \hat{\xi}(0) \ . \tag{7.34}$$

The other boundary condition can be derived by assuming the stress at $E_1 t = 0$ to be zero:

$$\overline{P}_{11} = \overline{P}_{33} = P'_{11} = 0 \ . \tag{7.35}$$

Combining Eqns. (7.19) and (7.27), and the resulting equation at t of zero is

$$\xi \frac{D}{Dt} (\overline{P}_{11} - \overline{P}_{33}) - 4\left[\frac{D\xi}{Dt} + E_1(1 + E_2/E_1)\xi\right] G = 0 \ . \tag{7.36}$$

And from Eqn. (7.25)

$$\frac{D}{Dt} (\overline{P}_{11} - \overline{P}_{33}) \Big|_{t=0} = 2G(2 + E_2/E_1)E_1 \ . \tag{7.37}$$

Then combining Eqns. (7.36) and (7.37) leads under constant strain rate deformation:

$$\frac{\partial \hat{\xi}}{\partial(E_1 t)} \Bigg|_{E_1 t=0} = -\frac{1}{2} (E_2/E_1)\hat{\xi}(0) \ . \tag{7.38}$$

A 5-th and 6-th order Runge-Kutta method can be used to obtain a solution of Eqn. (7.33) with the boundary conditions given by Eqns. (7.34) and (7.38).

The asymptote of $\tau E_1 \to 0$ in Eqn. (7.33) becomes

$$\frac{\partial \hat{\xi}}{\partial (E_1 t)} + \frac{1}{2} (E_2/E_1)\hat{\xi} = 0 \ . \tag{7.39}$$

This is the case of a Newtonian fluid which has been described in Chapter VI.

Eqn. (7.28) or (7.33) and Eqn. (7.29) show that the rate of the disturbance growth is determined three dimensionless groups, such as Weissenberg number τE_1, the strain rate softening parameter "a", the so-called Yamamoto number [W-20], and the degree of multiaxiality E_2/E_1.

There exist various levels of approximate solutions in Eqn. (7.33). First, we consider the case where τ' of zero, i.e., we neglect the variation of the relaxation time with deformation rate. The equation governing the growth of disturbances is

$$A \frac{\partial^2 \hat{\xi}}{\partial (E_1 t)^2} + B \frac{\partial \hat{\xi}}{\partial (E_1 t)} + C\hat{\xi} = 0 \ , \tag{7.40a}$$

where

$$A = \overline{P}_{11} + 3\overline{P}_{33} + 4G \ , \tag{7.40b}$$

$$B = 2(3+2E_2/E_1)\overline{P}_{11} - 3\overline{P}_{33} + 2[1/(\tau E_1) + E_2/E_1]G \ , \tag{7.40c}$$

$$C = (1+E_2/E_1)(5+3E_2/E_1)\overline{P}_{11} - 3(1+E_2/E_1)(3+E_2/E_1)\overline{P}_{33} + 2[(E_2/E_1)/(\tau E_1) - 2(1+E_2/E_1)]G \ . \tag{7.40d}$$

This is plotted in Figure 7.2 for various viscoelastic levels τE_1 and multiaxiality E_2/E_1. It is indicated that increasing multiaxiality, i.e., the larger the E_2/E_1 value, tends to make the disturbance growth rate small, i.e., disturbances are damped out by the lateral stretching. The effect of the Weissenberg number τE_1 is rather complex. In general, the disturbance growth rate decreases with increasing elasticity τE_1. However, the disturbance growth rate for a small Weissenberg number (for example, $\tau E_1 = 0.1$) is larger than that for $\tau E_1 = 0$ (i.e., the Newtonian fluids case).

We must in general consider the relaxation time to depend upon deformation rate, i.e., the deformation rate softening relaxation time as shown in Eqn. (7.2) or (7.29d). Figures 7.3a and 7.3b contain plots of $\hat{\xi}(E_1 t)/\hat{\xi}(0)$ versus $E_1 t$ computed from Eqns. (7.33) and (7.29) for various values of "a" and E_2/E_1 at $\tau_0 E_1$ of 0.5 and 10.0.

It is found that at a fixed Weissenberg number $\tau_0 E_1$, increasing "a" (greater strain rate softening character) increases the disturbance growth rate. At small "a", increasing $\tau_0 E_1$ tends to decrease the disturbance growth rate. However, above some intermediate "a" value (depending upon the multiaxiality E_2/E_1) a higher Weissenberg number increases the disturbance growth rate.

The present analysis is essentially equivalent to a generalization of the Chang and Lodge analysis [C-6], which was for finite disturbance growth in rods, to analysis for sheets with multiaxial stretching. An exact generalization of Chang and Lodge's finite disturbance solution requires numerical solution of a nonlinear

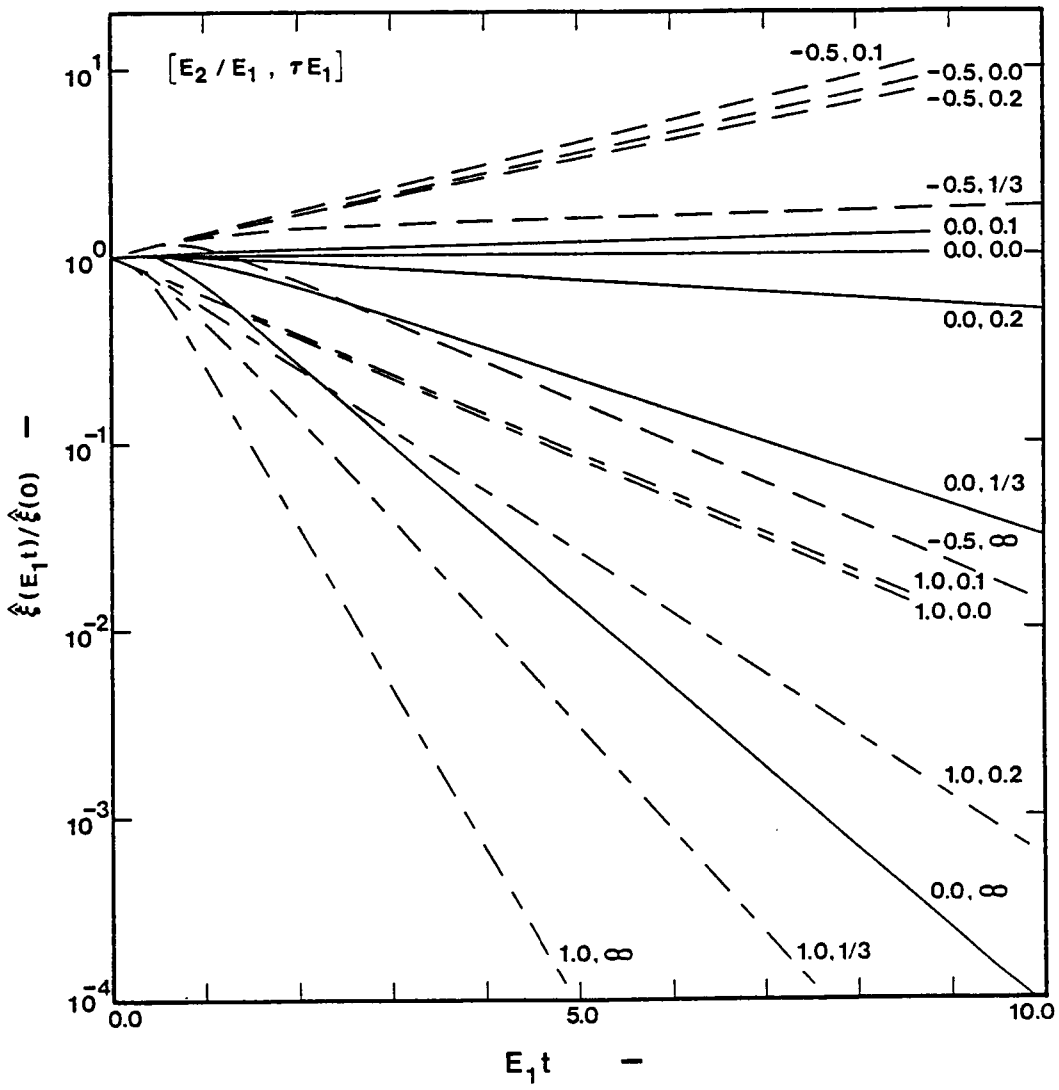

Figure 7.2. Growth of disturbances $\hat{\xi}(E_1t)/\hat{\xi}(0)$ as a function of E_1t for various E_2/E_1 and τE_1.

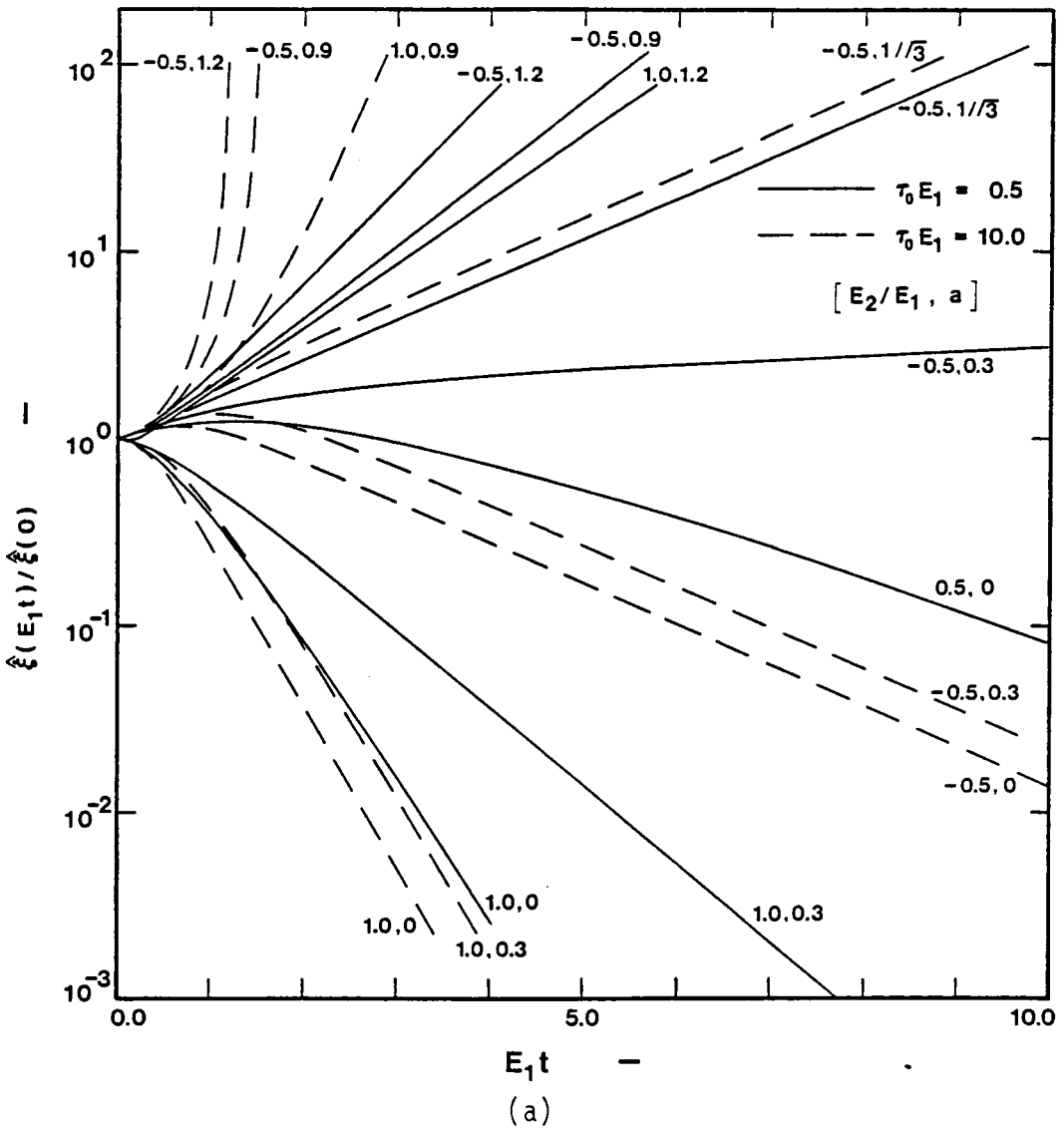

(a)

Figure 7.3. (a) Growth of disturbance $\hat{\xi}(E_1t)/\hat{\xi}(0)$ as a function of E_1t for various E_2/E_1 and "a" values (τ_0E_1 = 0.5 and 10.0); (b) growth of disturbance $\hat{\xi}(E_1t)/\hat{\xi}(0)$ as a function of E_1t for various E_2E_1 and "a" values (τ_0E_1 = 0.5 and 10.0).

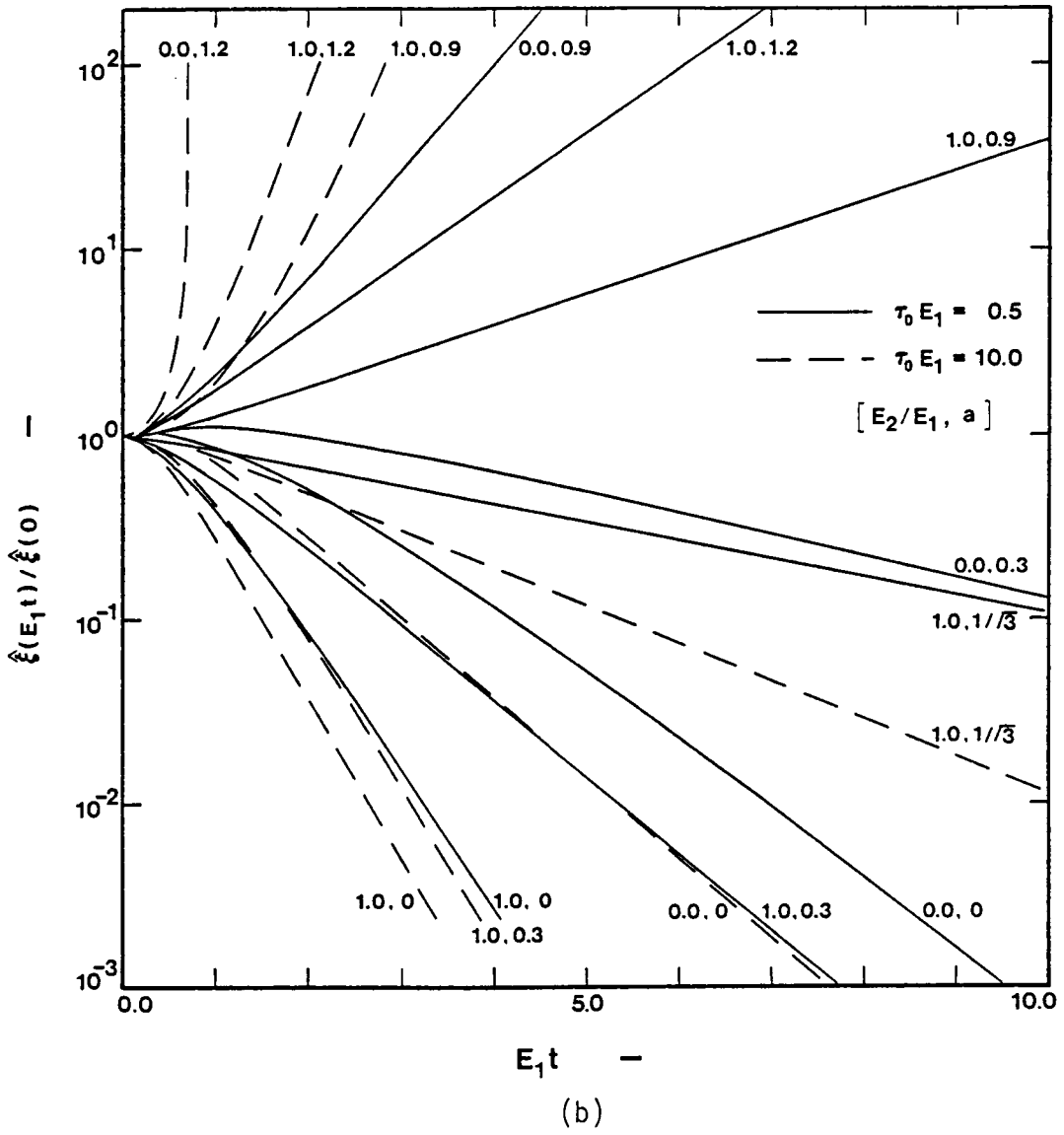

(b)

Figure 7.3 (continued)

integral equation. It is, however, possible to obtain an analytical solution for the asymptote of $\tau E_1 \to \infty$. This would be the case for a material such as vulcanized rubber [T-9].

Referring to Figure 7.4, the stress can be expressed as

$$\sigma_{11} = P_{11} - P_{33} = G\,(c_{11}^{-1} - c_{33}^{-1}) = G(\lambda_1^2 - \lambda_3^2)\,, \tag{7.41}$$

where $\underset{\sim}{c}^{-1}$ is the Finger deformation measure and λ_i is the extension rate. $\underset{\sim}{c}^{-1}$ is given as

$$c_{11}^{-1}(t) = \lambda_1^2 = \left[\frac{A(0)}{A(t)}\right]^2\,, \tag{7.42a}$$

$$c_{22}^{-1}(t) = \lambda_2^2 = \left[\frac{W(t)}{W(0)}\right]^2\,, \tag{7.42b}$$

$$c_{33}^{-1}(t) = \lambda_3^2 = \left[\frac{h(t)}{h(0)}\right]^2\,. \tag{7.42c}$$

A simple force balance of two sheets of different cross-section area A_1 and A_2 but with the same width W gives

$$A_1(\lambda_{1,1}^2 - \lambda_{3,1}^2) = A_2(\lambda_{1,2}^2 - \lambda_{3,2}^2)\,, \tag{7.43a}$$

where

$$A_1 = W \cdot h,\quad A_2 = W \cdot (h-\xi)\,. \tag{7.43b}$$

After neglecting P_{33} terms from Eqn. (7.43)

$$\frac{A_2(t)}{A_1(t)} = \left[\frac{A_2(0)}{A_1(0)}\right]^2\,. \tag{7.44}$$

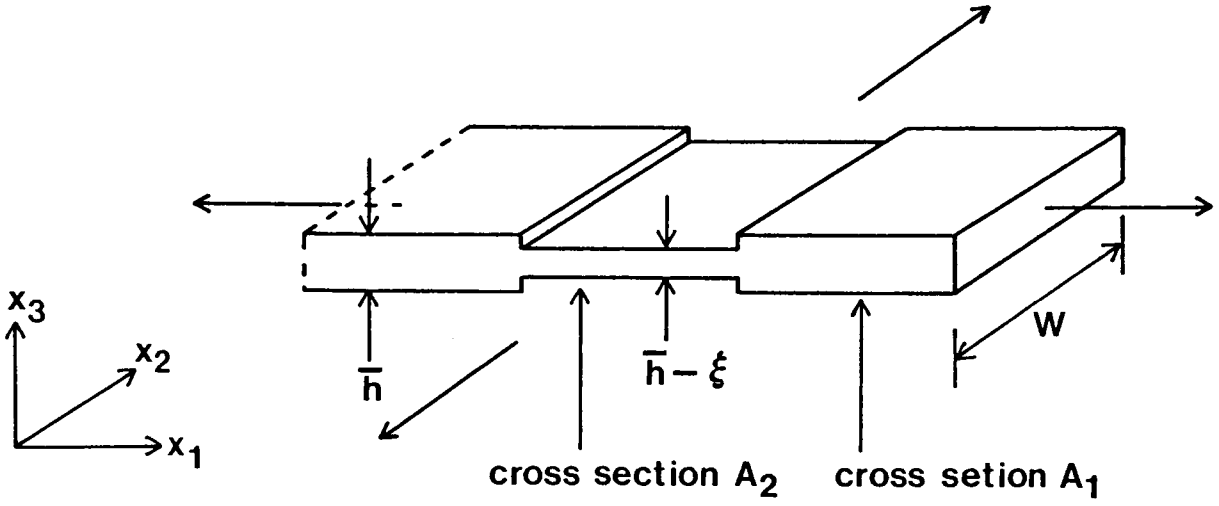

Figure 7.4. Disturbances in a stretched sheet: similar to Chang-Lodge model of disturbances.

The above expression seems to be able to approximate the disturbance growth of elastic solids. In terms of thickness, the above equation becomes

$$\frac{\hat{\xi}(t)}{\hat{\xi}(0)} = 2\,\frac{h(t)}{h(0)} = 2\lambda_3 \ . \tag{7.45}$$

For a constant strain rate deformation, the above equation may be expressed as

$$\frac{\hat{\xi}(E_1 t)}{\hat{\xi}(0)} = 2\,\exp\{-(1+E_2/E_1)E_1 t\} \ . \tag{7.46}$$

We are also able to obtain an analytical solution without neglecting the P_{33} term for this asymptotic case:

$$\frac{\xi(t)}{\xi(0)} = 2\,\frac{h(t)}{h(0)}\left[\frac{W^2(0)h^4(0) + W^2(t)h^4(t)}{W^2(0)h^4(0) + 3W^2(t)h^4(t)}\right]$$

$$= 2\lambda_3\left[\frac{1 + \lambda_2^2\lambda_3^4}{1 + 3\lambda_2^2\lambda_3^4}\right] \ . \tag{7.47}$$

For a constant strain rate deformation, the above equation may be rewritten as

$$\frac{\xi(E_1 t)}{\xi(0)} = 2\,\exp[-(1+E_2/E_1)E_1 t]\left[1 - \frac{2}{1+3\,\exp[2(2+E_2/E_1)E_1 t]}\right] \ . \tag{7.48}$$

The long-time asymptotic for growth of disturbance yields:

$$\frac{\xi(E_1 t)}{\xi(0)} \rightarrow 2\,\exp\left[-(1+E_2/E_1)E_1 t\right] \ . \tag{7.49}$$

We should note that neglecting P_{33} does not have an affect, but only when we are concerned with the long-time asymptote of a very highly elastic system. Eqn. (7.48) is shown in Figure 7.5 with the growth of disturbances in Newtonian fluid sheets, Eqn. (7.39).

One should note that the thickness reduction ratios of multiaxially stretched sheets are dependent upon the multiaxiality E_2/E_1 as follows:

$$\bar{h}(E_1 t) = \bar{h}(0) \exp\{-(1+E_2/E_1)E_1 t\} . \tag{7.50}$$

If we compare the disturbance growth without compensating for the thickness reduction, it might mislead us as to the effect of lateral stretching. It seems better to define another quantity, instead of $\hat{\xi}(E_1 t)/\hat{\xi}(0)$, to describe the growth of the disturbance. Let us define

$$\frac{\hat{\xi}(E_1 t)/\bar{h}(E_1 t)}{\hat{\xi}(0)/\bar{h}(0)}$$

to be a "normalized disturbance." Normalized disturbances of Newtonian fluids and elastic solids, and viscoelastic fluids with constant relaxation time are plotted in Figures 7.6a and 7.6b, respectively. These figures are replotted from Figures 7.5 and 7.2. It is found that the normalized disturbance increases with increasing multiaxiality E_2/E_1 (i.e., lateral stretching). Increasing the viscoelasticity τE_1 tends to reduce the growth rate of the normalized disturbance (i.e., tends to stabilize the system).

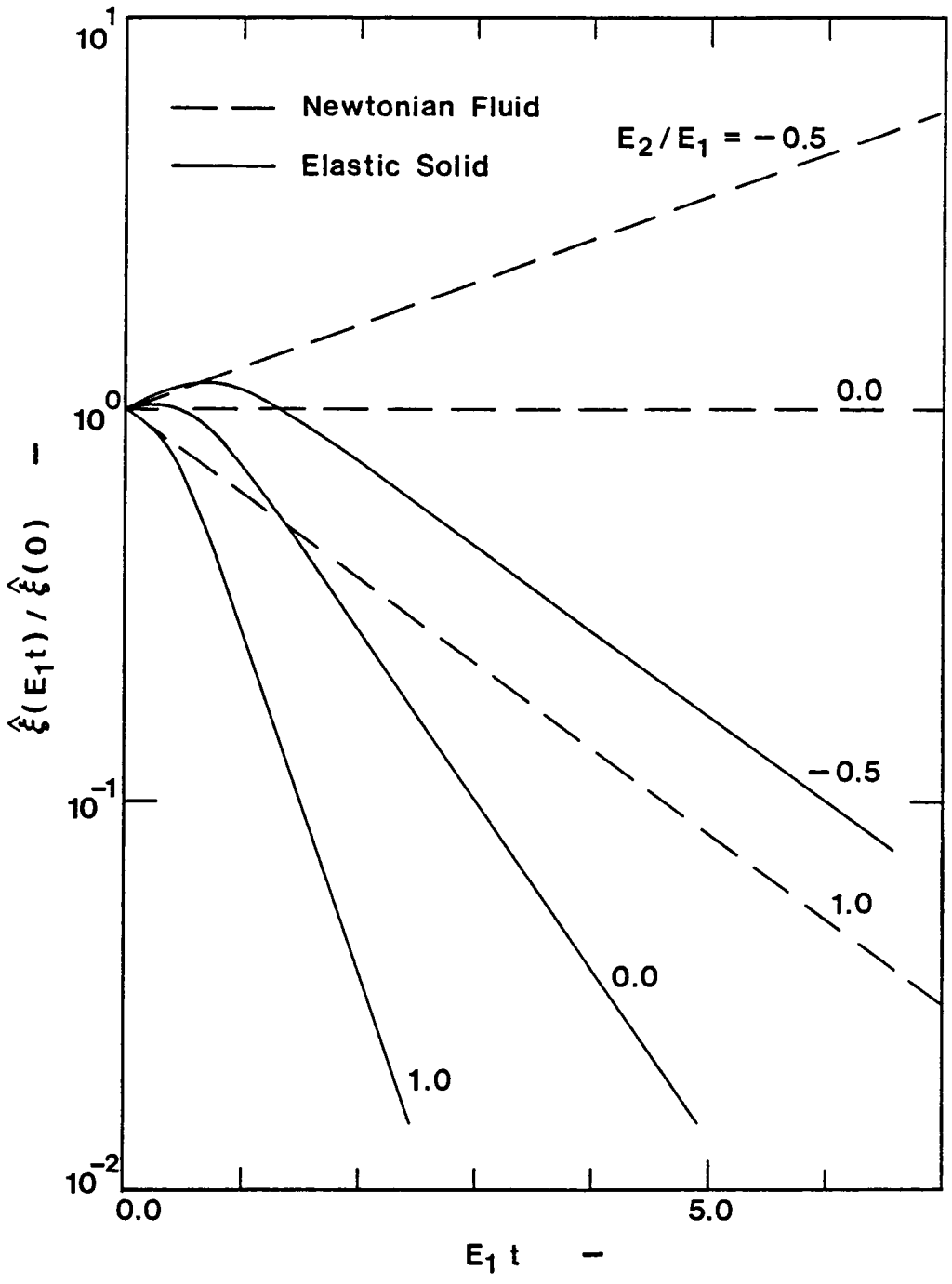

Figure 7.5. Growth of disturbance $\hat{\xi}(E_1t)/\hat{\xi}(0)$ as a function of E_1t for Newtonian fluids and elastic solids.

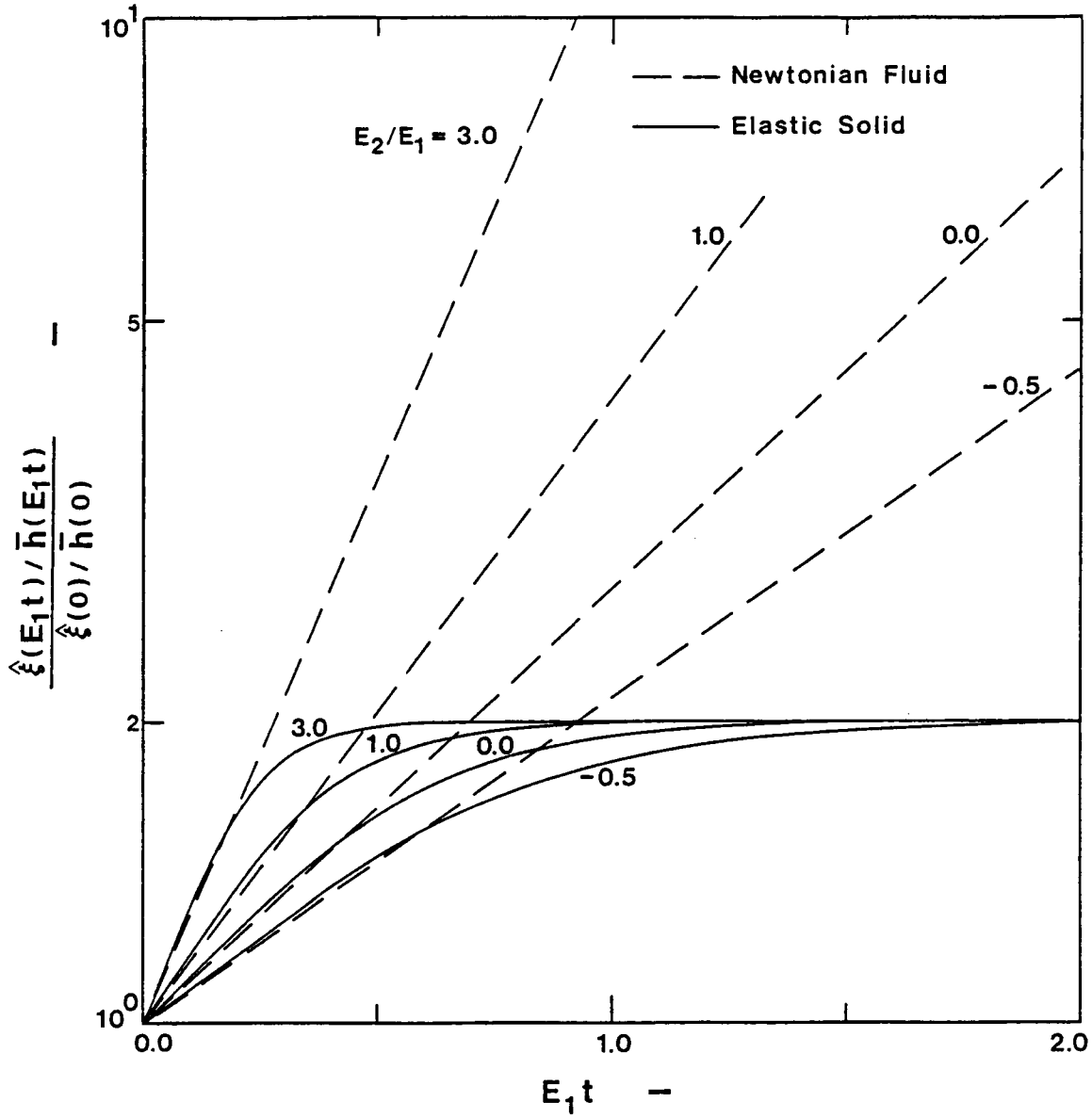

(a) Newtonian fluids and elastic fluids

Figure 7.6. Growth of "normalized disturbance" as a function of $E_1 t$.

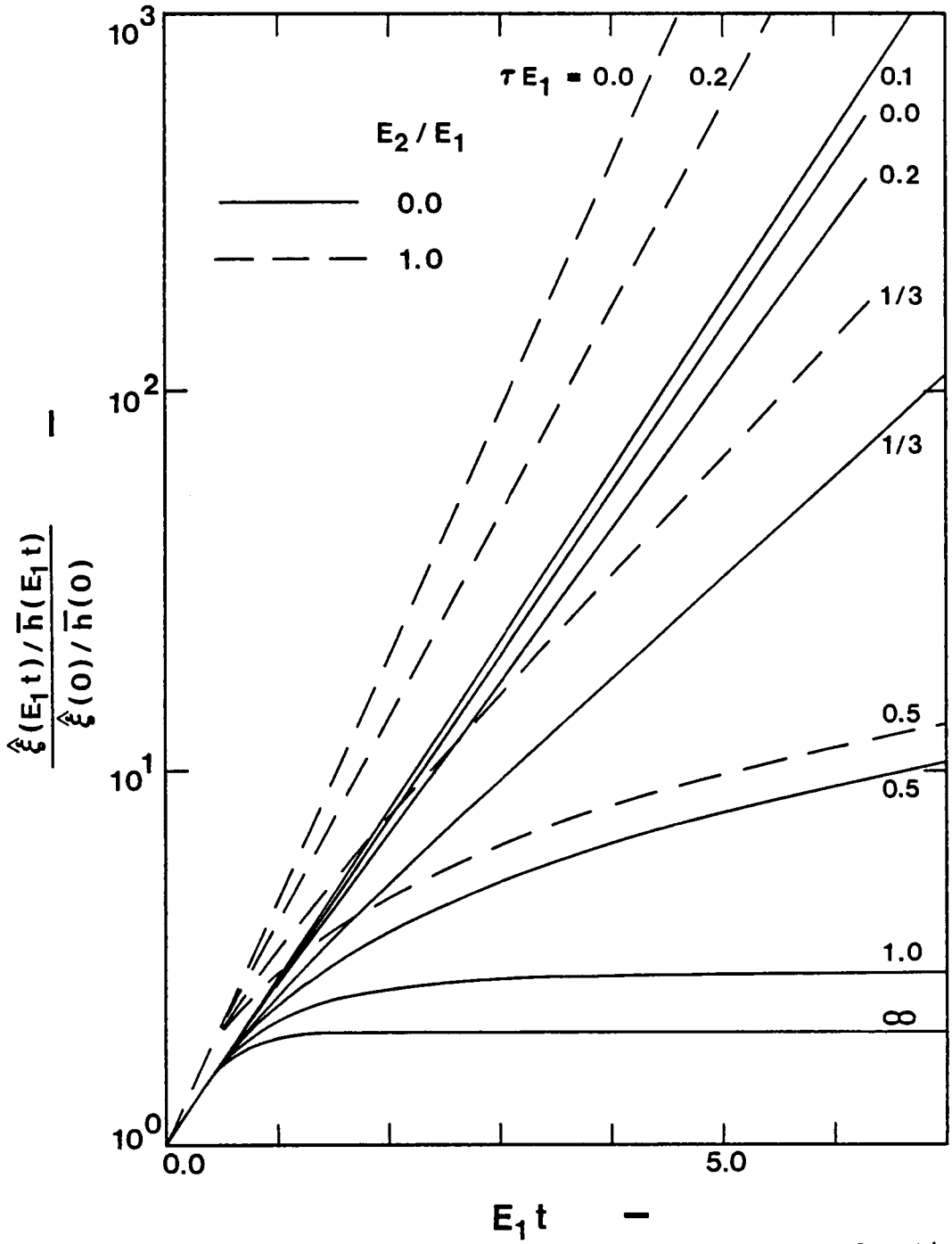

(b) A convected Maxwell model with a constant relaxation time

Figure 7.6 (continued)

Especially elastic solids (i.e., τE_1 of ∞) never make normalized disturbance more than 2.0. This suggests elastic solids will not fail even under conditions of finite disturbances.

C-4. Disturbances Along Lateral Direction

In previous sections, analyses for viscoelastic fluids have been made for disturbances which are only along the machine direction $\xi(t,x_1)$. This leads one to question whether it is necessary to also consider disturbance growths along the transverse direction $\xi(t,x_2)$.

Exact consideration and formulations have already been made in Chapter VI, Section B-5, for the disturbance growth of a Newtonian fluid, where the disturbances are along the transverse direction. The force balance and continuity equations for the perturbed state are

$$\sigma'_{22} + \bar{\sigma}_{33}\left(\frac{\xi}{\bar{h}}\right) = 0 \ , \tag{7.51a}$$

$$\frac{\partial v'_1}{\partial x_1} = 0 \quad , \quad \frac{\partial v'_2}{\partial x_2} = E'_2 \ ,$$

$$E'_2 = -\frac{\partial v'_3}{\partial x_3} = -\frac{1}{\bar{h}}\left(\frac{D\xi}{Dt} - \frac{\xi}{\bar{h}}\frac{\partial \bar{h}}{\partial t}\right) \ , \tag{7.51b}$$

where

$$\xi = \xi(t,x_2) \ . \tag{7.51c}$$

For a Newtonian fluid, the normalized disturbance is given

$$\frac{\hat{\xi}(t)/\bar{h}(t)}{\hat{\xi}(0)/\bar{h}(0)} = \exp[(1/2 + E_2/E_1)E_1 t] \ . \tag{7.52a}$$

where

$$1.0 \geq E_2/E_1 \geq 0.5 \ . \tag{7.52b}$$

If disturbances are along the machine direction, the normalized disturbance of Newtonian fluids is given by

$$\frac{\hat{\xi}(t)/\bar{h}(t)}{\hat{\xi}(0)/\bar{h}(0)} = \exp\left[(1 + \frac{E_2/E_1}{2})E_1 t\right] \ , \tag{7.53a}$$

where

$$E_2/E_1 \geq - 0.5 \ . \tag{7.53b}$$

It is indicated that the existence of disturbances along the machine direction propagates disturbances more rapidly than that along the transverse direction.

We now consider the defect growth in elastic solids where the disturbance exists along the transverse direction, i.e., $\xi(t,x_2)$. Referring to Figure 7.4 where the "1" and "2" directions are interchanged with each other, the stress in the "2" direction can be expressed as

$$\sigma_{22} = P_{22} - P_{33} = G(c_{22}^{-1} - c_{33}^{-1}) = G(\lambda_2^2 - \lambda_3^2) \ . \tag{7.54}$$

A simple force balance of two sheets of different cross-section areas A_1 and A_2, but with the same film length L, gives

$$A_1(\lambda_{2,1}^2 - \lambda_{3,1}^2) = A_2(\lambda_{2,2}^2 - \lambda_{3,2}^2) \ , \tag{7.55a}$$

where

$$A_1 = L \cdot h \ , \quad A_2 = L \cdot (h-\xi) \ . \tag{7.55b}$$

This leads to

$$\frac{\xi(t)}{\xi(0)} = 2\lambda_3 \left(\frac{1 + \lambda_1^2\lambda_3^4}{1 + 3\lambda_1^2\lambda_3^4} \right) \ . \tag{7.56}$$

For a constant strain rate deformation, the above equation may be rewritten as

$$\frac{\xi(E_1 t)}{\xi(0)} = 2 \exp[-(1+E_2/E_1)E_1 t] \left(1 - \frac{2}{3+\exp[2(1+2E_2/E_1)E_1 t]} \right) \ , \tag{7.57a}$$

$$\frac{\xi(E_1 t)/h(E_1 t)}{\xi(0)/h(0)} = 2 \left(1 - \frac{2}{3+\exp[2(1+2E_2/E_1)E_1 t]} \right) \ , \tag{7.57b}$$

where

$$1.0 \geq E_2/E_1 \geq 0.5 \ . \tag{7.57c}$$

Eqn. (7.57) has a character very similar to Eqn. (7.52), even though Eqn. (7.57) is for elastic solids and Eqn. (7.52) is for Newtonian fluids, provided we compare these equations with disturbances along the machine directions. The growth of the disturbance rate is slower and smaller for the cases where disturbances are along the transverse direction than that where disturbances are along the machine direction. And also the disturbance growth rate of

elastic solids along the transverse direction increases with increasing E_2/E_1; that is similar to the system where disturbances are along the machine direction. However, the rate of increase of disturbances are slower where disturbances are along the transverse direction. The normalized disturbances of elastic solids undergoing uniaxial stretching never grow, if disturbances are along the transverse direction. The disturbance growth of equal biaxial elongation is not affected by the direction of the disturbances.

We have examined the growth of disturbances, where disturbances are along the machine direction and along the transverse direction, for both Newtonian fluids and elastic solids. In both cases, disturbances in the direction which has the highest strain rate dominate the stability of multiaxialy deformed elongated sheets. Viscoelastic materials behave somewhere between Newtonian fluids and elastic solids. Therefore, the effects of the direction of disturbances for viscoelastic fluid are similar to those of Newtonian fluids and elastic solids. Finally, we can conclude that the investigation of disturbance growth is sufficient if we consider disturbances lying in the machine direction $\xi(t,x_1)$.

D. INTERPRETATION

D-1. Ductile Failure

The usefulness of the analysis developed in the previous section is that it allows the investigation of the relationship between rheological properties and the occurrence of ductile failure. If one takes the criterion of ductile failure to be

$$\hat{\xi}(E_1 t_b) = \bar{h}(E_1 t_b) = \bar{h}(0)\exp[-(1+E_2/E_1)E_1 t_b] \ , \qquad (7.58)$$

where t_b is the time to break, the length of sheet to failure in the machine direction and the total area to failure (i.e., the area of the 2-3 plane) are

$$L(t_b) = L(0)\ \exp(E_1 t_b) \ , \qquad (7.59a)$$

$$A(t_b) = A(0)\ \exp[(1+E_2/E_1)E_1 t_b] \ . \qquad (7.59b)$$

Figures 7.7 show plots of $L(t_b)/L(0)$ and $A(t_b)/A(0)$ of convected Maxwell materials with constant relaxation time as a function of τE_1, for various E_2/E_1. One assumes the magnitude of the initial disturbance $\hat{\xi}(0)/\bar{h}(0)$ to be 0.01.* It is seen that the elongation-to-break, both $L(t_b)/L(0)$ and $A(t_b)/A(0)$, first decreases with increasing τE_1, and after reaching minimum the elongation-to-break goes to infinity, i.e., one can roughly state that increasing τE_1 (i.e., the elasticity) makes the system more stable. The τE_1 value at which the elongation-to-break on a minimum value decreased with increasing E_2/E_1. Quite contrary results are observed in Figures 7.7a and 7.7b. $L(t_b)/L(0)$ decreases with increasing E_2/E_1, and tends to achieve minimum values which are close to the Newtonian asymptote. On the other hand, $A(t_b)/A(0)$ decreases and tends to show a more monotonic increasing function of τE_1 with decreasing E_2/E_1.

---

*An initial disturbance $\hat{\xi}(0)/\bar{h}(0)$ of 0.01 will be used throughout this chapter.

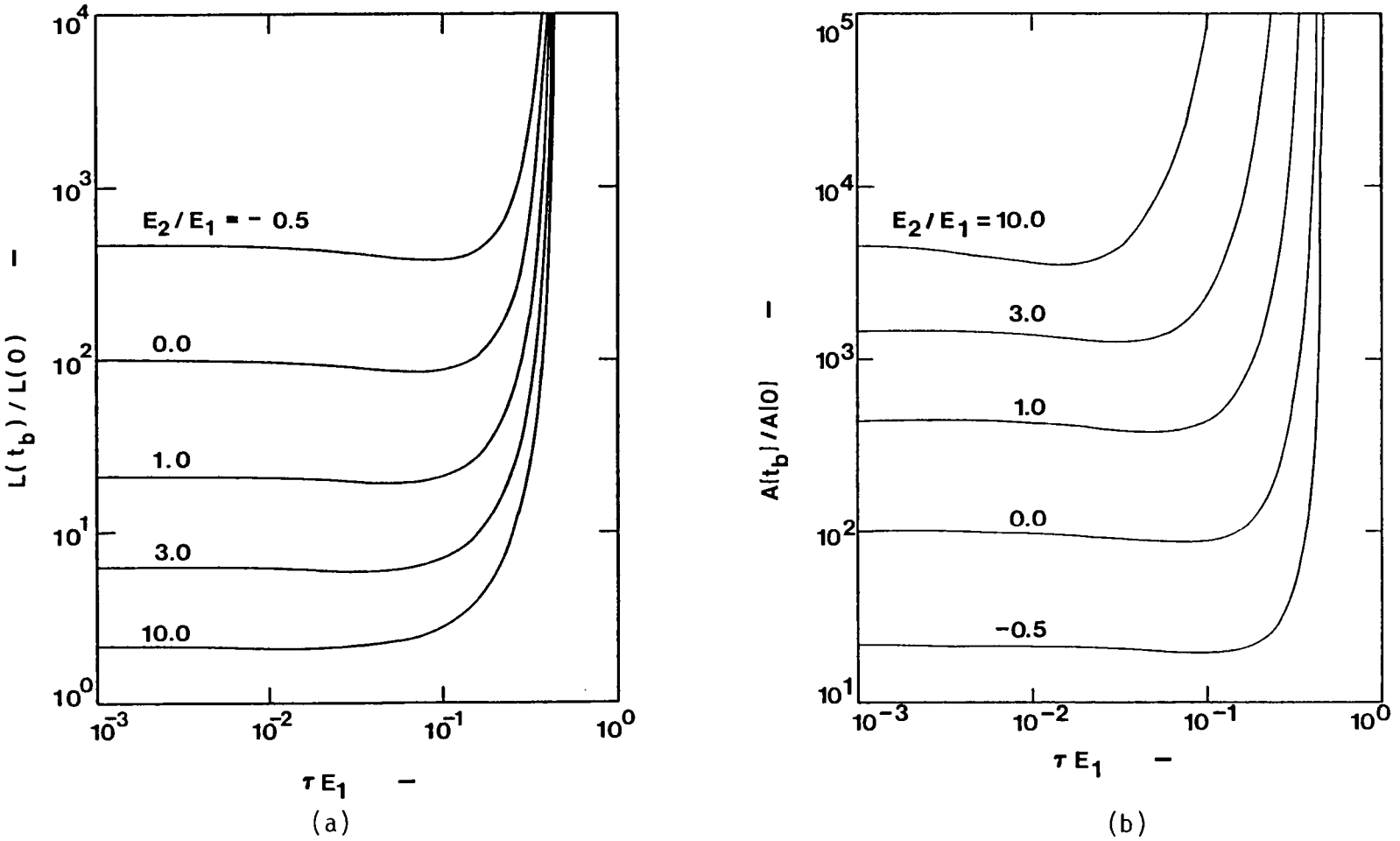

Figure 7.7. (a) Theoretical limiting strain $L(t_b)/L(0)$ caused by ductile failure as a function of τE_1 for various E_2/E_1 (constant relaxation time); (b) theoretical limiting area $A(t_b)/A(0)$ caused by ductile failure as a function of τE_1 for various E_2/E_1 (constant relaxation time).

The Ide and White analysis [I-2,I-3] disturbance growth of uniaxialy stretching filaments did not show any minimum in their limiting strain (elongation-to-break) curve as a function of τE_1 where initial defect sizes are taken as 1%. There exists two possibilities to explain the minimum in the present study. One is that one dimensional disturbances are considered in the present study instead of the two dimensional disturbances considered by Ide and White. Another one is that Ide and White have not considered the effect of the P_{33} or P_{rr} terms. To determine why the limiting strain due to the ductile failure has a minimum in the present study, the Ide and White analysis (involving growth of the disturbances of a convected Maxwell model for uniaxial elongational filaments) has been developed again and generalized to include the P_{33} (or P_{rr}) term with a strain rate dependent relaxation time τ of the form given by Eqn. (7.2).

The final disturbance growth equation is

$$A' \frac{\partial^2 \hat{\xi}}{\partial (E_1 t)^2} + B' \frac{\partial \hat{\xi}}{\partial (E_1 t)} + C' \hat{\xi} = 0 \ , \tag{7.60a}$$

where

$$A' = (1 - \sqrt{3}a)\bar{P}_{11} + (2 + \sqrt{3}a)\bar{P}_{33} + 3G \ , \tag{7.60b}$$

$$B' = 4(1 - \sqrt{3}a)\bar{P}_{11} - 2(2 + \sqrt{3}a)\bar{P}_{33} - \sqrt{3}aG + \frac{3G}{\bar{\tau} E_1} \ , \tag{7.60c}$$

$$C' = \frac{7}{4}(1 - \sqrt{3}a)\overline{P}_{11} - \frac{5}{4}(2 + \sqrt{3}a)\overline{P}_{33} - \frac{3}{4}(1 + 2\sqrt{3}a)G - \frac{3}{2}\frac{G}{\overline{\tau}E_1}, \tag{7.60d}$$

$$\overline{\tau} = \frac{\tau_0}{1 + \sqrt{3}a\overline{\tau}E_1}, \tag{7.60e}$$

$$\xi = R - \overline{R}, \tag{7.60f}$$

with boundary conditions given by

$$\hat{\xi}(E_1 t = 0) = \hat{\xi}(0), \tag{7.61a}$$

$$\frac{\partial \hat{\xi}}{\partial(E_1 t)}\bigg|_{E_1 t=0} = \frac{1}{2}E_1 t. \tag{7.61b}$$

Figure 7.8 shows a plot of the limiting strain $L(t_b)/L(0)$ caused by ductile failure by taking the initial defect size being 1% and by using a 5-th and 6-th order Runge-Kutta method. It is noted that $L(t_b)/L(0)$ of the convected Maxwell filament (with strain rate independent $\tau(a = 0)$) is a monotonic increasing function of $\tau_0 E_1$. Also the magnitude of $L(t_b)/L(0)$ for uniaxially stretched filaments is smaller than that of uniaxially stretched sheets with one dimensional disturbances; for example, $L(t_b)/L(0)$ of filaments has a value of only 21.54% of that of sheets at $\tau_0 E_1 = 0$. Therefore, it appears that the one dimensional disturbance is the cause of the minimum in the elongation-to-break plot as a function of τE_1.

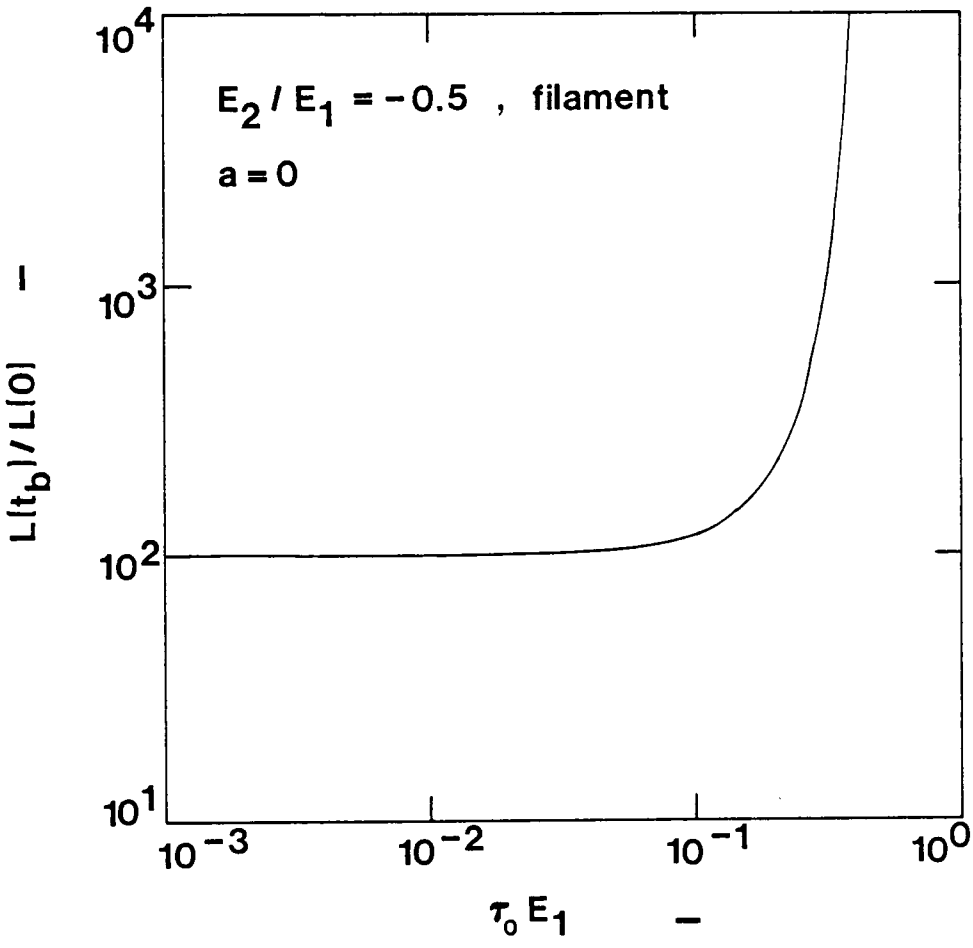

Figure 7.8. Theoretical limiting strain $L(t_b)/L(0)$ caused by ductile failure as a function of τE_1 for uniaxially extended filament (constant relaxation time).

Figures 7.9 and 7.19 show plots of $L(t_b)/L(0)$ and $A(t_b)/A(0)$, respectively, as a function of $\tau_0 E_1$ for different "a" values (i.e., strain rate softening parameter). Under any conditions, elongation-to-break, $L(t_b)/L(0)$ and $A(t_b)/A(0)$, decreases with an increasing "a" value (i.e., increasing strain rate softening character).

Certain interesting results concerning the $\tau_0 E_1$ dependence should be noted. When the dependence of τ upon strain rate is small (i.e., small "a"), increasing $\tau_0 E_1$ increases the elongation-to-break after the minimum. On the other hand, if the deformation rate dependence of τ is large (i.e., large "a") the elongation-to-break decreases as $\tau_0 E_1$ increases. However, the quantitative effect of "a" on elongation-to-break is rather complex.

Figures 7.11 and 7.12 show plots of $L(t_b)/L(0)$ caused by ductile failure as a function of multiaxiality E_2/E_1, for different $\tau_0 E_1$ and "a" values. In general $L(t_b)/L(0)$ decreases with increasing E_2/E_1. Weak strain rate softening τ (i.e., small "a") makes $L(t_b)/L(0)$ increase with increasing $\tau_0 E_1$ at fixed E_2/E_1, and decrease with increasing E_2/E_1 at fixed $\tau_0 E_1$. The strain rate softening character of τ being above intermediate (for example, "a" = 0.5) makes $L(t_b)/L(0)$ tend to have a minimum and then a maximum for high values of $\tau_0 E_1$. The minimum exists near $E_2/E_1 = 0$ (planar extension) and the maximum lies between $E_2/E_1 = 0.5$ and 2.0. This phenomenon is enhanced by increasing $\tau_0 E_1$. Quite different effects of the influence of $\tau_0 E_1$ on $L(t_b)/L(0)$ at small E_2/E_1 and large E_2/E_1 are also observed (see Figures 7.12d and 7.12e), especially for "a" = 0.6. Under small E_2/E_1, higher $\tau_0 E_1$

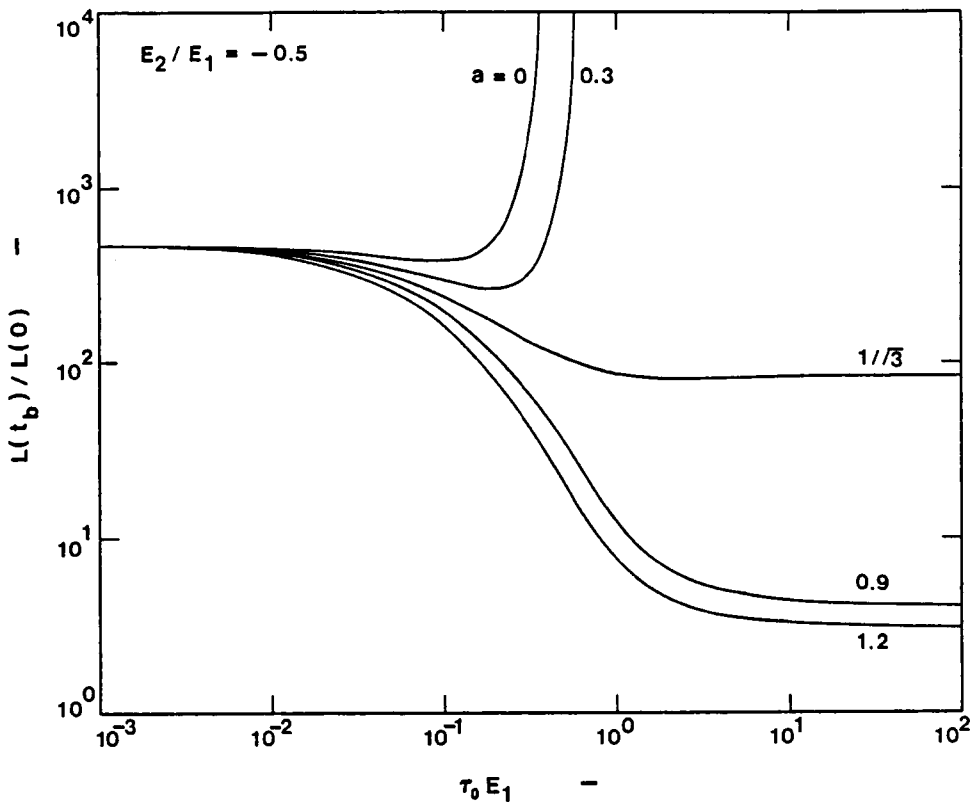

(a) E_2/E_1 = -0.5, uniaxial extension

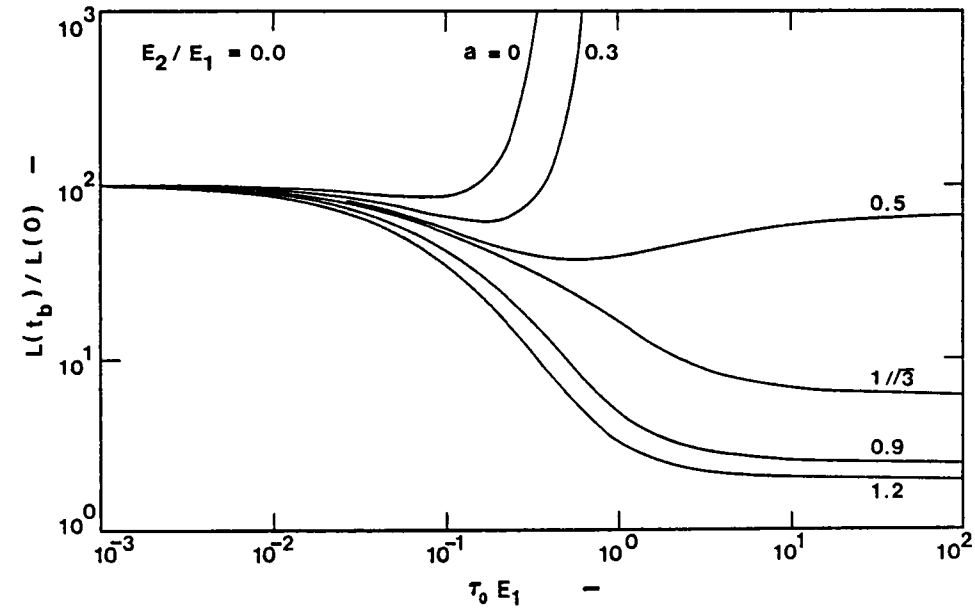

(b) E_2/E_1 = 0.0, planar extension

Figure 7.9. Theoretical limiting strain $L(t_b)/L(0)$ caused by ductile failure as a function of $\tau_0 E_1$ for various "a" values.

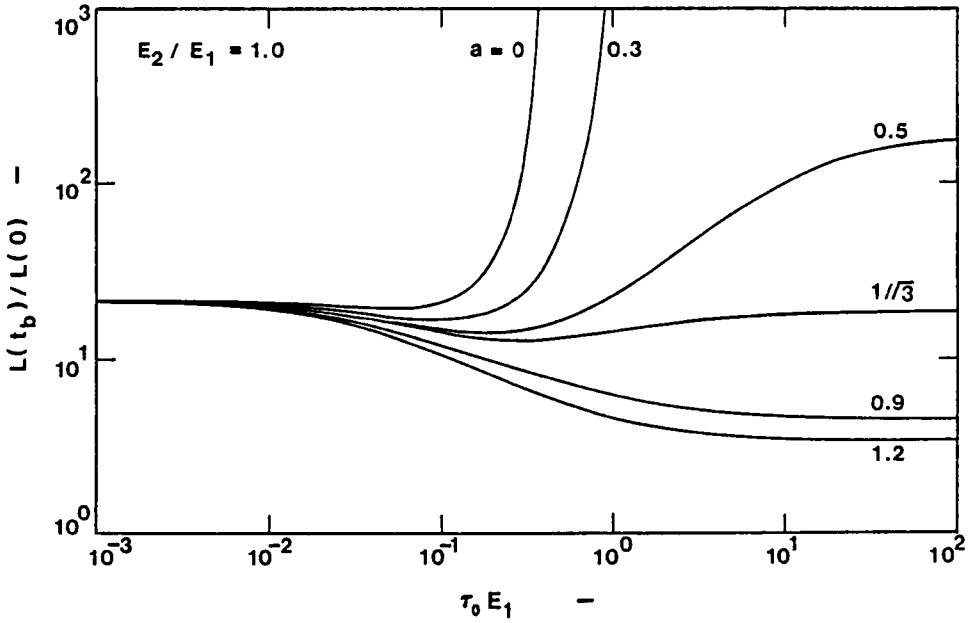

(c) E_2/E_1 = 1.0, equal biaxial extension

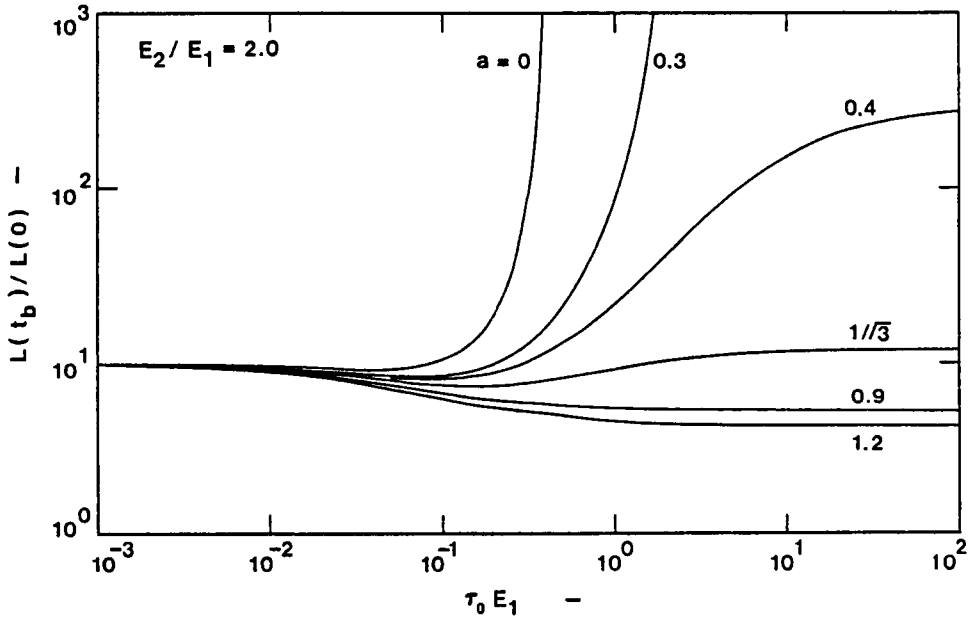

(d) E_2/E_1 = 2.0

Figure 7.9 (continued)

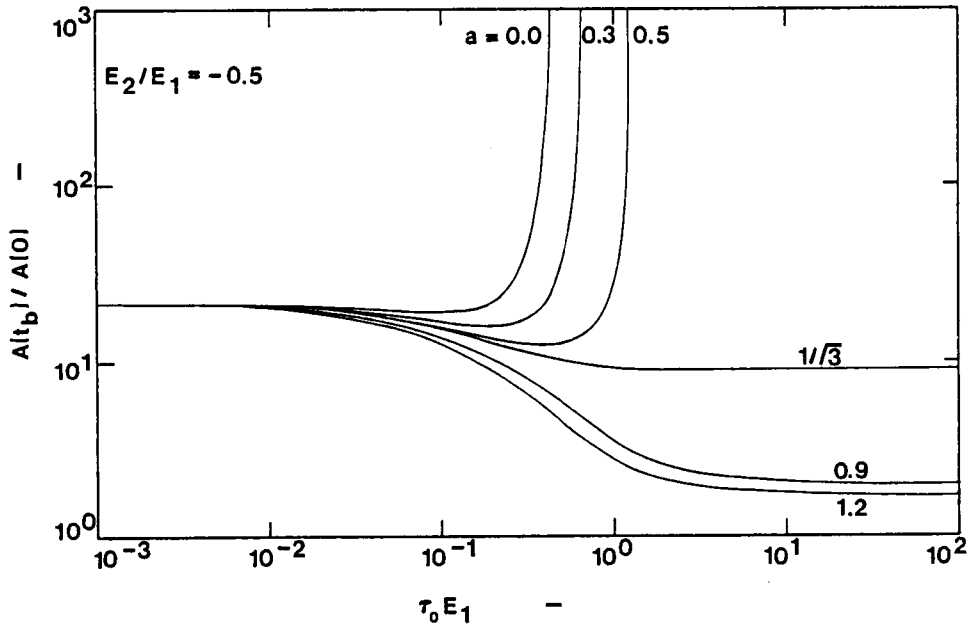

(a) E_2/E_1 = -0.5, uniaxial extension

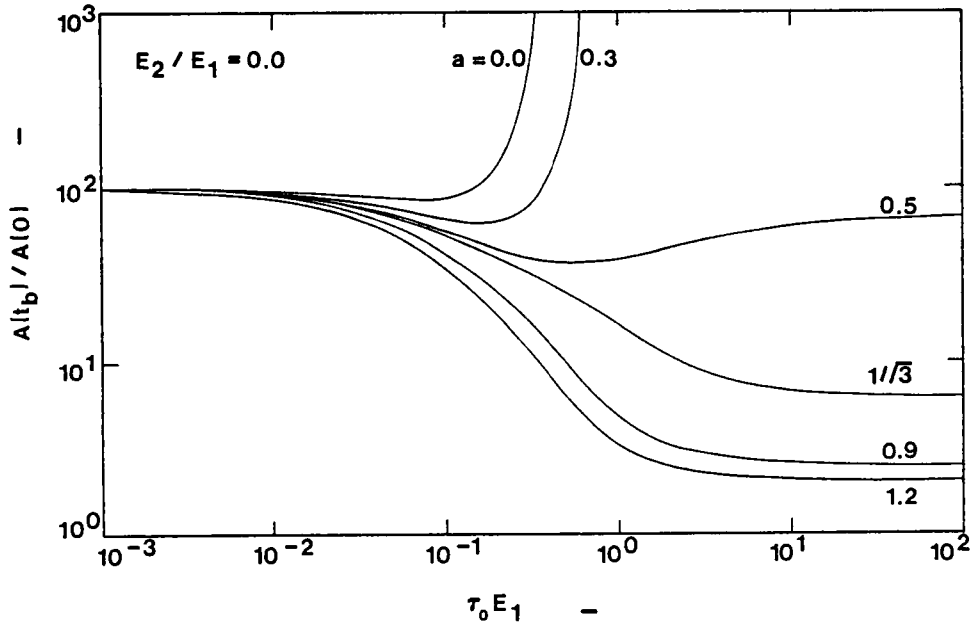

(b) E_2/E_1 = 0.0, planar extension

Figure 7.10. Theoretical limiting area $A(t_b)/A(0)$ caused by ductile failure as a function of $\tau_0 E_1$ for various "a" values.

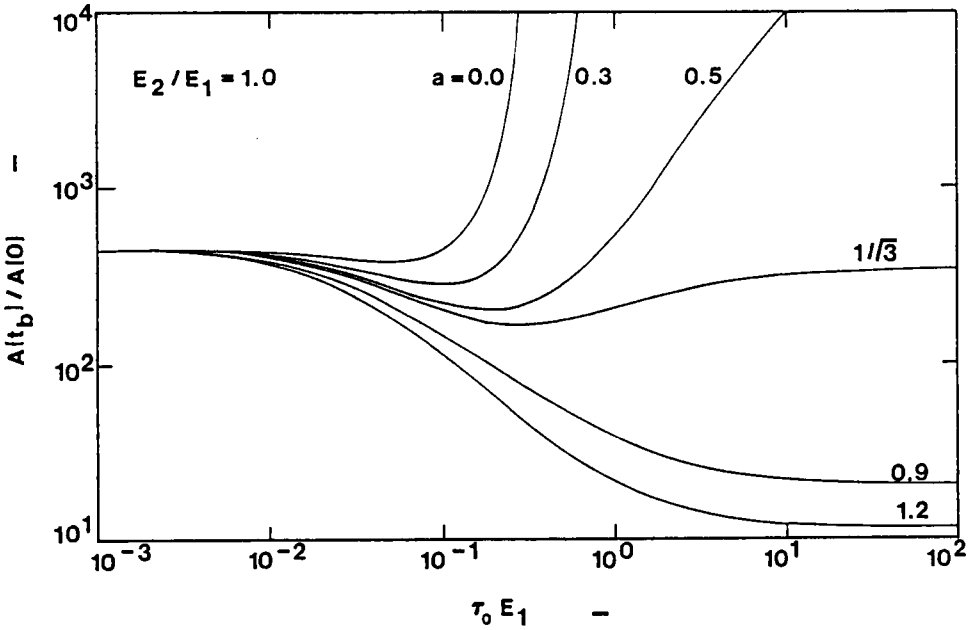

(c) E_2/E_1 = 1.0, planar extension

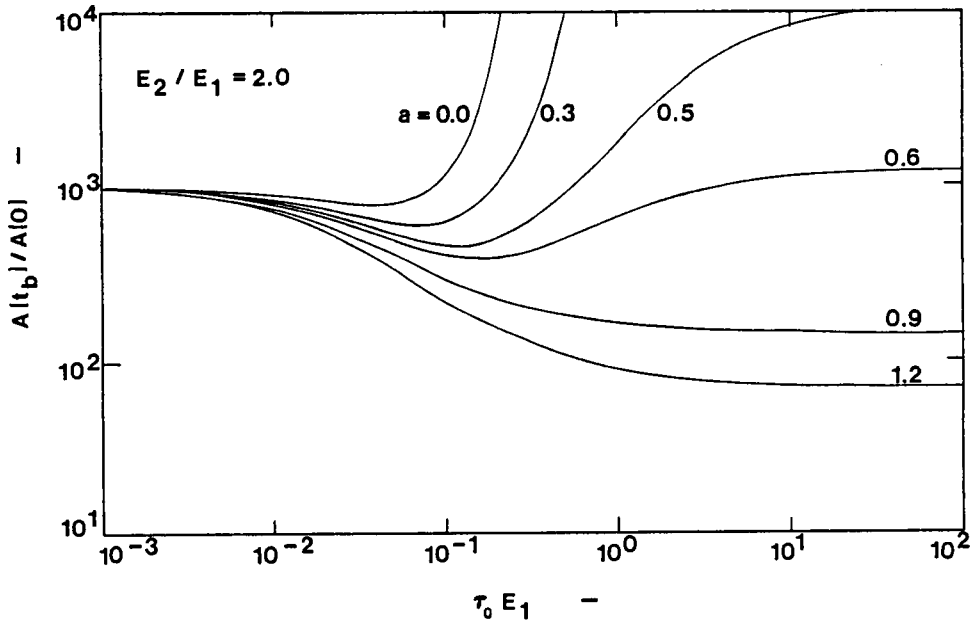

(d) E_2/E_1 = 2.0

Figure 7.10 (continued)

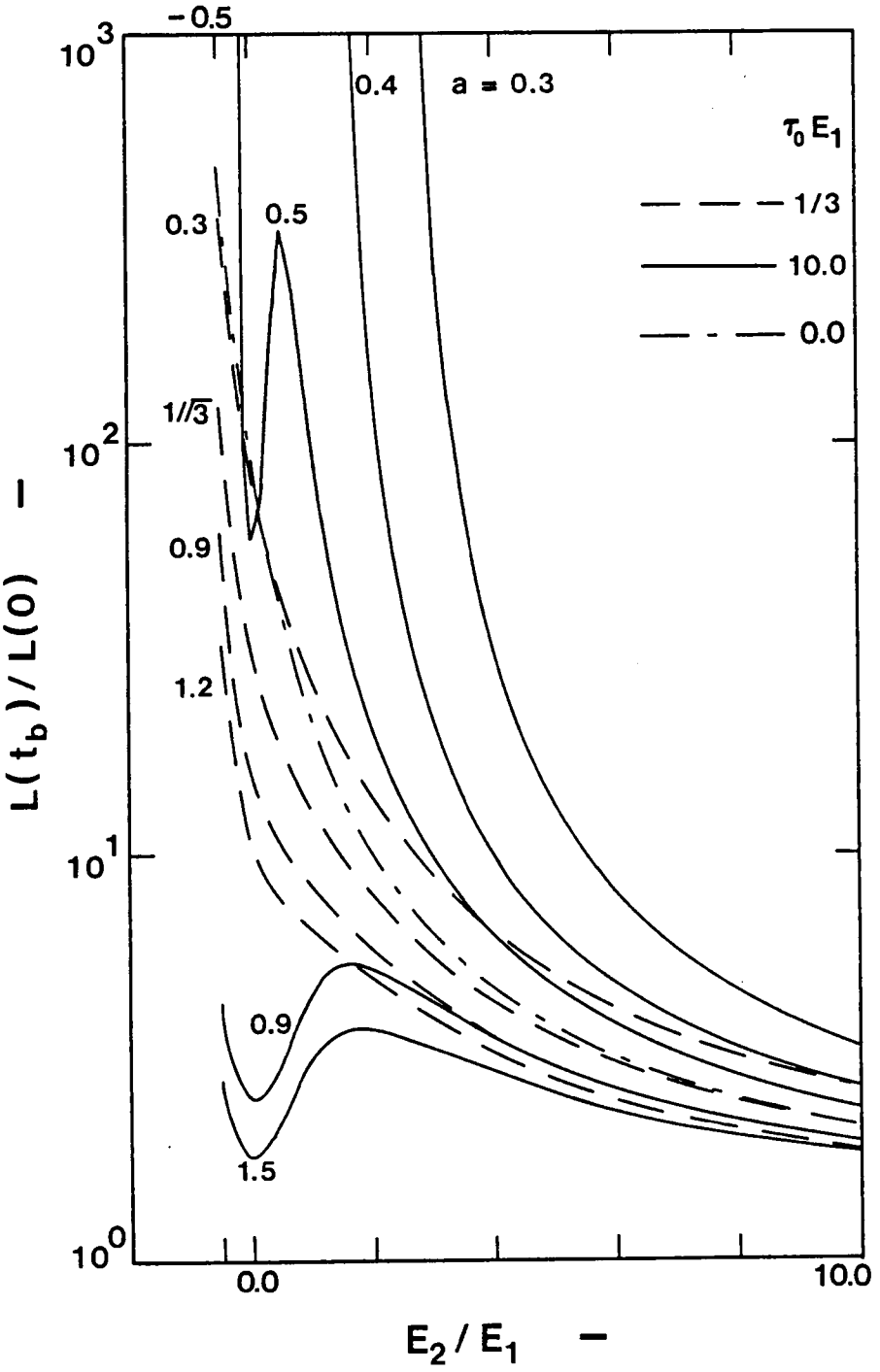

Figure 7.11. Theoretical limiting strain $L(t_b)/L(0)$ caused by ductile failure as a function of E_2/E_1 for various $\tau_0 E_1$ and "a".

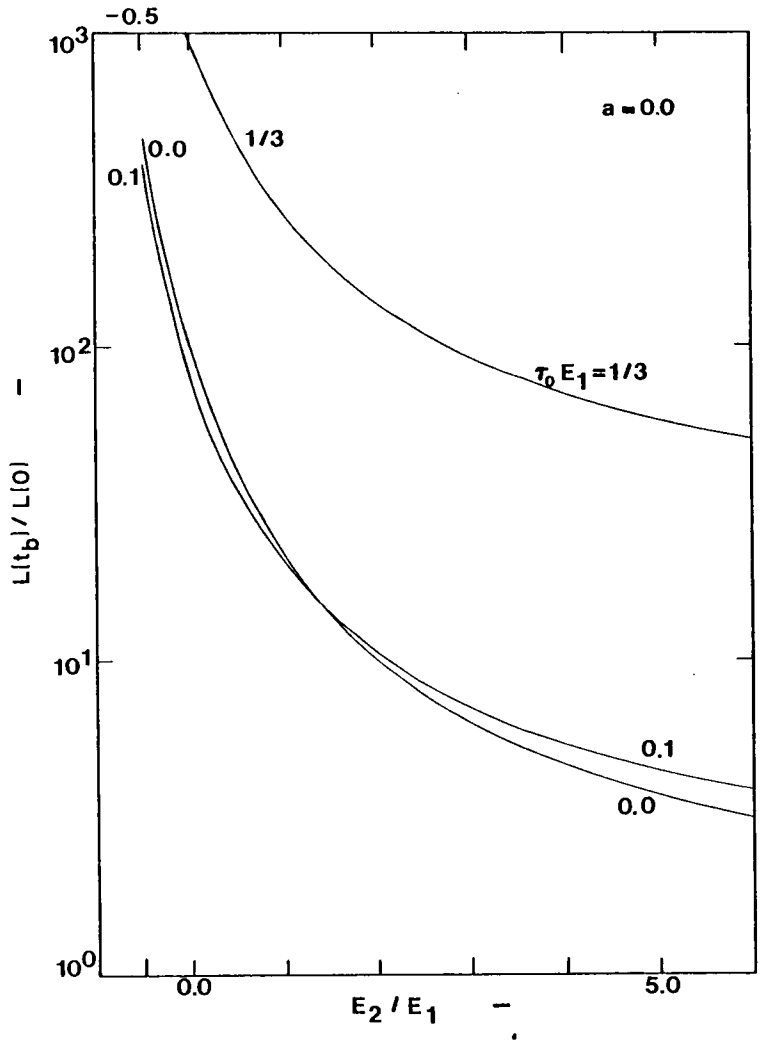

(a) "a" = 0.0

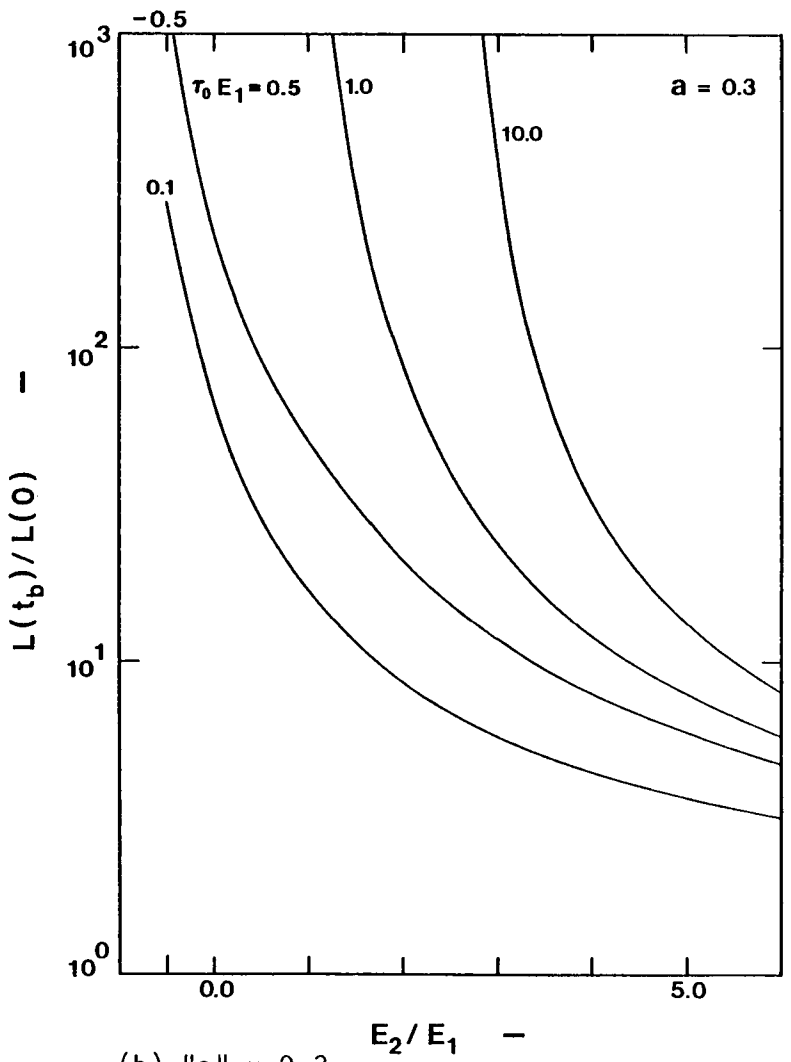

(b) "a" = 0.3

Figure 7.12. Theoretical limiting strain $L(t_b)/L(0)$ caused by ductile failure as a function of E_2/E_1 for various $\tau_0 E_1$.

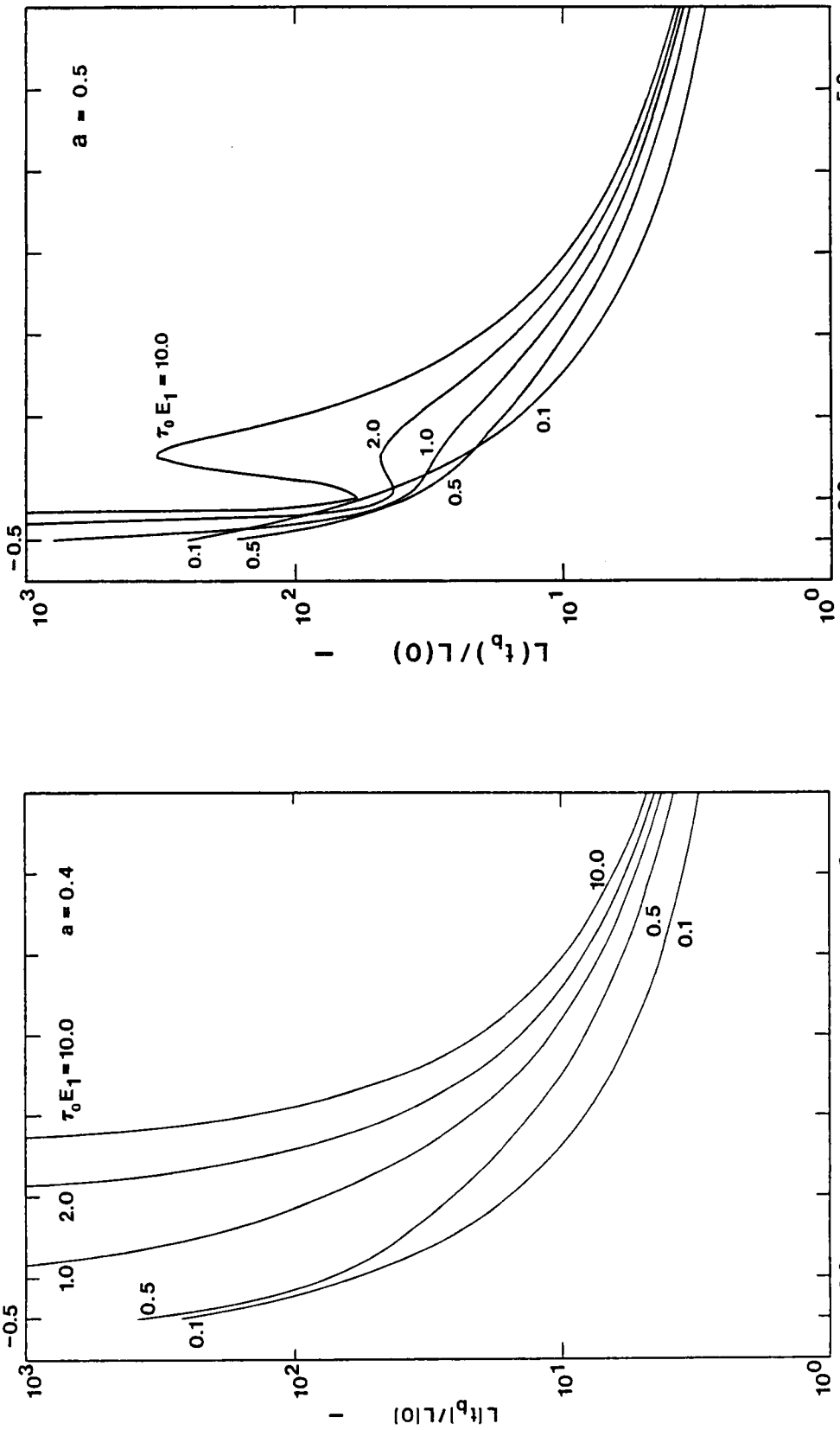

(c) "a" = 0.4

(d) "a" = 0.5

Figure 7.12 (continued)

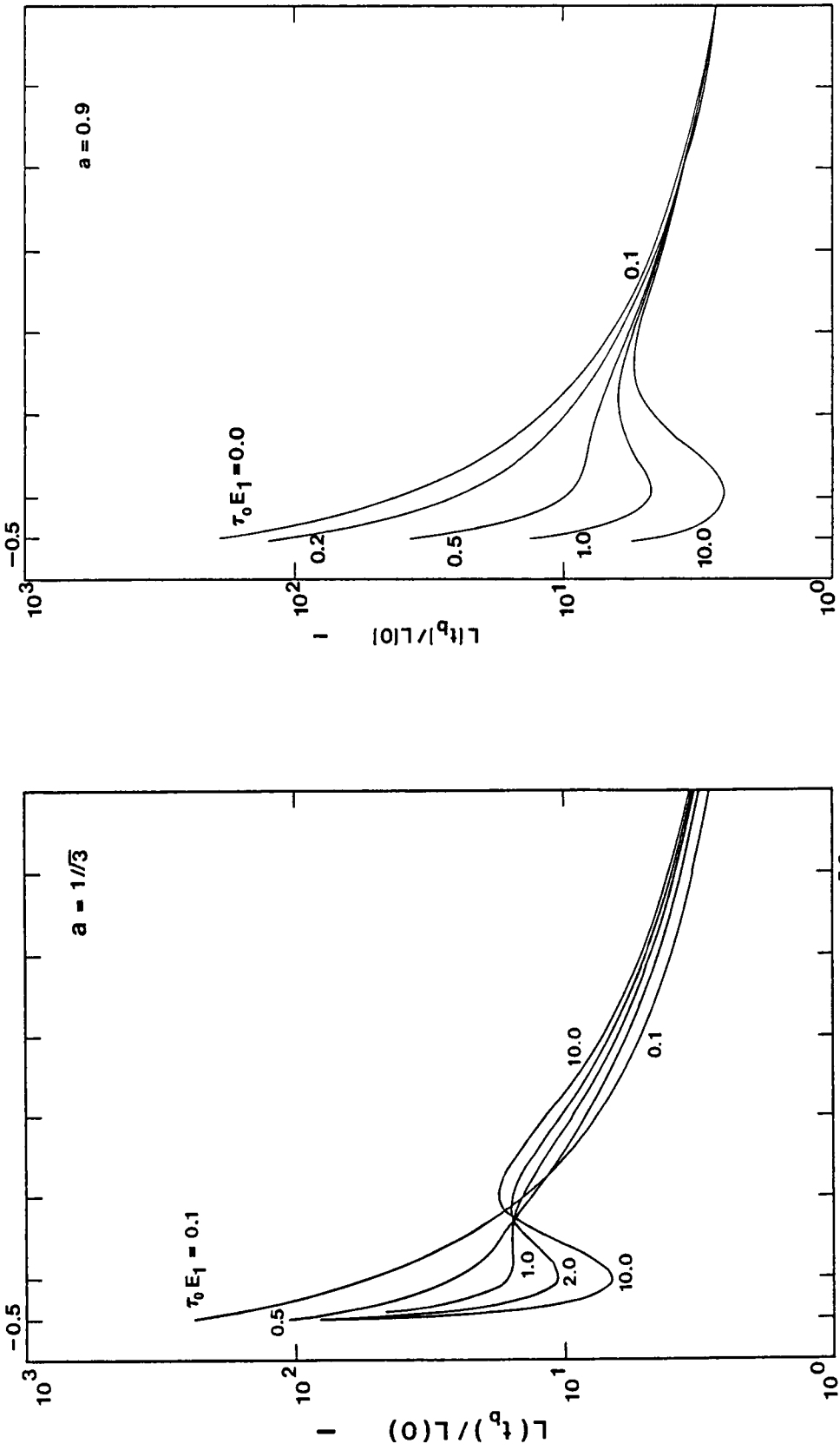

(e) "a" = $1/\sqrt{3}$

(f) "a" = 0.9

Figure 7.12 (continued)

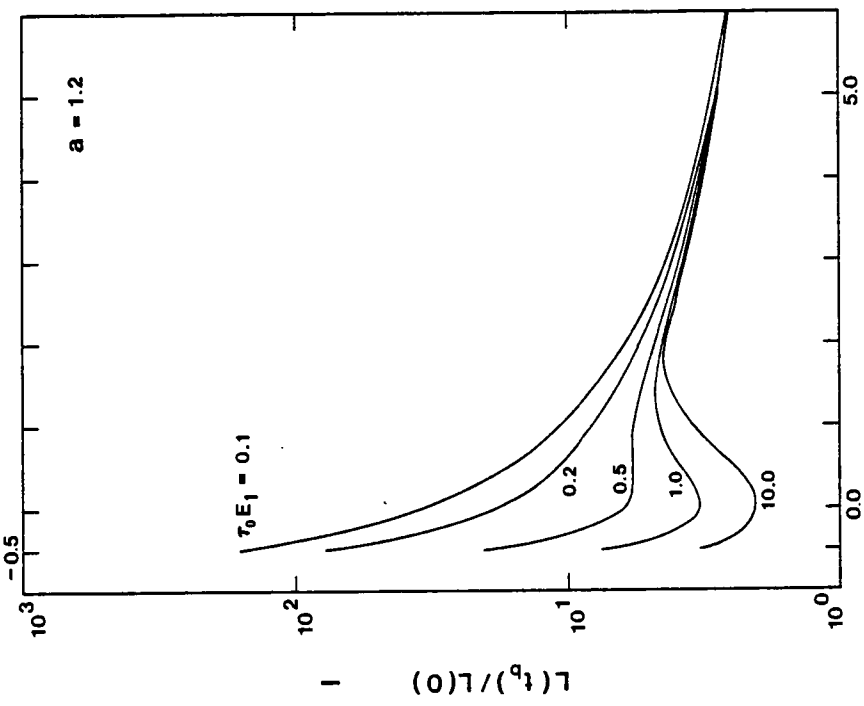

(g) "a" = 1.2

Figure 7.12 (continued)

tends to make $L(t_b)/L(0)$ smaller at fixed E_2/E_1; however, at large E_2/E_1, higher $\tau_0 E_1$ makes the system more stable at fixed E_2/E_1. The materials which have strong strain rate softening τ have smaller $L(t_b)/L(0)$ by increasing $\tau_0 E_1$, and still exhibit a minimum and a maximum on $L(t_b)/1(0)$ for a higher $\tau_0 E_1$ condition.

Figures 7.13 and 7.14 show plots of $A(t_p)/A(0)$ caused by ductile failure as a function of the multiaxiality E_2/E_1, for various values of $\tau_0 E_1$ and "a". One observes rather complex results compared with those of Figures 7.11 and 7.12. In general, $A(t_b)/A(0)$ increases with increasing E_2/E_1. Strain rate independent τ (i.e., "a" = 0) makes the system very stable and ductile failure occurs for $\tau_0 E_1$ of less than 0.5. Weak strain rate dependent τ (small "a") makes $A(t_b)/A(0)$ increase with increasing $\tau_0 E_1$, at fixed E_2/E_1. $A(t_b)/A(0)$ is a monotonic increasing function of E_2/E_1 for the condition of small $\tau_0 E_1$. However, $A(t_b)/A(0)$ is a monotonic decreasing function of E_2/E_1 for large $\tau_0 E_1$. For cases where "a" is not small (that is, for a significant strain rate softening effect on τ), $A(t_b)/A(0)$ for intermediate values of $\tau_0 E_1$ tend to exhibit minima (for example, when "a" is 0.4, $\tau_0 E_1$ of about 1.0 exhibits a minimum at E_2/E_1 of 0.2). This phenomenon becomes extreme at "a" = 0.5. Especially $\tau_0 E_1$ = 10.0 exhibits a maximum after the minimum in $A(t_b)/A(0)$. The effect of $\tau_0 E_1$ on $A(t_b)/A(0)$ at fixed E_2/E_1 gradually changes; $A(t_b)/A(0)$ decreases with increasing $\tau_0 E_1$ at small E_2/E_1, but higher $\tau_0 E_1$ still makes $A(t_b)/A(0)$ larger at larger E_2/E_1. A typical example is the case of "a" = $1/\sqrt{3}$. The value of E_2/E_1 at which $A(t_b)/A(0)$ exhibits

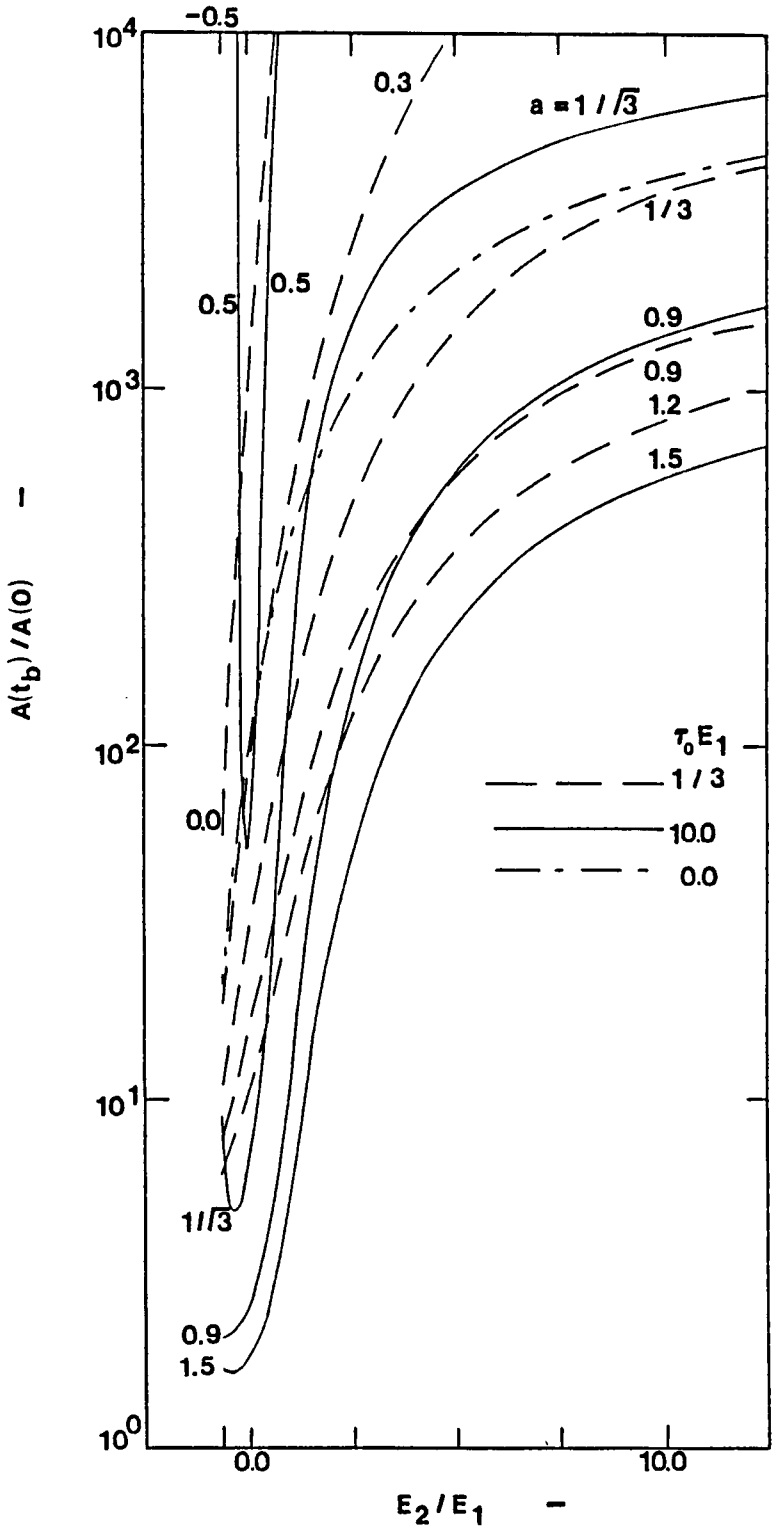

Figure 7.13. Theoretical limiting area $A(t_b)/A(0)$ caused by ductile failure as a function of E_2/E_1 for various $\tau_0 E_1$ and "a".

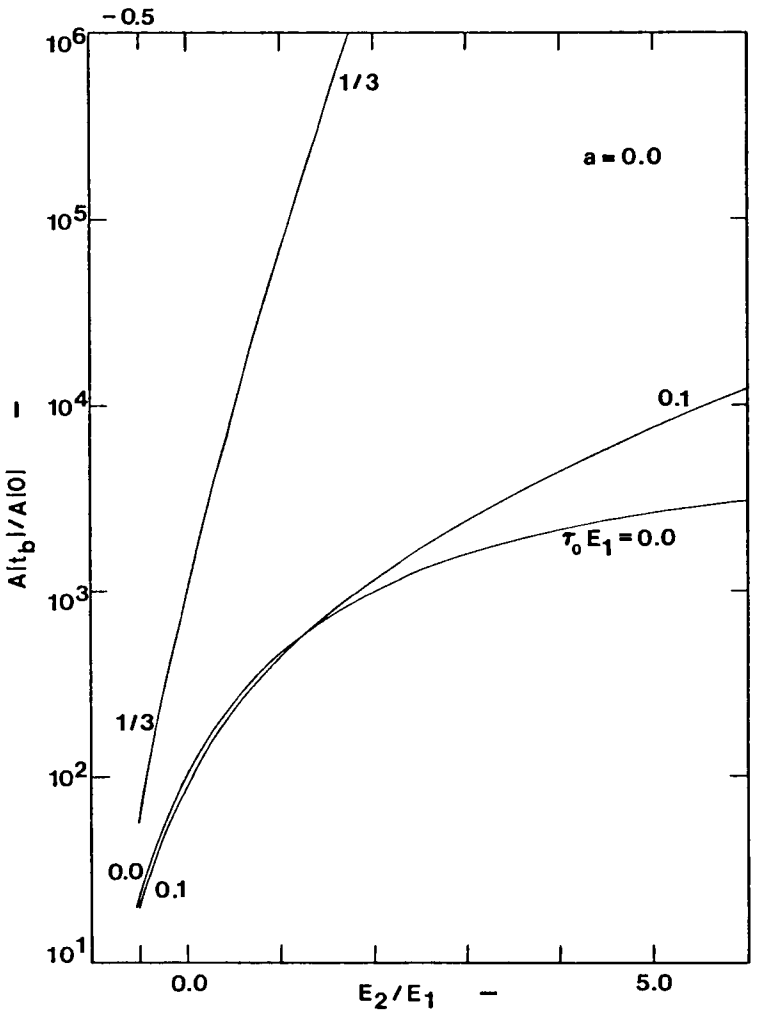

(a) "a" = 0.0

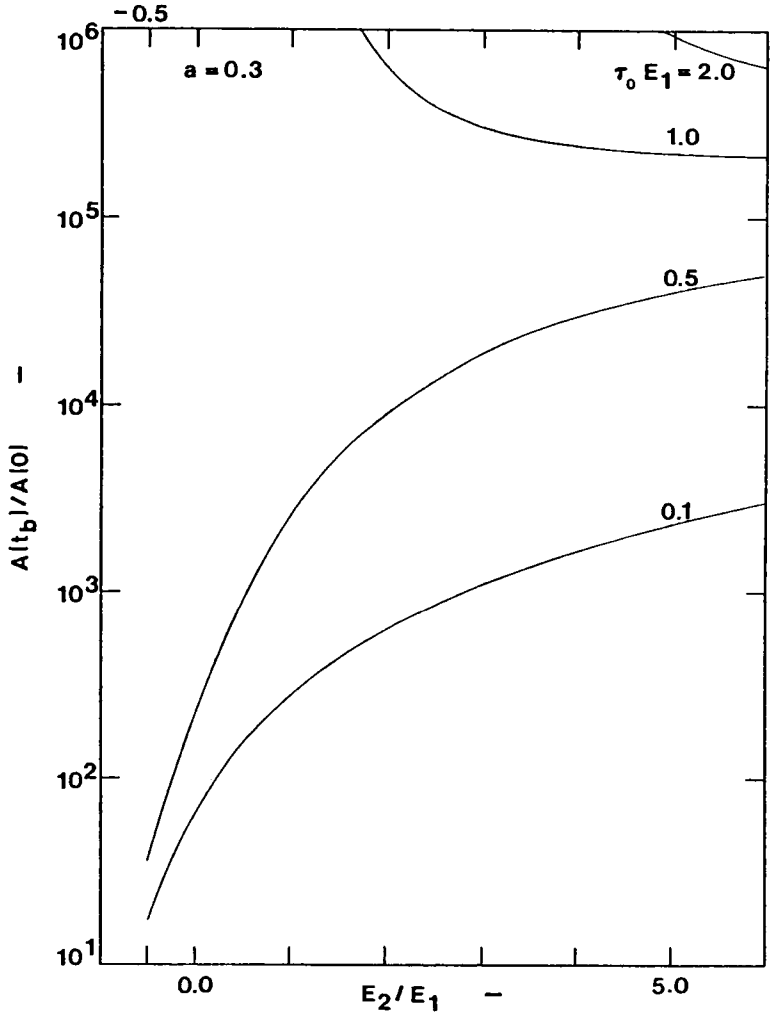

(b) "a" = 0.3

Figure 7.14. Theoretical limiting area $A(t_b)/A(0)$ caused by ductile failure as a function of E_2/E_1 for various $\tau_0 E_1$.

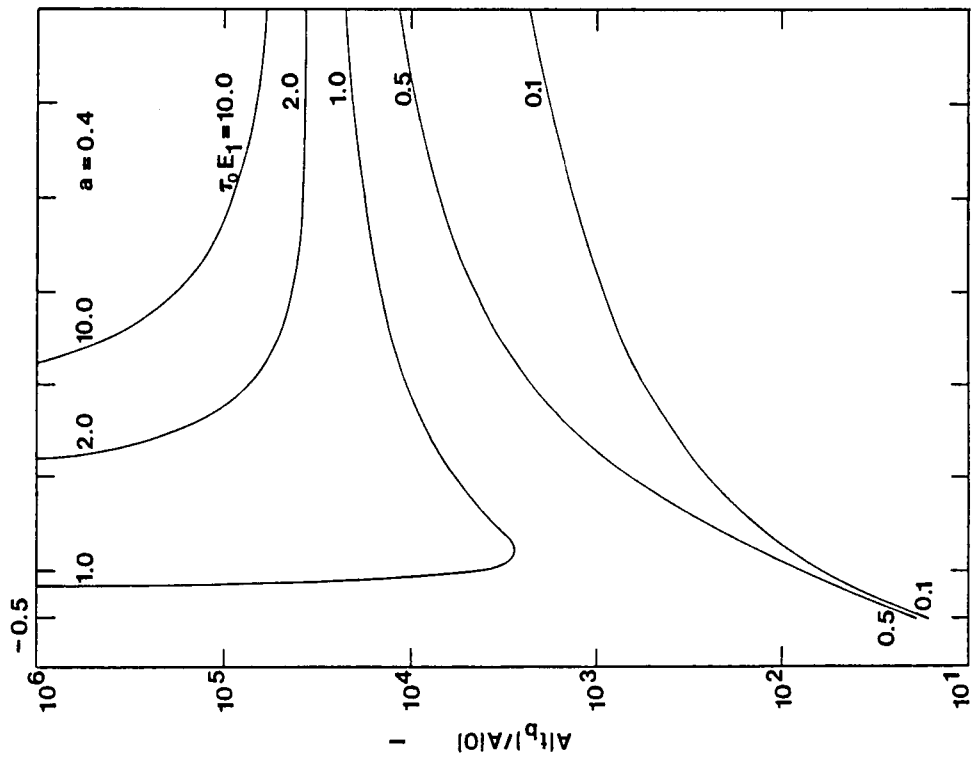

(c) "a" = 0.4

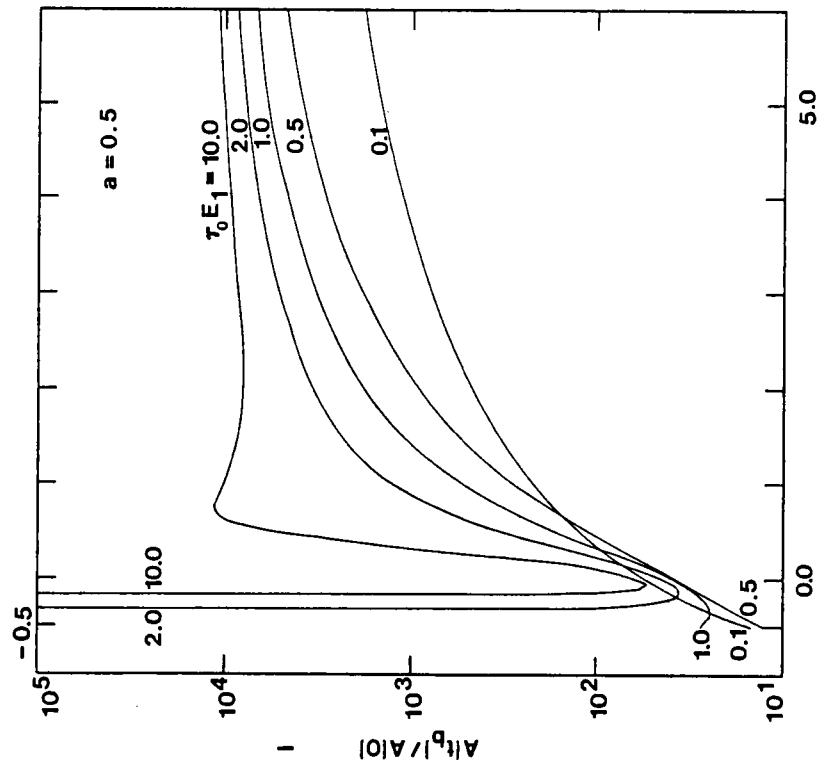

(d) "a" = 0.5

Figure 7.14 (continued)

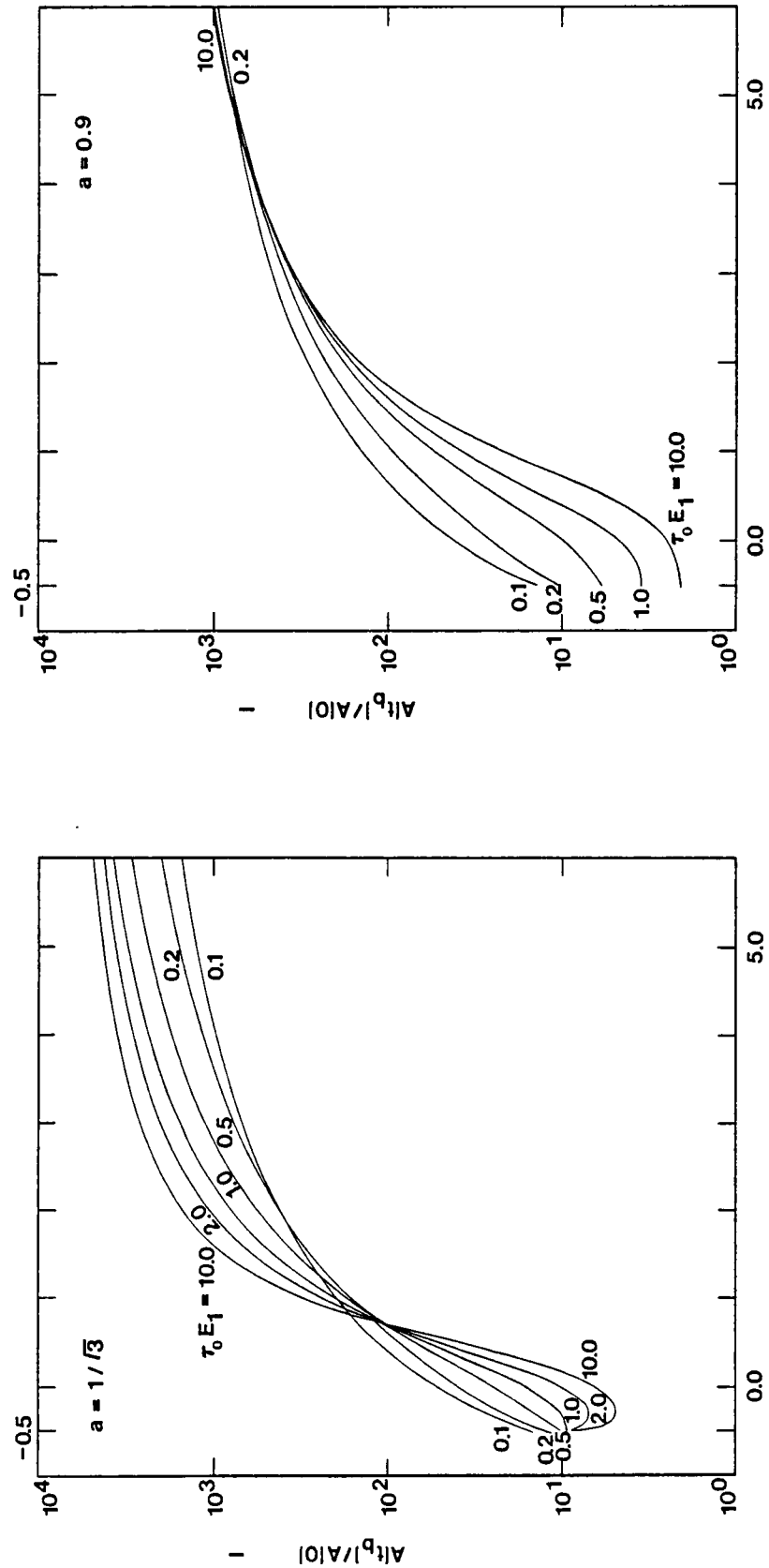

(e) "a" = $1/\sqrt{3}$ (f) "a" = 0.9

Figure 7.14 (continued)

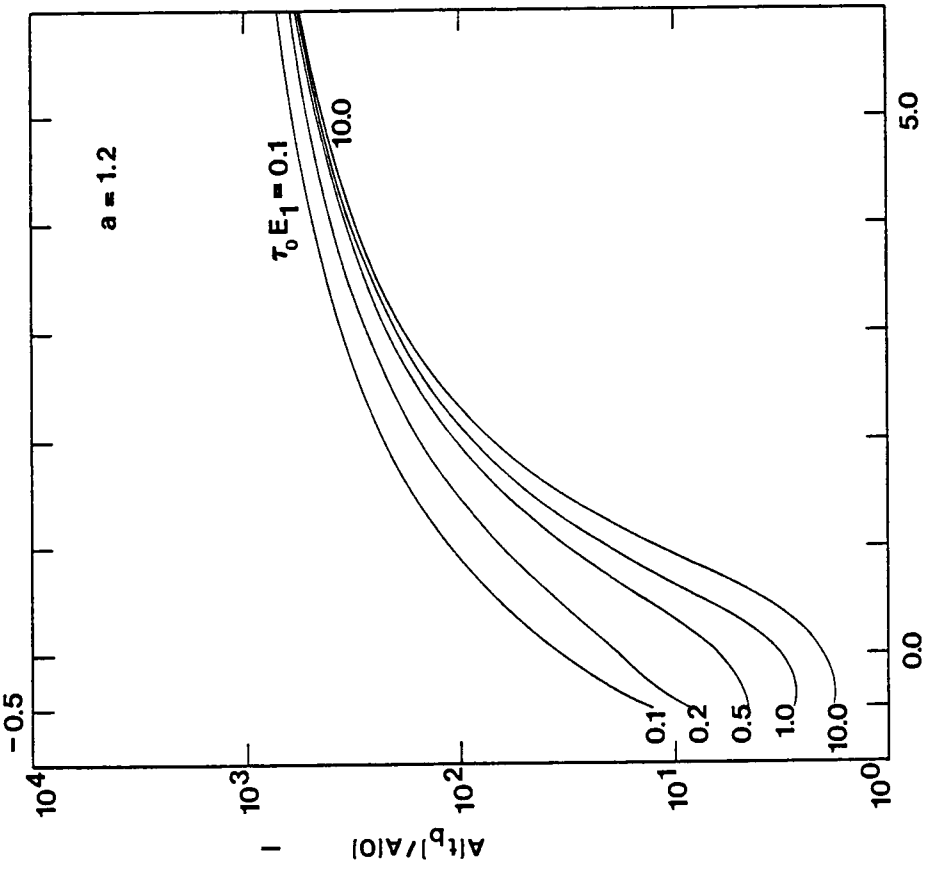

(g) "a" = 1.2

Figure 7.14 (continued)

a minimum decreases with decreasing $\tau_0 E_1$ and with increasing "a". A stronger strain rate softening τ makes $A(t_b)/A(0)$ small with increasing $\tau_0 E_1$ at fixed E_2/E_1.

D-2. Fracture

A viscoelastic fluid generally cannot be stretched rapidly because cohesive fracture occurs. If we may presume that failure occurs at a critical stress level or critical strain energy level, it might be useful to assume that the fracture surface is similar to the von Mises yield criterion [M-43,R-5] as:

$$2\sigma_{cr}^2 = \text{tr } T_{ij}^2 , \tag{7.62a}$$

where T_{ij} is the deviatoric stress tensor given by

$$T_{ij} = \sigma_{ij} - \frac{1}{3} \text{tr } \sigma_{ij} . \tag{7.62b}$$

It is expected that cohesive fracture occurs under a condition of high elasticity.

We assume $\sigma_{cr} = 6G$ and calculate the elongation-to-break due to fracture by combining Eqns. (7.7) and (7.62).

Figure 7.15 shows plots of $L(t_b)/L(0)$ and $A(t_b)/A(0)$ caused by cohesive fracture of a convected Maxwell material with constant relaxation time as a function of τE_1 for different E_2/E_1. It is found that the elongation-to-break decreases with increasing τE_1 and reaches a constant value at high τE_1. $L(t_b)/L(0)$ decreases with increasing E_2/E_1 at fixed τE_1 for E_2/E_1 of more than zero. $L(t_b)/L(0)$

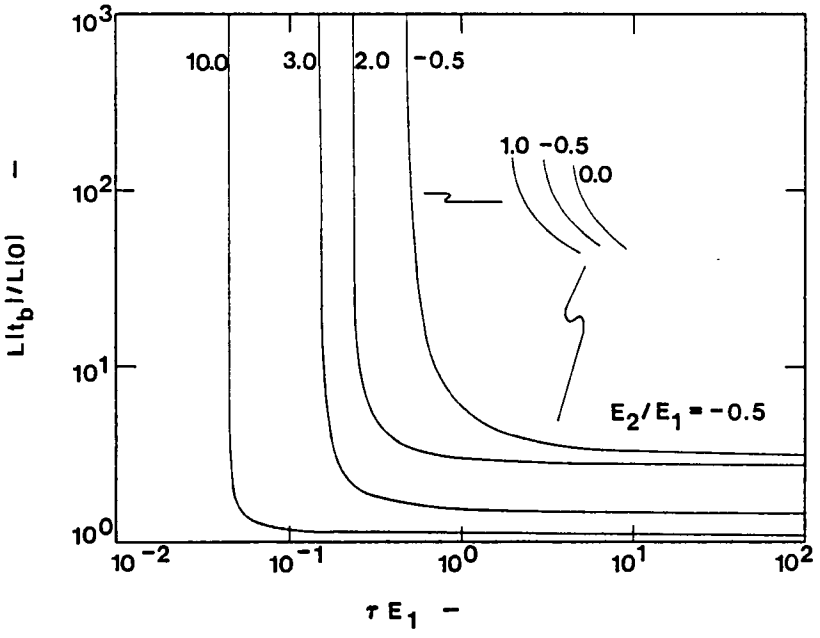

(a)

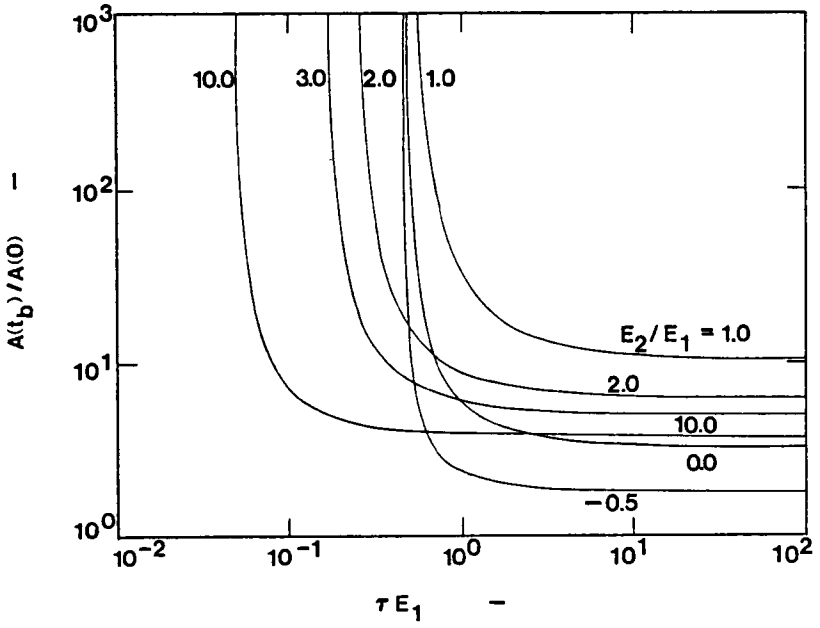

(b)

Figure 7.15. (a) Theoretical limiting strain $L(t_b)/L(0)$ caused by cohesive fracture as a function of τE_1 for various E_2/E_1 (constant relaxation time); (b) theoretical limiting area $A(t_b)/A(0)$ caused by cohesive fracture as a function of τE_1 for various E_2/E_1 (constant relaxation time).

for E_2/E_1 between -0.5 and 1.0 shows little variation. $A(t_b)/A(0)$ again exhibits complex behavior. At high τE_1, $A(t_b)/A(0)$ reaches asymptotic values which are highest for E_2/E_1 of 1.0 and lowest for E_2/E_1 of -0.5. $A(t_b)/A(0)$ has the same asymptotic values for the same value of E_2/E_1 and E_1/E_2. $A(t_b)/A(0)$ increases with decreasing τE_1, then finally goes to infinity at a critical value of $\tau E_{1,cr}$. The values of the critical τE_1 for each E_2/E_1 are related to the critical τE_1 for the inverse of each E_2/E_1 as

$$(\tau E_{1,cr}) \cdot (E_2/E_1) = \tau E_{1,cr}\Big|_{E_1/E_2} . \tag{7.63}$$

These phenomena suggest that elongation-to-break, in terms of stretched area due to cohesive fracture, is dependent on how the extra stress along the machine direction and the transverse direction balance each other. This explanation is reinforced by rewriting Eqn. (7.62) as

$$2\sigma_{cr}^2 = \frac{1}{3}\left[(P_{11} - P_{22})^2 + (P_{22} - P_{33})^2 + (P_{33} - P_{11})^2\right] . \tag{7.64}$$

Figures 7.16 and 7.17 show plots of elongation-to-break as a function of $\tau_0 E_1$ for various values of "a". It is clearly seen that increasing the strain rate softening character (i.e., increasing the "a" value or E_2/E_1) decreases the elongation-to-break due to cohesive fracture.

Figures 7.18 and 7.19 show plots of the limiting strain of the $L(t_b)/L(0)$ caused by cohesive fracture as a function of multiaxiality

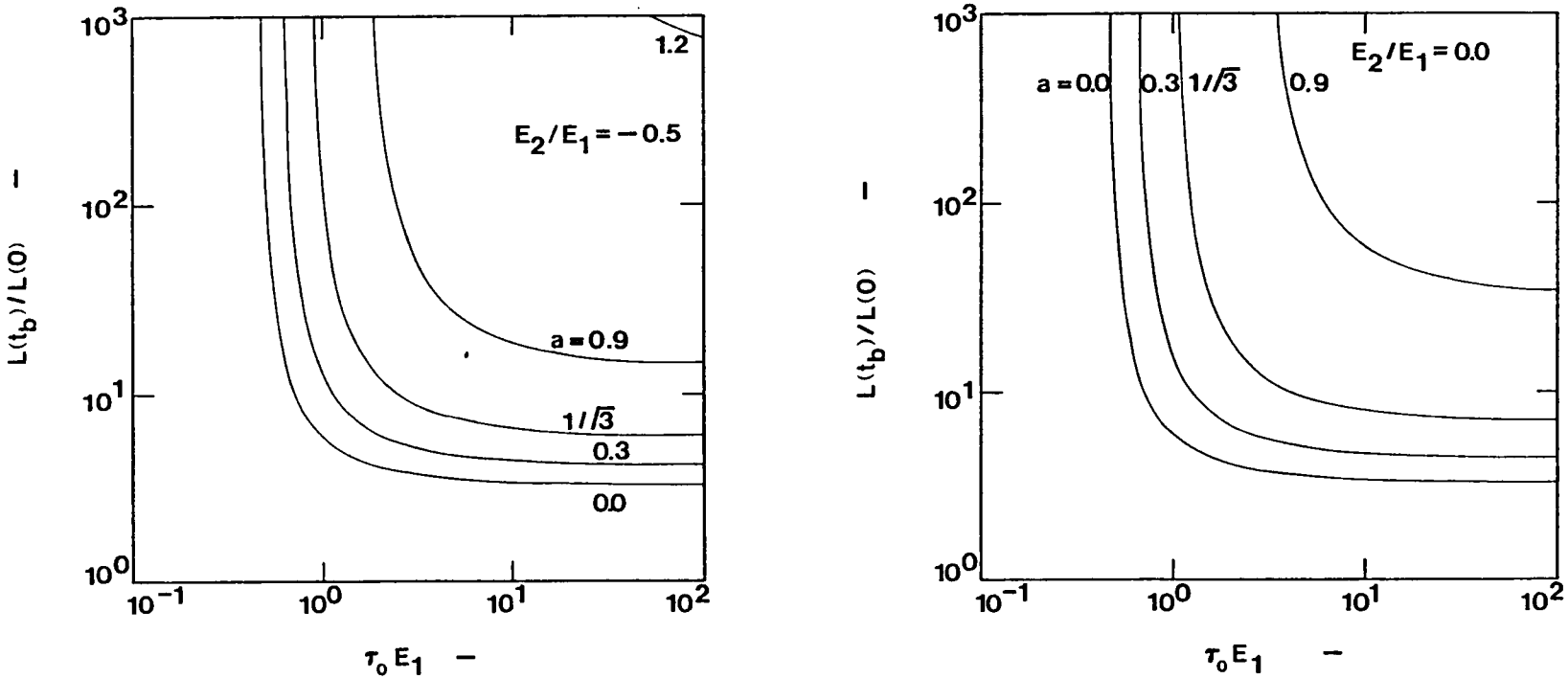

(a) E_2/E_1 = -0.5, uniaxial extension

(b) E_2/E_1 = 0.0, planar extension

Figure 7.16. Theoretical limiting strain $L(t_b)/L(0)$ caused by cohesive fracture as a function of $\tau_0 E_1$ for various "a" values.

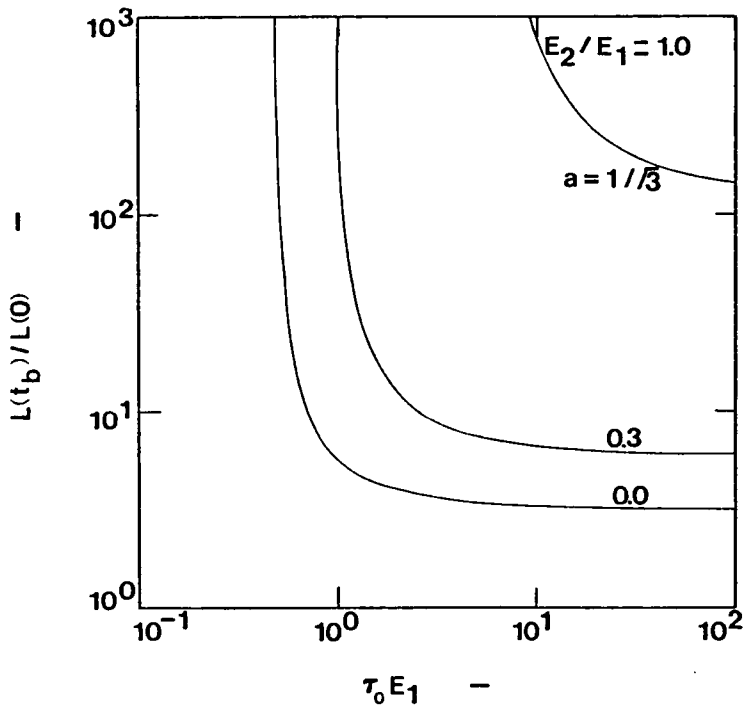

(c) E_2/E_1 = 1.0, equal biaxial extension

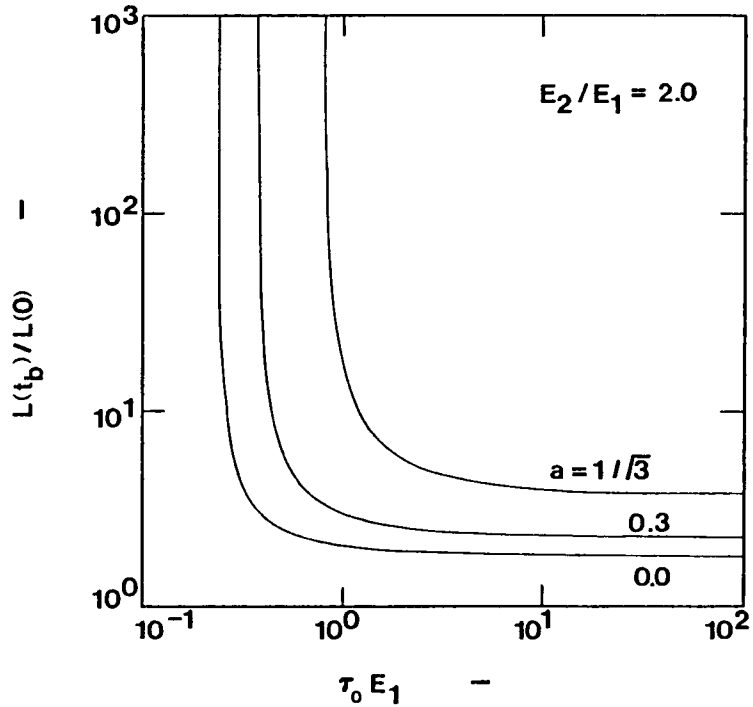

(d) E_2/E_1 = 2.0

Figure 7.16 (continued)

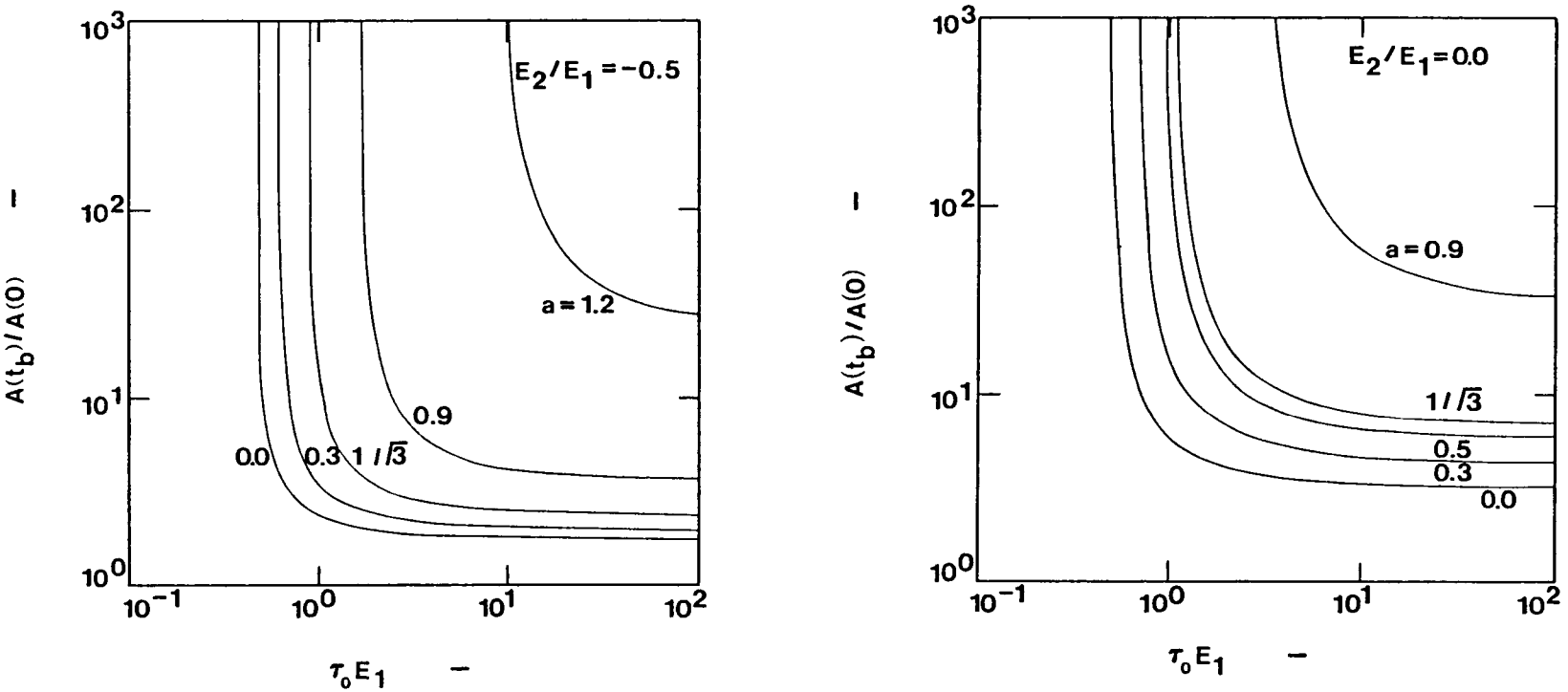

(a) E_2/E_1 = -0.5, uniaxial extension

(b) E_2/E_1 = 0.0, planar extension

Figure 7.17. Theoretical limiting area $A(t_b)/A(0)$ caused by cohesive fracture as a function of $\tau_0 E_1$ for various "a" values.

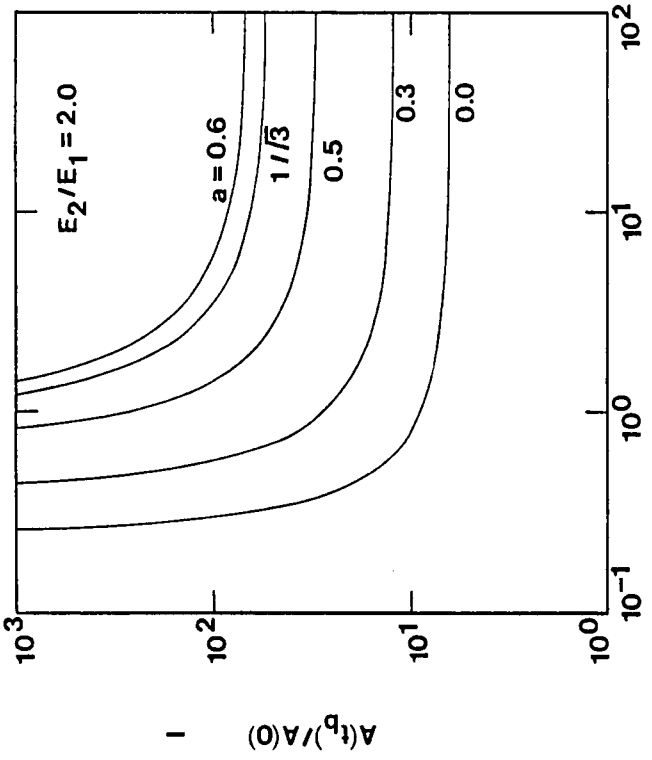

(d) $E_2/E_1 = 2.0$

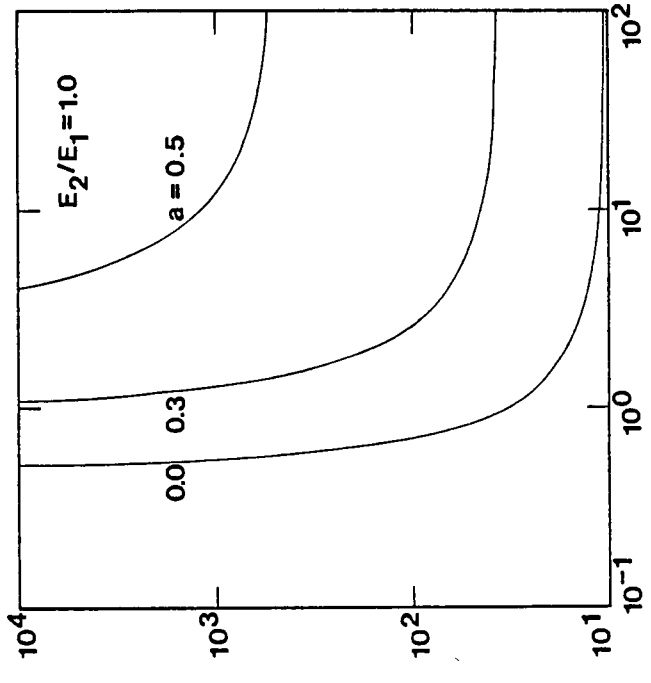

(c) $E_2/E_1 = 1.0$, equal biaxial extension

Figure 7.17 (continued)

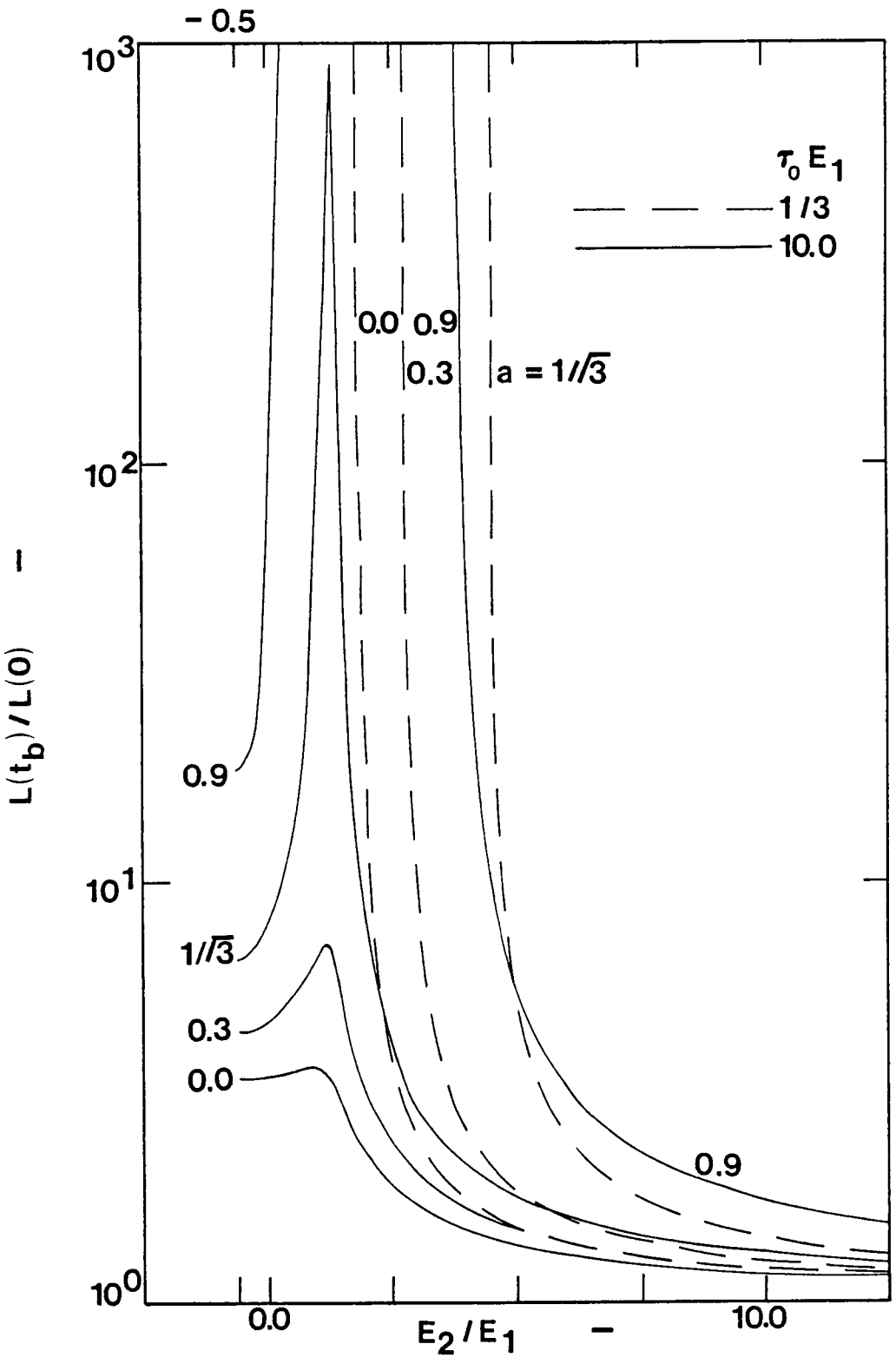

Figure 7.18. Theoretical limiting strain $L(t_b)/L(0)$ caused by cohesive fracture as a function of E_2/E_1 for various $\tau_0 E_1$ and "a" values.

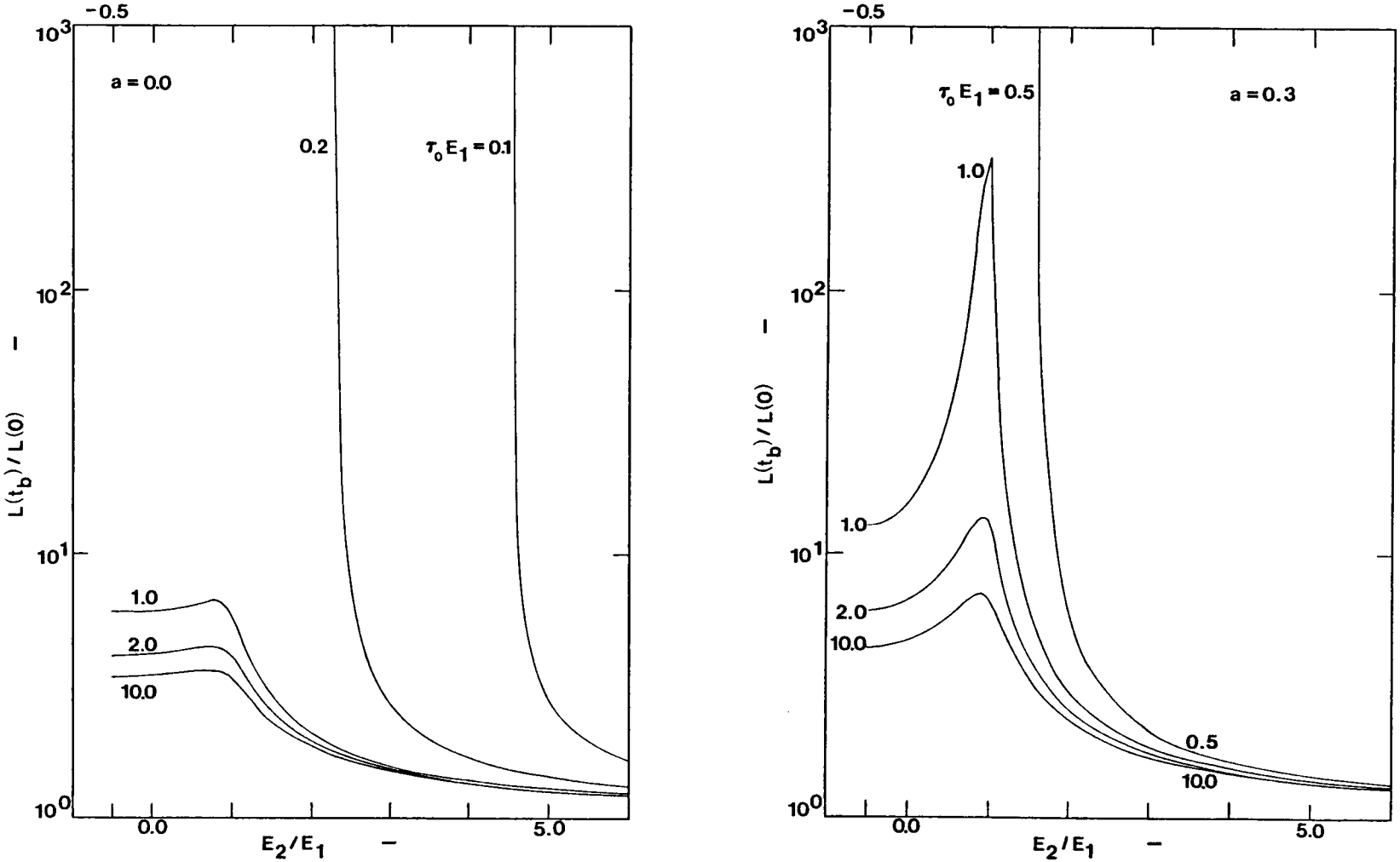

(a) "a" = 0.0 (b) "a" = 0.3

Figure 7.19. Theoretical limiting strain $L(t_b)/L(0)$ caused by cohesive fracture as a function of E_2/E_1 for various $\tau_0 E_1$.

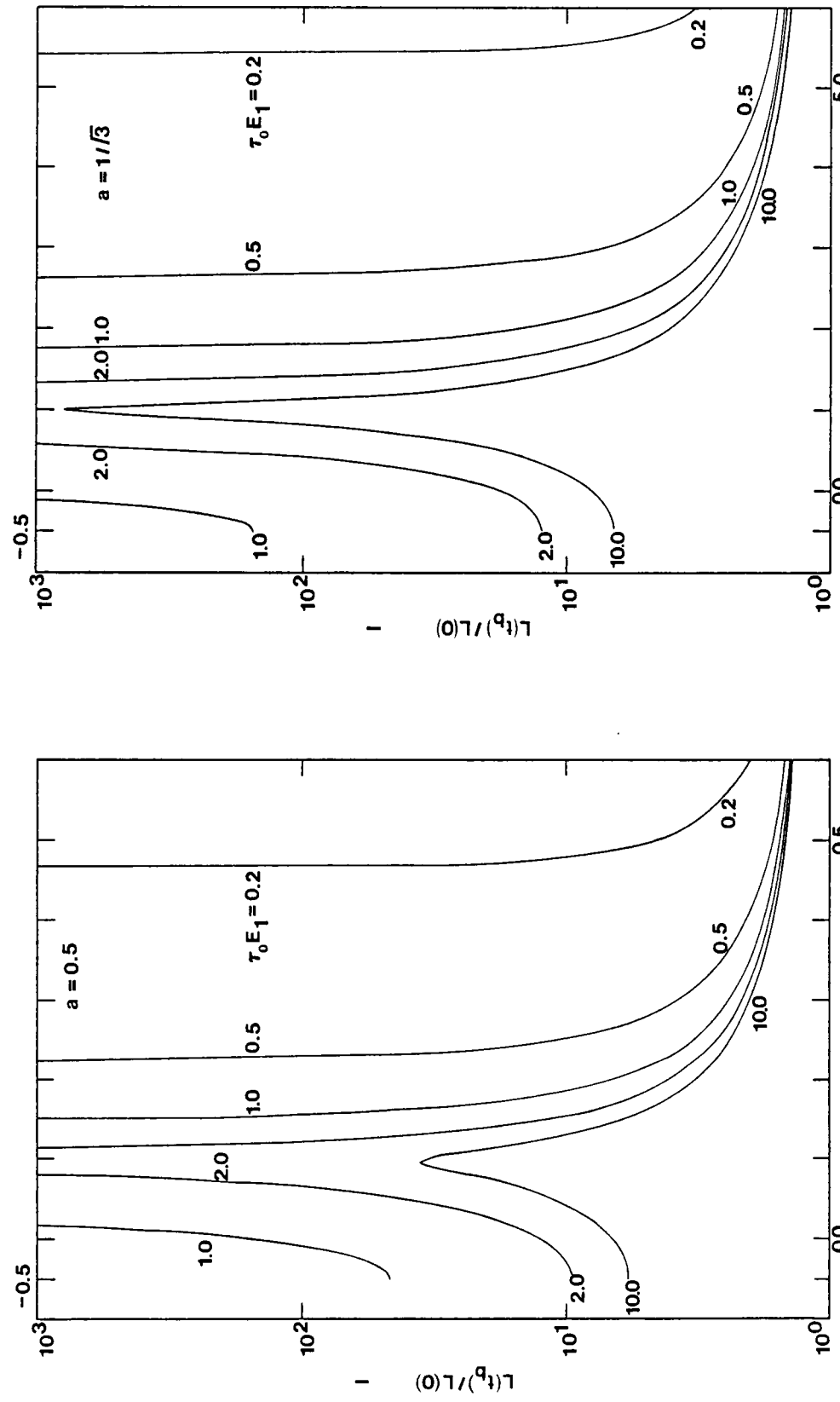

(c) "a" = 0.5

(d) "a" = $1/\sqrt{3}$

Figure 7.19 (continued)

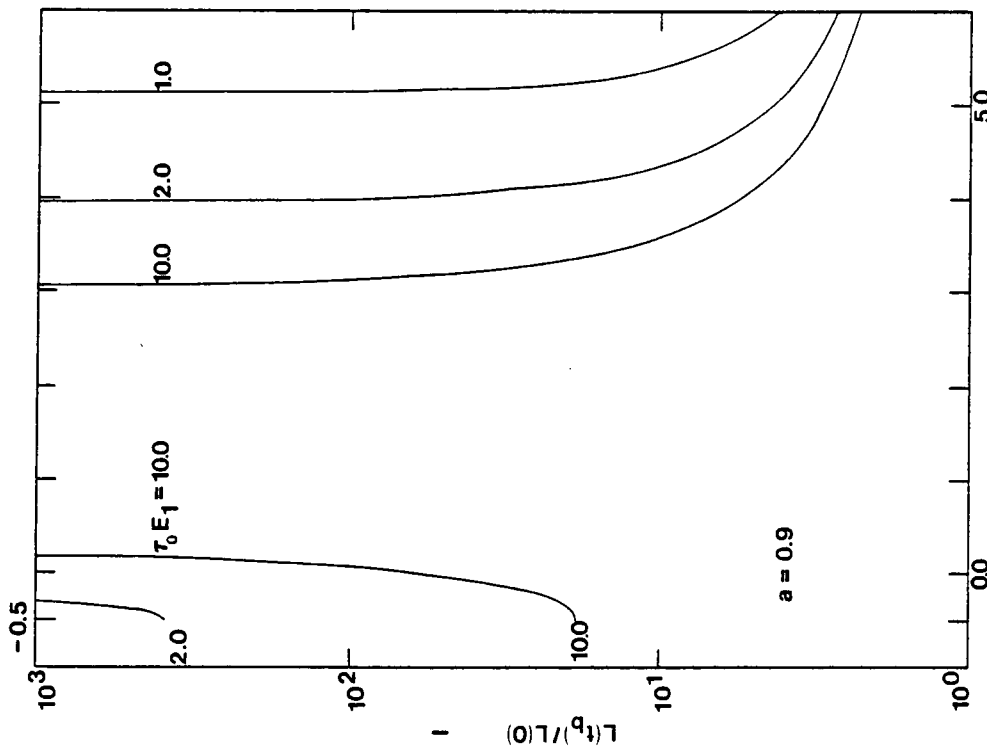

(e) "a" = 0.9

Figure 7.19 (continued)

E_2/E_1 for different values of $\tau_0 E_1$ and "a". Generally, $L(t_b)/L(0)$ is a decreasing function of E_2/E_1 with a maximum between E_2/E_1 = 1.0 and 0.7. Large $\tau_0 E_1$ or small "a" value makes $L(t_b)/L(0)$ exhibit a maximum at low E_2/E_1. The magnitude of the maximum value and the difference between this maximum value and the larger E_2/E_1 asymptotic value in $L(t_b)/L(0)$ increases with decreasing $\tau_0 E_1$ and increasing "a". Figures 7.20 and 7.21 show plots of the limiting stretched area $A(t_b)/A(0)$ due to cohesive fracture as a function of multiaxiality E_2/E_1 for different values of $\tau_0 E_1$ and "a". The $A(t_b)/A(0)$ curves exhibit a similar behavior to the $L(t_b)/L(0)$ plots. However, there are some differences. The existence of a maximum $A(t_b)/A(0)$ is more obvious than that for $L(t_b)/L(0)$. The E_2/E_1 value at which $A(t_b)/A(0)$ shows a maximum lies between 1.0 and 0.95. The larger $\tau_0 E_1$ and "a" values make the maximum point position near E_2/E_1 = 1.0.

E. COMPARISON WITH EXPERIMENT

The theoretical analyses developed in the previous sections will now be compared with certain experiments. In these experiments notched polystyrene sheets were stretched under various conditions. We give special attention to the growth of disturbances which lie along the machine direction. The defect development (thickness variation) was measured for various stretch ratio sheets.

E-1. Material and Experimental Conditions

The material which was used here was a commercial polystyrene, Dow Styron 685D with MI = 1.6, $M_w = 3.06 \times 10^5$, $M_w/M_n = 1.91$, and

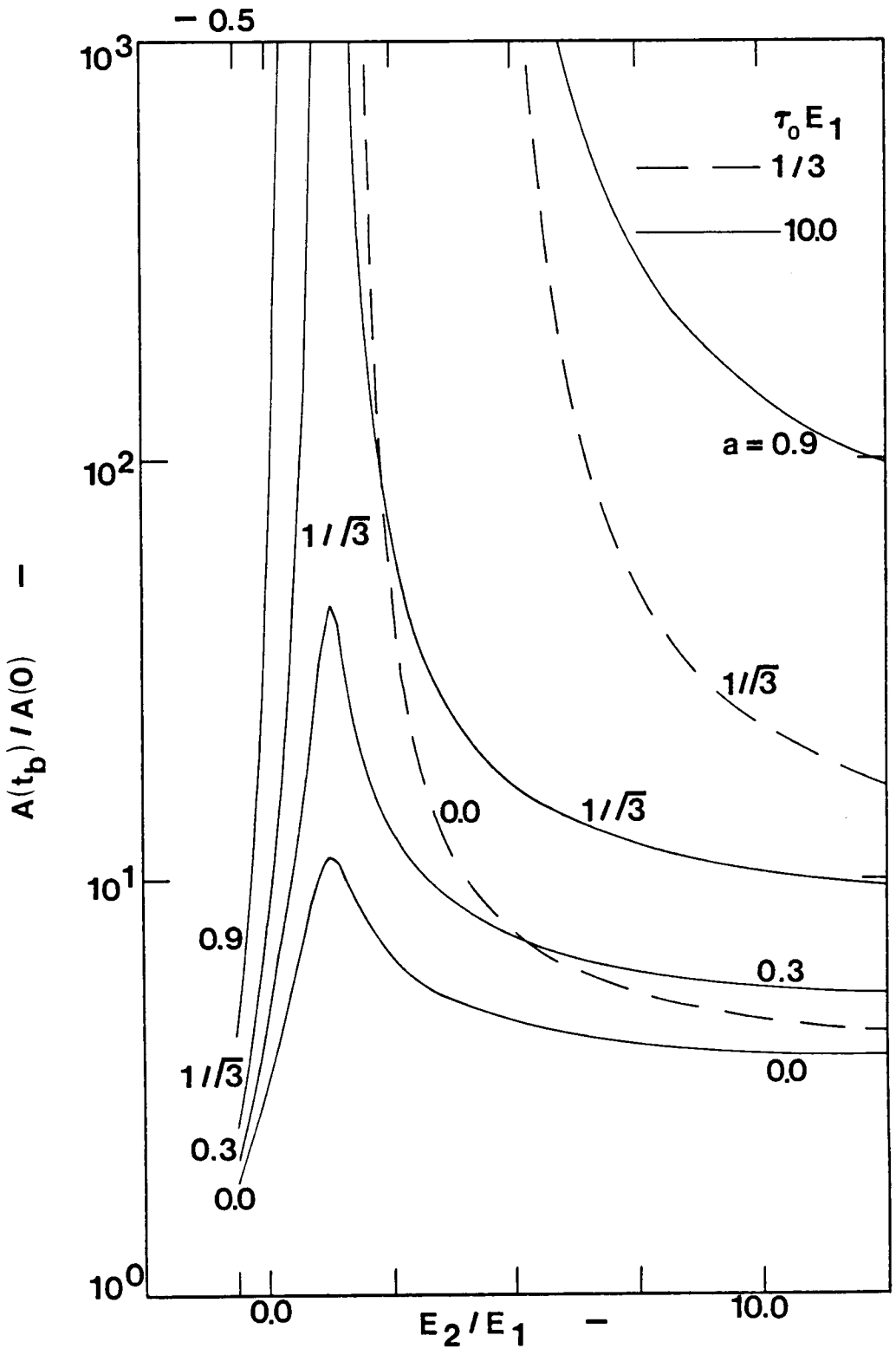

Figure 7.20. Theoretical limiting area $A(t_b)/A(0)$ caused by cohesive fracture as a function of E_2/E_1 for various $\tau_0 E_1$ and "a" values.

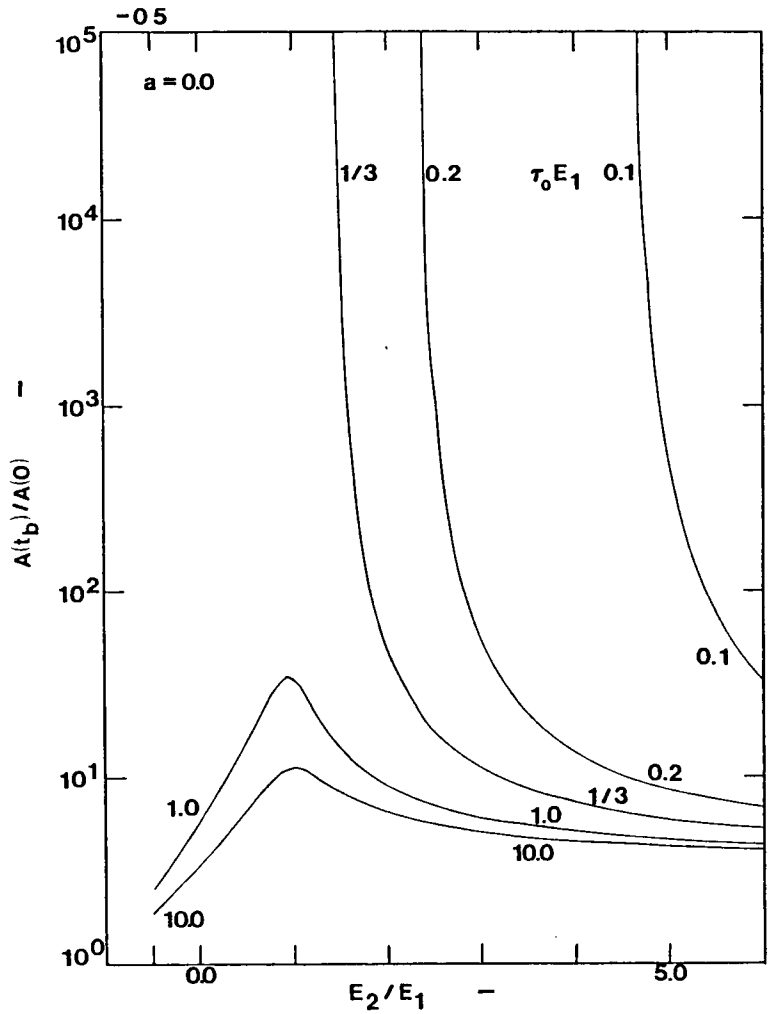

(a) "a" = 0.0

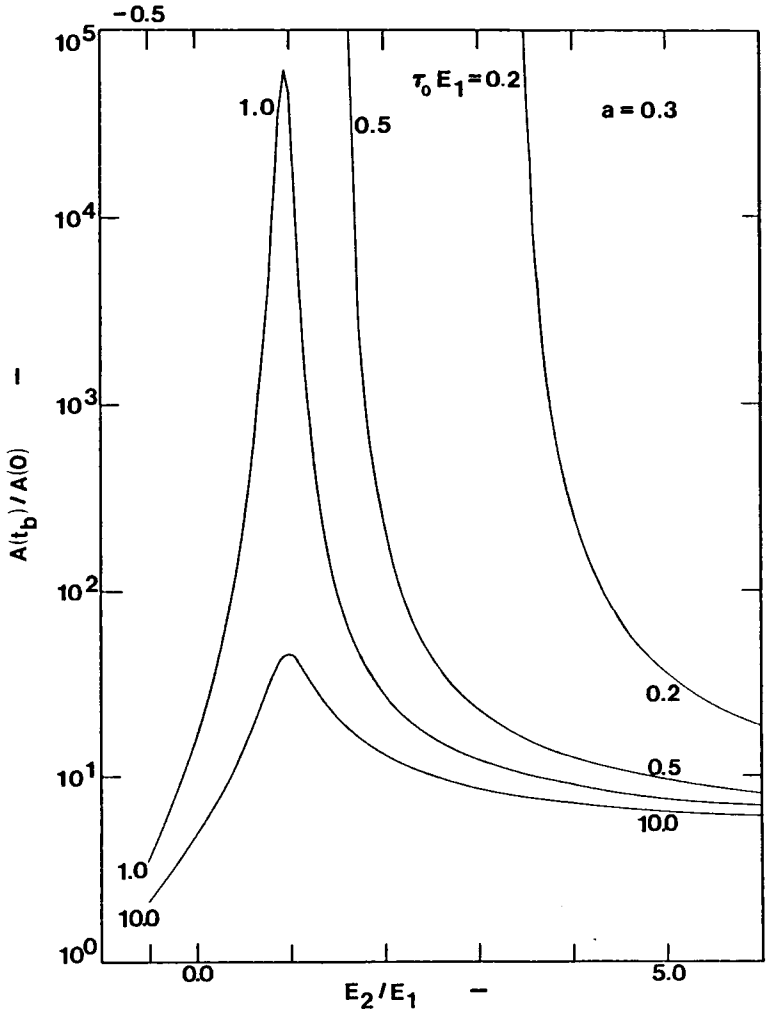

(b) "a" = 0.3

Figure 7.21. Theoretical limiting area $A(t_b)/A(0)$ caused by cohesive fracture as a function of E_2/E_1 for various $\tau_0 E_1$.

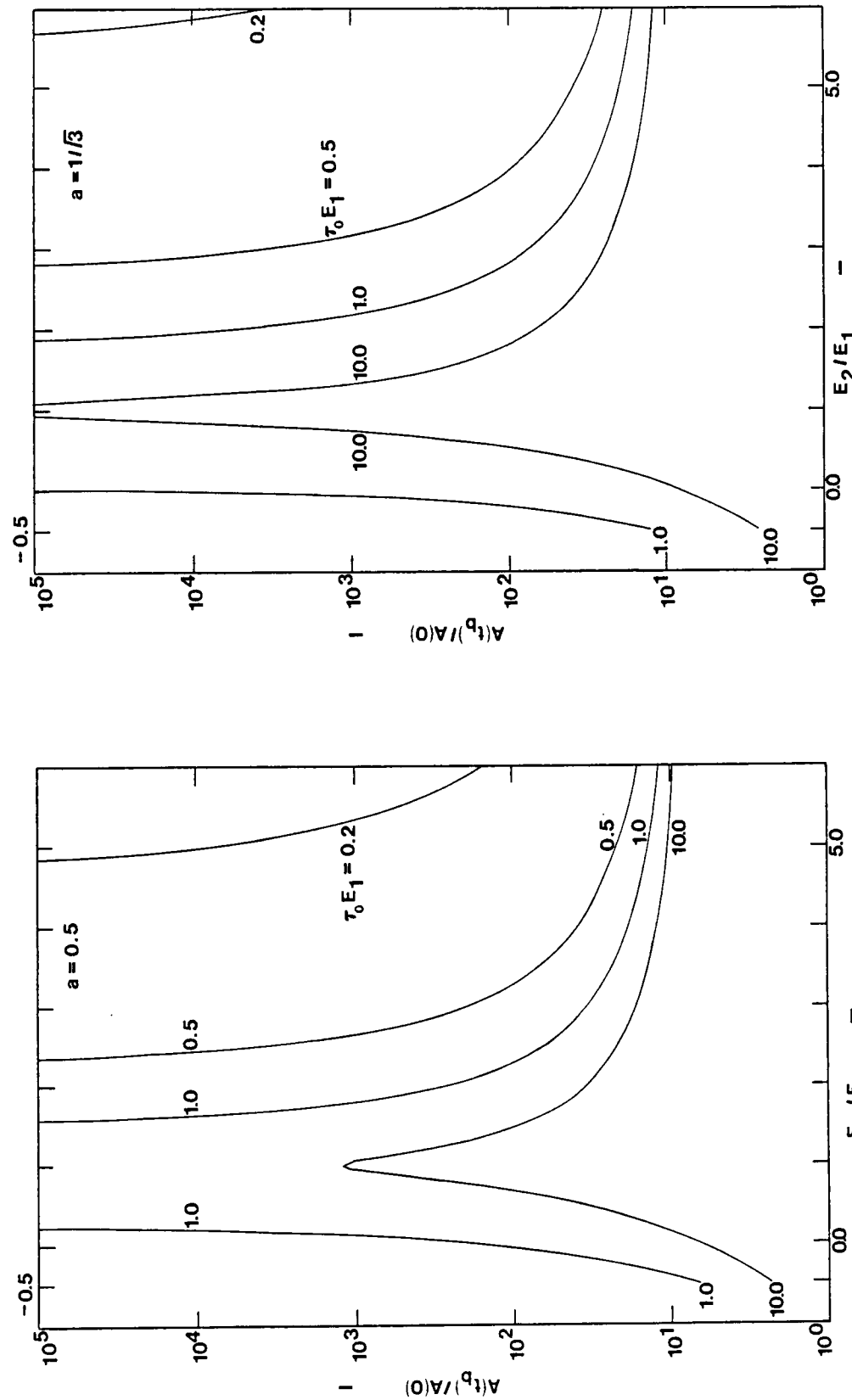

(c) "a" = 0.5

(d) "a" = $1/\sqrt{3}$

Figure 7.21 (continued)

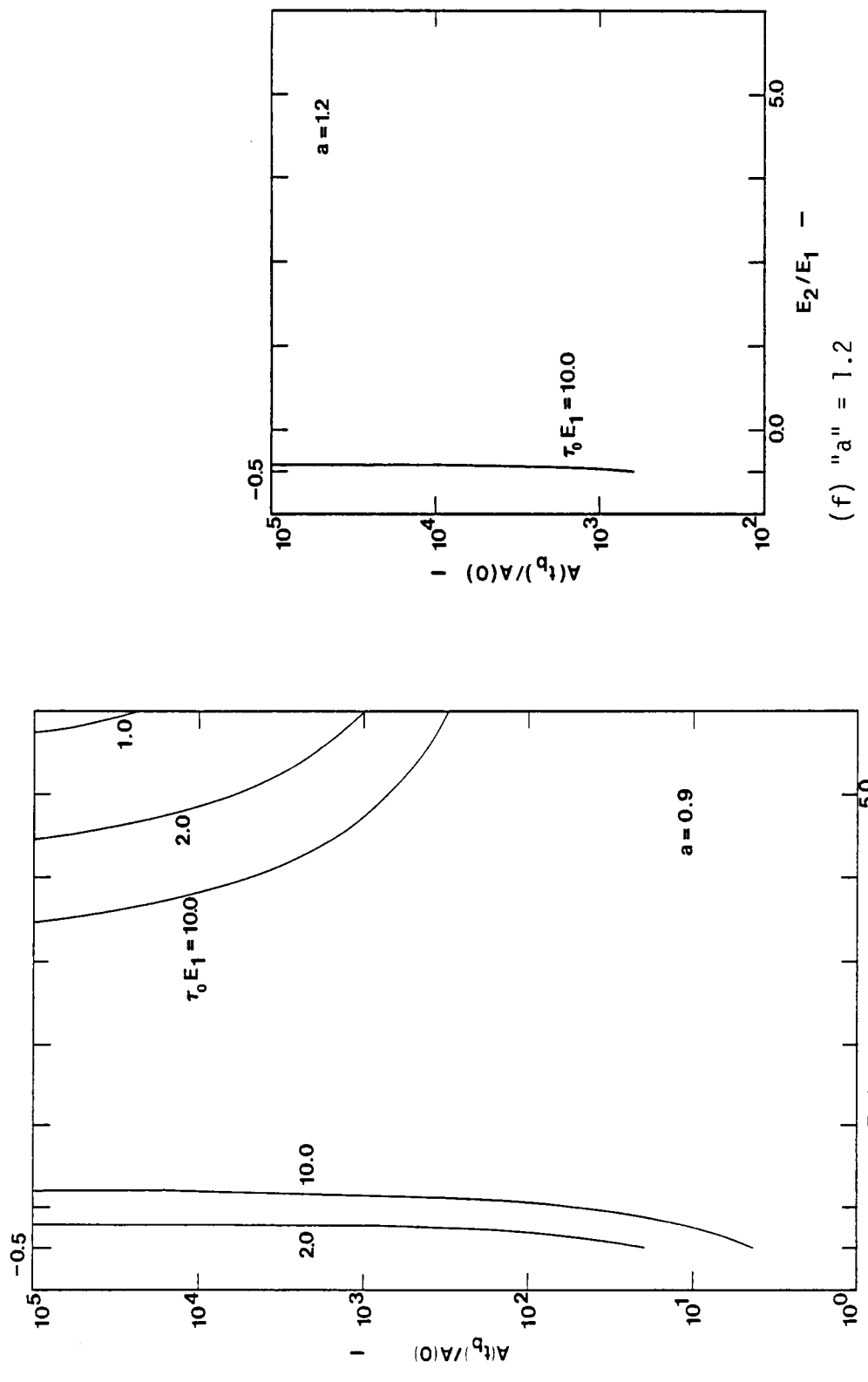

(f) "a" = 1.2

(e) "a" = 0.9

Figure 7.21 (continued)

M_z/M_w = 1.61. Molecular weight distribution data were supplied by Dr. J. M. Rieke of Dow Chemical Co. Linear viscoelastic properties (Figure 7.22) such as complex viscosity η^*, storage modulus G' and loss modulus G" were measured at 180°C in a sinusoidal oscillatory mode. The measurements were carried out by Mr. Peter Herh of Rheometrics, Inc., using a Rheometrics Mechanical Spectrometer (Rheometrics, Inc., Union, NJ).

The strain rate softening parameter "a", the so-called Yamamoto number [W-20], was determined with an assumption of one relaxation time and a Cox-Merz relation [C-24]. A shear modulus G of 1.37×10^4 Pascals was chosen, based on the correlation of molecular-weight distribution and steady state compliance J_e of polystyrene melts [M-40,M-42]. An "a" value of 0.2 was obtained. The estimated relaxation time τ at 180°C is about 8.3 sec. This leads by means of the WLF equation [W-25] to a relaxation time τ of 340 sec at 120°C.

The dimensions of the notched sheets are as follows (see Figure 7.23): 60.0 mm square, thickness of the flat part 0.67 $\sim$ 0.75 mm, defect depth 0.10 mm, defect width 12.7 mm, number average sheet thickness $\bar{h}$ of 0.644 $\sim$ 0.724 mm, and defect size ξ of 0.074 mm. Thickness fluctuations of less than $\pm$ 0.01 mm for the flat and notched parts were allowed. These notched sheets were prepared by using a hot press at a compression molding temperature of 180°C. A 10-minute molding time was used.

These sheets were placed in a T. M. Long Biaxial Tester (T. M. Long Co., Inc., Somerville, NJ) with thickness variation due to the

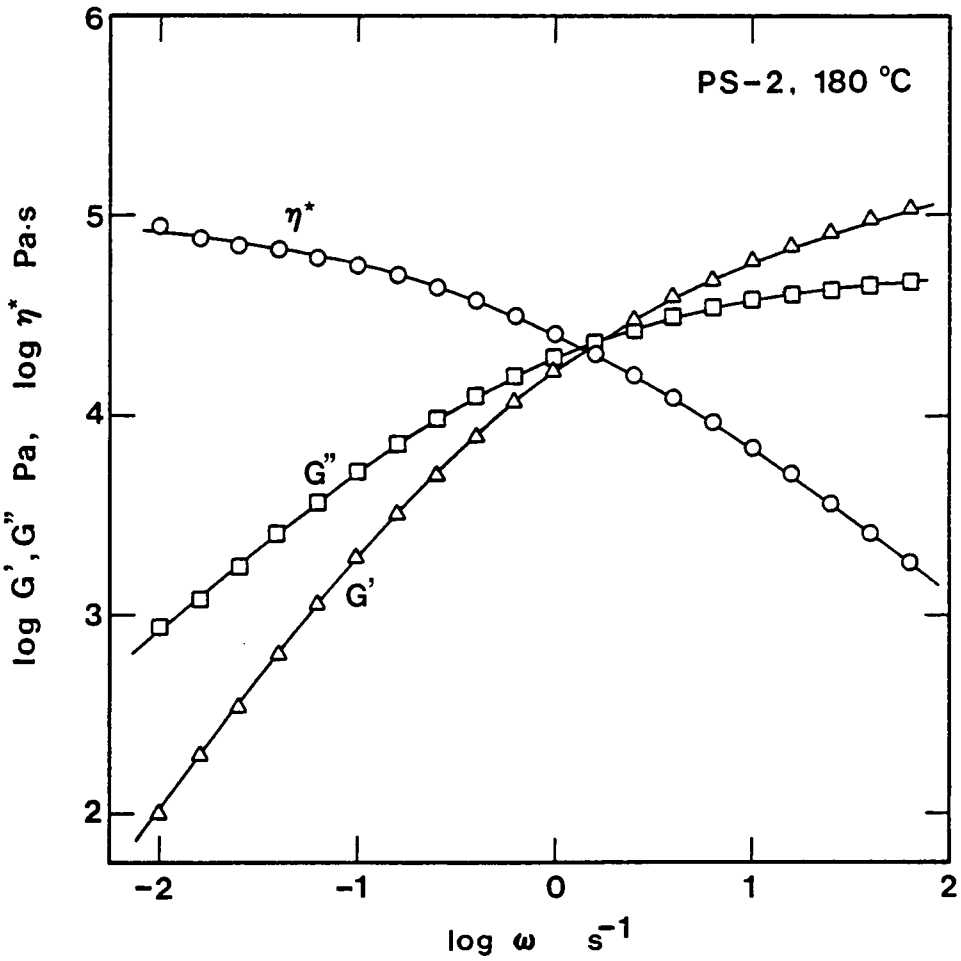

Figure 7.22. Dynamic property of polystyrene melts at 180°C.

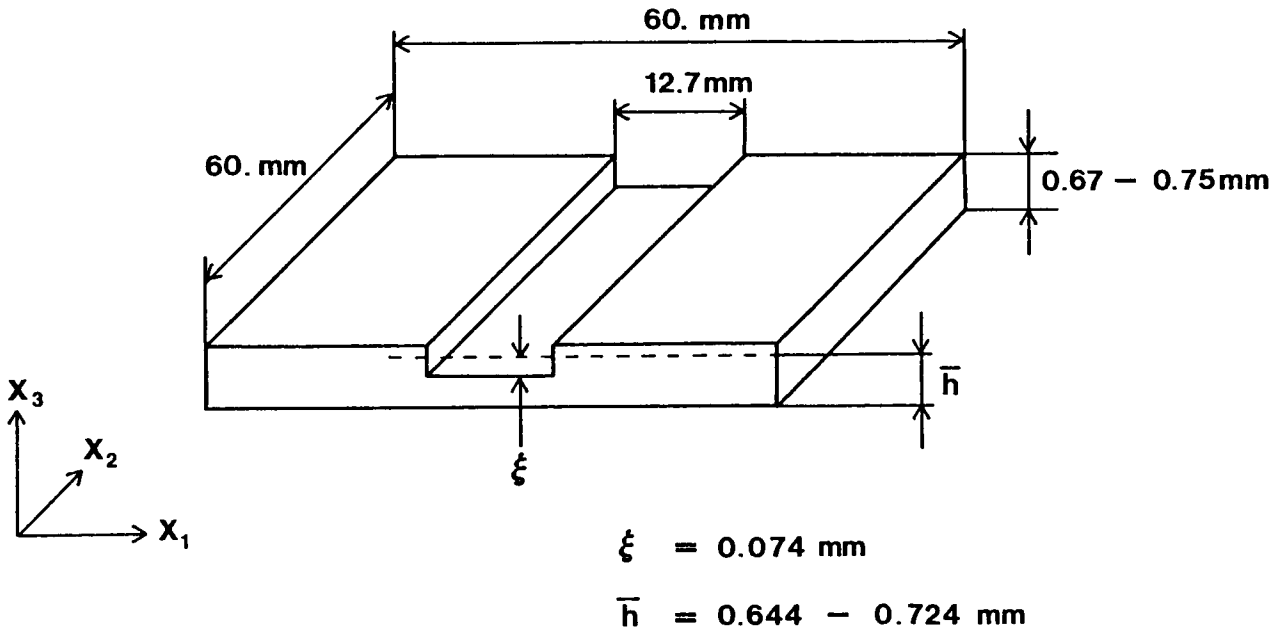

Figure 7.23. Dimensions of notched polystyrene sheet.

notch lying along the "1" direction (the machine direction). Gauge length between the grips was 49 mm. Sheets so placed were preheated for 7 minutes at 120°C to reach temperature equilibrium, then stretched at 120°C at a constant velocity of 460% and 1240% using an initial sample length (49 mm) per minute in the machine direction (the "1" direction) for various stretch ratio. The maximum stretch ratio achieved was 7.2 in terms of sheet length. These speeds produce an initial velocity gradient in the machine direction of 0.0767 sec^{-1} and 0.2067 sec^{-1}. Six different modes were employed: v_2/v_1 = 0.0, 0.5, 1.0, 2.0, and 3.0 and uniaxial extension (free transverse direction). v_2/v_1 = 0.0 and 1.0 could achieve E_2/E_1 of 0.0 and 1.0, respectively, during deformation. Other deformation modes (v_2/v_1 = 0.5, 2.0, and 3.0) resulted in values of E_2/E_1 of 0.5, 2.0, and 3.0 only at the start of deformation. These then gradually decreased with the deformation. However, to define and indicate these deformation modes, initial E_2/E_1 values will be used. After completing the extension, these stretched notched sheets were immediately quenched to room temperature using an air blower to prevent further deformation.

The thickness of the stretched sheet was measured along the centerline of the "1" direction (the machine direction) by means of a dial thickness gauge used every 0.5 cm. This dial thickness was graduated in increments of 0.0001 inch.

E-2. Results and Comparison with Theory

It should be noted that these experiments were carried out under constant velocity deformation conditions, not under constant strain rate deformation conditions. These experimental conditions are not the same as we used in the disturbance growth analyses of the previous sections. A linear stability analysis has been employed. Higher perturbation terms are neglected. Therefore, it may be possible to carry out a qualitative comparison between the experiments and the theoretical analyses.

As mentioned previously, only E_2/E_1 = -0.5, 0.0, and 1.0 can maintain the multiaxiality ratio E_2/E_1 at a constant value throughout the deformation. Special attention should be paid to the data for E_2/E_1 = -0.5, 0.0, and 1.0. However, the data for E_2/E_1 = 0.5, 2.0, and 3.0 may be used for qualitative or comparative purposes since the values for E_2/E_1 do not remain constant during the stretching.

A typical example for the thickness variation along the machine direction (the "1" direction) of a stretched notched sheet is shown in Figure 7.24. This sheet was stretched 4 x 4 at a velocity of 460% per minute, and the initial thickness of the flat part and the notched part were 0.7450 mm and 0.6425 mm, respectively. It is surprising that the stretched notched sheets still show a clear difference in thickness between the main part and the notched part. The number average thickness of the stretched sheet $\bar{h}$ (i.e., $\Sigma\, n_i h_i / \Sigma\, n_i$) and the notched part of the stretched sheet $\bar{h}_{de}$ were calculated. Defect size ξ was then determined by

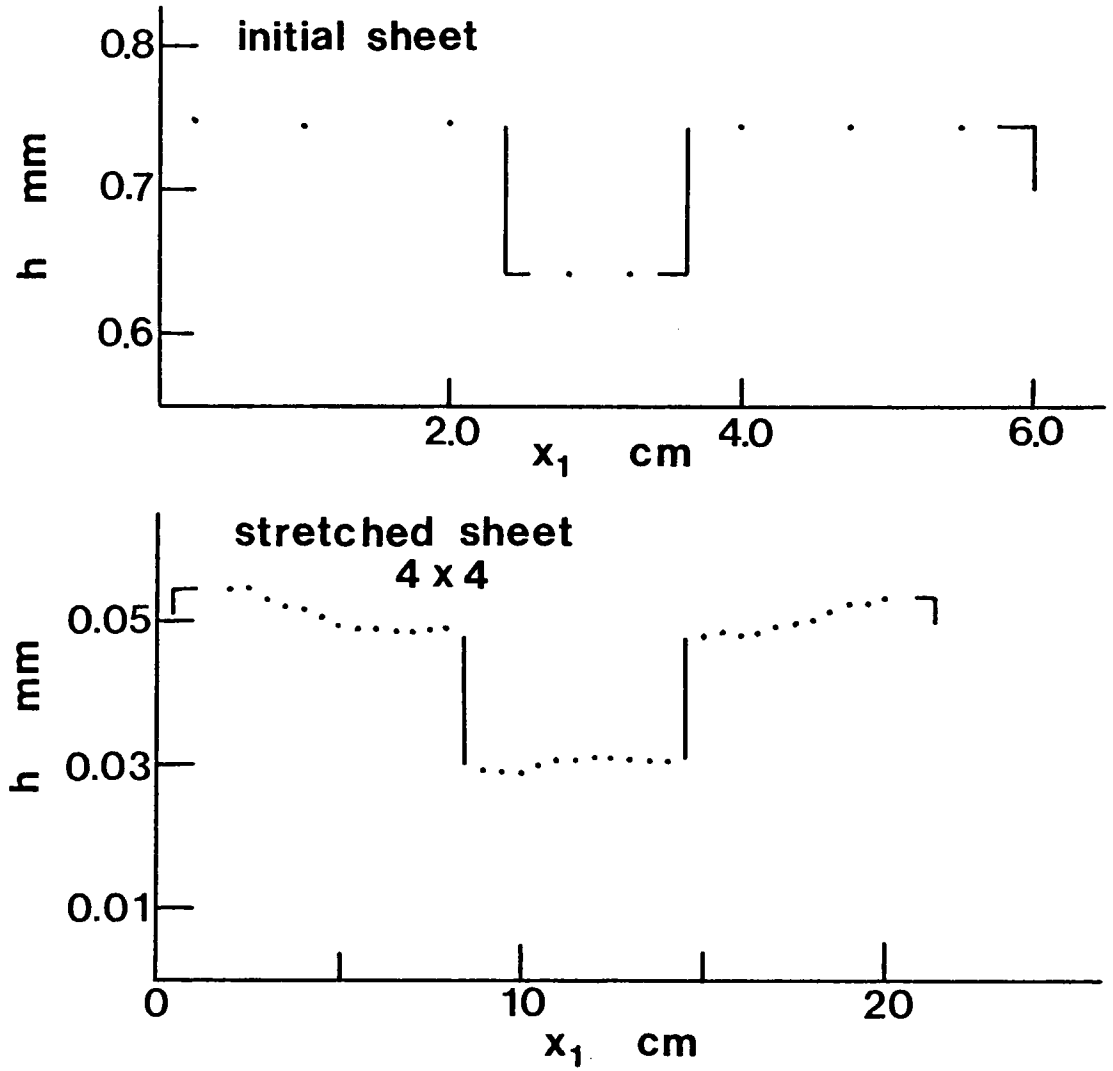

Figure 7.24. Thickness variation of an initial sheet and a stretched sheet (460% per minutes, 4 x 4).

$$\xi = \bar{h} - \bar{h}_{de} \ . \tag{7.65}$$

Eqn. (7.65) is the same as Eqn. (7.17a).

Figure 7.25 shows plots of the defect size change $\xi(\gamma_1)/\xi(0)$ as a function of the Hencky strain in the machine direction strain γ_1 for various stretching modes. The Hencky strain is defined by

$$\gamma_1 = \ell n\ (L/L_0) = \int_0^t E_1\ dt' = \int_0^t \frac{v_1}{L}\ dt' \ . \tag{7.66}$$

where L is the length of the stretching sheet along the machine direction, and L_0 is the initial sheet length. The effect of deformation mode is very clear, the larger E_2/E_1, the smaller $\xi(\gamma_1)/\xi(0)$ (i.e., the lateral stretching makes the growth of defect small). Increasing the strain rate E_1 also decreases the growth of the defect. We should remember that the average sheet thickness is also decreasing with stretching.

The "normalized defect" (or "normalized disturbance")

$$\frac{\xi(\gamma_1)/\bar{h}(\gamma_1)}{\xi(0)/\bar{h}(0)}$$

is plotted as a function of the stretch ratio γ_1 for various deformation modes in Figure 7.26. The normalized defect increases with increasing lateral stretching (larger E_2/E_1) and decreasing strain rate.

In most of the cases the failure occurred inside the notched part of the sheets in the 2-3 plane. The only exception was for the

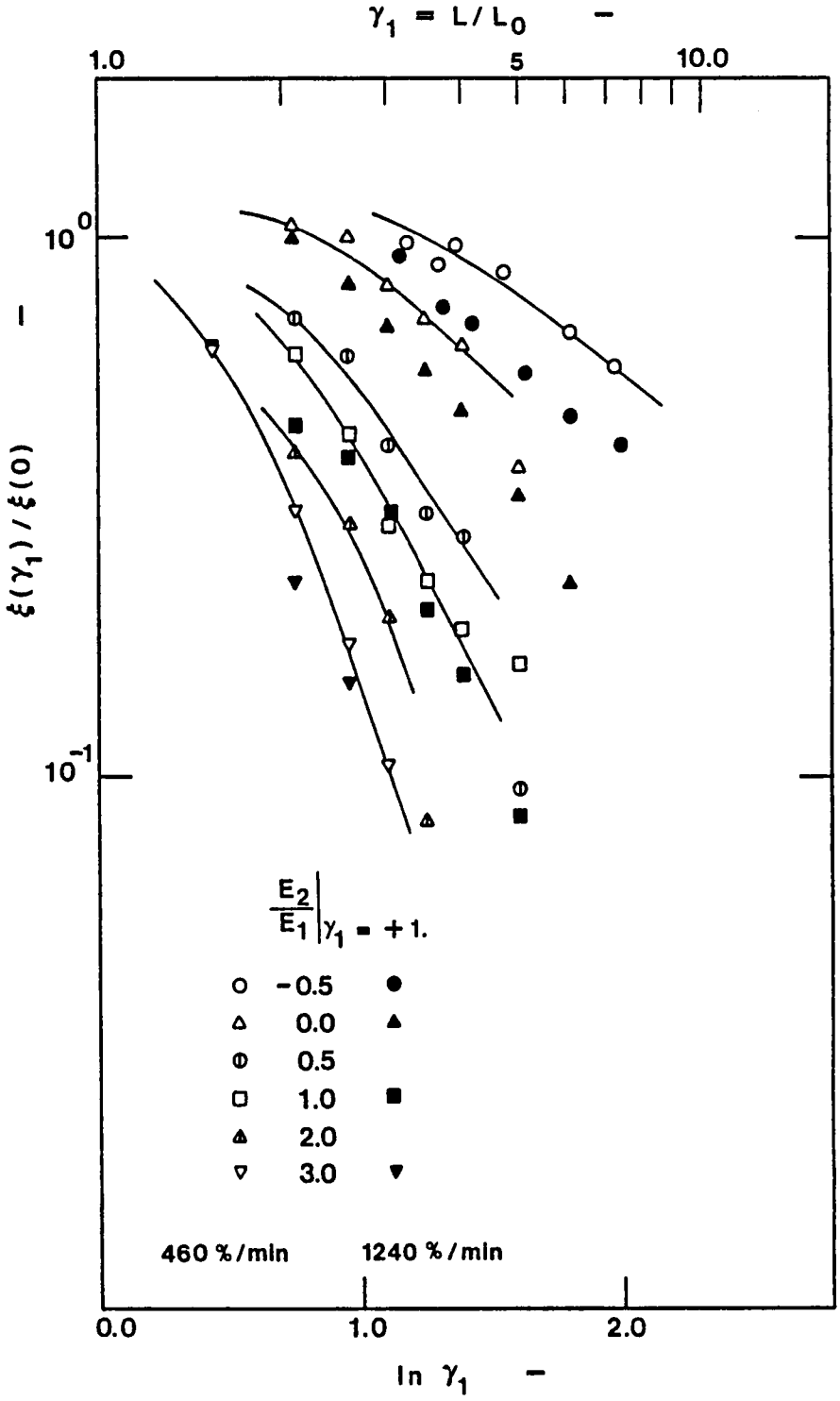

Figure 7.25. Defect growth of notched polystyrene sheets.

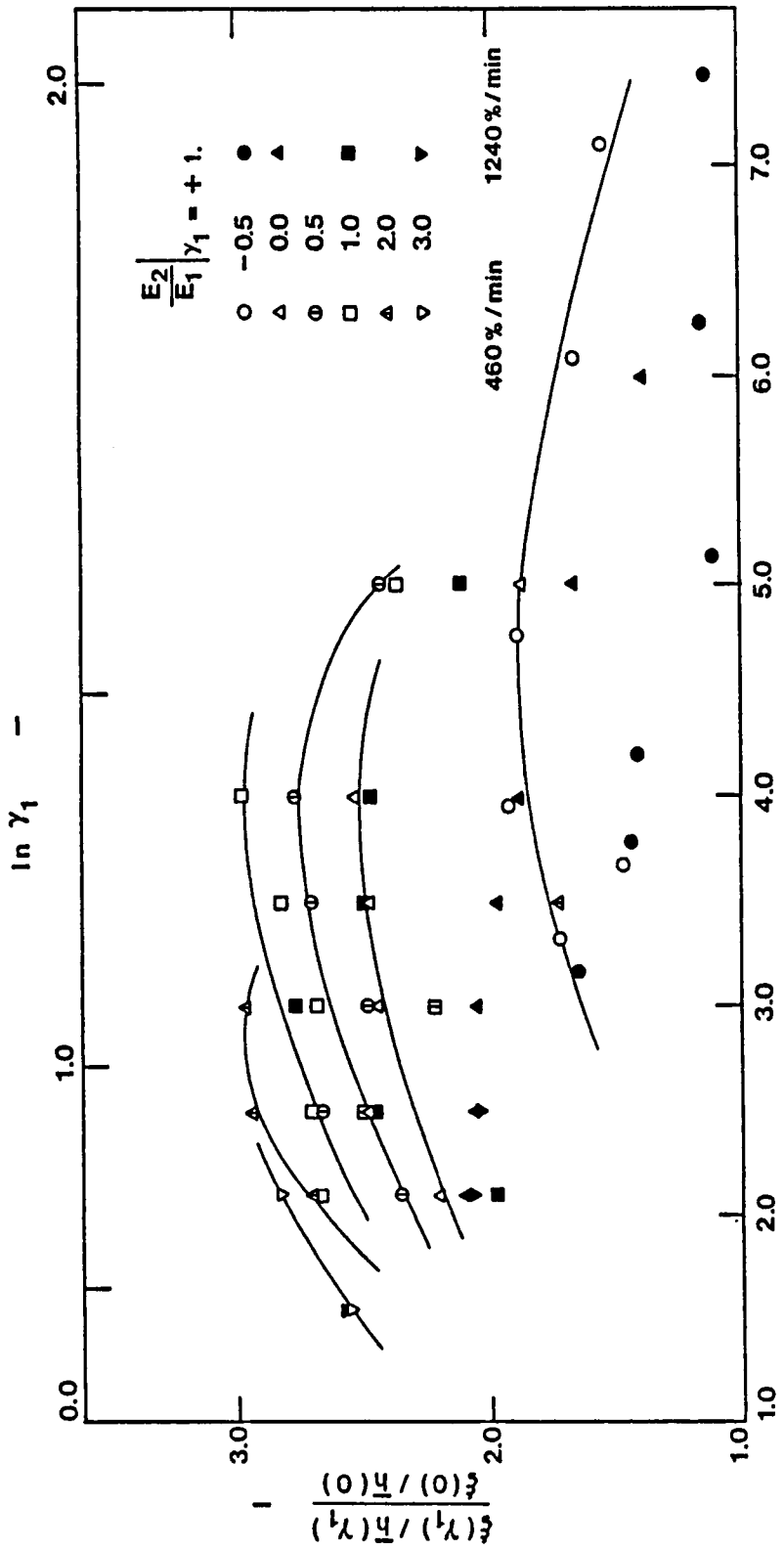

Figure 7.26. Growth of "normalized defect (disturbance)" of notched polystyrene sheets.

case of $E_2/E_1 = 3.0$ with $L/L_0 = 3.0$ at a stretching velocity v_1 of 1240% per minute. For this case one probably has cohesive failure instead of ductile failure; the fracture surface is along the 1-3 plane, not the 2-3 plane. The mechanism might be cohesive fracture instead of ductile failure, which was the failure mechanism of the other failures. Uniaxial extension never reached the failure point (the maximum stretch ratio L/L_0 was 7.2). Figure 7.27 shows plots of elongation-to-break as a function of E_2/E_1, deformation mode. Exact elongation-to-break could not be measured because of the limitation of the instrument drive system; that is, the machine can only be operated at discrete stretch ratio and therefore one can only estimate the stretch ratio at failure.

Figure 7.27 indicates that $L(t_b)/L(0)$ decreases with increasing lateral stretching while $A(t_b)/A(0)$ increases with increasing lateral stretching. The effects of strain rate on elongation-to-break are not clear. The Weissenberg number varies from 3.6 to 26 for a stretching velocity of 460% per minute and from 10 to 70 for a stretching velocity of 1240% per minute. The general tendency of the experimental results for elongation-to-break agree with the theoretical analyses developed in the previous sections.

F. SUMMARY

The growth of disturbances in viscoelastic fluid sheets undergoing multiaxial elongation has been analyzed. Linear stability analyses were carried out using a convected Maxwell model with a

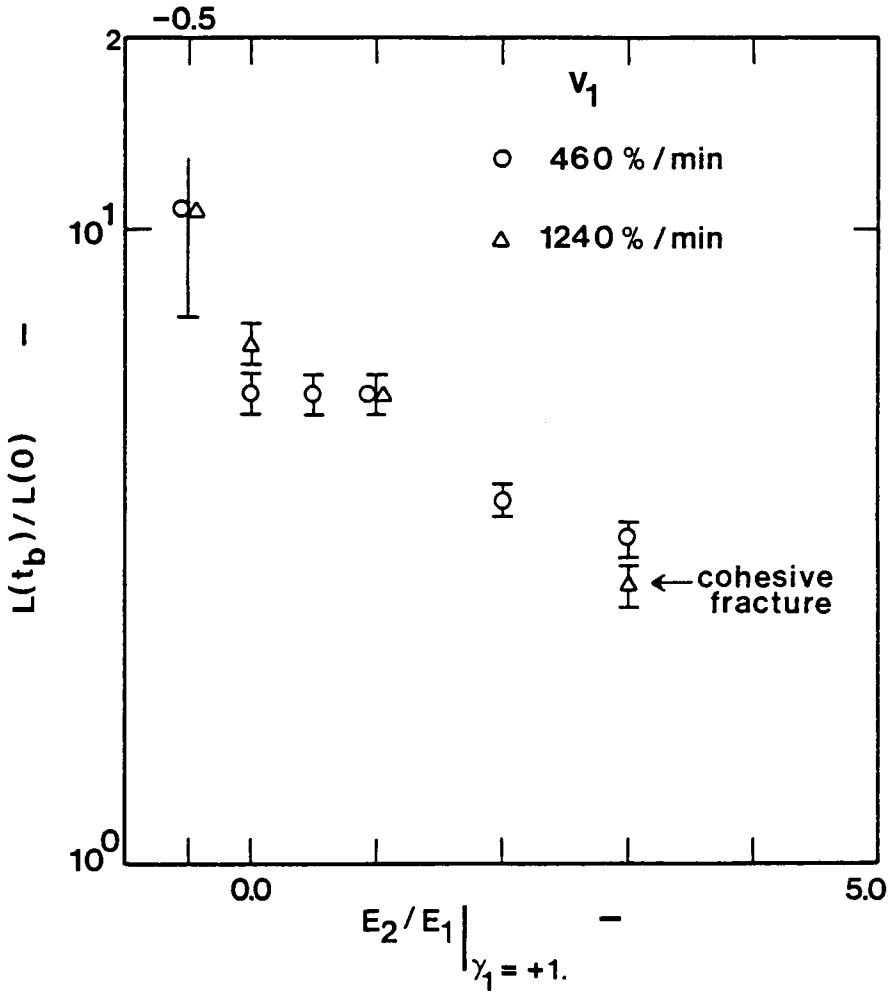

(a) Limiting strain $L(t_b)/L(0)$

Figure 7.27. Elongation-to-break of notched polystyrene sheets for various $E_2/E_1\Big|_{t=+0}$.

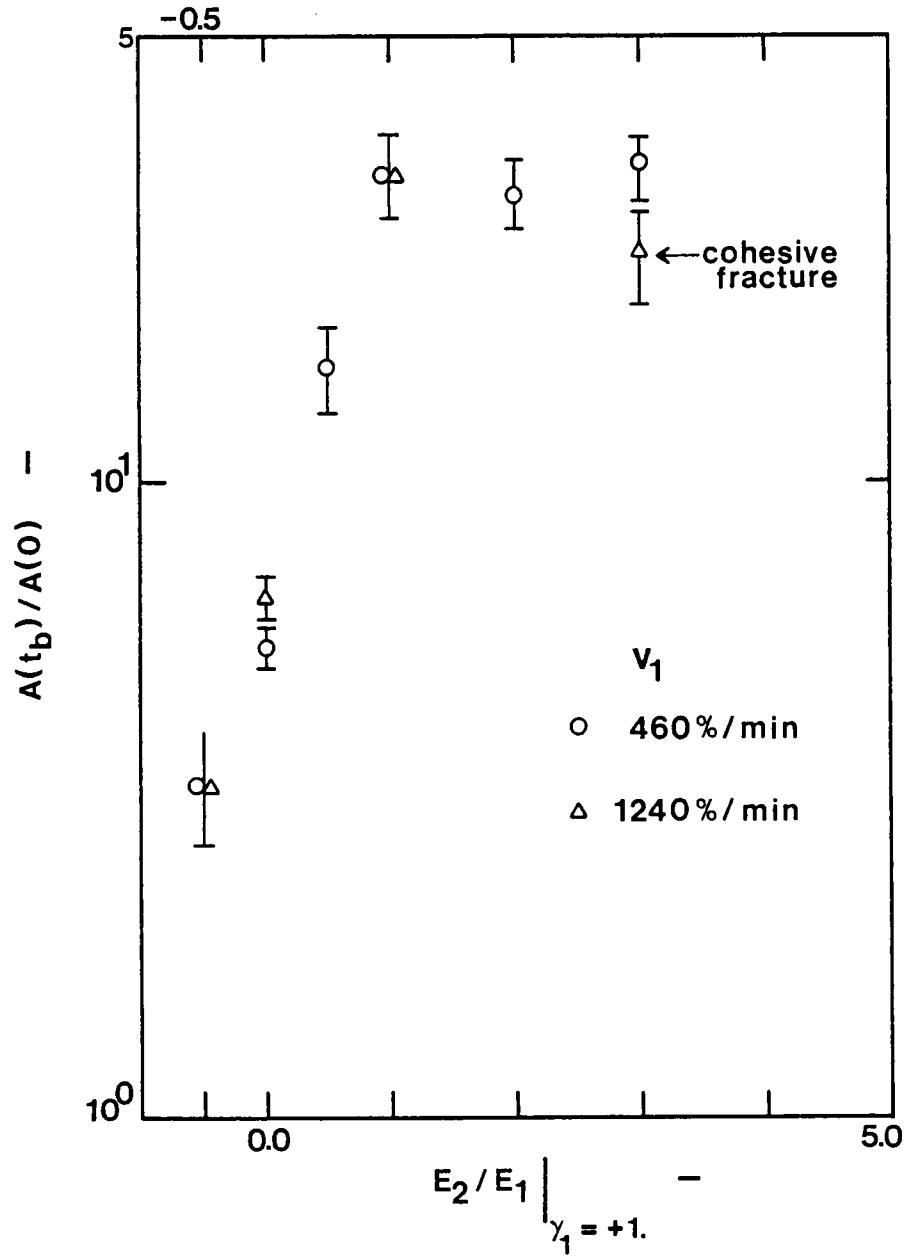

(b) Limiting area $A(t_b)/A(0)$

Figure 7.27 (continued)

strain rate dependent relaxation time, which varies according to $\tau = \tau_0/[1 + a\ \tau_0(2\ \text{tr}\ \underset{\sim}{d}^2)^{1/2}]$. Asymptote formulations, a Newtonian fluid and an elastic solid were also considered. It is shown that film stability and elongation-to-break depends upon the Weissenberg number $\tau_0 E_1$ (where E_1 is the elongation rate in the machine direction); on the strain rate softening parameter "a"; and on the multiaxiality factor E_2/E_1 (where E_2 is the strain rate in the transverse direction). In general, an increasing strain rate softening character (i.e., higher E_2/E_1 values or larger "a" values) decreases elongation-to-break in terms of length in the machine direction (i.e., decreases limiting strain in the machine direction). The limiting strain in the machine direction due to ductile failure has a minimum near $E_2/E_1 = 0.0$ (planar elongation) for larger "a" or higher $\tau_0 E_1$ conditions; however, larger "a" values are unstable under higher $\tau_0 E_1$ conditions. Material with smaller "a" values are stable under higher $\tau_0 E_1$ conditions; however, larger "a" values are unstable under higher $\tau_0 E_1$ conditions. The elongation-to-break, expressed in terms of area, exhibits a complex dependence upon E_2/E_1, $\tau_0 E_1$, and "a". A cohesive fracture criterion was hypothesized for various values of E_2/E_1, $\tau_0 E_1$, and "a". These results were compared with experiments involving the stretching of melted notched polystyrene sheets.

CHAPTER VIII

MULTIAXIAL ELONGATIONAL FLOW OF A BINGHAM PLASTIC FLUID: GROWTH OF DISTURBANCES

A. INTRODUCTION

Recently attention has been given to polymer melts filled with small particles, such as carbon black, titanium dioxide, talc, and calcium carbonate. These systems are found to exhibit yield values. It is of interest to investigate the effect of yield values on the growth of disturbances in flat sheets undergoing multiaxial elongation. The growth of disturbances in a Bingham plastic filament undergoing uniaxial stretching has already been described by White and Tanaka [W-21].

B. CONSTITUTIVE EQUATION OF A BINGHAM PLASTIC FLUID

The three dimensional Bingham plastic fluid, formulated by combining the von Mises yield surface and a Newtonian fluid, is written as [H-16,O-4,W-21]

$$\underset{\sim}{\sigma} = -p\underset{\sim}{I} + \underset{\sim}{P} , \tag{8.1a}$$

$$\underset{\sim}{d} = 0 \qquad \text{tr } \underset{\sim}{P}^2 < 2Y^2 , \tag{8.1b}$$

$$\underset{\sim}{P} = \left(1 + \frac{Y}{\sqrt{\frac{1}{2}\,\text{tr } \underset{\sim}{H}^2}}\right) \underset{\sim}{H} \qquad \text{tr } \underset{\sim}{P}^2 > 2Y^2 , \tag{8.1c}$$

$$\underset{\sim}{H} = 2\eta \underset{\sim}{d} \ , \tag{8.1d}$$

where Y is the yield stress. For elongational flow, Eqn. (8.1c) can be rewritten as

$$\underset{\sim}{P} = 2\eta \underset{\sim}{d} + \frac{Y/E_1}{\sqrt{(E_2/E_1)^2 + (E_2/E_1) + 1}} \underset{\sim}{d} \ . \tag{8.2}$$

In a biaxially stretched sheet, this is subjected to the boundary condition σ_{33} being zero. Therefore

$$\sigma_{11} = \frac{(2 + E_2/E_1)}{\sqrt{(E_2/E_1)^2 + (E_2/E_1) + 1}} Y + 2\eta(2 + E_2/E_1)E_1 \ . \tag{8.3}$$

The elongational viscosity is defined by

$$\chi = \frac{\sigma_{11}}{E_1} = \frac{(2 + E_2/E_1)}{\sqrt{(E_2/E_1)^2 + (E_2/E_1) + 1}} \frac{Y}{E_1} + 2\ (2\eta + E_2/E_1) \ . \tag{8.4}$$

For uniaxial extension,

$$\chi = 3\eta + \sqrt{3}\,\frac{Y}{E_1} \ . \tag{8.5a}$$

For planar elongation,

$$\chi = 4\eta + 2\,\frac{Y}{E_1} \ . \tag{8.5b}$$

For equal biaxial extension,

$$\chi = 6\eta + \sqrt{3}\,\frac{Y}{E_1} \ . \tag{8.5c}$$

The existence of yield values results in strain rate softening in elongational flow. The effect of yield values on elongational viscosity is a maximum for planar elongation ($E_2/E_1 = 0$), and decreases for other values of the multiaxiality E_2/E_1.

C. GROWTH OF DISTURBANCES

The conservation equations which represent the growth of disturbance of flat sheets, where the disturbances are in the machine direction ("1" direction), are given by

$$\sigma'_{11} + \bar{\sigma}_{11} \left(\frac{\xi}{\bar{h}}\right) = 0 \ , \tag{8.6a}$$

$$E'_1 = -E'_3 = -\frac{1}{\bar{h}} \left[\frac{D\xi}{Dt} + (1 + E_2/E_1)E_1\xi\right] \ , \tag{8.6b}$$

$$E'_2 = 0 \ , \tag{8.6c}$$

where

$$h(t,x_1) = \bar{h}(t) + \xi(t,x_1) \ . \tag{8.6d}$$

The perturbed stress along the "1" direction is

$$\sigma'_{11} = 2\eta(E'_1 - E'_3) = 4\eta E'_1 \ . \tag{8.7}$$

Combining Eqns. (8.3), (8.6), and (8.7) leads to

$$\frac{D \ \ell n \ \xi}{D(E_1 t)} = \left[-\frac{1}{2}\frac{E_2}{E_1} + \frac{(2 + E_2/E_1)}{4\sqrt{(E_2/E_1)^2 + (E_2/E_1) + 1}} \frac{Y}{\eta E_1} \right] \ , \tag{8.8}$$

while for a Newtonian fluid (i.e., $Y = 0$):

$$\frac{D \ell n \xi}{D(E_1 t)} = -\frac{1}{2}\frac{E_2}{E_1} . \tag{8.9}$$

If the disturbance is periodic along the "1" direction:

$$\xi(t,x_1) = \hat{\xi}(t)\, e^{ikx_1} . \tag{8.10}$$

This leads for a constant strain rate deformation to

$$\frac{D\xi}{Dt} = e^{ikx_1}\frac{\partial \hat{\xi}}{\partial t} . \tag{8.11}$$

This leads to

$$\hat{\xi}(E_1 t) = \hat{\xi}(0)\, \exp\left[\left(-\frac{1}{2}\frac{E_2}{E_1} + \frac{(2 + E_2/E_1)}{4\sqrt{(E_2/E_1)^2 + (E_2/E_1) + 1}}\frac{Y}{\eta E_1}\right)E_1 t\right] . \tag{8.12}$$

For uniaxial extension, we have

$$\hat{\xi}(E_1 t) = \hat{\xi}(0)\, \exp\left[\left(\frac{1}{4} + \frac{\sqrt{3}}{2}\frac{Y}{\eta E_1}\right)E_1 t\right] . \tag{8.13a}$$

For planar extension,

$$\hat{\xi}(E_1 t) = \hat{\xi}(0)\, \exp\left[(0.0 + \frac{1}{2}\frac{Y}{\eta E_1})E_1 t\right] . \tag{8.13b}$$

For equal biaxial extension,

$$\hat{\xi}(E_1 t) = \hat{\xi}(0)\, \exp\left[(-\frac{1}{2} + \frac{\sqrt{3}}{4}\frac{Y}{\eta E_1})E_1 t\right] . \tag{8.13c}$$

Existence of a yield value enhances the growth of disturbances.

The normalized disturbance of a Bingham plastic fluid sheet undergoing a constant strain rate multiaxial deformation is

$$\frac{\hat{\xi}(E_1 t)/\bar{h}(E_1 t)}{\hat{\xi}(0)/\bar{h}(0)} = \exp\left[\left(1 + \frac{E_2/E_1}{2}\right) E_1 t\right] \exp\left[\frac{(2 + E_2/E_1)}{4\,(E_2/E_1)^2 + (E_2/E_1) + 1} \frac{Y}{nE_1} E_1 t\right] . \quad (8.14)$$

For uniaxial extension, where E_2/E_1 is -0.5, one has

$$\frac{\hat{\xi}(E_1 t)/\bar{h}(E_1 t)}{\hat{\xi}(0)/\bar{h}(0)} = \exp\left[\left(\frac{3}{4} + \frac{\sqrt{3}}{4} \frac{Y}{nE_1}\right) E_1 t\right] . \quad (8.15a)$$

For planar extension, where E_2/E_1 is zero

$$\frac{\hat{\xi}(E_1 t)/\bar{h}(E_1 t)}{\hat{\xi}(0)/\bar{h}(0)} = \exp\left[\left(1 + \frac{1}{2} \frac{Y}{nE_1}\right) E_1 t\right] . \quad (8.15b)$$

For equal biaxial extension, where E_2/E_1 is 1.0,

$$\frac{\hat{\xi}(E_1 t)/\bar{h}(E_1 t)}{\hat{\xi}(0)/\bar{h}(0)} = \exp\left[\left(\frac{3}{2} + \frac{\sqrt{3}}{4} \frac{Y}{nE_1}\right) E_1 t\right] . \quad (8.15c)$$

Generally the existence of a yield value decreases the stability, the same as increasing the multiaxiality E_2/E_1. However, the quantitative effect of the Bingham number $Y/(nE_1)$ [0-5] is rather complex. The effect of the yield values are the highest for planar elongation, and decreases by decreasing or increasing multiaxiality E_2/E_1. Uniaxial and equal biaxial elongation are affected qualitatively to the same degree by the existence of a yield value.

D. SUMMARY

The growth of disturbances in Bingham plastic fluid sheets undergoing multiaxial elongation has been described. The existence of yield values acts to soften the material by a strain rate mechanism. As expected, yield values enhance growth of disturbances. The existence of yield values has the greatest effect for planar elongation and less as E_2/E_1 increases or decreases from zero.

CHAPTER IX

STABILITY OF CONTINUOUS FILM EXTRUSION PROCESSES, PART I: CONSTANT WIDTH PROCESSES AND MELT SPINNING

A. INTRODUCTION

Polymer processing operations involving post die deformations are known to exhibit a range of instabilities. Most striking are the draw resonance characteristics exhibited during the melt spinning of fibers [B-6,F-14,H-13,I-6,K-5,K-9,M-16,M-41,W-8,W-17]; similar instabilities in film casting [B-5,K-5,K-9]; bubble instabilities in tubular film extrusion [H-10,H-11]; and pleating of parisons in blow molding [C-14,H-15,S-6]. Of these phenomena only the draw resonance instability [C-8,F-3,F-4,F-5,F-6,G-1,H-13,I-6,K-5,K-9,S-11, S-12,S-14,W-17] has received significant extensive theoretical treatment.

We have initiated research to analyze the deformation and flow of a polymer system involving multiaxial deformations. Earlier considerations (Chapters VI, VII, and VIII) dealt with instabilities in the biaxial stretching of a sheet and an annulus. In the present chapter, we turn our concern to continuous process operations. Pioneering investigations of instabilities in film extrusion with multiaxial deformations have been made by Yeow [Y-8,Y-9]. These papers illustrate the complexity of the problems. In the present chapter we describe useful asymptotic solutions for the continuous

stability of films. We consider specifically cases in which the dynamic equations for film extrusion and stability are analogous to those of melt spinning fibers. The slit film problem has been specifically considered by Kase and his co-workers [K-5,K-9]. This chapter adds the consideration of other film extrusion processes, specifically certain limiting cases of annular film extrusion.

B. DYNAMICS OF FILM EXTRUSION AND MELT SPINNING

B-1. General Formulation of Conservation Equations

Consider the three processing operations described in Figure 9.1. These are the melt spinning of fibers, extrusion through a slit die with take-up, and annular extrusion without significant film curvature as in the case of extrusion over a lubricated mandrel. The continuity equation for each case may be expressed

$$\frac{\partial A}{\partial t} + \frac{\partial}{\partial z}(A\, v_z) = 0 \,, \tag{9.1a}$$

where A is the cross-sectional area of the fiber or film and v_z the linear velocity in the machine direction. We will speak of the draw-down DR as $v_z(L)/v_z(0)$. In the steady state we will have

$$DR = \frac{v_z(L)}{v_z(0)} = \frac{A(0)}{A(L)} \,. \tag{9.1b}$$

Neglecting air drag and gravity, the dynamics of each of these processes is described by

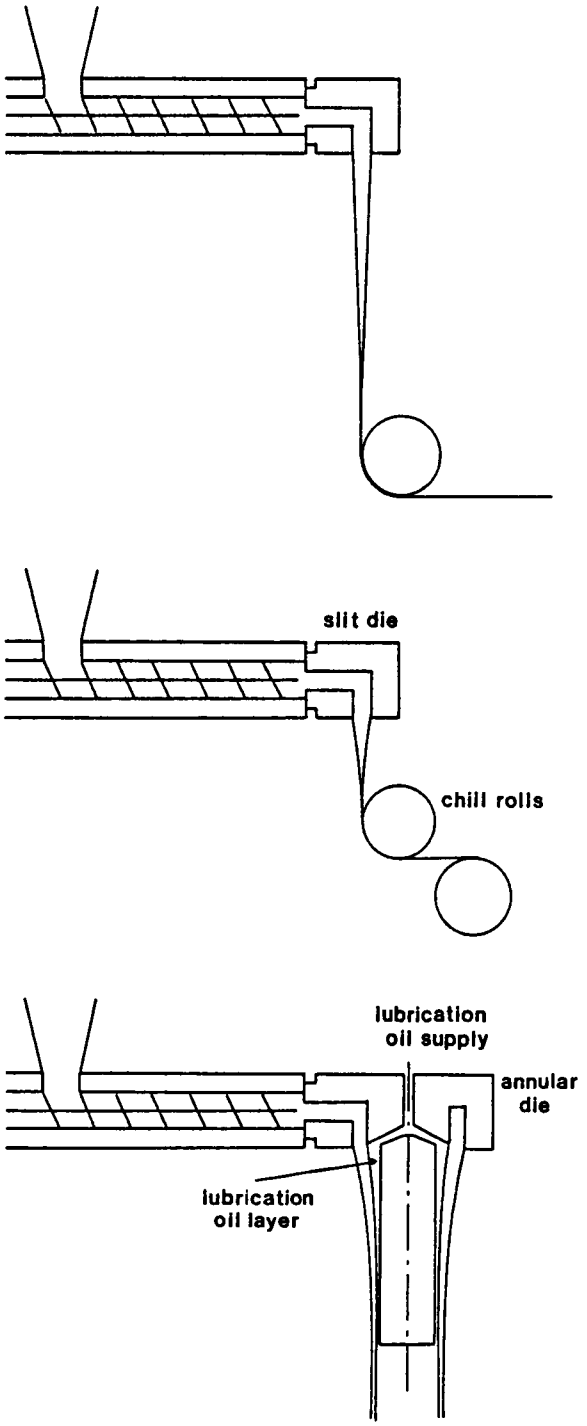

Figure 9.1. (a) Melt spinning; (b) flat film extrusion (film casting); (c) annular film extrusion over a lubricated straight mandrel.

$$\frac{\partial F_z}{\partial z} = \frac{\partial A\sigma_{zz}}{\partial z} = 0 \ , \tag{9.2a}$$

or

$$F_z = A\sigma_{zz} \ , \tag{9.2b}$$

where F_z is the applied tension and σ_{zz} the local stress.

The mean temperature, T, of the fibers and films is governed by the heat balance

$$\rho c \ A \left(\frac{\partial T}{\partial t} + v_z \frac{\partial T}{\partial z}\right) = - U \ C \ (T - T_{surr}) \ , \tag{9.3}$$

where ρ is the density, C is the heat capacity, U the local heat transfer coefficient, T_{surr} the temperature of the surroundings, and C the circumference available for heat transfer.

B-2. Comparison of Balance Equations for Fibers and Films

The balance equations for fibers and films may be further investigated by noting that the cross-sectional areas and circumferences can be expressed as

$$A_f = \frac{\pi d^2}{4} \ , \qquad C_f = \pi d \ , \tag{9.4a}$$

$$A_s = Wh_s \ , \qquad C_s = 2W \ , \tag{9.4b}$$

$$A_a = 2\pi R h_a \ , \qquad C_a = 4\pi R \ \text{(ambient temperature interior)}, \quad = 2\pi R \ \text{(adiabatic interior)}, \tag{9.4c}$$

where the subscripts "f", "s" and "a" refer to fiber, slit film and annular film. It may be seen that

$$C_f = \frac{A_f}{\pi d} = 2\sqrt{\pi A_f} \ , \tag{9.5a}$$

$$C_s = \frac{2}{h_s} A_s \ , \tag{9.5b}$$

$$C_a = \frac{2}{h_a} A_a \quad \text{or} \quad \frac{1}{h_a} A_a \ . \tag{9.5c}$$

The heat balance equations for the three cases are then:

$$\frac{\partial T}{\partial t} + v_z \frac{\partial T}{\partial z} = - \frac{2\sqrt{\pi}\, U}{\rho c \sqrt{A_f}} (T - T_{surr}) \ , \tag{9.6a}$$

$$\frac{\partial T}{\partial t} + v_z \frac{\partial T}{\partial z} = - \frac{2U}{\rho c h_s} (T - T_{surr}) \ , \tag{9.6b}$$

$$\frac{\partial T}{\partial t} + v_z \frac{\partial T}{\partial z} = - \frac{2U}{\rho c h_a} (T - T_{surr}) \qquad \text{(adiabatic interior)} \ . \tag{9.6c}$$

B-3. Newtonian Fluid Solutions

For the melt spinning of a fiber we have

$$\sigma_{zz} = 3\eta \frac{\partial v_z}{\partial z} \ . \tag{9.7}$$

Analogously for films with constant width dimension W (or radius R) we have

$$\sigma_{zz} = 4\eta \frac{\partial v_z}{\partial z} \ , \tag{9.8}$$

where the coefficient "4" rather than "3" follows from having planar extension rather than uniaxial extension. The force balance, Eqn. (9.2), becomes

$$F_f = 3\eta\, A\, \frac{\partial v_z}{\partial z}\,, \tag{9.9a}$$

$$F_s = 4\eta\, A_s\, \frac{\partial v_z}{\partial z}\,, \tag{9.9b}$$

$$F_a = 4\eta\, A_a\, \frac{\partial v_z}{\partial z}\,. \tag{9.9c}$$

For stable isothermal flow of constant viscosity fluids we obtain the solution

$$\frac{A_f(z)}{A_f(o)} = \left(\frac{d(z)}{d(o)}\right)^2 = \frac{v_f(o)}{v_f(z)} = \exp\left[-\frac{F_f\, z}{3\eta\, Q_f}\right]\,, \tag{9.10a}$$

$$\frac{A_s(z)}{A_s(o)} = \frac{h(z)}{h(o)} = \frac{v_s(o)}{v_s(z)} = \exp\left[-\frac{F_s\, z}{4\eta\, Q_s}\right]\,, \tag{9.10b}$$

$$\frac{A_a(z)}{A_a(o)} = \frac{h(z)}{h(o)} = \frac{v_a(o)}{v_a(z)} = \exp\left[-\frac{F_a\, z}{4\ Q_a}\right]\,. \tag{9.10c}$$

From Eqn. (9.1), Eqns. (9.10a,b,c) with z set equal to L correspond to reciprocal draw ratios "1/DR."

C. DISTURBANCES IN ELONGATIONAL FLOW

C-1. General Formulation of Conservation Equations

In this section we consider the introduction of disturbances into a slit or annular film.

We begin by introducing infinitesimal disturbances, which we take to be axisymmetric in the case of the annulus and not to vary through the thickness. We take:

$$h(z,t) = \bar{h}(z,t)\,[1 + \alpha(z,t)]\ , \tag{9.11a}$$

$$v_z(z,t) = \bar{v}_z(z,t)\,[1 + \beta(z,t)]\ , \tag{9.11b}$$

$$\sigma_{zz}(z,t) = \bar{\sigma}_{zz}(z,t) + \sigma'_{zz}(z,t)\ , \tag{9.11c}$$

$$F_z(t) = \bar{F}_z(t) + F'_z(t)\ , \tag{9.11d}$$

where the overbar denotes the steady state. The form of Eqn. (9.11d) is suggested by the force balance equation of Eqn. (9.2).

We use Eqns. (9.1) and (9.2) as continuity and force balances defining the dynamics of the system. If we introduce the disturbances of Eqn. (9.11) and subtract out the steady state form, we obtain, after linearization

$$\frac{D\alpha}{Dt} + \frac{1}{\bar{h}}\,\frac{\partial(\bar{v}_z\,\bar{h}\,\beta)}{\partial z} = 0\ , \tag{9.12a}$$

$$\frac{F'_z}{2\pi\,\bar{R}\,\bar{h}} = \Phi_z = \sigma'_{zz} + \bar{\sigma}_{zz}\,\alpha\ . \tag{9.12b}$$

C-2. Tensile Stretching of an Isolated Film or Annulus

To proceed further, we need to introduce greater restrictions on the kinematics of the system. For the tensile stretching of an isolated film or annulus

$$\frac{\partial \bar{h}}{\partial z} = 0 \ , \qquad \frac{\partial \bar{v}_z}{\partial z} = E_z \ . \tag{9.13a,b}$$

the continuity equation, Eqn. (9.12a), reduces to

$$\frac{D\alpha}{Dt} + \frac{\partial \beta \bar{v}_z}{\partial z} = 0 \ , \tag{9.14a}$$

or

$$\frac{\partial \alpha}{\partial t} + \bar{v}_z \frac{\partial (\alpha+\beta)}{\partial z} + \beta E_z = 0 \ . \tag{9.14b}$$

Eqn. (9.14) is the continuity equation for a disturbance equivalent to the form used in Chapters VI and VII for constant elongation rate stretching.

C-3. Slit and Annular Tubular Film Extrusion Over a Lubricated Mandrel

For continuous extrusion

$$\frac{\partial \bar{h}}{\partial t} = 0 \ , \qquad \frac{\partial \bar{v}_z \bar{h}}{\partial z} = 0 \ . \tag{9.15a,b}$$

Eqn. (9.12a) becomes

$$\frac{D\alpha}{Dt} + \bar{v}_z \frac{\partial \beta}{\partial z} = 0 \ . \tag{9.16}$$

D. ISOTHERMAL NEWTONIAN FLUID SOLUTIONS

C-1. Isolated Sheet and Annular Cylinder

For the case of constant strain rate stretching, Eqn. (9.12b) can be simplified using Eqn. (9.8) and by the aid of the continuity equation, Eqn. (9.13a), to

$$\Phi_z = 4\eta\left(\alpha \frac{\partial \bar{v}_z}{\partial z} - \frac{D\alpha}{Dt}\right) = 4\eta\left(\alpha E_z - \frac{D\alpha}{Dt}\right) . \tag{9.17}$$

Therefore

$$\frac{D\alpha}{Dt} = \alpha E_z - \frac{\Phi_z}{4\eta} = \alpha E_z - \frac{F'_z}{8\pi \bar{R}\, \bar{h}\, \eta} . \tag{9.18}$$

The stability behavior is determined by Eqn. (9.18). Let the disturbance be periodic along the "z" direction so that we may write:

$$\alpha(z,t) = \hat{\alpha}(t)\, e^{ikz} . \tag{9.19}$$

The wave number k varies with time because of the extension of the annulus. With a constant deformation rate E_z, we have

$$k(t) = k(o)\, e^{-E_z t} . \tag{9.20}$$

This leads to

$$\frac{D\alpha}{Dt} = \frac{\partial \alpha}{\partial t} + \bar{v}_z \frac{\partial \alpha}{\partial z} = \frac{\partial \hat{\alpha}}{\partial z} e^{ikz} . \tag{9.21}$$

Eqn. (9.18) can be rewritten with the aid of Eqns. (9.19) and (9.20) for a constant strain rate deformation, when Φ_z is zero:

$$\frac{1}{\hat{\alpha}} \frac{\partial \hat{\alpha}}{\partial t} = E_z . \tag{9.22}$$

The disturbance varies exponentially in time according to

$$\hat{\alpha}(t) = \hat{\alpha}(o)\, \exp(E_z t) . \tag{9.23}$$

This is equivalent to the result originally obtained in Chapter VI, where we set $\xi = \alpha\, \bar{h}$.

D-2. Slit and Continuous Annular Film Extrusion Over a Lubricated Mandrel

For the case of continuous slit film and annular extrusion, Eqn. (9.12b) can be reduced by the aid of Eqns. (9.8) and (9.16) to give:

$$\Phi'_z = \frac{F'_z}{\bar{F}_z} = \frac{\Phi_z}{4\eta\ \partial \bar{v}_z/\partial z} = (\alpha+\beta) - \frac{1}{\partial \bar{v}/\partial z}\frac{D\alpha}{Dt}\ , \tag{9.24}$$

where

$$\frac{\partial \bar{v}_z}{\partial z} = \frac{\bar{F}_z\ \bar{v}_z}{4\eta\ Q}\ . \tag{9.25}$$

Substituting the steady state solution of $\partial \bar{v}_z/\partial z$ into Eqn. (9.24) and differentiating it with respect to "z" gives

$$\frac{\partial \Phi'_z}{\partial z} = \frac{1}{\bar{F}_z}\frac{\partial F'_z}{\partial z} = \frac{\partial(\alpha+\beta)}{\partial z} + \frac{1}{\bar{v}_z}\frac{D\alpha}{Dt} - \frac{1}{\partial \bar{v}_z/\partial z}\frac{\partial}{\partial z}\left(\frac{D\alpha}{Dt}\right) = 0 \tag{9.26}$$

Combining Eqns. (9.16), (9.25), and (9.26), and then eliminating the $\partial\beta/\partial z$ term, we obtain:

$$\frac{\partial^2 \alpha}{\partial z^2} + \frac{1}{\bar{v}_z}\frac{\partial^2 \alpha}{\partial z\ \partial t} = 0\ , \tag{9.27a}$$

or

$$\left(\frac{\partial}{\partial t} + \bar{v}_z\ \frac{\partial}{\partial z}\right)\frac{\partial \alpha}{\partial z} = \frac{D}{Dt}\left(\frac{\partial \alpha}{\partial z}\right) = 0\ . \tag{9.27b}$$

This is exactly the same equation as derived by Pearson and Matovich [P-2] for the stability of the isothermal melt spinning of a Newtonian fluid.

Eqn. (9.27) may be solved under various boundary conditions. The solution obtained $\alpha(v_z(L)/v_z(o), t)$ generally represents a forced oscillation due to the applied boundary condition (i.e., applied infinite disturbances to the system). The natural oscillation (or draw resonance phenomenon) is the special or extreme case of the forced oscillation which occurs when the time average of $\alpha(v_z(L)/v_z(o), t)$ exhibits singular points in the boundary condition domain. Therefore, Eqn. (9.27) is the equation which represents the sensitivity of disturbances on the system.

The stability of slit film and continuous annular extrusion and drawdown over a lubricated mandrel is determined by Eqn. (9.27). Introducing dimensionless time t* and distance Y* leads to

$$t^* = t\,\bar{v}_z(o)\,\frac{\bar{F}_z}{4\eta\,Q} = t\,\frac{\bar{v}_z(o)}{L}\,\ell n\ DR\ , \tag{9.28a}$$

$$Y^* = z\,\frac{\bar{F}_z}{4\eta\,Q} = \frac{z}{L}\,\ell n\ DR\ , \tag{9.28b}$$

where we have used Eqns. (9.1b) and (9.10). This allows us to reduce Eqn. (9.27) to

$$\left(\frac{\partial}{\partial t^*} + e^{Y^*}\,\frac{\partial}{\partial Y^*}\right)\frac{\partial \alpha}{\partial Y^*} = 0\ . \tag{9.29}$$

This has the solution

$$\frac{\partial \alpha}{\partial Y^*} = f(t^* + e^{-Y^*}) \ , \tag{9.30}$$

$$\alpha = \int_0^{Y^*} f(t^* + e^{-Y^*}) dY^* + g(Y^*) \ . \tag{9.31}$$

The above result was obtained for the case of melt spinning by Pearson and Matovich [P-2]. These authors evaluate Eqn. (9.31) with an input of $\alpha(o, t^*)$ equal to $\sin \omega t^*$ and have shown that the time average value of $\alpha(v_z(L)/v_z(o), t^*)$ exhibits singular points in the ω, $v_z(L)/v_z(o)$ domain. There is an unstable operating point at a drawdown ratio DR of 20.2. Similar conclusions have been obtained by Kase et al. [K-5,K-9] and Gelder [G-1]. They predict that stable melt spinning is not possible above a drawdown ratio of 20.2.

The results of the above paragraph indicate that a similar solution should be valid here. Kase et al. [K-9] specifically considered slit film casting. The phenomenon of draw resonance should also occur in annular extrusion over a lubricated circular cylindrical mandrel. The critical drawdown ratio for an isothermal Newtonian fluid should be the same as in melt spinning.

E. OTHER PROCESSES LEADING TO THE PEARSON-MATOVICH EQUATION

It has been found that the equation which describes the thickness fluctuation in an annular tubular film being drawn down over a lubricated straight cylindrical mandrel is exactly the same as for slit film extrusion and melt spinning. We now consider this problem more

generally. Let us reconsider the balance and stability equations for extensional flow continuous polymer processing where the force balance equation can be represented as

$$F_z = A\,\sigma_{zz} \,. \tag{9.32}$$

It seems useful to consider the cross section perturbation instead of dimension perturbation which we used earlier. Let

$$A(z,t) = \bar{A}(z)[1 + \alpha(z,t)] \,. \tag{9.33}$$

This leads to the perturbed continuity equation

$$\frac{D\alpha}{Dt} + \bar{v}_z \frac{\partial \beta}{\partial z} = 0 \,. \tag{9.34}$$

where β is defined in Eqn. (9.11b) and a perturbed force balance equation of

$$\Phi_z' = \alpha + \frac{\sigma_{zz}'}{\bar{\sigma}_{zz}} = \Phi_z'(t) \,. \tag{9.35}$$

We can write the kinematics of extensional flow as:

$$\frac{\partial v_2}{\partial x_2} = K_1 \frac{\partial v_z}{\partial z} \,, \tag{9.36a}$$

$$\frac{\partial v_3}{\partial x_3} = -(1 + K_1) \frac{\partial v_z}{\partial z} \,, \tag{9.36b}$$

where "z" is in the machine direction and "2", "3" are in the cross-section perpendicular to flow. For the case of annular tubular

film on a lubricated straight cylindrical mandrel and slit film extrusion "2" corresponds to the transverse direction of the film and "3" is in the free surface direction.

We may write

$$\frac{\partial \bar{v}_2}{\partial x_2} = \bar{K} \frac{\partial \bar{v}_z}{\partial z} , \tag{9.37a}$$

$$\frac{\partial v'_2}{\partial x_2} = K' \frac{\partial v'_z}{\partial z} , \tag{9.37b}$$

$$\frac{\partial \bar{v}_3}{\partial x_3} = -(1 + \bar{K}) \frac{\partial \bar{v}_z}{\partial z} , \tag{9.37c}$$

$$\frac{\partial v'_3}{\partial x_3} = -(1 + K') \frac{\partial v'_z}{\partial z} . \tag{9.37d}$$

For a Newtonian fluid

$$\bar{\sigma}_{zz} = 2\eta \left(\frac{\partial \bar{v}_z}{\partial z} - \frac{\partial \bar{v}_3}{\partial x_3} \right) = 2\eta(2 + \bar{K}) \frac{\partial \bar{v}_z}{\partial z} \tag{9.38a}$$

$$\sigma'_{zz} = 2\eta \left(\frac{\partial v'_z}{\partial z} - \frac{\partial v'_3}{\partial x_3} \right) = 2\eta(2 + K') \frac{\partial v'_z}{\partial z} . \tag{9.38b}$$

Substituting Eqn. (9.38) into Eqn. (9.35) and combining with Eqn. (9.34) gives

$$\Phi'_z = \alpha + \frac{2\eta Q}{\bar{F}_z \bar{v}_z} (2 + K') \left[\beta \frac{\partial \bar{v}_z}{\partial z} - \frac{D\alpha}{Dt} \right] . \tag{9.39}$$

This can be further reduced if K' is not a function of "z".

$$\frac{\partial \Phi_z}{\partial z} = \frac{\partial \alpha}{\partial z} - \left(\frac{2+K'}{2+\bar{K}}\right) \frac{\partial \alpha}{\partial z}$$

$$- \frac{2\eta Q}{\bar{F}_z \bar{v}_z} (2+K')\left[\frac{\partial^2 \alpha}{\partial z \, \partial t} + \bar{v}_z \frac{\partial^2 \alpha}{\partial z^2}\right] = 0 \ . \qquad (9.40)$$

Eqn. (9.40) becomes the same as Eqn. (9.27) only when

$$K' = \bar{K} \neq f(z) \ , \qquad (9.41a)$$

or

$$\frac{\partial \bar{v}_3 / \partial x_3}{\partial \bar{v}_z / \partial z} = \frac{\partial v_3' / \partial x_3}{\partial v_z' / \partial z} \neq f(z) \ . \qquad (9.41b)$$

Both slit film extrusion and annular film extrusion over a lubricated mandrel satisfy these conditions.

F. NON-ISOTHERMAL RESPONSE

In order for the dynamic stability under non-isothermal conditions to be the same for film and fiber spinning, the heat transfer conditions and temperature profiles must be the same. Different rates of cooling will result in different degrees of process stability.

The conservation equations, Eqns. (9.1), (9.2), and (9.3), for a Newtonian fluid may be written by assuming temperature independent fluid density and heat capacity:

$$\frac{\partial A^*}{\partial t^*} + \frac{\partial}{\partial Z^*} (A^* V^*) = 0 , \tag{9.42a}$$

$$F^* = \eta^*(\theta) A^* \frac{\partial V^*}{\partial Z^*} , \tag{9.42b}$$

$$\frac{\partial \theta}{\partial t^*} + V^* \frac{\partial \theta}{\partial Z^*} = - N_{St} \frac{C^*}{A^*} \theta , \tag{9.42c}$$

where

$$A^* = \frac{A}{L^2} , \qquad C^* = \frac{C}{L} ,$$

$$V^* = \frac{v_z}{v_z(o)} \qquad t^* = \frac{t\, v_z(o)}{L} ,$$

$$Z^* = \frac{z}{L} , \tag{9.43}$$

$$F^* = \frac{F_z}{4\eta(o)\, v_z(o)\, L} , \qquad \eta^* = \frac{\eta(\theta)}{\eta(o)} \sim e^{-B\theta} ,$$

$$N_{St} = \frac{U}{\rho\, c\, v_z(o)} , \qquad \theta = \frac{T - T_{surr}}{T(o) - T_{surr}} .$$

Here N_{St} is a Stanton number [E-1]. θ may be seen to depend upon the value of the dimensionless group $N_{St}\, C^*/A^*$ if fluids of the same $\eta^*(\theta)$ are investigated.

If we specify the drawdown ratio DR for each case, we have from Eqn. (9.10):

$$DR = \frac{v_z(L)}{v_z(o)} = \frac{A(o)}{A(L)} , \tag{9.44}$$

$$DR = \frac{h(o)}{h(L)} \qquad \text{(film)}, \tag{9.45a}$$

$$DR = \left(\frac{d(o)}{d(L)}\right)^2 \qquad \text{(fiber)}, \tag{9.45b}$$

the film thickness h has been drawn down by a factor of $\sqrt{DR}$ more than the fiber diameter. In terms of the variation of C*/A* with position, we have for an isothermal Newtonian model:

$$\frac{C^*}{A^*} \sim \exp\left(\frac{1}{2} Z^* \ln DR\right) \qquad \text{(fiber spinning)}, \tag{9.46a}$$

$$\frac{C^*}{A^*} \sim \exp(Z^* \ln DR) \qquad \text{(slit film and annular film extrusion)}, \tag{9.46b}$$

$$V^* = \exp\left(\frac{F^*}{\eta^* Q} Z^*\right) = \exp(Z^* \ln DR) \ . \tag{9.46c}$$

Eqn. (9.46) suggests that the cooling rate of the slit film and annular film extrusion is greater than that of fiber spinning at the same drawdown ratio DR.

To get a more detailed view of the cooling effect, we have to consider the nature of heat transfer coefficient U or Stanton number N_{St}. Using Kase and Matsuo's correlation [K-6,K-7] between U and v_z (or velocity difference between thread and cooling air) of fiber, we may express the heat transfer coefficient of fiber and film as

$$U = \Gamma H^{-\frac{2}{3}} v_z^{\frac{1}{3}} , \tag{9.47}$$

where H is film thickness h or fiber diameter d and Γ is a constant.

Introducing Eqn. (9.47) into Eqn. (9.42c) of the steady state condition gives

$$\frac{\partial \theta}{\partial Z^*} = - \frac{\Gamma}{\rho c \, (v_z(o) \, L)^{2/3}} (V^* \, H^*)^{-\frac{2}{3}} \frac{C^*}{A^*} \theta \, . \tag{9.48}$$

Let

$$U^* = (V^* \, H^*)^{-\frac{2}{3}} \frac{C^*}{A^*} \, . \tag{9.49}$$

The value U^* varies as for fiber spinning

$$U^* \sim \exp(\frac{Z^*}{6} \ell n \, DR) \sim V^{*1/6} \, , \tag{9.50a}$$

and for slit film or annular tubular film extrusion on a lubricated straight cylindrical mandrel

$$U^* \sim \exp(Z^* \ell n \, DR) \sim V^* \, . \tag{9.50b}$$

Eqn. (9.50) again suggests that cooling rate of film processes are greater than that of melt spinning of a fluid of the same $\eta^*(\theta)$ at the same drawdown ratio.

G. SUMMARY

The stability of annular and cast film extrusion is analyzed and contrasted to melt spinning. Generally melt spinning and slit film extrusion are governed by the same equations in the isothermal case. This is also true for other film processes including annular

film extrusion under limited circumstances, notably extrusion over a lubricated mandrel. Draw resonance observed in melt spinning and slit film extrusion under similar circumstances should be observed here. Detailed arguments are given for Newtonian fluid models.

CHAPTER X

STABILITY OF CONTINUOUS FILM EXTRUSION: PART II

A. INTRODUCTION

Polymer melt operations involving post die deformation are well known to exhibit a range of instabilities. The most significant ones are natural oscillation effects, draw resonance in melt spinning of fibers [B-6,F-14,H-13,I-6,K-5,K-9,M-16,M-41,W-8,W-17], surging in film casting [B-6,K-5,K-9], and bubble instabilities in tubular blown film extrusion. Of these phenomena only the draw resonance instability [C-8,F-3,F-4,F-5,F-6,G-1,H-13,I-6,K-5,K-9,S-11,S-12,S-14, W-17] has received significant theoretical treatment.

We have initiated research to analyze the deformation and flow of polymer systems involving multiaxial deformations. Earlier considerations (Chapters VI, VII, VIII and IX) dealt with instabilities in biaxially stretched isolated sheets and annuli, and some of the simpler continuous film processings, such as constant width film extrusions, including annular film extrusion over a lubricated straight mandrel. Two of the most important film processing operations are the tubular blown film extrusion process and the flat film extrusion process, the latter involving a tentering frame [A-8,M-4,W-23]. Pioneering investigations of instabilities in film extrusion, such as film casting and tubular blown film extrusion, have been made by Yeow [Y-8,Y-9] for an isothermal Newtonian fluid.

These papers illustrate the complexity of the problem including film width fluctuation in the film casting process, and complex changes of kinematics along the machine direction with bubble diameter fluctuation in the tubular blown film extrusion process. In the present chapter, we consider two different flat film extrusion processes with tentering frames, one involving a linearly varying width change along the machine direction and the other involving a constant ratio of kinematics between the machine direction and the transverse direction throughout the process. And also an annular film extrusion over a lubricated conical mandrel and annular unblown film extrusion will be considered as part of tubular film extrusion processes. The last two film processes are the asymptotic cases of a tubular blown film extrusion. Special interest will be paid to the differences of processing geometries and kinematics of the stability equations. To make the problems simpler, isothermal Newtonian fluids will be considered.

B. DISTURBANCES IN FLAT FILM OR SHEET

In this section we consider the conservation equations for a flat film or sheet to which disturbances are imposed. First we consider the general case, then simplify them to certain special cases: the isolated stretching case and the continuous film extrusion case.

B-1. Conservation Equations for Homogeneous Deformation

Consider a flat fluid film or sheet being stretched multiaxially. Let the film thickness be h and the width be W, and imagine a Cartesian coordinate system where "1" or "z" is the machine direction; "2" is the transverse direction and "3" is the normal to sheet. If we could assume that the flow field is completely elongational, the continuity equation is given as follows, by assuming isothermal conditions and incompressibility:

$$\frac{\partial v_1}{\partial x_1} + \frac{\partial v_2}{\partial x_2} + \frac{\partial v_3}{\partial x_3} = 0 \ . \tag{10.1}$$

Eqn. (10.1) can be rewritten by neglecting the velocity gradient along the "3" direction:

$$\frac{\partial v_1}{\partial x_1} + \frac{\partial v_2}{\partial x_2} + \frac{v_3}{h} = 0 \ , \tag{10.2a}$$

or

$$\frac{\partial v_1}{\partial x_1} + \frac{\partial v_2}{\partial x_2} + \frac{1}{h}\frac{Dh}{Dt} = 0 \ , \tag{10.2b}$$

or

$$\frac{\partial h}{\partial t} + \frac{\partial v_1 h}{\partial x_1} + \frac{\partial v_2 h}{\partial x_2} = 0 \ . \tag{10.2c}$$

For the special case of a molten polymer sheet where inertia, gravity, and surface tension are small and may be neglected, the force balance equation is

$$\frac{\partial hW\sigma_{11}}{\partial x_1} = \frac{\partial F_1}{\partial x_1} = 0 \ , \tag{10.3a}$$

and

$$\frac{\partial h\sigma_{22}}{\partial x_2} = \frac{\partial F_2}{\partial x_2} = 0 \ . \tag{10.3b}$$

B-2. Conservation Equations for Perturbed States

B-2-a. General formulation. We now introduce infinite disturbances into the flow of a flat sheet or film, which we take not to vary through the thickness. We take

$$h(x_1,x_2,t) = \bar{h}(x_1,t)[1 + \alpha(x_1,x_2,t)] \ , \tag{10.4a}$$

$$v_1(x_1,x_2,t) = \bar{v}_1(x_1,t)[1 + \beta(x_1,x_2,t)] \ , \tag{10.4b}$$

$$v_2(x_1,x_2,t) = \bar{v}_2(x_1,x_2,t)[1 + \gamma(x_1,x_2,t)] \ , \tag{10.4c}$$

$$\sigma_{11}(x_1,x_2,t) = \bar{\sigma}_{11}(x_1,t) + \sigma'_{11}(x_1,x_2,t) \ , \tag{10.4d}$$

$$\sigma_{22}\ (x_1,x_2t) = \bar{\sigma}_{22}(x_1,x_2,t) + \sigma'_{22}(x_1x_2,t) \ , \tag{10.4e}$$

$$F_1(t) = \bar{F}_1(t) + F'_1(t) \ , \tag{10.4f}$$

where the bar denotes the steady state. The form of Eqn. (10.4f) is proposed based on the force balance of Eqn. (10.3).

If we introduce the disturbances of Eqn. (10.4) into the continuity equation of Eqn. (10.2) and subtract out the steady state results, we obtain

$$\frac{D\alpha}{Dt} + \frac{1}{\bar{h}} \left(\frac{\partial \bar{v}_1 \bar{h} \beta}{\partial x_1} + \frac{\partial \bar{v}_2 \bar{h} \gamma}{\partial x_2} \right) = 0 \ , \tag{10.5a}$$

where

$$\frac{D\alpha}{Dt} = \frac{\partial \alpha}{\partial t} + \bar{v}_1 \frac{\partial \alpha}{\partial x_1} + \bar{v}_2 \frac{\partial \alpha}{\partial x_2} \ . \tag{10.5b}$$

The perturbed force balance equations are

$$\Phi_1 = \frac{F_1'}{\bar{h}\,\bar{W}} = \sigma_{11}' + \bar{\sigma}_{11} \left(\alpha + \frac{W'}{\bar{W}} \right) = f(t) \ . \tag{10.6}$$

For the system where width W is constant (i.e., W' is zero), Eqn. (10.6) is rewritten as

$$\Phi_1 = \sigma_{11}' + \bar{\sigma}_{11} \alpha = \frac{F_1'}{\bar{h}\,\bar{W}} \ . \tag{10.7a}$$

And the force balance along the transverse direction is

$$\Phi_2 = \sigma_{22}' + \bar{\sigma}_{22} \alpha \ . \tag{10.7b}$$

Eqn. (10.7) might be reduced to

$$\Phi_1' = \alpha + \frac{\sigma_{11}'}{\bar{\sigma}_{11}} = \frac{F_1'}{\bar{F}_1} = \Phi_1'(t) \ , \tag{10.8a}$$

$$\Phi_2' = \alpha + \frac{\sigma_{22}'}{\bar{\sigma}_{22}} = \Phi_2'(t) \ . \tag{10.8b}$$

To proceed further, we need to introduce more restrictions on the kinematics of the system.

B-2-b. Tensile stretching of an isolated sheet. For the tensile stretching of an isolated sheet

$$\frac{\partial \bar{h}}{\partial x_1} = 0, \qquad \frac{\partial \bar{h}}{\partial x_2} = 0 \ , \tag{10.9a,b}$$

and

$$\frac{\partial \bar{v}_1}{\partial x_1} = E_1, \qquad \frac{\partial \bar{v}_2}{\partial x_2} = E_2 \ . \tag{10.9c,d}$$

The continuity equation Eqn. (10.5) is reduced to

$$\frac{D\alpha}{Dt} + \frac{\partial \bar{v}_1 \beta}{\partial x_1} + \frac{\partial \bar{v}_2 \gamma}{\partial x_2} = 0 \ , \tag{10.10a}$$

or

$$\frac{\partial \alpha}{\partial t} + \bar{v}_1 \frac{\partial(\alpha+\beta)}{\partial x_1} + \bar{v}_2 \frac{\partial(\alpha+\gamma)}{\partial x_2} + \beta E_1 + \gamma E_2 = 0 \ . \tag{10.10b}$$

Eqn. (10.10) is the equivalent equation for continuity whicy has been used in Chapters VI and VII where either β or γ are assumed to be zero.

B-2-c. Continuous film extrusion process. For a continuous film extrusion process we have

$$\frac{\partial \bar{h}}{\partial t} = 0, \qquad \frac{\partial \bar{h}}{\partial x_2} = 0 \ , \tag{10.11a,b}$$

$$\frac{\partial \bar{v}_1 \bar{h}}{\partial x_1} + \frac{\partial \bar{v}_2 \bar{h}}{\partial x_2} = 0 \ . \tag{10.11c}$$

The continuity equation, with the aid of Eqn. (10.11), becomes

$$\frac{D\alpha}{Dt} + \frac{\partial \bar{v}_1 \beta}{\partial x_1} + \frac{\partial \bar{v}_2 \gamma}{\partial x_2} - \beta\left(\frac{\partial \bar{v}_1}{\partial x_1} + \frac{\partial \bar{v}_2}{\partial x_2}\right) = 0 \ , \tag{10.12a}$$

or

$$\frac{\partial \alpha}{\partial t} + \bar{v}_1 \frac{\partial(\alpha+\beta)}{\partial x_1} + \bar{v}_2 \frac{\partial(\alpha+\gamma)}{\partial x_2} + (\gamma-\beta)\frac{\partial \bar{v}_2}{\partial x_2} = 0 \ . \tag{10.12b}$$

B-3. Newtonian Fluid Solution

B-3-a. General solution. In the case of a Newtonian fluid, the stress field is given by

$$\bar{\sigma}_{11} = 2\eta\left(2\frac{\partial \bar{v}_1}{\partial x_1} + \frac{\partial \bar{v}_2}{\partial x_2}\right) \ , \tag{10.13a}$$

$$\bar{\sigma}_{22} = 2\eta\left(\frac{\partial \bar{v}_1}{\partial x_1} + 2\frac{\partial \bar{v}_2}{\partial x_2}\right) \ , \tag{10.13b}$$

$$\sigma'_{11} = 2\eta\left(2\frac{\partial \bar{v}_1}{\partial x_1} + \frac{\partial \bar{v}_2 \gamma}{\partial x_2}\right) \ , \tag{10.13c}$$

$$\sigma'_{22} = 2\eta\left(\frac{\partial \bar{v}_1}{\partial x_1} + 2\frac{\partial \bar{v}_2 \gamma}{\partial x_2}\right) \ . \tag{10.13d}$$

Introducing Eqn. (10.13) into Eqns. (10.6) and (10.7b) yields

$$\Phi_1 = 2\eta\left((2\frac{\partial \bar{v}_1}{\partial x_1} + \frac{\partial \bar{v}_2}{\partial x_2})(\alpha + \frac{W'}{\bar{W}}) + 2\frac{\partial \bar{v}_1 \beta}{\partial x_1} + \frac{\partial \bar{v}_2 \gamma}{\partial x_2}\right) \ , \tag{10.14a}$$

$$\Phi_2 = 2\eta\left[\left(\frac{\partial \bar{v}_1}{\partial x_1} + 2\,\frac{\partial \bar{v}_2}{\partial x_2}\right)\alpha + \frac{\partial \bar{v}_1 \beta}{\partial x_1} + 2\,\frac{\partial \bar{v}_2 \gamma}{\partial x_2}\right] . \qquad (10.14b)$$

The sensitivity of the system to the applied disturbances, whose constitutive relation may be represented as a Newtonian fluid, can be derived from Eqn. (10.14) with the aid of the continuity equation Eqn. (10.5) and further restrictions on the kinematics.

B-3-b. Stretching of isolated sheets. For the case of constant strain rate stretching and with the neglect of W', Eqn. (10.14a) becomes

$$\Phi_1 = 2\eta\left[E_1[2\alpha + \frac{E_2}{E_1}(\alpha+\gamma)] - \bar{v}_2\,\frac{\partial \gamma}{\partial x_2} - 2\,\frac{D\alpha}{Dt}\right] . \qquad (10.15)$$

Eqn. (10.15) can be simplified, with the aid of the continuity equation Eqn. (10.10) and neglecting the v_2 variation (i.e., $v_2' = 0$ or $\gamma = 0$), to

$$\frac{D\alpha}{Dt} = \alpha(1 + \frac{1}{2}\,\frac{E_2}{E_1})E_1 - \frac{\Phi_1}{4\eta} . \qquad (10.16)$$

If we set Φ_1 equal to zero (i.e., $F_1' = 0$), Eqn. (10.16) is reduced to

$$\frac{1}{\alpha}\,\frac{D\alpha}{Dt} = (1 + \frac{1}{2}\,\frac{E_2}{E_1})E_1 . \qquad (10.17)$$

Eqn. (10.17) has been already described in Chapter VI.

B-3-c. Continuous film extrusion. For continuous film or sheet extrusion processes, Eqn. (10.14) can be reduced with the aid of Eqn. (10.12) to

$$\frac{\Phi_1}{2\eta} = \left(2 \frac{\partial \bar{v}_1}{\partial x_1} + \frac{\partial \bar{v}_2}{\partial x_2} \right) \left(\alpha + \beta + \frac{W'}{\bar{W}} \right) - 2 \frac{D\alpha}{Dt} + (\beta - \gamma) \frac{\partial \bar{v}_2}{\partial x_2} - \bar{v}_2 \frac{\partial \gamma}{\partial x_2} , \tag{10.18a}$$

$$\frac{\Phi_2}{2\eta} = \left(\frac{\partial \bar{v}_1}{\partial x_1} + 2 \frac{\partial \bar{v}_2}{\partial x_2} \right) (\alpha + \beta) - 2 \frac{D\alpha}{Dt} - \bar{v}_1 \frac{\partial \beta}{\partial x_1} . \tag{10.18b}$$

If disturbances occur only along the machine direction ("1" direction) and γ and W' are assumed to be zero (i.e., $v_2' = 0$ and $W' = 0$), Eqn. (10.18) leads to

$$\frac{\Phi_1}{2\eta} = \left(2 \frac{\partial \bar{v}_1}{\partial x_1} + \frac{\partial \bar{v}_2}{\partial x_2} \right) (\alpha + \beta) - 2 \frac{D\alpha}{Dt} + \beta \frac{\partial \bar{v}_2}{\partial x_2} . \tag{10.19}$$

Eqn. (10.19) will be differentiated with respect to "x_1" (i.e., $\Phi_1 = f(t)$, therefore $\partial \Phi_1 / \partial x_1 = 0$) and β will be eliminated from the resulting equation by using continuity equation Eqn. (10.12); then the steady state solution will be substituted in order to obtain the equation which represents the stability of the system.

C. FLAT FILM EXTRUSION PROCESS WITH TENTERING FRAME: CONSTANT RATIO OF KINEMATICS

We now consider the flat film extrusion process where the film is stretched not only in the machine direction but also in the transverse direction with the aid of a tentering frame. The ratio of the velocity gradient between the machine direction and the

transverse direction is kept constant in any place (i.e., kept constant along the machine direction) (see Figure 10.1). We shall analyze the steady state and the unsteady state of this film process.

A Newtonian fluid assumption will be made for the constitutive equation.

C-1. Steady State Solution

A "z,2,3" Cartesian coordinate system with its origin at the center of the die exit is used where "z" is in the machine direction, "2" is in the transverse direction, and "3" is normal to the film.

We may represent the force balance by neglecting inertia, gravity and friction effects as

$$\frac{\partial F_z}{\partial z} = Q \frac{\partial}{\partial z}\left(\frac{\sigma_{zz}}{v_z}\right) = 0 \ , \tag{10.20a}$$

or

$$F_z = \frac{Q}{v_z}\sigma_{zz} = \frac{Q}{v_z}(P_{zz} - P_{33}) \tag{10.20b}$$

where Q is the volumetric flow rate. The stress field of a Newtonian fluid is given by

$$P_{zz} = 2\eta \frac{\partial v_z}{\partial z} \ , \tag{10.21a}$$

$$P_{33} = 2\eta \frac{\partial v_3}{\partial x_3} = -2\eta\left(\frac{\partial v_z}{\partial z} + \frac{\partial v_2}{\partial x_2}\right) = -2\eta(1+K)\frac{\partial v_z}{\partial z} \ , \tag{10.21b}$$

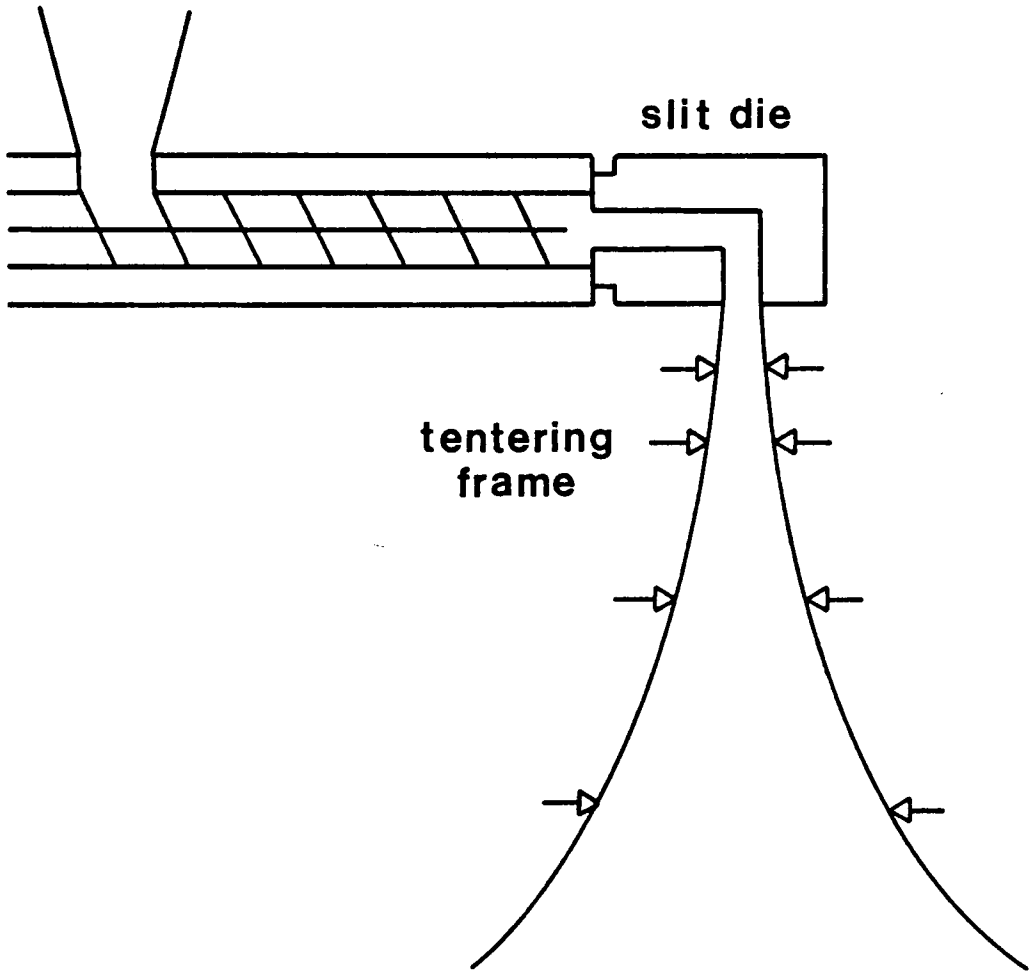

Figure 10.1. Flat film extrusion with tentering frame (the ratio of deformation rate is independent of position).

where

$$K = \frac{\partial v_2}{\partial x_2} \Big/ \frac{\partial v_z}{\partial z} \neq f(z) \ . \tag{10.21c}$$

The force balance equation becomes

$$F_z = 2\eta(2+K) \frac{\partial v_z}{\partial z} \frac{Q}{v_z} \ , \tag{10.22}$$

which leads to the exponential solution

$$v_z = v_z(0) \exp\left[\frac{z}{2\eta(2+K)} \frac{F_z}{Q}\right] \ . \tag{10.23}$$

The solution can be non-dimensionalized by using the following dimensionless groups

$$Z^* = \frac{z}{L}, \qquad V^* = v_z(z)/v_z(0) \ , \tag{10.24a,b}$$

where L is the distance between the die exit and the take-up position. Eqn. (10.24) requires us to introduce another dimensionless group for F_z motivated by the fact that V* is DR(= $v_z(L)/v_z(0)$) at Z* = 1.0:

$$F^* = \frac{L}{2\eta(2+K)} \frac{F_z}{Q} = \ell n \ DR \ . \tag{10.25}$$

Finally, the dimensionless solution of the velocity profile of this process is given with the aid of Eqns. (10.24) and (10.25) by:

$$V^* = \exp(Z^* \ \ell n \ DR) \ . \tag{10.26}$$

The velocity profile of this process is the same as that already described in Chapter IX, such as annular film extrusion over a lubricated straight cylindrical mandrel, constant width film casting, and melt spinning processes. In a case of melt spinning K in Eqn. (10.21c) is -0.5 and the other two film extrusion processes have K of 0.0.

In this process, we assume that

$$\frac{\partial v_2}{\partial x_2} = K \frac{\partial v_z}{\partial z} \neq f(z) \ . \tag{10.27}$$

By neglecting the deformation rate distribution along the transverse direction (i.e., "2" direction)

$$\frac{\partial v_2}{\partial x_2} = \frac{1}{W} \frac{DW}{Dt} = \frac{v_z}{W} \frac{\partial W}{\partial z} \ . \tag{10.28}$$

Eqns. (10.28) and (10.27) lead to

$$\ell n \frac{W(z)}{W(0)} = K \ \ell n \frac{v_z(z)}{v_z(0)} \ . \tag{10.29}$$

Eqn. (10.29) is also non-dimensionalized to

$$W^* = V^{*K} \ , \tag{10.30a}$$

where

$$W^* = \frac{W(z)}{L} \ . \tag{10.30b}$$

C-2. Stability of the System

We now consider the perturbed state with disturbances being only in the machine direction and no fluctuation along the width of film. Therefore the applied disturbances, Eqn. (10.4), may be simplified to

$$h(z,t) = \bar{h}(z)[1 + \alpha(z,t)] \ , \tag{10.31a}$$

$$v_z(z,t) = \bar{v}_z(z)[1 + \beta(z,t)] \ , \tag{10.31b}$$

$$v_2(z,x_2,t) = \bar{v}_2(z,x_2) \ , \tag{10.31c}$$

$$\sigma_{zz}(z,t) = \bar{\sigma}_{zz}(z) + \sigma'_{zz}(z,t) \ , \tag{10.31d}$$

$$F_z(t) = \bar{F}_z + F'_z(t) \ . \tag{10.31e}$$

The form of Eqn. (10.31e) is suggested from the force balance equation of Eqn. (10.20).

The perturbed conservation equations are (see Section B):

$$\frac{D(\alpha+\beta)}{Dt} - \frac{\partial\beta}{\partial t} = 0 \ , \tag{10.32a}$$

or

$$\frac{\partial \bar{v}_z \beta}{\partial z} - \beta \frac{\partial \bar{v}_z}{\partial z} + \frac{D\alpha}{Dt} = 0 \ , \tag{10.32b}$$

and

$$\Phi'_z = \alpha + \frac{\sigma'_{zz}}{\bar{\sigma}_{zz}} = \Phi'_z(t) = \frac{F'_z}{\bar{F}_z} \ . \tag{10.33}$$

The stress field of a Newtonian fluid is

$$\bar{\sigma}_{zz} = 2\eta\left(\frac{\partial \bar{v}_z}{\partial z} - \frac{\partial \bar{v}_3}{\partial x_3}\right) = 2\eta(2+K)\,\frac{\partial \bar{v}_z}{\partial z} \quad , \tag{10.34a}$$

$$\sigma'_{zz} = 2\eta\left(\frac{\partial v'_z}{\partial z} - \frac{\partial v'_3}{\partial z}\right) = 2\eta\left(2\,\frac{\partial \bar{v}_z\beta}{\partial z} + \frac{\partial v'_2}{\partial x_2}\right) \quad . \tag{10.34b}$$

We have assumed v'_2 to be zero; therefore, Eqn. (10.34b) may be simplified to

$$\sigma'_{zz} = 4\eta\,\frac{\partial v'_z}{\partial z} = 4\eta\,\frac{\partial \bar{v}_z\beta}{\partial z} \quad . \tag{10.34c}$$

Substituting Eqn. (10.34) into Eqn. (10.33) gives

$$\Phi'_z = \alpha + \left(\frac{2}{2+K}\right)\frac{1}{\partial \bar{v}_z/\partial z}\,\frac{\partial \bar{v}_z\beta}{\partial z} \quad . \tag{10.35}$$

With the aid of Eqn. (10.32), this leads to

$$\Phi'_z = \alpha + \left(\frac{2}{2+K}\right)\beta - \left(\frac{2}{2+K}\right)\frac{1}{\partial \bar{v}_z/\partial z}\left(\frac{D\alpha}{Dt}\right) . \tag{10.36}$$

Substituting the steady state solution of $\partial \bar{v}_z/\partial z$ into Eqn. (10.36) and differentiating it with respect to "z", then eliminating β with the aid of Eqn. (10.32) leads to

$$\frac{\partial \Phi'_z}{\partial z} = \frac{1}{\bar{F}_z}\,\frac{\partial F'_z}{\partial z} = \frac{\partial \alpha}{\partial t} - \left(\frac{2}{2+K}\right)\frac{1}{\partial \bar{v}_z/\partial z}\,\frac{\partial}{\partial z}\left(\frac{D\alpha}{Dt}\right) = 0 \quad . \tag{10.37}$$

Eqn. (10.37) can be rewritten as

$$\frac{D}{Dt}\left(\frac{\partial\alpha}{\partial z}\right) - \frac{K}{2}\frac{\partial\bar{v}_z}{\partial z}\left(\frac{\partial\alpha}{\partial z}\right) = 0 \ , \tag{10.38a}$$

where

$$\frac{D}{Dt} = \frac{\partial}{\partial t} + \bar{v}_z \frac{\partial}{\partial z} \ , \tag{10.38b}$$

$$K = \frac{\partial\bar{v}_2/\partial x_2}{\bar{\partial}_2/\partial z} \neq f(z) \ . \tag{10.38c}$$

By introducing the following dimensionless groups

$$Z^* = \frac{z}{L}, \qquad V^* = \frac{v_z}{v_z(0)} \ , \tag{10.39a,b,c}$$

$$t^* = \frac{t}{L} v_z(0) \ .$$

Eqn. (10.38) leads to

$$\frac{D}{Dt^*}\left(\frac{\partial\alpha}{\partial Z^*}\right) - \frac{K}{2}\frac{\partial V^*}{\partial Z^*}\left(\frac{\partial\alpha}{\partial Z^*}\right) = 0 \ , \tag{10.40a}$$

or

$$\frac{\partial^2\alpha}{\partial Z^* \partial t^*} + V^* \frac{\partial^2\alpha}{\partial Z^{*2}} - \frac{K}{2}\frac{\partial V^*}{\partial Z^*}\frac{\partial\alpha}{\partial Z^*} = 0 \ , \tag{10.40b}$$

where

$$V^* = \exp(Z^* \ \ell n \ DR) \ , \tag{10.41a}$$

$$\frac{\partial V^*}{\partial Z^*} = \ell n \ DR \exp(Z^* \ \ell n \ DR) \ . \tag{10.41b}$$

Eqn. (10.40) is the equation which represents the sensitivity of the system for the applied disturbances to the system. It is expected that this flat film extrusion process could exhibit natural oscillation phenomena on the film thickness (draw resonance), when the time average value of α exhibits singular points in the applied boundary conditions, including the drawdown ratio DR and the kinematics constant K. Other cases are the response of a forced oscillation.

D. FLAT FILM EXTRUSION PROCESS WITH TENTERING FRAME: LINEARLY VARYING WIDTH

We consider another flat film extrusion process where the film is stretched also in the transverse direction by the tentering frame and the width of the film W changes linearly along the machine direction (i.e., dW/dz = constant) (see Figure 10.2). This process has been used for the production of biaxially oriented polymer films of polyethylene terephthalate, polypropylene and polystyrene. There are roughly two different manners of stretching. One is simultaneous stretching and the other is two-stage successive stretching. Here only the simultaneous stretching process of a Newtonian fluid will be analyzed.

D-1. Steady State Solution

A "z,2,3" Cartesian coordinate system with an origin at the center of the die exit is used where "z" is in the machine direction,, "a" is in the transverse direction, and "3" is normal to the film.

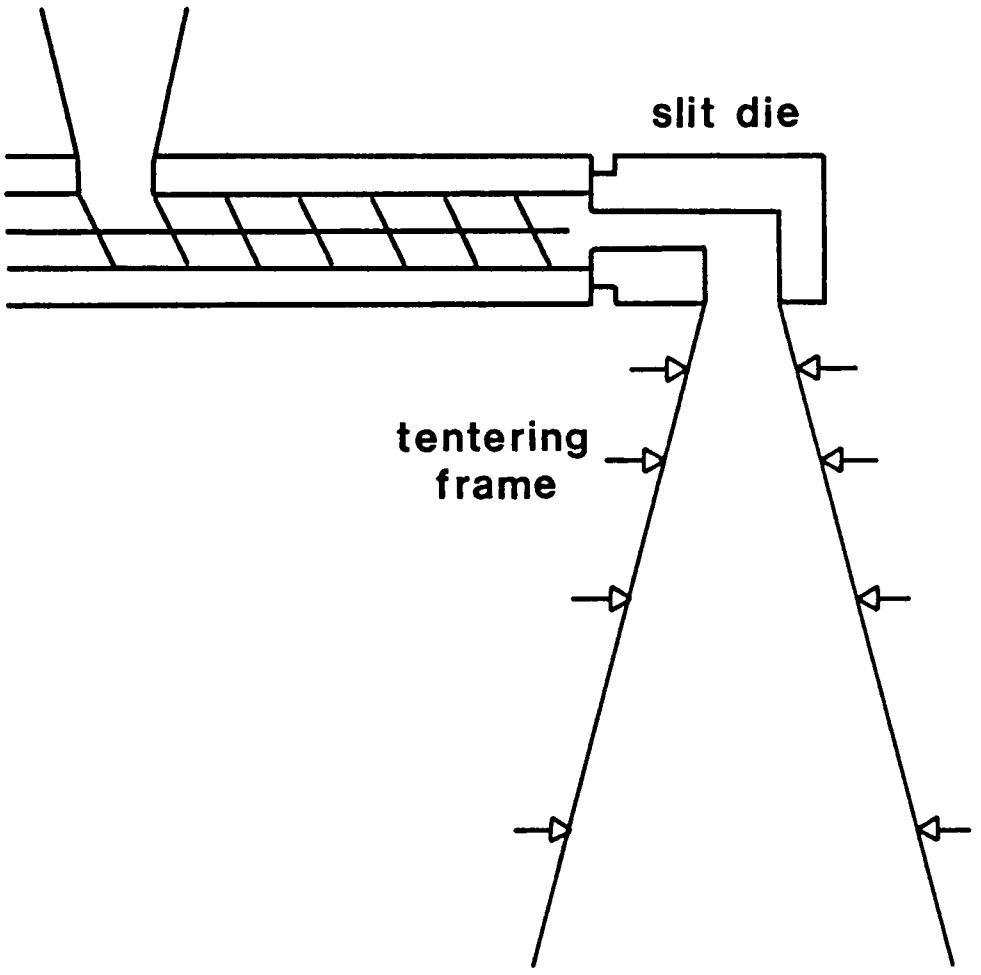

Figure 10.2. Flat film extrusion with tentering frame (linearly varying width along the machine direction).

The velocity field of the flow between the die exit and the freezing point (take-up position) has been treated by assuming a flat velocity profile. The film width W changes according to

$$W(z) = W_0 + 2z \tan \theta \ , \tag{10.42}$$

where W_0 is the film width at the die exit and θ is the angle between the film edge and the machine direction.

The strain rate tensor $\underset{\sim}{d} = \frac{1}{2} [\nabla \underset{\sim}{v} + (\nabla \underset{\sim}{v})^T]$ is given by neglecting the variation of $\partial v_2/\partial x_2$ with "x_2" and v_3/ x_3 with "x_3" as

$$d_{zz} = \frac{\partial v_z}{\partial z} \ , \tag{10.43a}$$

$$d_{22} = \frac{\partial v_2}{\partial x_2} = \frac{1}{W} \frac{dW}{Dt} = \frac{v_z}{W} \frac{\partial W}{\partial z} = 2 \tan \theta \frac{v_z}{W} \ , \tag{10.43b}$$

$$d_{33} = \frac{\partial v_3}{\partial x_3} = \frac{1}{h} \frac{Dh}{Dt} = \frac{v_z}{h} \frac{\partial h}{\partial z} \ , \tag{10.43c}$$

$$d_{zz} + d_{22} + d_{33} = 0 \ . \tag{10.43d}$$

By neglecting inertia, gravity, friction and shear effects, the force balance becomes:

$$F_z = Wh\sigma_{zz} = Wh(P_{zz} - P_{33}) \ . \tag{10.44}$$

For a Newtonian fluid, Eqn. (10.44) can be rewritten as

$$F_z = 4\eta \frac{Q}{v_z} \left[\frac{\partial v_z}{\partial z} + \frac{\partial v_z}{W} \tan \theta \right] \ , \tag{10.45}$$

where Q is the volumetric flow rate.

Eqn. (10.45) has the solution

$$v_z = v_z(0) \exp\left[- \frac{1}{2} \ell n \left| \frac{W}{W_0} \right| + \frac{z F_z}{4\eta Q} \right] , \qquad (10.46a)$$

or

$$v_z = v_z(0) \exp\left[- \frac{1}{2} \ell n \left| 1 + \frac{2 \tan \theta}{W_0} z \right| + \frac{z F_z}{4\eta Q} \right] . \qquad (10.46b)$$

From Eqn. (10.43b), the velocity in the transverse direction is

$$v_2 = \frac{2 \tan \theta \, v_z}{W(0) + 2z \tan \theta} x_2 + c . \qquad (10.47a)$$

By taking the origin of the coordinate at the center of the die exit, $v_z(z = 0, x_2 = 0)$ is zero. Therefore

$$v_2 = \frac{2 \tan \theta \, v_z}{W(0) + 2z \tan \theta} x_2 = \frac{2 \tan \theta \, v_z}{W} x_2 . \qquad (10.47b)$$

The solution can be non-dimensionalized by introducing the following dimensionless groups:

$$Z^* = \frac{z}{L} , \quad V^* = \frac{v_z}{v_z(0)} , \quad W^* = \frac{W}{L} , \qquad (10.48a,b,c)$$

$$DR = V^*(1.0) = \frac{v_z(L)}{v_z(0)} , \quad B = \frac{W^*(1.0)}{W^*(0)} = \frac{W(L)}{W(0)} , \qquad (10.48d,e)$$

where L is the distance between the die exit and the take-up position. Eqn. (10.48e) leads to

$$\frac{W^*(Z^*)}{W^*(0)} = (B-1)Z^* + 1 . \qquad (10.48f)$$

Eqn. (10.48) requires us to introduce another dimensionless group related to the take-up force F_z, the drawdown ratio DR and the transverse stretch ratio B at Z* being unity as

$$F^* = \frac{F_z L}{4\eta Q} = \ell n\ DR + \frac{1}{2}\ \ell n|B| \ . \tag{10.49}$$

Eqn. (10.49) is led by

$$F^* = \frac{F_z L}{4\eta Q} = \frac{1}{V^*}\frac{\partial V^*}{\partial Z^*} + \frac{B-1}{2[(B-1)Z^* + 1]} \ , \tag{10.50a}$$

or

$$F^* = \frac{F_z L}{4\eta Q} = \frac{1}{V^*}\frac{\partial V^*}{\partial Z^*} + \frac{\tan\theta}{W^*} \ . \tag{10.50b}$$

The dimensionless velocity profile is

$$V^* = [(B-1)Z^* + 1]^{-1/2} \exp\left[(\ell n\ DR + \frac{1}{2}\ \ell n|B|)Z^*\right] \ . \tag{10.51}$$

D-2. Stability of System: Disturbances in the Machine Direction

We now consider the perturbed state with disturbances being only in the machine direction and no fluctuation in the width of film. The imposed disturbances are the same as the one in Section C.

The perturbed conservation equations are (see Section B):

$$\frac{D(\alpha+\beta)}{Dt} - \frac{\partial\beta}{\partial t} = 0 \ , \tag{10.52a}$$

or

$$\frac{\partial\ \bar{v}_2\beta}{\partial z} - \beta\frac{\partial\bar{v}_z}{\partial z} + \frac{D\alpha}{Dt} = 0 \ , \tag{10.52b}$$

and

$$\Phi_z' = \alpha + \frac{\sigma_{zz}'}{\bar{\sigma}_{zz}} = \Phi_z'(t) \ . \tag{10.53}$$

The stress field of a Newtonian fluid is

$$\bar{\sigma}_{zz} = 2\eta\left(\frac{\partial \bar{v}_z}{\partial z} - \frac{\partial \bar{v}_3}{\partial x_3}\right) = 2\eta\left(2\,\frac{\partial \bar{v}_z}{\partial z} + \frac{\partial \bar{v}_2}{\partial x_2}\right) \ , \tag{10.54a}$$

$$\sigma_{zz}' = 2\eta\left(\frac{\partial v_z'}{\partial z} - \frac{\partial v_3'}{\partial x_3}\right) = 2\eta\left(2\,\frac{\partial \bar{v}_z}{\partial z} + \frac{\partial v_2'}{\partial x_2}\right) \ . \tag{10.54b}$$

We have assumed v_2' to be zero; therefore, Eqn. (10.54b) may be simplified to

$$\sigma_{zz}' = 4\eta\,\frac{\partial \bar{v}_z \beta}{\partial z} \ . \tag{10.54c}$$

Substituting Eqn. (10.54) into Eqn. (10.53) leads to

$$\Phi_z' = (\alpha+\beta) - \frac{2}{\left(2\,\frac{\partial \bar{v}_z}{\partial z} + \frac{\partial \bar{v}_z}{\partial x_2}\right)}\frac{D\alpha}{Dt} \ . \tag{10.55}$$

The force balance equation of the steady state of a Newtonian fluid is (see also Section D-1):

$$\bar{F}_z = 2\eta\,\frac{Q}{\bar{v}_z}\left(2\,\frac{\partial \bar{v}_z}{\partial z} + \frac{\partial \bar{v}_2}{\partial x_2}\right) \ . \tag{10.56}$$

Differentiating Eqn. (10.55) with respect to "z", and then eliminating $(2\ \partial\bar{v}_z/\partial z + \partial\bar{v}_2/\partial x_2)$ and β from the resulting equatioh (with the aid of Eqns. (10.56) and (10.52)) gives finally

$$2\frac{\partial}{\partial z}\left(\frac{D\alpha}{Dt}\right) + \frac{1}{\bar{v}_z}\frac{\partial \bar{v}_2}{\partial x_2}\frac{D\alpha}{Dt} - \frac{\bar{F}_z\,\bar{v}_z}{2\eta Q}\frac{\partial \alpha}{\partial z} = 0 \ . \qquad (10.57)$$

Eqn. (10.57) can be further reduced to

$$\frac{D}{Dt}\left(\frac{\partial \alpha}{\partial z}\right) + \frac{\partial \bar{v}_2}{\partial x_2}\frac{\partial \alpha}{\partial t} = 0 \ , \qquad (10.58a)$$

or

$$\frac{D}{Dt}\left(\frac{\partial \alpha}{\partial z}\right) + \frac{\tan\theta}{\bar{W}}\frac{\partial \alpha}{\partial t} = 0 \ . \qquad (10.58b)$$

Eqn. (10.58) may be non-dimensionalized with the aid of Eqn. (10.48) to

$$\frac{\partial^2 \alpha}{\partial Z^{*2}} + \frac{1}{V^*}\frac{\partial^2 \alpha}{\partial Z^*\,\partial t^*} + \frac{(B-1)}{2V^*[(B-1)Z^*+1]}\frac{\partial \alpha}{\partial t^*} = 0 \ , \qquad (10.59a)$$

where

$$t^* = t\,\frac{v_1(0)}{L} \ . \qquad (10.59b)$$

And V^* is given as

$$V^* = [(B-1)Z^*+1]^{-1/2}\exp\left[\left(\ell n\ DR + \frac{1}{2}\ell n|B|\right)Z^*\right] \ . \qquad (10.60)$$

Eqn. (10.59) is the equation which represents the sensitivity of this system to the imposed disturbances. It is expected that this flat film extrusion process could exhibit natural oscillation phenomena on the film thickness (draw resonance), when the time average of α exhibits singular points in the applied boundary

conditions, including drawndown ratio DR and transverse stretching ratio B. Other types of solutions for α include the response of a forced oscillation.

D-3. Stability of System: General Case

We now increase the complexity of the disturbances to include those which vary in both the machine direction and the transverse direction. Still no fluctuation of the width of film is assumed. The imposed disturbances are

$$h(z,x_2,t) = \bar{h}(z)[1 + \alpha(z,x_2,t)] , \tag{10.61a}$$

$$v_z(z,x_2,t) = \bar{v}_z(z)[1 + \beta(z,x_2,t)] , \tag{10.61b}$$

$$v_2(z,x_2,t) = \bar{v}_2(z,x_2)[1 + \gamma(z,x_2,t)] , \tag{10.61c}$$

$$\sigma_{zz}(z,t) = \bar{\sigma}_{zz}(z) + \sigma'_{zz}(z,t) , \tag{10.61d}$$

$$F_z(t) = \bar{F}_z + F'_z(t) . \tag{10.61e}$$

The velocity along the transverse direction of this system is given in Eqn. (10.47). The perturbed velocity of v_2 is

$$v'_2 = \bar{v}_2\gamma = \frac{2 \tan \theta \, v'_z}{W} x_2 = \frac{2 \tan \theta \, \bar{v}_z \, \beta}{W} x_2 . \tag{10.62}$$

This leads to a simple relationship between β and γ, namely

$$\beta = \gamma . \tag{10.63}$$

The perturbed conservation equations are (see Section B):

$$\frac{D(\alpha+\beta)}{Dt} - \frac{\partial \beta}{\partial t} = 0 \ . \tag{10.64a}$$

or

$$\frac{\partial \alpha}{\partial t} + \bar{v}_z \frac{\partial(\alpha+\beta)}{\partial z} + \bar{v}_2 \frac{\partial(\alpha+\beta)}{\partial x_2} = 0 \ . \tag{10.64b}$$

The perturbed force balance equation is

$$\Phi_z' = \alpha + \frac{\sigma_{zz}'}{\bar{\sigma}_{zz}} = \Phi_z'(t) \ , \tag{10.65a}$$

$$\Phi_2' = \alpha + \frac{\sigma_{22}'}{\bar{\sigma}_{22}} = \Phi_2'(t) \ . \tag{10.65b}$$

The stress field of a Newtonian fluid is

$$\bar{\sigma}_{zz} = 2\eta\left(\frac{\partial \bar{v}_z}{\partial z} - \frac{\partial \bar{v}_3}{\partial x_3}\right) = 2\eta\left(2\,\frac{\partial \bar{v}_z}{\partial z} + \frac{\partial \bar{v}_2}{\partial x_2}\right) \ , \tag{10.66a}$$

$$\bar{\sigma}_{22} = 2\eta\left(\frac{\partial \bar{v}_2}{\partial x_2} - \frac{\partial \bar{v}_3}{\partial x_3}\right) = 2\eta\left(\frac{\partial \bar{v}_z}{\partial z} + 2\,\frac{\partial \bar{v}_2}{\partial x_2}\right) \ , \tag{10.66b}$$

$$\sigma_{zz}' = 2\eta\left(\frac{\partial v_z'}{\partial z} - \frac{\partial v_3'}{\partial x_3}\right) = 2\eta\left(2\,\frac{\partial \bar{v}_z\beta}{\partial z} + \frac{\partial \bar{v}_2\gamma}{\partial x_2}\right) \ , \tag{10.66c}$$

$$\sigma_{22}' = 2\eta\left(\frac{\partial v_2'}{\partial x_2} - \frac{\partial v_3'}{\partial x_3}\right) = 2\eta\left(\frac{\partial \bar{v}_z\beta}{\partial z} + 2\,\frac{\partial \bar{v}_2\gamma}{\partial x_2}\right) \ . \tag{10.66d}$$

Eqns. (10.66c) and (10.66d) can be simplified with the aid of Eqn. (10.63) to:

$$\sigma'_{zz} = 2\eta\left(2\frac{\partial\bar{v}_z\beta}{\partial z} + \frac{\partial\bar{v}_2\beta}{\partial x_2}\right) . \tag{10.66e}$$

$$\sigma'_{22} = 2\eta\left(\frac{\partial\bar{v}_z\beta}{\partial z} + 2\frac{\partial\bar{v}_2\beta}{\partial x_2}\right) . \tag{10.66f}$$

Substituting Eqn. (10.66) into Eqn. (10.65) leads to

$$\Phi'_z = (\alpha+\beta) - \frac{2}{(2\frac{\partial\bar{v}_z}{\partial z} + \frac{\partial\bar{v}_2}{\partial x_2})}\left(\frac{D\alpha}{Dt} + \frac{\bar{v}_2}{2}\frac{\partial\beta}{\partial x_2}\right) , \tag{10.67a}$$

$$\Phi'_2 = (\alpha+\beta) - \frac{2}{(\frac{\partial\bar{v}_z}{\partial z} + 2\frac{\partial\bar{v}_2}{\partial x_2})}\left(\frac{D\alpha}{Dt} + \frac{\bar{v}_1}{2}\frac{\partial\beta}{\partial x_1}\right) . \tag{10.67b}$$

Differentiating Eqn. (10.67a) with respect to "z" and Eqn. (10.67b) with "x_2", eliminating $\partial^2\beta/\partial z\,\partial x_2$ from the resulting equation, and assuming zero shear components leads us to

$$2\frac{D}{Dt}\left(\frac{\partial\alpha}{\partial z} - \frac{\partial\alpha}{\partial x_2}\right) - \left(2\frac{\partial\bar{v}_z}{\partial z} + \frac{\partial\bar{v}_2}{\partial x_2}\right)\frac{\partial(\alpha+\beta)}{\partial z}$$
$$+ \left(\frac{\partial\bar{v}_z}{\partial z} + 2\frac{\partial\bar{v}_2}{\partial x_2} - \frac{\bar{v}_2}{\bar{v}_z}\frac{\partial\bar{v}_z}{\partial z}\right)\frac{\partial(\alpha+\beta)}{\partial x_2}$$
$$- \frac{\bar{v}_2}{\bar{v}_z}\frac{\partial\bar{v}_z}{\partial z}\frac{\partial\alpha}{\partial x_2} - \frac{2}{\bar{v}_z}\frac{\partial\bar{v}_z}{\partial z}\frac{\partial\alpha}{\partial t} = 0 . \tag{10.68}$$

The solution α in Eqn. (10.68) may possibly be available by solving simultaneously Eqns. (10.68) and (10.64) with the aid of the steady state solution for the velocity profile.

E. ANNULAR FILM EXTRUSION OVER A LUBRICATED CONICAL MANDREL

In this section, we consider annular film extrusion over a lubricated conical mandrel with half cone angle θ (see Figure 10.3). This process has been analyzed by Gutteridge [G-14]; she considered a post inflation, biaxially stretched process, in which tubular blown films are again subjected to deformation just below their melting points. An elastic solid model and a Kelvin-Voigt type viscoelastic model were used. A slightly different process, where conical mandrel was used without a lubrication layer, has also been analyzed for a Newtonian fluid including a friction effect between the mandrel and the deforming film layer [W-10]. This process has actually been used by Flood et al. [F-7] to produce biaxially oriented Kevlar® film.

One of the interesting features is that this process is the asymptote of tubular blown film extrusion processes, including annular film extrusion over a lubricated straight cylindrical mandrel. Both steady state and unsteady state solutions for a Newtonian fluid will be examined.

E-1. Steady State Solution

The most natural choice of a coordinate system for this process is spherical coordinates. However, the choice of spherical coordinates is not the most suitable one from the practical points of view. The next best choice of coordinate systems is the "z,ϕ,r" cylindrical coordinate system.

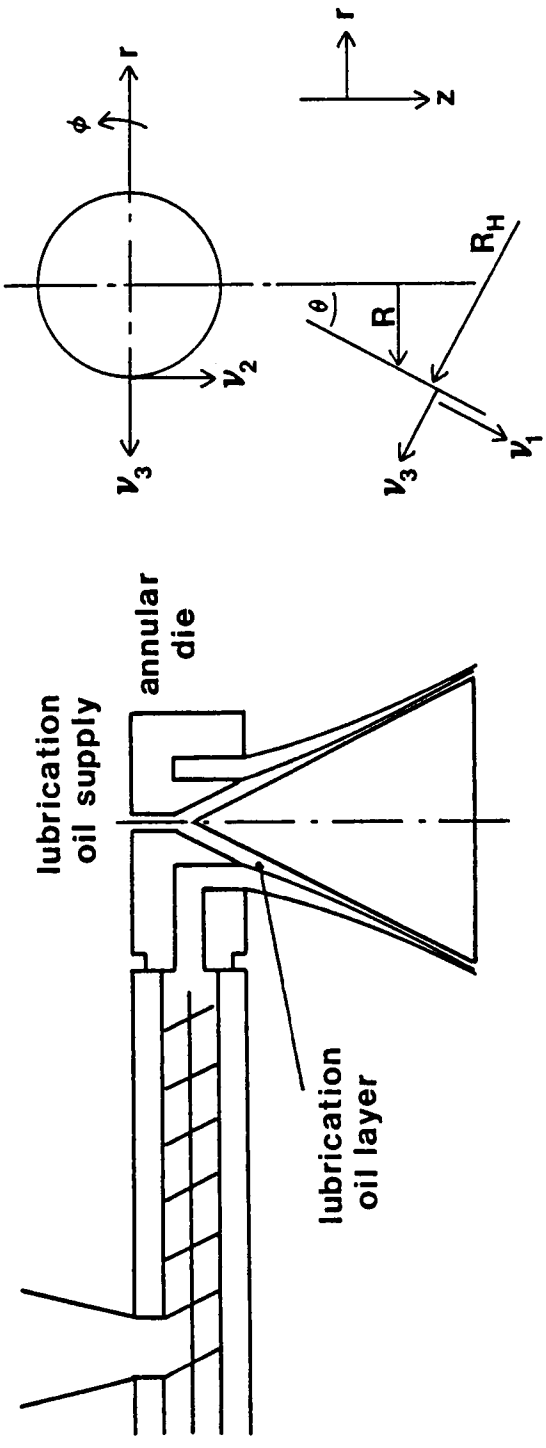

Figure 10.3. Annular film extrusion over a lubricated conical mandrel and employed coordinate system.

The diameter of an annular film R (distance between the inner surface of film and the center line of the conical mandrel) varies according to

$$R(z) = R(0) + z \tan \theta \ , \tag{10.69}$$

where R_0 is the diameter at the die exit.

The assumption which we made here is that the film thickness h is small compared to the other dimensions of an annular film. This permits us to approximate the curved film by a plane film, and the velocity gradients are approximated locally by those of a plane film.

The cylindrical coordinates (z,ϕ,r) are related to the local Cartesian coordinates (ν_1,ν_2,ν_3) at point p in the film where ν_1 is in the "z" direction; however, parallel to the film, ν_2 is in the hoop direction, and ν_3 is normal to the film. The origin p is taken on the inner surface, and the ν_3-axis meets the outer surface at ν_3 of h.

Let (v_1,v_2,v_3) be the velocity components in the coordinate system (ν_1,ν_2,ν_3). The deformation rate is

$$d_{ij}(\nu_1,\nu_2,\nu_3) = \frac{1}{2}\left[\frac{\partial v_i}{\partial \nu_j} + \frac{\partial v_j}{\partial \nu_i}\right] \ , \tag{10.70}$$

where "i" or "j" is "1", "2", or "3". The subscript "M" will be used where "i" or "j" is "1", "2", or "3". The subscript "M" will be used instead of the subscripts "1" or "11" to eliminate confusion and to indicate the machine direction (i.e., the ν_1 direction). The "H" will be used for the subscripts "2" or "22".

The physical components of deformation rate tensor are

$$d_M = d_{11} = \frac{\partial v_M}{\partial \nu_1} = \cos\theta \ \frac{\partial v_M}{\partial z} , \tag{10.71a}$$

and using the axisymmetry condition assumption

$$d_H = d_{22} = \frac{1}{R}\frac{DR}{Dt} = \frac{v_M}{R}\frac{dR}{d\nu_1} = \sin\theta \frac{v_M}{R} \tag{10.71b}$$

Also, by neglecting the variation of $\partial v_3/\partial \nu_3$ with ν_3

$$d_{33} = \frac{1}{h}\frac{Dh}{Dt} = \frac{v_M}{h}\frac{dh}{d\nu_1} = \cos\theta \frac{v_M}{h}\frac{dh}{dz} . \tag{10.71c}$$

Eqn. (10.71) must satisfy the continuity equation. For incompressible fluids

$$d_M + d_H + d_{33} = 0 . \tag{10.72}$$

Eqn. (10.72) leads to the following differential equation between the velocity v_M and the film thickness h:

$$\frac{\partial v_M}{\partial z} + v_M \left(\frac{\tan\theta}{R} + \frac{1}{h}\frac{\partial h}{\partial z}\right) = 0 . \tag{10.73}$$

Eqn. (10.73) has a solution with the aid of Eqn. (10.69) and the definition of the volumetric flow rate $Q = 2\pi r h v_M$:

$$h(z) = \frac{v_M(0)h(0)R(0)}{v_M(z)[R(0) + z\tan\theta]} . \tag{10.74}$$

For the special case where inertia, gravity and friction effects are negligible, the thin shell theory [F-8,L-10] involves the following two force balance equations, one a differential type and the other one integral type:

$$\frac{\partial \sigma_M hR}{\partial z} - \sigma_H \, h \tan\theta = 0 \tag{10.75a}$$

where

$$\sigma_M hR = \frac{F_M}{2\pi} \tag{10.75b}$$

and

$$(\sigma_M hR)\Big|_{\overline{z}} = \frac{F_{M,L}}{2\pi} - \int_z^L \sigma_H \, hR \tan\theta \, dz \ , \tag{10.76}$$

where F_M is the take-up force along the v_1 direction and $F_{M,L}$ is F_M at the take-up position L.

For a Newtonian fluid, the stress field, with σ_{33} being zero, is given by

$$\sigma_M = 2\eta\left(2\cos\theta \frac{\partial v_M}{\partial z} + \sin\theta \frac{v_M}{R}\right) , \tag{10.77a}$$

$$\sigma_H = 2\eta\left(\cos\theta \frac{\partial v_M}{\partial z} + 2\sin\theta \frac{v_M}{R}\right) . \tag{10.77b}$$

Substituting Eqn. (10.77) into the differential type force balance equation leads to

$$\frac{\partial^2 \ell n \ v_M}{\partial z^2} - \frac{\tan\theta}{2R} \frac{\partial \ell n \ v_M}{\partial z} - \frac{3}{2} \frac{\tan^2\theta}{R^2} = 0 \ . \tag{10.78}$$

Eqn. (10.78) has the solution

$$\ell n\ v_M = -\ \ell n\ R + \frac{2}{3}\frac{R^{3/2}}{\tan\theta} C_1 + C_2 \tag{10.79}$$

where C_1 and C_2 are the integral constants. These integral constants may be determined with the boundary conditions of v_M at the die exit, z of zero, and the take-up position, z of L. However, our interest is also in the relationship between the velocity "v_M" and the take-up force "F_M".

Substituting Eqn. (10.77) into the integral type force balance equation, with the aid of the volumetric flow rate, and integrating from the position "z" to the take-up position "L" leads to

$$\frac{\partial\ \ell n(v_M^2 R)}{\partial z} = \left(\frac{F_{M,L}}{2\eta Q\cos\theta}\right) - \tan^2\theta \int_z^L \frac{1}{R^2}\, dz - \tan\theta \int_z^L \frac{1}{R}\frac{\partial\ \ell n(v_M R)}{\partial z}\, dz\ . \tag{10.80}$$

Integration of the right-hand side of Eqn. (10.80) is carried out by substituting Eqn. (10.79); then we have

$$C_1 = \left(\frac{F_{M,L}}{4\eta Q\cos\theta}\right) R(L)^{-1/2} + \frac{\tan\theta}{2} R(L)^{3/2}\ . \tag{10.81}$$

Combining Eqn. (10.79) and Eqn. (10.81) with the boundary condition $v_M(z = 0) = v_M(0)$ leads to

$$C_2 = \ell n[v_M(0)R(0)] - \frac{1}{3 \sin \theta}\left(\frac{F_{M,L}}{2\eta Q}\right) R(0)^{3/2}\, R(L)^{-1/2}$$

$$- \frac{1}{3}\left[\frac{R(0)}{R(L)}\right]^{3/2} . \qquad (10.82)$$

Therefore, the velocity profile of this process is

$$v_M = v_M(0)\left[1 + \frac{\tan \theta}{R(0)} z\right]^{-1} \exp\left\{\frac{B^{-3/2}}{3}\left(\frac{R(0)B}{\sin \theta}\,\frac{F_{M,L}}{2\eta Q} + 1\right)\left[\left(1 + \frac{\tan \theta}{R(0)} z\right)^{3/2} - 1\right]\right\}, \qquad (10.83a)$$

where

$$B = \frac{R(L)}{R(0)} . \qquad (10.83b)$$

The solution can be non-dimensionalized by using the following dimensionless groups:

$$Z^* = \frac{z}{L} , \qquad V^* = \frac{v_M}{v_M(0)} , \qquad R^* = \frac{R}{L} , \qquad (10.84a,b,c)$$

$$DR = V^*(1.0) = \frac{v_M(L)}{v_M(0)} , \qquad R_0^* = \frac{R(0)}{L} \qquad (10.84d,e)$$

$$F^* = \frac{L\, F_{M,L}}{2\eta Q} . \qquad (10.84f)$$

The dimensionless velocity profile is

$$V^* = \left[1 + \frac{\tan \theta}{R_0^*} Z^*\right]^{-1} \exp\left\{\frac{B^{-3/2}}{3}\left(\frac{R_0^* B}{\sin \theta} F^* + 1\right)\left[\left(1 + \frac{\tan \theta}{R_0^*} Z^*\right)^{3/2} - 1\right]\right\}. \qquad (10.85)$$

Or, noting the relationship between the drawdown ratio DR and the take-up force F*:

$$\left(\frac{F^*}{\sin\theta}\,(R_0^* + \tan\theta) + 1\right) B^{-3/2} = 3(B^{3/2} - 1)^{-1}\,\ell n(DR \cdot B)\ . \qquad (10.86)$$

Eqn. (10.85) can be rewritten in terms of the drawdown ratio DR and the transverse stretching ratio B as

$$V^* = (1 + \frac{\tan\theta}{R_0^*} Z^*)^{-1}\ \exp\left[(B^{3/2} - 1)^{-1}\ \ell n(DR \cdot B) \cdot \left[(1 + \frac{\tan\theta}{R_0^*} Z^*)^{3/2} - 1\right]\right]. \qquad (10.87)$$

E-2. Stability of System

We now consider the perturbed state with disturbances also satisfying the axisymmetry condition.

The imposed disturbances are:

$$h(z,t) = \bar{h}(z)[1 + \alpha(z,t)]\ , \qquad (10.88a)$$

$$v_M(z,t) = \bar{v}_M(z)[1 + \beta(z,t)]\ , \qquad (10.88b)$$

$$\sigma_M(z,t) = \bar{\sigma}_M(z) + \sigma_M'(z,t)\ , \qquad (10.88c)$$

$$\sigma_H(z,t) = \bar{\sigma}_H(z) + \sigma_H'(z,t)\ , \qquad (10.88d)$$

$$F_M(z,t) = \bar{F}_M(z) + F_M'(z,t)\ , \qquad (10.88e)$$

where the bar denotes the steady state. The form of Eqn. (10.88e) is based upon the force balance equation of Eqn. (10.75).

If we introduce disturbances given by Eqn. (10.88) into the strain rate tensor of Eqn. (10.71), and subtract out the steady state form, we obtain

$$d'_M = \cos\theta \frac{\partial \bar{v}_{M\beta}}{\partial z} , \tag{10.89a}$$

$$d'_H = \sin\theta \frac{\bar{v}_{M\beta}}{R} , \tag{10.89b}$$

$$d'_{33} = \frac{D\alpha}{Dt} + \beta \frac{\bar{v}_M}{\bar{h}} \frac{\partial \bar{h}}{\partial z} , \tag{10.89c}$$

where

$$\frac{D}{Dt} = \frac{\partial}{\partial t} + \cos\theta \, v_M \frac{\partial}{\partial z} . \tag{10.89d}$$

Substituting Eqns. (10.89) and (10.71) into the continuity equation Eqn. (10.72), we obtain the perturbed continuity equation given by

$$\frac{D\alpha}{Dt} + \frac{\cos\theta}{\bar{h}} \frac{\partial \bar{h}\, \bar{v}_{M\beta}}{\partial z} + \frac{\sin\theta}{R} \bar{v}_{M\beta} = 0 . \tag{10.90}$$

Similarly, after introducing disturbances into the force balance equation Eqn. (10.75), the perturbed force balance equation of the differential type becomes

$$\frac{\partial \sigma'_M \bar{h} R}{\partial z} + \bar{\sigma}_M \bar{h} R \frac{\partial \alpha}{\partial z} - \sigma'_H \bar{h} \tan\theta = 0 . \tag{10.91}$$

The stress field of a Newtonian field is

The stress field of a Newtonian field is

$$\bar{\sigma}_M = 2\eta\left(2\cos\theta\,\frac{\partial \bar{v}_M}{\partial z} + \frac{\sin\theta}{R}\,\bar{v}_M\right), \tag{10.92a}$$

$$\sigma'_M = 2\eta\left(2\cos\theta\,\frac{\partial \bar{v}_{M\beta}}{\partial z} + \frac{\sin\theta}{R}\,\bar{v}_{M\beta}\right), \tag{10.92b}$$

$$\sigma'_H = 2\eta\left(\cos\theta\,\frac{\partial \bar{v}_{M\beta}}{\partial z} + 2\,\frac{\sin\theta}{R}\,\bar{v}_{M\beta}\right). \tag{10.92c}$$

Substituting Eqn. (10.92) into Eqn. (10.91) with the aid of Eqn. (10.90) yields

$$2\,\frac{\partial}{\partial z}\left(\frac{D\alpha}{Dt}\right) - 3A\,\frac{D\alpha}{Dt} + \cos\theta\,\bar{v}_{M\beta}\,\frac{\partial A}{\partial z} - \frac{\sin\theta}{R}\,\bar{v}_{M\beta}\,B = 0, \tag{10.93a}$$

where

$$A = \frac{2}{\bar{v}_M}\,\frac{\partial \bar{v}_M}{\partial z} + \frac{\tan\theta}{R}, \tag{10.93b}$$

$$B = \frac{1}{\bar{v}_M}\,\frac{\partial \bar{v}_M}{z} + 2\,\frac{\tan\theta}{R}. \tag{10.93c}$$

Eqn. (10.93a) leads to

$$\cos\theta\cdot\bar{v}_{M\beta} = \frac{1}{\left(\frac{\partial A}{\partial z} - \frac{\tan\theta}{R}\,B\right)}\left(3A\,\frac{D\alpha}{Dt} - 2\,\frac{\partial}{\partial z}\left(\frac{D\alpha}{Dt}\right)\right). \tag{10.94}$$

Differentiating Eqn. (10.93a) with respect to "z", $\partial\beta/\partial z$ term in the resulting equation is subtracted out, with the aid of Eqn. (10.94). After considerable tedious manipulation and non-dimensionalizing the

resulting equation, with the dimensionless groups of Eqns. (10.84) and (10.83b), gives us

$$2\left(2\frac{\partial^2 \ell nV^*}{\partial Z^{*2}} - f\frac{\partial \ell nV^*}{\partial Z^*} - 3f^2\right)\frac{\partial^3 \alpha}{\partial Z^{*3}}$$

$$-\left(4\frac{\partial^3 \ell nV^*}{\partial Z^{*3}} + 4\left(2\frac{\partial \ell nV^*}{\partial Z^*} + f\right)\frac{\partial^2 \ell nV^*}{\partial Z^{*2}} - \left(4f\frac{\partial \ell nV^*}{\partial Z^*} + 13f^2\right)\frac{\partial \ell nV^*}{\partial Z^*} - 5f^3\right)\frac{\partial^2 \alpha}{\partial Z^{*2}}$$

$$+\left(2\left(4\frac{\partial \ell nV^*}{\partial Z^*} + 3f\right)\frac{\partial^3 \ell nV^*}{\partial Z^{*3}} + \left(4f\frac{\partial \ell nV^*}{\partial Z^*} + 19f^2\right)\frac{\partial^2 \ell nV^*}{\partial Z^{*2}} + \left(3f^2\frac{\partial \ell nV^*}{\partial Z^*} + 2f^2\right)\frac{\partial \ell nV^*}{\partial Z^*} - 12f^4\right)\frac{\partial \alpha}{\partial Z^*}$$

$$+ 2\sec\theta\left(2\frac{\partial^2 \ell nV^*}{\partial Z^{*2}} - f\frac{\partial \ell nV^*}{\partial Z^*} - 3f^2\right)\frac{\partial^3 \alpha}{V^*\,\partial Z^{*2}\,\partial t^*}$$

$$-\sec\theta\left(4\frac{\partial^3 \ell nV^*}{\partial Z^{*3}} + 4\left(4\frac{\partial \ell nV^*}{\partial Z^*} + f\right)\frac{\partial^2 \ell nV^*}{\partial Z^{*2}} - \left(8f\frac{\partial \ell nV^*}{\partial Z^*} + 25f^2\right)\frac{\partial \ell nV^*}{\partial Z^*} - 5f^3\right)\frac{\partial^2 \alpha}{V^*\,\partial Z^*\,\partial t^*}$$

$$+\sec\theta\left(6\left(2\frac{\partial \ell nV^*}{\partial Z^*} + f\right)\frac{\partial^3 \ell nV^*}{\partial Z^{*2}} - \left(4\frac{\partial^3 \ell nV^*}{\partial Z^{*2}} - 2\left(6\frac{\partial \ell nV^*}{\partial Z^*} + 5f\right)\frac{\partial \ell nV^*}{\partial Z^*} - 25f^2\right)\frac{\partial^2 \ell nV^*}{\partial Z^{*2}}\right)$$

$$-\left(2\left(3f\frac{\partial \ell nV^*}{\partial Z^*} + 8f^2\right)\frac{\partial \ell nV^*}{\partial Z^*} + 3f^2\right)\frac{\partial \ell nV^*}{\partial Z^*} - 12f^4\Bigg)\frac{\partial \alpha}{V^*\,t^*} = 0, \quad (10.95a)$$

where

$$f = \frac{\tan \theta}{R^*} = \frac{(B - 1)}{1 + Z^*(B-1)} , \tag{10.95b}$$

$$t^* = t \frac{v_M(0)}{L} . \tag{10.95c}$$

The differential equation describing the responses of the system on the imposed disturbances α is a third-order, instead of a second-order, differential equation. A second-order equation was previously derived for the flat film extrusion processes (see Sections B, C, and D). The difference comes from the force balance equations. For flat film extrusion processes

$$\frac{\partial \bar{F}}{\partial z} = 0 . \tag{10.96a}$$

However, this process has

$$\frac{\partial \bar{F}_M(z)}{\partial z} \neq 0 . \tag{10.96b}$$

The steady state take-up force $\bar{F}_M(z)$ $(=2\pi \bar{R}\ \bar{h}\ \bar{\sigma}_M)$ of this process changes with position "z" according to Eqn. (10.75). This feature increases the order of the differential equation.

F. TUBULAR UNBLOWN FILM EXTRUSION

We now turn to the unblown tubular film extrusion process (see Figure 10.4). This process is a special case of the tubular blown

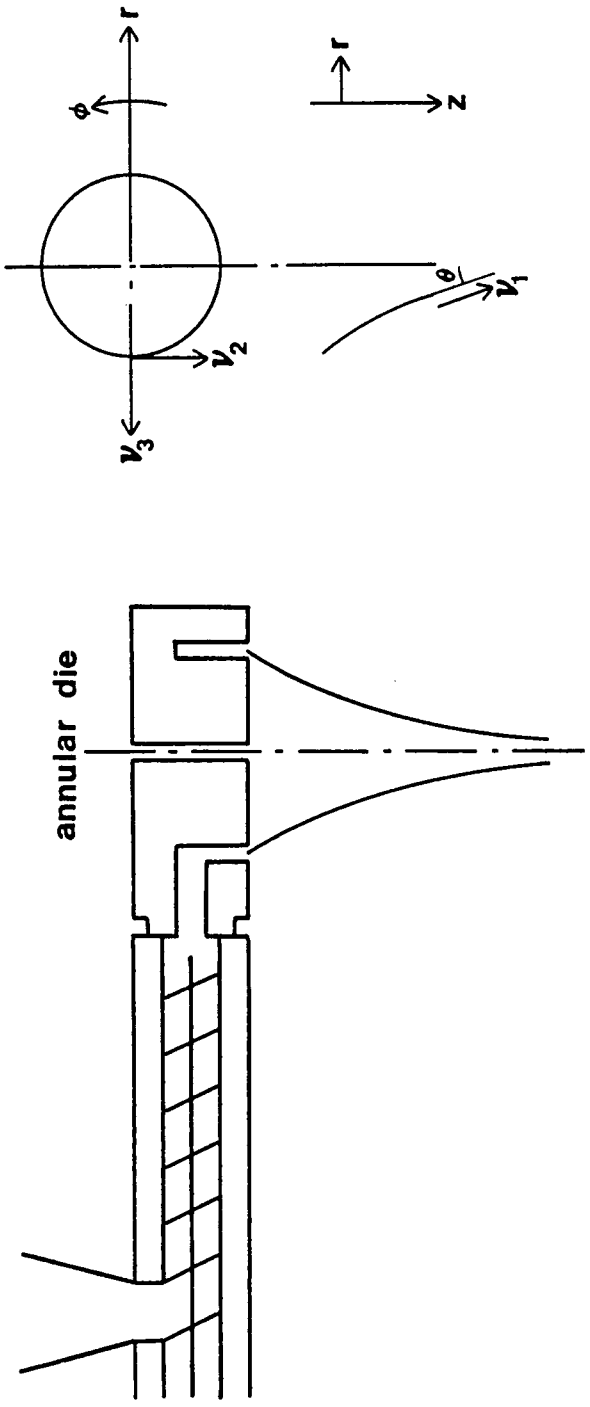

Figure 10.4. Tubular unblown film extrusion and employed coordinate system.

film extrusion process, where there is not any pressure difference between the inside of the bubble or tube and the outside.

F-1. Steady State Solution

The assumption which is made here is that the film thickness h is small compared with the other dimensions of the annulus film. This permits us to approximate the curved film by a plane film, and the velocity gradients are approximated locally by those of a plane film.

The cylindrical coordinates (z,ϕ,r) are related to the local Cartesian coordinates (ν_1,ν_2,ν_3) at a point p in the film, where ν_1 is in the "z" direction; however, parallel to the film, ν_2 is in the hoop direction, and ν_3 is normal to the film. The origin p is taken on the inner surface, the ν_3-axis meets the outer surface at ν_3 of h.

Let (v_1,v_2,v_3) be the velocity components in the coordinates (ν_1,ν_2,ν_3). The subscript "M" will be used instead of the subscripts "1" or "11" to eliminate confusion, and the subscript "H" will be used for the subscripts "2" or "22".

The physical components of the deformation rate tensor are

$$d_M = d_{11} = \frac{\partial v_M}{\partial \nu_1} = \cos\theta \frac{\partial v_M}{\partial z} , \tag{10.97a}$$

and using the axisymmetry condition assumption

$$d_H = d_{22} = \frac{1}{R}\frac{DR}{Dt} = \frac{v_M}{R}\frac{dR}{d\nu_1} = \sin\theta \frac{v_M}{R} . \tag{10.97b}$$

Also, by neglecting the variation of $\partial v_3/\partial \nu_3$ with ν_3

$$d_{33} = \frac{1}{h}\frac{Dh}{Dt} = \frac{v_M}{h}\frac{dh}{d\nu_1} = \cos\theta\ \frac{v_M}{h}\frac{dh}{dz} . \qquad (10.97c)$$

Eqn. (10.97) must satisfy the continuity equation. For incompressible fluid:

$$d_M + d_H + d_{33} = 0 , \qquad (10.98a)$$

or

$$\frac{\partial v_M}{\partial z} + v_M\left(\frac{\tan\theta}{R} + \frac{1}{h}\frac{\partial h}{\partial z}\right) = 0 . \qquad (10.98b)$$

For the special case where inertia, gravity and drag effects are negligible, the thin shell theory [F-8,L-10] gives the force balance equation:

$$\frac{\partial 2\pi R\ h\ \sigma_M \cos\theta}{\partial z} = \frac{\partial \cos\theta\ F_M}{\partial z} = \frac{\partial F_z}{\partial z} = 0 , \qquad (10.99a)$$

or

$$2\pi R\ h\ \sigma_M = F_M = \sec\theta\ F_z , \qquad (10.99b)$$

where F_M is the take-up force along the ν_1 direction and F_z along the "z" axis.

To proceed further with the analysis of the velocity profile, we will make an additional assumption about the kinematics; that is, we will assume that the unblown tubular film extrusion process is approximately in uniaxial extension:

$$d_M = -\frac{1}{2} d_H = -\frac{1}{2} d_{33} \ . \qquad (10.100)$$

Combining Eqns. (10.98), (10.100), and the volumetric flow rate Q ($=2\pi R\ h\ v_M$) yields

$$\frac{\partial h}{\partial z} - \frac{2\pi}{Q} \tan\theta\ h^2\ v_M = 0 \ . \qquad (10.101)$$

Substituting Eqn. (10.100) into Eqn. (10.101) gives

$$\frac{1}{v_M} \frac{\partial v_M}{\partial z} + \frac{2}{h} \frac{\partial h}{\partial z} = 0 \ . \qquad (10.102)$$

Eqn. (10.102) has a solution, with the aid of volumetric flow rate Q, as follows:

$$h(z) = \frac{2\pi}{Q} h^2(0) v_M(0) R(z) \ , \qquad (10.103a)$$

or

$$h^2(z) = \frac{h^2(0)\ v_M(0)}{v_M(z)} \ . \qquad (10.103b)$$

The angle θ is given with the aid of Eqn. (10.103) as

$$\tan\theta = \frac{\partial R}{\partial z} = -\frac{Q}{4\pi h(0)\sqrt{v_M(0) v_M}} \frac{\partial \ell n v_M}{\partial z} \ . \qquad (10.104)$$

For a Newtonian fluid, the stress field of this process is

$$\sigma_M = 3\eta \cos\theta \frac{\partial v_M}{\partial z} \ . \qquad (10.105)$$

Substituting Eqn. (10.105) into Eqn. (10.99) yields

$$F_z = 3\eta\, Q \cos^2\theta \frac{\partial \ell n v_M}{\partial z} . \qquad (10.106)$$

The differential equation for the velocity profile is obtained by combining Eqns. (10.104) and (10.106):

$$\left(\frac{\partial v_M}{\partial z}\right)^2 - \frac{24\eta\pi}{F_z} \frac{h(0)}{R(0)} v_M^2 \frac{\partial v_M}{\partial z} - \frac{8\pi}{Q} \frac{h(0)}{R(0)} v_M^3 = 0 . \qquad (10.107)$$

The non-dimensionalized form of Eqn. (10.107) is also available:

$$\left(\frac{\partial V^*}{\partial Z^*}\right)^2 - \frac{V^{*2}}{kQ^* F_z^*} \left(\frac{\partial V^*}{\partial Z^*}\right) + \frac{1}{kQ^*} V^{*3} = 0 , \qquad (10.108)$$

where

$$V^* = \frac{v_M}{v_M(0)} , \qquad Z^* = \frac{z}{L} , \qquad (10.109a,b)$$

$$Q^* = \frac{Q}{8\pi\, v_M(0) L^2} , \qquad F_z^* = \frac{LF_z}{3\eta Q} \qquad (10.109c,d)$$

$$k = \frac{R(0)}{h(0)} \qquad (10.109e)$$

and L is the distance between the die exit and the take-up position. The solution of Eqn. (10.108) can be obtained only by numerical methods, such as the Runge-Kutta method.

F-2. Stability of System

We now introduce disturbances into the system, while continuing to assume the axisymmetric condition:

$$h(z,t) = \bar{h}(z)[1 + \alpha(z,t)] \ , \tag{10.110a}$$

$$v_M(z,t) = \bar{v}_M(z)[1 + \beta(z,t)] \ , \tag{10.110b}$$

$$R(z,t) = \bar{R}(z)[1 + \gamma(z,t)] \ , \tag{10.110c}$$

$$\theta(z,t) = \bar{\theta}(z)[1 + \delta(z,t)] \ , \tag{10.110d}$$

$$\sigma_M(z,t) = \bar{\sigma}_M(z) + \sigma'_M(z,t) \ , \tag{10.110e}$$

$$F_z(t) = \bar{F}_z + F'_z(t) \ , \tag{10.110f}$$

$$F_M(z,t) = \bar{F}_M(z) + F'_M(z,t) \ . \tag{10.110g}$$

The form of Eqns. (10.110f) and (10.110g) is suggested from the force balance equation of Eqn. (10.99). Eqns. (10.110c) and (10.110d) can be rewritten as

$$R(z,t) = k\ \bar{h}(z)[1 + \gamma(z,t)] \ , \tag{10.110h}$$

$$\theta(z,t) = \bar{\theta}(z)\left[1 + \frac{\dfrac{\partial \bar{R}\gamma(z,t)}{\partial z}}{1 + (\partial \bar{R}/\partial z)^2}\right] \ . \tag{10.110i}$$

If we introduce the disturbances of Eqn. (10.110) into the continuity equation Eqn. (10.98) and subtract out the steady state equations, we obtain the following, after neglecting diameter and angle fluctuations (i.e., γ is zero):

$$\frac{D(\alpha+\beta)}{Dt} - \frac{\partial \beta}{\partial t} = 0 \ , \tag{10.111a}$$

or

$$\frac{D\alpha}{Dt} + \cos\ \theta\ \bar{v}_M \frac{\partial \beta}{\partial z} = 0 \ , \tag{10.111b}$$

where

$$\frac{D}{Dt} = \frac{\partial}{\partial t} + \cos\ \theta\ \bar{v}_M \frac{\partial}{\partial z} \ . \tag{10.111c}$$

Similarly, after introducing disturbances into the force balance equation Eqn. (10.99), then subtracting out the steady state, we have a perturbed force balance of

$$\Phi'_z = (\alpha + \frac{\sigma'_M}{\bar{\sigma}_M}) \cos\ \theta = \frac{F'_z}{\bar{F}_z} = \Phi'_z(t) \ . \tag{10.112}$$

In the case of a Newtonian fluid, the stress field is

$$\bar{\sigma}_M = 3\eta \cos\ \theta \frac{\partial \bar{v}_M}{\partial z} \ , \tag{10.113a}$$

$$\sigma'_M = 2\eta(d'_M - d'_{33}) \ , \tag{10.113b}$$

where

$$d'_M = \cos\ \theta \frac{\partial \bar{v}_M \beta}{\partial z} \ , \tag{10.114a}$$

$$d'_{33} = \frac{1}{h}\frac{Dh}{Dt} - \frac{1}{\bar{h}}\frac{D\bar{h}}{Dt} \ . \tag{10.114b}$$

Eqn. (10.114b) is simplified with the help of Eqn. (10.100):

$$d'_{33} = \frac{D\alpha}{Dt} - (\alpha + \frac{\beta}{2}) \cos\theta \frac{\partial \bar{v}_M}{\partial z} . \qquad (10.114c)$$

Therefore, Eqn. (10.113b) becomes

$$\sigma'_M = 2\eta \left[\cos\theta \, \bar{v}_M \frac{\partial \beta}{\partial z} - \frac{D\alpha}{Dt} + (\alpha + \frac{\beta}{2}) \cos\theta \frac{\partial \bar{v}_M}{\partial z} \right] . \qquad (10.115)$$

Substituting Eqns. (10.113a) and (10.115) into the perturbed force balance equation Eqn. (10.112), with the aid of Eqn. (10.111), yields

$$6\Phi'_z = \Phi''_z = (5\alpha + 3\beta) \cos\theta - \frac{4}{(\partial \bar{v}_M / \partial z)} \frac{D\alpha}{Dt} = \Phi''_z(t) . \qquad (10.116)$$

Eqn. (10.116) is differentiated with respect to "z", then the $\partial\beta/\partial z$ term is eliminated with the aid of Eqn. (10.111). The resulting equation is combined with Eqn. (10.106). After tedious manipulation and non-dimensionalizing the resulting equation, with the dimensionless groups of Eqn. (10.109), yields

$$\frac{\partial^3 \alpha}{\partial Z^{*3}} + \left[\frac{6}{g} \left(\frac{\partial g}{\partial Z^*}\right) - \frac{\partial^2 g / \partial Z^{*2}}{\partial g / \partial Z^*} - \frac{F^*_z}{2g^2} \right] \frac{\partial^2 \alpha}{\partial Z^{*2}}$$

$$+ \frac{1}{g^2} \left[6\left(\frac{\partial g}{\partial Z^*}\right)^2 + \frac{3F^*_z}{2g} \left(\frac{\partial g}{\partial Z^*}\right) + \frac{F^*_z}{2} \frac{(\partial^2 g / \partial Z^{*2})}{(\partial g / \partial Z^*)} \right] \frac{\partial \alpha}{\partial Z^*}$$

$$+ \frac{1}{gV^*} \frac{\partial^3 \alpha}{\partial Z^{*2} \partial t^*} + \frac{1}{gV^*} \left[\frac{4}{g} \left(\frac{\partial g}{\partial Z^*}\right) - \frac{\partial^2 g / \partial Z^{*2}}{\partial g / \partial Z^*} - \frac{5F^*_z}{4g^2} \right] \frac{\partial^2 \alpha}{\partial Z^* \partial t^*}$$

$$+ \frac{1}{gV^*} \left[\frac{F^{*2}_z}{4g^4} + \frac{5F^*_z}{4g^3} \left(\frac{\partial g}{\partial Z^*}\right) + \frac{1}{2g^2} \left(\frac{\partial g}{\partial Z^*}\right) + \frac{F^*_z}{4g^2} \frac{(\partial^2 g / \partial Z^{*2})}{(\partial g / \partial Z^*)} \right] \frac{\partial \alpha}{\partial t^*}$$

$$= 0 , \qquad (10.117a)$$

where

$$g = \cos\theta \quad . \tag{10.117b}$$

And the angle θ defined by Eqn. (10.104) becomes

$$\tan\theta = 2\,\frac{Q^*}{h_0^*}\,V^{*-1/2}\,\frac{\partial \ell n V^*}{\partial Z^*}\ , \tag{10.118a}$$

where

$$h_0^* = \frac{h(0)}{L}\ . \tag{10.118b}$$

We have again obtained a third-order differential equation which represents the response of the system to the imposed disturbances. The steady state force take-up force $\bar{F}_M(=2\pi\bar{R}\,\bar{h}\,\bar{\sigma}_M)$ of this process again changes with position z. This feature increases the order of the differential equation for the stability analysis.

G. ADDITIONAL COMMENTS

From the previous discussion on the stability of continuous film extrusion processes (see Sections C through F), it has been found that the stability equations for flat film extrusion processes are second-order partial differential equations (see Eqns. (10.40) and (10.59)); however, those for annular film extrusion processes are third-order partial differential equations (see Eqns. (10.95) and (10.117)).

The simplified form of these stability response equations are listed below, including melt spinning processes (see Chapter IX):

1. Flat film extrusion process, with $\partial v_2/\partial x_2 \Big/ \partial v_z/\partial z$ constant at any position:

$$\alpha = f_1\left(\frac{\partial^2\alpha}{\partial z^2}, \quad \frac{\partial\alpha}{\partial z}, \quad \frac{\partial^2\alpha}{\partial z\ \partial t}\right) . \tag{10.119}$$

2. Flat film extrusion process, with a linearly varying width change ($\partial W/\partial z$ = constant):

$$\alpha = f_2\left(\frac{\partial^2\alpha}{\partial z^2}, \quad \frac{\partial^2\alpha}{\partial z\ \partial t}, \quad \frac{\partial\alpha}{\partial t}\right) . \tag{10.120}$$

3. Annular film extrusion over a lubricated conical mandrel:

$$\alpha = f_3\left(\frac{\partial^3\alpha}{\partial z^3}, \quad \frac{\partial^2\alpha}{\partial z^2}, \quad \frac{\partial\alpha}{\partial z}, \quad \frac{\partial^2\alpha}{\partial z^2\ \partial t}, \quad \frac{\partial^2\alpha}{\partial z\ \partial t}, \quad \frac{\partial\alpha}{\partial t}\right) . \tag{10.121}$$

4. Unblown annular film extrusion:

$$\alpha = f_4\left(\frac{\partial^3\alpha}{\partial z^3}, \quad \frac{\partial^2\alpha}{\partial z^2}, \quad \frac{\partial\alpha}{\partial z}, \quad \frac{\partial^3\alpha}{\partial z^2\ \partial t}, \quad \frac{\partial^2\alpha}{\partial z\ \partial t}, \quad \frac{\partial\alpha}{\partial t}\right) . \tag{10.122}$$

5. Melt spinning and special case of processes "2" and "3", where film with or diameter is constant along the machine direction:

$$\alpha = f_5\left(\frac{\partial^2\alpha}{\partial z^2}, \quad \frac{\partial^2\alpha}{\partial z\ \partial t}\right) . \tag{10.123}$$

It is noted that the time derivative of the disturbance α is first-order in any of the processes. However, the position derivative of α varies in a second-order manner for flat film extrusion processes

(processes "1", "2", and "5") and in a third-order manner for annular film extrusion processes (processes "3" and "4").

The differences in the order of these partial differential equations is caused by the force balance equations. For flat film extrusion processes (including the melt spinning and an annular film extrusion over a lubricated straight cylindrical mandrel) the force balance equation is

$$\frac{\partial \overline{F}_M}{\partial z} = 0 \qquad \text{or} \qquad \overline{F}_M \neq \overline{F}_M(z) \ . \tag{10.124a}$$

In contrast, the force balance equation for annular film extrusion over a lubricated conical mandrel and for unblown tubular film extrusion is

$$\frac{\partial \overline{F}_M}{\partial z} + y_1(z) = 0 \qquad \text{or} \qquad \overline{F}_M = \overline{F}_M(z) \ . \tag{10.124b}$$

where F_M is the take-up force in the direction of the main (or primary) deformation (i.e., v_1-axis direction) and "y_1" is some function of "z", which is dependent upon the geometry of the system.

With the aid of Eqn. (10.8), Eqn. (10.124a) suggests that we have

$$\frac{\partial \Phi'_z}{\partial z} = \frac{\partial}{\partial z}\left(\frac{F'_M(t)}{\overline{F}_M}\right) = \frac{\partial \Phi'_M(t)}{\partial z} = 0 \ . \tag{10.125}$$

On the other hand Eqn. (10.124b) leads us to

$$\frac{\partial \Phi_z'}{\partial z} = \frac{\partial}{\partial z}\left[\frac{F_M'(z,t)}{\bar{F}_M(z)}\, y_2(z,t) + y_3(z,t)\right] , \qquad (10.126)$$

where "y_2" and "y_3" are functions of "z" and "t". Eqn. (10.126) is rewritten as

$$\frac{\partial \Phi_z'}{\partial z} = \frac{F_M'(z,t)}{\bar{F}_M(z)}\,\frac{\partial y_2(z,t)}{\partial z} + y_2(z,t)\,\frac{\partial}{\partial z}\left[\frac{F_M'(z,t)}{\bar{F}_M(z)}\right] + \frac{\partial y_3(z,t)}{\partial z} . \qquad (10.127)$$

y_2 and y_3 are functions of "α", "β" and $\bar{v}_M$ (or $\bar{v}_z$); this functionality comes about because "v_M" (or v_z) are functions of "z" and "t". The stability equation should be a function of α, not α and β, so that Eqn. (10.127) has to be differentiated again by "z"; then eliminating the y_2 term from the resulting equation, by substituting Eqn. (10.127), leads to

$$\begin{aligned}\frac{\partial^2 \Phi_z'}{\partial z^2} = \frac{1}{\partial^2 F_M'(z,t)/\partial \bar{F}_M(z)^2}\Bigg[&\frac{\partial \Phi_z'}{\partial z} - \frac{F_M'(z,t)}{\bar{F}_M(z)}\,\frac{\partial y_2(z,t)}{\partial z} \\ &- \frac{\partial y_3(z,t)}{\partial z}\Bigg]\,\frac{\partial^2}{\partial z^2}\left[\frac{F_M'(z,t)}{\bar{F}_M(z)}\right] \\ &+ \left[2\,\frac{\partial y_2(z,t)}{\partial z} + \frac{\partial^2 y_2(z,t)}{\partial z^2}\right]\frac{\partial}{\partial z}\left[\frac{F_M'(z,t)}{\bar{F}_M(z)}\right] + \frac{\partial^2 y_3(z,t)}{\partial z^2} .\end{aligned} \qquad (10.128)$$

In Eqn. (10.128), the β terms appearing in $y_2(z,t)$ and $y_3(z,t)$ are differentiated by "z" at least once or twice, so that these β terms can be eliminated by using perturbed continuity equations, such as

Eqns. (10.90) or (10.111), by themselves or combined with the perturbed force balance equations.

If we compare Eqns. (10.125) and (10.128), it is seen that the order of the differential equation of α derived from Eqn. (10.128) for a Newtonian fluid is at least one order higher than that from Eqn. (10.125). In the last case the take-up force F_M is not a function of position.

In this chapter, we have derived the differential equations which deal with the sensitivity of various continuous film extrusion systems to the imposed disturbances. As we have described earlier, those differential equations are very complicated, even though an isothermal Newtonian fluid assumption has been used. The solutions of these partial differential equations are not available in analytical form. Numerical solutions, however, might be possible. One of the objectives deriving those differential equations was to specify the conditions (i.e., in terms of drawdown ratio and transverse stretching ratio) where natural oscillation occurs. For this purpose, an eigenvalue treatment of the differential equations might be the only way to proceed.

Especially we are interested in obtaining the solution of Eqn. (10.40) for a flat film extrusion with tentering frame in order to achieve a kinematics ratio independent of position (i.e., $(\partial v_2/\partial x_2)/(\partial v_z/\partial z)$ independent of position). Once we obtain that solution, we could compare the differences of the continuity equations between continuous processing systems and batch processing systems; the

stability of the latter systems has been discussed in Chapters VI and VII for both Newtonian fluids and viscoelastic fluids.

H. SUMMARY

The stability equations of various flat film and annular film extrusion processes are analyzed and compared to each other. The processes include: (1) flat film extrusion with tentering frames to achieve a constant ratio of kinematics (i.e., the ratio of deformation rates is independent of positions); (2) flat film extrusion with tentering frames to achieve a linearly varying width along the machine direction; (3) annular film extrusion over a lubricated conical mandrel; (4) annular unblown film extrusion. A detailed discussion has been presented for Newtonian fluids.

CHAPTER XI

INFLUENCE OF MOLECULAR STRUCTURE ON ISOTHERMAL MELT SPINNING

A. INTRODUCTION

Melt spun filaments are often nonuniform, exhibiting fluctuating diameters along their lengths. These diameter fluctuations may be due to heterogeneities or forced oscillations on the system, induced by temperature, extrusion rate, or tension variations. However, "natural oscillations," in the sense of a basic hydrodynamic instability, may also occur under some circumstances and give rise to periodic diameter fluctuations of large magnitude. This kind of instability is known as draw resonance. Similar thickness fluctuations are observed in extruded ribbons, cast films, and extrusion coating processes [B-5,B-6,C-13,I-6,K-5,K-9].

Oscillations in fiber diameter due to fluctuations in system parameters (such as heat transfer, spinline tension, extrusion rate, etc.) were first clearly discussed by Kase and Matsuo [K-8]. These researchers carried out experiments in which they suddenly changed the rate of the cooling air being applied to a descending polypropylene fiber. Diameter fluctuations in the fiber resulted. The existence of small amplitude random diameter fluctuations in melt spun fibers has also been observed by various researchers. However, such results are rarely reported in the literature. Such a study is

presented by Minoshima, White and Spruiell [M-41], who noted that the amplitude of the fluctuations depend upon the rheological properties of the polymer. In the case of polypropylene larger amplitude fluctuations are observed with moderate and broad molecular weight distribution materials than with narrow molecular weight distribution materials. They noted that this amplitude correlates with the uniaxial elongational flow behavior of the polymer melt and with the spinline elongational behavior. A rapid rate of decrease in the spinline elongational viscosity function results in a larger amplitude fluctuation.

Regular fiber diameter oscillations of large amplitude have been described by various authors, beginning with the study of Freeman and Coplan's study [F-14]. In more recent years studies have appeared for polyethylene terephthalate [I-6,K-5], polypropylene [B-6,F-14, G-5,H-4,H-13,I-6,K-5,M-41,W-8,W-17,Y-1], polystyrene [H-4,M-16,W-21], high density polyethylene [H-4,H-13,W-8,W-17], and other melts. There are only two studies on the effects of molecular weight distributions with various molecular weights which are carried out for polypropylene [G-5,M-41].

In the present chapter, we will examine the effects of molecular structure, such as molecular weight, molecular weight distribution, and degree of long chain branching, on the draw resonance phenomenon for a variety of polymers (polyethylenes, polypropylenes, and polystyrenes). The steady state spinline behavior will be described.

B. EXPERIMENTAL

B-1. Materials

A series of seven high density polyethylenes (HDPE), four linear low density polyethylenes (LLDPE), four (long chain branched) low density polyethylenes (LDPE), five polypropylenes (PP) and two polystyrenes (PS) were used. These materials are listed in Tables III-1, III-2, III-3, III-4, and III-5 (pp. 49, 50, 51, 52, and 53), with molecular characterization data. Rheological properties of polyethylenes (PE) were presented in Chapter IV. We also included polypropylenes which were previously used in the melt spinning experiments and had been rheologically characterized by the author [M-41, M-42]. One of the polystyrene samples (PS-2) was used in Chapter VII. The other polystyrene sample (PS-1) had been used for the melt spinning studies and rheologically characterized by Tanaka and White [T-3, W-21].

B-2. Isothermal Melt Spinning

Isothermal melt spinning was carried out at 180°C using an Instron capillary rheometer as a delivery device (Figure 11.1). The polymer was extruded at 180°C through a die of diameter 0.029 inch, having a length/diameter ratio of 53.88. The extrudate directly passes into an isothermal heated chamber (2.5 cm inside diameter and 6.0 cm long). It emerges from this chamber into a water quench bath. Two sets of electrical heaters were used to heat the chamber. Both sets of heaters were controlled using two temperature controllers by

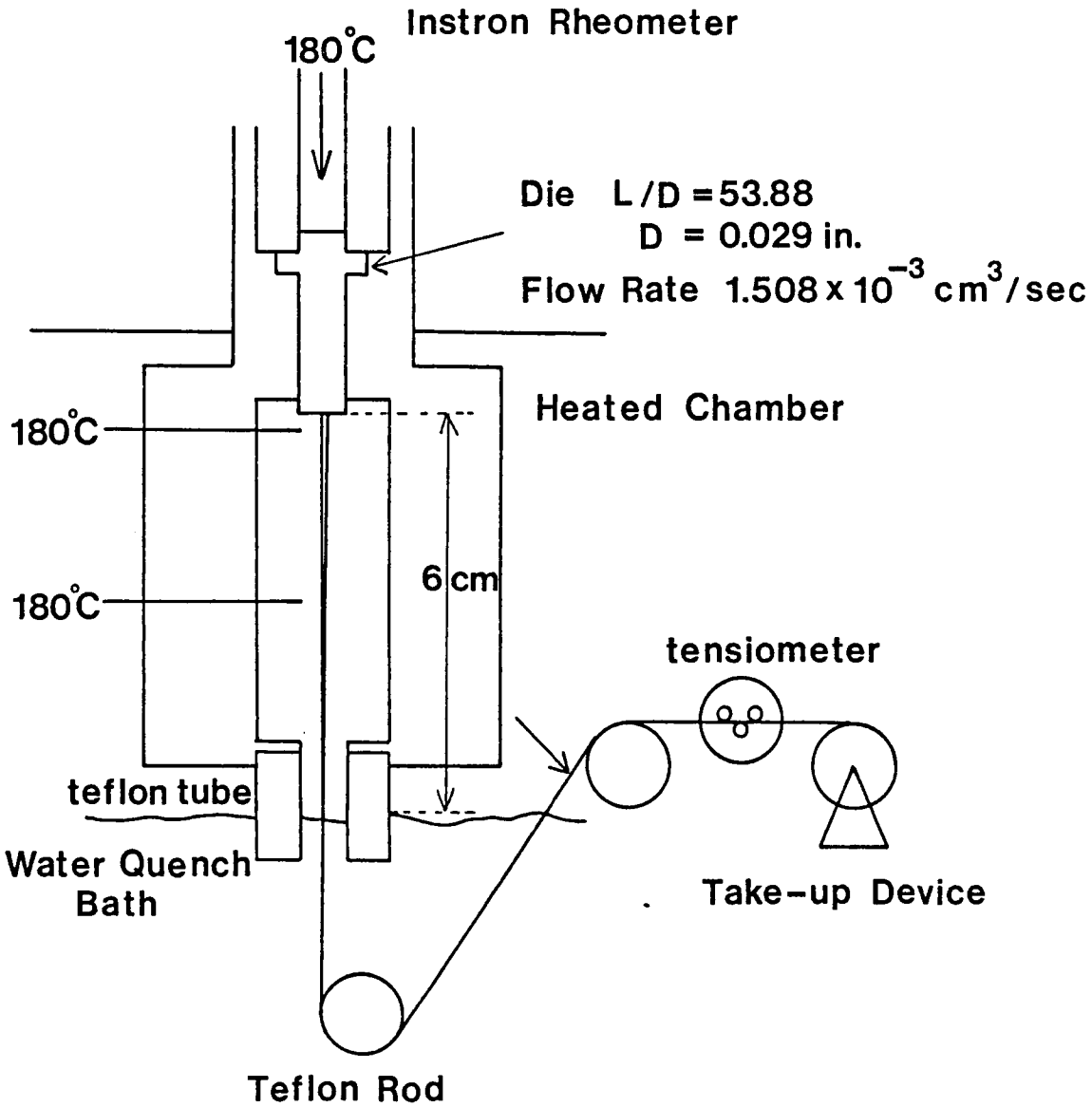

Figure 11.1. Apparatus for isothermal melt spinning.

means of two thermocouples, which were placed 0.5 cm and 3.0 cm below the die exit. The take-up roll, which had a diameter of 8.77 cm, was driven by a 1/15 Hp B & B motor (12 rpm and 86 rpm maximum speed) with a B & B controller type ST-12. A volumetric throughput of 9.05×10^{-2} cm^3/min. (v_0 = 21.236 cm/min.) was used.

A Rothschild tensiometer (100 mV full scale, 4 g and 40 g measuring head) was placed near the take-up device to measure spin-line tension. The measured tension was recorded on a strip chart recorder (model EV-205-11, Heath Company, Benton Harbor, MI) with a potentiometric amplifier (model EV-200-01, Heath Company, Benton Harbor, MI). The development of diameter variations along the fiber was detected by the tension measuring device, which instantaneously provided a qualitative measure of the diameter fluctuation. Diameter variations as observed directly on the spun fiber and indirectly by means of the tensiometer readings agree well with each other. That the on-line tensiometer readings gave the same periodicity and a reasonable approximating of the diameter fluctuations has been noted previously [M-40,M-41,N-1].

The onset of draw resonance was defined as the point where periodic tension fluctuations first appeared. In our experiments draw down ratio was gradually increased. The rate of increased take-up speed was approximately 2 cm/min.^{2} (10.5 min. was necessary to increase one unit of drawn down ratio). When the periodic tension fluctuations detected were very small, compared with the average tension, or had little periodicity, the draw down ratio was

momentarily increased by pulling the solidified fiber by hand (the position for doing so is indicated with an arrow in Figure 11.1). If the draw down ratio was in an unstable (draw resonance) region, the tension fluctuation grew rapidly to a very large value with time. If the draw down ratio was in a stable region, the tension fluctuation did not grow further.

B-3. Isothermal Ribbon Extrusion

Isothermal ribbon extrusion was carried out at 180°C. The same setup as described in Section B-2 was used. A slit die (thickness 0.015 inch, width 0.15 inch, length/thickness ratio of 53.33 and aspect ratio of 10.0) was used in place of the capillary die. A volumetric throughput of 1.81×10^{-1} cm^3/min (v_0 = 12.468 cm/min.) was used. This produced an apparent wall shear rate of 32.7 sec^{-1} instead of 38.4 sec^{-1} for the capillary die.

C. RESULTS

At the start of the melt spinning process, the descending extrudate is pulled onto a take-up roll. It was found that moderate and broad molecular weight distribution (MWD) linear polymers have to be pulled very carefully to avoid ductile failure; this failure occurs somewhere between the extrudate swell region and the middle of the spinline.

Two types of extrudate diameter fluctuations were observed. One of these is random in character, of small amplitude, and seems to occur to a certain extent under all spinning conditions. This

behavior is not a die flow instability nor due to fluctuations in the extrusion system, because we are using an apparatus which delivers a constant volumetric throughput. The second type of diameter fluctuation has a well-defined wavelength (or period) and a much larger amplitude (see Figure 8 in Ref. [M-41]). It was this second type of diameter fluctuation which was investigated in detail.

The draw down ratio DR is defined as

$$DR = v_L/v_0 \ , \tag{11.1}$$

where v_L is the velocity of fiber at the take-up position (or the solidification point) and v_0 is the average velocity at die exit. The critical draw down ratios (DR_c) (onset of draw resonance) in isothermal melt spinning are shown in Table XI-1 as molecular weight distribution (MWD) and material parameters in a convected Maxwell model (see Eqns. (11.2), (11.3) and (11.4)).

Among the linear polymers (HDPE, LLDPE, PP, and PS) the onset of draw resonance generally decreases with the breadth of the molecular weight distribution (MWD). The existence of long chain branching (LCB) delays the onset of draw resonance. However, the LDPE threadline was fractured just above DR_c.

The onset of draw resonance DR_c in an isothermal ribbon extrusion is shown in Table XI-2. The aspect ratio of solidified ribbon are approximately 10.0 at any draw down ratio; the kinematics of ribbon extrusion appear to be uniaxial elongation, as in the case of melt spinning. HDPE-13 could not be spun into a ribbon shape; the

Table XI-1. Onset of Draw Resonance in Terms of Molecular Weight Distribution and Material Parameters

Material	Onset of Draw Resonance, DR_c	M_w/M_n	M_z/M_w	τ_0 sec	a*
HDPE-1	6.9_1	9.64_6	6.35_5	36.5	0.55
HDPE-2	5.7_2	14.10_8	8.28_9	25.3	0.6
HDPE-3	7.6_9	7.10_4	7.84_1	1.95	0.6
HDPE-5	6.1_3	4.66_8	6.55_6	0.548	0.5
HDPE-11	10.2_7	3.35_5	2.97_4	0.690	0.1
HDPE-12	10.6_3	3.59_2	3.11_3	0.253	0.1
HDPE-13	10.1_5	3.05_9	2.70_6	0.0549	0.1
LLDPE-1	12.3_1	3.81	--	1.07	0.3
LLDPE-2	12.6_6	3.36	--	0.828	0.35
LLDPE-3	14.1_8	--	--	0.744	0.3
LLDPE-4	11.6_2	--	--	0.670	0.4
LDPE-1	20.6_8	11.19	--	5.42	0.25
LDPE-2	39.7_3	8.35_6	5.26_3	3.43	0.4
LDPE-11	36.7_6	4.11	--	1.74	0.3
LDPE-12	39.7_3	3.29_3	5.61_4	0.673	0.3
PP-1	6.8_7	9.04	3.57	5.96	0.8
PP-2	6.2_8	7.83	4.82	3.23	0.7
PP-11	9.8_7	6.37	2.59	1.36	0.4
PP-12	9.4_3	4.67	2.81	0.841	0.45
PP-13	12.1_1	4.62	2.47	0.237	0.45
PS-1	11.1_6	2.6	--	4.0	0.4
PS-2	7.2_0	1.91	1.61	8.3	0.2

*Best fit from shear viscosity and principle normal stress difference data.

Table XI-2. Onset of Draw Resonance in Isothermal Melt Spinning and Ribbon Extrusion

Material	Onset of Draw Resonance, DR_c	
	Ribbon Extrusion	Fiber Spinning
HDPE-1	6.2_3	6.9_1
HDPE-2	5.7_2	5.7_2
HDPE-3	7.4_0	7.6_9
HDPE-5	5.8_4	6.1_3
HDPE-11	11.4_2	10.2_7
HDPE-12	11.5_4	10.6_3
HDPE-13	--*	10.1_5
LLDPE-1	10.8_9	12.3_1
LLDPE-2	11.9_5	12.6_6
LDPE-1	20.3_3	20.6_8
PP-1	6.5_4	6.8_7
PP-2	5.9_7	6.2_8
PP-11	10.8_9	9.8_7
PP-12	9.9_8	9.4_3

*Indicates ribbon could not be spun; spun material had a circular cross-section.

cross-section of the solidified extrudates was circular. Narrow MWD HDPE and PP show slightly higher critical draw down ratio in ribbon extrusion, compared with melt spinning, using isothermal conditions in both cases. On the other hand, moderate and broad MWD HDPE and PP, LLDPE, and LDPE show slightly lower critical draw down ratio in ribbon extrusion compared with melt spinning.

When the spinline length for the isothermal ribbon extrusion was reduced to 1.5 cm from 6.0 cm, the aspect ratio of the solidified extrudate was still about 10.0.

D. INTERPRETATION

D-1. Effects of Molecular Weight Distribution and Long Chain Branching

Values for the onset draw resonance (DR_c) for PE, PP and PS are plotted against M_w/M_n and M_z/M_w in Figures 11.2 and 11.3, respectively. These indicate that the narrowing MWD makes the threadline more stable. The plot of DR_c vs. M_z/M_w for PP exhibits a better correlation than the others. This may be due to the relatively simpler MWD shape of PP compared to HDPE.

The occurrence of LCB makes the spinline stable: critical draw down ratios of LDPE's are 20 to 40 (20.7 for LDPE-1 and 36.8 to 39.7 for LDPE-1, -11, and -12); on the other hand, critical draw down ratios for linear polymers (HDPE, LLDPE, PP and PS) are less than 12.7. The effect of LCB appears more dominant on the spinline stability than that of MWD.

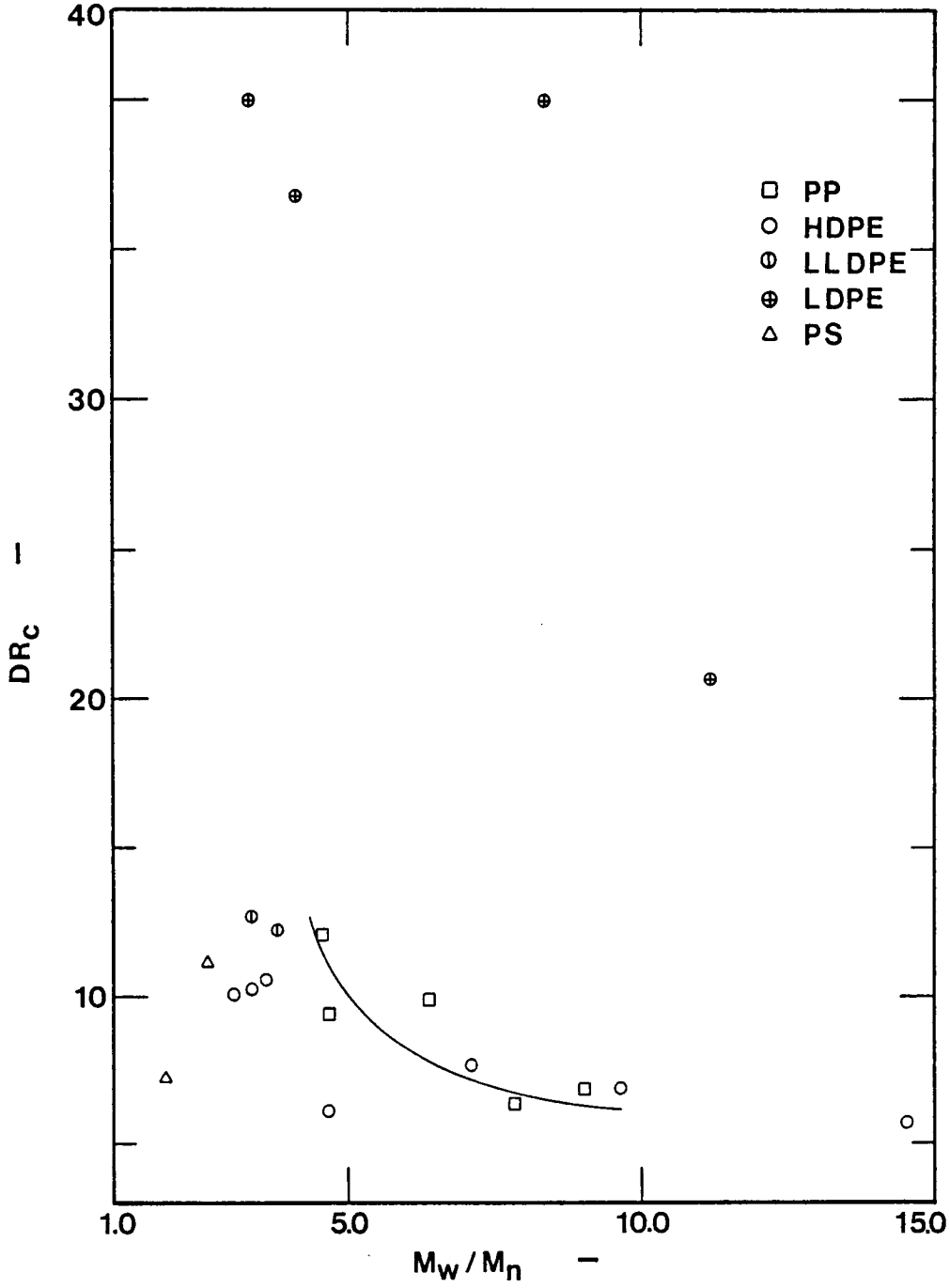

Figure 11.2. Onset of draw resonance as a function of M_w/M_n for high density polyethylene and polypropylene.

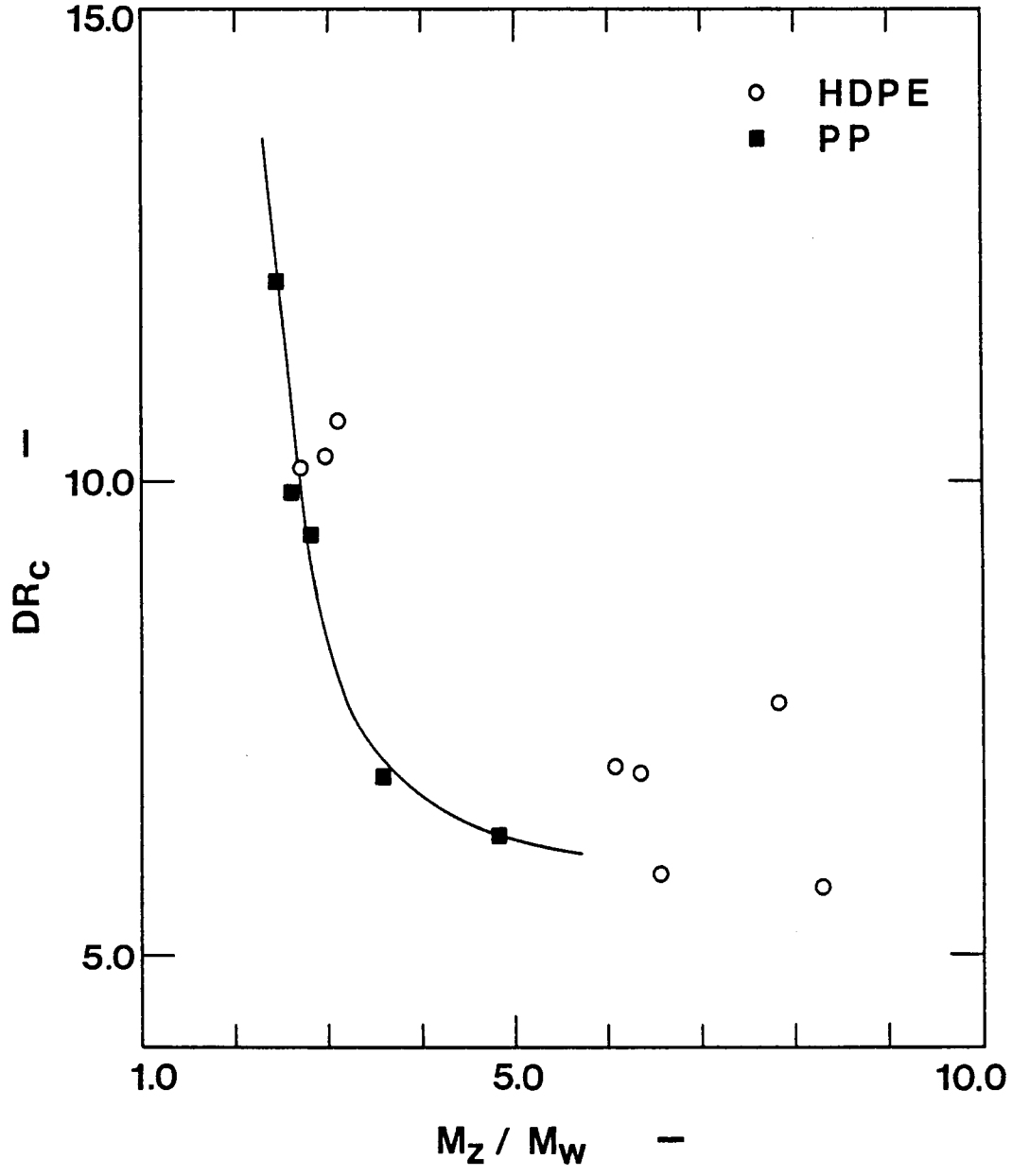

Figure 11.3. Onset of draw resonance as a function of M_z/M_w for high density polyethylene and polypropylene.

In Figure 11.4, the values of the onset of draw resonance are plotted as a function of elongation-to-break during uniaxial elongation under constant strain rate conditions (elongation-to-break data for PE's are in Chapter IV, data for PP samples from Minoshima, White and Spruiell [M-42], and PS-1 from Tanaka and White [T-3]). Elongation-to-break data at $E = 0.002 \sim 0.1\ sec^{-1}$ are used. Melts having a lower elongation-to-break in uniaxial extension tend to exhibit draw resonance at lower DR. White and Ide [W-17], later Minoshima, White and Spruiell [M-41] and White and Tanaka [W-21] argue that draw resonance is a continuous form of the neck development accompanying a ductile failure. Melts which exhibit ductile failure in uniaxial stretching tend to exhibit draw resonance at low DR. This is indeed the case. Melts which failed in cohesive fracture in uniaxial extension (at relatively high E) tend not to exhibit draw resonance; they have higher values of onset of draw resonance such as DR_c of 40. Also their spinline broke just above critical draw down ratio.

The softening effect of deformation rate on relaxation time may be represented by expressing a relaxation time of the form

$$\tau = \frac{\tau_0}{1 + a\,\tau_0\,II_d^{1/2}}\ , \qquad (11.2)$$

where II_d is the second invariant of the deformation rate tensor and "a" indicates the extent of deformation rate dependency (or deformation rate softening) on the relaxation time τ. Values of τ_0 and "a"

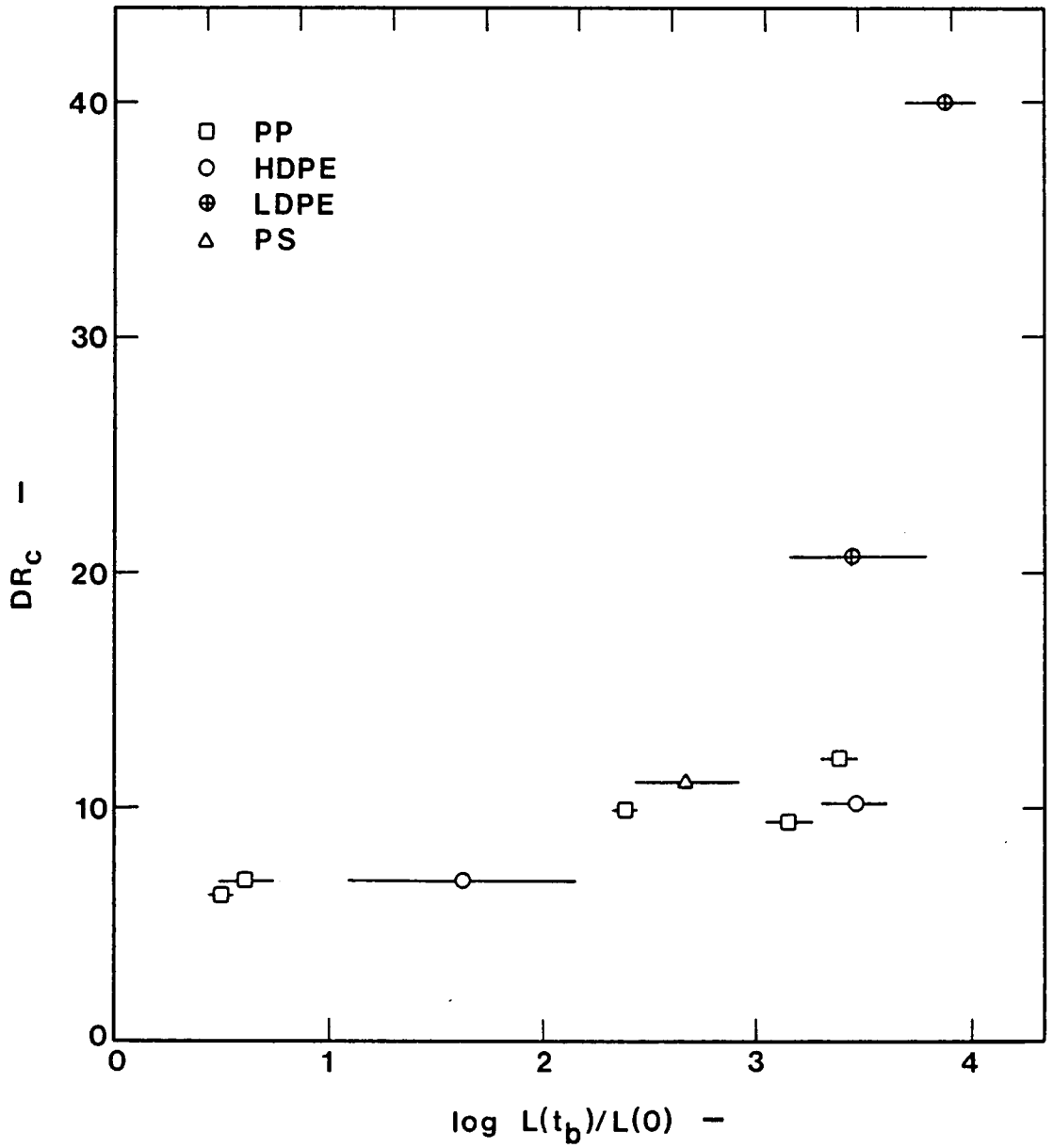

Figure 11.4. Onset of draw resonance as a function of elongation-to-break (in uniaxial elongational flow).

in Eqn. (11.2) in a convected Maxwell (White-Metzner) model are also shown in Table XI-1. Table XI-1 and Figure 11.4 indicate that increasing the deformation rate softening character (i.e., a larger "a" value in Eqn. (11.2)) is destabilizing in the spinline and induces draw resonance at lower draw down ratios. However, the effect of a rate softening relaxation time always appears accompanied by the effect of the Weissenberg number (or values of τ_0). This combination of effects will be discussed in the following section.

D-2. Draw Resonance and Steady State Solutions

It would appear that there are two separate phenomena giving rise to fluctuations in filament diameter in the threadline. There are fluctuations brought on by system disturbances, as proposed by Kase and Matsuo [K-8], which may be termed "forced oscillations." Secondly, there are the fluctuations known as "draw resonance" or "natural oscillations." This latter phenomenon was first analyzed by Kase, Matsuo, and Yoshimoto [K-9] and has since been treated by various investigators. The former phenomenon has received treatment for the case of a nonisothermal Newtonian fluid only. The latter, where the work is more extensive, has been studied for an isothermal Newtonian fluid [K-9,P-2], an isothermal power law fluid [I-6,S-13], an isothermal viscoelastic fluid represented by a convected Maxwell model [C-7,F-5], and various nonisothermal models [F-6,K-5,S-11, S-12].

From analyzing the various papers listed above, it would seem that modifying any rheological model would give a more elongation

rate thinning behavior. This results in draw resonance occurring at lower DR. Following White and Ide's formulation [W-14], the "a" parameter represents this deformation rate softening. Clearly, as "a" increases (see Table XI-1, page 345), the spinline destabilizes and the critical DR decreases. Analyzing Kase and Matsuo's formulation [K-8] leading to forced oscillations, it would seem clear that a similar influence on the spinline elongational viscosity function would lead to accentuation of the diameter fluctuations. This suggests that a steady state solution of the spinline behavior will give us at least qualitative information on draw resonance.

The basic problem with the integral constitutive equation formulation is its complexity. It is desirable to be able to use a more simple model for such analyses. Zeichner [Z-2] has shown that such a theory can be developed from the convected Maxwell model. This view has been developed in succeeding papers by Denn, Petrie, and Avenas [D-4], Fisher and Denn [F-5], Petrie [P-10], Chang and Denn [C-7], and White and Ide [W-17].

Let us begin with the convected Maxwell (White-Metzner) model constitutive equation [C-7,D-4,F-5,I-3,M-35,M-41,M-42,P-10,W-17,W-19]:

$$\underset{\sim}{\sigma} = -p\underset{\sim}{I} + \underset{\sim}{P} \,, \tag{11.3a}$$

$$\underset{\sim}{P} = 2G\tau\underset{\sim}{d} - \tau \frac{\delta \underset{\sim}{P}}{\delta t} \tag{11.3b}$$

where $\underset{\sim}{P}$ is the extra stress, $\underset{\sim}{d}$ is the rate of deformation, and G and τ parameters where τ is assumed to be a function of II_d, the second invariant of $\underset{\sim}{d}$. This may usefully be taken as [I-3,M-41,M-42,W-17]:

$$\tau = \frac{\tau_0}{1 + a\,\tau_0\,II_d^{1/2}} , \tag{11.4}$$

a functional form suggested by Bogue in connection with an integral formulation [B-12]. In the study of Fisher and Denn [F-5] and Chang and Denn [C-7], power law forms are used to represent the deformation rate dependence of τ (and G). This is unsatisfactory because it leads to improper low deformation rate behavior.

For isothermal melt spinning [C-7,D-4,F-5,W-17,Z-2], where the force acting is assumed to be only the rheological force, we have

$$v_z = v_z(z) , \tag{11.5a}$$

$$v_r = v_r(r) , \tag{11.5b}$$

$$\frac{\partial v_z}{\partial z} + 2\,\frac{\partial v_r}{\partial r} = 0 , \tag{11.5c}$$

$$F = \sigma_{zz}\pi R^2 = (P_{zz} - P_{rr})\pi R^2 = (P_{zz} - P_{rr})\,\frac{Q}{v_z} . \tag{11.6}$$

We follow now the analysis of White and Ide [W-17]. If we take P_{zz} to dominate P_{rr} and neglect the latter (Zeichner's asymptote), the spinline behavior is given by combining Eqns. (11.3), (11.4), and (11.6)

$$\tau\left[v\,\frac{d}{dz}\left(\frac{Fv}{Q}\right) - 2\,\frac{Fv}{Q}\,\frac{dv}{dz}\right] = 2G\tau\,\frac{dv}{dz} - \frac{Fv}{Q} , \tag{11.7}$$

where F is the take-up force, Q is the volumetric flow rate,

$v(=v_z)$ is the spinline velocity along the machine (z) direction, and z is the distance from the die exit (or the maximum extrudate swell position). Eqn. (11.7) is the case at high stress levels and for highly elastic systems (Zeichner's asymptote).

Eqn. (11.7) can be nondimensionalized to

$$[(1 - \sqrt{3}\,a)F^*V^* + 2]N_{ws}\frac{\partial V^*}{\partial Z^*} - F^*V^* = 0 \ . \tag{11.8}$$

Here

$$F^* = \frac{Fv(0)}{GQ}, \tag{11.9a}$$

$$N_{ws} = \tau_0 v(0)/L \ , \tag{11.9b}$$

$$V^* = v(z)/v(0) \quad \text{or} \quad v(z)/v_0 \ , \tag{11.9c}$$

$$Z^* = z/L \ , \tag{11.9d}$$

where L is the spinline length and $v(0)$ (or v_0) is the velocity at the die exit (or at the maximum extrudate swell position). The solution to Eqn. (11.8) may be expressed alternatively as

$$F^* = \frac{2N_{ws}\ \ell n\ V^*}{Z^* - \alpha(V^* - 1)} \tag{11.10a}$$

or

$$Z^* = \frac{1 - \alpha(DR - 1)}{\ell n\ DR}\ \ell n\ V^* + \alpha(V^* - 1) \ , \tag{11.10b}$$

where

$$\alpha = (1 - \sqrt{3}\, a)N_{ws} = (1 - \sqrt{3}\, a)\, \frac{\tau v(0)}{L} , \qquad (11.11a)$$

and

$$V^* = DR = v(L)/v(0) \quad \text{at} \quad Z^* = 1,0 ,$$
$$V^* = 1.0 \quad \text{at} \quad Z^* = 0.0 . \qquad (11.11b)$$

For $a = 1/\sqrt{3}$, an exponential response is obtained similar to that of a Newtonian fluid. For $a = 0$, Zeichner's solution [Z-2] is obtained.

The characteristics of Eqn. (11.10) are illustrated in Figure 11.5. Figure 11.5 gives us some information about limits on melt spinning. These are (i) the take-up force should be finite (an infinite or negative take-up force is not allowed), and (ii) the spinline velocity should change continuously (a discontinuity in the velocity profile is not allowed).

Finite take-up force requires (Eqn. (11.10a))

$$Z^* - \alpha(V^* - 1) > 0 . \qquad (11.12)$$

Discontinuities in the spinline velocity may occur only at $Z^* = 0.0$ and 1.0. When a discontinuity in the spinline velocity occurs, the velocity gradient becomes negative (see Fig. 11.4 and Eqn. (11.10b)) at $Z^* = 0.0$ and 1.0. Eqn. (11.6b) leads to

$$\frac{\partial V^*}{\partial Z^*} = \frac{V^* \ln DR}{1 - \alpha(DR - 1 - V^* \ln DR)} . \qquad (11.13)$$

Eqn. (11.13) suggests

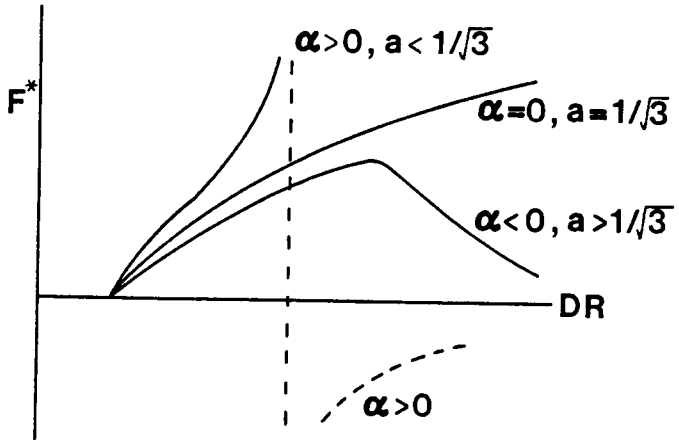

(a) Take-up force-draw down ratio relationship for various α

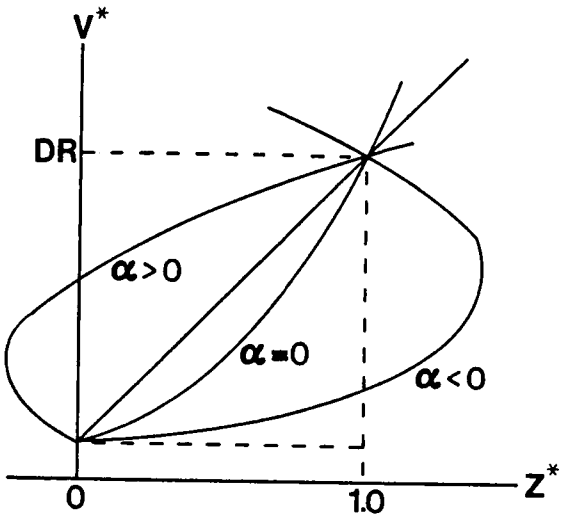

(b) Velocity profile for various α

Figure 11.5. Theoretical prediction for isothermal melt spinning.

$$\frac{\partial V^*}{\partial Z^*} > 0 \quad \text{at} \quad 0 < Z^* < 1 \quad \text{and} \quad 1.0 < V^* < DR \ . \tag{11.14}$$

Therefore, the velocity profile is continuous when

$$1 - \alpha(DR - 1 - \ell n\ DR) > 0 \quad \text{for} \quad \alpha > 0 \ , \tag{11.15a}$$

and

$$1 - \alpha(DR - 1 - DR\ \ell n\ DR) > 0 \quad \text{for} \quad \alpha < 0 \ . \tag{11.15b}$$

Zeichner [Z-2], Denn, Petrie ane Avenas [D-4], and later White and Ide [W-17], discussed the existence of a critical draw down rations due to the development of an infinite stress (or infinite take-up force) which cause cohesive fracture on the spinline. The critical draw down ratio is

$$DR_c = \frac{1}{\alpha} + 1 \ . \tag{11.16}$$

This is the same case as described in Eqn. (11.12). Nam and Bogue [N-2] suggest that a computation using an integral formulation for isothermal melt spinning is possible below the critical draw down ratio when F* in Eqn. (11.10a) is below the maximum. After examining Eqn. (11.10a), based on the convected Maxwell model, they concluded that melt spinning is possible below the maximum take-up force.

The condition where melt spinning is possible (not unattainable) is given by combining Eqns. (11.12), (11.15a), and (11.15b). This is given as

$$\frac{1}{DR - 1 - DR\ \ell n\ DR} < \alpha < \frac{1}{DR - 1} . \qquad (11.17)$$

The condition given by Eqn. (11.17) also corresponds to

$$F^* \geq 0 \quad \text{and} \quad \frac{\partial F^*}{\partial DR} > 0 . \qquad (11.18)$$

The physical meaning of Eqn. (11.17) may be interpreted as follows: (i) the right-hand side is due to cohesive fracture on the spinline, and (ii) the left-hand side (discontinuity of the spinline velocity at the take-up position) may imply ductile failure in the spinline at the take-up position because $\partial V^*/\partial Z^* \to \infty$ when $\alpha = 1/(DR - 1 - DR\ \ell n\ DR)$.

It is necessary to carry out a stability analysis to determine the critical draw down ratio for the phemenon of draw resonance. However, White ane Ide [W-16] described the difficulty of obtaining an analytical solution (or a single differential equation) for stability in the isothermal melt spinning of a convected Maxwell model. Although a stability analysis is not involved in Eqns. (11.17) and (11.18), they do, nonetheless, provide a limiting case for stable melt spinning and so it would be interesting to compare experimental data for the onset of draw resonance and Eqn. (11.17), especially the inequality in the left side. This is plotted in Figure 11.6. Generally the critical draw down ratio increases with increasing $\alpha(=(1 - \sqrt{3}\ a)N_{w_s})$, except for LDPE's. The positions of LDPE's in the $DR_c - \alpha$ plot (well above the limitation caused by the right side of Eqn. (11.6)) seem qualitatively reasonable; because the spinline

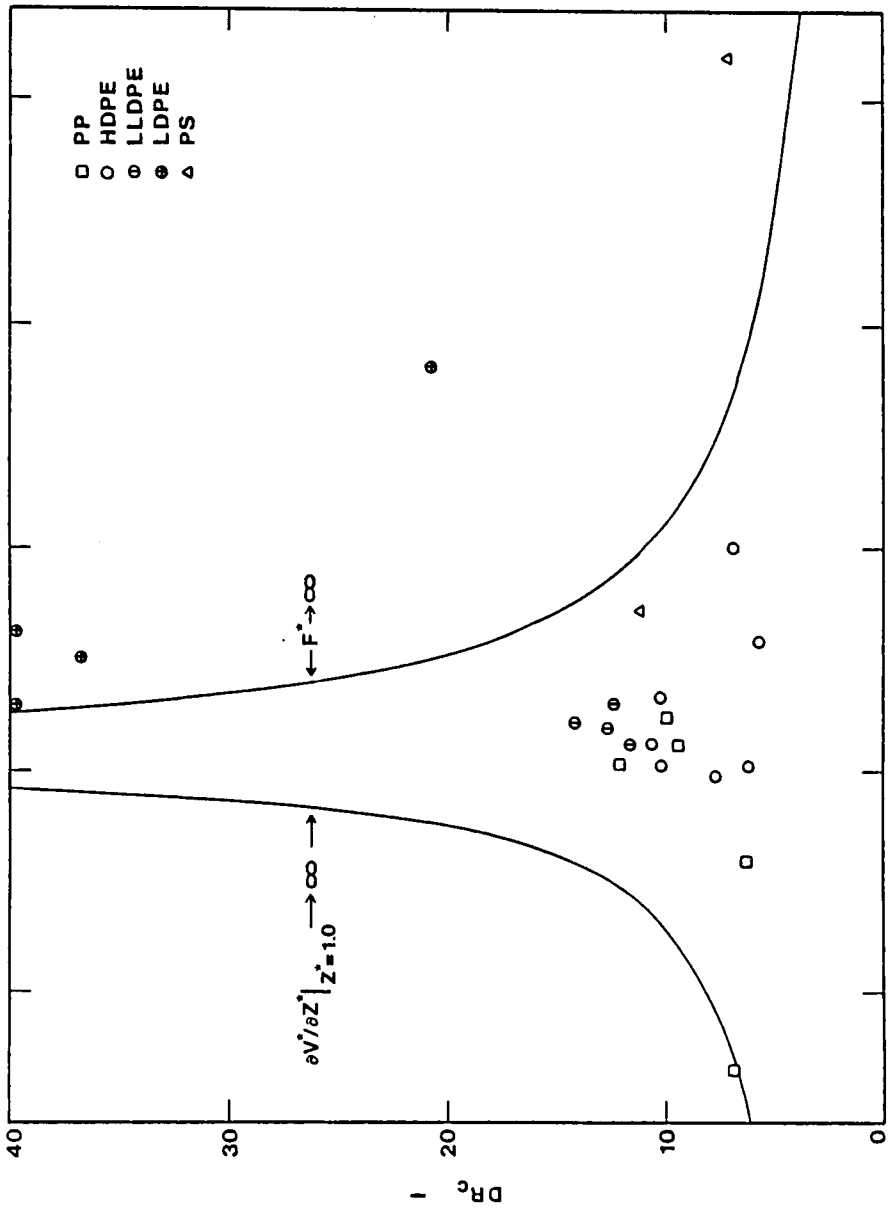

Figure 11.6. Onset of draw resonance as a function of α.

for the LDPE samples fractured just above the critical draw down ratio in a cohesive manner, after exhibiting the usual draw resonance behavior. It is not clear whether there is a good correlation among the linear polymers when the rheological constants in the convected Maxwell model (rheological properties) are different. The following are possible reasons for the scatter in the plots: (i) Eqn. (11.17) is based on an assumption that neglects the extra stress in the radial direction (assumed to be a highly elastic system); (ii) Eqn. (11.17) or Eqn. (11.3) neglects the distribution of relaxation times; (iii) $\alpha(=(1 - \sqrt{3}\ a)N_{W_S} = (1- \sqrt{3}a)\tau_0 v(0)/L)$ is too sensitive to the difference of "a" values as determined from shear flow data; and (iv) the steady state solution for a hydrodynamic problem cannot tell us anything about the qualitative tendency for hydrodynamic instabilities. Weissenberg numbers ($N_{W_S} = \tau_0 v(0)/L$) for the isothermal melt spinning varied from 2.15 to 0.00324. The relaxation time used in Eqn. (11.3) is the second moment of the relaxation spectrum. Yamane [Y-1] reported that the spinline velocity profiles of thermally degraded PP is predicted by Eqn. (11.10b) but not for the original nondegraded PP, which is believed to have a broad MWD. The velocity profiles were measured well below the critical draw down ratio (DR_c) for thermally degraded PP, and just below DR_c for the original PP. Therefore, the first, second, and third reasons may be the cause of the scatter on the $DR_c - \alpha$ plot.

Eqns. (11.8) and (11.9) give a dimensionless spinline elongational viscosity as

$$\chi^*_{sp} = \frac{2N_{w_s}}{1 - \alpha N_{w_s} \partial V^*/\partial Z^*} \sim \frac{F^* V^*}{\partial V^*/\partial Z^*} , \tag{11.19a}$$

where

$$\chi^*_{sp} = \frac{\chi_{sp}}{G} \frac{v(0)}{L} + \frac{\sigma_{zz}}{\partial v/\partial z} \frac{v(0)}{GL}. \tag{11.19b}$$

At the conditions where the velocity gradient goes to infinity near the take-up position, α is

$$\alpha \to \frac{1}{DR - 1 - DR \ln DR} . \tag{11.20}$$

Eqn. (11.19a) is modified under the condition of Eqn. (11.20)

$$\chi^*_{sp}\Big|_{Z^*=1.0} \to 0 \quad . \tag{11.21}$$

And Eqn. (11.19a) also suggests that the spinline elongational viscosity tends to rapidly decrease near the take-up position with the value of α decreasing toward $1/(DR - 1 - DR \ln DR)$. $C\chi^*_{sp}$ vs. Z^* (in linear scale) is plotted in Figure 11.7 for different values of α, where C is an arbitrary constant (which is dependent on α and DR). It is shown that (i) χ^*_{sp} changes from increasing functions of the spinline position to decreasing functions of the position by decreasing the value of α; (ii) χ^*_{sp} increases linearly along the spinline at $\alpha \to 1/(DR-1)$; (iii) χ^*_{sp} is constant at $\alpha = 0$ (where the velocity profile is the same as a Newtonian fluid); (iv) χ^*_{sp} falls off

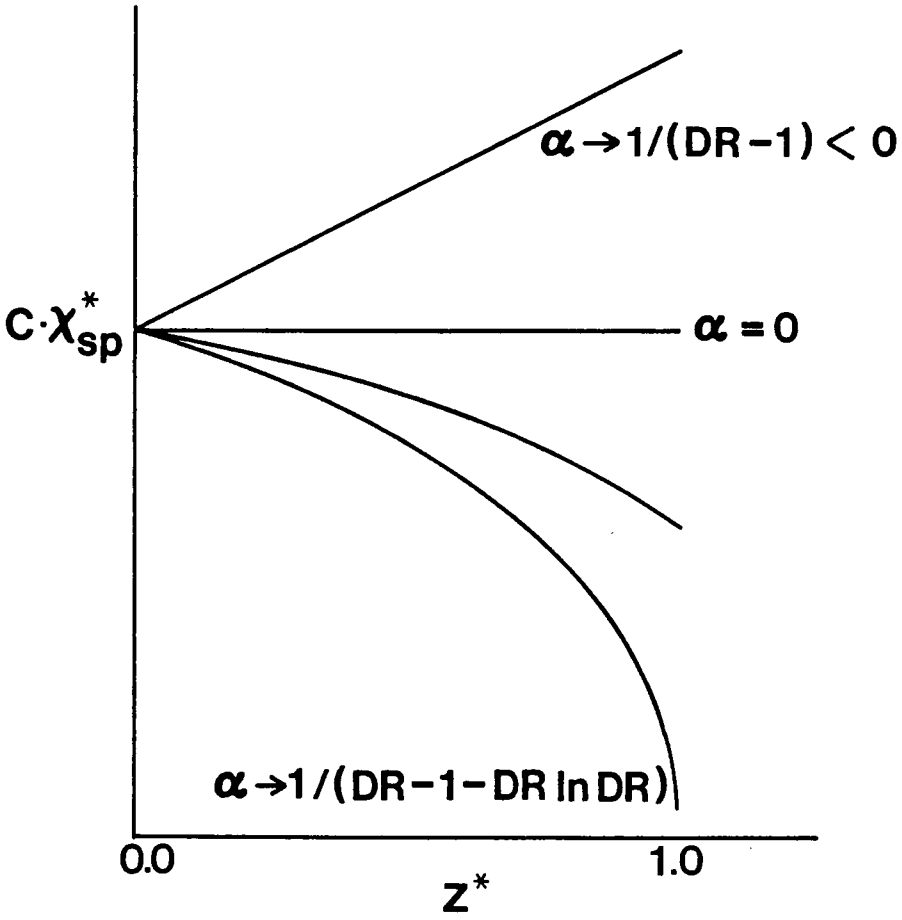

Figure 11.7. Spinline elongational viscosity as a function of spinline for various α (based on a convected Maxwell model).

more rapidly along the spinline position by decreasing the value of α (α is less than zero); and (v) χ^*_{sp} falls to zero at (or near) the take-up position when $\alpha \to 1/(DR - 1 - DR\ \ell n\ DR)$. It becomes clear again that the spinline may exhibit necking at $\alpha \to 1/(DR - 1 - DR\ \ell n\ DR)$; because at the take-up position the velocity gradient approaches infinity and the spinline elongational viscosity decreases to zero. This may imply the draw resonance phenomenon which is believed to be a continuous form of the neck.

E. SUMMARY

An experimental study of the influence of molecular structure (molecular weight, molecular weight distribution, and degree of long chain branching) on the onset of draw resonance in a series of polyolefins and polystyrenes is reported. The materials include high density polyethylene, linear low density polyethylene, low density polyethylene, polypropylene and polystyrene. Narrowing the molecular weight distribution and the occurrence of long chain branching stabilizes the spinline disturbances. The results are interpreted in terms of viscoelastic fluid mechanics and earlier experimental studies on rheological properties.

CHAPTER XII

INSTABILITIES IN TUBULAR FILM EXTRUSION

A. INTRODUCTION

The most important continuous film process is tubular blown film extrusion which is widely used for polyethylenes. There have been, however, few basic experimental studies of this process. Some measurements of bubble shape, velocity or strain rate as functions of the operating variables (draw down ratio, blowup ratio, take-up tension, blowing air pressure, flow rate of polymer melts) were studied by Ast [A-13,A-14,A-15], Farber and Dealy [F-1], Han and Park [H-8], Wagner [W-1,W-2,W-3], Swerdlow, Cogswell and Krul [S-31], and Kanai and White [K-2]. Experimental studies of heat transfer in blown film extrusion have been reported by Zeppenfeld [Z-4], Menges and Predohl [M-29,M-30,M-31], Ast [A-13,A-14,A-15], and Kanai and White [K-2]. There have only been three reports in the literature about stabilities in tubular blown film extrusion. Han et al. [H-10,H-11] found the development of periodic variations in bubble diameter. This wavy surface is imparted to the bubble when the size of disturbance was greater than some critical value. Kanai and White [K-2] studied an operational space (drawn down ratio, blowup ratio, and frost line height) for three polyethylenes. These were high density, linear low density, and low density polyethylene. The relative stability of different melts over a range of operating

conditions is not clear. There still appear to be some questions on (i) the type of instabilities which exist, (ii) the effects of the operating conditions, (iii) the influence of material properties of polymer melts (rheological properties, heat transfer properties, etc.). There is only one theoretical study on bubble instability. Yeow [Y-9] presented an analysis for isothermal Newtonian fluids, using the assumption of infinitesimal disturbances with axisymmetry,

In the present chapter, we describe comparative studies of the stabilities of tubular blown film extrusion for a series of polyethylenes, including high density polyethylenes, linear low density polyethylenes, and low density polyethylenes.

B. EXPERIMENTAL

B-1. Materials

A series of four high density polyethylenes (HDPE), two linear low density polyethylenes (LLDPE), and two low density polyethylenes (LDPE) were used. These are HDPE-1, -2, -3, and -11, LLDPE-1 and -2, and LDPE-1 and LDPE-11 and are listed in Tables III-1, III-2, and III-3 (pp. 49, 50, 51) with molecular characterization data. In addition to these tables, HDPE-1, LLDPE-1 and -2, and LDPE-1 and -11 are film grade, HDPE-2 is a blow molding resin and HDPE-3 and -11 are injection molding grade. The rheological properties (steady shear viscosity, principal normal stress difference, and uniaxial elongational flow) are described in Chapter IV. HDPE-2, LLDPE-2,

and LDPE-11 were already used by Kanai and White [K-2] for their tubular blown film extrusion investigations.

B-2. Tubular Film Extrusion

The tubular film extrusion was carried out at 180°C using a Kissam single screw extruder (Ed-X-Truder, model 75 x 20:1, screw diameter 3/4 inch, L/D = 20, Kissam Manufacturing, Inc., Mountainside, NJ) with an annular blown film die (outer diameter = 5/8 inch, inner diameter = 9/16 inch). The die was designed by the author in cooperation with Y. Shimomura. A volumetric flow rate of 1100 cm^3/ hour was used. An extruded bubble was surrounded and covered by a cardboard "protector" between the nip rolls and the annular die in order to minimize the influence of the surroundings. In addition to the guide rolls, two sets of stabilizing bars were added to minimize the sliding motion of the bubble along the nip rolls. Films were extruded with a range of values for the draw down ratio (DR), the blowup ratio (BUR), and the frost line height (FLH). These are defined as

$$DR = v_L/v_0 \ , \tag{12.1a}$$

$$BUR = R_L/R_0 \ , \tag{12.1b}$$

where v_L and v_0 is the velocity of the solidified polymer film and at the die exit, respectively, and R_L is the diameter of the final film and

$$R_0 = (\text{outer diameter of the annular die} + \text{inner diameter of the annular die})/2 \ . \qquad (12.1c)$$

The draw down ratio was controlled by take-up speed. The blow up ratio was controlled by changing the air pressure (indicated as Δp in Figure 12.1). The frost line height varied by the cooling air coming from an air ring. The experiments on the observation of stability are carried out by the following procedures: (1) find stable operating conditions, (2) the operating conditions are gradually changed to set certain values for FLH and DR, (3) if this operating condition is unstable, the operating parameters are again set at a stable operating condition, (4) step (2) is again carried out. Two different frost line heights were used (FLH = 5 cm and 12 cm). For the case of FLH = 5 cm, film extrusion without internal pressure could not be carried out because of insufficient cooling.

C. RESULTS

There would seem to be three important kinematic variables to represent tubular blown film extrusion in a global manner. These are the draw down ratio (DR), the blowup ratio (BUR) and the frost line height (FLH). The former two quantities determine the machine direction stretching rates and the hoop direction stretching rates, respectively. FLH represents the distance through which the deformation occurs. We note that this is a first approximation of the kinematics.

One of the most surprising experimental results in our studies of the stability of tubular blown film extrusion is that the response

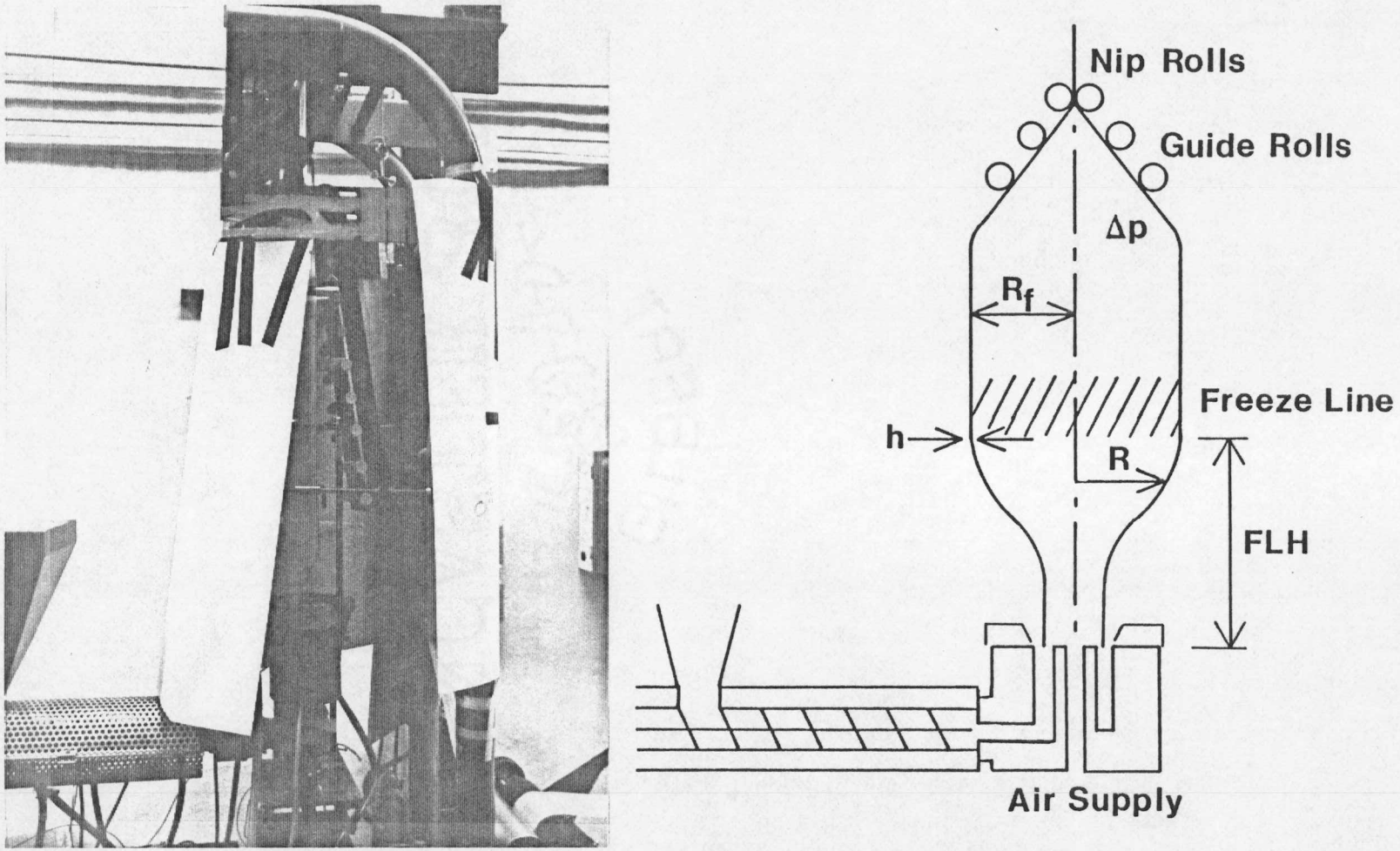

(a)

(b) Schematic diagram

Figure 12.1. Apparatus for tubular film extrusion.

of the system is very slow, compared with an isothermal melt spinning of the same polymer melt. Sometimes it takes more than 30 minutes after setting operating variables to find out whether a system is stable or not.

Four different types of unstable bubble shapes were observed. In unblown film extrusion, there exists a periodic diameter fluctuation whose period (ℓ) corresponds to the length between the first nip rolls and the die exit (see Figure 12.2). The magnitude of diameter fluctuation is almost constant with time change. This phenomenon appears only at very high DR. The phenomenon has exactly the same character as "draw resonance" in melt spinning and film casting. We will therefore again refer to it as "draw resonance." The maximum DR of the present study is 11.0 and this type of instability never occurred in any of the samples.

In blown film extrusion there are three types of unsteady state operation. The first is the so-called "bubble instability" which has been described by Han et al. [H-10,H-11] and Kanai and White [K-2].

Photographs are shown in Figure 12.3. The characteristics of this instability are (i) the period of diameter fluctuation corresponds to the length between the first nip rolls and die exit, (ii) the magnitude of the diameter fluctuation increases with time and finally causes breakage of the tubes, and (iii) the fluctuations are axisymmetric. The second type may be called a "meta-stable condition" (see Figure 12.4). The characteristics of this type are

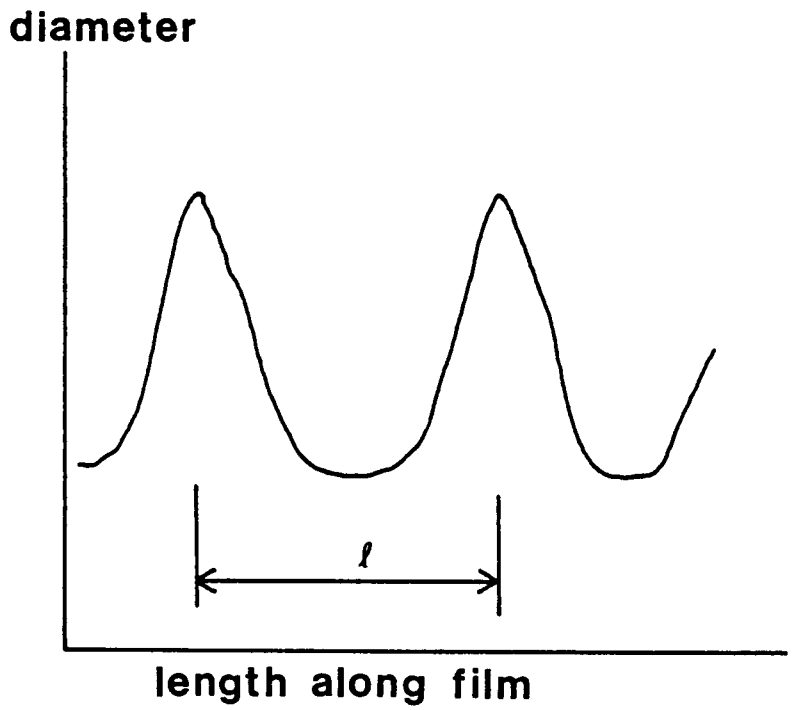

Figure 12.2. Schematics for unstable operation of an unblown film extrusion.

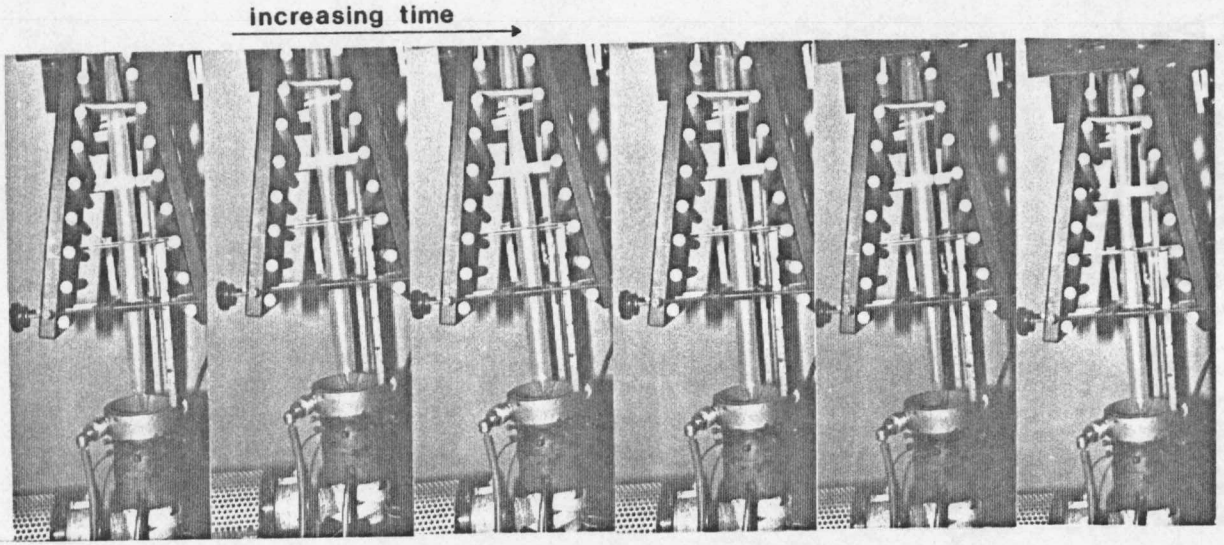

Figure 12.3. Photographs for bubble instability of tubular blown film extrusion.

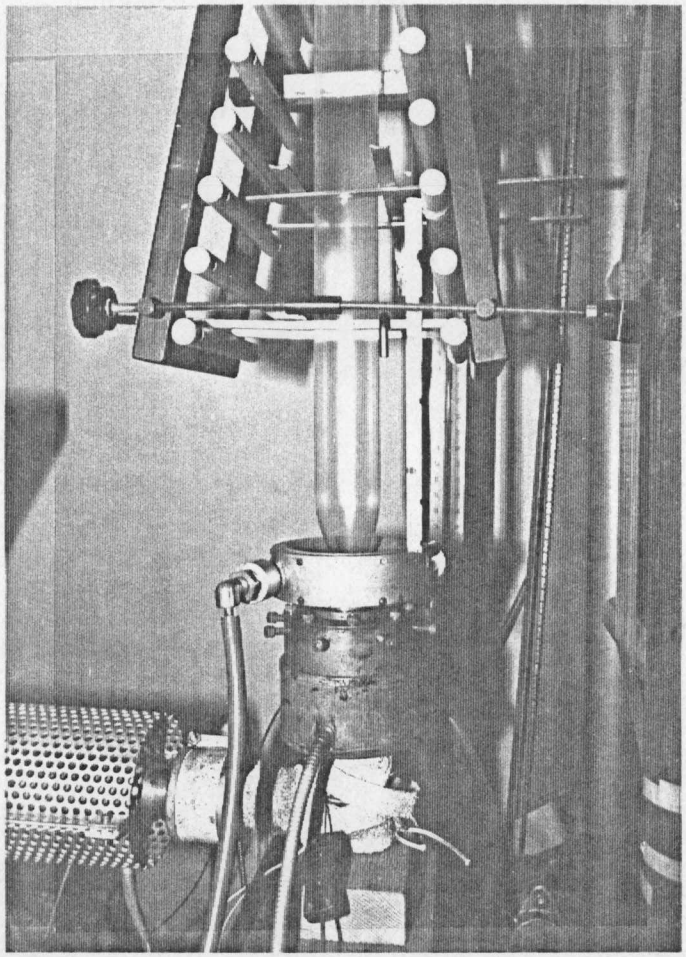

State (A)

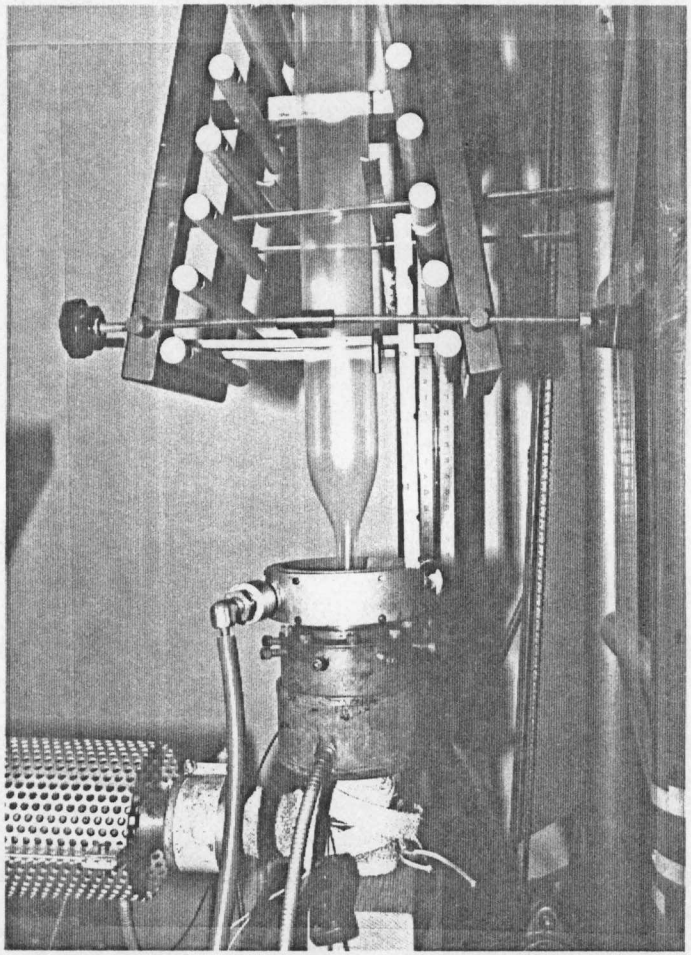

State (B)

Figure 12.4. Photographs for meta-stable condition of tubular blown film extrusion.

(i) the final diameter of bubble is constant (R_L does not change with time), (ii) the frost line height (FLH) fluctuates between two positions, (iii) the value of the tension (measured by a Tensitron Web Tensiometer) for the low FLH case is larger than the higher FLH case, (iv) the transition time between one bubble shape to the other is relatively quick (less than 10 sec), and (v) the period does not correspond to the length between the first nip rolls and the die exit (the period is of the order of minutes). These are schematically shown in Figure 12.5. The "bubble instability" and the "meta-stable condition" are easily distinguished by noting the period and the magnitude of the diameter fluctuation. The third type may be called a "helical bubble" (see Figure 12.6). The characteristics are (i) the bubble rotates in a helical manner (not axisymmetric), (ii) this phenomena appears only at higher blow up ratios (BUR), (iii) when BUR is increased from a stable operating condition to high BUR, the bubble first starts to rotate between the nip rolls and the die exit, before showing an obvious helically rotated bubble if any bubble stabilizing bars were not added, and (iv) once it achieves a certain level of helical movement, the magnitude never grew.

In Figure 12.7, the DR-BUR diagrams are shown with open circles representing stable operating conditions, circles with straight lines through them helical bubble behavior, closed squares unstable operation (bubble instability), and open squares meta-stable operating conditions. LDPE and LLDPE samples could not have their FLH lowered to 5 cm for BUR of about 1.5 because of insufficient cooling air (this is indicated by the oblique lines in Figure 12.7).

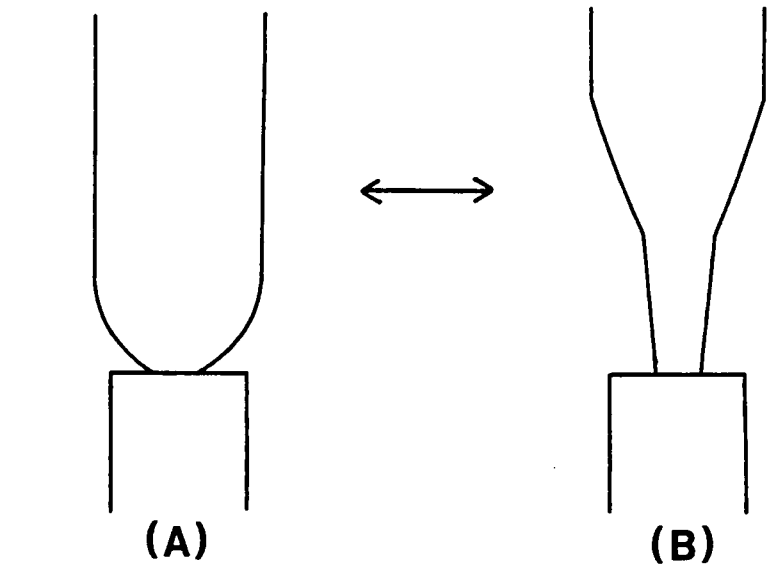

Figure 12.5. Schematics for meta-stable condition of tubular blown film extrusion.

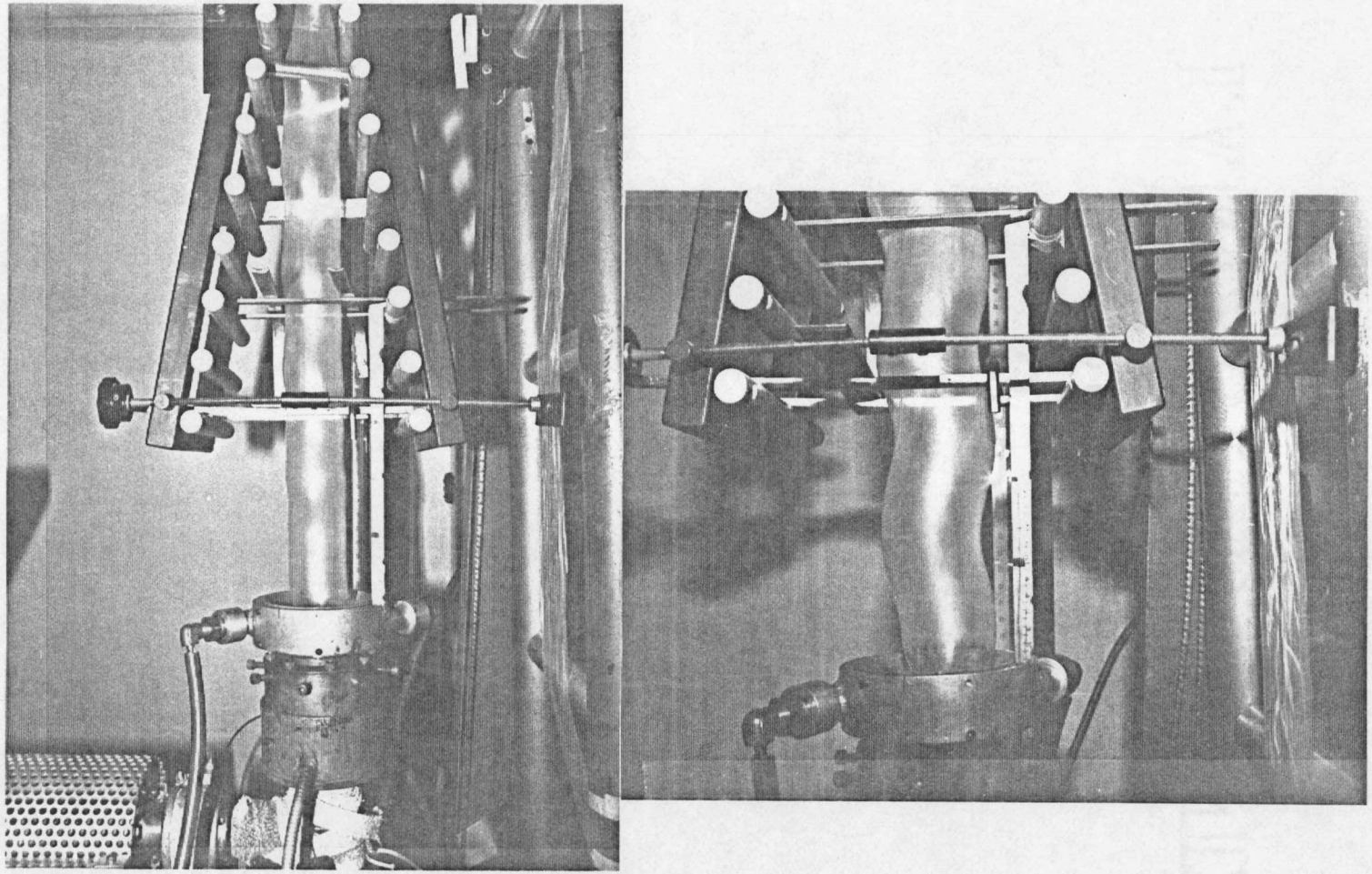

Figure 12.6. Photographs for helical bubble of tubular blown film extrusion.

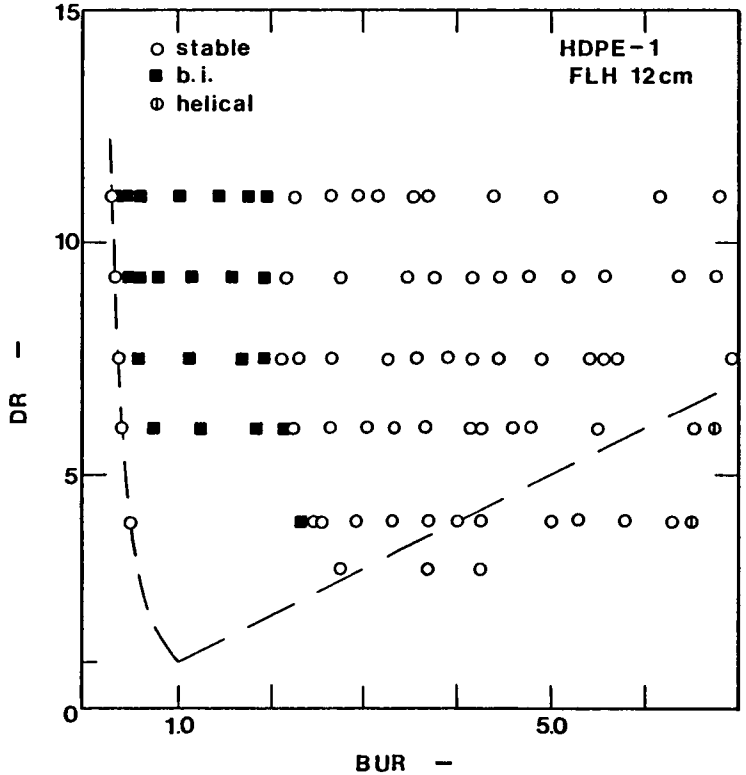

(a) HDPE-1, FLH = 12 cm

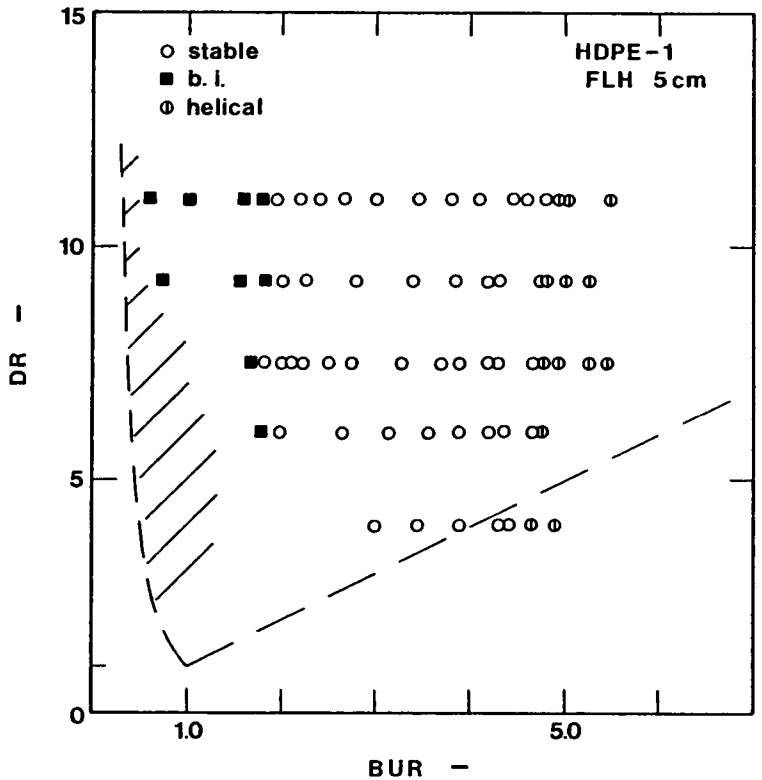

(b) HDPE-1, FLH = 5 cm

Figure 12.7. Operational diagram (draw down ratio DR-blow-up ratio BUR) for tubular film extrusion.

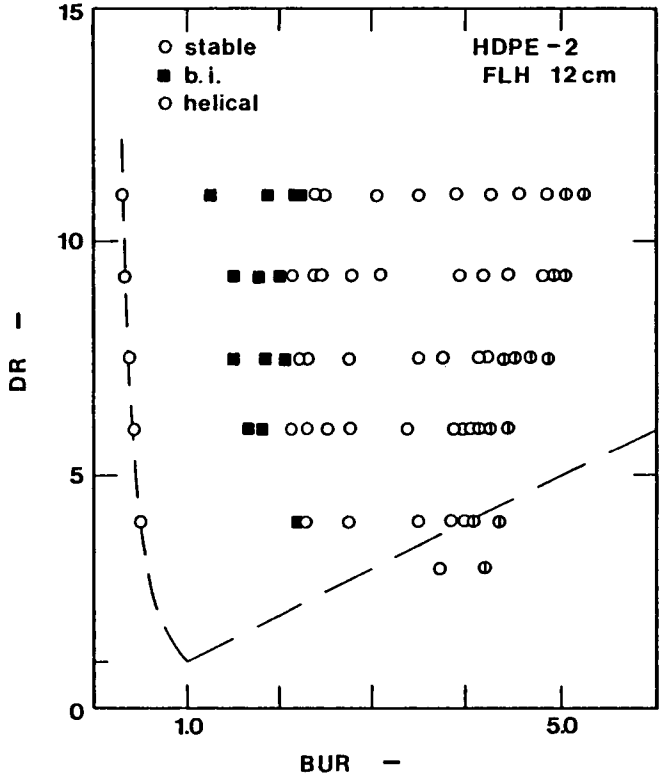

(c) HDPE-2, FLH = 12 cm

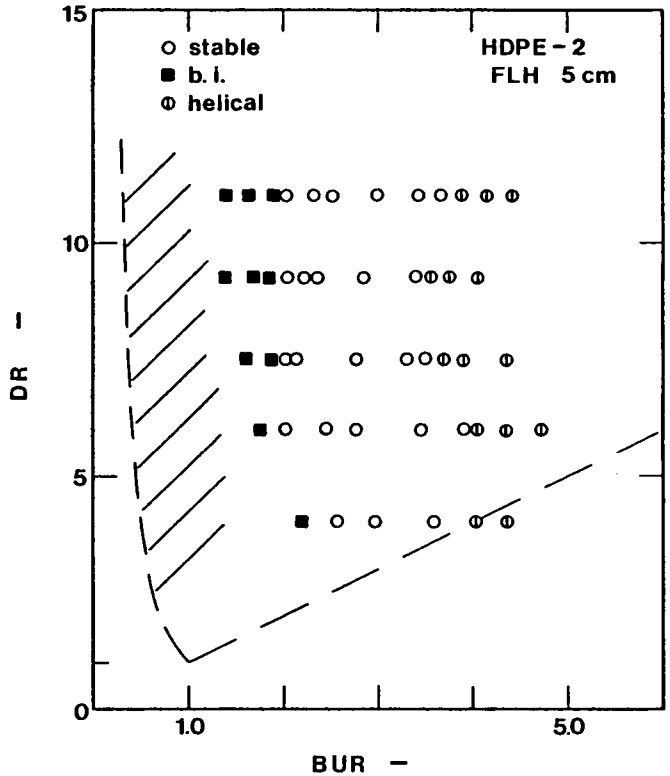

(d) HDPE-2, FLH = 5 cm

Figure 12.7 (continued)

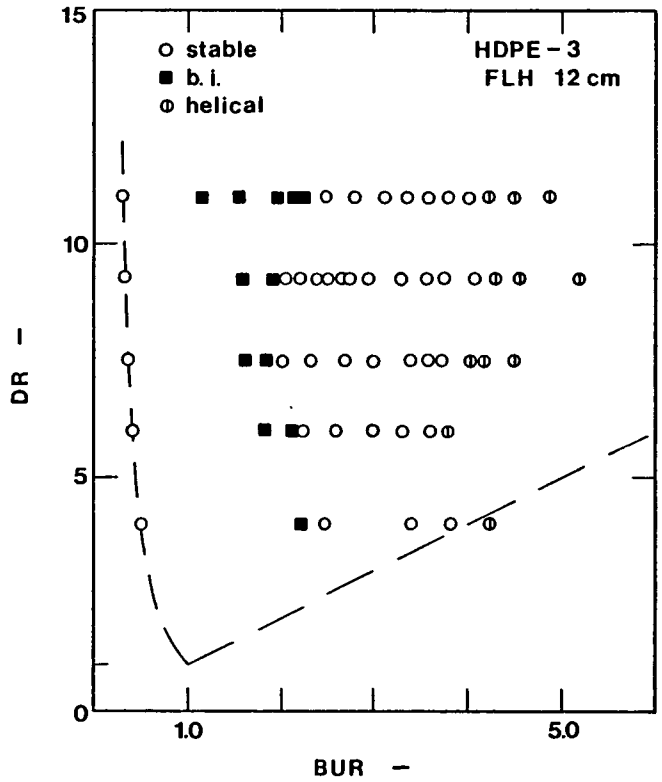

(e) HDPE-3, FLH = 12 cm

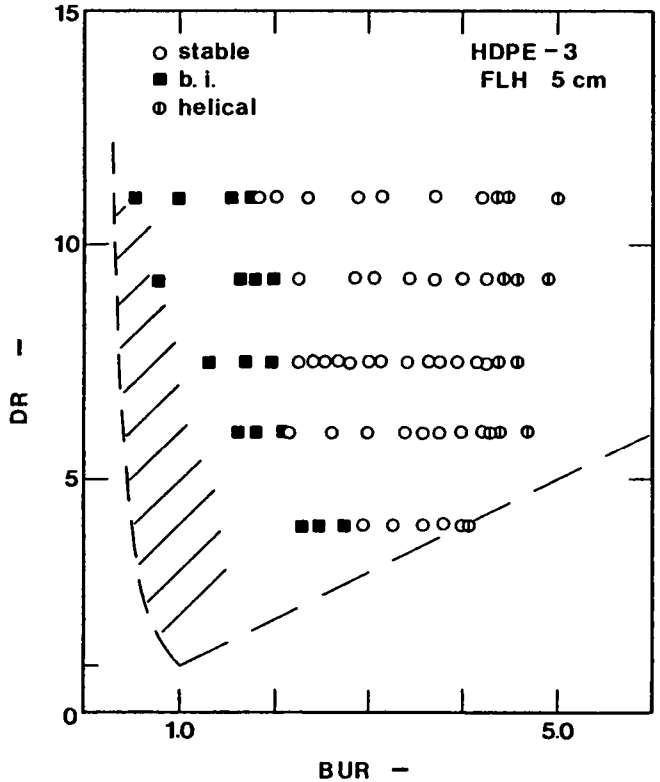

(f) HDPE-3, FLH = 5 cm

Figure 12.7 (continued)

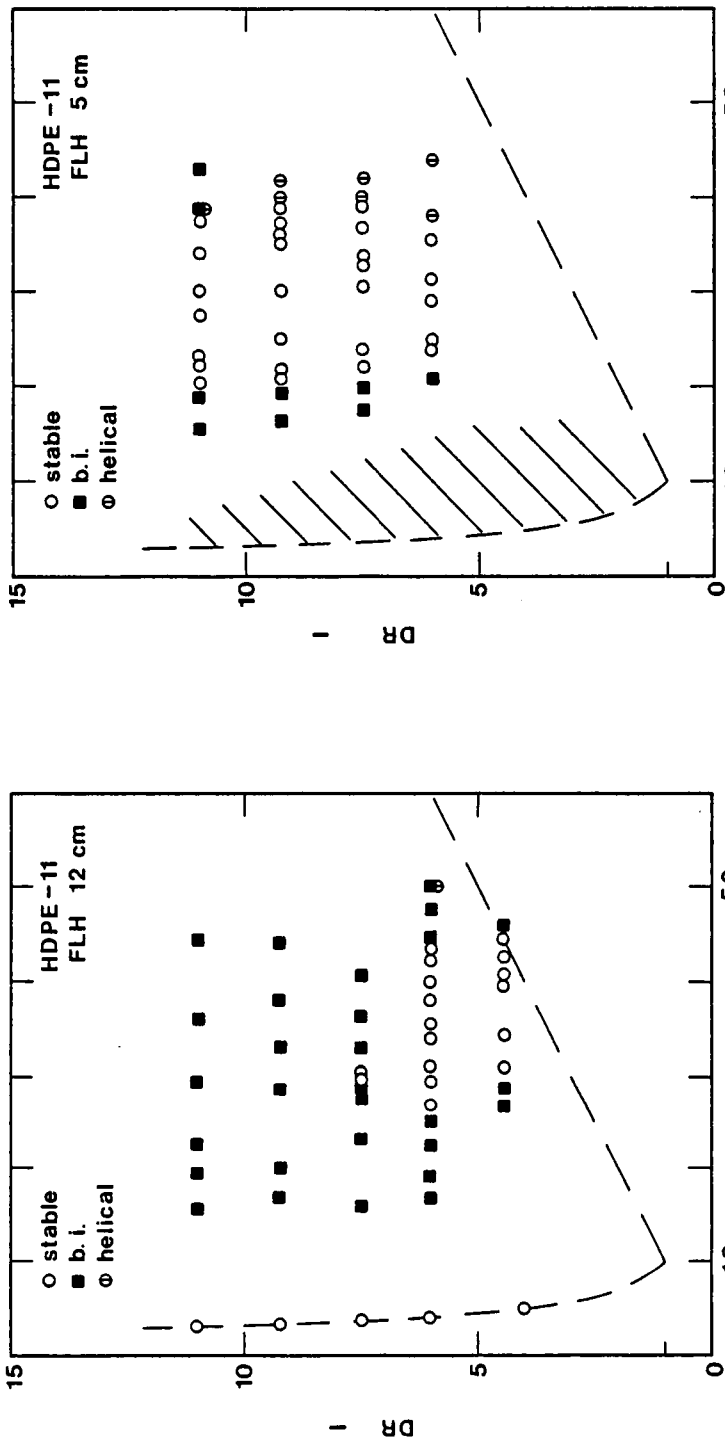

(g) HDPE-11, FLH = 12 cm

(h) HDPE-11, FLH = 5 cm

Figure 12.7 (continued)

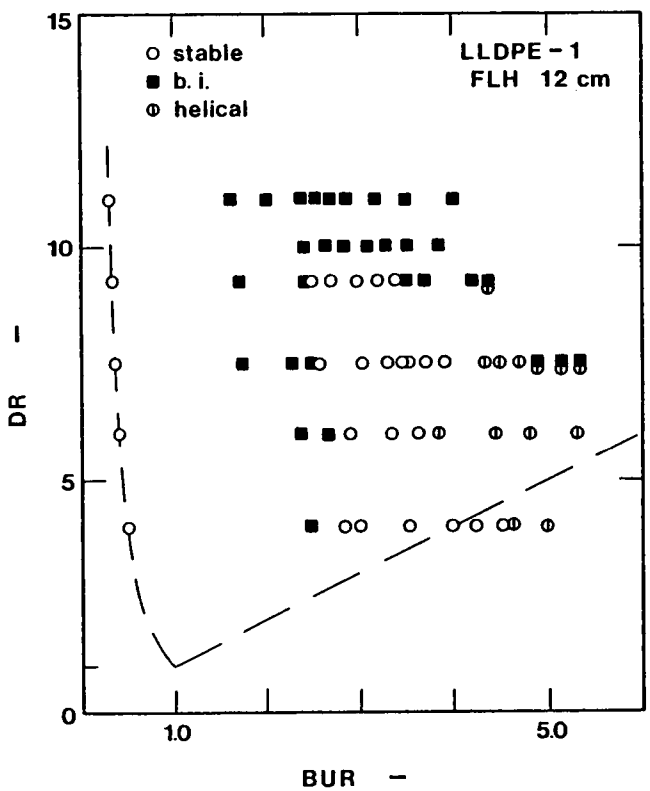

(i) LLDPE-1, FLH = 12 cm

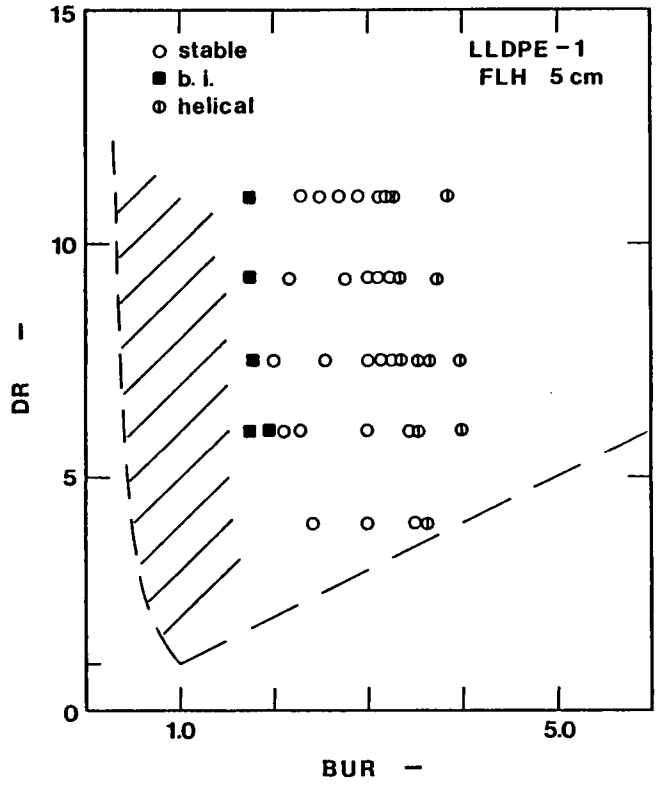

(j) LLDPE-1, FLH = 5 cm

Figure 12.7 (continued)

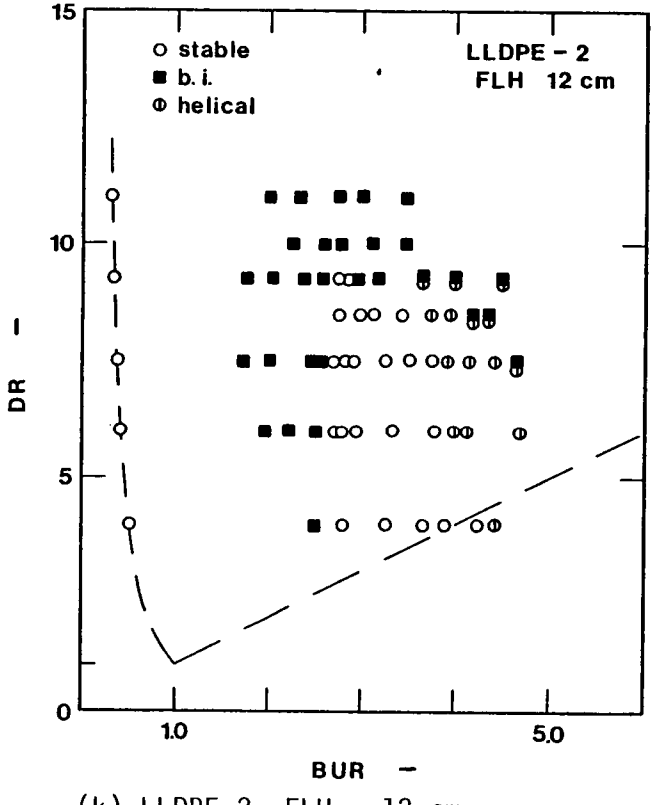

(k) LLDPE-2, FLH = 12 cm

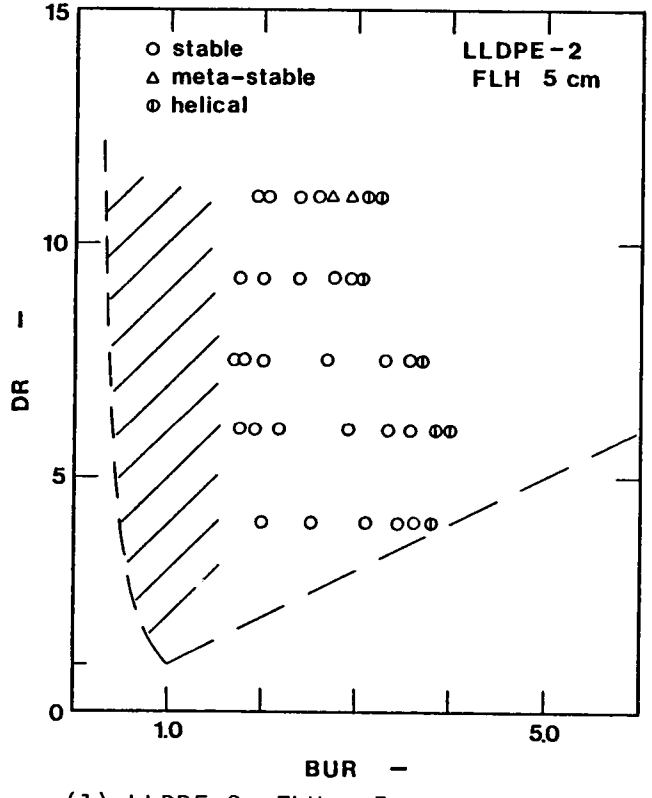

(l) LLDPE-2, FLH = 5 cm

Figure 12.7 (continued)

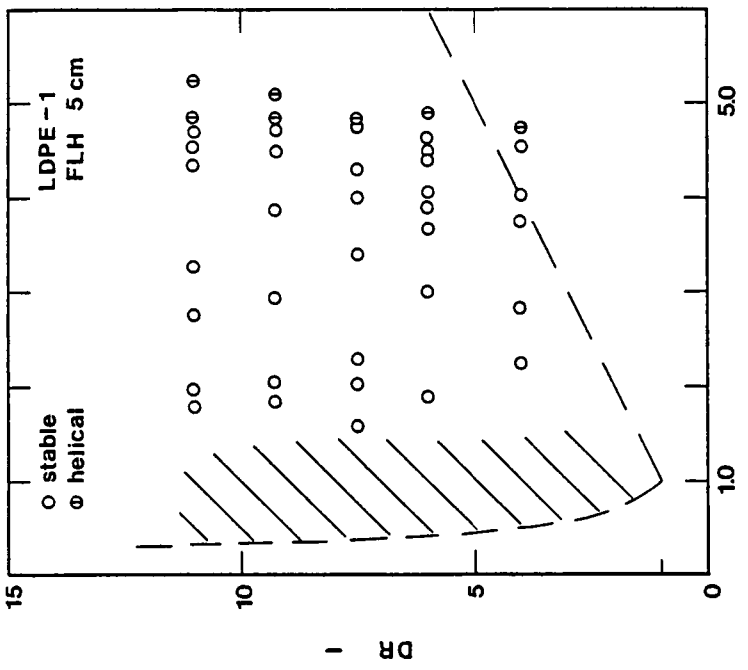

(n) LDPE-1, FLH = 5 cm

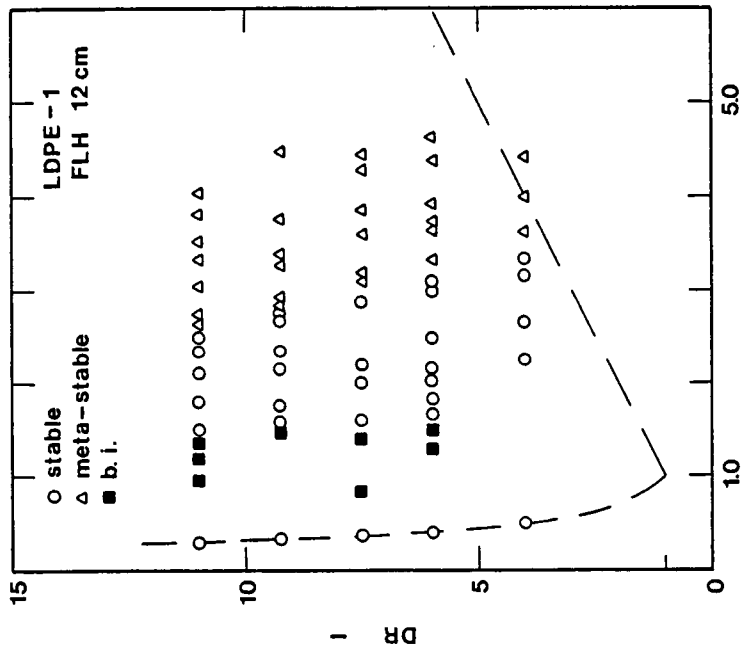

(m) LDPE-1, FLH = 12 cm

Figure 12.7 (continued)

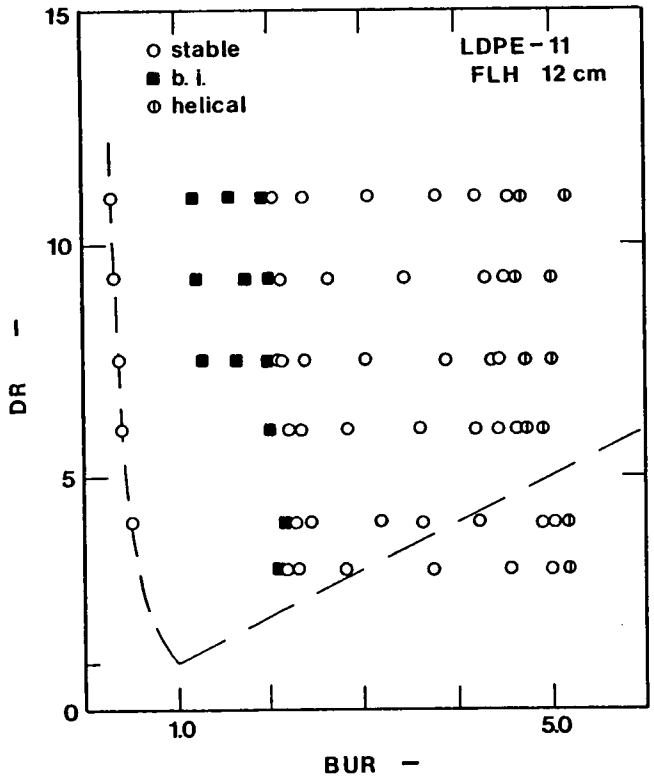

(o) LDPE-11, FLH = 12 cm

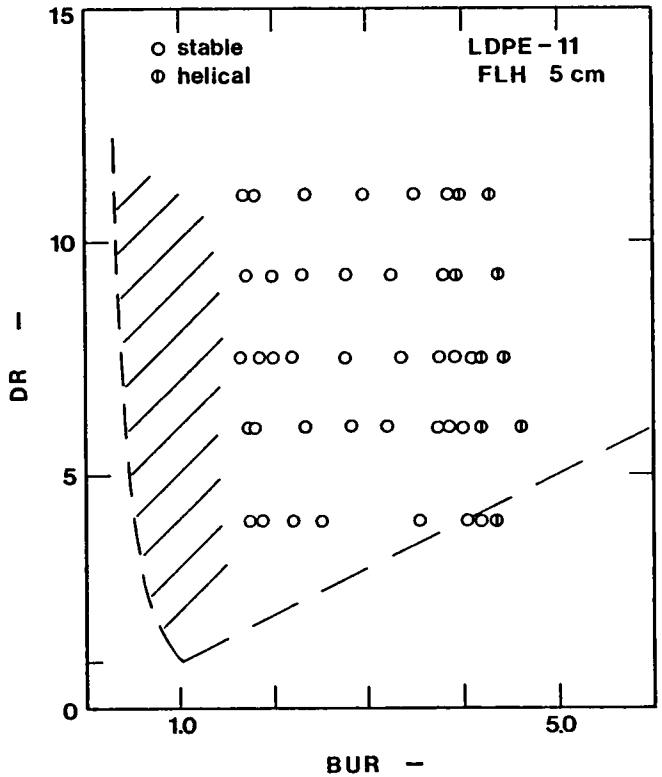

(p) LDPE-11, FLH = 5 cm

Figure 12.7 (continued)

"Unblown" film extrusion (uniaxial stretching of a tube) is always stable under the experimental conditions. Investigated bubble instabilities (unstable behavior) are observed at relatively low BUR, and sometimes continue to higher (BUR x DR) regions. Meta-stable behaviors are observed in only LDPE-1 and LLDPE-2 at larger BUR and higher (BUR x DR) regions. Helical bubble behaviors appear only at high BUR regions.

Generally a shorter FLH makes the stable operating regions expand to lower BUR and higher DR regions; however, the helical bubble regions become broader toward a lower DR. The effects of FLH on the unstable operating regions for HDPE samples are small compared with those for LLDPE and LDPE samples. Meta-stable behaviors only appear LDPE-1 and LLDPE-2 (FLH = 5 cm).

For any sample, bubble instability was observed in the regions between the unblown film extrusion condition and a BUR of less than 2.5; planar extension or near planar extension condition always exhibits bubble instability.

D. INTERPRETATION

The problem of bubble stability was first described in a paper by Han and Park [H-10] and later by Han and Shetty [H-11]. They examined only the effects of applied disturbances (sudden change in take-up speed and the air pressure of bubble) in tubular blown film extrusion. Kanai and White [K-2] examined the effect of operational variables such as DR, BUR, and FLH.

A theoretical stability analysis of instabilities due to axisymmetric disturbances in an isothermal Newtonian fluid has been given by Yeow [Y-9]. Yeow's results are presented in terms of kinematic and dynamic variables, specifically for each input infinitesimal disturbance frequency, the instability occurs at a corresponding value of

$$BUR = R_L/R_0, \quad H = 1/(DR \times BUR), \quad X = FLH/R_0 \ . \tag{12.2}$$

Yeow presents neutral stability curves on plots of H-BUR for specific X. It is not possible to carry out a detailed comparison of this theory with our experimental results, because our system is nonisothermal viscoelastic polymer fluids.

The H-BUR plots for unstable behavior (bubble instability) are in Figures 12.8 and 12.9. Figures 12.8(a) and 12.8(b) are for HDPE samples at FLH = 12 cm and 5 cm, respectively. Figure 12.9 is for LLDPE and LDPE at FLH = 12 cm. LLDPE samples and LLDPE-2 do not show any unstable behavior (bubble instability) at FLH = 5 cm. Figure 12.10 is the H-BUR plots for meta-stable behavior. Figure 12.11(a) and 12.11(b) are the H-BUR plots for helical bubble behavior of HDPE samples at FLH = 12 cm and 5 cm, respectively. Figures 12.12(a) and 12.12(b) are the H-BUR plots for the helical behavior of LLDPE and LDPE samples at FLH = 12 cm and 5 cm, respectively. LDPE-1 does not show any helical bubble shapes at FLH = 12 cm.

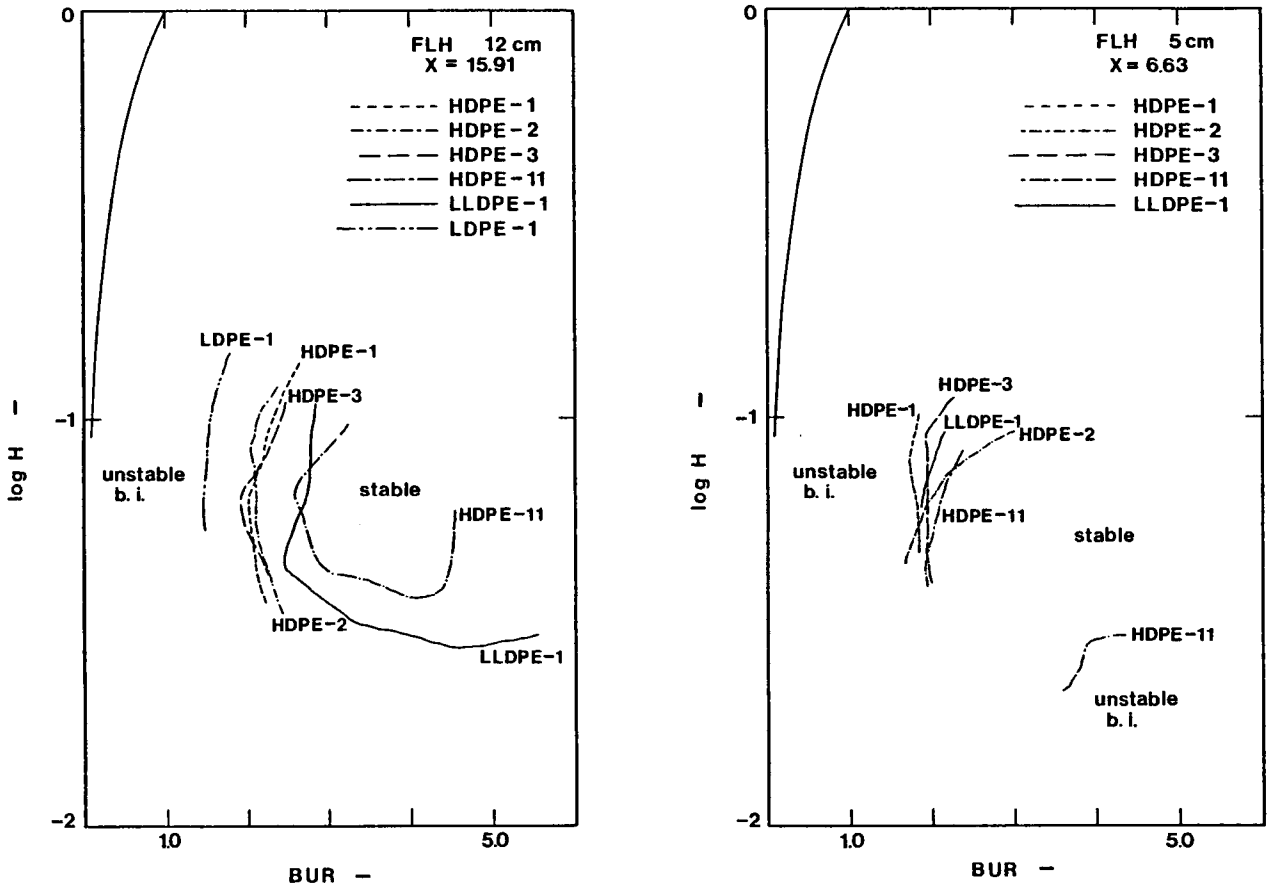

Figure 12.8. Plots of H versus BUR showing regions of stable and bubble instability; HDPE.

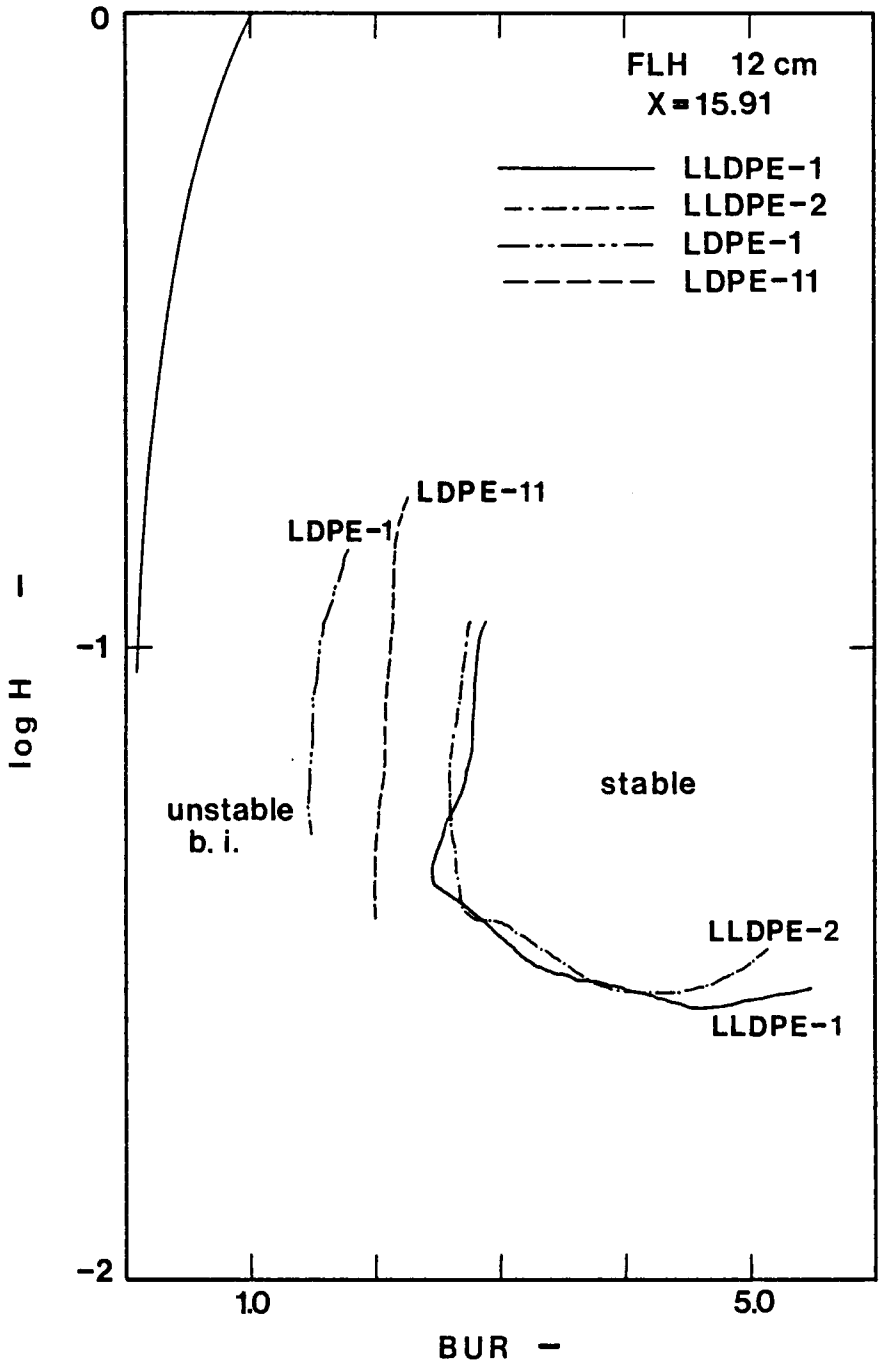

Figure 12.9. Plots of H versus BUR showing regions of stable and bubble instability; LLDPE and LDPE, X = 15.91.

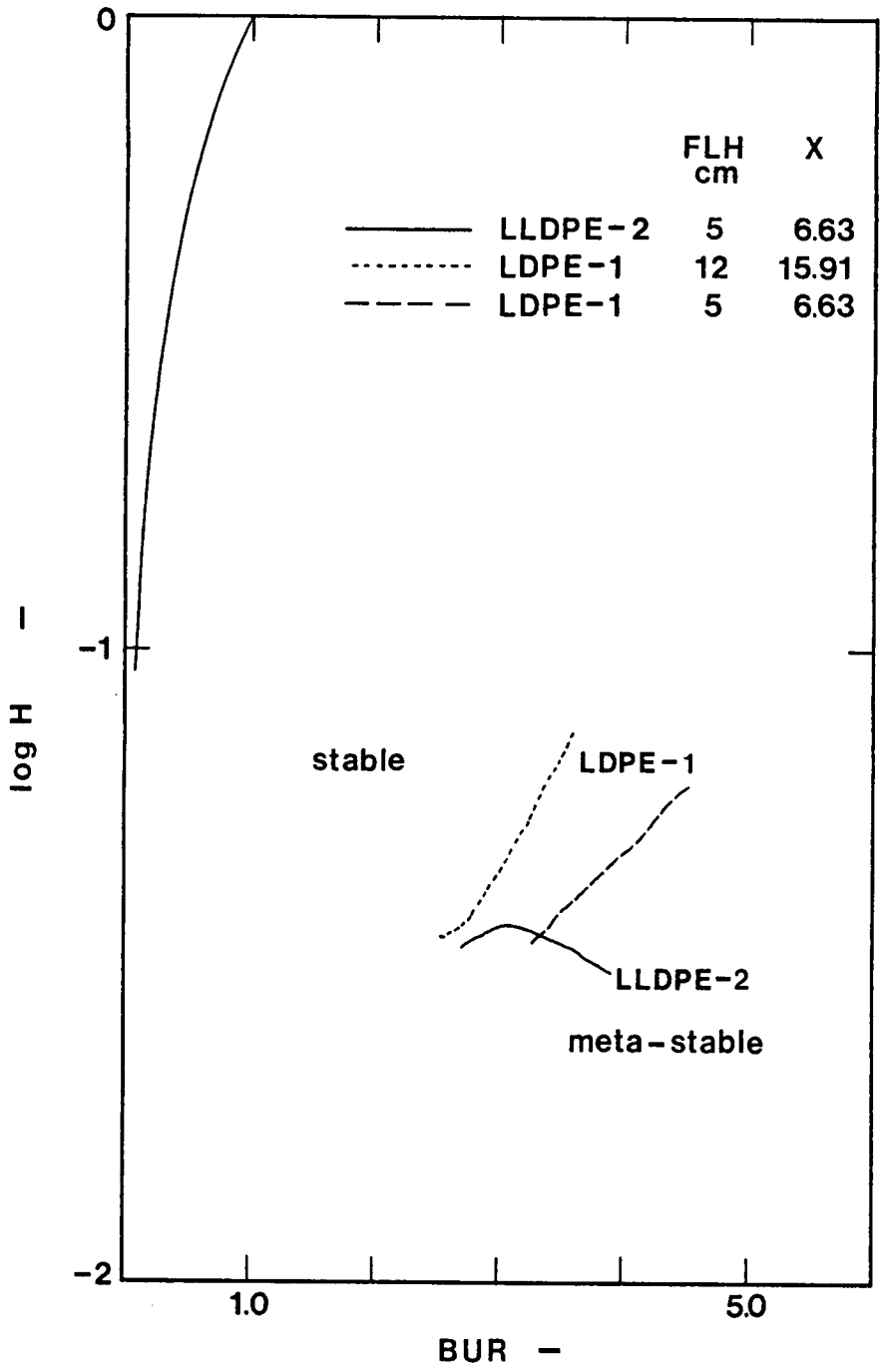

Figure 12.10. Plots of H versus BUR showing regions of stable and meta-stable condition.

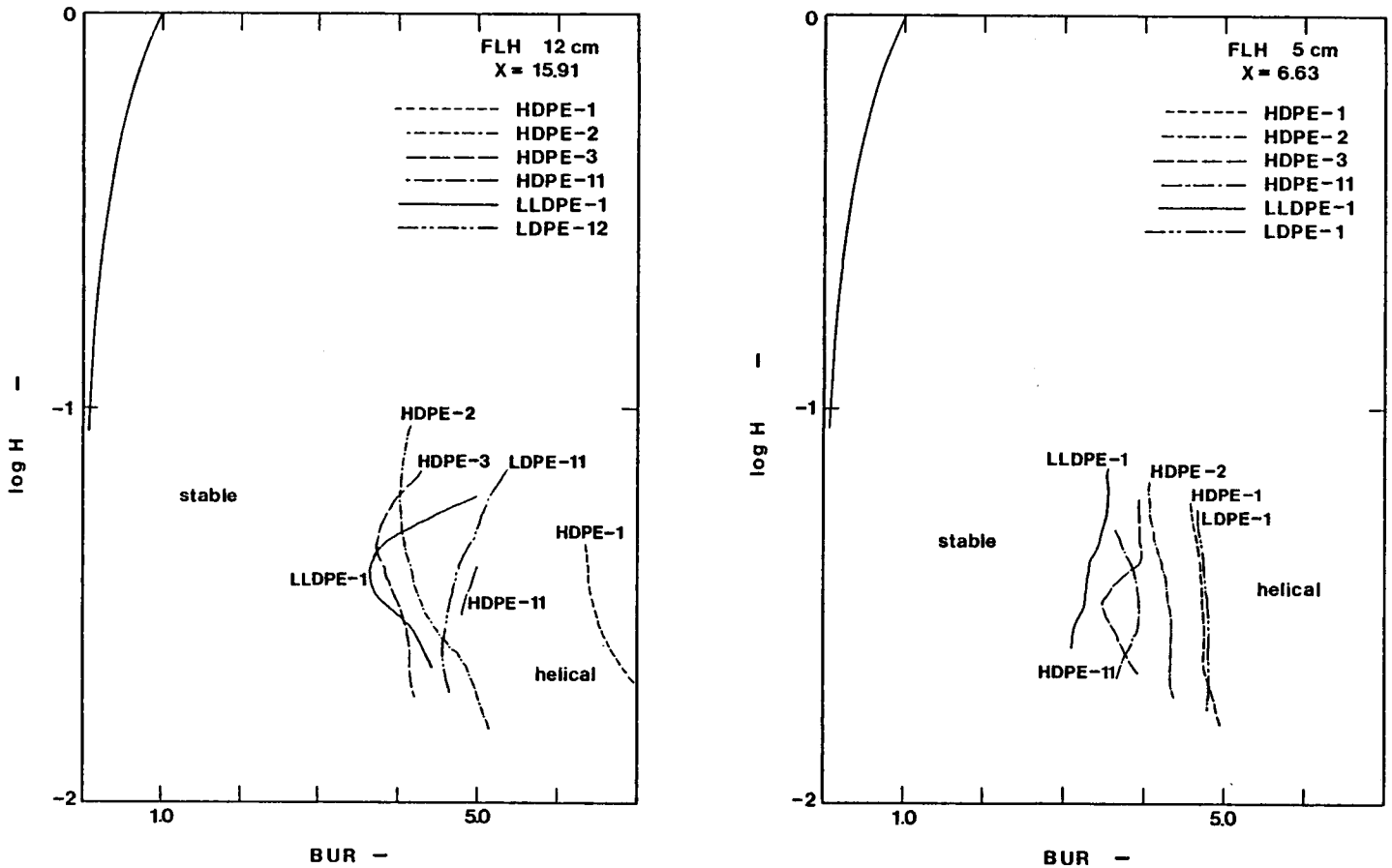

(a) X = 15.91

(b) X = 6.63

Figure 12.11. Plots of H versus BUR showing regions of stable and helical bubble for HDPE.

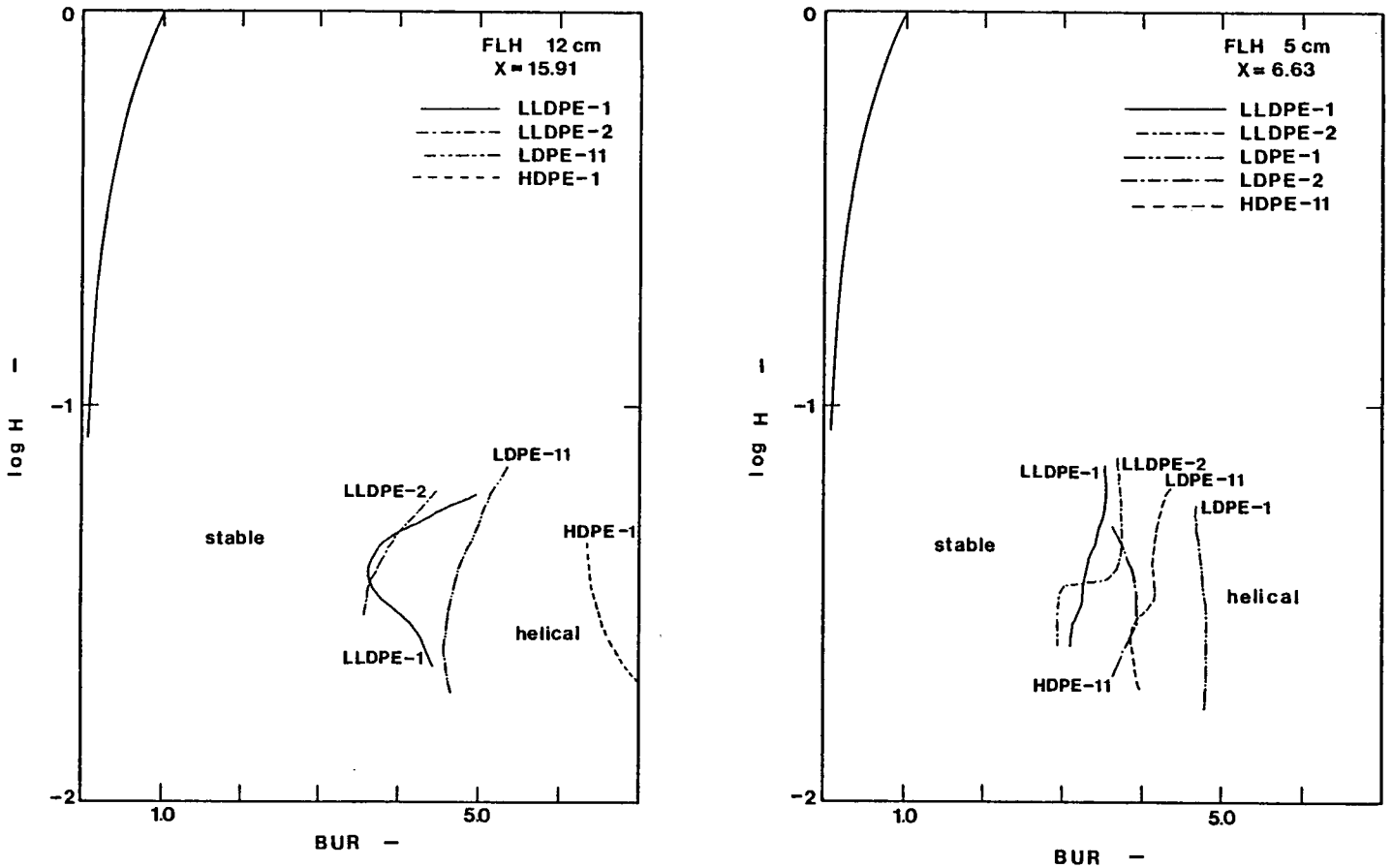

(a) X = 15.91

(b) X = 6.63

Figure 12.12. Plots of H versus BUR showing regions of stable and helical bubble for LLDPE and LDPE.

The general tendency of stability in the H-BUR plots is illustrated in Figure 12.13. The experimental data do not correspond to Yeow's prediction (Figure 12.14(a)). Figure 12.14(b) plots the DR-BUR based upon the Yeow's theoretical prediction of the H-BUR plot [Y-9]. Experimental data on tubular blown film extrusion (Figure 12.14(c)) indicate that a stable operating condition exists above certain BUR and below some DR. The differences between Yeow's theoretical prediction and our experimental data are not surprising, because Yeow's analysis is for an isothermal Newtonian fluid.

It is clear that the stable operating limits (region) (bubble instability vs. stable bubble) at FLH = 12 cm fall in the order:

LDPE - 1 > LDPE - 11 >

moderate and broad MWD HDPE

> LLDPE > narrow MWD HDPE

where MWD indicates molecular weight distribution. The effect of MW (molecular weight) is not clear. At FLH = 5 cm, the stable operating limits (region) fall in the order:

LDPE, LLDPE - 2 > LLDPE - 1, moderate

and broad MWD HDPE > narrow MWD HDPE.

It would be reasonable to describe the differences of bubble stabilities or instabilities of these samples in terms of uniaxial elongational flow behavior.

There are two types of stress build-up. One type, shown by narrow MWD HDPE, LLDPE [K-2], and LDPE of low degree of long chain branching (LCB), exhibits monotonic increasing stress build-up to an

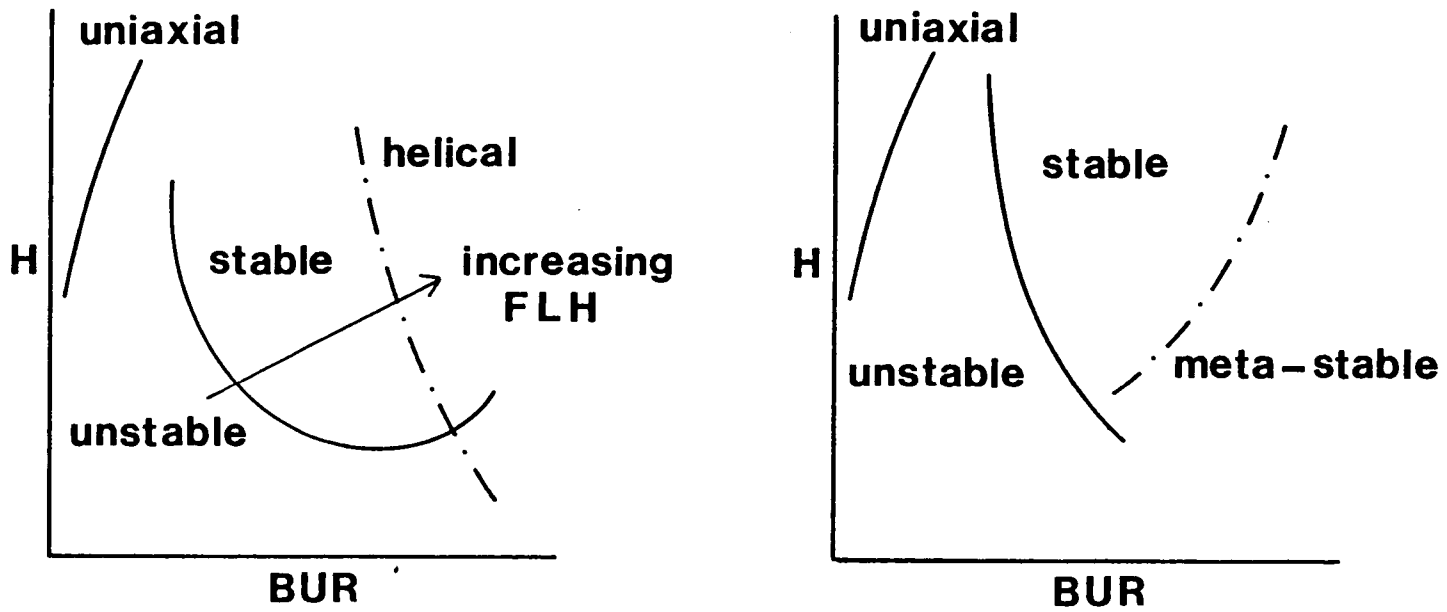

Figure 12.13. Schematic diagram of experimental data on bubble stability: H versus BUR plots.

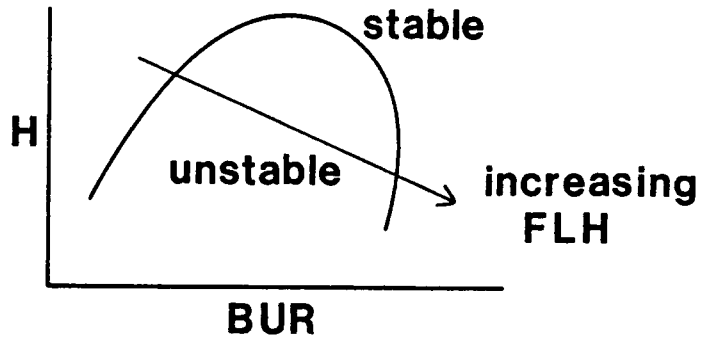

(a) H versus BUR plots of Yeow's theoretical analysis

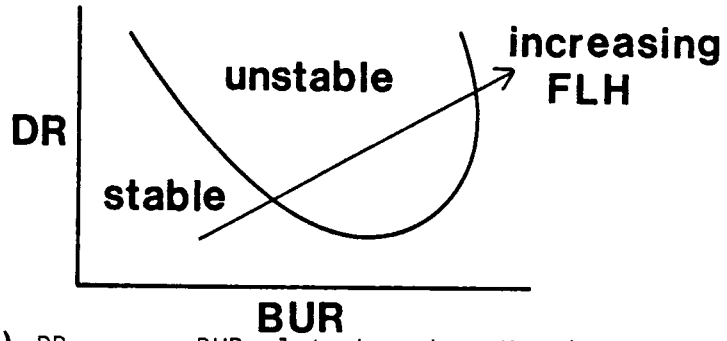

(b) DR versus BUR plots based on Yeow's theoretical analysis

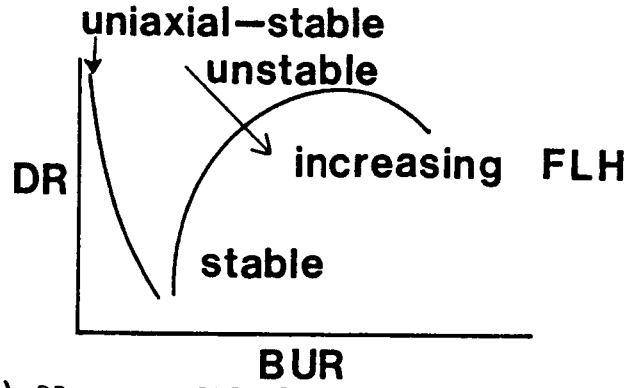

(c) DR versus BUR plots of actual experimental data

Figure 12.14. Yeow's theoretical prediction on bubble stability [Y-3] and comparison with actual experimental data.

asymptotic value; this value is close to three times the zero shear viscosity ($3\eta_0$) at low elongation rate. It shows higher values at higher deformation rate (deformation rate hardening). The other type, shown by HDPE of moderate and broad MWD and by LDPE of high degree of LCB, exhibits a strong strain hardening effect (on log $\chi(E,t)$ - log t plots) after achieving a certain strain level. However, the later type shows two subclassifications. One, shown by moderate and broad MWD HDPE, exhibits the maximum elongational viscosity decrease with increasing elongation rate (deformation rate softening). The other, shown by LDPE with high degree of LCB, exhibits the steady state (or maximum) elongational viscosity increase with increasing elongation rate (deformation rate hardening).

The material (LDPE-1) which exhibits strain hardening and deformation rate hardening is the most stable. The intermediate group (moderate and broad MWD HDPE) exhibits strain hardening but deformation rate softening behavior in uniaxial elongational flow. The most unstable materials (narrow MWD HDPE and LLDPE) show strain softening but deformation rate hardening in uniaxial elongational flow. By lowering FLH, LLDPE becomes relatively stable. By lowering FLH (namely, by increasing the heat transfer or by imposing rapid cooling), LLDPE becomes relatively stable.

It might be useful if we interpret the above discussion in terms of viscoelastic fluid mechanics using a convected Maxwell (White-Metzner) model. There are two dimensionless groups which determine the characteristics of the system. These are the Weissenberg number

(having to do with elasticity) and the Yamamoto number (having to do with the deformation rate dependency of the relaxation time) [W-20]. Here, relaxation time is taken as

$$\tau = \frac{\tau_0}{1 + a\,\tau_0\,II_d^{1/2}}\,, \tag{12.3}$$

where II_d is the second invariant of deformation rate tensor and "a" is a so-called Yamamoto number. This functional form was suggested by Bogue in connection with an integral formulation [B-12].

Values of the Weissenberg number and "a" in Eqn. (12.3) are shown in Table XII-1 including molecular weight distribution, degree of long chain branching, and flow activation energy. The Weissenberg number is defined as

$$N_{w_s} = \tau_0\, v_0/L\,, \tag{12.4}$$

where v_0 is the average melt velocity at the die exit and L is the distance between the frost line and the die exit. Values of τ_0 and "a" were obtained based on shear flow measurements at 180°C (see Chapter IV) (variation of temperature along the machine direction was not considered). Bubble instability is considered to be a function of the Weissenberg number, the "a" value and the heat transfer (more specifically the flow activation energy). We may roughly state that the material (or system) which has a larger N_{w_s}, or a smaller "a" value, or a higher flow activation energy has a

Table XII-1. Weissenberg Number, "a" Value, and Molecular Characterization Data

Polymer	Weissenberg Number FLH = 12 cm	Weissenberg Number FLH = 5 cm	"a"	M_w/M_n	M_z/M_w	Degree of Long Chain Branching* per 10^3 C Atoms	Flow Activation Energy Kcal/mole
HDPE-1	2.47	5.93	0.55	9.65	6.36	--	--
HDPE-2	1.71	4.11	0.6	14.11	8.29	0.011	7.40***
HDPE-3	0.132	0.317	0.6	7.10	7.84	0.010	7.32***
HDPE-11	0.0371	0.0891	0.1	3.36	2.97	--	--
LLDPE-1	0.0725	0.174	0.3	3.81	--	less than 0.1	--
LLDPE-2	0.0561	0.135	0.35	3.36	--	less than 0.1	11.1**
LDPE-1	0.367	0.881	0.25	11.19	--	3.4	--
LDPE-11	0.118	0.283	0.3	4.11	--	1.6	16.1**

*See Tables III-1, III-2, and III-3.

**Data from Kanai and White [K-3].

***Data are supplied to us from Mr. Wekman [W-9].

wider operating region. However, the functionality of these parameters on bubble instability is not known.

Previously we interpreted bubble instability in terms of uniaxial elongational flow behavior. "Strain hardening" behavior is responsible for a large value of τ_0 (which leads to a larger Weissenberg number) and "deformation rate softening" behavior is responsible for a large value of "a", and conversely, "deformation rate hardening" behavior is caused by a small value of "a".

Meta-stable behavior appears only in LDPE-1 (FLH = 12 and 5 cm) and LLDPE-2 (FLH = 5 cm). In these materials, stable operation was possible at lower FLH and at the same DR and BUR. The FLH was gradually increased from the stable operating condition by adjusting the cooling air. After reaching a certain FLH, the bubble tended to exhibit passage between two stable states. The cause is not known; however, heat transfer processes must certainly play a role.

HDPE-1 and LDPE-1 have the strongest resistance for helical bubble behavior. However, there is not any tendency to exhibit helical bubble behavior among the other polymers. Increasing FLH inhibits the helical bubble behavior. A helical stream line of cooling air around inflating tube could be the cause of this phenomenon. The maximum BUR of commercial tubular blow film extrusion is less than 4.0. Therefore, the helical bubble behavior may not be so important as other instabilities (bubble instability and meta-stable behavior).

Our experimental data on stability of tubular blown film extrusion are very confusing, if we try to correlate with rheological

properties of these polymers. In uniaxial stretching (including uniaxial elongational flow and melt spinning), the deformation rate softening character dominates the stability of the system [M-41,W-17] (see Chapters IV and XI). This may be due to the complex elongational flow fields of tubular blown film extrusion (see Kanai and White [K-2]) and highly nonisothermal processing conditions.

It is necessary to investigate the change of dynamics and kinematics in tubular film extrusion by gradually changing the operational variables toward the unsteady conditions from the stable operating conditions. This will give a more complete picture of the behavior of bubbles.

E. SUMMARY

An experimental study was carried out to investigate the effects of rheological properties and molecular structure on unstable flow behavior in tubular film extrusion. High density, linear low density, and low density polyethylenes were used. Four types of unsteady state behavior are observed. These are: (i) a draw resonance-type of instabilities in unblown film extrusion; (ii) a draw resonance-type of (wavy diameter fluctuation); (iii) meta-stable behavior; and (iv) helical bubble behavior in tubular blown film extrusion. Regions of stability and instability are described and discussed in connection with the rheological properties of polymer melts. Attention is given to uniaxial elongational flow behavior. The existence of strain hardening and deformation rate hardening gives a system more stable operating regions.

CHAPTER XIII

NON-ISOTHERMAL CONSTITUTIVE EQUATION: DIFFERENTIAL TYPE

A. INTRODUCTION

Almost all polymer processing operations involve the cooling of a polymer, during or after deformation and shaping, from the molten state to the solid state. In order to make a complete model of a polymer processing operation, we should have a constitutive relation of polymer melts which includes the effects of temperature change.

In most mathematical modeling of polymer processing the rheological responses are handled by simply assuming temperature dependent (and sometimes deformation rate dependent) viscous fluids. Examples of this kind of mathematical modeling are the melt spinning analysis of Kase and Matsuo [K-2,K-7,K-8], Ziabicki and Kedzierska [Z-5,Z-7], Yasuda, Sugiyama and Yanagawa [Y-6], and Toriumi, Konda and Shimizu [T-6], the models of tubular blown film extrusion process of Han and Park [H-9], Petrie [P-8], Wagner [W-1] and Kanai and White [K-3], and the modeling of injection molding, as summarized by White [W-12]. These simple viscous fluids models seem to work in many cases. However, it is not clear that neglecting elastic effects (memory effects) can be done in general.

Efforts to develop a constitutive equation for viscoelastic fluids which account for the histories of temperature and deformation

have been made by various researchers. A more general perspective is suggested by the time-temperature superposition behavior observed in small strain viscoelastic behavior [F-2,W-24]. This approach was formalized by Morland and Lee [M-44] in terms of the linear viscoelasticity theory, and by Bernstein, Kearsley and Zapas [B-9] in terms of a non-equilibrium thermodynamics to describe a viscoelastic fluid of finite deformation. From the view of continuum mechanics, a series of papers by Crochet and Naghdi [C-25,C-26] present the most general non-isothermal theory based upon Coleman's thermodynamics of simple materials [C-21]. A specific non-linear formulation of integral type was developed by Matsui and Bogue [M-14] and Matsumoto and Bogue [M-15]. It was used to represent the rheological behavior of molten polystyrene in experiments with programmed temperature fields. They proposed a constitutive equation of form similar to the model of Carreau [C-3] except relaxation time varies according to temperature changes. A similar constitutive equation, where the relaxation time was assumed to be deformation independent, was also proposed by Wagner [W-2]. Marrucci [M-5] has approached this problem using the elastic dumbbell (bead-spring) model for a dilute polymer solution and derived a differential type constitutive equation. A slightly different form of Marrucci's equation has been derived by Gupta and Metzner [G-12] using the flexible dumbbell model for a dilute polymer solution. A convected Maxwell model with free volume dependent relaxation time was applied by La Mantia [L-1] to represent the rheological behavior of molten polyisobutylene under heating.

Applications to the mathematical modeling of polymer processing operations of these non-isothermal viscoelastic fluids are very few. Marrucci's model was applied to the melt spinning analysis by Fisher and Denn [F-6]. Matsui and Bogue's model has been used for the injection molding process by Dietz and White [D-8] and for a tubular blown film extrusion process by Wagner [W-2]. Less sophisticated approaches for the modeling have been carried out by Matsui and Bogue [M-13] for a melt spinning process and Gupta and Metzner [G-13] for a tubular blown film extrusion process using their own proposed non-isothermal constitutive equations. In both cases, the calculated stress distribution based on the actual measured temperature profiles were compared with experimentally determined stress profiles.

In the mathematical modeling of polymer processing operations, three conservation equations such as the force balance, the continuity or mass balance, and the energy balance have to be coupled with a rheological equation which can represent the material behavior of viscoelastic fluids undergoing both deformation and temperature change. The three conservation equations are often expressed in differential forms, so that for most of the cases, the differential type is more convenient to solve (in connection with conservation equations) than is the integral type. It is also possible to carry out stability analyses of processing operations using differential types but not integral types.

It is our object here to develop a differential type non-isothermal constitutive equation using a phenomenological approach.

B. ISOTHERMAL VISCOELASTIC THEORY

The total stress is usually divided into two parts for convenience:

$$\underset{\sim}{\sigma} = -p\underset{\sim}{I} + \underset{\sim}{P} , \tag{13.1}$$

where p is an isotropic pressure and $\underset{\sim}{P}$ is the extra stress tensor associated with deformation. When a fluid is in the static condition, i.e., $\underset{\sim}{P}$ being zero, p is identified as the hydrostatic pressure. In a dynamic situation for incompressible fluid p should be considered as a scalar value to be determined by boundary conditions.

The historical development of viscoelastic constitutive models begins with Maxwell's equation [M-17].

$$P + \tau \frac{dP}{dt} = G\,\tau \frac{d\gamma}{dt}, \quad G\tau = \eta \tag{13.2}$$

where P is the stress, γ the strain, G the elastic modulus, and τ denotes the relaxation time. This is the simplest viscoelastic fluid model in one dimensional linear form.

The first generalization of Eqn. (13.2) which is independent of the coordinate system and valid for large deformation was given by Zaremba [Z-1]. He considered an embedded coordinate system which translates and rotates with a material point (i.e., corotational coordinates). Zaremba's theory predicts non-Newtonian viscosity and normal stresses in simple shear flow. Oldroyd [O-6] considered a coordinate system which translates, rotates, and deforms with the fluid which he termed a convected coordinate system. In succeeding

years other generalizations were described by various researchers [N-4,S-25,S-26,W-18,W-24]. The expression developed by White and Metzner [W-19] is the simplest but still describes many important features of nonlinear viscoelasticity. This is written as

$$\underset{\sim}{P} + \tau \frac{\delta \underset{\sim}{P}}{\delta t} = 2G\tau \underset{\sim}{d}, \quad \eta = G\tau \tag{13.3}$$

where $\underset{\sim}{d}$ is the deformation rate tensor, $\delta(\ )/\delta t$ is Oldroyd's contravariant convected derivative, and relaxation time τ is a function of the second invariant of the deformation rate tensor.

Integral theories are based on Boltzmann's superposition principle [B-14] which represents the stress response to a series infinitesimal strains

$$\underset{\sim}{P}(t) = \sum_i G^{\dagger}(t-t_i)\Delta\gamma = \int_{-\infty}^{t} G^{\dagger}(t-t') \frac{d\underset{\sim}{\gamma}}{dt} dt' , \tag{13.4}$$

where $G^{\dagger}(t-t')$ is a time dependent elastic modulus, γ is strain, and t' is past time (the variable of integration). With an exponential form for $G(t-t')$ the Boltzmann's equation can be a solution to the differential equation for the Maxwell model. The expansion of the Boltzmann's equation to large deformation has been discussed by Oldroyd [O-6], Lodge [L-7], Yamanoto [Y-3,Y-4,Y-5], Lodge [L-8], and Green and Rivlin [G-11], respectively. Most of the integral type constitutive equations have the form

$$\underset{\sim}{P}(t-t') = \int_{-\infty}^{t} [m_1(t-t')\underset{\sim}{c}^{-1}(t-t') + m_2(t-t')\underset{\sim}{c}(t-t')]dt' , \tag{13.5}$$

where $m_1(t-t')$ and $m_2(t-t')$ are memory functions, and $\underset{\sim}{c}^{-1}$ and $\underset{\sim}{c}$ are the relative Finger and Cauchy deformation tensors, respectively. The memory functions for Eqn. (13.5) (for example, m_1) may be expressed in terms of a discrete spectrum of the form

$$m_1(t-t') = \sum_i \frac{G_i}{\tau_i} \exp[-(t-t')/\tau_i] \ , \tag{13.6}$$

where G_i are the elastic moduli, τ_i are the relaxation times.

There exists a large literature dealing with deformation dependent (nonlinear) memory functions within the framework of Eqns. (13.5) and (13.6). The memory functions are expanded to be dependent upon the invariants of $\underset{\sim}{c}^{-1}$, $\underset{\sim}{c}$, $\underset{\sim}{d}$ or $\underset{\sim}{P}$ by various researchers. In general, the memory function of m_1 of most of these constitutive equations may be written in terms of a discrete spectrum of the form

$$m_1(t-t') = \sum_i \frac{G_i}{\tau_i \ f_i} \exp\left(- \int_{-t'}^{t} \frac{dt''}{\tau_i \ g_i}\right) \ . \tag{13.7}$$

Here f_i and g_i are functions of tensor invariants at time t' and t" ($t' \leq t'' \leq t$) and indicate the change of relaxation intensity and relaxation times due to deformation, respectively.

C. NON-ISOTHERMAL CONSTITUTIVE EQUATION: DIFFERENTIAL TYPE

Time and temperature are closely related variables which have been recognized for many years. Leaderman [L-5] first stated explicitly the temperature superposition principle which allows one

to normalize experiments carried out at different rates (or times) and temperature. For example, the relaxation moduli at different temperatures can be superposed by shifting the times in logarithmic scale. Later Ferry [F-2] generalized the change of modulus with temperature for viscoelastic fluid, after the similar work by Tobolsky and Andrews [T-5] with vulcanized rubbers. Time-temperature superposition has been widely used and applied, even when we lack convincing molecular theory.

In summary, the "vertical" shift of modulus G and the "horizontal" shift of the time constant τ can be expressed by the following equations, where the subscript "0" denotes a reference state:

$$\frac{\tau(T)}{\tau_0} = \frac{a_T(T)}{a_{T_0}} , \tag{13.8}$$

and

$$\frac{G(T)}{G_0} = \frac{\rho T}{\rho_0 T_0} . \tag{13.9}$$

The shift factor $a_T(T)$ is usually correlated with an equation due to Williams, Landrel, and Ferry [W-25] which has the form

$$\log a_T(T) = \frac{-C_1(T-T_0)}{C_2+T-T_0} . \tag{13.10}$$

In the present work, we use the same ideas applied by Matsui and Bogue [M-14] in developing their integral type of non-isothermal constitutive equation. However, our intention is to develop a differential type.

The stress field of Eqn. (13.1), which is expressed in a fixed space coordinate, can be written in terms of a convected coordinate system*

$$\pi^{\alpha\beta} = -p\,\gamma^{\alpha\beta} + \pi'^{\alpha\beta} \ , \tag{13.11}$$

where $\pi^{\alpha\beta}$ and $\pi'^{\alpha\beta}$ are total stress and extra stress, respectively, and $\gamma^{\alpha\beta}$ is the conjugate metric tensor.

Boltzmann's superposition equation of Eqn. (13.4) may also be expressed in terms of a convected coordinate:

$$\pi'^{\alpha\beta}(t) = \int_{-\infty}^{t} G^{\dagger}(t-t')\,\frac{d\gamma^{\alpha\beta}}{dt}\,dt' \ . \tag{13.12}$$

The time dependent modulus $G^{\dagger}(t-t')$ can generally be expressed after introducing the time-temperature superposition principle of Eqns. (13.8) and (13.9)

$$G^{\dagger}(t-t') = G_0\,\frac{\rho T}{\rho_0\,T_0}\,\phi\left[\frac{t-t'}{\tau(T)}\right] = G_0\,\frac{\rho T}{\rho_0\,T_0}\,\phi\left[\frac{t-t'}{a_T(T)\tau_0}\right] \ , \tag{13.13}$$

where ϕ is an aribtrary function of time but with the requirement

$$\phi(t' = t) = 1.0, \quad \phi(t' = -\infty) = 0 \ . \tag{13.14}$$

---

*Following Oldroyd [0-6], stresses are taken to transform by a contravariant law. In this chapter tensors in a convected coordinate will be expressed by using component notation.

Let us consider the case where the temperature changes stepwise from T_2 to T_1 at time t_1, i.e., the time constant of the material changes $\tau(T_2)$ to $\tau(T_1)$ at time t_1. This temperature change can be translated into a change in time scale by the time-temperature superposition as

$$G^{\dagger}(t-t') = G_0 \frac{\rho_1 T_1}{\rho_0 T_0} \phi\left[\frac{t-t_1}{a_T(T_1)\tau_0} + \frac{t_1-t'}{a_T(T_2)\tau_0}\right], \quad t' < t_1 < t \ . \tag{13.15}$$

If the temperature change is continuous, Eqn. (13.13) leads to

$$G^{\dagger}(t-t') = G_0 \frac{\rho(t)T(t)}{\rho_0 T_0} \phi\left[\lim_{\Delta t \to 0} \sum_{k=1}^{n} \frac{t_k - t_{k+1}}{a_T(T_k)\tau_0}\right] , \tag{13.16a}$$

where

$$t_1 = t, \quad t' = t_n \ . \tag{13.16b}$$

In continuous form

$$G^{\dagger}(t-t') = G_0 \frac{\rho(t)T(t)}{\rho_0 T_0} \phi\left[\int_{t'}^{t} \frac{dt''}{a_T[T(t'')]\tau_0}\right] ,$$

$$= G(t)\ \phi\left[\int_{t'}^{t} \frac{dt''}{\tau[T(t'')]}\right] , \tag{13.17a}$$

where

$$G(t) = G_0 \frac{\rho(t)T(t)}{\rho_0 T_0}, \quad \tau[T(t)] = a_T[T(t)]\tau_0 \ . \tag{13.17b}$$

Substituting Eqn. (13.17) into Eqn. (13.12) yields

$$\pi'^{\alpha\beta}(t) = \int_{-\infty}^{t} G(t)\ \phi\left[\int_{t'}^{t} \frac{dt''}{\tau[T(t'')]}\right] \frac{d\gamma^{\alpha\beta}}{dt'}\, dt' \ . \tag{13.18}$$

Integrating Eqn. (13.18) by parts follows:

$$\pi'^{\alpha\beta}(t) = G(t) \left[\phi\left[\int_{t'}^{t} \frac{dt''}{\tau[T(t'')]}\right] \gamma^{\alpha\beta}(t')\right]_{-\infty}^{t} \quad (\phi \to 0)$$

$$- G(t)\int_{-\infty}^{t} [\gamma^{\alpha\beta}(t') - \gamma^{\alpha\beta}(t)]d\phi\left[\int_{t'}^{t} \frac{dt''}{\tau[T(t'')]}\right] \ . \tag{13.19}$$

In Eqn. (13.19), ϕ is generally assumed to have an exponentially decreasing form that is then to be a solution of the differential equation for the simple Maxwell model. Therefore, Eqn. (13.19) may be expressed as

$$\pi'^{\alpha\beta}(t) = -G(t)\int_{-\infty}^{t} \frac{1}{\tau[T(t')]} \exp\left[-\int_{t'}^{t} \frac{dt''}{\tau[T(t'')]}\right][\gamma^{\alpha\beta}(t') - \gamma^{\alpha\beta}(t)]dt' \ . \tag{13.20}$$

After counting the distribution of time constants, Eqn. (13.20) can be rewritten in terms of a fixed spaced coordinate with neglecting m_2 terms in Eqns. (13.5) and (13.6) as

$$\underset{\sim}{P}(t) = \sum_{n} G_n(t)\int_{-\infty}^{t} \frac{1}{\tau_n[T(t')]} \exp\left[-\int_{t'}^{t} \frac{dt''}{\tau_n[T(t'')]}\right] \underset{\sim}{\zeta}^{-1}(t,t')dt' \ , \tag{13.21a}$$

where

$$\tau_n[T(t)] = a_T[T(t)]\ \tau_{n,0} \ , \tag{13.21b}$$

and

$$G_n(t) = G_{n,0} \frac{\rho(t)T(t)}{\rho_0 T_0} , \qquad (13.21c)$$

with $\tau_{n,0}$ and $G_{n,0}$ designating the time constants and moduli at some reference temperature T_0 at which a_T is unity, respectively, and $\underset{\sim}{c}^{-1}$ is the relative Finger deformation tensor. Eqn. (13.21) is the same integral type non-isothermal constitutive equation which Matsui and Bogue [M-14] has derived. They also assumed that relaxation time is a function of the second invariant of the strain rate tensor.

Eqn. (13.20) is equivalent to

$$\pi'^{\alpha\beta}(t) \exp\left[\int_{-\infty}^{t} \frac{dt'}{\tau[T(t')]}\right] = -G(t) \int_{-\infty}^{t} \exp\left[\int_{-\infty}^{t'} \frac{dt''}{\tau[T(t'')]}\right] \frac{d\gamma^{\alpha\beta}(t')}{dt'} dt' . \qquad (13.22)$$

Differentiating Eqn. (13.22) with respect to present time t using Leibnitz's rule yields

$$\begin{pmatrix}\text{left side of}\\ \text{Eqn. (13.22)}\end{pmatrix} = \exp\left[\int_{-\infty}^{t} \frac{dt'}{\tau[T(t')]}\right]\left(\frac{d\pi'^{\alpha\beta}(t)}{dt} + \frac{\pi'^{\alpha\beta}(t)}{\tau(t)}\right) , \qquad (13.23a)$$

$$\begin{pmatrix}\text{right side of}\\ \text{Eqn. (13.22)}\end{pmatrix} = \pi'^{\alpha\beta}(t) \exp\left[\int_{-\infty}^{t} \frac{dt'}{\tau[T(t')]}\right] \frac{d \ell n\, G(t)}{dt}$$

$$- G(t) \exp\left[\int_{-\infty}^{t} \frac{dt'}{\tau[T(t')]} \frac{d\gamma^{\alpha\beta}(t)}{dt}\right] . \qquad (13.23b)$$

Eqn. (13.23) leads (combine Eqns. (13.23a) and (13.23b)) to

$$\frac{d\,\pi'^{\alpha\beta}}{dt} + \left(\frac{1}{\tau} - \frac{d \ell n\, G(t)}{dt}\right)\pi'^{\alpha\beta} = -G(t) \frac{d\gamma^{\alpha\beta}}{dt} , \qquad (13.24a)$$

or

$$\frac{\pi'^{\alpha\beta}}{\tau} + G(t)\,\frac{d}{dt}\left[\frac{\pi'^{\alpha\beta}}{G(t)}\right] = -G(t)\,\frac{d\gamma^{\alpha\beta}}{dt}\,. \tag{13.24b}$$

In terms of a fixed space coordinate Eqn. (13.24) is expressed (convected derivative for scalar is the same as the material derivative of that scalar):

$$\frac{\delta \underset{\sim}{P}}{\delta t} + \left(\frac{1}{\tau} - \frac{D\ \ell n\ G(T)}{Dt}\right) \underset{\sim}{P} = 2G(T)\ \underset{\sim}{d}\,, \tag{13.25a}$$

or

$$\underset{\sim}{P} + G(T)\tau\,\frac{\delta}{\delta t}\left(\frac{\underset{\sim}{P}}{G(T)}\right) = 2G(T)\,\tau\,\underset{\sim}{d}\,, \tag{13.25b}$$

where

$$G(T) = G_0\,\frac{\rho(T)\ T}{\rho_0\ T_0}\,, \tag{13.25c}$$

and

$$\frac{\delta \underset{\sim}{P}}{\delta t} = \frac{D\underset{\sim}{P}}{Dt} - \nabla\underset{\sim}{v}\cdot\underset{\sim}{P} - \underset{\sim}{P}\cdot\nabla\underset{\sim}{v}\,. \tag{13.25d}$$

If we neglect the density change with temperature, Eqn. (13.25) becomes

$$\frac{\delta \underset{\sim}{P}}{\delta t} + \left(\frac{1}{\tau} - \frac{d\ \ell n\ T}{Dt}\right) \underset{\sim}{P} = 2G\underset{\sim}{d}\,, \tag{13.26a}$$

or

$$\underset{\sim}{P} + G\,\tau\,\frac{\delta}{\delta t}\left(\frac{\underset{\sim}{P}}{G}\right) = 2G\tau\underset{\sim}{d}\,, \tag{13.26b}$$

where

$$G = G_0\,\frac{T(t)}{T_0}\,. \tag{13.26c}$$

Eqn. (13.26) is the identical form of which Marrucci [M-5] has derived from the elastic dumbbell (bead-spring) model for a dilute polymer solution.

Isothermal forms of Eqn. (13.25) or (13.26) cannot predict non-Newtonian shear viscosities nor shear rate dependence on first normal stress difference coefficients. Therefore, it is necessary to expand Eqns. (13.25) and (13.26) to be able to predict this additional nonlinear character. Let us assume that the relaxation intensity and relaxation time changes by deformation with factor of "f" or "g" which are functions of tensor invariants, respectively. The Boltzmann's superposition equation, Eqn. (13.19), may be written

$$\pi'^{\alpha\beta} = -G(t)\int_{-}^{t} \frac{1}{f(t')} [\gamma^{\alpha\beta}(t') - \gamma^{\alpha\beta}(t)]d\phi[\int_{t'}^{t} \frac{dt''}{\tau[T(t'')]g(t'')}] . \tag{13.27}$$

After assuming ϕ being a Maxwell type exponentially decreasing form, Eqn. (13.26) becomes:

$$\pi'^{\alpha\beta}(t) = -G(t)\int_{-\infty}^{t} \frac{1}{\tau[T(t')]f(t')} \exp\left[-\int_{-t'}^{t} \frac{dt''}{\tau[T(t'')]g(t'')}\right] \left[\gamma^{\alpha\beta}(t') - \gamma^{\alpha\beta}(t)\right]dt' . \tag{13.28}$$

After counting the distribution of time constants, Eqn. (13.28) can be rewritten in terms of a fixed spaced coordinate with neglect of the m_2 term in Eqns. (13.5) and (13.6) as

$$\underset{\sim}{P}(t) = \sum_n G_n(t) \int_{-}^{t} \frac{1}{\tau_n[T(t')]f(t')} \exp\left[- \int_{t'}^{t} \frac{dt''}{\tau_n[T(t'')]g(t'')} \right] \underset{\sim}{c}^{-1}(t,t')dt' . \tag{13.29}$$

For an isothermal condition, Eqn. (13.29) can be reduced to Eqn. (13.7).

Eqn. (13.28) leads to

$$\pi'^{\alpha\beta}(t) = -G(t) \int_{-}^{t} \exp\left[- \int_{t'}^{t} \frac{dt''}{\tau[T(t'')]f(t'')} \right] \frac{d}{dt'} \left[\gamma^{\alpha\beta}(t') \frac{g(t')}{f(t')} \right] dt' . \tag{13.30}$$

Differentiating Eqn. (13.30) with respect to "t" gives

$$\frac{d\pi'^{\alpha\beta}}{dt} + \left[\frac{1}{\tau(t)g(t)} - \frac{d \ln G(t)}{dt} \right] \pi'^{\alpha\beta} = -G(t) \frac{d}{dt} \left[\gamma^{\alpha\beta} \frac{g(t)}{f(t)} \right] . \tag{13.31}$$

Eqn. (13.31) leads to

$$\frac{\pi'^{\alpha\beta}}{\tau(t)g(t)} + G(t) \frac{d}{dt} \left[\frac{\pi'^{\alpha\beta}}{G(t)} \right] = -G(t) \frac{g(t)}{f(t)} \frac{d\gamma^{\alpha\beta}}{dt} - \cancel{G(t)\gamma^{\alpha\beta}(t)}^{\,0} \frac{d}{dt} \left[\frac{g(t)}{f(t)} \right] . \tag{13.32}$$

In terms of a fixed space coordinate, Eqn. (13.32) becomes

$$\underset{\sim}{P} + G(T)\tau(t)g(t) \frac{\delta}{\delta t} \left[\frac{\underset{\sim}{P}}{G(T)} \right] = 2G(T)\tau(t) \frac{g^2(t)}{f(t)} \underset{\sim}{d} . \tag{13.33}$$

When f and g are unities, Eqn. (13.33) is equivalent with Eqn. (13.25). As a special case we may assume that

$$g(t) = f(t) = \frac{\tau(II_d)}{\tau(II_d=0)} , \tag{13.34a}$$

when II_d is the second invariant of deformation rate tensor. More specifically, we may choose Bogue's type expression for a deformation dependent relaxation time [M-14,W-20] in the following form:

$$\frac{\tau[II_d(t)]}{\tau[II_d(t)=0]} = \frac{1}{1 + a\,\tau(t)\,II_d(t)^{1/2}} , \tag{13.34b}$$

or

$$\tau(t)g(t) = \frac{a_T[T(t)]\tau_0}{1 + a\,II_d(t)^{1/2}\,a_T[T(t)]\tau_0} . \tag{13.34c}$$

Eqn. (13.33) may be simplified using Eqn. (13.34):

$$\frac{\delta \underset{\sim}{P}}{\delta t} + \left(\frac{1}{\tau g} - \frac{D\,\ell n\,G(T)}{Dt}\right) \underset{\sim}{P} = 2G(T)\underset{\sim}{d} , \tag{13.35a}$$

or

$$\underset{\sim}{P} + G(T)\tau g\,\frac{\delta}{\delta t}\left(\frac{\underset{\sim}{P}}{G(T)}\right) = 2G(T)\tau g\underset{\sim}{d} . \tag{13.35b}$$

Eqns. (13.33) and (13.35) are the generalized White-Metzner type convected Maxwell model including temperature change.

The differential type constitutive equations, Eqns. (13.25) and (13.35), which have been derived based upon the Boltzmann's superposition principle to describe non-isothermal behaviors of viscoelastic fluids are identical to the integral type non-isothermal constitutive equation developed by Matsui and Bogue [M-14]. The developed non-isothermal differential type constitutive equation is purely phenomenological equation, however, Eqn. (13.25) has the same form developed from the elastic dumbbell (bead-spring) model

for a dilute polymer solution by Marrucci [M-5], and special form of Gupta and Metzner's [G-12] where parameter B is taken as zero. However, molecular models used by Marrucci and Gupta and Metzner are essentially for dilute polymer solutions so that there is not any motivation to apply those models to regions where intermolecular forces exist.

It is also possible to include the distribution of time constants in Eqns. (13.25), (13.33), and (13.35) by employing multiple relaxation times and moduli, as applied by Spearot and Metzner [S-24] and Ide [I-1].

The developed constitutive equations indicate the temperature dependence of relaxation time has more dominant effects on the viscoelastic behavior than that of modulus, i.e., the effect of temperature dependent modulus is affected only by natural logarith. The choice of the shift factor a_T for cooling rate has been discussed by Matsumoto and Bogue [M-15] and later by Carey, Wust and Bogue [C-1] in terms of the equilibrium glass transition temperature and a cooling rate dependent glass transition temperature. They argue that the higher cooling rate makes shift factor larger than the slower cooling rate conditions or isothermal conditions even though fluid still remains above the glass transition temperature.

The comparison of these developed constitutive equations with experimental data such as Matsumoto and Bogue's [M-15] will appear elsewhere.

D. SUMMARY

A convected Maxwell model which accounts for the temperature history was developed in a phenomenological way, based upon the Boltzmann superposition method and the time-temperature superposition principle. It was shown that the non-isothermal convected Maxwell model so developed is equivalent to Matsui and Bogue's non-isothermal integral model [M-14].

CHAPTER XIV

CONCLUSIONS AND RECOMMENDATIONS

A. CONCLUSIONS

The influence of the rheological properties of polymer melts on the processing behavior undergoing multiaxial extension (including uniaxial elongation) was investigated both theoretically and experimentally. Major attention was given to the effects of the geometry, conservation equations (such as the continuity and the force balance equation), rheological properties, and molecular structure (such as molecular weight, molecular weight distribution, and degree of long chain branching).

A-1. Studies on Extensional Polymer Processings and Multiaxial Elongational Flows

Various multiaxial elongational flows, including compressive flow, were classified in terms of two individual elongation rates E_1, the strain rate along the machine direction, and E_2, the strain rate along the transverse direction, for various geometries. Elongational viscosities were described for a Newtonian fluid and a convected Maxwell model. It is shown that increasing the lateral stretching (larger E_2/E_1 values) makes the elongational viscosities more deformation rate softening.

The growth of disturbances in sheets and annular cylinders undergoing multiaxial elongational flow was described. The governing

equations (force balance and continuity) were derived for two different disturbances, one along the machine direction and the other along the transverse (or hoop) direction. It was found that the governing equations for flat sheets and annular cylinders were essentially the same. Detailed analyses were given for a Newtonian fluid and an elastic solid undergoing constant stretch rates. Disturbances in the highest strain rate direction dominate the stability of the system. When disturbances are in the machine direction, lateral (or hoop) stretching of sheets decreases the size of the disturbances but at a less rapid rate than the homogeneous decrease in thickness. The elongation-to-break (limiting strain) in the machine direction is actually decreased. However, the relative stretched area at break increases with increasing strain rates in the transverse (or hoop) direction. Disturbances in the transverse (or hoop) direction cause diametrically opposite effects in the disturbance growth and the elongation-to-break on the lateral stretching of sheets.

The growth of disturbances in viscoelastic fluid sheets and Bingham plastic fluid sheets undergoing multiaxial elongation was also analyzed. Linear stability analyses were carried out using a convected Maxwell model with a strain rate dependent relaxation time, which varies according to $\tau = \tau_0/[1 + a\,\tau_0\,(2\,\mathrm{tr}\,\underset{\sim}{d}^2)^{1/2}]$. It is shown that film stability and elongation-to-break depends upon the Weissenberg number $\tau_0 E_1$ (where E_1 is the elongation rate in the machine direction); on the deformation rate softening parameter "a";

and on the multiaxiality factor E_2/E_1 (where E_2 is the strain rate in the transverse direction). In general, an increasing strain rate softening character (i.e., higher E_2/E_1 values or larger "a" values, and also large yield values in the case of a Bingham plastic fluid) decreases elongation-to-break in terms of length in the machine direction (i.e., decreases limiting strain in the machine direction). The limiting strain in the machine direction due to ductile failure has a minimum near $E_2/E_1 = 0$ (planar elongation) for larger "a" or higher $\tau_0 E_1$ conditions; however, larger "a" values are unstable under higher $\tau_0 E_1$ conditions. Material with smaller "a" values are stable under higher $\tau_0 E_1$ conditions; however, larger "a" values are unstable under higher $\tau_0 E_1$ conditions. The elongation-to-break, expressed in terms of area, exhibits a complex dependence upon E_2/E_1, $\tau_0 E_1$, and "a". A cohesive fracture criterion was hypothesized for various values of E_2/E_1, $\tau_0 E_1$, and "a". These results were compared with experiments involving the stretching of melted notched polystyrene sheets.

The stability of continuous film extrusion processes was analyzed and contrasted to melt spinning. The processes included: (1) cast film extrusion; (2) annular film extrusion over a straight cylindrical mandrel; (3) flat film extrusion with tentering frames to achieve a constant ratio of kinematics; (4) flat film extrusion with tentering frames to achieve a linearly varying width along the machine direction; (5) annular film extrusion over a lubricated conical mandrel; (6) annular unblown film extrusion. A detailed

discussion is presented for Newtonian fluids. Generally melt spinning and flat film extrusion (with constant film width) are governed by the same equations in the isothermal case. This is also true for other film processes including annular film extrusion under limited circumstances, notably extrusion over a lubricated straight cylindrical mandrel. Draw resonance observed in melt spinning and film extrusion under similar circumstances should be observed here.

An experimental study of the influence of molecular structure (molecular weight, molecular weight distribution, and degree of long chain branching) on the onset of draw resonance in a series of polyolefins and polystyrenes was carried out. The materials include high density polyethylene, linear low density polyethylene, low density polyethylene, polypropylene and polystyrene. Narrowing the molecular weight distribution and the occurrence of long chain branching stabilize the spinline disturbances. The results are interpreted in terms of viscoelastic mechanics and experimental studies on rheological properties.

An experimental study was also carried out to investigate the effects of rheological properties and molecular structure on unstable flow behavior in tubular film extrusion. High density, linear low density, and low density polyethylenes were used. Four types of unsteady state behaviors are observed. These are: (1) a draw resonance-type of instabilities in unblown film extrusion; (2) bubble instability (wavy diameter fluctuation); (3) meta-stable behavior; and (4) helical bubble behavior in tubular blown film

extrusion. Regions of stability and instability were described and discussed in connection with the rheological properties of polymer melts. Attention is given to uniaxial elongational flow behavior. The existence of strain hardening (which was caused by large τ_0 values) and deformation rate hardening (which was caused by small "a" values) gives a system more stable operating regions.

A convected Maxwell model which accounts for the temperature history was developed in a phenomenological way, based upon the Boltzmann superposition method and time-temperature superposition principle. It was shown that the non-isothermal convected Maxwell model so developed is equivalent to Matsui and Bogue's non-isothermal model.

A-2. Rheological Properties of Polyethylene Melts

An experimental study of steady shear and uniaxial elongational flow rheological properties of a series of high density, linear low density, and low density polyethylene melts of varying molecular weight and distribution and different degree of long chain branching was carried out. Broadening the molecular weight distribution increased the non-Newtonian character of the shear viscosity functions and increased the principal normal stress differences at fixed shear stress. Increasing the degree of long chain branching increased the non-Newtonian character of shear viscosity functions and increased the principal normal stress differences at fixed shear stress. However, the existence of long chain branching in polydisperse systems makes the principal normal stress difference-

shear stress relationship more linear than linear polydisperse systems. Uniaxial elongational flow studies indicated that linear polyethylenes of moderate and broad molecular weight distribution readily fail by neck development; also the elongational viscosity appeared to decrease with increasing elongation rate. For polyethylenes of narrow molecular weight distribution (including low density polyethylenes), the elongational viscosity is an increasing function of elongational rate and never fails. Highly branched low density polyethylene exhibits cohesive fracture at high elongation rate and the elongational viscosity strongly increases with elongation rate. Finally, the implications of these experimental results in developing a constitutive equation was discussed.

B. RECOMMENDATIONS

Several of the most important polymer processing operations involve the deformation of melt streams in the absence of walls result in elongation of polymer melts. This includes uniaxial elongation for melt spinning, but multiaxial elongation for film casting, tubular film extrusion, flat film extrusion with tentering frames, thermoforming, blow molding and stretch blow molding. These processes are operated not only under extensional flow (generally multiaxial elongational flow) but also under non-isothermal conditions. A range of materials, having varying molecular structure and rheological properties, have been used for these processes to produce desired products.

B-1. Rheological Properties of Polymer Melts

The following further studies are recommended:

1. The development of new instruments to measure planar and equal biaxial elongational viscosities under constant strain rate conditions. Orthogonal stagnation flow within a lubricated die method [W-26,A-6,A-7] is the most feasible one.

2. An upgrading of an uniaxial elongational viscometer. This should operate wider elongation rates (either constant elongation rate or constant stress), measure an actual sample diameter in on-line, and eliminate ends effects.

3. The development of a new instrument to measure uniaxial elongational viscosity of low viscosity materials.

4. Further study of cooling effects during various kinds of flows, including multiaxial extension.

5. Experimental studies on rheological properties of linear, star-branched, comb-branched and randomly branched monodispersed hydrogenated polybutadine melts and their blends. This should include not only linear viscoelastic properties but also simple shear and elongational flow properties.

6. The investigation of rheological properties of intermediate polyethylenes. Comparison should be made with other types of polyethylenes including fractionated samples and their blends.

7. The development of a new differential type constitutive equation whose parameters can reflect the molecular structure (such

as molecular weight distribution, degree of long chain branching and short chain branching, and structure of branchings).

B-2. Studies on Polymer Processing Operations

The following further studies are recommended:

1. Experimental and theoretical studies on kinematics, dynamics, heat transfer, and crystallization of film extrusion processes (including tubular film extrusion and melt spinning). The data obtained should be compared in terms of dimensionless operating variables from stable operating conditions toward unsteady state operating conditions.

2. Experimental and theoretical studies of crystallization under elongational flows in not only uniaxial extensional flow but alco complex stretching field. The flow field should be highly nonisothermal.

3. Stability analyses of various continuous film extrusion processes including melt spinning. Emphases should be given for geometrical effects, elasticity (Weissenberg number), deformation rate softening characteristics, and cooling effects.

4. Experimental and theoretical studies on thickness variation of various batch extensional processes (such as blow molding, stretch blow molding and thermoforming).

REFERENCES

REFERENCES

A-1. Abbott, L. E. and J. L. White, Appl. Polym. Symp., 20, 247 (1973).

A-2. Acierno, D., J. N. Dalton, J. M. Rodriguez and J. L. White, J. Appl. Polym. Sci., 15, 2395 (1971).

A-3. Acierno, D. and F. P. La Mantia, J. Non-Newt. Fluid Mech., 4, 99 (1978).

A-4. Acierno, D., F. D. La Mantia and G. Titomanlio, Rheol. Acta, 15, 642 (1976).

A-5. Agrawal, P. K., W. K. Lee, J. M. Lorntson, C. I. Richardson, K. F. Wissbrun and A. B. Metzner, Trans. Soc. Rheol., 21, 355 (1977).

A-6. van Aken, J. A. and H. Janeschitz-Kriegl, Rheol. Acta, 19, 744 (1980).

A-7. van Aken, J. A. and H. Janeschitz-Kriegl, Rheol. Acta, 20, 419 (1981).

A-8. Alfrey, T., SPE Trans., April, 162 (1965).

A-9. Alfrey, T., K. J. Cleereman and W. J. Schrenk, U.S. Patent 3,739,052 (1973).

A-10. Alles, F. P. and K. A. Heilman, U.S. Patent 2,728,941 (1956).

A-11. Anderson, S. L., J. Text. Inst., 49, T53, 1383 (1965).

A-12. Au-Yeung, J. S., C. W. Macosko and V. R. Raju, J. Rheol., 25, 445 (1981).

A-13. Ast, W., Kunststoffe, 63, 427 (1973).

A-14. Ast, W., Kunststoffe, 64, 146 (1974).

A-15. Ast, W., Ph.D. Dissertation, University of Stuttgart (1976).

A-16. Axelson, D. E. and W. C. Knapp, J. Appl. Polym. Sci., 25, 119 (1980).

B-1. Bagley, E. B., Trans. Soc. Rheol., 5, 355 (1961).

B-2. Baily, E. D., Trans. Soc. Rheol., 18, 635 (1974).

B-3. Ballman, R. L., Rheol. Acta, 4, 137 (1965).

B-4. Bankar, V. G., J. E. Spruiell and J. L. White, J. Appl. Polym. Sci., 21, 2135 (1977).

B-5. Bergonzoni, A. and A. J. DiCresce, Polym. Eng. Sci., 6, 45 (1966).

B-6. Bergonzoni, A. and A. J. DiCresce, Polym. Eng. Sci., 6, 50 (1966).

B-7. Bergstrom, C. and E. Avela, J. Appl. Polym. Sci., 23, 163 (1979).

B-8. Bernstein, B., E. A. Kearsley and L. J. Zapas, Trans. Soc. Rheol., 7, 391 (1963).

B-9. Bernstein, B., E. A. Kearsley and L. J. Zapas, J. Res. Nat. Bur. St., B68, 103 (1964).

B-10. Bewley, H., English Patent 10,825 (1845).

B-11. Bird, R. B., O. Hassager, R. C. Armstrong and C. F. Curtiss, "Dynamics of Polymer Liquid: Vol. 1 and Vol. 2," Wiley, New York (1977).

B-12. Bogue, D. C., Ind. Eng. Chem. Fund., 5, 253 (1966).

B-13. Bogue, D. C. and J. L. White, "Engineering Analysis of Non-Newtonian Fluid," NATO Agardograph #144 (1970).

B-14. Boltzmann, L., Sitzungber, Akad. Wiss. Wien., 70, 275 (1874).

B-15. Bovey, F. A., F. C. Schilling, F. L. McCrackin and H. L. Wagner, Macromol., 9, 76 (1976).

B-16. Brooman, R. A., English Patent 10,582 (1845).

B-17. Bueche, W. F., J. Chem. Phys., 20, 1959 (1952).

B-18. Bueche, W. F., J. Polym. Sci., A-2, 5, 1261 (1967).

C-1. Carey, D. A., C. J. Wust and D. C. Bogue, J. Appl. Polym. Sci., 25, 575 (1980).

C-2. Carpenter, W. B., U.S. Patent 237,168 (1881).

C-3. Carreau, P. J., Trans. Soc. Rheol., 16, 99 (1972).

C-4. Cbristman, L. and W. Knappe, Colloid and Polym. Sci., 252, 705 (1974).

C-5. Chan, Y. M., J. L. White and Y. Oyanagi, J. Rheol., 22, 507 (1978).

C-6. Chang, H. and A. S. Lodge, Rheol. Acta, 10, 448 (1971).

C-7. Chang, J. C. and M. M. Denn, J. Non-Newt. Fluid Mech., 5, 369 (1979).

C-8. Chang, J. C., M. M. Denn and F. T. Geyling, I.E.C. Fund., 20, 147 (1981).

C-9. Chatraei, S. H., C. W. Macosko and H. H. Winter, J. Rheol., 25, 433 (1981).

C-10. Chen, I. J. and D. C. Bogue, Trans. Soc. Rheol., 16, 59 (1972).

C-11. Chen, I. J., G. E. Hagler, L. E. Abott, D. C. Bogue and J. L. White, Trans. Soc. Rheol., 16, 473 (1972).

C-12. Chen, C. H., J. L. White, J. E. Spruiell and B. C. Goswami, Textile Res. J., 53, 44 (1983).

C-13. Christensen, R. E., SPE J., 18, 751 (1962).

C-14. Clifford, T. H., M. L. Corser and R. J. Johl, SPE J., 25, November, 53 (1969).

C-15. Cogswell, F. N., Rheol. Acta, 8, 187 (1968).

C-16. Cogswell, F. N., Polym. Eng. Sci., 12, 64 (1972).

C-17. Cogswell, F. N., Trans. Soc. Rheol., 16, 383 (1972).

C-18. Cogswell, F. N., in "Fiber and Yarn Processing," ed. by J. L. White, Appl. Polym. Symp., 27, 1 (1975).

C-19. Cogswell, F. N., J. Non-Newt. Fluid Mech., 4, 23 (1978).

C-20. Cogswell, F. N. and D. R. Moore, Polym. Eng. Sci., 14, 573 (1974).

C-21. Coleman, B. D., Arch. Rat. Mech. Anal., 17, 1 (1964).

C-22. Coleman, B. D. and H. Markovitz, J. Appl. Phys., 35, 1 (1964).

C-23. Coleman, B. D. and W. Noll, Arch. Rat. Mech. Anal., 6, 355 (1960).

C-24. Cox, W. P. and E. H. Merz, J. Polym. Sci., 28, 619 (1958).

C-25. Crochet, M. J., in "Theoretical Rheology," ed. by J. F. Hutton, J. R. A. Pearson, and K. Walters, Applied Science Publishers, London, 111 (1975).

C-26. Crochet, M. J. and P. M. Naghdi, Int. J. Eng. Sci., 10, 775 (1972); Rheol. Acta, 12, 237 (1973); J. de Mecanique, 13, 97 (1974).

C-27. Cudby, M. E. A. and A. Bunn, Polymer, 17, 345 (1976).

C-28. Cutler, D. J., P. J. Hendra, M. E. A. Cudby and H. A. Willis, Polymer, 18, 1005 (1977).

D-1. Dealy, J. M., J. Non-Newt. Fluid Mech., 4, 9 (1978).

D-2. Denn, M. M. and G. Marrucci, A.I. Ch.E.J., 17, 101 (1971).

D-3. Denn, M. M. and G. Marrucci, J. Non-Newt. Fluid Mech., 2, 159 (1977).

D-4. Denn, M. M., C. J. S. Petrie and P. J. Avenas, A.I.Ch.E.J., 21, 791 (1975).

D-5. Denson, C. D. and D. L. Crady, J. Appl. Polym. Sci., 18, 1611 (1974).

D-6. Denson, C. D. and R. J. Gallo, Polym. Eng. Sci., 11, 174 (1971).

D-7. Denson, C. D. and D. C. Hylton, 7th Int. Cong. Rheol., 386 (1976).

D-8. Dietz, W. and J. L. White, Polym. Eng. Sci., 18, 273 (1978).

D-9. Dow Chem. Co., British Patent 656,735.

E-1. Eckert, E. R. G. and R. M. Drake, "Heat and Mass Transfer," McGraw-Hill, New York (1959).

E-2. Everage, A. E., Jr. and R. L. Ballman, J. Appl. Polym. Sci., 20, 1137 (1976).

E-3. Everage, A. E., Jr. and R. L. Ballman, J. Appl. Polym. Sci., 21, 841 (1977).

E-4. Everage, A. E., Jr. and R. L. Ballman, Nature, 273, 213 (1978).

F-1. Farber, R. and J. M. Dealy, Polym. Eng. Sci., 14, 435 (1974).

F-2. Ferry, J. D., J. Amer. Chem. Soc., 72, 3746 (1950).

F-3. Fisher, R. J. and M. M. Denn, Chem. Eng. Sci., 30, 1129 (1975).

F-4. Fisher, R. J. and M. M. Denn, in "Fiber and Yarn Processing," ed. by J. L. White, Appl. Polym. Symp., 27, 103 (1975).

F-5. Fisher, R. J. and M. M. Denn, A.I.Ch.E.J., 22, 237 (1976).

F-6. Fisher, R. J. and M. M. Denn, A.I.Ch.E.J., 23, 23 (1977).

F-7. Flood, J. E., J. L. White and J. F. Fellars, J. Appl. Polym. Sci., 27, 2965 (1982).

F-8. Flugge, W., "Stresses in Shells," Springer-Verlag, Berlin (1960).

F-9. Foster, G. N., Personal Communication (1982).

F-10. Foster, G. N., A. E. Hamielec and T. B. MacRury, ACS Symposium Series 138, 131 (1980).

F-11. Fraser, W. A. and G. S. Cieloszyk, U.S. Patent 4,243,619 (1981).

F-12. Fraser, W. A., L. S. Scarola and M. Concha, TAPPI Paper Synthetics Course Proceedings, 237 (1980).

F-13. Fredrickson, A. G., "Principles and Applications of Rheology," Prentice-Hall, Englewood Cliffs (1964).

F-14. Freeman, H. I. and M. J. Coplan, J. Appl. Polym. Sci., 8, 2389 (1964).

F-15. Fujiki, T., J. Appl. Polym. Sci., 13, 233 (1969).

F-16. Fujiki, T. and M. Rokudai, J. Rheol., Japan, 6, 146 (1978).

F-17. Fujimoto, T., H. Narukawa and M. Nagasawa, Macromol., 3, 57 (1970).

F-18. Fujimoto, T., H. Kajiura, M. Hirose and M. Nagasawa, Polym. J., 3, 181 (1972).

F-19. Fujiyama, M., Y. Kagiyama, K. Shikata and K. Azuma, Zairyo, Japan, 21, 445 (1975).

F-20. Fukuda, K., Seni Gakkaishi, Japan, 22, 53 (1966).

F-21. Fuller, E. D., U.S. Patent 2,461,975 (1949).

F-22. Furuta, I., V. M. Lobe and J. L. White, J. Non-Newt. Fluid Mech., 1, 207 (1976).

G-1. Gelder, D., Ind. Eng. Chem. Fund., 10, 534 (1971).

G-2. George, H. H., Polym. Eng. Sci., 22, 292 (1982).

G-3. Gerow, M. R., U. S. Patent 2,720,680 (1955).

G-4. Geyling, F. T., Bell System Tech. J., 55, 1011 (1976).

G-5. Ghijsels, A. and J. J. S. M. Ente, "Rheology, Proc. 8th Int. Rheol. Cong.," 3, 15, ed. by G. Astarita, G. Marrucci and L. Nicolais, Plenum, London (1980).

G-6. Graessley, W. W., J. Chem. Phys., 43, 2696 (1965).

G-7. Graessley, W. W., J. Chem. Phys., 54, 5143 (1971).

G-8. Graessley, W. W., Advances in Polym. Sci., Vol. 16, Springer-Verlag, Berlin (1974).

G-9. Graessley, W. W., T. Masuda, J. E. L. Roovers and N. Hadjichristidis, Macromol., 9, 127 (1976).

G-10. Graessley, W. W. and L. Segal, Macromol., 2, 49 (1969).

G-11. Green, A. E. and R. S. Rivlin, Arch. Rat. Mech. Anal., 1, 1 (1957).

G-12. Gupta, R. K. and A. B. Metzner, J. Rheol., 26, 181 (1982).

G-13. Gupta, R. K. and A. B. Metzner, Polym. Eng. Sci., 22, 172 (1982).

G-14. Gutteridge, P. A., J. Non-Newt. Fluid Mech., 4, 73 (1978).

H-1. Hadjichristidis, N. and J. E. L. Roovers, J. Polym. Sci., Polym. Phys. Ed., 12, 2521 (1974).

H-2. Hamana, I., M. Matsui and S. Kato, Meilland Textilber, 5, 382 (1969).

H-3. Han, C. D., "Rheology in Polymer Processing," Academic Press, New York (1976).

H-4. Han, C. D. and S. M. Apte, J. Appl. Polym. Sci., 24, 61 (1979).

H-5. Han, C. D. and T. H. Kwack, Private Communication (1982).

H-6. Han, C. D. and Y. M. Kim, J. Appl. Polym. Sci., 20, 1555 (1976).

H-7. Han, C. D. and R. R. Lamonte, Trans. Soc. Rheol., 16, 447 (1972).

H-8. Han, C. D. and J. Y. Park, J. Appl. Polym. Sci., 19, 3257 (1975).

H-9. Han, C. D. and J. Y. Park, J. Appl. Polym. Sci., 19, 3277 (1975).

H-10. Han, C. D. and J. Y. Park, J. Appl. Polym. Sci., 19, 3291 (1975).

H-11. Han, C. D. and R. Shetty, Ind. Eng. Chem. Fund., 16, 49 (1977).

H-12. Han, C. D., K. V. Kim, N. Siskovic and C. R. Huang, Rheol. Acta, 14, 533 (1975).

H-13. Han, C. D., R. R. Lamonte and Y. T. Shah, J. Appl. Polym. Sci., 16, 3307 (1972).

H-14. Hoffmann, W. D., G. Eckhardt, E. Brauer and F. Keller, Acta Polym., 31, 233 (1980).

H-15. Hogan, J. P., C. T. Levett and R. T. Werkman, SPE J., 23, November, 87 (1967).

H-16. Hohenemser, K. and W. Prager, ZFAMM, 12, 216 (1932).

H-17. Howard, J. B. and M. M. Gilroy, SPE J., 24, January, 68 (1968).

H-18. Hyun, J. C., A.I.Ch.E.J., 24, 418 (1978).

H-19. Hyun, J. C., A.I.Ch.E.J., 24, 423 (1978).

H-20. Hyun, J. C. and R. L. Ballman, J. Rheol., 22, 349 (1978).

I-1. Ide, Y., Ph.D. Dissertation, The University of Tennessee, Knoxville (1976).

I-2. Ide, Y. and J. L. White, J. Appl. Polym. Sci., 20, 2511 (1976).

I-3. Ide, Y. and J. L. White, J. Non-Newt. Fluid Mech., 2, 281 (1977).

I-4. Ide, Y. and J. L. White, J. Appl. Polym. Sci., 22, 1061 (1978).

I-5. Ishida, N., I. Shiga and K. Sakamoto, Kobunshi Kagaku, Japan, 28, 834 (1971).

I-6. Ishihara, H. and S. Kase, J. Appl. Polym. Sci., 20, 167 (1976).

I-7. Ishizuka, O. and K. Koyama, Polymer, 21, 164 (1980).

I-8. Ishizuka, O. and K. Koyama, Polymer, 21, 691 (1980).

I-9. Isono, Y., T. Fujimoto, H. Inagaki, M. Shishido and M. Nagasawa, Polym. J., 12, 131 (1980).

I-10. Iwakura, K., M. Yoshinari and T. Fujimura, J. Rheol., Japan, 3, 134 (1975).

J-1. Joye, D. D., G. W. Poehlein and C. D. Denson, Trans. Soc. Rheol., 16, 421 (1972).

J-2. Joye, D. D., G. W. Poehlein and C. D. Denson, Trans. Soc. Rheol., 17, 287 (1973).

K-1. Kajiura, H., Y. Ushiyama, T. Fujimoto and M. Nagasawa, Macromol., 11, 894 (1978).

K-2. Kanai, T. and J. L. White, "Kinematics, Dynamics and Stability of Tubular Film Extrusion of Various Polyethylenes," PATRA Report #203 (1983).

K-3. Kanai, T. and J. L. White, unpublished research.

K-4. Kase, S., J. Appl. Polym. Sci., 18, 3267 (1974).

K-5. Kase, S., J. Appl. Polym. Sci., 18, 3279 (1974).

K-6. Kase, S. and T. Matsuo, J. Polym. Sci., A3, 2541 (1965).

K-7. Kase, S. and T. Matsuo, Sen-i Gakkaish. 18, 188 (1965).

K-8. Kase, S. and T. Matsuo, J. Appl. Polym. Sci., 11, 251 (1967).

K-9. Kase, S., T. Matsuo and Y. Yoshimoto, Sen-i-Kikai Gakaishi, Japan, 19, T63 (1966).

K-10. Kataoka, T. and S. Ueda, J. Appl. Polym. Sci., 12, 939 (1968).

K-11. King, R. G., Rheol. Acta, 5, 35 (1966).

K-12. Kobayashi, S. and K. Murata, Kogyo-Kagaku, Japan, 74, 641 (1970).

K-13. Koyama, K. and O. Ishizuka, Sen-i Gakkaishi, Japan, 36, T472 (1980).

K-14. Koyama, K, and O. Ishizuka, Sen-i Gakkaishi, Japan, 37, T258 (1981).

K-15. Koyama, K. and O. Ishizuka, Sen-i Gakkaishi, Japan, 38, T239 (1982).

K-16. Kumazaki, M., I. Shiga and A. Hashimoto, J. Rheol., Japan, 3, 97 (1975).

K-17. Kume, K., M. Takahashi, T. Masuda and S. Onogi, J. Rheol., Japan, 8, 18 (1980).

K-18. Kuraus, G. and T. Gruver, J. Polym. Sci., A3, 105 (1965).

L-1. La Mantia, F. P., Rheol. Acta, 16, 302 (1977).

L-2. Lamonte, R. R. and C. D. Han, J. Appl. Polym. Sci., 16, 3285 (1972).

L-3. Laun, H. M. and H. Munstedt, Rheol. Acta, 15, 517 (1976).

L-4. Laun, H. M. and H. Munstedt, Rheol. Acta, 17, 415 (1978).

L-5. Leaderman, H., Text. Res., 11, 171 (1941).

L-6. Lobe, V. M. and J. L. White, Polym. Eng. Sci., 19, 617 (1979).

L-7. Lodge, A. S., Proc. 2nd Int. Rheol. Cong., 229 (1952).

L-8. Lodge, A. S., Trans. Faraday Soc., 52, 120 (1956).

L-9. Lodge, A. S., "Elastic Liquid," Academic Press, New York (1964).

L-10. Love, A. E. H., "A Treatise of the Mathematical Theory of Elasticity," 4th ed., Cambridge Univ. Press (1927).

M-1. Macosko, C. W. and J. M. Lorntson, SPE ANTEC Tech. Papers, 22, 461 (1973).

M-2. Macosco, C. W., Rheol. Acta, 13, 814 (1974).

M-3. Maerker, J. M. and W. R. Schowalter, Rheol. Acta, 13, 627 (1974).

M-4. Martin, R. C., U.S. Patent 2,328,827 (1943).

M-5. Marrucci, G., Trans. Sco. Rheol., 16, 321 (1972).

M-6. Masuda, T., K. Kitagawa and S. Onogi, Macromol., 3, 116 (1970).

M-7. Masuda, T., Y. Ohta and S. Onogi, Macromol., 4, 763 (1971).

M-8. Masuda, T., M. Takahashi and S. Onogi, Appl. Polym. Symp., 20, 49 (1973).

M-9. Masuda, T., Y. Nakagawa, Y. Ohta and S. Onogi, Polym. J., 3, 92 (1972).

M-10. Masuda, T., Y. Ohta, M. Kitamura, Y. Saito, K. Kato and S. Onogi, Macromol., 14, 354 (1981).

M-11. Matovich, M. and J. R. A. Pearson, Ind. Eng. Chem. Fund., 8, 512 (1969).

M-12. Matsui, M., Trans. Soc. Rheol., 20, 465 (1976).

M-13. Matsui, M. and D. C. Bogue, Polym. Eng. Sci., 16, 735 (1976).

M-14. Matsui, T. and D. C. Bogue, Trans. Soc. Rheol., 21, 133 (1977).

M-15. Matsumoto, T. and D. C. Bogue, Trans. Soc. Rheol., 21, 453 (1977).

M-16. Matsumoto, T. and C. C. Bogue, Polym. Eng. Sci., 18, 564 (1978).

M-17. Maxwell, J. C., Phil. Trans. Roy. Soc., 157, 249 (1866).

M-18. Meissner, J., Rheol. Acta, 8, 78 (1969).

M-19. Meissner, J., Trans. Soc. Rheol., 13, 123 (1969).

M-20. Meissner, J., Rheol. Acta, 10, 230 (1971).

M-21. Meissner, J., Trans. Soc. Rheol., 16, 405 (1972).

M-22. Meissner, J., Pure and Appl. Chem., 42, 553 (1975).

M-23. Meissner, J., T. Raible and S. E. Stephenson, J. Rheol., 25, 1 (1981).

M-24. Meissner, J., S. E. Stephenson, A. Demarmels and P. Portmann, J. Non-Newt. Fluid Mech., 11, 221 (1982).

M-25. Mendelson, R. A. and F. L. Finger, J. Appl. Polym. Sci., 17, 797 (1973).

M-26. Mendelson, R. A. and F. L. Finger, J. Appl. Polym. Sci., 19, 1061 (1975).

M-27. Mendelson, R. A., W. A. Bowles and F. L. Finger, J. Polym. Sci., A2, 8, 105 (1970).

M-28. Mendelson, R. A., F. L. Finger and E. B. Bagley, J. Polym. Sci., Part C, 35, 177 (1971).

M-29. Menges, G. and W. Predohl, Plastverarbeiter, 21, 433 (1970).

M-30. Menges, G. and W. Predohl, Plastverarbeiter, 23, 388 (1972).

M-31. Menges, G. and W. Predohl, Polym. Eng. Sci., 15, 394 (1975).

M-32. Mewis, J. and A. B. Metzner, J. Fluid Mech., 62, 593 (1974).

M-33. Middleman, S., "The Flow of High Polymers," Wiley, New York (1968).

M-34. Middleman, S., Trans. Soc. Rheol., 13, 123 (1969).

M-35. Middleman, S., "Fundamental of Polymer Processing," McGraw-Hill, New York (1977).

M-36. Mieras, H. J. M. A. and C. F. H. van Rijn, Nature, 218, 865 (1968).

M-37. Mills, N. J., European Polym. J., 5, 675 (1969).

M-38. Mills, N. J. and A. Nevin, J. Polym. Sci., A2, 9, 267 (1971).

M-39. Miltz, J. and A. Ram, Polym. Eng. Sci., 13, 273 (1973).

M-40. Minoshima, W., M.S. Thesis, The University of Tennessee, Knoxville (1978).

M-41. Minoshima, W., J. L. White and J. E. Spruiell, J. Appl. Polym. Sci., 25, 287 (1980).

M-42. Minoshima, W., J. L. White and J. E. Spruiell, Polym. Eng. Sci., 20, 1166 (1980).

M-43. von Mises, R., Gottiger Nachrichten, Math.-Phys. Klasse, 582 (1913).

M-44. Morland, L. W. and E. H. Lee, Trans. Soc. Rheol., 4, 233 (1960).

M-45. Munstedt, H., Rheol. Acta, 14, 1077 (1975).

M-46. Munstedt, H., J. Rheol., 23, 421 (1979).

M-47. Munstedt, H., J. Rheol., 24, 847 (1980).

M-48. Munstedt, H. and H. M. Laun, Rheol. Acta, 18, 492 (1979).

M-49. Munstedt, H. and H. M. Laun, Rheol. Acta, 20, 211 (1981).

N-1. Nam, S., Ph.D. Dissertation, The University of Tennessee Knoxville (1982).

N-2. Nam, S. and D. C. Bogue, "The Dynamics of Steady and Unsteady Melt Spinning," PATRA Report #187 (1983).

N-3. Nemoto, N., Polym. J., 1, 485 (1970).

N-4. Noll, W., Rat. Mech. Anal., 4, 13 (1955).

N-5. Noordermer, J. W. M., O. Kramer, F. H. M. Nestler, J. L. Schrag and J. D. Ferry, Macromol., 8, 539 (1975).

O-1. Oda, K., J. L. White and E. S. Clark, Polym. Eng. Sci., 18, 25 (1978).

O-2. Ohta, Y., M. Kitamura, T. Masuda and S. Onogi, Polym. J., 13, 859 (1981).

O-3. Okumura, M., T. Nishikawa and N. Nishikawa, U.S. Patent 3,649,611 (1972).

O-4. Oldroyd, J. G., Proc. Camb. Phil. Soc., 43, 100 (1947).

O-5. Oldroyd, J. G., Proc. Camb. Phil. Soc., 43, 383 (1947).

O-6. Oldroyd, J. G., Proc. Roy. Soc. (London), A, 200, 523 (1950).

O-7. Onogi, S., T. Masuda and K. Kitagawa, Macromol., 3, 109 (1970).

P-1. Pearson, J. R. A., "Mechanical Principles of Polymer Melt Processing," Pergamon Press, Oxford (1966).

P-2. Pearson, J. R. A. and M. A. Matovich, Ind. Eng. Chem. Fund., 8, 605 (1969).

P-3. Pearson, J. R. A. and C. J. S. Petrie, J. Fluid Mech., 40, 1 (1970).

P-4. Pearson, J. R. A. and C. J. S. Petrie, J. Fluid Mech., 42, 609 (1970).

P-5. Pearson, J. R. A. and C. J. Petrie, Plastics and Polymers, April, 85 (1970).

P-6. Pedersen, S. and A. Ram, Polym. Eng. Sci., 18, 990 (1978).

P-7. Petrie, C. J. S., Rheol. Acta, 12, 92 (1973).

P-8. Petrie, C. J. S., A.I.Ch.E.J., 21, 275 (1975).

P-9. Petrie, C. J. S., J. Non-Newt. Fluid Mech., 2, 221 (1977).

P-10. Petrie, C. J. S., J. Non-Newt. Fluid Mech., 4, 137 (1978).

P-11. Petrie, C. J. S., "Elongational Flows," Pittman, London, (1979).

P-12. Petrie, C. J. S. and M. M. Denn, A.I.Ch.E.J., 22, 209 (1976).

P-13. Prest, W. W., Jr., J. Polym. Sci., A-2, 8, 1897 (1970).

P-14. Prichard, J. H. and K. F. Wissbrun, J. Appl. Polym. Sci., 13, 233 (1969).

R-1. Racin, R. and D. C. Bogue, J. Rheol., 23, 263 (1979).

R-2. Raible, T., A. Demarmeis and J. Meissner, Polym. Bulletin, 1, 397 (1979).

R-3. Raju, V. R. and W. W. Graessley, J. Polym. Sci., Polym. Phys. Ed., 17, 1223 (1979).

R-4. Raju, V. R., G. G. Smith, G. Marin, J. R. Knox and W. W. Graessley, J. Polym. Sci., Polym. Phys. Ed., 17, 1183 (1979).

R-5. Reiner, M. and A. M. Freudenthal, Proc. 5th Inter. Cong. Appl. Mech., 228 (1938).

R-6. Rhi-Sausi, J. and J. Dealy, Polym. Eng. Sci., 21, 227 (1981).

R-7. Rivlin, R. S. and D. W. Saunders, Phil. Trans. Roy. Soc., 243A, 251 (1951).

R-8. Rochefort, W. E., G. G. Smith, H. Rachapudy, V. R. Raju and W. W. Graessley, J. Polym. Sci., Polym. Phys. Ed., 17, 1197 (1979).

R-9. Rokudai, M., J. Appl. Polym. Sci., 23, 463 (1979).

R-10. Rokudai, M., J. Rheol., Japan, 8, 161 (1980).

R-11. Rokudai, M., J. Appl. Polym. Sci., 26, 1427 (1981).

R-12. Rokudai, M. and T. Fujiki, J. Appl. Polym. Sci., 23, 3295 (1979).

R-13. Rokudai, M., S. Mihara and T. Fujiki, J. Appl. Polym. Sci., 23, 3289 (1979).

R-14. Ronca, G., Rheol. Acta, 15, 149 (1976).

R-15. Ronca, G., Rheol. Acta, 15, 628 (1976).

S-1. Sabia, R. W. R., J. Appl. Polym. Sci., 7, 347 (1963).

S-2. Saeda, S., T. Suzuki and K. Yamaguchi, Zairyo, Japan, 20, 621 (1971).

S-3. Saeda, S., J. Yotsuyanagi and K. Yamaguchi, J. Appl. Polym. Sci., 15, 277 (1971).

S-4. Sakamoto, K. and R. S. Porter, Polym. Lett., 8, 177 (1970).

S-5. Sano, Y. and K. Orii, Seni Gakkaishi, Japan, 24, 212 (1968).

S-6. Schaul, J. S., M. J. Hannon and K. F. Wissburn, Trans. Soc. Rheol. 19, 351 (1975).

S-7. Schenk, B. H., U.S. Patent 2,461,976 (1949).

S-8. Schreiber, H. P. and E. B. Bagley, J. Polym. Sci., 58, 29 (1962).

S-9. Schwartz, S. S. and S. H. Goodman, "Plastics Materials and Processes," Van Nostrand Reinhold Co., New York (1982).

S-10. Sebastian, D. H. and J. R. Dearborn, SPE ANTEC Tech. Papers, 40, 66 (1982).

S-11. Shah, Y. T. and J. R. A. Pearson, Ind. Eng. Chem. Fund., 11, 145 (1972).

S-12. Shah, Y. T. and J. R. A. Pearson, Ind. Eng. Chem. Fund., 11, 150 (1972).

S-13. Shah, Y. T. and J. R. A. Pearson, Polym. Eng. Sci., 16, 219 (1972).

S-14. Shah, Y. T. and J. R. A. Pearson, Trans. Soc. Rheol., 16, 519 (1972).

S-15. Shiga, I., N. Ishida, J. Hashimoto and K. Sakamoto, Kobunshi Kagaku, Japan, 28, 839 (1971).

S-16. Shirayama, K. and S. Kita, Kohbunshi Kagaku, Japan, 28, 307 (1971).

S-17. Shirayama, K. and T. Okada, Kohbunshi Kagaku, Japan, 28, 325 (1971).

S-18. Shirayama, K., S. Kita and M. Kakugo, Kohbunshi Kagaku, Japan, 28, 312 (1971).

S-19. Shirayama, K., T. Okada and S. Kita, J. Polym. Sci., A3, 907 (1965).

S-20. Shroff, R. N. and M. Shida, J. Polym. Sci., A2, 8, 1917 (1970).

S-21. Shroff, R. N. and M. Shida, Polym. Eng. Sci., 11, 200 (1970).

S-22. Shroff, R. N. and M. Shida, Trans. Sco. Rheol., 21, 327 (1977).

S-23. Shroff, R. N., L. V. Cancio and M. Shida, Trans. Soc. Rheol., 21, 429 (1977).

S-24. Spearot, J. A. and A. B. Metzner, Trans. Soc. Rheol., 16, 495 (1972).

S-25. Spriggs, T. W., Chem. Eng. Sci., 20, 931 (1965).

S-26. Spriggs, T. W. and R. B. Bird, Ind. Chem. Fund., 4, 182 (1964).

S-27. Stephenson, S. E. and J. Meissner, "Rheology, Proc. 8th Int. Rheol. Cong," Vol. 2, 431, ed. by G. Astarita, G. Marrucci, and L. Nicolais, Plenum, London (1980).

S-28. Stevenson, J. F., A.I.Ch.E.J., 18, 540 (1972).

S-29. Stevenson, J. F., S. C-K. Chung and J. T. Jenkins, Trans. Sco. Rheol., 19, 397 (1975).

S-30. Suetsugu, Y. and J. L. White, "The Influence of Particle Size and Surface Coating of Calcium Carbonate on the Rheological Properties of Its Suspensions in Molten Polystyrene," PATRA Report #186 (1982).

S-31. Swerdlow, M., F. N. Cogswell and N. Krul, Plast. Rubber Processing, March, 11 (1980).

T-1. Takahashi, M. and S. Onogi, J. Rheol., Japan, 3, 1 (1975)

T-2. Takaki, T. and D. C. Bogue, J. Appl. Polym. Sci., 19, 419 (1975).

T-3. Tanaka, H. and J. L. White, Polym. Eng. Sci., 20, 949 (1980).

T-4. Thurber, C., U.S. Patent 699,330 (1901).

T-5. Tobolsky, A. V. and R. D. Andrews, J. Chem. Phys., 13, 3 (1945).

T-6. Toriumi, K., A. Konda and J. Shimizu, Sen-i Gakkaishi, Japan, 38, T49 (1982).

T-7. Tung, L. H., J. Polym. Sci., 46, 409 (1960).

T-8. Treloar, L. R. G., Trans. Inst. Rubber Ind., 19, 201 (1944).

T-9. Treloar, L. R. G., "Physics of Rubber Elasticity," 2nd ed., Clarendon Press, Oxford (1958).

T-10. Trouton, F., Proc. Roy. Soc., A, 77, 426 (1906).

T-11. Trusdell, C. and W. Noll, "The Nonlinear Field Theories of Mechanics," in Handuch der Physik, Springer-Verlag, Berlin (1965).

U-1. Utracki, L. A. and J. E. L. Roovers, Macromol., 6, 366 (1973).

U-2. Utracki, L. A. and J. E. L. Roovers, Macromol., 6, 373 (1973).

V-1. Vinogradov, G. V., J. Polym. Sci., A-2, 8, 1 (1970).

V-2. Vinogradov, G. V., Rheol. Acta, 12, 272 (1973).

V-3. Vinogradov, G. V. and A. Y. Malkin, J. Polym. Sci., A-2, 4, 135 (1966).

V-4. Vinogradov, G. V., V. D. Fikhman and V. Raduchkevich, Rheol. Acta, 11, 386 (1972).

V-5. Vinogradov, G. V., V. D. Fikhman, R. V. Raduchkevich and A. Y. Malkin, J. Polym. Sci., A-2, 8, 657 (1970).

V-6. Vinogradov, G. V., A. Y. Malkin, V. V. Volosevitch, V. P. Shatabv and V. P. Yudin, J. Polym. Sci., A-2, 13, 1741 (1975).

V-7. Vinogradov, G. V., V. E. Dreval, E. K. Borisenkova, M. K. Kurbanaliev and V. G. Shalganova, Rheol. Acta, 20, 433 (1981).

W-1. Wagner, M. H., Rheol. Acta, 15, 40 (1976).

W-2. Wagner, M. H., Ph.D. Dissertation, University of Stuttgart (1976).

W-3. Wagner, M. H., Kunststoffe, 68, 362 (1978).

W-4. Wagner, H. L. and F. L. McCrackin, J. Appl. Polym. Sci., 21, 2833 (1977).

W-5. Wales, J. L. S., Pure and Appl. Chem., 20, 231 (1969).

W-6. Wales, J. L. S., "The Application of Flow Birefringence to Rheological Studies of Polymers," Delft University Press, Netherlands (1976).

W-7. Walter, K., "Rheometry," Chapman and Hall, London (1975).

W-8. Weinberger, C. B., G. F. Cruz-Saenz and G. J. Donnelly, A.I.Ch.E.J., 22, 441 (1976).

W-9. Werkman, R. T., personal communication (1979).

W-10. Wessling, R. A., Trans. Soc. Rheol., 9, 95 (1965).

W-11. White, J. L., J. Appl. Polym. Sci., 8, 1129 (1964).

W-12. White, J. L., Polym. Eng. Sci., 15, 144 (1975).

W-13. White, J. L., Rheol. Acta, 14, 600 (1975).

W-14. White, J. L., Appl. Polym. Symp., 33, 31 (1978).

W-15. White, J. L., in "Rubber Science and Technology," ed. by F. R. Eirich, Academic Press, New York (1978).

W-16. White, J. L. and Y. Ide, in "Fiber and Yarn Processing," ed. by J. L. White, Appl. Polym. Symp., 27, 61 (1975).

W-17. White, J. L. and Y. Ide, J. Appl. Polym. Sci., 22, 3057 (1978).

W-18. White, J. L. and A. Kondo, J. Non-Newt. Fluid Mech., 3, 41 (1977).

W-19. White, J. L. and A. B. Metzner, J. Appl. Polym. Sci., 8, 1367 (1963).

W-20. White, J. L. and W. Minoshima, Polym. Eng. Sci., 21, 1113 (1981).

W-21. White, J. L. and H. Tanaka, J. Appl. Polym. Sci., 26, 579 (1981).

W-22. Wild, L., R. Banganath and D. C. Knobeloch, Polym. Eng. Sci., 16, 811 (1976).

W-23. Wiley, F. E., R. W. Canfield, R. S. Jesionowski and J. Bailey, U.S. Patent 2,412,187 (1946).

W-24. Williams, M. C. and R. B. Bird, Phys. Fluid, 5, 1126 (1962).

W-25. Williams, M. L., R. F. Landel and J. D. Ferry, J. Amer. Chem. Soc., 77, 3701 (1955).

W-26. Winter, H. H., C. W. Macosko and K. E. Bennett, Rheol. Acta, 18, 323 (1979).

W-27. Wyman, D. P., L. J. Elyash and W. J. Frazer, J. Polym. Sci., A3, 681 (1965).

W-28. Wyeth, N. C. and R. N. Roseveare, U.S. Patent 3,733,309 (1973); 3,849,530 (1974).

Y-1. Yamane, H., M.S. Thesis, The University of Tennessee, Knoxville (1982).

Y-2. Yamane, H. and J. L. White, Polym. Eng. Reviews, 2, 167 (1982).

Y-3. Yamamoto, M., Busseiron Kenyu, Japan, 59, 1 (1953); 60, 38 (1953); 67, 17 (1953); 73, 1 (1954); 78, 51 (1954).

Y-4. Yamamoto, M., J. Phys. Soc., Japan, 11, 413 (1956).

Y-5. Yamamoto, M., J. Phys. Soc., Japan, 12, 1148 (1957).

Y-6. Yasuda, H., H. Sugiyama and H. Yanagawa, Sen-i Gakkaishi, Japan, 35, T-370 (1979).

Y-7. Yasuda, K., R. C. Armstrong and R. E. Cohen, Rheol. Acta, 20, 163 (1981).

Y-8. Yeow, Y. L., J. Fluid Mech., 66, 613 (1974).

Y-9. Yeow, Y. L., J. Fluid Mech., 75, 577 (1976).

Z-1. Zaremba, S., Bull. Acad. Cracovie, 594 (1903).

Z-2. Zeichner, G., M.S. Thesis, The University of Delaware, Newark (1973).

Z-3. Zeichner, G. R. and P. D. Patel, 2nd World Congress of Chemical Engineering, 334 (1981).

Z-4. Zeppenfeld, R., Kunststoffe, 61, 147 (1971).

Z-5. Ziabicki, A. and K. Kedziersha, Kolloid A., 171, 51 (1960).

Z-6. Ziabicki, A. and K. Kedziersha, Kolloid A., 171, 111 (1960).

Z-7. Ziabicki, A. and K. Kedziersha, Kolloid Z., 175, 14 (1961).

APPENDIX

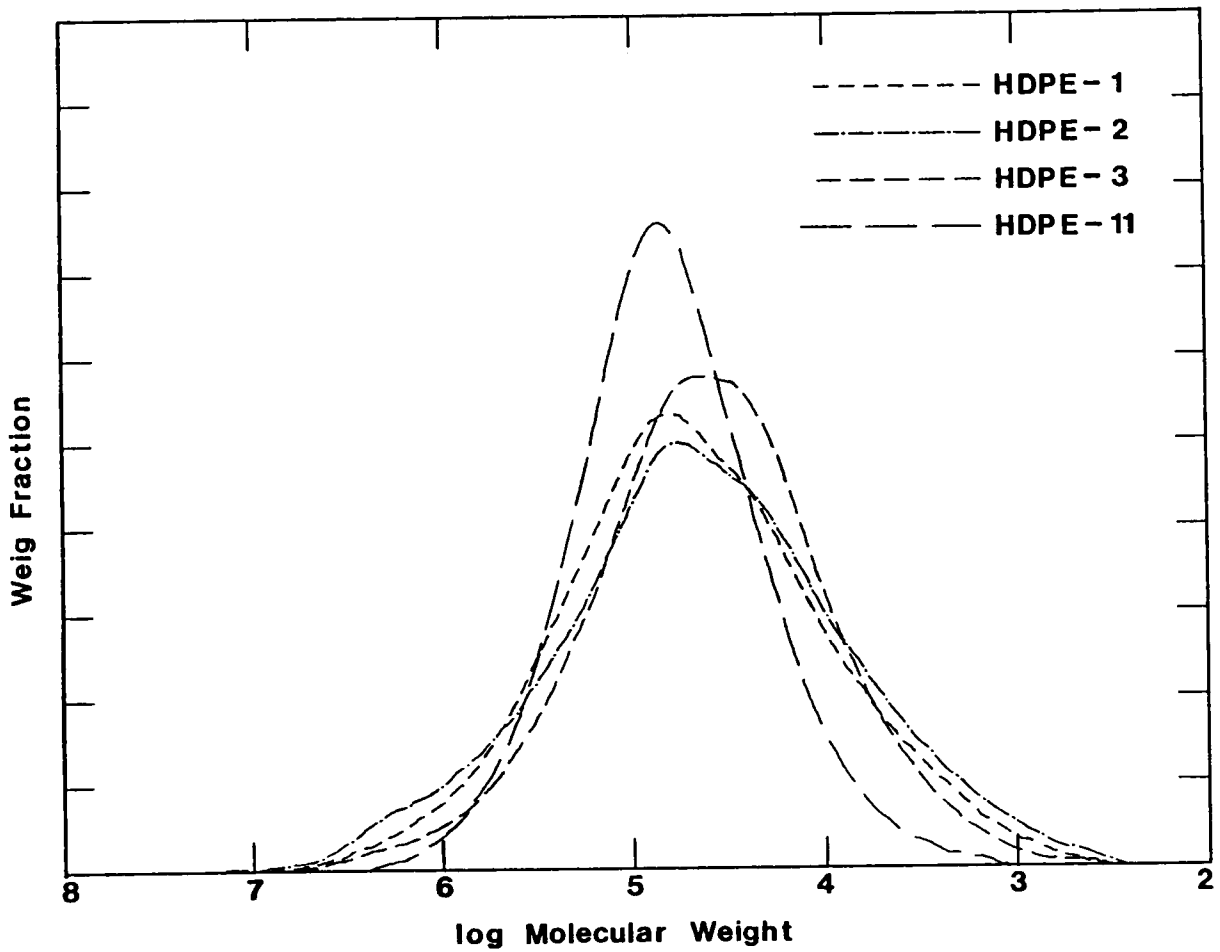

Figure A.1. Molecular weight distribution curves for four high density polyethylenes investigated (HDPE-1, HDPE-2, HDPE-3, HDPE-11).

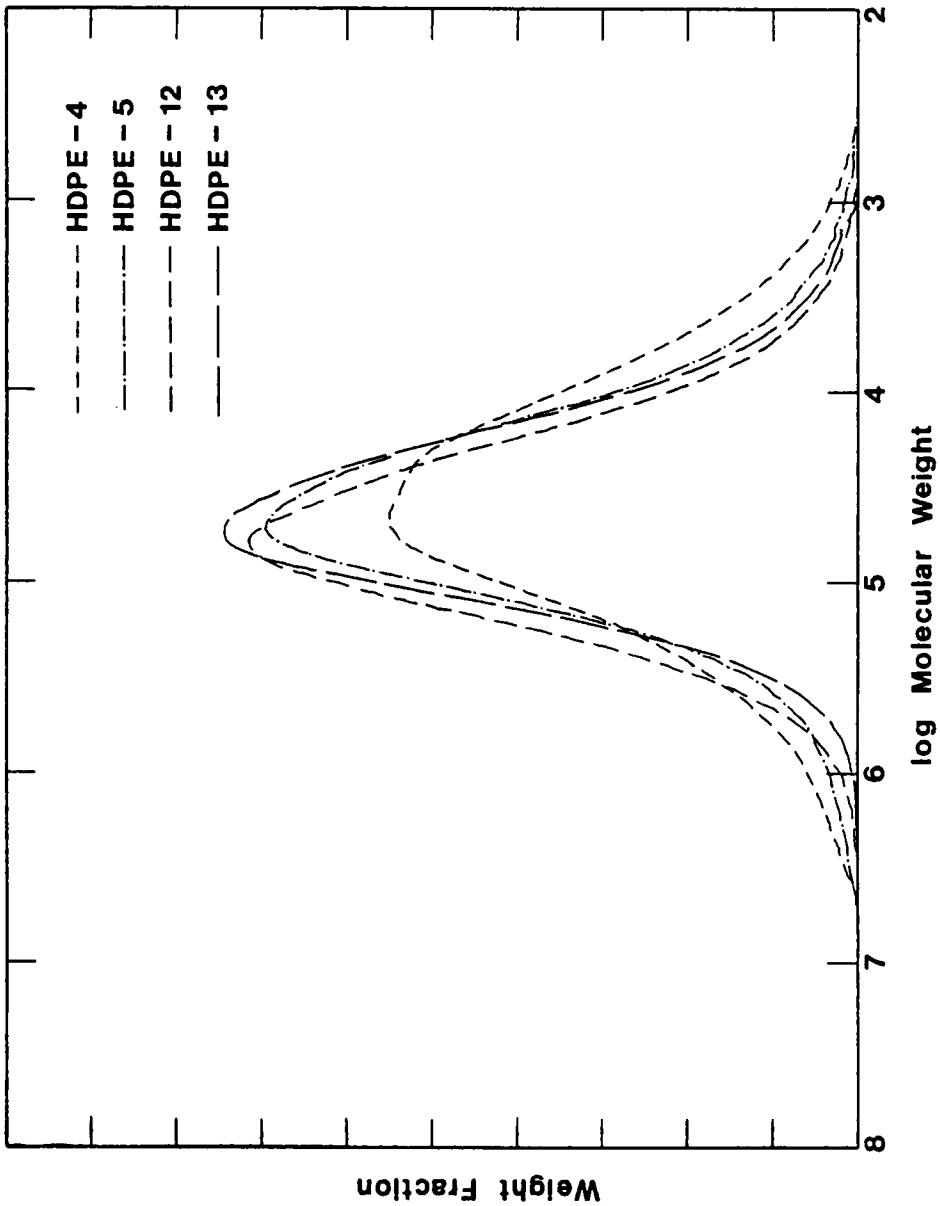

Figure A.2. Molecular weight distribution curves for four high density polyethylenes investigated (HDPE-4, HDPE-5, HDPE-12, HDPE-13).

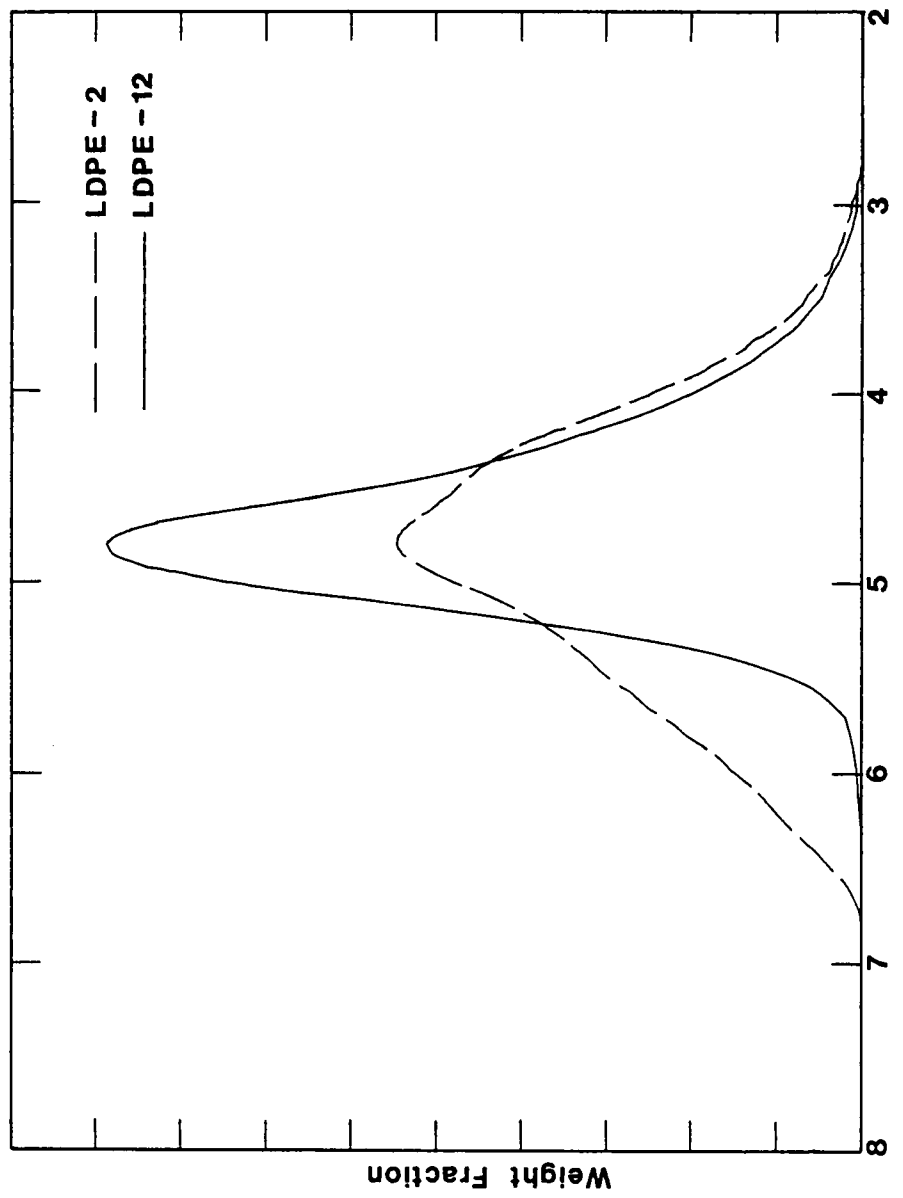

Figure A.3. Molecular weight distribution curves for two high density polyethylenes investigated (LDPE-2, LDPE-12).

VITA

The author, Wataru Minoshima (箕島 亘) was born in Kobe, Japan, on November 27, 1952, as the eldest son of Mr. and Mrs. Yasuhiko Minoshima. After completing his elementary education from kindergarten to high school in Fukuyama, Japan, he was admitted to the Kyoto University of Industrial Arts and Textile Science in April, 1971. He studied polymer processing for his bachelor's thesis at that university and received a Bachelor of Science in Fiber Chemistry in March, 1975.

He continued his education in graduate school at the same university until August, 1976. He entered The University of Tennessee, Knoxville, in the Fall of 1976. He received the Master of Science degree in Polymer Engineering in December, 1978. His Master of Science thesis involved the rheological properties and processing of polypropylene melts of varying molecular weight and distribution.